Multi-purpose gel:

From supramolecular envirogel to high-value applications

Babatunde Omosehin Okesola

A thesis submitted for the degree of

Doctor of Philosophy

University of York

Department of Chemistry

December 2015

Abstract

Dibenzylidene-D-sorbitol (DBS) has remained a well-known low molecular weight gelator of organic solvents for over 100 years. As such, it constitutes a very early example of supramolecular gels. It has found widespread applications such as personal care products and high-tech applications.

Despite the versatility of DBS as an organogelator and industrial feedstock, none of its existing derivatives could gel water. Herein, functionalization of the aromatic 'wings' with various functionalities and their gelation profiles were described. None of the synthesized derivatives but **DBS-COOH** and **DBS-CONHNH$_2$** could undergo gelation in water. **DBS-COOH** formed a stable hydrogel by pH-switching while the **DBS-CONHNH$_2$** formed stable hydrogels across a wide range of pH values by a heat-cool cycle. CD spectroscopy and SEM were used to show that these functionalities control the aggregation mode of the parent DBS.

DBS-COOH and **DBS-CONHNH$_2$** hydrogels demonstrated a significant uptake of dyes from model polluted water and hence we call them supramolecular envirogels. **DBS-COOH** demonstrated higher affinity towards methylene blue at ambient conditions but **DBS-CONHNH$_2$** demonstrated a pH-dependent selectivity towards various dyes. Lead, cadmium and mercury were significantly adsorbed by **DBS-CONHNH$_2$** .The maximum metal loading of 1:1 molar ratio was obtained at neutral ambient pH condition and 2:1 molar ratio at basic pH. The adsorption processes fit pseudo-second-order kinetic and the Langmuir isotherm models.

DBS-CONHNH$_2$ were used to recover precious metals from a model mine tailing with greater selectivity towards precious metals than earth-abundant metals. The adsorbed precious metals were reduced in situ to nanoparticulate form. Interestingly, the hydrogel–NPs exhibited higher conductance and electrocatalytic activities than bare gels and/or carbon electrodes.

Solubility of the APIs in water was enhanced by forming complexes with the **DBS-CONHNH$_2$** while the mechanical stability and morphology of the native hydrogel was influenced by the presence of APIs. APIs were released under basic pH conditions in a controlled-manner.

Table of Contents

List of Figures

List of Schemes

List of Tables

Acknowledgement

I would like to thank Professor David K. Smith for giving me the opportunity to study under his supervision. His supports especially when I was unable to secure financial support towards my study will ever remain indelible on my mind. The benevolence of Dr Tony Wild through his generous Wild fund scholarship for international students in the Department of Chemistry was a saving grace for me. It is hard to forget Nigerian's gari and palm oil bought for me many times by Dr Avtar Matharu whenever he travels to Manchester or Leeds. I would like to thank past and present members of the group who have contributed to my success story. In particular, Dr William Edwards who mentored me when I newly started in the group, Dr Bromfield Stephen for helping me to understand some synthetic strategies and Ching Wan Chan who I always refer to as my 'back-up' both financial and material wise. I would also like those who helped me with the technical aspects of my project; Sindhu Krishna for designing the bottomless vials, Dr Alison Parkin for electrochemical characterization of conductive nanogels, Heather Fish (NMR), Dr Karl Heaton (Mass spec), Dr Andrew Leach (CD), Meg Stark (SEM/TEM), Dr Kellye Curtis (XPS), Darren Philips (ICP-MS), Dr Helen Parker (ICP-MS), Dr Rebecca Sutton (AAS), Dr Laurence Abbott (Fluorescence), Paul Elliot (FTIR), Chris Mortimer (mechanical), Abigail Storey (Glass blowing). It is hard to forget the contributions of the undergraduate student, Edwards Howe whose MChem project was supervised by me, for immense contributions. Mrs Abimbola K Okesola (my wife), John Iseoluwa Okesola (my son), Mr and Mrs Ade & Alice Okesola (my parent), Joseph Ogunjobi's family, Adegboyega Ehinmowo's family, Pastor Reuben & Roseline Inwe, Mr Babatunde Oyeniyan's family, Mr David Crooks' family, Mr Askew Michael's family and all members of RCCG (Hope centre, York and Chapel of Grace, Dewsbury) for emotional, spiritual and financial supports. Most importantly, I would like to thank the Almighty God, who gives me life and grace to complete my study against all odds.

Declaration

I declared that the work presented within this thesis is entirely my own, except where otherwise acknowledged. This work has not been submitted in part or fully for examination towards any other degrees or qualifications.

Babatunde O. Okesola

1 Chapter 1 - Supramolecular Envirogels: Emerging nanosorbents for water purification

1.1 Introduction

Water is one of the abundant natural resources the earth is endowed with, yet the world is "thirsty", with the scarcity of safe water being a serious challenge confronting mankind in the 21st century. Water is an essential commodity for both fauna and flora. Even though, water constitutes about 70% of the Earth's surface, it is not evenly distributed across the globe. Therefore, despite the numerous large bodies of water that surround humanity, only 2.5% is available in a useable form as freshwater while a larger percentage has no direct usefulness to man because of its high salt content. However, 68% of this meagre amount of freshwater is frozen in the ice cap, leaving about 30% for the diversity of human uses (such as agriculture, recreation, industrial processes, drinking and domestic purposes).[1]

Freshwater might have been assumed infinite by our predecessors in past centuries when the population was sparse, but the Earth can no longer supply water that will be sufficient for her inhabitants.[2] Since late 19th century, a little under a billion (748 million) people from different parts of the World do not have access to improved sources of clean water to meet their basic needs.[3] Nearly half of this population are in sub-Saharan Africa. Therefore, it has been projected that if this trend continues in the region, the number of people that lack access to improved sources of clean water would have risen to 547 million by the end of 2015.[4] According to the World Health Organization (WHO), an improved source of clean water is characterized by (i) a significantly increased probability that the water is safe (ii) easy accessibility (iii) protective measures against potential sources of contamination.[5] It is important to emphasise the praise-worthy jobs done by the United Nations (UN); an organization that proposed in its Millennium Development Goals (MDGs) to reduce the number of people that lack access to improved sources of safe water by half by 2015, a target that was met in 2010.[4] Nevertheless, due to the increasingly alarming impacts of climate change, increasing water scarcity, population growth and urbanization, it has been speculated that by 2025, half of the world's population will be residing in water-stressed areas if the existing trends persist.[6] Hence water demand will increase against the finite volume of global water in the near future if no drastic measures are taken to control global population or devise water purification technologies that will help sustain the available water.[1]

Because the state of the well-being of humanity hinge on the state of the environment, a close relationship has been established between the quantity of water consumed and the alarming annual death rate caused by water-related diseases and chemical poisoning. For instance, more than 3 million people are estimated to die annually from water-related diseases such as diarrhoea as a result of unsafe drinking water, lack of sanitation and hand hygiene.[6]

1.2 Causes of global water scarcity

A number of factors have been identified as potential reasons for the scarcity of freshwater; primarily among them are agriculture, climate change and pollution.[7]

1.2.1 Agriculture

Agriculture is the chief "culprit'' among the factors draining global water, hence it is responsible for global water scarcity. Freshwater is consumed in a variety of agricultural practices ranging from fertilizer and pesticide applications to irrigation of farmlands. Irrigation, which is the artificial supply of water to farmland so as to aid crop growth, especially in drought, accounts for about 70% global freshwater consumption. The Food and Agriculture Organization of the United Nations (FAO, 2007),[8] has reported that because of the need to meet the rising demands for foods and industrial raw materials, agriculture is under severe threat with respect to global freshwater scarcity. Considering the trend of declining global water, the future of water and food is uncertain.[9]

1.2.2 Climate change and pollution

The impact of climatic variability on the Earth's freshwater quantity and quality cannot be overemphasized. Climate change can occur as a result of natural occurrences or anthropogenic activities. Because there is a direct connection between climate and water cycle, variation in climatic factors such as temperature, wind, precipitation and sunshine have significant impact on the World's freshwater.[10] Bonsor and co-workers, reported that an increase in water temperature leads to a higher rate of freshwater withdrawal from rivers, lakes, reservoir, and oceans via evapo-transpiration and as a result of this, the self-purification ability of the water is compromised, leading to an increase in water-borne diseases. The temperature of water bodies can be increased by the direct impact of climate change (drought) or indirectly from human activities in the form of thermal pollution. Increase in the sea level (due to global

warming), also leads to higher freshwater salinity; an event that contributes to global water scarcity. The vulnerability of the Earth's freshwater to climate variability varies from one region of the World to another with respect to seasonality.[11]

The indiscriminate release of harmful substances directly or indirectly into water bodies is known as water pollution. Any substance which is present in the environment at a quantity beyond the tolerance level, causes offensive effects, impairs the quality of the environment, reduces the quality of life and is capable of causing death, is called a pollutant. Water pollutants can be categorised into biological, chemical and radiological pollutants on the basis of their constituents.[12, 13]

1.2.3 Biological water pollution

Biological water pollution occurs when large numbers of harmful microorganisms (bacteria, viruses and fungi), worms, algae, protozoa etc. are present in water. Decaying organic matter in wastewater, which results from animal and human wastes, are potential sources of these microorganisms.[12, 14] It has recently been reported that 2.5 billion people lack access to improved sanitation, hence 1 billion people (9 out of 10 dwellers of rural areas) engage in open defecation.[3, 15] Open defecation is responsible for a vicious cycle of disease and poverty that is prevalent in low and middle income countries. For instance, if these pathogens are released into water bodies, it results into an epidemic of water-borne diseases such as diarrhoea, typhoid, cholera and onchocerciasis upon exposure to the contaminated water. WHO estimated that about 1.8 billion people use sources of such water that are contaminated by faecal discharge and this has led to a high death rate, especially child mortality rate among inhabitants of the affected geographical locations.[4, 16]

1.2.4 Chemical water pollution

The industrial revolution brought to humanity both benefits and associated woes. Many of the largest global water pollutants come from chemical, petrochemicals, pesticides, metal smelting, food processing, textile, pharmaceutical, pulp and paper industries. According to the toxics release inventory (TRI) published by the United State Environmental Protection Agency (US EPA), more than 2.95 million metric tons of hazardous chemicals are discharged yearly from about 2000 industrial communities into the environment, and about 43,360 metric tons have been documented as cancer-inducing substances.[17] Crude oil and petroleum products,

metalloids (nitrate, perchlorate, and phosphate), chlorinated solvents, metals and their compounds, pesticides and herbicides (e.g DDT), dyes and dyestuffs, endocrine disruptors and pharmaceuticals are the most prominent among the chemicals that contaminate global waters when discharged deliberately or unintentionally into the environment.[18]

The presence of pharmaceutical compounds as parent compounds or metabolites in the aquatic environment is increasingly becoming an environmental concern, hence attracting global attention.[19, 20] Because drugs are not usually completely assimilated into human or animal bodies after use, they are often introduced into sewage systems by human excretion and soil/ground water by animal excretion as liquid manure. Therefore, pharmaceuticals reach surface water as a result of incomplete removal during sewage treatment and run-off from agricultural sites.[21] Disposal of unused drugs and direct discharge of effluents from pharmaceutical industries are alternative routes by which they also enter into aquatic systems.[22] Their presence in the rivers, lakes, and oceans could elicit adverse health risks to the aquatic animals and the people that feed on harvested fish from such rivers.[23] Levaquin **1.0** [24] and sulphanilamide **1.1** (Figure 1.2.1)[25] are examples of antibiotics of which adverse effects on aquatic organisms have been reported.[26]

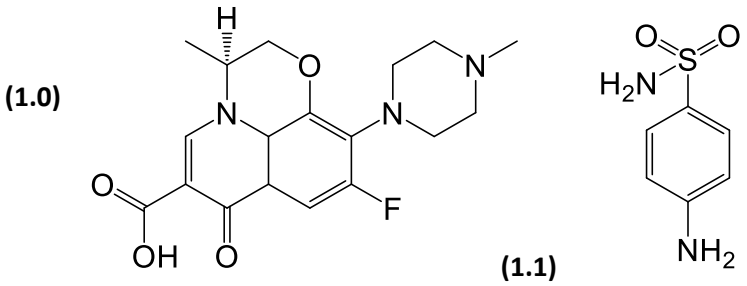

Figure 1.2.1 Chemical structure of Levaquin **1.0** and Sulfanilamide **1.1**

In recent times, Rúa-Gómez and Püttmann demonstrated that wastewater treatment plants are active dischargers of pharmaceuticals such as the analgesic tramadol **1.2** and **1.3**, the anaesthetic lidocaine **1.4**, the anti-depressant venlafaxine **1.5** and their metabolites; *O*-desmethyltramadol **1.6** and **1.7** and *O*-desmethylvenlafaxine **1.8** into surface water.[27]

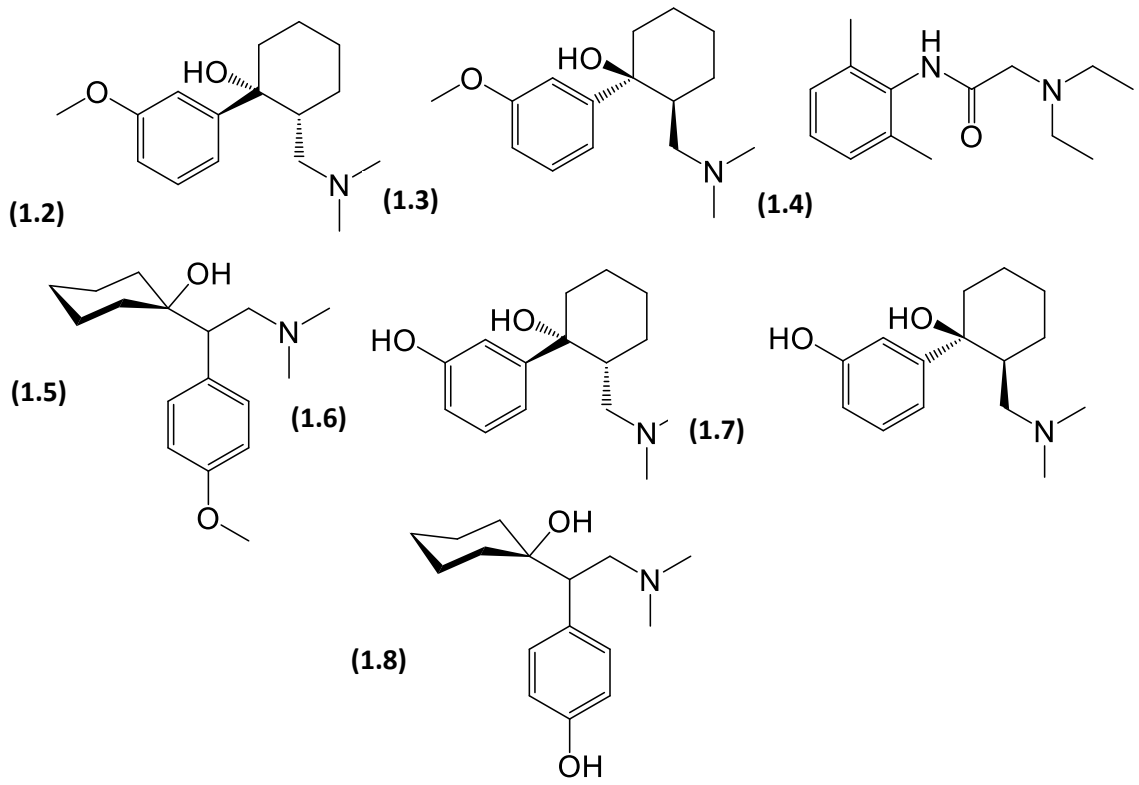

Figure 1.2.2 Chemical structure of (a) *R*-tramadol **1.2** (b) *S*-tramadol **1.3** (c) lidocaine **1.4** (d) venlafaxine **1.5** (e) *R*-O-desmethyltramadol **1.6** (f) *S*-O-desmethyltramadol **1.7** (g) O-desmethylvenlaflaxine **1.8**

Heavy metals are another class of chemical water pollutants. These are metallic elements or metalloids with relatively high densities. Their densities are greater than 4 g/cm^3 or more than five times the density of water.[28] Prominent in this category of toxic metals are mercury (Hg), lead (Pb), cadmium (Cd) and arsenic (As). Heavy metals enter water bodies as a result of geogenic factors or anthropogenic activities. For instance, heavy metals such as arsenic enter groundwater from the natural sources in the form of arsenate-iron oxide.[29] Human beings discharge heavy metals into the environment through industrial processes such as battery manufacturing, mining, smelting, electroplating, metal finishing, refining, forging, automobile exhausts[30] The alarming rate of heavy metal discharge into the environment is a global concern because they are resistant to degradation, and thus bio-accumulate in the food chain.[31] They cause health hazards to plants and animals upon exposure. Such hazards include reproductive disorders, congenital disorders, cancer, brain retardation, and lethargy.[32] Heavy metals enter the blood, kidney, liver, bones, brains and muscles through the gastrointestinal tract or nasal tract.[33]

1.2.5 Radioactive water pollution

Naturally occurring radionuclides such as those from the family of the uranium-238 nuclear fission chain; uranium-238 (^{238}U), uranium-234 (^{234}U), radium-226 (^{226}Ra) and radon-222 (^{222}Rn) and those from the family of the thorium-232 series; thorium-232 (^{232}Th), thorium-230 (^{230}Th), thorium-229 (^{229}Th), radium-228 (^{228}Ra) and lead-208 (^{208}Pb) are usually present in different concentrations in drinking water, as they are normally released from rocks and minerals that constitute the aquifer.[34, 35] Even though, thorium is 3-4 times more abundant than uranium in the earth's crust, it rarely exists in water due to its poor solubility. However, its descendant, radium-228 is more highly radiotoxic, hence a critical contaminant in water. The beta-gamma emitter, potassium-40 (^{40}K) of primordial origin and the cosmogenic tritium (^{3}H or T) which occurs in rain water as tritiated water are also widely distributed in water bodies.[36] Besides the predisposition to radiotoxicity caused by nature, anthropogenic activities such as radioactive fallout triggered by accidents or nuclear explosions have added significantly to the discharge of radioelements into rivers, oceans, streams and lagoons. A recent example is the massive contamination of water in Tokyo during the Fukushima Daiichi nuclear plant accident.[37] It is important to note that radionuclides can become ionised by displacing electrons in various organs in the body such as lung, kidney and also the DNA, thereby disrupting their functions which gives rise to organ dysfunctions and genetic disorders in the human body.[38] Therefore, WHO has set out a provisional guidance for a maximum concentration level of uranium in drinking water as 30 µg/l (ppb) based on its chemical toxicity, corresponding to a ^{238}U concentration of 186 mBq/l which is about 16 times lower than the reference level (3 Bq/l) for its radio-toxicity. Also, the amount of U-234 present in water is greater or equal to that of the U-238.[39]

1.3 Conventional methods for water purification

In order to remove toxic substances from contaminated water systems, conventional physicochemical methods such as chemical precipitation, coagulation-flocculation, ion exchange, solvent extraction and filtration, evaporation, electrochemical treatment, oxidation processes and membrane methods have been used.[40-47] However, all of these conventional methods are characterized with some inherent drawbacks such as limited concentration of pollutants, generation of large amount of toxic sludge, and high capital costs. Therefore, adsorption of water pollutants onto solid materials is currently attracting global interest due to

features such as; simplicity, ease of operation and handling, regeneration, near-to complete removal of pollutants and economic feasibility.[48] Activated carbon (AC) is an adsorbent which has demonstrated huge success in the past century due to its high surface area.[41] Commercial AC is often obtain by carbonising raw materials such as wood, bitumen, and anthracite. However, the use of commercial activated carbon for removing pollutants from water is gradually disappearing because its regeneration and reuse is costly.[49] Therefore, a number of non-conventional sorbents such as zeolite, cyclodextrin, chitin, chitosan, mineral clay and sawdust are currently being considered as replacements for commercial AC due to factors such as low-cost, high abundance, high adsorption capacities and benignity.[48, 50] Ramakrishna *et al* (2012) have recently reviewed the use of nanomaterials such as carbon nanotubes, graphene, dendrimers, metal nanoparticles and polymer nanocomposites as emerging adsorbents for environmental remediation.[51] Nonetheless, these materials are expensive and difficult to make.

1.4 Supramolecular gels; emerging nanosorbents for water purification

Gels are colloidal soft materials which demonstrate the continuous flow properties of liquid-phase materials and the rheological properties of solid-phase materials on the analytical time-scale.[52] Gels are easily recognised soft materials with a wide range of different applications, for example, being used in cosmetics, pharmaceutical preparation, as greases/lubricants, electrolytes, sealants and in the food industry.[53-55] A scientifically acclaimed and emerging class of gels called supramolecular gels[56-58] encompass all gel materials that are formed via the interplay of non-covalent interactions - hydrogen bonds, van der Waals forces, solvophobic effects, π-π stacking, dipole-dipole, charge-transfer and coordination interactions. Common among this class are the low molecular weight gelators (LMWG), also known as molecular gelators.[52, 59] Low molecular weight gelators are organic compounds with a molecular weight below 2000 Da having the potential to gel organic solvents or water. They are known as organogelators if they gel organic solvents and hydrogelators if they gel water. Over the past century, a wide range of molecular building blocks including peptides, ureas, sugars, steroids and bile acids, lipids, nucleobases, and simple alkanes have demonstrated their potential as efficient gelators.[60-62]

In this type of supramolecular gel, the molecular-scale information incorporated into the LMWG molecules is translated into the nanofibres via a hierarchical self-assembly process, and the fibres tangle with one another to form an extended nanofibrillar network which

immobilizes a large volume of solvent under the influence of capillary forces (**Error! Reference source not found.**).[63]

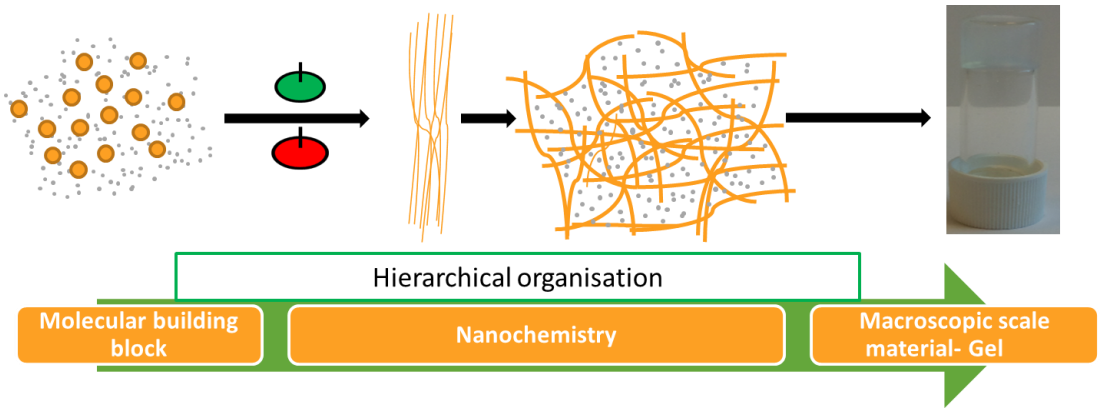

Figure 1.4.1 ON/OFF switching of supramolecular gelation

Light, pH switching, heat-cool cycle, solvents, analytes, ligands, oxidant and sonication *inter alia* other factors capable of switching on or off the gelation of potential LMWGs have been widely demonstrated. For example, a molecular hydro/organogel is formed when a hot solution (hydrosol or organosol) of a LMWG is cooled to a certain temperature, known as phase transition temperature (T_{gel}). Intriguingly, gels of LMWGs in water or organic solvents have been investigated for high-tech applications in area as diverse as nanomedicine, catalysis, drug delivery, light harvesting, cell culturing, tissue engineering, nanoelectronics, templating and sensing.[64, 65] These applications, among many others, are attributed to the inherent properties such as the responsiveness, tunability, biocompatibility and easy modification of the molecular motifs of the gelators, and the dynamics of supramolecular interactions that uphold the three-dimensional self-assembled nanofibrillar networks.

As part of global efforts tailored toward combating the rapid pace of environmental damage, supramolecular gels have attracted some attention in the past decades as emerging nanodevices for water purification. These materials can therefore be referred to as *supramolecular envirogels*; a generic term coined for the first time to describe supramolecular gels capable of sequestering pollutants from the environment. There are many different LMWGs with different structures that are capable of forming supramolecular envirogels. As such, the use of supramolecular envirogels to remove oils, dyes and heavy metals from water are discussed in subsequent sections.

1.4.1 Supramolecular envirogels for oil spill remediation

Marine pollution mostly through accidental discharge of crude oil and petrochemicals is a serious environmental problem confronting the 21st century. For instance, waterways have witnessed an alarming rate of oil spills since 2000, especially the 5 billion barrels of crude oil released in the Gulf of Mexico in 2010.[66] This is problematic from both the economic perspective through wastage of valuable non-renewable oil and the alarming impacts on health through the consumption of sea foods obtained from oil polluted seas, impacts on climate change as a result of the accumulation of the volatile hydrocarbons in the stratosphere and devastating effects on the delicate balance of marine ecosystem due to the residual toxic oil.[67] Conventional methods for remediating oil spills include; absorption, dispersion, bioremediation and solidification.[68-73] Sorbents are solids that absorb the oil, dispersants emulsify the oil and solidifiers are polymeric materials that gel the oil. However, they are not economically viable for a large scale solution, or themselves leave behind toxic residues which bioaccumulate through food webs. Therefore, low molecular weight gels offer promising potentials for congealing oil spills owing to their inherent properties such as; (i) selective gelation of oil phase from oil-water biphasic mixture (ii) simple synthesis at low cost (iii) environmental benignity (iv) thermoreversibility to facilitate oil recovery from the gel (v) recyclability and reusability.[74]

The use of small organic molecules to gel oil and oil spills have been known since 1970s but they are not usually cited in literatures. An early example of gelling oils with small organic molecules was demonstrated by Saito in 1976.[75] In the original patent, certain derivatives of *N*-acetyl amino acids was admixed with non – polar organic solvents such as kerosene with stirring at an elevated temperature (120 °C). Interestingly, a stable gel was formed within 2 min as the solution cools to room temperature. As a proof of principle for oil-spill remediation, a solution of *N*-lauroylglutamic acid- α γ -di-n-octylamide (1 g) in benzene (5 mL) selectively gelled about 25 g of heavy oil suspension in the presence of seawater within 20 min. The aromatic solvent was also entrapped with a small amount of water. The solidified oil was filtered off through a wire gauze (20 mesh). As such, this technology should extend the frontier of knowledge in the area of oil-spill remediation but there was no follow-up research in this area until 1985 when the use of acetalized D-sorbitol derivatives (structures and chemistry of sorbitol derivatives are comprehensively discussed in Chapter 2) to gel crude oil in the presence of seawater was patented. For instance, when a slick of kerosene on the surface of seawater

was treated by spraying with a mixture of hydrophilic solvents such as *N*–methyl-2-Pyrrolidone (NMP) and hydrophobic solvents such as liquid palm oil containing 5% dibenzylidene – D – sorbitol (DBS) and polyoxyethylene lauryl alcohol ether (1%) for 10 min. In this way, the oil phase was selectively gelled by DBS within 10 min, leading to recovery of 100% of the kerosene with only 1% water content. In another composition, 6 wt% 1,3:2,4-di(*p*-methylbenzylidene)-D-sorbitol enables the 95% recovery of gasoline in seawater with only 0.3% water content. The immobilised oil was scooped off the surface of the seawater using a net having 2 mm x 2 mm mesh opening and easily recovered by either dilution or distillation.

In the past decades, several molecular building blocks such as sugars alcohols, amino acid amphiphiles, aromatic amino acids, 12-hydroxyl-*N*-alkyloctadecanamide, and glucosamines have been well-exploited to fabricate envirogels for this application.[74] Low-molecular-weight gelators may find real-life applications such as mopping oil leaking on contaminated surfaces and perhaps enhance safety associated with transportation of oil. This approach has been extended to oil spill remediation via a phase-selective in situ gelation of the oil from an oil-water biphasic mixture.

The first example of phase-selective gelation of oil from oil-water mixture was reported by Bhattacharya and co-workers.[76] In their investigation, an amino acid, *N*-lauroyl-L-alanine **1.9** (Figure 1.4.2) was synthesized and its ability to selectively gel aromatic, aliphatic hydrocarbons and commercial oils such as kerosene, petrol and paraffin oils were demonstrated. In this case, a requisite amount of the gelator was added to the biphasic oil-water mixture either by dissolving the gelator in the solvent mixture by heating, or by adding its ethanolic solution. As a result of this, the oil-phase was selectively gelled leaving the aqueous phase unaffected. Interestingly, the oil-gels remained stable for one week. Moreover, the presence of NaCl, $CuSO_4$, $KMnO_4$ and other impurities had no significant effect on the selective gelation event.

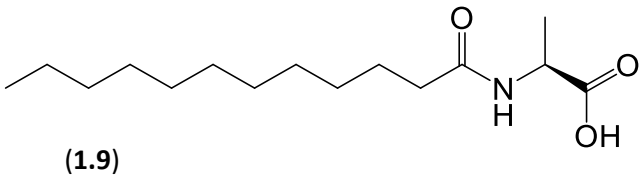

(**1.9**)

Figure 1.4.2 Chemical structure of *N*-lauroyl-L-alanine **1.9**

Dastidar and co-workers reported a series of organic salts that demonstrated selective gelation of oils from oil-water mixture.[77, 78] For instance, one of the gelators **1.20a** (Figure 1.4.3)

selectively congealed petrol, kerosene, cottonseed oil, sunflower oil and coconut oil in a biphasic oil-water mixture. The traditional heating-cooling circle with or without some drops of methanol added was employed to achieve gelation process. Interestingly, the presence of inorganic salts did not significantly affect the gelation process. Similarly, another series of organic salts **1.20** – **1.22** (Figure 1.4.3) synthesized by the authors exhibited phase-selective gelation of petrol or coconut oil from their mixture with water. The preferential dissolution of the gelators in the oil-phase mediated the phase-selective gelation. It is noteworthy that such two component gels are not usually strong due to the weak intermolecular interaction(s) between the two components and such, the gels might not be able to withstand the rigour of separating the immobilized oil from the mother aqueous liquor.

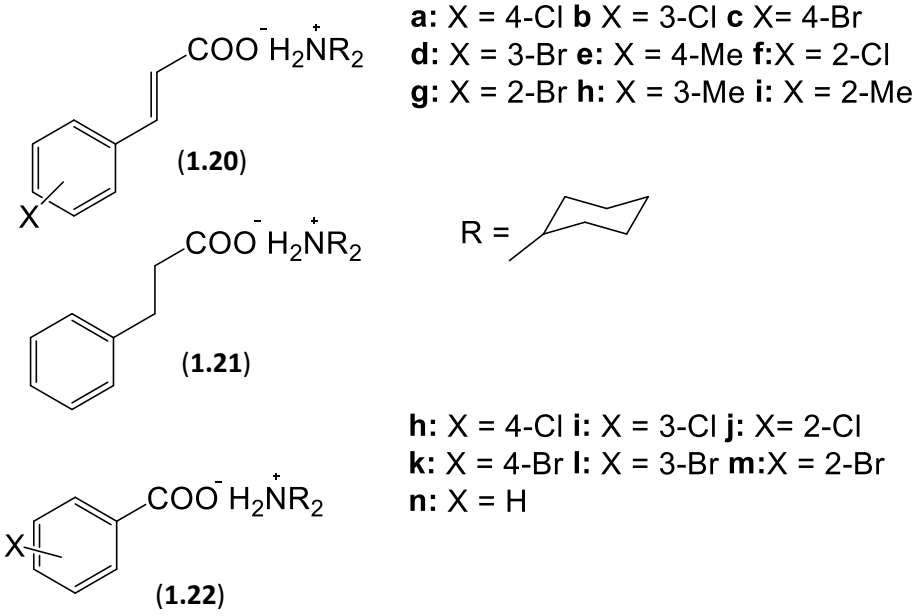

Figure 1.4.3 Chemical structures of organic salt based gelators **1.20**, **1.21** and **1.22**

In 2006, Dastidar and co-workers developed a combinatorial library of 40 primary ammonium monocarboxylate salts derived from cinnamic acid derivatives **1.23** and *n*-hexadecyl amines **1.24** (Figure 1.4.4).[79] A few among them **1.23a-c** exhibited selective gelation of petrol, kerosene and diesel from their corresponding mixtures with water (as shown in Figure 1.4.4d).

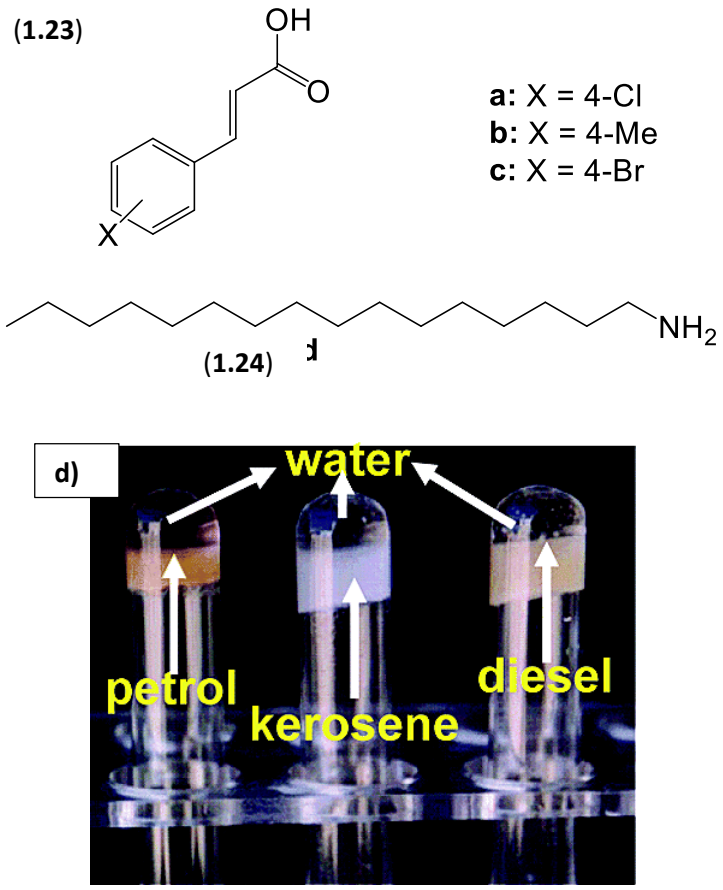

Figure 1.4.4 Chemical structures of cinnamic acid derivatives **1.23** (a-c) that form gel with primary amine **1.24** and (d) the photo of phase-selective gelation of commercial oils from their mixtures with water [Reproduced from ref. 79].

John and co-workers,[80] reported a class of sugar-based gelators that efficiently immobilized diesel, mineral oil, silicone oil, crude oil fractions (alkanes with $n > 9$ carbon atoms) and mixture of hydrocarbon solvents (aromatic and aliphatic) from their mixtures with water at room temperature. In this case, a solution of selected gelators **1.25** and **1.26** (Figure 1.4.5) in ethanol at a high concentration was added to 1:1 mixture of oil and water. The gelator spontaneously migrated into the oil-phase thereby forming strong and self-supported gels at room temperature. Interestingly, the purity of the gelator or the presence of impurities or pH conditions (basic, acidic or neutral) did not have any significant effect on the gelation process. Hydrogen-bonding was the prime intermolecular interaction that mediated selective gelation. John and co-workers[81] have recently demonstrated how essential the philosophy of green chemistry is in designing and developing materials, especially molecular gelators for

environmental remediation. As such, sugar-based gelators are ideal candidates for such eco-friendly oil-spill remediation and design of biorefinery.

(**1.25**)

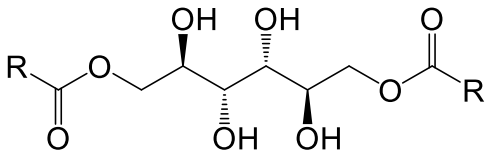

a: R = C_3H_7
b: R = C_7H_{15}

(**1.26**)

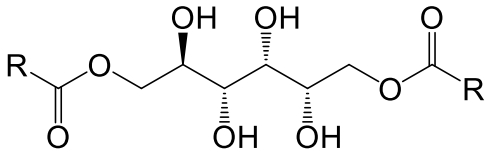

c: R = C_3H_7
d: R = C_7H_{15}

Figure 1.4.5 Chemical structures of sugar-based gelators **1.25** and **1.26**

Phase-selective gelation systems that involve a heating-cooling cycle or addition of a co-solvent are not especially practical for a real-life applications. The heating-cooling method is not applicable to oil recovery from sea while the use of co-solvents leads to further addition of large volume of toxic carrier solvents into the sea.[82] Therefore, Fang and co-workers reported a family of cholesterol-based gelators **1.27** (Figure 1.4.6a-c) that exhibited superior phase-selective gelation of xylene and / or kerosene from their mixtures with water at room temperature.[83] In both cases, the gelators demonstrated remarkable gelation of the oil-phase by simple mixing with the oil-water mixture and neither heating nor addition of a co-solvent was required. Interestingly, one of gelators **1.27a** (Figure 1.4.6a) demonstrated selective gelation of xylene at a temperature as low as 0 °C and another **1.27b** could only gel kerosene between 25 – 30 °C. The rheological properties of the gelator / xylene systems show that exhibited an enhanced mechanical strength. Therefore, if we want to think of suitable candidates for a real-life immobilization of oil slick in the presence of water under ambient conditions without introducing a secondary pollutant, the gelators **1.27a-c** would probably be ideal.

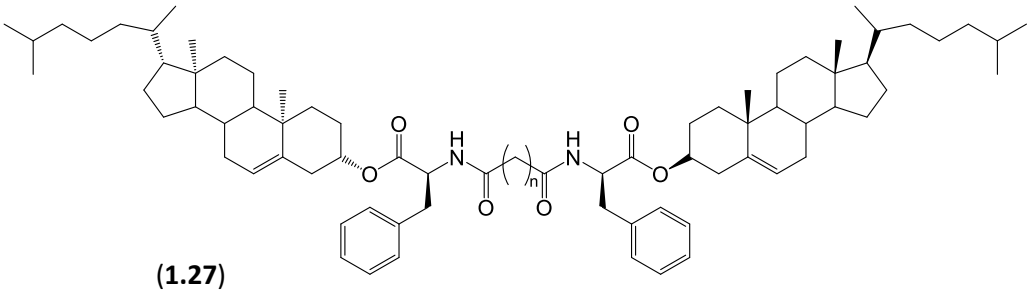

(**1.27**)

a: *n* = 2, LL; **b:** *n* = 3, LL; **c:** *n* = 2, DD

Figure 1.4.6 Molecular structures of the diacid amides of dicholesteryl L-phenylalaninate **1.27**.

In 2009, Fang and co-workers have also reported the ability of $A(LS)_2$ type cholesteryl derivatives **1.28** and **1.29** (Figure 1.4.7) to selectively gel chloroform, tetrachloromethane, toluene or xylene from their mixtures with water at room temperature.[84] In all cases, neither heating nor addition of a co-solvent was employed. Interestingly, the gelators exhibited a significant resistance to salts, confirming their possible suitability for a real-life applications. However, it should be noted that they did not exhibit gelation of crude oil and it is important to be able to translate gelation events precisely into different solvents.

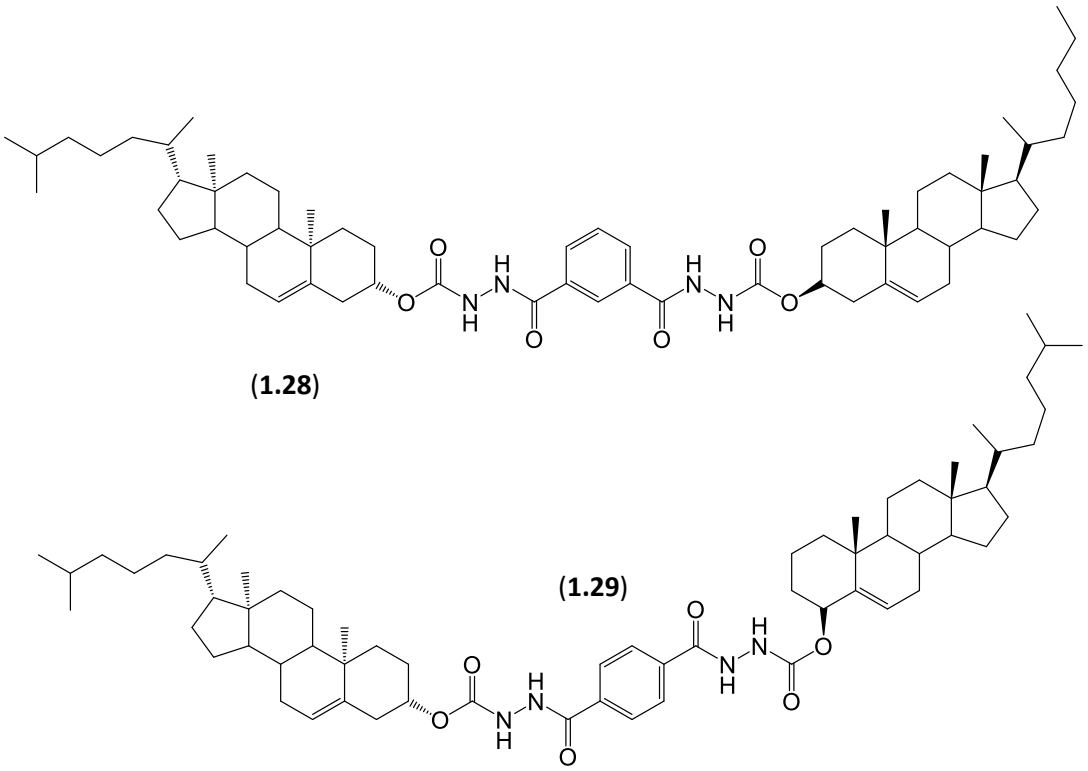

Figure 1.4.7 Molecular structures of cholesteryl-based gelators **1.28** and **1.29**

Interestingly, Prathap and Sureshan reported a novel approach which is practical to a real-life scenario of oil spill recovery from sea using a sugar-based organogelator.[82] In this case the gelator **1.30** (Figure 1.4.8) was initially dissolved in a small volume of commercial petrol or diesel and aerially sprayed onto the oil-phase of the oil-water biphasic mixture such that the carrier solvent and the oil slick are both immobilised by the gel. The gelator demonstrated an efficient gelation of the oil-layer at 2 to 4 wt % minimum gelation concentration for the petrol but a much lower concentration for the diesel (0.75 wt %). The gels were exceptionally strong as they could be taken out of the water surface with forceps, could withstand the weight of a metallic coin for several days (as shown in Figure 1.4.8a-d) and exhibited a high elastic modulus (~100,000 Pa). The presence of NaCl and other ions did not affect the gelation system. It was further demonstrated that hydrogen-bonding is the driving force for the phase-selective gelation.

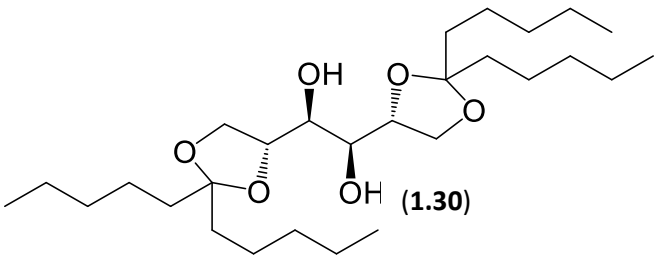

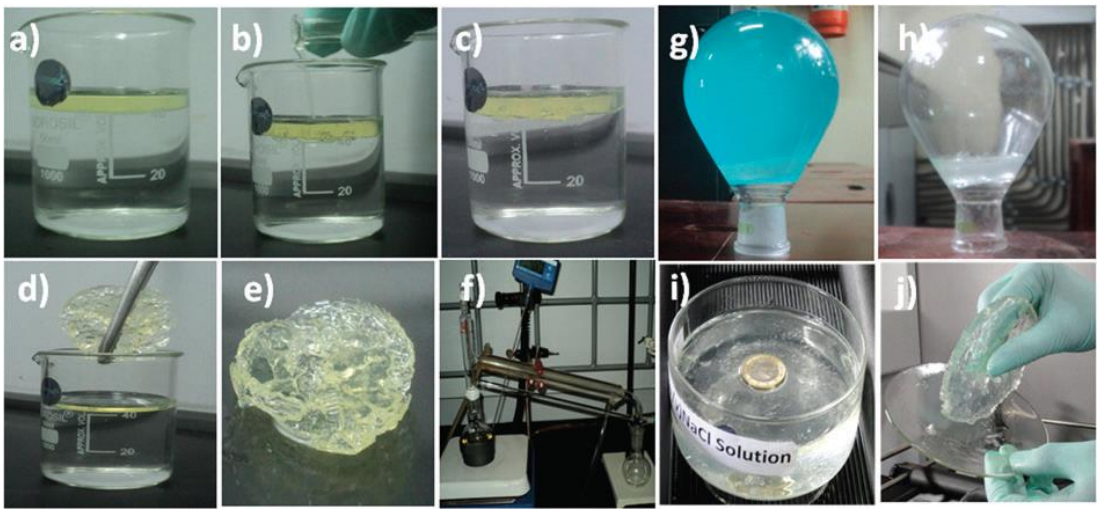

Figure 1.4.8 Molecular structure of the sugar-based gelator **1.30**. (a) Biphasic mixture of diesel and water. (b) Introduction of a gelator solution into the biphasic mixture. (c) The solidified oil phase (d) Removal of congealed oil phase. (e) Isolated gel. (f) Recovery of diesel by distillation. (g) A 3 wt% gel holding the weight of a litre of a dilute $CuSO_4$ solution. (h) The gel after removing the $CuSO_4$ solution. (i) A metal coin (1 Euro) on the surface of a 1.5 wt% diesel gel on the surface of water. (j) The gel disc formed on the surface of water being taken with hand [Reproduced from ref. 82]

Despite the rapid progress that has been reported in this field of application, supramolecular envirogels that can exhibit instant phase-selective gelation of oils from their biphasic mixtures with water are still rare. Therefore, Fang and co-workers have recently demonstrated two simple gelators **1.31a** and **b** (Figure 1.4.9) that exhibit efficient and instant gelation of petrol, kerosene, diesel, silicone oil, pump oil and pure organic solvents and which they claim to be eco-friendly.[85]

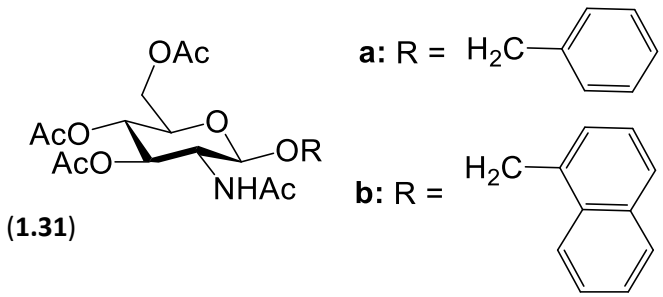

(**1.31**)

Figure 1.4.9 Chemical structures of β-glycosides of *N*-acetyl glucosamine **1.31a** and **b**)

In the initial investigation, the gelation of **1.31a** and **1.31b** in petrol and diesel respectively were carried out using the traditional heating-cooling method. Strong gels (G' ~10^4 Pa) were formed in both cases with critical gelation concentrations (CGCs) ranging from 0.23 - 3.5% wt /vol. In order to demonstrate the practicality of these systems to a real life situation, a concentrated solution of the gelators in THF was added by syringe at the interface of 0.8:2 mixture of diesel / petrol and water in a glass vial at room temperature. Interestingly, gelation occurs within 10 s and full strength gels were formed within 45 s. The oils were recovered from the gels by distillation and the gelators reused more than three times without losing their gelation ability. It was further established that neither the presence of salts in the biphasic mixtures nor low temperature (0- 5 °C) affected the gelation of the oil phase.

In 2013, Lee and Rogers demonstrated the use of 12-hydroxystearic acid (12-HSA) xerogels to adsorb non-polar solvents and various commercial oils from their mixtures with water.[86] The xerogels were prepared by evaporating the solvent component of the organogels of 12-HSA in low boiling solvents; acetonitrile, pentane and diethyl ether under atmospheric pressure for at least 24 h. A known amount of the xerogel from acetonitrile was suspended in the oil phase of the simulated oil spill consisting 3 g of oil and 3 g of water or sea water in a 10 mL beaker. The set-up was left undisturbed for about 1 h and the mass gained was measured afterwards. Interestingly, the xerogel increased in weight by 459 ± 33 wt % and 583 ± 42 wt % in diesel and gasoline respectively against 3.85 ± 0.5 wt % and 5.23 ± 1.2 wt % in distilled and seawater respectively. However, the xerogels of 12-HSA from pentane is not as effective as that of the gelator from acetonitrile due to the differences in the gel networks formed in both solvents. The xerogel from diethyl ether was not used because it is very fragile. The xerogels are thermoreversible, therefore the adsorbed oil can be simply recovered and the xerogel re-used. This study demonstrated that drying gels from different solvents really does yield xerogels with different properties – not just simple powders.

1.4.2 Supramolecular envirogels for sequestering dyes from water

Gels are particularly good candidates for dye removal because they are solvated, yet highly porous materials with nanoscale fibres. This ensures a high surface area of contact between the solid-like network and the liquid-like phase, potentially offering attractive pollutant extraction. Furthermore, they are amphiphilic, making them suitable for removing dyes as the hydrophilic moiety interacts with water while the hydrophobic core adsorb the dyes or vice versa. The gelators are easy to synthesize, cheap and the gels are reversible in nature.[87]

In 2007, Banerjee and co-workers reported the synthesis of phenylalanine based bolaamphiphilic hydrogelator **1.32** (Figure 1.4.10) which exhibits divalent hydrogelation induced by divalent metals within a physiological pH range (6.5-7.2) on sonication, hence the resulting gels were called smart metallo-hydrogels.[88]

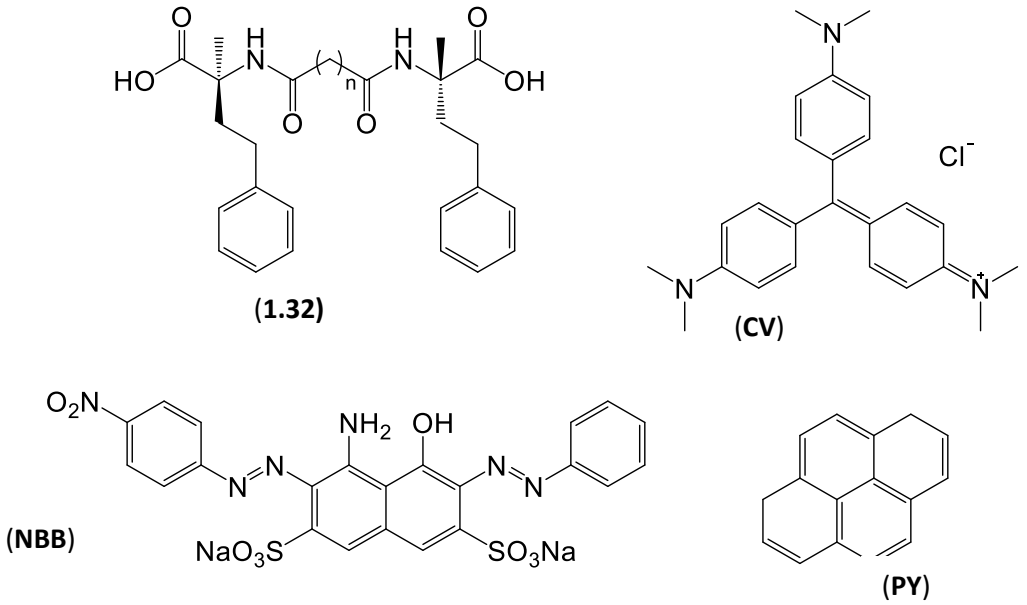

Figure 1.4.10 Chemical structure of a) phenylalanine based bolaamphiphilic hydrogelator **1.32** (b) crystal violet **CV** (c) naphthol blue black **NBB** and (d) pyrene **PY**

Interestingly, the dried gel (xerogel) of this molecule demonstrate efficient uptake of crystal violet **CV** (cationic dye), naphthol blue black **NBB** (anionic dye) and pyrene **PY** (non-ionic dye) (Figure 1.4.10) - it sequestered 63, 84 and 2.8 mgg^{-1} respectively from their aqueous solutions over a period of 24 h. As such, this was first among the various low molecular weight organo/hydrogels, otherwise known as supramolecular ‘‘envirogels’’, for this application. The suitability of this material for a real-world water purification process is limited by its

responsiveness to pH as the pH values of polluted water are not always within a physiological range.[89] However, the supposed limitation has been harnessed to tailor the hydrogels for the entrapment and controlled release of a biological molecule, vitamin B_{12}. At a lower pH (pH 2), the metallo-hydrogel transformed into a precipitate and sol but completely into sol at a higher pH (pH 9), hence vitamin B_{12} is released at pH 9. The ability of this material to demonstrate this application is predicated on the entrapment of the adsorbate within the porous framework of the gel (as shown in Figure 1.4.11) – this was demonstrated using TEM.

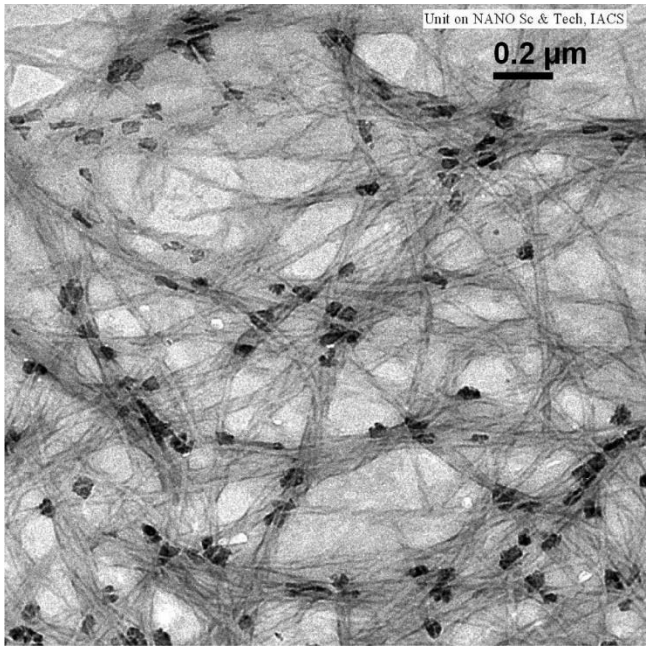

Figure 1.4.11 TEM image of the metallo-hydrogel prepared from bolaamphiphile 1−Co salt at pH 6.5 in the presence of vitamin B12 showing the trapped vitamin molecules within the gel nanofiber network. [Reproduced from ref. 88]

At about the same time, Kang and co-workers demonstrated the ability of a silanated terpyridine-based metallo-organogelator **1.33** (Figure 1.4.12a) which exhibited strong affinity and high uptake for the various model dye candidates - basic blue 41 **BB41**, crystal violet **CV** and bromocresol green **BCG** (anionic) (Figure 1.4.12).[90] The gelator formed stable organogels with and without divalent metal ions in a wide range of organic solvents when prepared via the traditional heat-cool cycle. The presence of metal ions did not have any effect on the morphology of the fibrillar network. However, the amount of the **CV** and **BB41** adsorbed onto the xerogels of **1.33** decreased from 115 and 141 mg^{-1} to 90 and 116 mgg^{-1} in the presence of Cu^{2+} and to 93 and 70 mgg^{-1} in the presence of Zn^{2+} respectively. Conversely, for the anionic

dye, **BCG**, the maximum uptake increases from 87 mgg^{-1} to 159 and 162 mgg^{-1} in the presence of Cu^{2+} and Zn^{2+} respectively. It is assumed that the xerogel is neutral in the absence of the metals but becomes cationic when doped with metal salts, hence electrostatic repulsion between the cationic dyes and the cationic gel could be a reason for the declining uptake while the reverse is the case for the anionic dye. The hydrophobic interaction between the aromatic moieties of the gelator and that of the dyes was reasoned to be the principal driving force for the adsorption process.

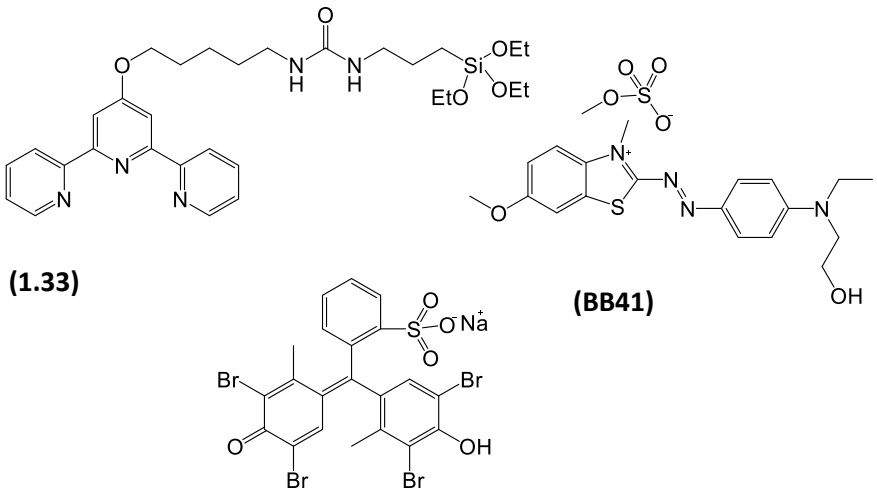

Figure 1.4.12 Chemical structure of (a) terpyridine-based metallo-organogelator **1.33** (b) basic blue 41 **BB41** and (c) bromocresol green **BCG**

A family of dipeptide organogelators which selectively gelled aromatic organic solvents in the presence of water via a heat-cool cycle have been reported by Das and co-workers.[91] The authors demonstrated that structural variation also affects the structure-properties relationships of the organogelators as they differ not only in their fibres network morphologies but also dye uptake abilities. In order to demonstrate the effect of molecular architecture on the dye uptake efficiency of the gelators, the xerogels of dipeptide-based gelators **1.34**, **1.35** and **1.36** (Figure 1.4.13) were interacted with aqueous solutions of **CV** and rhodamine 6G, **Rh6G** (Figure 1.4.13).

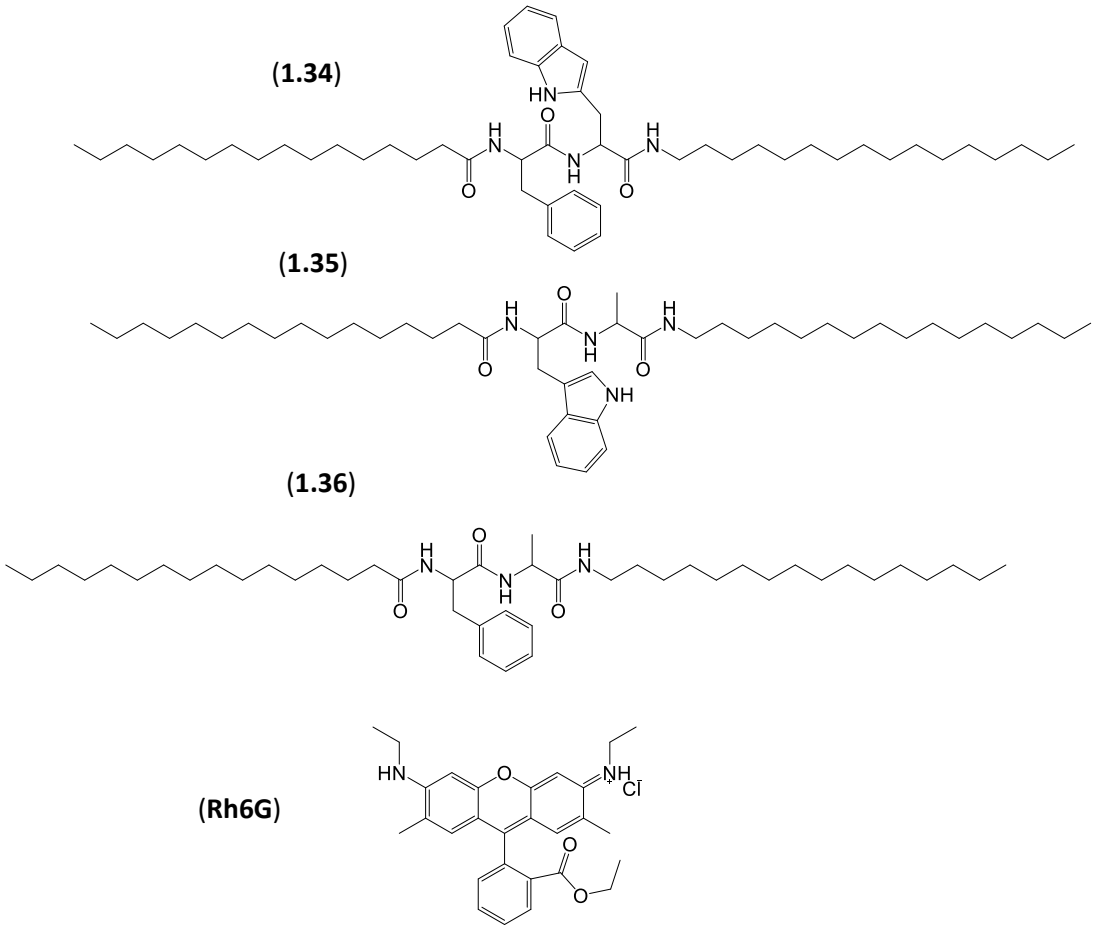

Figure 1.4.13 Chemical structures of dipeptide gelators **1.34** – **1.36** and rhodamine 6G **Rh6G**

It was interesting to observe the highest uptake of crystal violet onto the xerogels of **1.34** (21.7 mgg^{-1}) and **1.35** (14.3 mgg^{-1}) over a period of 10 and 15 h respectively while the other gelators only adsorbed 4-9 mgg^{-1}. However, it took a longer time for both xerogels to adsorb 13.1 and 9.4 mgg^{-1} of **Rh6G**, respectively. It is noteworthy that, the presence of tryptophan moiety as one of the peptide units in the two gelators **1.34** and **1.35** was attributed to the better uptake of both dyes than the non-tryptophan based gelator **1.36**. However, it should be noted that some of the toluene might be expected to leach from the organogel into the purified water, which would obviously be undesirable for application of this technology. Furthermore, the loading levels were relatively low.

A library of tripeptide based hydrogelators **1.37a-c** (Figure 1.4.14) among many others were synthesized and the ability of their wet hydrogels to capture and remove rhodamine B **RhB**, reactive blue 4 **RB4** and direct red 80 **DR80** (Figure 1.4.15) from water was reported by Banerjee and co-workers.[92]

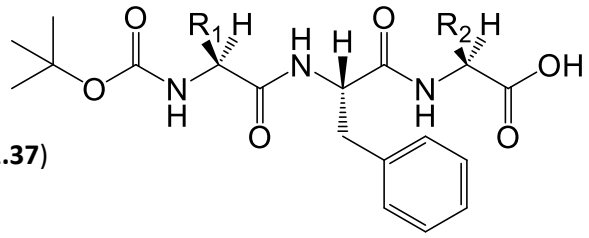

(**1.37**)

(a) R_1= —$CH_2CH(CH_3)_2$ R_2= —CH_2Ph

(b) R_1= —CH_2Ph R_2= —$CH_2CH(CH_3)_2$

(c) R_1= —$CH_2CH(CH_3)_2$ R_2= —$CH_2CH(CH_3)_2$

Figure 1.4.14 Chemical structures of phenylalanine-based tripeptide gelators **1.37a-c**

Unlike the pH responsive metallo-hydrogels earlier reported by the authors,[88] the tripeptide hydrogelators formed thermoreversible hydrogels at basic pH (pH 11.5- 13.5). However, below pH 11.5, the gelators remained insoluble in water; this may imply that the presence of excess of hydroxide ion has a synergistic benefit on the self-aggregation of these tripeptides into anti-parallel β-sheet supramolecular conformations.

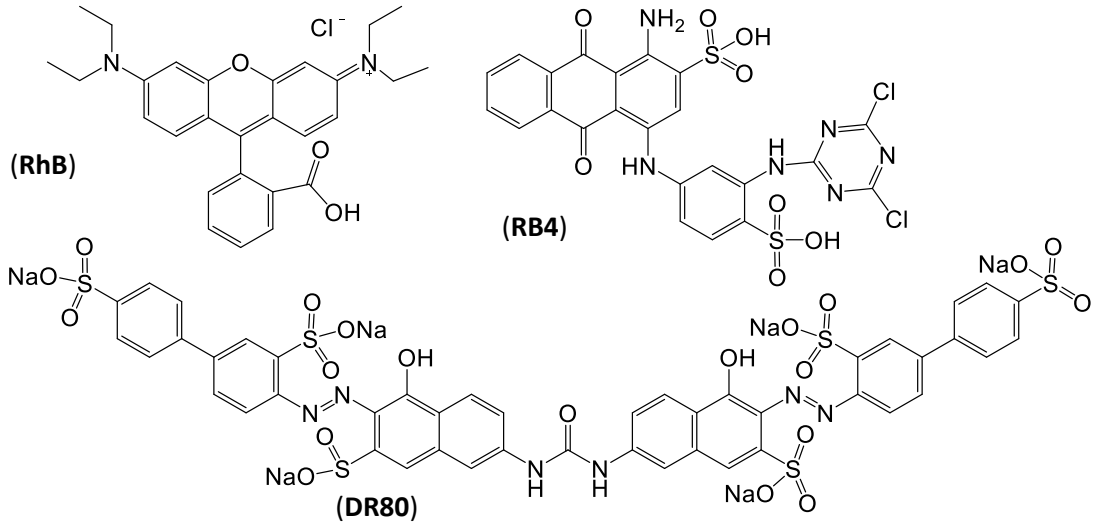

(**RhB**) (**RB4**) (**DR80**)

Figure 1.4.15 Chemical structures of (a) rhodamine B **RhB**, (b) reactive blue 4 **RB4** and (c) direct red 80 **DR80**

The hydrogels of gelator **1.37b** demonstrated removal of each of the dyes from their aqueous solutions as it adsorbed 7.4, 9.8 and 10.6 mgg^{-1} of **RhB**, **RB4** and **DR80** over a period of 28, 30 and 32 h, respectively. Surprisingly, despite the fact that hydrophobic interactions are solely responsible for the adsorption of **DR80** onto the hydrogel nanofibres, it was better adsorbed

than **RhB** and **RB4** in which both hydrophobic and acid-base interactions drive their adsorption. Complete adsorption of the three dyes from their equimolar aqueous mixture of was achieved within two days. Interestingly, the spent gelators were regenerated by dropwise addition of 1 M HCl. The gelator peptides precipitated out when the pH was adjusted to 7.5, leaving behind the organic dyes in the aqueous medium and the gelator was filtered-off, washed repeatedly with deionized water and dried. However, it should be noted that acidic conditions may well be expected to lead to cleavage of the Boc group on these gelators, and therefore multi-cycle re-use may become difficult.

In 2010, Das and co-workers investigated the tunability of a single non-gelator **1.38** precursor to furnish a hydrogelator **1.39**, organogelator **1.40** and ionogelator **1.41** (as shown in Figure 1.4.16).[93] Quaternization of the amine group of the **1.38** with methyl iodide and a further ion exchange with chloride ions produced the **1.39** whereas coupling of the same precursor with a long-chain acid yielded the **1.40**. Interestingly, when the same amine was coupled with a cyclic acid, it yielded **1.41** which is capable of immobilizing a wide range of ionic liquids (IL), hence it is termed an ionogelator and the resulting gels, ionogels.

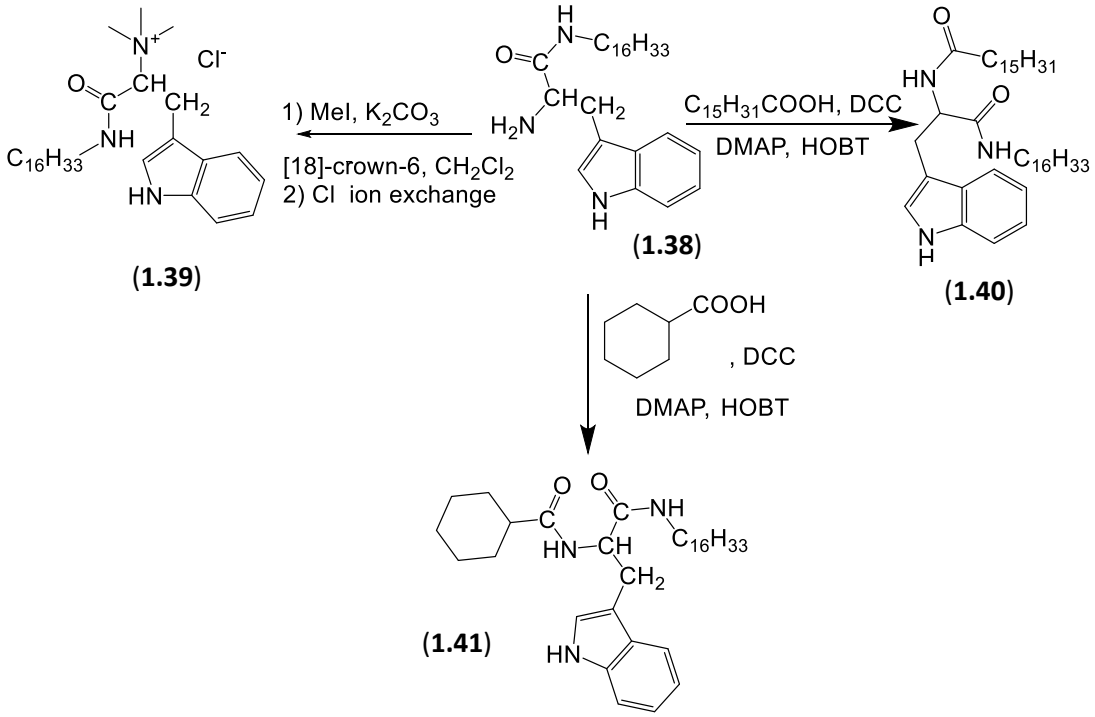

Figure 1.4.16 Tuning the amphiphilicity of a non-gelator (a) to (b) a hydrogelator, (c) an organogelator and (c) an ionogelator by simple chemical modifications

To this end, xerogels of the organogels and hydrogels (but not the ionogels) were then used to remove various dyes from water. The ionogels of the IL **$BMIMPF_6$** (Figure 1.4.17) prepared via a traditional heat-cool cycle were used to sequester **CV** (0.01 mM) and **NBB** (0.01 mM) from their aqueous solutions.

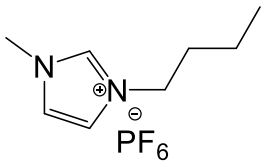

$BMIMPF_6$

Figure 1.4.17 Chemical structure of imidazolium-based ionic liquid

It was observed that more than 90% of both the **CV** and the **NBB** were adsorbed by the ionogel within 8 h and 20 h respectively. On the other hand, the organogels of **1.40** made in toluene slowly adsorbed 50% of both dyes within 6 h and 20 h, respectively. It was suggested that the excellent performance of the ionogel could be a result of the inherent ionic character of the ionic liquid used to make the gel.

A two-component gelator system in which chiral amphiphilic lithocholic acid **1.42** (Figure 1.4.18a) and the non-ionic surfactant dodecyl (dimethyl) amine oxide **1.43** (Figure 1.4.18b), which are not capable of achieving gelation in their own rights to has been reported. This mixture electrostatically form an intermediate complex which forms a pH responsive chiral supramolecular gel in water at room temperature, when mixed in the right stoichiometric ratio as shown in Scheme 1.4.1.[94] The xerogels of the two-component hydrogel demonstrated an excellent affinity and adsorption of amido black 10B (also known as naphthol blue black) adsorbing 202 mgg^{-1} of the dye from its aqueous solution within 15 h. However, the nanofibres of the gel only adsorbed a slight amount of methyl red **MR**, chrome azurol S **CAS** (Figure 1.4.18) and **Rh6G,** which suggests that the adsorption of **NBB** is primarily driven by hydrophobic interaction between the nanofibres and the dye molecules.

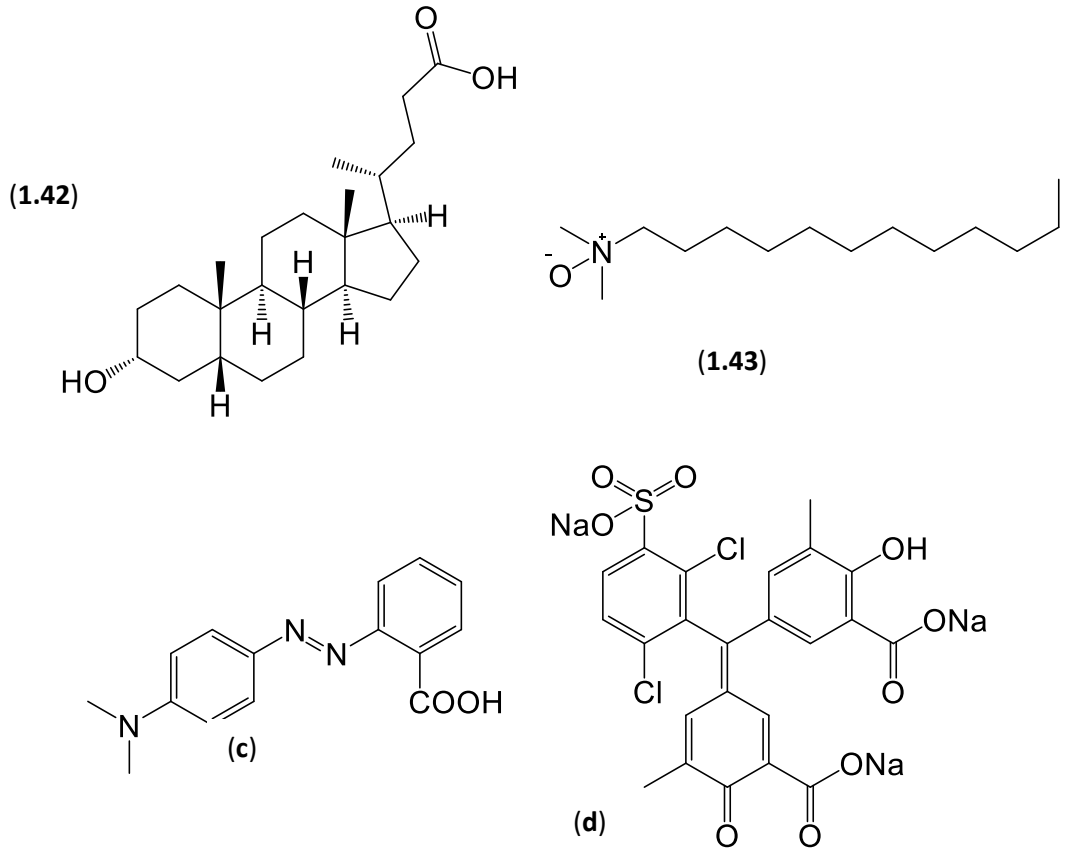

Figure 1.4.18 Chemical structures of (a) amphiphilic lithocholic acid **1.42** and (b) dodecyl (dimethyl) amine oxide **1.43** (c) methyl red **MR** (d) chrome azurol S **CAS**

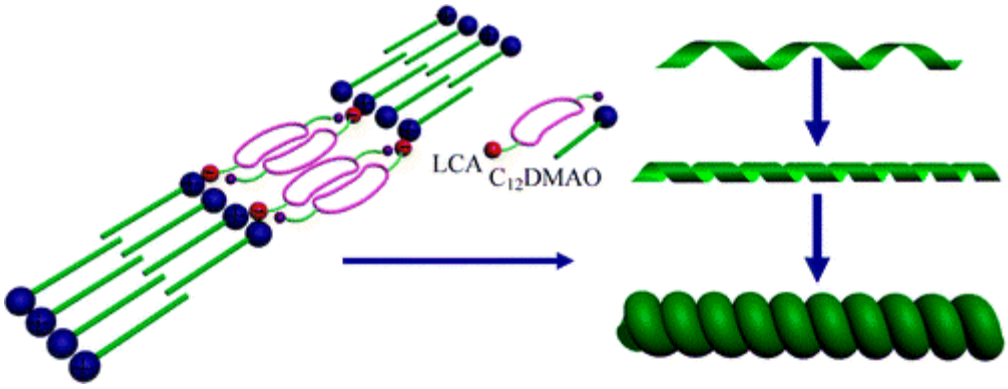

Scheme 1.4.1 Formation of a complex hydrogelator from two nongelators and the subsequent formation of a chiral aggregate.

Song and co-workers have also recently demonstrated that pH-responsive hydrogels and metallo-hydrogels of lithocolate (**LC$^-$)** formed when an aqueous solutions is mixed with solutions of **LC$^-$** is mixed with solutions of different monovalent cations, exhibited a very high

adsorption capacity and efficiency for cationic dyes; methylene blue **MB** (0.87-1.10 g g^{-1}) and **Rh6G** (1.12- 1.42 g g^{-1}) within 20 min.[95]

A family of novel pH-tunable hydrogelators among which are compounds **1.44** and **1.45** (Figure 1.4.19) having a urea and two aromatic rings with nitro/ nitrile and carboxylic acid functional groups appended were reported in 2012 by Hayes and co-workers.[96] Methylene blue **MB** (Figure 1.4.19b) was used as a model candidate for the adsorption studies. In this case, the adsorption was done in an unconventional way as the basic solutions of the gelators were added to the aqueous solutions of the dye and acidification using a diluted solution of HCl added dropwise or slow hydrolysis of glucono-δ-lactone to induce the in situ gelation of both gelators in the presence of the dye. As a result of this, the hydrogels demonstrated extremely high adsorption efficiencies, with maximum dye uptakes of 1020 mgg^{-1} making them the most effective hydrogels amongst the various supramolecular gels reported up-to-date for extracting dyes from water.

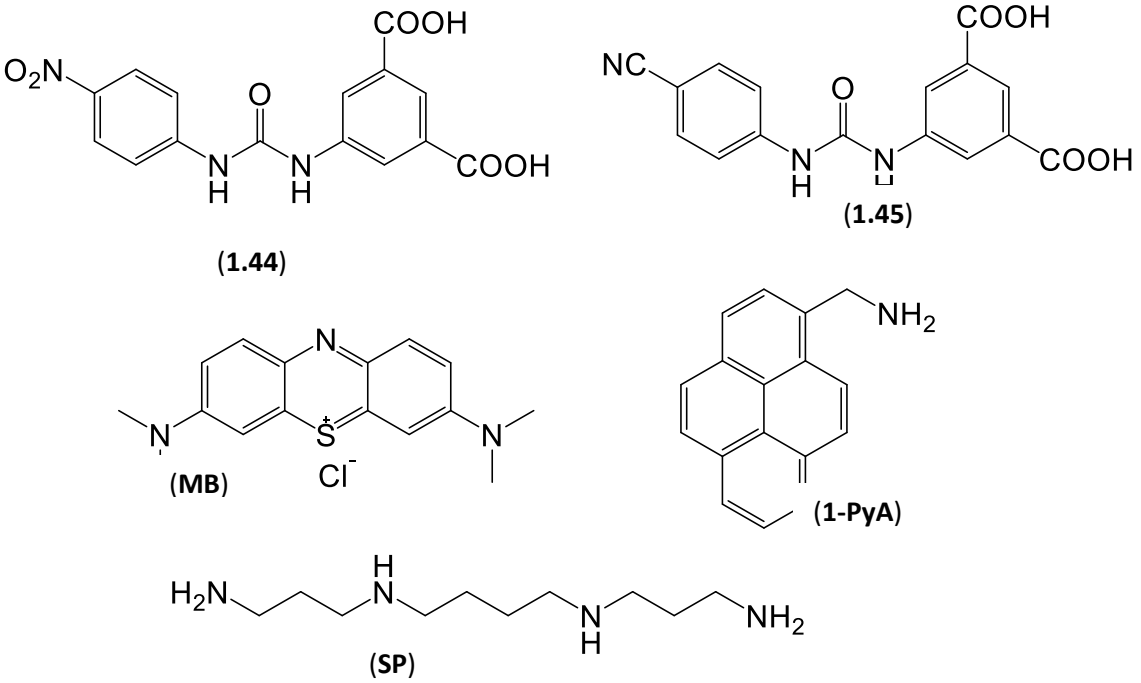

Figure 1.4.19 Chemical structure of urea based gelators **1.44** and **1.45**, (b) methylene blue **MB**, (c) 1-pyrenemethyl amine **1-PyA** and (d) spermine (**SP**)

It was further demonstrated that the gel nanofibres are highly selective towards the nature of the aromatic moiety in the chemical structure and the charge of the dye. Intercalation was adjudged to be the main driving force for the adsorption of methylene blue onto the hydrogel

nanofibres due to its planar geometry whereas acid-base interaction between the amine group of the dye and the carboxylic acid groups of the gelator were suggested to be responsible for the 62 % of 1-pyrenemethyl amine **1-PyA** (Figure 1.4.19c) adsorbed by the gel fibres. In order to counter-investigate the validity of the proposed intercalation hypothesis, spermine **SP** (Figure 1.4.19d), a tetracationic amine was interacted with the hydrogel fibres but there was only very small amount of spermine **SP** adsorbed. This is the justification that other dyes were adsorbed purely by inclusion/intercalation into the gel fibres. Interestingly, the inclusion of methylene blue into the gel fibres had significant impact on the strength of the fibres as the length of the fibres decreases from 10 μm to 600 nm when 20 % **MB** was added as measured by TEM.[96]

In an attempt to optimise the structure-property relationships and dye uptake efficiency, analogues of compound **1.44** and **1.45** were synthesized such that the number of the acid groups increase from 2 to 4 as shown in the structure of the bis amide-aromatic-urea **1.46a-c** with a bola-amphiphilic structure (Figure 1.4.20).[97] The hydrogels of the derivatised gelators were formed via a pH-switching protocol. Their minimum gelation concentrations were lower than that of the parent bis-aromatic urea and the mechanical stability of the hydrogels were enhanced. Interestingly, the hydrogels of the bis amide-aromatic-urea did not demonstrate dye adsorption capability at gelator concentration > 20 mM in contrast to the parent analogues, possibly because of the change in aggregation mode at higher concentrations which impaired permeability within the gel network required for the intercalation of **MB**.[98] However, at a lower gelator concentrations, the hydrogels of the bis amide-aromatic-urea gelators demonstrated a more effective molar uptake of the dye than the parent bis-aromatic urea gelators due to the increase in the number of available sites for intercalation; i.e., the aromatic acid units per molecule.

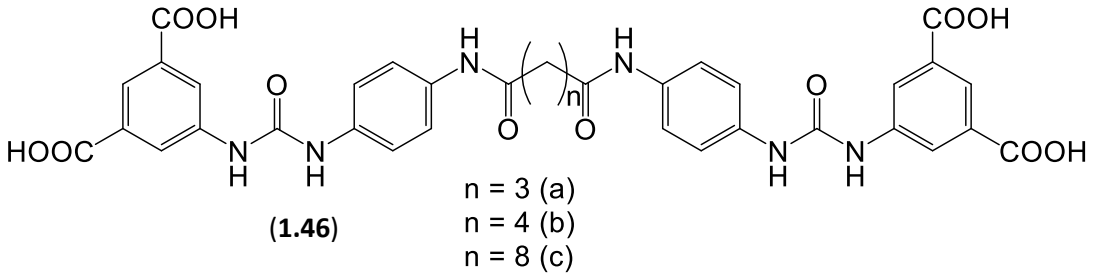

Figure 1.4.20 Chemical structure of bis amide-aromatic-urea based hydrogelators **1.46a-c**

In 2013, Sukul and Malik reported the design of thermoreversible bi-component hydrogels comprising a purine nucleobase, adenine **1.47** and tricarboxylic acids **1.48** and **1.49** (Figure 1.4.21).[99] Interestingly, the interactions between adenine and each of the tricarboxylic acids produced hydrogels with different morphologies. For instance, the hydrogels comprising the 1,3,5-tris (4-carboxyphenyl)benzene **1.48** yielded slim belt-like nanofibres having diameters of *ca*. 20-100 nm while those of biphenyl-3,4',5-tricarboxylic acid **1.49** had large belt-like fibres with diameter of 500-600 nm.

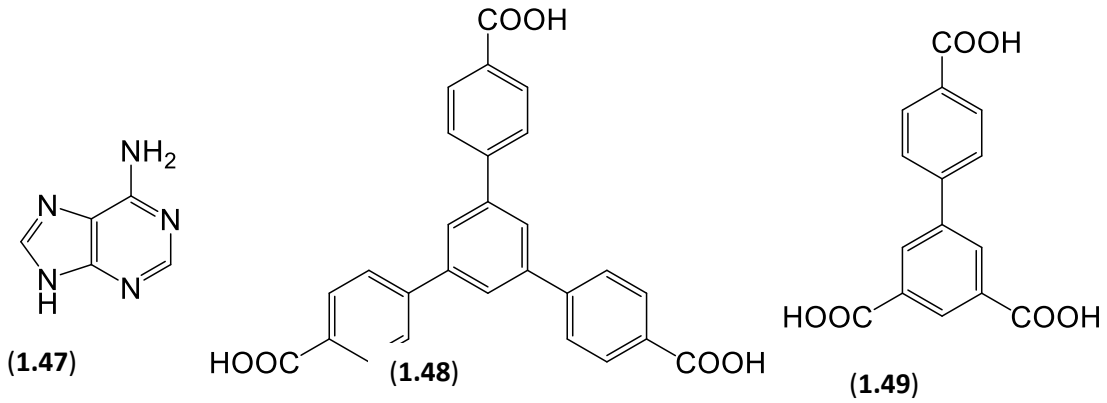

Figure 1.4.21 Chemical structure of (a) adenine **1.47** (b) 1, 3, 5-tris (4-carboxyphenyl) benzene **1.48** (c) biphenyl-3, 4', 5-tricarboxylic acid **1.49**

Such morphological variations have been attributed to differences in the conformations of the aromatic ring of the acids. The formation of longitudinal π-π stacking between two aromatic rings in compound **1.48** is restricted due to flipping of the benzene plane, hence the reason for the formation of slim nanofibres, whereas extended π-π stacking occurs in the hydrogels of compound **1.49** which gives rise to the formation of large fibres (as shown in Scheme 1.4.2).

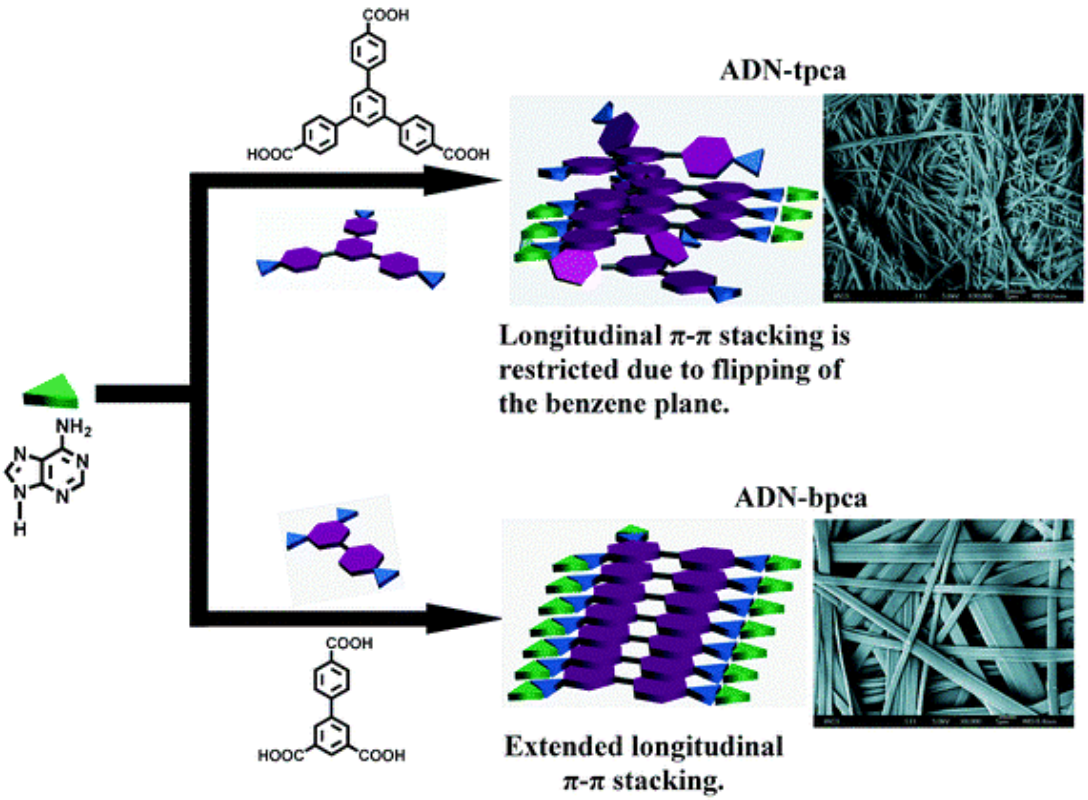

Scheme 1.4.2. Plausible modelling for the formation of different size of belt for different gel and their growth in the longitudinal direction. [Reproduced from ref. 99]

These bicomponent gelator systems demonstrated a high efficiency for dye adsorption capability when the hydrogels were contacted with aqueous solutions of **MB**, **CV** and **Rh6G** for a period of 48 h. The maximum uptake of **MB**, **Rh6G** and **CV** onto the hydrogels **1.48** was 6.3, 7.2 and 7.9 mg of dye / g of gelator respectively while 6.0, 7.2 and 7.5 mg of the same dyes was adsorbed onto 1.0 g of gelator **1.49**. Hydrophobic interactions have been propounded as the driving force for the adsorption process.

In 2013, a pH-responsive C_2-symmetric cyclohexane-based hydrogelator **1.50** (Figure 1.4.22) was designed by Feng and co-workers.[100] The hydrogels were prepared by pH-switching; under basic conditions, the carboxylic acid groups become deprotonated and subsequent addition of HCl led to instantaneous gelation due to the reprotonation of the gelator. It was further demonstrated that the pH_{gs} (pH value at which the gel begins to lose its integrity) increased from 3.6 to 6.4 as the gelator concentration increased until a plateau was attained. Interestingly, the wet hydrogels demonstrated rapid adsorption of methylene blue within 2-3 min when mixed with aqueous solutions of the dye, making the hydrogel the most kinetically efficient among its kinds as many gels usually take 20- 40 h to adsorb similar dyes. The nanofibres of the

hydrogels decorated with dye were filtered off to obtain clean water. In order to understand the mechanism underpinning the adsorption interactions between dyes and hydrogel nanofibres, the Langmuir isotherm model was used to estimate the most appropriate equilibrium curve by plotting the reciprocal of the equilibrium concentration of the dye against the against the experimental amount of dye adsorbed per unit hydrogel. From the isotherm, the maximum amount of dye adsorbed was estimated as 47 mg g^{-1} and the correlation coefficient R^2 was close to 1. As such, although uptake was very fast, only relatively low level of dye loading were achieved. In order to demonstrate the recyclability of the hydrogels, the gelator was dissolved in basic aqueous medium followed by acidification and the dye was recovered by repeated washing with chloroform. Amazingly, the hydrogel with this simple approach demonstrated a higher recyclability (90%) than that of the conventional adsorbent- activated carbon (73.5%). However, it should be noted that repeated washing is not an environmentally friendly protocol.

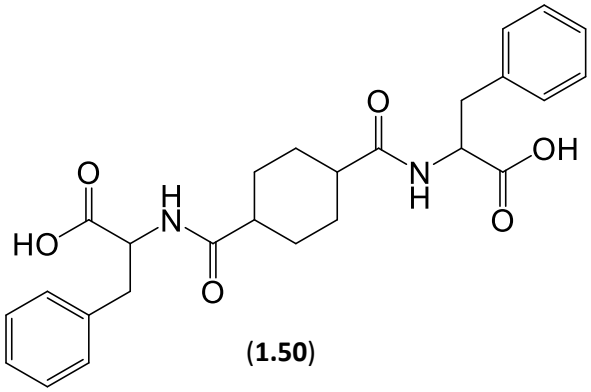

(**1.50**)

Figure 1.4.22 Chemical structure of C_2-symmetric cyclohexane-based hydrogelator **1.50**

1.5 General features of supramolecular envirogelators

Supramolecular envirogelators are structurally diverse, nonetheless, they share common features such as (i) amphiphilicity (ii) nanostructuring (iii) molecular programming (iv) insolubility and (v) biocompatibility with regards to their design and applications. Due to the importance of these parameters, their roles and relevance are described in the following subsections.

1.5.1 Amphiphilicity

Amphiphilicity[101, 102] is an indispensable requirement for the self-assembly of a molecular building block to occur in water or mixtures of water and organic solvents. An amphiphile is a molecule that contains both ‘‘water-loving’’ (hydrophilic) and water-hating (hydrophobic) parts. They can self-assemble in solution or at the interface between two solvents to form myriads of molecular architectures such as micelles, vesicles, bilayers and gels. Generally, the hydrophilic part always resides in the aqueous phase while the hydrophobic core is preferentially immersed in the nonpolar solvents or in the air. This concept has been widely exploited by many authors in the past century, especially in oil spill remediation technology whereby a LMWGs, selectively gels an oil slick from the surface of water leading to phase-separation with little or no water being incorporated into the resulting gel matrix (as shown in Figure 1.5.1).[76, 82, 103, 104] The immobilized oil can be recovered by distillation.

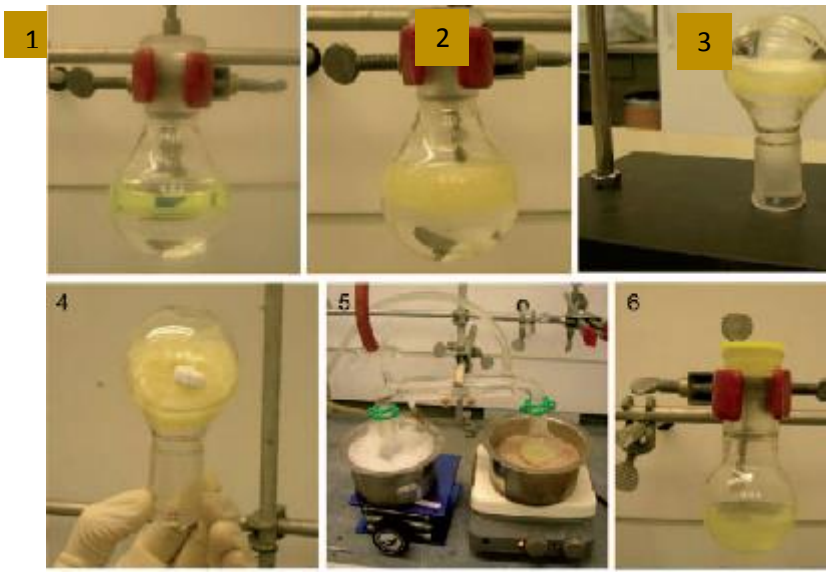

Figure 1.5.1 Gelation of bulk diesel in the presence of water, and its quantitative recovery through vacuum distillation. Photographs: 1) diesel and water form a two-phase system; 2) gel forms instantaneously upon addition of gelator by syringe; 3) Owing to the strength of the diesel gel, the flow of water is stopped upon inversion of flask; 4) Diesel gel remains after removal of the bottom water layer; 5) The entrapped diesel is recovered by vacuum distillation; 6) Recovered diesel. [Reproduced from ref. 80].

The hydrophobic effect is the primary factor underpinning self-aggregation.[105, 106] It is noteworthy that a balance between the hydrophilic and hydrophobic units is vital to the

controlling of the morphology and the spatiotemporal structure of the resulting nanostructured gel-phase material.[107, 108] Moreover, by tuning the amphiphilicity of the molecular building blocks (gelators), self-assembly can be controlled. In most cases, this is done by an inter-conversion between the hydrophilic and hydrophobic regimes. Such conversion is usually done reversibly or irreversibly by chemical modification. In this way, the transformation of LMW organogelators to more biocompatible hydrogelators have been demonstrated by some authors in this field.[109-111] For a representative example, Das and co-workers tuned the amphiphilicity of a single non-gelator to obtain a hydrogelator, an organogelator, and an ionogelator (Figure 1.4.16).[93] It is important to mention that such modification is a very useful approach for increasing the existing library of LMWG as most LMWGs are usually discovered serendipitously. It also significantly increases the scope of their applications.[87]

As being discussed in section 1.4.2 of this thesis Chapter, some supramolecular envirogels have recently demonstrated high uptake of dissolved organic (dyes)[88, 91-93, 96, 97, 112] and inorganic (heavy metals)[113, 114] pollutants from water in the past decades due to their amphiphilicity. In most cases, the hydrophilic part of the envirogel interacts with water while the hydrophobic part preferentially interact with the pollutants, thereby enabling their better performance than the conventional hydrophobic adsorbents such as activated carbon.

1.5.2 Nanostructuring

The hierarchical self-assembly of low molecular weight gelators is a sophisticated supramolecular approach for fabricating complex supramolecular architectures that spontaneously produce orderly assembled molecular components.[115] This nanofabrication approach is can also be refer to as nanostructuring. Nanostructuring helps increase the surface area of nanofibres; thus, the inherent solid-like fibrillar network of a supramolecular envirogel is a potential highly accessible surface for high uptake of pollutants.[112] Due to the structure-property relationships of these nanofibres, self-assembled nanofibrillar networks (SAFiNs) with a desired macroscopic properties can be designed.[116] The morphology, hence the mechanical properties of a fibrillar network can be engineered by controlling fibre and network formation.[117] For example, the storage or elastic modulus, *G'* is dependent on the correlation length ξ, i.e. average mesh size of fibre networks (Figure 1.5.2). As ξ, an important parameter determined by the average mesh size of SAFiNs, increases, *G'* of the gel decreases.[118]

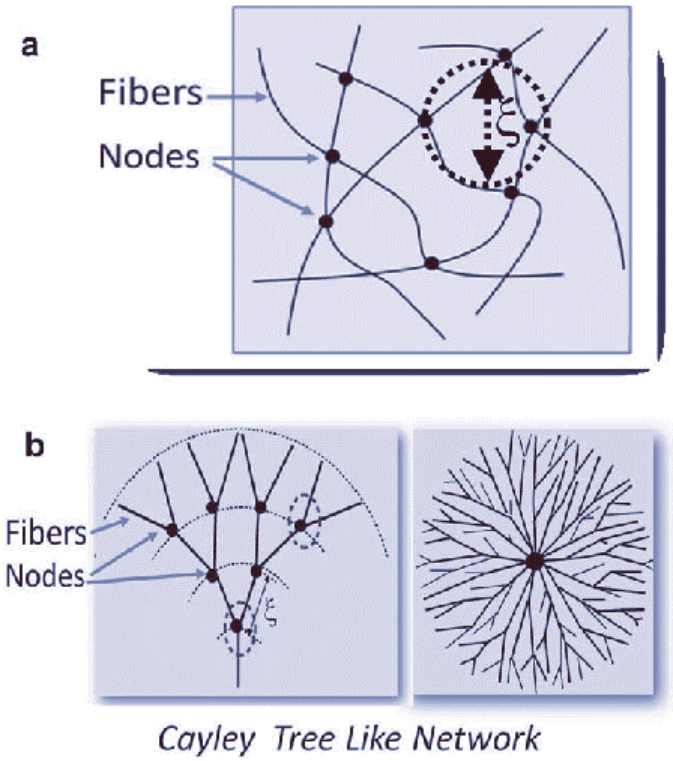

Figure 1.5.2 Illustration of fibre networks commonly observed in supramolecular materials. a) Interconnecting fibre network consisting of fibres and joints (or nodes) with closed loops. b) Cayley tree-like network (left) with open loops, and spherulite. [Reproduced from ref. 118].

It is noteworthy that there are two different types of fibre networks- single fibre network and multi-domain networks, obtainable when gelation is completed. Single fibre network emerges when numerous fibre networks mutually interpenetrate and are interlocked with one another to form a homogeneous SAFiN, therefore the mechanical strength is strong (Figure 1.5.3a). On the other hand, a multi-domain fibre networks is a collection of disjointed single fibre networks. Hence, multi-domain fibre network usually exhibit a high value of ξ and have low mechanical properties (Figure 1.5.3b).

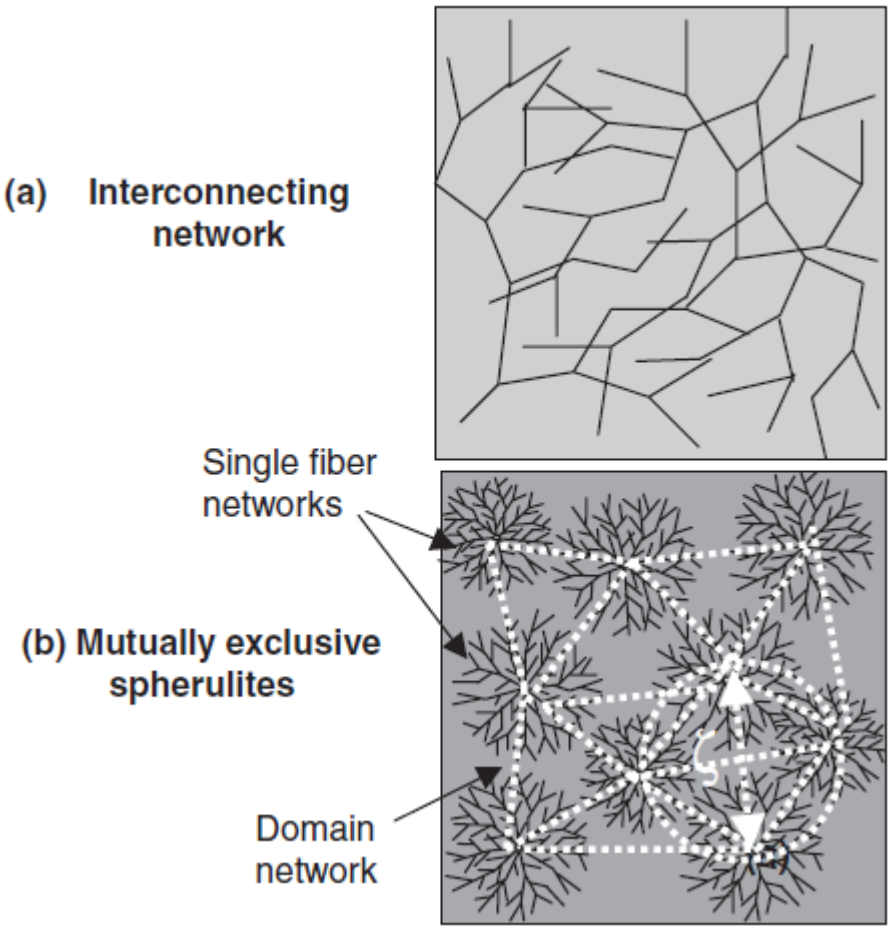

Figure 1.5.3 Illustration of (a) single fibre (b) multi-domain fibre networks

Due to the mechanical strength requirements for the applications of a supramolecular envirogel in water purification processes and also the need for the stability of the nanofibres under the weight of adsorbed pollutants, it is important that the networks of supramolecular envirogels be engineered to suit this purpose. Approaches such as supersaturation/supercooling, thermal processing, seeding, additives and ultrasound have been widely employed to tune the network and rheological properties of functional molecular gels.[117, 119-123]

Besides tuning the mechanical properties of nanofibres, the specific surface area of a supramolecular envirogel nanofibrillar network can also be tuned by simple chemical modifications which in turn affect the nanostructuring processes. Feng and co-workers employed the nitrogen adsorption technique to investigate the structure effect on specific surface area nanofibrillar networks. Interestingly, it was observed that the BET surfaces for the xerogels of C_2-symmetric benzene-based gelator **1.51** (Figure 1.5.4) decrease from 14.7 m^2g^{-1} to 3.8 m^2g^{-1} when the carboxylic acid group on **1.51G1**was replaced with a terminal diglycol

group to obtain the gelator **1.51G2**. As a result of the relatively large surface area of the xerogel of **1.51G1**, the amount of cationic dyes uptake onto the xerogels of **1.51G1** was about 80 times the amount adsorbed onto the xerogel of **1.51G2**.[124]

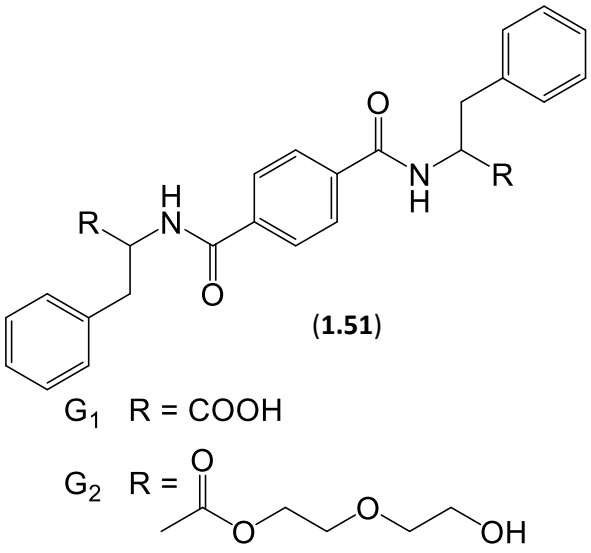

Figure 1.5.4 Chemical structures of C_2-symmetric benzene based gelators

1.5.3 Molecular programming and molecular recognition

Molecular recognition underpin of biological systems and mediates interactions for instance, between receptor-ligand, antigen-antibody, DNA-protein, protein-protein, enzyme-substrate and RNA-ribosome.[125] Molecular recognition is the specific interaction between two or more molecules mediated by complementary non-covalent interactions such as hydrogen bonding, van der Waals forces, metal coordination, solvophobic, π-π and electrostatic interactions.[126] Molecular recognition involves information storage and readout at the macroscopic level. Information can be molecularly programmed into the building blocks. Such information could include the nature, number and arrangement of the binding sites, or the ligands enveloping the substrate.[127] The advent of supramolecular chemistry[128, 129] has birthed numerous artificial systems wherein the concepts of molecular recognition are employed.[130, 131] Interestingly, van Esch and co-workers have emphasised that gelation of LMWGs is a ‘‘supramolecular system par excellence’’. In order to further support this profound truth, Smith[63] and other researchers[132, 133] in this field have reported that molecular-scale information such as chirality programmed into a gelator is usually translated onto and expressed by the supramolecular nanofibres. In the light of this, supramolecular envirogels having pre-determined energetics

and geometry can be designed from the molecular level. For example, a number of authors have demonstrated that LMWGs adsorb one class of dye better than another due to electronic interaction and geometric differences.[88, 92, 134] Wayne and co-workers demonstrated that isophthalic acid based hydrogelators **1.52** (Figure 1.5.5) exhibits high selectivity for the uptake of cationic dyes- methylene blue and methyl violet and a negligible uptake of indigo carmine, an anionic dye - suggesting selective interactions between LMWG and dye. It was also hypothesised that intercalation is a key part of the mechanism underpinning the selective uptake of cationic dyes as the aliphatic tetracation spermine shows <1 % uptake.[134]

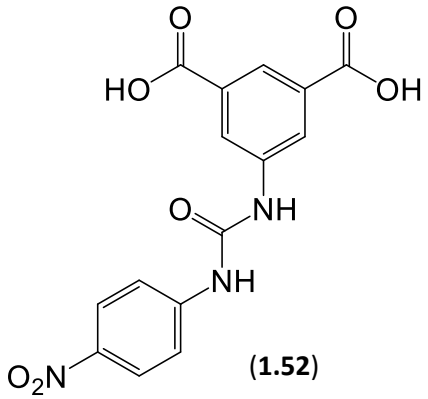

Figure 1.5.5 Chemical structure of isophthalic acid based hydrogelator **1.52**

Programming the self-assembly properties of a supramolecular envirogelator via the molecular geometry and intermolecular interactions is a paradigm of supramolecular devices purposed for selective and efficient capture of pollutants.

1.5.4 Nanoporosity

In most cases, applications of gel matrices are diffusion-driven.[135] A high porosity and the consequent large surface area with more specific adsorption sites are the fundamental important characteristics of a good adsorbent. When a LMWG is nanostructured by gelation in an appropriate solvent, a nanonet having a mesh with a range of diameters ξ, usually emerges (as shown in Figure 1.5.3a).[58, 136] Extraneous materials can diffuse into, through and out of the gel SAFiN. The mesh size of the fibrillar networks controls the dynamics and mechanisms of diffusion in the gel.[137] It is important to note that the size of the resulting mesh depends on the nature of the gelator, gelator loading, solvent and the gelation process employed.[98] Imaging techniques such as scanning electron microscopy (SEM), transmission electron microscopy

(TEM) and atomic force microscopy (AFM) are commonly used tools for measuring the mesh size of molecular gels (really all kinds of gels).[138, 139] However, these techniques have inherent limitation such as sample preparation-induced damage or alteration to the morphology of the gels. When the samples are dried prior to imaging, they collapse internally. With the advent of environmental scanning electron microscopy (ESEM), it is possible to image a gel in its native (wet) state or by converting it into an aerogel through drying under a reduced pressure without any disruption.[140]

In the hunt for non-invasive techniques, the use of nuclear magnetic resonance (NMR) spectroscopy for the characterization of gels has recently witnessed enormous growth. Spin relaxation times, magic angle spinning (MAS), nuclear Overhauser enhancements (NOE) and pulse field gradient (PFG) are the NMR measurements commonly used nowadays to gain detailed insight about the molecular organization, specific interactions and internal mobility of constituents in a gel.[141] Adams and Iggo *et al*, have recently demonstrated the use of PFG-NMR spectroscopy to analyse the SAFiN mesh size in micellar solutions and in stable molecular hydrogels formed upon addition of Ca^{2+} to a solution of naphthalene diphenylalanine **1.53** (Figure 1.5.6).[98] Dextran guests of various masses and hydrodynamic radii ($2R_h$) were used to probe diffusion in both the networks of the precursor micellar solutions and the hydrogels. Interestingly, the diffusivities of smaller dextran having a nominal mass 6 kDa, and glucose, through the two networks are similar to their dilute aqueous solutions and no retardation was observed. Similarly, for the dextran having a nominal mass, $Mr < 500$ kDa and $2Rh < 40$ nm, the diffusivity was only slightly restricted in both cases compare to its dilute aqueous solution. However, the heaviest dextran having an approximate mass and hydrodynamic diameter 3300 kDa and 84 nm respectively was almost completely retarded by the gels, making this consistent with the mesh size of the gel (40 - 100 nm) but the restriction was much weaker in the micellar solution, probably due its very short-lived networks. It was also observed that the mesh size decreases in the micellar solutions but increases in the gels when the gelator concentration was doubled. Increased fibre aggregation at higher concentrations was concluded to be the reason for this observation.

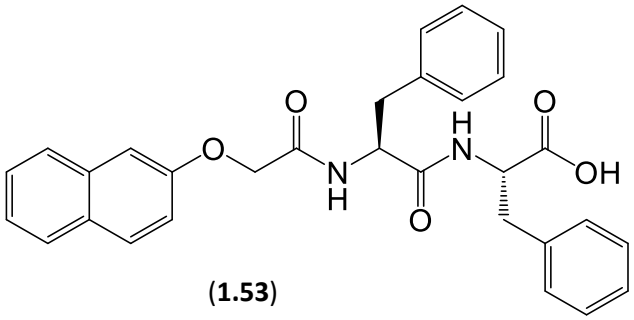

(**1.53**)

Figure 1.5.6 Chemical structure of naphthalene diphenylalanine **1.53**

With this information, new applications can be envisaged for supramolecular envirogels. For instance, bacterial contamination of drinking water is a significant problem. Bacteria are relatively large objects (micron-scale) whereas the mesh size of a nanostructured envirogel certainly prevents the diffusion of objects in excess of 100 nm. As such, the envirogel should act as an effective barrier to the passage of biological toxins. Indeed the ability of a LMW hydrogel to act as an effective barrier has recently been demonstrated by Xu and co-workers.[136] In this case, enzyme-instructed hydrogelation was employed to build gel nanonets in the pericellular space of a cancer HeLa cell. The nanonets could obstruct extracellular mass exchange, in this case even including the blockage of a dye having an average mass of 277 Da from entering into the cell.

1.5.5 Others

When a LMWG undergoes gelation in an appropriate solvent, phase separation between the 'solid-like' nanofibres and the solvent occurs.[142] Therefore, the nanofibres can be filtered-off and recycled afterward. Hence, the 'insolubility' of an envirogel is an important parameter worthy of note while designing a LMWG for water purification process.

It is expedient that an envirogel be water-compatible, hence biocompatible. Therefore, biocompatible molecular motifs such as peptides, sugar and nucleic acids are potential building blocks essential for designing supramolecular envirogels for water purification.[143] On the other hand, organogelators that are capable of sequestering pollutants from water can sometimes be tuned by simple chemical modification to obtain a gelator capable of forming gels in biocompatible media without losing their adsorption efficiency.[144]

1.6 Thesis aims

Supramolecular Envirogels hold a great promise owning to their inherent properties such as large surface area, specificity for selectivity, high porosity and tunability. Several molecular building blocks have been designed into supramolecular envirogels in the past decades, however many of them are not suitable for real-life water purification processes due to their dependence on pH, multi-step synthesis and poor biocompatibility. Therefore, in this project, pioneer hydrogelators of 1,3:2,4-dibenzylidine-d-sorbitol (DBS) will be synthesized and characterized. The hydrogelation of the gelators will be investigated and the hydrogels characterized using various techniques.

In the second and third phases of the project, the ability of the hydrogel nanofibres to sequester various types of dye and heavy metals from a model polluted water will be probed under various pH conditions. Batch and flow-through bench-scale adsorption methods will be employed. Parameters such as selectivity for pollutants, maximum pollutant uptake, adsorptive kinetics and isotherms, limit of pollutant removal, regeneration and reusability will be investigated.

Amongst metal waste, there is a particular awakening of research into e-wastes (waste electrical and electronic equipment) in the past decade brings along with it, a significant economic incentive for gold recovery not only from the ores and consumer electronics but also from wastewater near, for example, mines.[145, 146] However, the conventional leaching method, which involves the use of inorganic cyanides, to recover gold from spent liquors often results in contamination of the environment via leakages.[147] Therefore, developing environmentally benign process for binding silver and gold from water, reducing them and converting them into a more useful nanostructured gold and nanoparticles is not only important from a green chemistry point of view but could also lead to a more technologically viable nanodevices. Although several techniques exist for converting noble metals to nanoparticles,[148-151] we rarely find any that could function as a self-reducing and stabilizing agent for silver and gold nanoparticles synthesis without adding external reducing agents such as sodium borohydride ($NaBH_4$) – this area will be reviewed in full in Chapter 5. Therefore, the ability of the DBS based hydrogels to act as potential templates for *in situ* reduction, capping and binding of silver and gold in an aqueous medium- a simple and veritable technique for converting 'waste to wealth', will be exploited. We will then investigate the conductivity of these organic-inorganic

hybrid nanomaterials via electrochemical and electroconductivity techniques in order to determine whether in the process of decontaminating the waste we have created new hybrid soft / hard electronic nanomaterials.

.

2 Chapter 2 - Dibenzylidene-D-sorbitol and the new-born DBS-based hydrogelators

Most of the information in this Chapter has been published. For example, a review of DBS and its derivatives has recently been published in *Soft Matter*, 2015, 11, 4768 – 4787. An article on DBS-COOH, one of the novel pioneer DBS-based hydrogelators has been published in *Soft Matter*, 2013, 9, 8730 - 8736 and also featured in *ChemistryWorld* magazine on August 30, 2013.

2.1 *Introduction*

DBS is a chiral low molecular weight amphiphile having a 'butterfly-shape' conformation – it can be considered that the sorbitol backbone is the body and the phenyl rings are the 'wings' (Figure 2.1.1). It is a white, crystalline substance derived from the naturally occurring hexose sugar, D-sorbitol,[152] and can be synthesized by a condensation reaction between D-sorbitol and benzaldehyde.[153] In the earliest reports, DBS was synthesized by Meunier who proposed that the acid-catalysed condensation of D-sorbitol and benzaldehyde yielded a mixture of two isomeric diacetals, each having a unique solubility in boiling water and different melting points, one of which formed a gel while the other did not.[154] In 1926, Thomas and Sibi also investigated the gelation potential of DBS in organic solvents and water.[155]

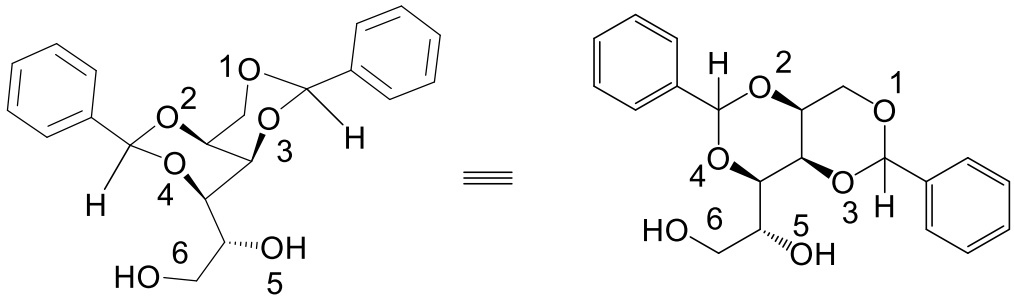

Figure 2.1.1 Chemical structure of DBS

Since mid-20th century, a number of studies have explored the reactivity, and hence the structure of DBS. Wolfe and co-workers[156] re-investigated DBS and by conversion of the free alcohols into variety of esters were able to demonstrate that it existed as a single species having both the mono- and the tri-substituted derivatives (MBS and TBS, Figure 2.1.2) of the protected D-sorbitol as by-products rather than being a mixture of isomers as reported earlier.

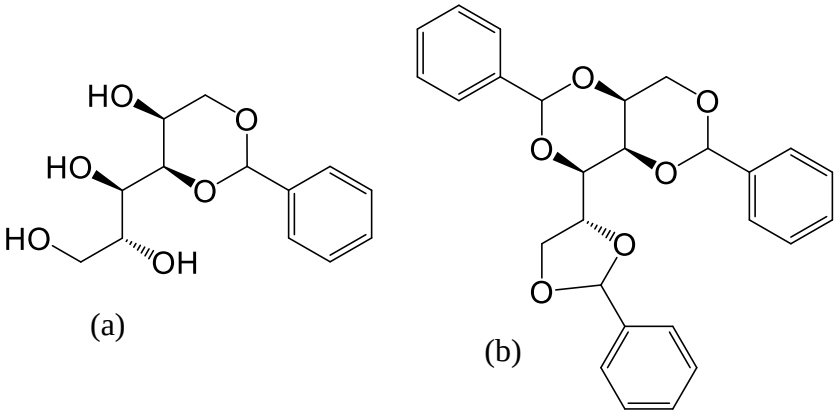

Figure 2.1.2 Structure of (a) 1,3-monobenzylidene-D-sorbitol (MBS) (b) 1,3:2,4:5, 6-tribenzylidene-D-sorbitol (TBS)

Treatment with lead tetra-acetate demonstrated the presence of a glycol group within the DBS structure, which suggests it has either 1,2,3,4 or 3,4,5,6 acetal functionalisation patterns (Figure 2.1.3a and b). When an equivalent of triphenylmethyl chloride was reacted with DBS, a mono-trityl derivative was formed which confirmed the presence of a single primary hydroxyl group in the structure of DBS against the possible 2,3:4,5-diacetal derivative which would have two primary hydroxyl groups (Figure 2.1.3b), supporting the proposed structure of 1,3:2,4-dibenzylidene-D-sorbitol.

By subjecting the molecule to acid hydrolysis, they converted six-carbon protected sugar DBS into the dibenzylidene-protected five-carbon sugar L-xylose. Therefore, the observation of this product rather than five-carbon sugar D-arabinose confirmed the acetal functionalization pattern of DBS as 1,2,3,4 not 3,4,5,6.

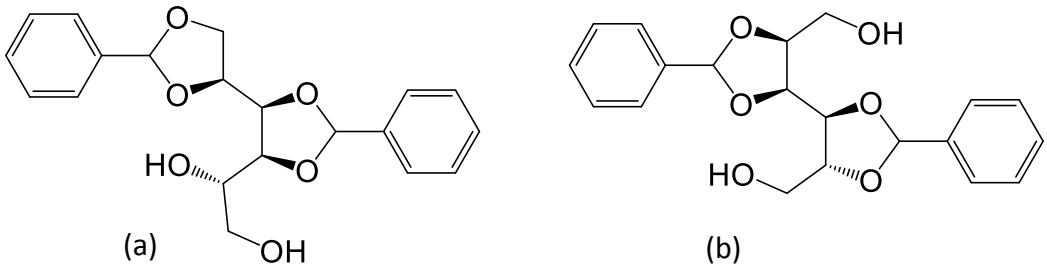

Figure 2.1.3 Proposed chemical structures (a) 1,2,3,4-dibenzylidene-D-sorbitol (b) 3,4,5,6-dibenzylidene-D-sorbitol

Even though the backbone was well-established, the exact pattern of attachment of the benzylidene moieties to the backbone remained elusive. In 1944, Angyal and

Lawler confirmed the structure of DBS as having a 1,3:2,4 connection pattern. This was achieved by careful hydrolysis of DBS to yield 2,4-monobenzylidene-D-sorbitol,[157] a compound that has previously been structurally established and reported by Vargha.[158] This compound has been shown to form via the rearrangement of a less stable intermediate, 2,3-monobenzylidene-D-sorbitol.[159]

It is important to note that the carbon atoms within the ring structure of DBS are themselves new chiral centres. Knowing that their formation is thermodynamically controlled, it can be assumed that the bulky phenyl groups occupy the equatorial positions as shown in (Figure 2.1.1). As such, Brecknell and co-workers explored the use of NMR to validate the definitive structure of DBS, and finally assigned it as 1,3(*R*):2,4(*S*)-dibenzylidene-D-sorbitol (shown in Figure 2.1.1).[160]

2.2 *DBS and its derivatives: A chronicle of synthetic strategies*

Since the early 1970s, the synthesis of DBS has attracted numerous patents with respect to the variation of reaction media, choice of catalysts, stoichiometric balance of the reacting species and product purification procedures.[161-167]

In 1973, Akazome and co-workers kick-started this field by demonstrating a process of preparing DBS in which case an aqueous solution of sorbitol and benzaldehyde was dispersed in a large volume of cyclohexane and the reaction was performed at an elevated temperature furnishing water under the azeotropy of cyclohexane, thereby causing the reaction to proceed while separating water from the reaction system to obtain the crude product as a slurry in cyclohexane.[161] However, the formation of a considerable amount of MBS and trace amounts of TBS as by-products was observed. It has been reported that MBS has a deleterious effect on the industrial applications of DBS. Therefore, it is important it is removed as fully as possible. However, its removal from the crude product is always complicated and difficult.

Uchiyama improved on the previous invention such that practically no MBS was formed. This was achieved by splitting the reaction procedures into two stages. In the first stage, reactants were heated to 50- 70 °C.[163] When the conversion reached 10-40%, water and additional amount of acid catalyst were added, and the reaction performed under controlled concentration conditions at room temperature. The product was obtained as an aqueous suspension.

In 1985, Machell disclosed a method in which sorbitol was initially mixed with mineral acid, and in the subsequent step, an effective amount of an aromatic aldehyde was incrementally added to the homogeneous aqueous solution of sorbitol at an appropriate rate to allow a substantially spontaneous reaction to occur.[168]

Murai and co-workers demonstrated a method for making DBS and its derivatives using benzaldehydes, acetal derivatives of benzaldehyde, D-sorbitol and an acid catalyst in a reaction solvent medium comprising a mixture of hydrophobic solvent (such as cyclohexane) and a hydrophilic polar organic solvent (e.g., alcohols) – the hydrophobic solvent helps precipitate the product while the hydrophilic solvent helps dissolve the reacting species.[162] The reaction was performed under forced agitation conditions in the gel/solid phase. This method was further developed with the use of long chain amines for the neutralization step – it is supposed that the surfactant-like properties of these bases help control solubilities during reaction and work-up.[169]

In the hunt for more environmentally friendly reaction conditions, Salome and co-workers reported an alternative approach to DBS.[165] They used water as the solvent medium and arylsulfonic acid as the catalyst. This allowed the authors to synthesise DBS and simple derivatives in good purities (>90%). Even though the method of Salome appears to be environmentally friendly through its use of water, Gardlik and co-workers improved on the method using C_1-C_3 aliphatic alcohols with no hydrophobic co-solvent.[170] The crude DBS was purified by simple washing with alcohol to remove the mono- and tri-acetal derivatives as previously demonstrated by Uchiyama *et al* in which case the authors increased the percentage purity of the a crude DBS from 95 to 98 % by simple washing with a mixture of aliphatic alcohols.[164] This approach yielded DBS (and meta-substituted halogenated derivatives) largely free of solvent, catalyst impurities or mono and tri-substituted by-products. However, Gardlik's approach uses relatively large amount of solvent, therefore, Scrivens and Salley patented a method in which 2-15 wt% (compared to reactants) of a glycol solvent was present during the reaction. They referred to this solvent as a 'processing agent', and also noted that its presence assisted during the reaction work-up, which could effectively be condensed down to a single simple step.[171]

In 2001, Lever and co-workers reported the addition of surfactant to the reaction as a way of enhancing solubility, which can be particularly suitable for the formation of a

more hydrophobic DBS derivatives – the solubility of these derivatives is lower in polar solvents.[172]

In 2006, Xie *et al* [166] demonstrated the use of Lewis acid catalysts such as $AlCl_3$, $ZnCl_2$, $SnCl_2$, $Bi(OTf)_3$, $FeCl_3$ and BF_3 either in addition to the Brønsted acid catalysts more typically used, or in replacement for them.

Given the inherent drawbacks associated with the some of the previously reported methods; (i) use of large volume of organic solvents, (ii) difficult purification processes, (iii) large usage of acid catalysts, (iv) high cost of operations, and (v) long reaction times, Uppara and co-workers recently patented an improved synthetic method for DBS and its derivatives.[173] The authors used an ionic liquid as reaction medium and catalyst for the reaction between various benzaldehydes and D-sorbitol. The products were obtained in good yield (>60%) and high purity without any trace of residual acid or alkaline residues following neutralization.

It should be noted that when derivatives of DBS are synthesised, this can either be done by (i) modification of the aromatic 'wings', or (ii) modification of the free alcohol groups on the sorbitol 'backbone' of the amphiphile. Both of these approaches have been employed.

In 2007, Feng *et al*[174] reported a different synthetic method for making DBS and numerous new derivatives (Figure 2.2.1). Similar to the method of Gardlik *et al* (*vide supra*),[170] a dual solvent reaction medium (cyclohexane-methanol) and acid catalyst (p-TSA. $3H_2O$) were employed in the syntheses of various derivatives, but Dean-Stark apparatus was incorporated, thereby circumventing the problem of solvent recycling. The crude product was neutralized by sodium carbonate (Na_2CO_3), sodium chloride (NaCl) and hexadecane/stearyl dimethylamine – an approach similar to that previously reported by Kobayashi described above.[169] The products were obtained in good yield (69-99%). When using different benzaldehydes to react with sorbitol, it is noteworthy that electron withdrawing substituents (e.g., CN, NO_2) promote faster reactions than electron-donating ones (e.g., OH, OMe), as a consequence of the electron-withdrawing effect rendering the aldehyde more electrophilic and hence, more reactive.[175]

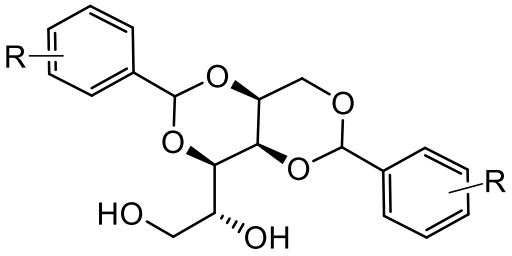

R = H, CH_3, OCH_3, NO_2, F, Cl

Figure 2.2.1 Chemical structure of DBS modified on the 'wings'.

The nitro groups were converted to amino groups by Pd/C catalysed hydrogenation reaction. Further derivatization of the amino groups of the amino DBS by *N, N'*-dicyclohexylcarbodiimide (DCC) mediated amide coupling with carboxylic acids yielded DBS amide derivatives (as shown in Scheme 2.2.1).

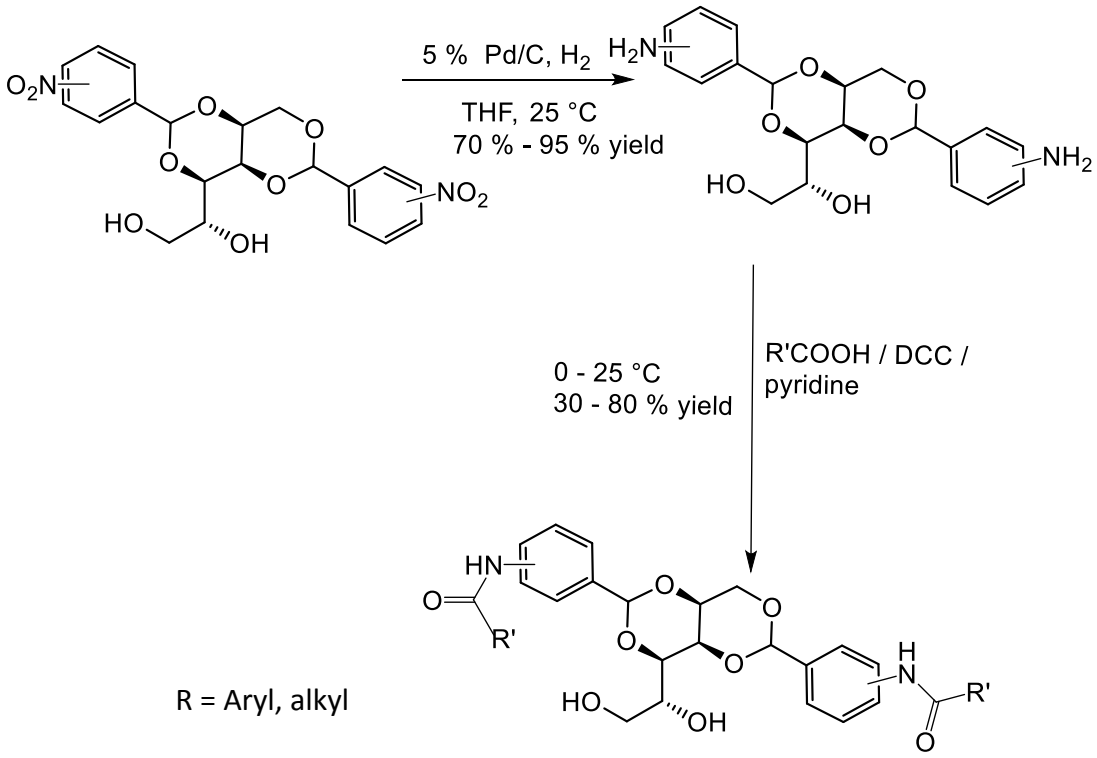

Scheme 2.2.1 Formation of DBS amido derivatives.

In 2008, Stan and co-workers reported the syntheses and gelation behaviours of cationic organogelators based on 1,3:2,4-di-*O*-(*p*-ammoniumbenzylidene)-D-sorbitol (Figure 2.2.2, *p*- DBS-NH_3^+) counterbalanced by the carboxylate anions of one four of natural fatty acids; stearic acid (SA), 12-hydroxystearic acid (HSA), *erythro*-9, 10-dihydroxystearic acid (DHSA) and *erythro*, *erythro*-9,10,12,13-tetrahydroxystearic acid (THSA).[176] Although salt formation impaired the inherent gelation ability of p-

DBS-NH_2 due to the disruptive effect of the positive charge on the π-π stacking of the benzylidene groups, the complex with HSA formed stable organogels in chloroform, ethanol, ethyl acetate and acetonitrile. This could be attributed to the fact that HSA, a natural fatty acid and active component of castor oil, is an active gelator on its own right. These salt-type gelators can be considered as examples of two-component gels.[177]

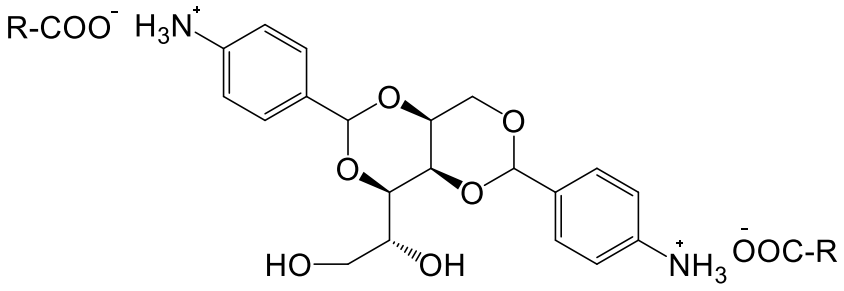

R= $-C_{17}H_{35}$; SA

$-(CH_2)_{10}CH(OH)-(CH_2)_6-CH_3$; HSA

$-(CH_2)_7(CH)(OH)-CH(OH)-(CH_2)_7-CH_3$; DHSA

$-(CH_2)CH(OH)-CH(OH)-CH_2-CH(OH)-CH(OH)-(CH_2)_4-CH_3$; THSA

Figure 2.2.2 Structure of cationic organogelators derived from D-sorbitol and natural fatty acids

In addition to modifying the aromatic wings of DBS, there has been significant number of interest in functionalizing the free alcohol groups of the DBS backbone. This is not surprising as this approach was even demonstrated in the earliest reports in which such derivatisation helped elucidate the structure of DBS.[156] Generally, the primary alcohol is more reactive than the secondary, and hence more easily modified using methods such as tosylation, esterification, etc. In order to demonstrate this, Feng and co-workers reacted acid chlorides with DBS (with or without modified wings) to furnish mono- or bis-esters, depending on the molar ratio of base and acid chloride used.[174] In the presence on one equivalent, 6-substituted product was formed, whereas when more acylating agent was present, the 5,6-disubstituted product was obtained (Scheme 2.2.2).

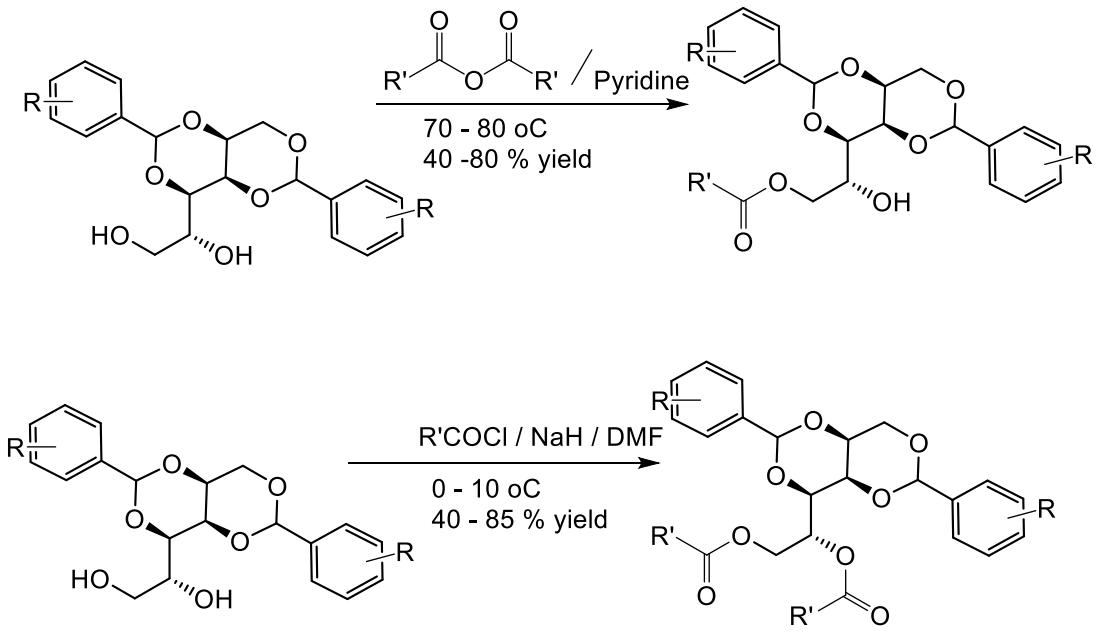

Scheme 2.2.2 Esterification of the free hydroxyl groups of DBS and derivatives with acid anhydride and/or by acylation.

In 2009, Stan and co-workers demonstrated the functionalization of the primary and secondary alcohol groups of the sorbitol backbone with acrylate groups, potentially capable of polymerization. The DBS-based organogelator, 1,3:2,4-bis-(*O*-benzylidene)-5,6-bis-(carbonylaminoethylmethymethacrylate)-D-sorbitol (Figure 2.2.3, IEM-DBS) was synthesized by reacting 3 moles of DBS with 1 mole of 2-isocynanatoethylmethacrylate and dibutyltin dilaurate as a catalyst in THF under argon at 60 °C. This derivative of DBS has been exploited as a dental composite by the same author (*vide infra*).[178]

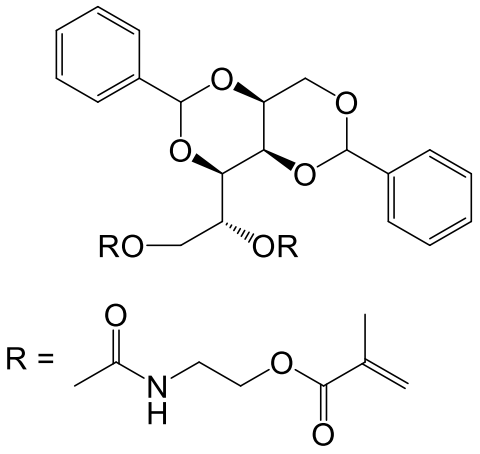

Figure 2.2.3 Chemical structure of IEM-DBS [Adapted from ref. 23]

In an attempt to find a replacement for waxes commonly used in the formulation of personal care products and pharmaceuticals, due to their inherent brittleness, Malle and Luukas have recently patented esters of DBS in which the modification lies on the primary alcohol of the sorbitol backbone.[179] Varieties of ester groups with a range of alkyl chain lengths (Figure 2.2.4 (a-d)) were attached to these groups. In this case, a derivative of DBS is reacted with an acid chloride such as stearoyl chloride, isostearoyl chloride or isohexadecanoyl chloride in an aprotic solvent such as acetonitrile, tetrahydrofuran or ethyl acetate in the presence of a tertiary amine and the reaction mixture refluxed for 5-10 h. For the diesters (such as shown in Figure 2.2.4d) having tails of different chain lengths, two different acid halides were simultaneously or sequentially reacted with the DBS derivatives.

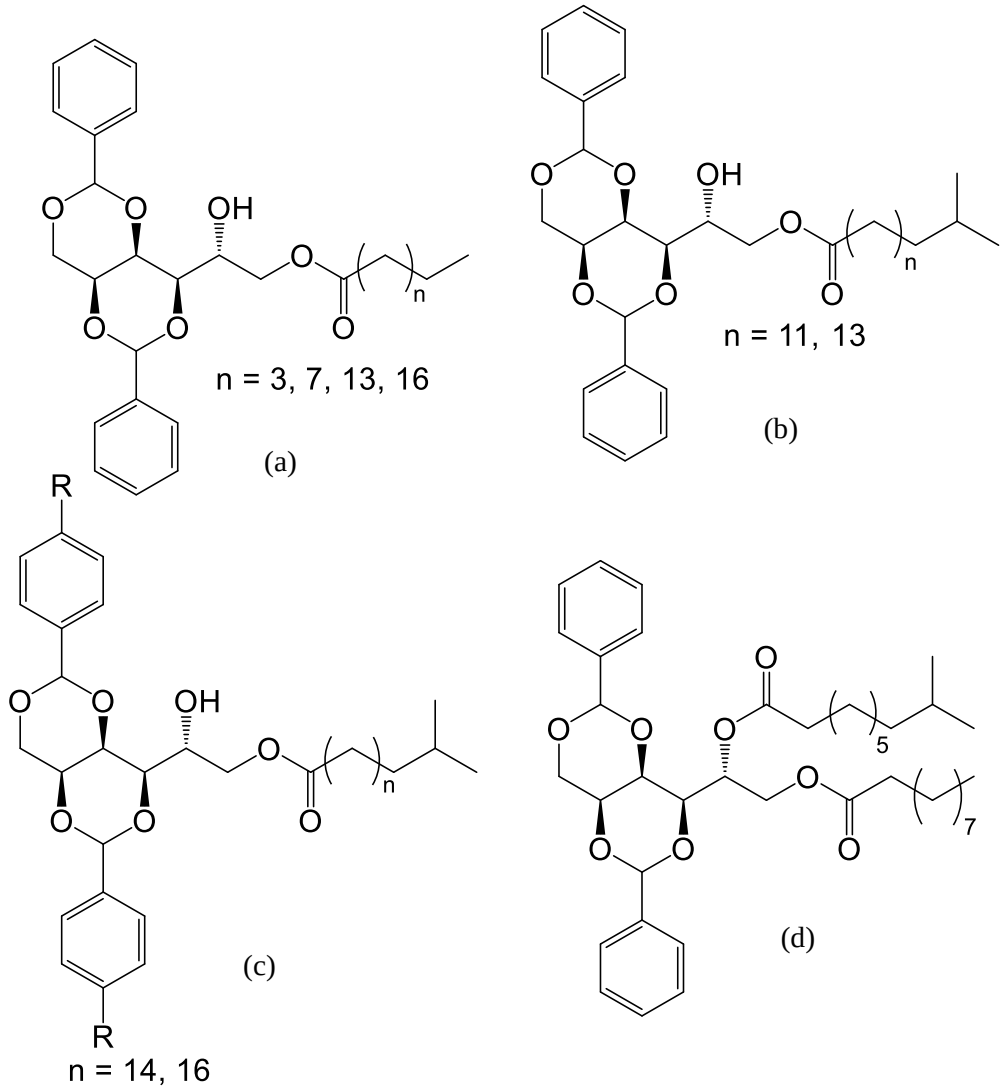

Figure 2.2.4 Chemical structures of DBS derivatives with modified "tails"

This approach was also used to tether together the primary alcohol units of two DBS molecules in order to form bolaamphiphiles[111, 180] (two-headed amphiphiles) with DBS head groups (Figure 2.2.5 (a-c)). In this case, a diacid chloride such as sebacoyl chloride were reacted with DBS derivatives as previously discussed or α, ω-dicarboxyl silicone (also known as Tegomer C-Si 2342) were reacted with the DBS derivative under microwave conditions for about 30 min. The potential advantages of these novel materials in formulating cosmetics over conventional thickeners and dispersants lies in their high transparency, good adhesion to supports, appropriate flexibility and good strength.

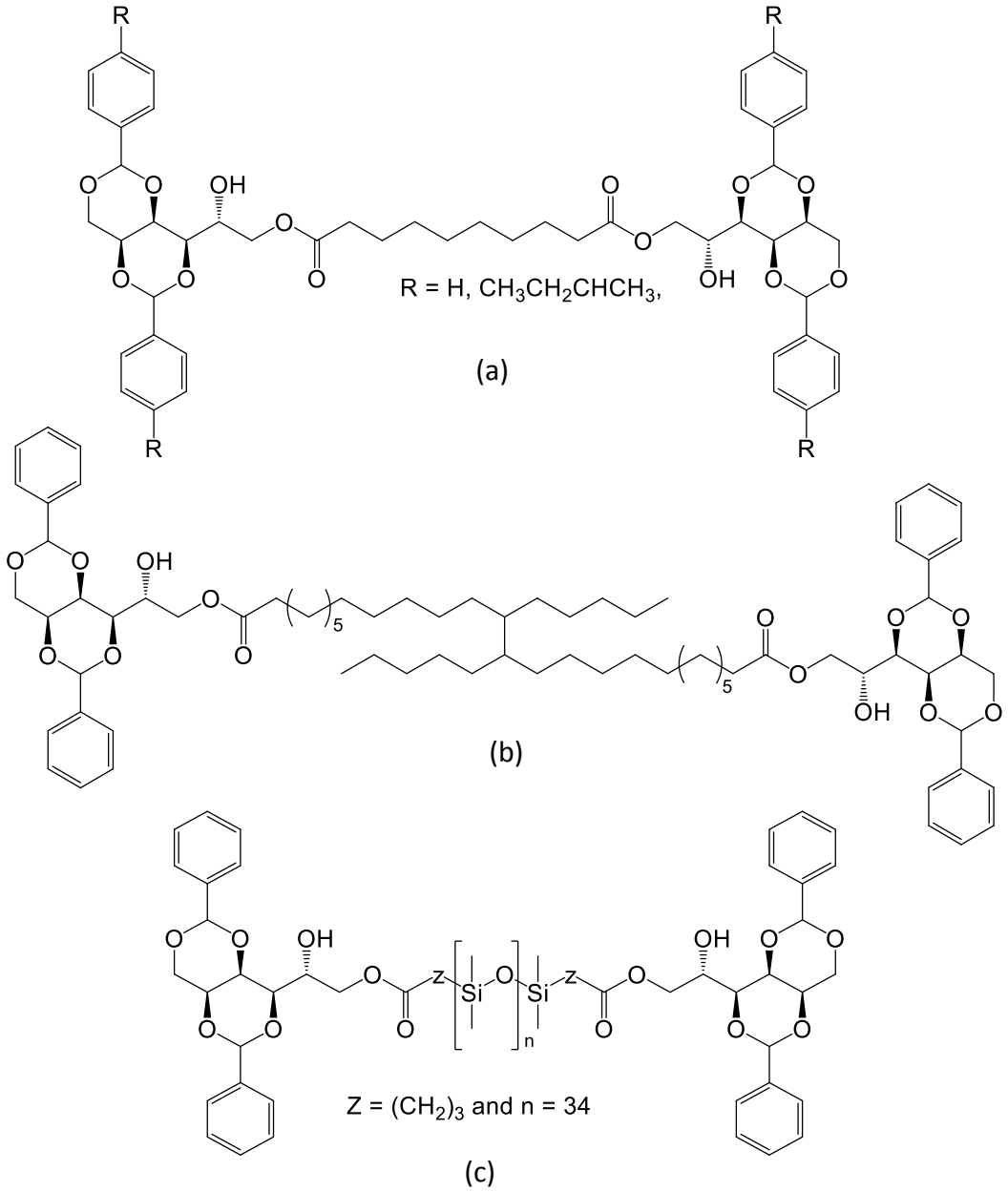

Figure 2.2.5 Chemical structures of DBS-based bolaamphiphiles

Most efforts to-date have focused on modifying the substitution pattern of the substituents appended onto the benzylidene ring and / or the free hydroxyl groups of the sugar backbone but Xie and co-workers have demonstrated that even the first carbon atom of the sorbitol skeleton is not unmodifiable.[181] In a novel approach, tin mediated allylation of glucose (Scheme 2.2.3, A) with allylbromide in an aqueous medium was employed to synthesise allyl-sorbitol (Scheme 2.2.3, B). The allyl-sorbitol was subjected to catalytic reduction to yield n-propyl sorbitol (Scheme 2.2.3, C). Dehydrocondensation reaction of 1 mole of the modified sorbitols with 2 moles of

various substituted benzaldehydes yielded the novel DBS derivatives (Scheme 2.2.3, D and E).

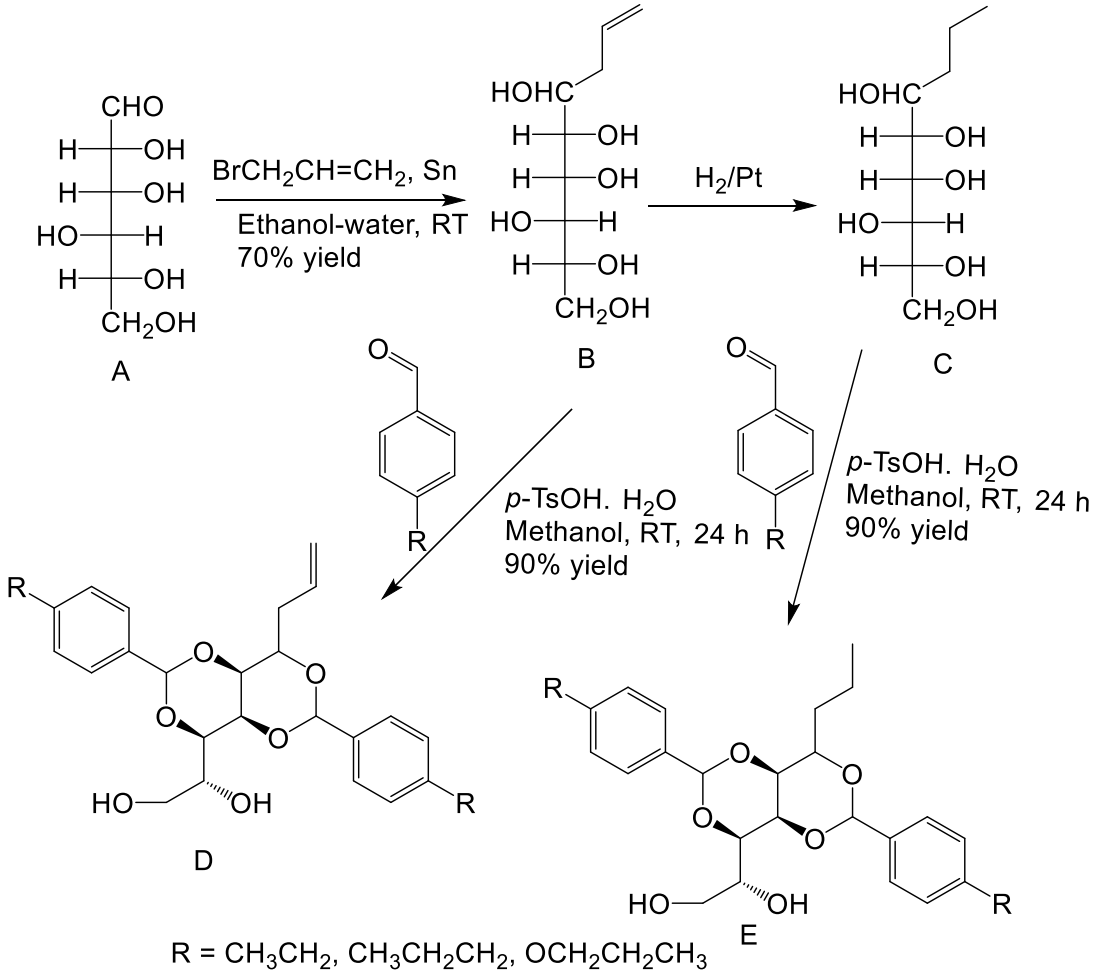

Scheme 2.2.3 Synthesis of Bis-1, 3: 2, 4-(4'-alkyl/alkoxylbenzylidene)-1-allyl sorbitol (D) and Bis-1, 3: 2, 4-(4'-alkyl/alkoxylbenzylidene)-1-propyl sorbitol (E) from glucose (A).

As described in this section, syntheses of DBS are well established. The compound is of industrial importance, and as such, there have been a number of attempts to enhance the methodology in terms of making it more environmentally friendly, for example by changing solvents and catalysts. At heart, however, the synthesis is a relatively straightforward one-step process, and purification can be achieved through simple optimised washing procedures, with no chromatography being required. Furthermore, DBS is a versatile building block for further synthetic modification. As has been discussed, the aromatic 'wings' of DBS offer considerable scope for modification, as do the free hydroxyl groups of the sorbitol backbone. Obviously such derivatisation

can impact, either positively or negatively, on gelation potential, and in order to understand the ways in which this can occur, it is vital to understand the gelation mechanism of native DBS, as explored in the following section.

2.3 *Insight into the Molecular self-assembly of DBS: Computational and experimental concepts*

As discussed in the Chapter 1 of this thesis, for supramolecular gelation to occur, a potential gelator must be capable of forming self-complementary non-covalent interactions which lead to the formation of one-dimensional nanostructures called nanofibrils while the nanofibrils tangle together to form nanofibres. The nanofibres support a sample-spanning three-dimensional network with solvent as the major component.

Several investigations into the molecular self-assembly of DBS have shed light on the mechanisms underpinning the self-assembly processes that mediate its gelation. In an attempt to understand the gelation of DBS, many authors have employed experimental and *in silico* approaches. In essence, the butterfly-like structure of DBS has two potential molecular recognition motifs: (i) hydrogen bonding involving the 'body' of the structure between 5-OH/6-OH groups of one molecule and the 5-OH/6-OH or the ten (10) member acetal ring of another, and (ii) π-π stacking or solvophobic interactions between the aromatic 'wings' of the gelator group of one molecule and those of another. Curiosity to establish the precise structure and mechanism of DBS aggregation has triggered some controversy – some authors propose π-π stacking as the major driving force responsible for the molecular assembly of DBS, while others emphasise the interplay of both π-π stacking and hydrogen bonding.

Yamasaki and co-workers demonstrated that the polarity of a solvent can have a remarkable effect on the nature of the hydrogen bonding responsible for self-assembly. In low polarity solvents, intra- and intermolecular H-bonding of DBS was favoured, whilst in high polarity solvents, H-bonding between DBS and the solvent, which does not underpin gelator assembly, instead became favoured.[182] In order to probe the roles of the free OH in self-assembly, a selective conversion of each of the 5-OH group and the terminal 6-hydroxyl group into methoxy groups to obtain 5-methoxy and 6-methoxy DBS respectively was demonstrated. The 5-methoxy derivative of DBS was

synthesised through the reaction of L-glucono-1, 5-lactone with two equivalents of benzaldehyde dimethyl acetal to first yield the intermediate 3,5:4,6-dibenzylidene-L-gluconic acid. This was further reacted with NaH and MeI to give 3,5:4,6-dibenzylidene-L-glucono acid methyl ester, then finally reduction of the carboxylic acid with $LiAlH_4$ yielded 5-methoxy-1,3:2,4-dibenzylidene-D-Sorbitol. (Scheme 2.3.1).

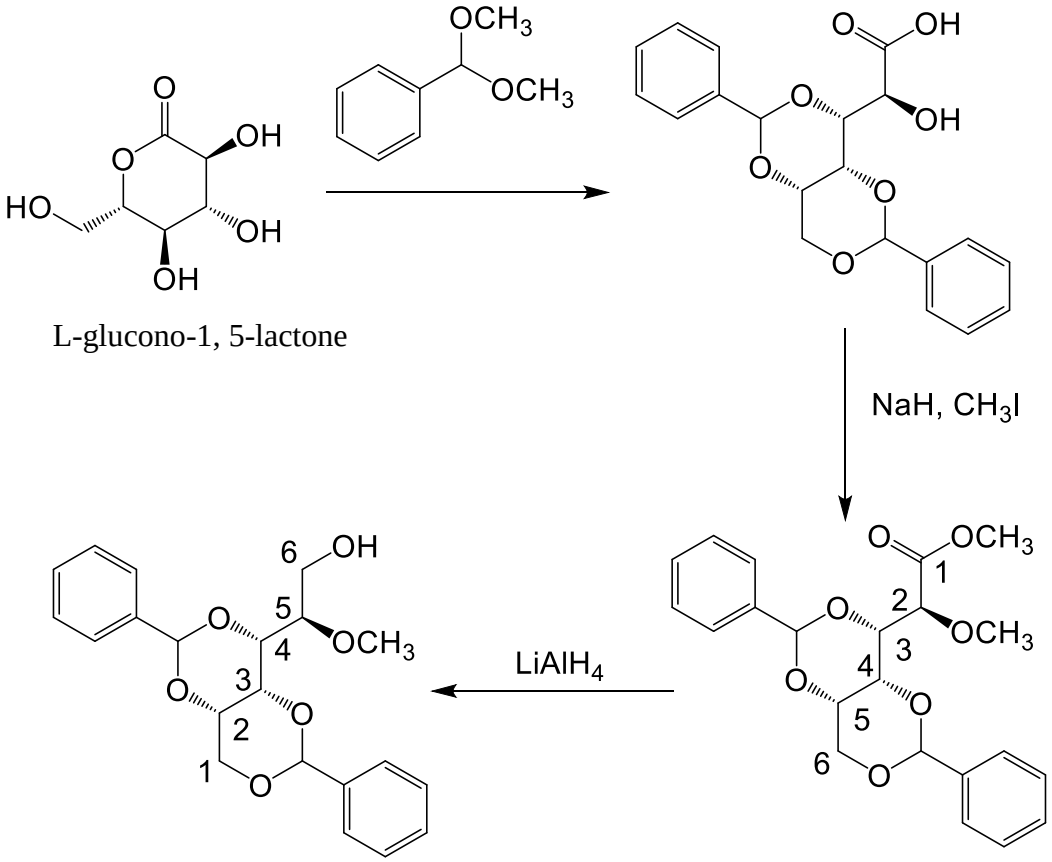

Scheme 2.3.1 Synthesis of DBS derivative functionalised selectively as an ether in the 5-position. Note: the priority order of the numbering changes on conversion from gluconic acid to the sorbitol derivative.

Yamasaki et al[183] observed that no gelation occurred when the terminal (6-OH group) was protected, while gelation still occurred with the 5-OH group protected. This observation suggests that 6-OH is more important for the self-assembly of DBS, most probably because it forms an intermolecular hydrogen bond with the acetal groups of another molecule of DBS. The authors also used IR, UV, and CD spectroscopies to establish that; (i) the 5-OH group either hydrogen-bonds intramolecularly to an acetal oxygen, or intermolecularly to the surrounding solvent and is indeed not involved in

the molecular recognition pathways that underpin gelation, (ii) the 6-OH group is intermolecularly hydrogen-bonded to an acetal oxygen and supports self-assembly, (iii) the phenyl groups are ordered side by side around the aggregate axis, and (iv) helical fibres are formed. The authors concluded that whilst this model, where H-bonding primarily contributes towards DBS self-assembly, is corroborated by the available experimental data, it might not be the only correct model.[184] In a separate study, it was noted that, if the 6-OH group is functionalized with a hydrogen bonding acceptor or donor moiety, gelation can still occur.[178]

In 1999, Watase et al,[185] investigated the ground state dimerization of DBS molecules in relatively polar alcoholic solvents using fluorescence spectroscopy. It was concluded from this study that the self-assembly of DBS was mediated by π-π stacking of the molecules on top of one another to form a molecular fibre. The 1,3–phenyl ring overlapped that of another molecule, while the 2,4-phenyl ring overlapped that of another molecule within a distance of 0.35 nm. It was further established by the same authors that the stabilization of DBS gel is not only a function of the interplay of the non-covalent interactions but rather a molecular structural balance that favours the formation of crystals[152] – indeed, the solubility of gelators is known to be of primary importance in controlling their ability to form solvent-compatible yet 'solid-like' gel phase colloidal materials.[186-188]

In 2003, Wilder and co-workers for the first time used a computational approach – molecular mechanics calculations and molecular dynamics simulations – to determine the configuration of DBS and the intermolecular interactions which underpin its self-assembly.[189] Molecular mechanics analysis of a single DBS molecule produces an energy minimized structure (Figure 2.3.1). However, conformational searches to explore structural variation showed four other possible energy-minimized structures of DBS (Figure 2.3.2), suggesting that the molecular configuration of DBS can potentially switch between several low-energy structures. This provides a significant challenge for modelling as subtle changes in (e.g.) solvent, or derivatisation of DBS, may favour or disfavour one or other of these conformations.

Figure 2.3.1 Energy minimized configuration of DBS as determined by Wilder et al. through the use of molecular mechanics; two different angles are shown. Phenyl rings are in an equatorial positions, 5-OH group forms intramolecular hydrogen bond with acetal oxygen, and 6-OH group shows rotational flexibility C = black, H = grey, O = white. [Images adapted from ref. 189]

With respect to intermolecular interactions, these authors found that for the initial energy-minimized configuration of DBS, the only interaction in the dimer was the formation of a hydrogen bond between the 6-OH group of one DBS molecule and an acetal oxygen of the other – in agreement with the model proposed by Yamasaki.[184] For the alternative energy-minimized conformations of DBS, it was found that π-π interactions (between phenyl groups in the equatorial position) were also present, in some agreement with the results of Itagaki.[185] The authors therefore concluded that both H-bonding and π-π interactions must be considered in the mechanism of DBS self-assembly, as well as the degree of fluxionality of DBS (Figure 2.3.3). However, it should be noted that these computational calculations and simulations were carried out in a vacuum, and hence did not take solvent effects into account – solvent may well be expected to affect the relative strengths of non-covalent interactions and hence the conformation of DBS.

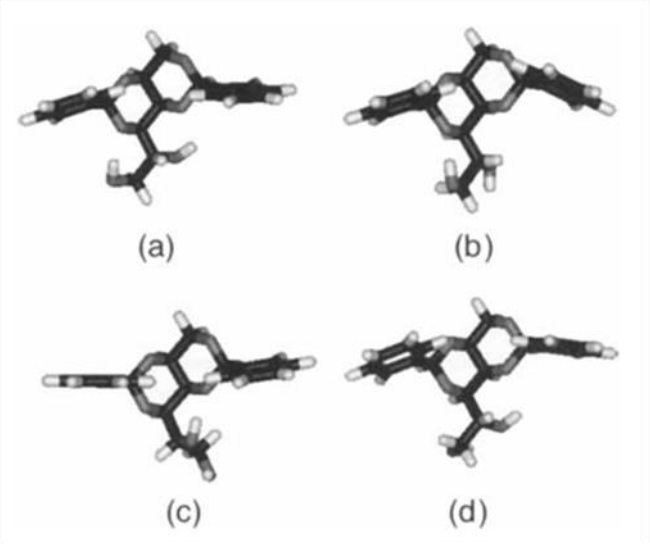

Figure 2.3.2 Alternative energy-minimized structures of DBS as determined by Wilder et al. through molecular mechanics, showing that DBS is flexible and can adopt several low-energy conformations. [Image reproduced from ref. 189]

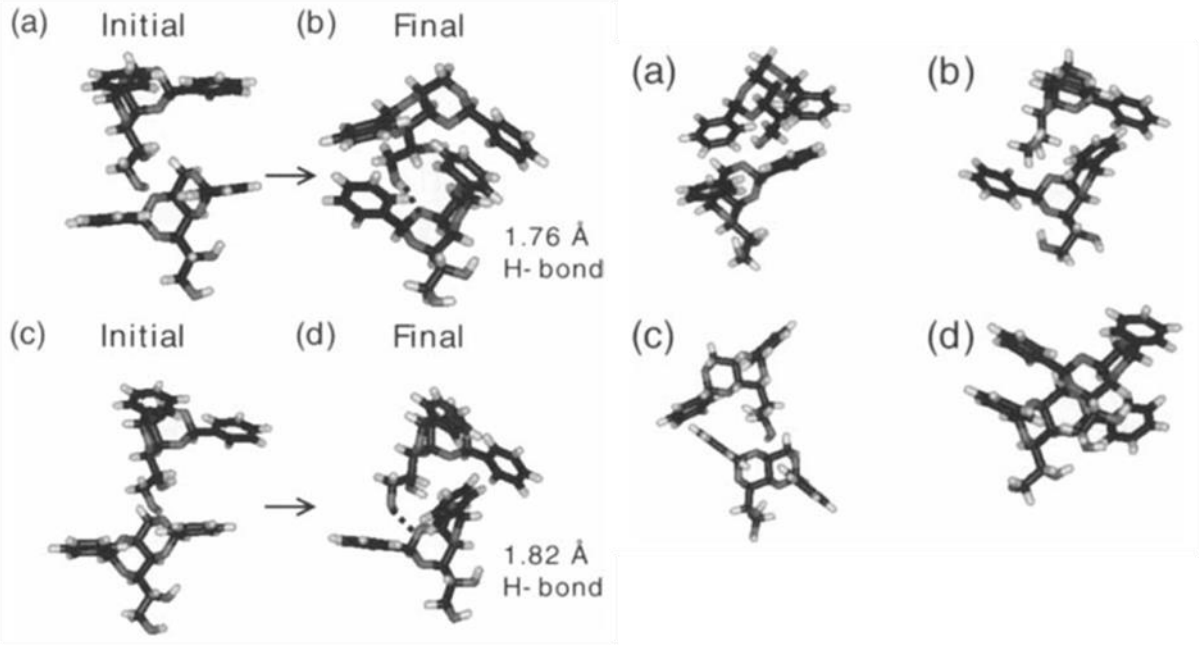

Figure 2.3.3 Left: DBS dimers of initial energy-minimized configuration (as determined by Wilder et al.) before and after energy minimization; the formation of intermolecular hydrogen bonds are shown for (b) and (d) by a dashed line. Right: dimers formed by alternative energy-minimized configurations of DBS; potential edge-to-face π-π interactions can be seen for (a), (b) and (c), whilst definite face-to-face π-π interactions are present in (d). [Images reproduced from ref. 189]

In 2013, Alperstein and Knani[190] used quantum mechanics to determine the molecular configuration of a single molecule and a dimer of DBS, and reported that the energy-minimized conformation of a single DBS molecule had phenyl rings in an almost equatorial position, in close agreement with the results of Wilder, but in contrast, they found that the 5-OH group points towards the 6-OH group with an intramolecular hydrogen bond forming between them. By employing molecular mechanics and molecular dynamics simulations to probe the predominant intra- and intermolecular interactions in DBS as a gelator for polypropylene, an industrially relevant system, they found that the major intermolecular interaction was hydrogen bonding between the O6 and H-O6 groups, with O5/H-O6 and O5/H-O5 interactions also contributing. This agrees with the reports from Yamasaki and Wilder about the importance of the 6-OH group, but in this case the proposed destination of the intermolecular hydrogen bond is different. The authors reasoned that due to the H-bonds, DBS forms a rigid structure, which might aid fibre formation. No significant π-π interactions were observed in their gelation simulations, and they argued that the main contribution from phenyl groups was to stiffen the molecular structure. It is noteworthy that the hydrogen bonding interactions were much stronger in the hydrophobic environment of polypropylene, suggesting that the nature of the solvent can affect the intermolecular interactions in DBS fibre formation – this may also be the reason that the π-π interactions were less significant in this simulation.

Song and co-workers[191] used SEM to experimentally demonstrate that the nanofibres of the xerogels of a derivative of DBS; 1,3:2,4-di(3,4-dichlorobenzylidene)-D-sorbitol (DCDBS) exhibited different structures in polar solvents (non-helical fibre aggregates) and non-polar solvents (rope-like helical fibres) (Figure 2.3.4). They also used molecular mechanics to show that the gelator molecules adopted a planar-type conformation in polar solvents, causing the molecules to stack on top of each other, with π-π interactions being responsible for self-assembly. They suggested that these π-π interactions prevent the individual molecules from bending, leading to the observed non-helical fibres. However, in non-polar solvents H-bonding between the 6-OH and an acetal oxygen was found to be the driving force responsible for the self-assembly; with the intermolecular interactions having different effects on each side of the molecule, hence twisting the fibres in a helical way to minimize energy.

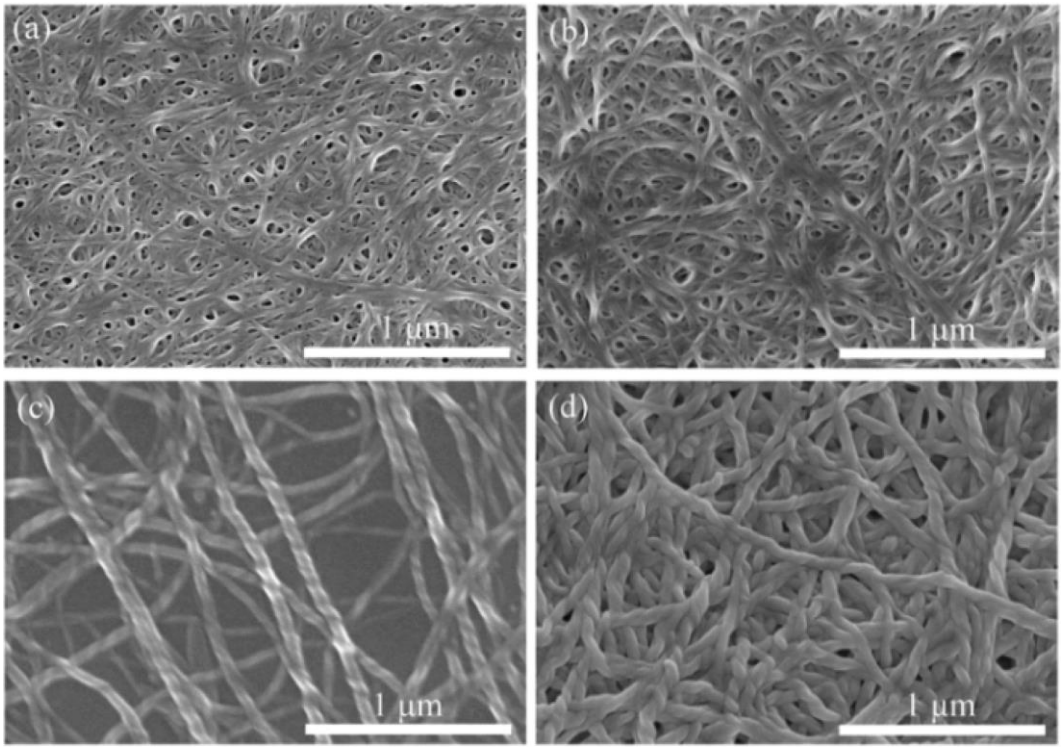

Figure 2.3.4 SEM images of DCDBS xerogels made from (a) DMSO−H_2O (7:3 v/v), (b) ethylene glycol, (c) n-octanol and, (d) *o*-dichlorobenzene.

In terms of DBS derivatives, Song and co-workers reported that the precise positioning of the substituents on the aromatic 'wings' of DBS determines whether it will form gels or not as demonstrated by 1,3:2,4-di(2,4,6-trimethylbenzylidene)-D-sorbitol (2,4,6-TMDBS, Figure 2.3.5a) and 1,3:2,4-di (2,4,5-trimethylbenzylidene)-D-sorbitol (2,4,5-TMDBS; Figure 2.3.5b).[192] The former is an efficient organogelator but the later does not form gels in the solvents tested. The inability of the later could be attributed to the substituents at the meta-position sterically disrupting the interactions between one molecule of DBS and another during gelation – or alternatively could be due to the substitution inducing conformational changes or slight differences in overall solubility.

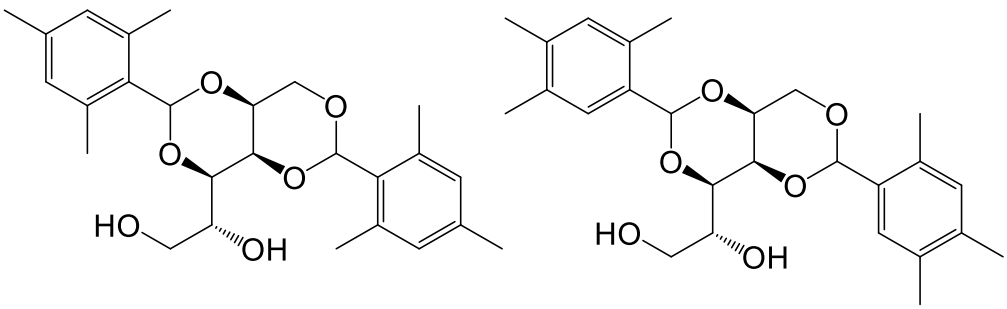

Figure 2.3.5 Chemical structure of (a) 2, 4, 6-TMDBS (b) 2, 4, 5-TMDBS

Taking these experimental and theoretical results in combination, the following factors clearly emerge:

(i) DBS is a relatively fluxional molecule with a number of low-lying energy conformations – the relative populations of these will be affected by a number of factors, and self-assembly may specifically favour any of these conformations.

(ii) In non-polar solvents hydrogen bonding, predominantly from the 6-OH group play a key role in underpinning self-assembly.

(iii) In polar, protic solvents, hydrogen bonding becomes less significant, owing to competition for these interactions from the solvent, and self-assembly is primarily driven by stacking and/or solvophobic interactions between the aromatic faces of the gelator.

Clearly, DBS is a versatile and responsive gelator which can, to some extent, adapt to the environment in which it finds itself. This means that as a gelation system it has a relatively broad scope, and clearly synthetic derivatisation, can extend this yet further. In order to probe the structural and solvent effects on gelation in more detail, a number of important studies have been carried out, as described in the following section.

2.4 *DBS-based gelators: Effects of medium on gelation*

2.4.1 DBS-based Gelators: Medium Effects on Gelation

As described above, DBS is a highly versatile gelator, indeed it has demonstrated exemplary ability to induce gelation in a wide range of organic solvents,[182, 184, 192-194] monomers,[195, 196] polymer melts,[197-203] oils,[204] liquid crystals,[205] and ionic liquids.[206] This unusual ability is governed by factors such as the concentration of DBS, temperature, solvent polarity, chirality and the positioning of substituents on the benzene rings. All of these factors have significant effects on, for instance, the phase transition temperature and the rheology of the resulting gel.

2.4.2 Solvent Effects on DBS Gelation

Solvent effects have been of considerable interest in gel-phase materials. In general terms it is often considered that a gelator must be sufficiently soluble for it to be compatible with the solvent, but sufficiently insoluble for self-assembly into a ‘solid-

like' network to be desirable.[187, 188, 207, 208] Most gelators sit on a knife-edge between solubility and precipitation. DBS is somewhat unusual in the breadth of solvents which it can immobilise, and given the industrial importance, the gelation properties have been widely explored in a range of organic solvents by many authors.[182, 184, 192-194, 206, 209-211] However, there are fewer studies in which a rational approach to understanding solvent effects on its gelation is attempted.

In 1995, Yamasaki and Tsutsumi reported that solvent polarity could have a significant effect on self-assembly, tuning the relative importance of hydrogen bonding and π-π stacking.[182] However, they did not fully quantify the effects of solvent on gelation, and their results still make it hard to understand why DBS is unable to form gels in highly polar, hydrogen bonding solvents, such as water. Nonetheless, their pioneering work set up much of the understanding of the gelation behaviour of DBS – both in terms of nanoscale morphology and rheological performance.

In fact, as early as 1991, rheological analysis had been used to show that the time requires for DBS to form stable organogels in esters of diacids such as dimethyl phthalate, dibutyl phthalate, and dibutyl adipate depended significantly both on the solvent polarity and the concentration of DBS.[193] The minimum concentration of DBS required to induce gelation, the gel-sol transition temperature and the mechanical properties of the resulting organogels all depended on the polarity of the solvent.[152, 194] In a recent extension of this early work, Liu and co-workers investigated DBS organogels in liquid paraffin (LP), diisodecyl phthalate (DIDP) and poly (ethylene glycol) (PEG). [210] Interestingly, regardless of the polarity of the of the solvent used, the elastic moduli (*G*') of the resulting gels remained identical, but the phase transition temperature increased significantly with solvent polarity (Figure 2.4.1b). This suggests that the thermodynamics of nucleation/assembly change with solvent, but the mechanical nature of the network, once assembled, is equivalently independent of solvent. This would suggests that solvent primarily affects network growth. However, both of these parameters increase with the concentration of the gelator – as the network becomes more heavily entangled (Figure 2.4.1a).

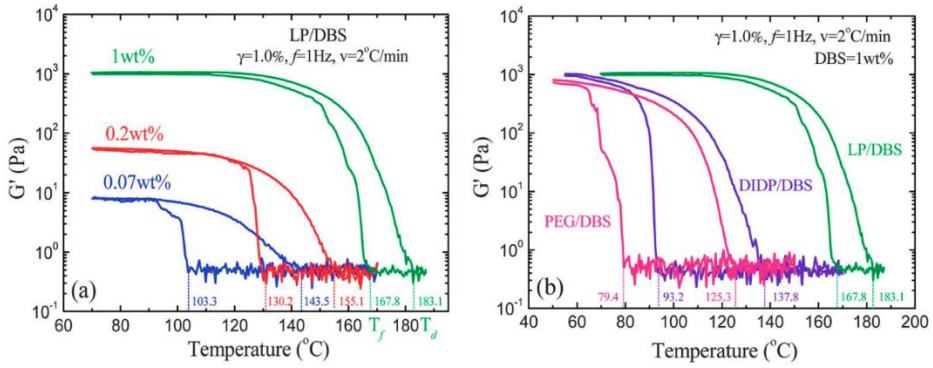

Figure 2.4.1 The dependence of *G*' on the temperature at a heating and cooling rate of 2 °C min^{-1}: (a) LP–DBS gels containing 0.07 wt%, 0.2 wt% and 1 wt% DBS. (b) 1 wt% DBS in LP–DBS, DIDP–DBS and PEG–DBS gel systems, respectively. The strain amplitude and frequency are 1.0% and 1 Hz.

In sharp contrast, Santos and co-workers demonstrated that the choice of organic solvent did have significant effects on the rheology of DBS organogels by using chlorobenzene, mineral oil, ethylene glycol, glycerol and ethanol as model solvents.[212] As shown in Figure 2.4.2, the elastic moduli (*G*') of the organogel of 2% DBS in the tested solvents are in the order of chlorobenzene > ethylene glycol > glycerol > mineral oil > ethanol and the stiffness are 12.6, 10.7, 7.3, 4.0 and 3.6 (nm^{-1} x 10^3) respectively. This order seems difficult to rationalise as it does not simply correlate with solvent polarities. It was suggested that including hydrogen bonding effects could account for this, although a multi-parameter approach of this type was not applied in any quantitative way.

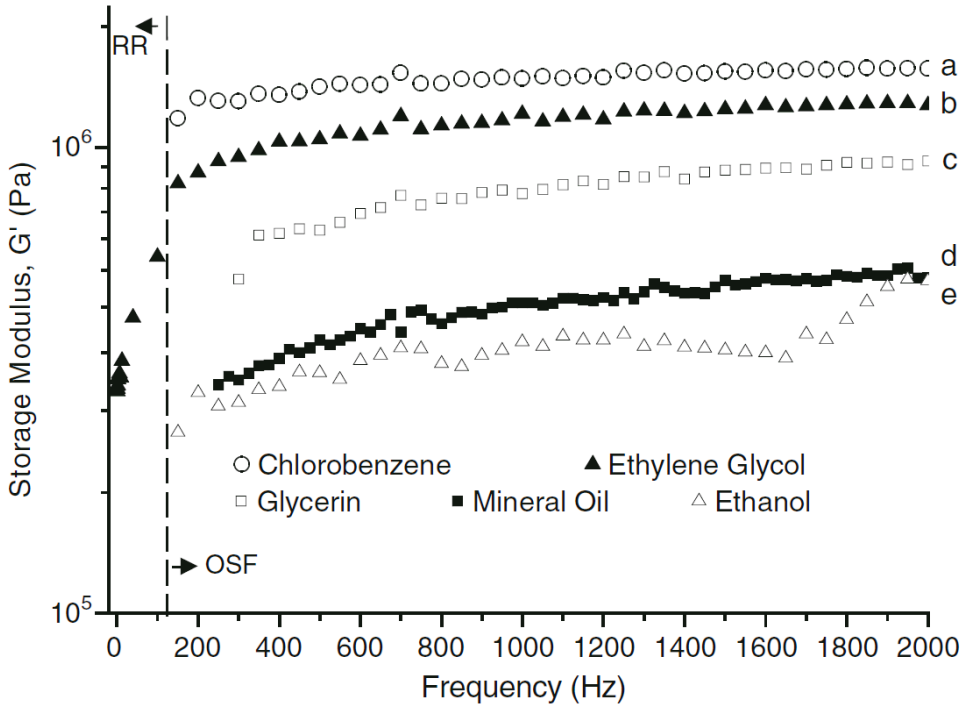

Figure 2.4.2 Storage modulus (*G'*) versus frequency for (a) chlorobenzene, (b) ethylene glycol, (c) glycerol, (d) mineral oil, and (e) ethanol containing 2% DBS. The storage modulus (*G''*) of ethylene glycol was also measured at lower frequencies using a rotational rheometer. [Adapted from ref. 122]

In the late 1990s, Watase and co-workers proposed that a weak gel would be formed if the solvent has little or no tendency to form interactions with the aggregates.[185] In a relatively simplistic approach, the authors attempted to correlate the gel forming ability with the hydrogen bond density of the solvent. In low hydrogen bonding solvents, the gels formed had lower strength. However, despite the extremely high dielectric constant (ε = 80) and polarity of water, DBS could not form a gel in water, although the use of water as a co-solvent enhanced the strength of its ethanol gel. In order to clearly understand the gelation of the highly versatile DBS, the use of multiple solvent parameters will be required.

Deng and co-workers have demonstrated the gelation ability of DBS in over numerous organic solvents.[192] They showed that DBS generally precipitated out of non-polar organic solvents (except *o*-xylene), but was able to form stable organogels in glycerol, ethylene glycol, propylene glycol, propanol, butanol, octanol and benzyl alcohol. However, when dissolved in highly polar solvents such as DMSO or DMF, the gelator

remained soluble. These observations are consistent with a view in which the solvent compatibility of the gelator must be just right in order for gelation to occur. In highly polar solvents, the interactions between DBS and solvent becomes stronger than that between one molecule of DBS and the other, thereby leading to the formation of a weak gel or a homogeneous solution, whereas if the solvent is too apolar, the gelator is unable to dissolve.

The qualitative understanding of Deng and co-workers was put onto a more quantitative footing by the landmark research of Raghavan and co-workers, who published a powerful predictive gelation model for DBS in a wide range of organic solvents using a multi – parameter treatment of solvent properties.[213] By fitting practically-obtained data from the gelation of DBS at given temperatures and concentrations, into 'Hansen space', which is designed based on Hansen solubility parameters (HSPs) they could generate a 3-D colour co-ordinated maps (Figure 2.4.3) of gelation performance. Hansen space takes account of solvent polarity, and the ability to accept and donate hydrogen bonds.[214] These parameters had previously been used to model the performance of other low molecular weight gelators.[215] Using this approach, it became possible to predict the region of Hansen space where DBS will either remain soluble (S), form gels slowly (SG), form gels instantly (IG) or remain insoluble (I). The distance (R_o) from the centre of the sphere effectively determines the degree of compatibility between gelator and solvent, the speed of gelation and the mechanical properties of the resulting gels. As R_o increases, DBS-solvent compatibility and speed of gelation decrease while the mechanical properties increase, up to a point when the gelator ultimately becomes insoluble. This is in agreement with the simple qualitative solubility-driven model of self-assembly and gelation, in which sufficient insolubility to nucleate gel fibres, and sufficient compatibility of the fibres with the solvent, are both essential characteristics. The authors also considered the effect of DBS concentration on the Hansen Space treatment, and as would be expected, found that the insolubility region became increasingly dominant as the concentration of DBS was increased.

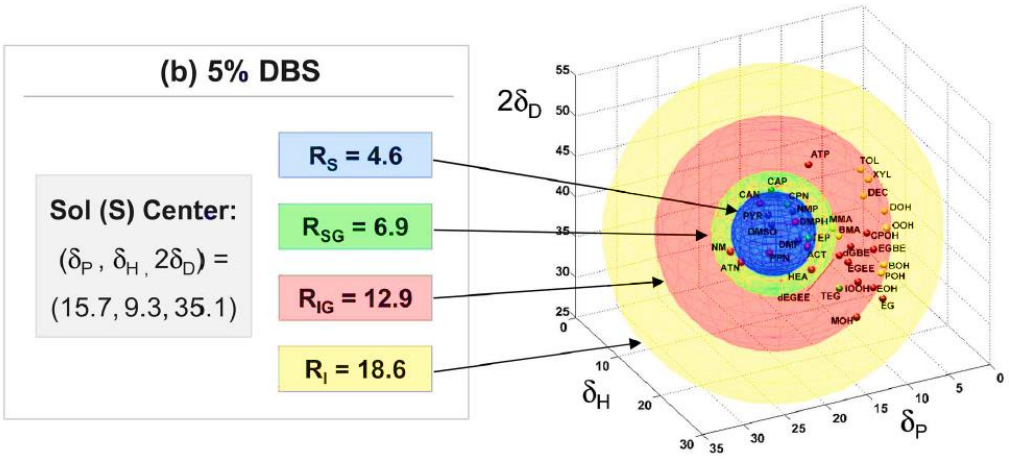

Figure 2.4.3 Results for DBS in various solvents, plotted in 3-D Hansen space for 5% DBS. The axes represent the three Hansen solubility parameters (d_D = dispersive, d_P = polar, and d_H = hydrogen-bonding interactions). Each solvent is represented as a color-coded point on these plots. The results show a pattern of concentric spheres, i.e., the central sol (S) sphere in blue, followed in order by spheres corresponding to slow gel (SG) in green, instant gel (IG) in red, and insoluble (I) in yellow. The co-ordinates for the centre of the S sphere and the radii of each sphere are indicated. [Reproduced from Ref. 213]

Rogers and co-workers also demonstrated the importance of a solvent's hydrogen bond acceptor/donor character in determining whether DBS will form a solution, transparent or an opaque gel – properties which are connected strongly to gelator solubility.[115] They found that individual HSPs, especially the hydrogen bonding HSP, δ_h strongly influences the physical properties of the DBS organogel. A solvent with a larger δ_h than that of DBS will yield a transparent gel while a lower δ_h , an opaque gel.[115] It is also noteworthy that unlike for polymer gel counterparts, the appearance of DBS organogels is dependent on both the distance between the HSPs for DBS and the HSPs of the solvent and the directionality of Hansens distance (R_{ij}).

The by-products of DBS synthesis; mono- and tri-acetals (MBS and TBS) also have the capability to induce the gelation of organic solvents and / or water. In 1999, Watase and co-workers demonstrated with the use fluorescence spectroscopy to show that for TBS, the 5, 6-*O*-bezylidene groups interacted with 1,3- and 2,4-benzylidene groups thereby disrupting the π-π stacking of 1,3- and 2,4-benzylidene groups. As a result of this interaction, the organogels of TBS are less stable than those of the DBS as revealed

by the T_{gel} values and rheological measurements. In order to further establish the general solvation differences between the trio (MBS, DBS and TBS), Song and co-workers investigated the structure-gelation relationships among the gelators by using 30 organic solvents and water.[167] It was observed that the gelator with more hydroxyl groups (MBS) could gel water due to increasing hydrophilicity and those with more aromatic rings could gel aromatic solvents most efficiently because the aromatic ring enhances the strength of the π-π interactions between gelators. Besides gelling water, MBS could also gel long-chain alcohols such as hexanol, decanol and dodecanol or aromatic alcohols such as anisole and benzyl alcohol, hence it is an ambidextrous gelator. It is important to mention that hydrogen bonding interaction is the main driving force for the formations of the gels by MBS, DBS and TBS. [167, 216]

2.4.3 DBS Gels formed in a Polymeric Medium

Instead of using simple solvents for gel formation, it is possible to use a liquid phase which is more functional in nature – in the case of DBS, polymer melts have been quite widely investigated as the DBS network can potentially enhance the mechanical properties of the polymer (see following section for applications of this technology). In this way, polymer gels using polymer matrices including but not limited to isotactic polypropylene (iPP),[201] poly(propyleneglycol) (PPG),[197, 198, 203, 217] poly(ethyleneglycol) (PEG),[202] poly(dimethylsiloxane) (PDMS),[198] poly(propyleneoxide) (PPO),[198] poly(styrene) (PS), poly(methylmethacrylate) (PMMA),[198] silicone fluids,[199, 218] copolymers and triblock polymers,[199] have been reported. The morphological and thermal properties of some polymer gels do not differ significantly from that of the organogels in simple organic solvents as evidenced in the phase transition temperature of the resulting gel and the shapes/sizes of their nanofibres.[197] For example, Wilder and co-workers demonstrated that the nanofibrils of PPG/DBS gel systems were 10-70 nm in diameter with a primary nanofibrillar diameter of 10 nm; identical to those of gels of DBS in low-molar-mass organic solvents.[217]

In large part, the polymeric melt phase does effectively behave just like a solvent. For example, it has been reported that PEG derivatives with a pendant methoxy group at one end, being less polar, tend to enhance the speed of gelation, which indicates that 'solvent-like' effects also apply in the gelation of polymer melts.[217, 219] Indeed, capping one end of PEG as a methyl ether will clearly modify its hydrogen bond potential and

affect its solvent-like parameters. As is commonly found in organic solvents, the speed of gelation, elastic modulus (*G*') and sol-gel/gel-sol transition temperature of polymer/DBS gel systems increases with an increase in DBS concentration. Spontak and co-workers demonstrated with PPG/DBS systems that an increase in DBS concentration will consistently promote an increase in *G*' until the concentration reaches about 4 wt%, at which point *G*' plateaus. Further increase beyond 4 wt% in the PPG systems yielded a heterogeneous matrix which indicates a saturated gel network (i.e. the gelator effectively becomes insufficiently soluble for further network formation).[197, 199]

However, the molecular weight of the polymer can affect the stability of the gel.[220] Mercurio and co-workers demonstrated that the higher the molecular weight of poly(propyleneglycol) (PPG), the less the amount of DBS required for onset of gelation.[197] It was suggested that the solubility of DBS decreased significantly as the molecular weight of PPG increased and it was argued that this underpinned the observed behaviour. It should also be noted that the gelation process in polymer matrices is particularly time-dependent, requiring a fixed period of time to attain equilibrium, depending on the concentration of DBS.[203]

2.5 *Applications of DBS and derivatives: The most patented supramolecular gelators of all time*

DBS has a long history of industrial use, and as such, this compound has attracted more patents than any other low molecular weight gelators, and has been employed in a wide range of different industrial sectors. Furthermore, as gel chemists increasingly consider high-tech applications for these responsive self-assembled materials,[64, 65, 221, 222] DBS and its derivatives are well placed for potential future use, given the long history of precedent, and studies to expand the scope of DBS applications are well underway.[179, 221]

2.5.1 Personal and health care products

DBS has long been employed in the formulation of cosmetics (e.g. Figure 2.5.1) due to its ability to gel the cosmetic condiments, thereby imparting the product with the desired thickness, adhesion, strength, and consistency and its use in the field is widespread.

Figure 2.5.1 'RightGuard' antiperspirant products containing DBS as a gel matrix

In development of simple DBS technology, between 1979 and 1982, Roeh[223, 224] patented DBS-mediated gelation of glycols with acidic aluminium antiperspirant salts, in which DBS was used to give a clear solid antiperspirant composition, with suitable stick hardness and adhesion. However, it was noticed that these formulations were not stable over time, did not have adequate shelf life and deteriorated at elevated temperatures. These drawbacks could be adduced to the instability of the 10-membered acetal ring of DBS in acidic media.[225] Therefore, several patents were developed in which less reactive solvents were used and stabilizing agents were added into the DBS gel. Schamper et al describe the use of alcohols which would be less reactive in the presence of acidic antiperspirant salts and a gel stabilizer such as zinc acetate. This formulation was an improvement over the earlier versions as it retards degradation of the gel sticks and enhanced stability at elevated temperatures.[226] Stabilizing and coupling agents such as guanidines,[227] polypropylene glycol ethers of fatty alcohols,[228] *N*-(2-hydroxyethyl) fatty acid amides, zinc and magnesium acetate,[229] silicone elastomers,[230] and amino acid salts,[231] have also been used to stabilize deodorants containing DBS gels in the past decades – demonstrating the vitality of this area of industrial research and the significant market for these products.

The use of DBS derivatives in formulating other personal care products has also recently begun to find expression. For examaple, Malle and Luukas have recently patented a library of DBS esters (Figure 2.2.4 andFigure ***2.2.5***) which demonstrated tremendous ability as thickeners for lipophilic media. The lipstick sticks made with

these esters exhibited better properties such as transparency, flexibility, good adhesion to supports, good coverage, good stability, glossiness and adequate strength over more conventional waxy lipsticks.[232] Similarly, DBS has recently been used as oil-soluble thickener in oil-in-water emulsions that is currently finding application in products as diverse as milky lotion, cream, foundation, sunscreen and makeup base.[233]

In terms of healthcare, Furuishi and co-workers patented a pharmaceutical formulation containing an organogel, a fatty acid ester and a glycerolglycerin fatty acid ester that incorporates drugs, such as non-narcotic analgesics for external applications.[234] The use of DBS with 30% ethanol as gel presented good skin permeability, together with high drug release, leading to efficient transdermal absorbable pharmaceutical composition. A recent patent uses DBS to formulate pseudoephedrine, preventing easy extraction of the API for use in the synthesis of illicit drugs.[235]

Applications of DBS and its derivatives in healthcare are not simply limited to drug delivery systems but also explored in clinical testing laboratories. Graper and co-workers have demonstrated that the use of DBS gel, a blood compatible and shear-sensitive gel, can facilitate the separation of serum from the cellular portion of blood.[236] In this patent, a block copolymer was gelled by DBS in the bottom of a tube and a blood sample was added on top. The thermoreversible, shear-sensitive properties of the obtained gel enables the formation of a viscous liquid when centrifuged, with the gel being capable of recovering and reforming once centrifugation is complete. At this point, the re-formation of a solid gel barrier helps separate the solid and the liquid constituents of blood according to their densities.

2.5.2 Polymers with Embedded DBS Networks for Enhanced Performance

DBS-based compounds are widely used as nucleating and clarifying agents in plastic or thermoplastic materials – indeed this remains one of the primary industrial applications of this class of material.[200, 237-239] Importantly, the presence of DBS or DBS derivatives shortens processing times, improves the mechanical properties and reduces the 'haze' in these materials.[240-242] DBS acts as a nucleating agent, by dissolving in the molten polymer and homogeneously dispersing in the polymer matrix, and on cooling forms a thermoreversible nanofibrillar network in the polymer,

resulting in faster and more organized crystal growth of the polymer matrix, which leads to the desirable properties.[243, 244] In addition, in the case of polyolefins it exists in epitaxial interaction between the nucleating agent and the polymer which also influence the efficiency of the nucleation.[245] There have been a number of developments of this technology which are described in more detail below.

Titus and co-workers[246] patented a polyolefin composition with improved clarity, which is desirable in certain plastic products such as syringes, made by injection moulding. The presented polyolefin composition contained fluorinated DBS as clarifying agent, which contributed to the improved clarity, resistance to shrinkage and heat deterioration, without loss of mechanical and chemical properties. Other patents had proven the ability of DBS and derivatives to improve transparency and reduce moulding shrinkage of polyolefins that make them suitable for packaging, containers for cosmetics, transparent doors and electrical component parts.[247-249]

Despite its efficiency as a nucleating/clarifying agent for polyolefin production, DBS is not suitable for food packaging due to the transfer of taste and odour to the food. On researching this problem, Rekers et al.[250] found that substitution on the aromatic rings to make bis-dialkylbenzylidene sorbitols is crucial for the performance of this type of compound as clarifying agents and also overcome the organoleptic problems associated with the native DBS (unsubstituted). As a result, the commercial product sold under the trade name Millard®3988 (1,3;2,4-bis(3,4-dimethylbenzylidene)sorbitol (Figure 2.5.2) led to compositions with suitable taste and odour transfer properties for food packaging. Xie et al[181] have also made DBS derivatives, in this case having an allyl group attached to the first carbon of the sorbitol chain which have found applications in polyolefin formulation with an improved organoleptic profile (Figure 2.5.2b).

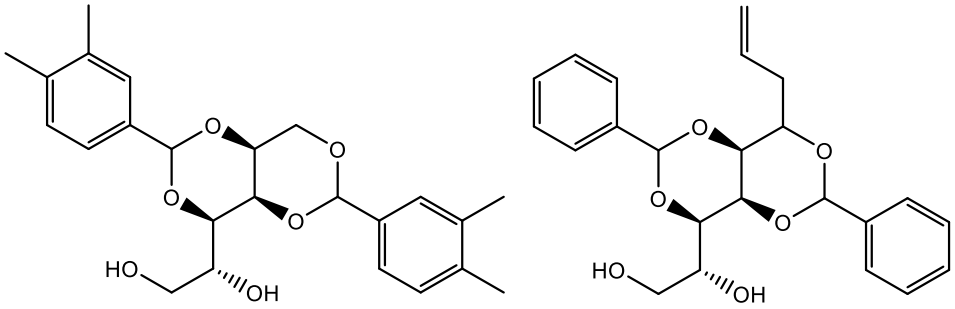

Figure 2.5.2 Chemical structure of (a) Millard®3988 (b) Structure of 1-allyl-1:3, 2:4-Dibenzylidene-D-Sorbitol

Simultaneous use of DBS as a nucleating agent, and poly(ethylene glycol) (PEG) as a plasticizer, in order to improve the rate of crystallization of poly(lactic acid) (PLA) has been reported by You and co-workers.[251] Due to the presence of the DBS nanofibrils that acted as heterogeneous nucleating sites for crystallization, it was possible to observe a crystallization peak after cooling, even at a very high cooling rate (40˚C/ min) – therefore enabling rapid polymer processing. The influence of DBS self-assembly on the liquid-liquid phase separation and crystallization of ultrahigh molecular weight polyethylene (UHMWPE)/ liquid paraffin (LP) blends was also studied and confirmed that DBS nanofibrils can be an effective heterogeneous nucleating agent and accelerate the crystallization of UHMWPE. Furthermore, the competition between the liquid-liquid phase separation and crystallization of UHMWPE can be controlled by the amount of DBS.[252]

In addition to simply modifying the kinetics of polymer crystallisation, DBS gel networks can also play a more active role in directing the structure of polymeric materials. Indeed, the 3D fibrillar networks of DBS organogels can be used as self-assembled templates for the polymerization of a monomer, inducing its crystal orientation and contributing to the formation of nanoporous polymer matrix, suitable for a variety of applications, after the removal of the DBS scaffold (as shown in Scheme 2.5.1).[196, 253-256]

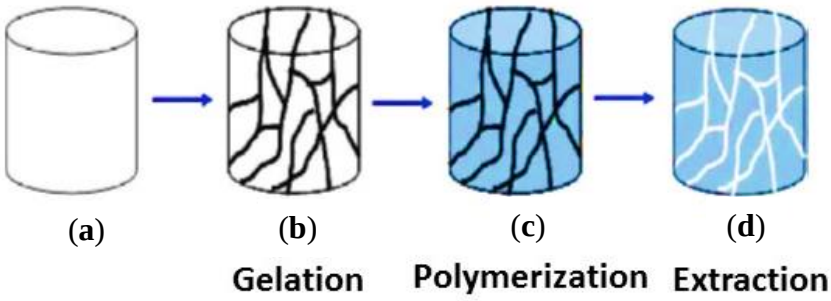

Scheme 2.5.1 Schematic representation of (a) a homogeneous solution containing DBS molecules, (b) the formation of DBS nanofibrils, (c) polymers within DBS organogels and (d) porous polymers after DBS organogel extraction.

Lai and Tseng demonstrated the polymerization of styrene using DBS as a template.[255] DBS nanofibrils were formed in styrene followed by the free-radical polymerization of the monomer in the presence of a chemical cross-linker, divinyl benzene. The obtained material remained transparent and homogeneous and it was proved that the DBS fibrils remained intact in the final product, showing that the thermal polymerization process did not affect the DBS network. Subsequently, a nanoporous polymer was successfully obtained by solvent-mediated extraction of the DBS, suggesting the feasibility of DBS as a template – as has also been demonstrated for other low molecular weight gelators.[257, 258] The concentration of DBS influences the crystallization and the morphology of the resulting polymer. In a similar manner, Lai *et al* demonstrated that the gelation of DBS in methyl (methacrylate) (MMA), a hydrophilic monomer, takes a longer time to attain equilibrium than the hydrophobic styrene monomer due to the *in situ* hydrogen bonding interaction between DBS and the MMA and as a result of this, the average pore diameter of the resulted porous material was larger than the diameter of the nanofibres of the gel sample.[259] In 2009, Lai and co-workers carried out BET analysis of the nano-imprinted polystyrene which showed that the specific surface area (3.1 m^2/g) of the templated polymer was about six times that of the untemplated counterpart.[196]

Another approach using DBS derivative 1,3:2,4-di(3,4-dimethylbenzylidene)-D-sorbitol to orientate the crystallization of polypropylene (PP), reported better orientation when 0.4% (instead of 1%) of the DBS-based gelator was used. This was

attributed to the fact that low concentrations of the gelator produce longer fibres which could be more effectively aligned and organized, leading to a good orientation of the polymer chain. [253]

It is certainly clear that DBS offers a low cost method for modification of polymer matrix properties. Obviously, there is significant further scope for the active templating of polymer matrices with DBS and its derivatives in which the nanoscale network introduced activity or function to the overall system rather than simply modifying kinetics and structure. This approach to modifying well-established materials with a self-assembled nanoscale network offers high potential for future high-tech applications, a number of which are currently being explored for DBS and other self-assembled gel-phase materials.[260]

2.5.3 Dental composite

Dental composites can be obtained by photopolymerization of several dimethacrylate monomers, such as bisphenol-A-glycidyl dimethacrylate (bis-GMA) and urethane dimethacrylate (UDMA). However, polymeric composites are vulnerable to shrinkage and incomplete vinyl conversion that can lead to the presence of free monomers or unbound species and cause oral health problems. In order to overcome this problems, DBS and DBS derivatives have been used to gel dental monomers, resulting in a reduced volumetric shrinkage and increased vinyl conversion for photopolymerization.[261, 262] Clearly this application is related to other examples of DBS-modified polymers.

Şulcă et al. used DBS, 1,3:2,4-bis-(p-methoxybenzylidene)-D-sorbitol (MeO-DBS) and 1,3:2,4-bis-(benzylidene-5,6-biscarbonylamino-ethylmethacrylate)-D-sorbitol (IEM-DBS) to gelate bis-GMA and UDMA.[178, 263] They verified that regardless of the type of DBS derivative, the use of 2 wt% of organogelator contributed to increase vinyl conversion. Furthermore, it was observed that in the presence of IEM-DBS (2 wt%) the samples revealed a compact structure, most likely due to the additional methacrylic groups that contribute to a better compatibility with the polymer matrix. Wilder and co-workers also designed a dental composite consisting DBS, photopolymerisable ethoxylated bisphenol A (EBPADMA) and zirconium-modified amorphous calcium phosphate (Zr-ACP) suitable for assisting the remineralisation of teeth.[261] Besides, increasing the monomer conversion rate (by increasing viscosity, limiting radical

termination and enhancing free radical propagation), introduction of DBS into the dental composite, also enhanced the strength and reduced shrinkage of the nanocomposite. However, the incorporation of DBS retarded the leaching of calcium and phosphate ions from the Zr-ACP.[262]

2.5.4 Gel Electrolytes for Future Battery Technology

Many of the examples of applications described above are established technologies, used in the real world. However, there are a number of developing potential applications of DBS derivatives which are of great interest. Amongst these, the development of gel electrolytes has been of great interest in the past decades due to the inherent drawbacks with the use of liquid and solid electrolytes in energy storage technology – an area of vital technological importance in a world increasingly filled with mobile devices and energy storage problems. Liquid electrolytes use volatile organic solvents which may lead to leakage and volatilization problems, while solid electrolytes present much lower conductivity when compared to their liquid counterparts. Gels offer a potential solution to this dichotomy.

In this regard, recently Raghavan and co-workers have demonstrated the combination of a DBS derivative; 1,3;2,4-bis(4,4'-dimethylbenzylidene)sorbitol (MDBS) with a nanoparticulate material, fumed silica (FS), suspended in propylene carbonate (PC) containing lithium perchlorate salt ($LiClO_4$) as a source of lithium ions for lithium-ion batteries.[264] FS did not form a gel in the mentioned solvent, but helped rigidify the resulting organogel via non-covalent cross-linking between the silanol (Si-OH) groups of FS and the free hydroxyl groups of MDBS. This produced a robust 'solid-like' electrolyte with high 'liquid-like' ionic conductivity, and an electrochemical stability window and good interfacial stability against Li (Figure 2.5.3). This clearly demonstrates how the solid-like/liquid-like properties of gel phase materials can be harnessed within this application.

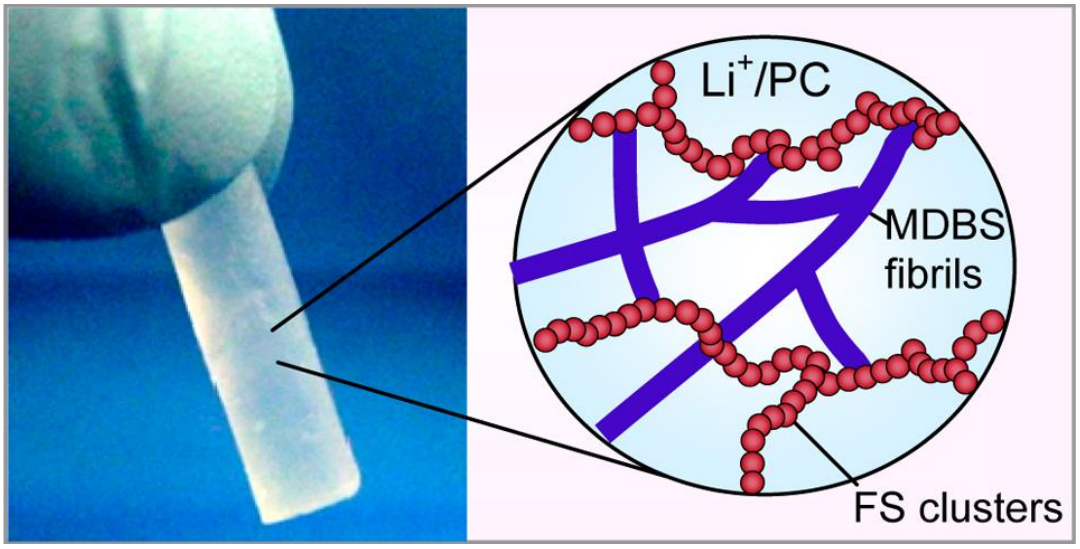

Figure 2.5.3 Schematic depicting the synergistic interaction between FS in Li^+/PC electrolyte and MDBS and the resulting free-standing gel. [Reproduced from ref. 264].

Very recently, gel electrolytes comprising various concentrations of DBS in poly (ethylene glycol) (PEG) containing iodide/iodine (I^-/I^{3-}) redox couples have been devised by Lai and Chen.[265] The molecular weight and the end groups of the PEG influenced the ionic mobility and hence the conductivity of the hybrid organogels. A low molecular weight PEG with terminal methyl groups exhibited the highest conductivity, energy conversion and stability because it does not undergo intermolecular interactions with other components in the gel. It was further demonstrated that the addition of DBS to PEG increased the thermal stability of the gel and led to better dissolution of the electrolyte ions, therefore making it possible to obtain similar high conductivity for these electrolyte gels as for liquid electrolytes.

The ability of DBS to immobilise organic solvents can also be applied to electrolyte systems used in dye-sensitized solar cells. Mohmeyer et al demonstrated that less polar gelators than DBS, such as methyl-substituted DBS (MDBS) and dimethyl-substituted DBS (DMDBS), were optimal to solidify the polar organic solvents, like 3-methoxypropionitrile, frequently used in dye sensitized solar cells.[266] In addition, DMDBS proved to have a higher T_{gel} value and viscoelastic behaviour than MDBS, making it an appropriate gelator for these electrolyte systems. The quasi-solid-state dye sensitized solar cells yielded identical overall solar energy conversion efficiency using DMDBS gel electrolyte as the cell which used liquid electrolyte, combined with

excellent thermal stability. With these novel designs in hand, the application of DBS organogel-based electrolytes in a more biologically related area such as enzymatic electrochemical processes is being explored.[267] For instance, the development and characterization of an amperometric detector based on gelled 2-nitrophenyl octyl ether (NPOE) with DBS has been reported[268] and the obtained electrochemical response was in the range of a typical enzymatic electrode.

It is clear that this field offers significant potential for high-tech application of DBS gels. It seems likely that as the area develops, there will be an increasing focus on introducing activity into these electrodes via DBS modification, rather than simply using the gel matrix for immobilisation of the overall electrode.

2.5.5 Liquid-Crystal Gels

The use of low molecular weight gelators to immobilize liquid crystals and the associated properties has attracted significant scientific attention in the past decades.[222, 269, 270] The presence of a nanoscale gel network is able to impact on liquid crystal properties such as switching times and voltages, and the liquid crystal organisation is also able to impact upon the nanoscale morphology of the gel.

In 2000, Jansen and co-workers demonstrated that DBS could be used to gel liquid crystals in order to obtain a thermo-reversible and electro-responsive hybrid soft material having electro-optical characteristics appropriate for use in projection systems.[205, 271] The development of a white light-scattering film constituted by a commercial liquid crystal, LC-E7 and DBS, caused the orientation of the liquid crystal molecules in the direction of the electric field when an alternating current electric field was applied, leading to the alignment of the molecules and consequently the transmission of light (Scheme 2.5.2). [272] The gel plays a key role in controlling the phase diagram of these materials to provide the desired electro-optical properties. On the contrary, Kato and co-workers expressed a preference for gelators which possess a mesogen within their network, unfortunately, DBS was not their preferred embodiment for the invention.[64, 273]

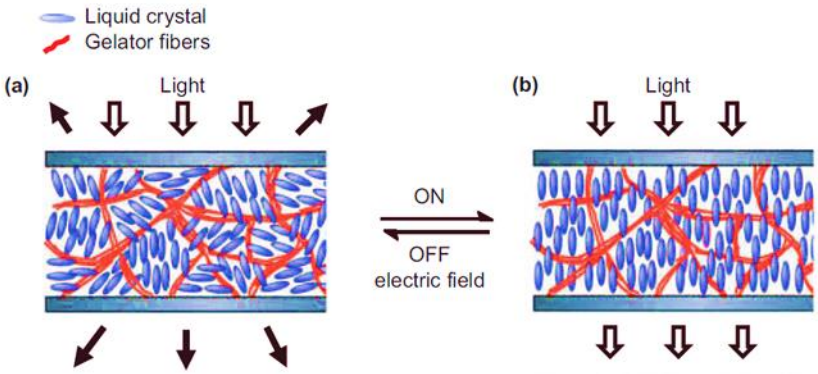

Scheme 2.5.2 Schematic representation of the orientation of liquid crystal molecules in the presence of DBS nanofibrils, when an electric field is applied. (Adapted from Ref.[222])

In an interesting patent, DBS gel was used to enhance the performance of liquid crystal displays (LCDs) when deposited onto an optical olefin film in the presence of rough strippable layers.[274] The strippable layers, mostly polymers, are attached to the optical film in order to protect the surfaces against damage during storage, handling and transport and later removal by users. DBS was incorporated as a nucleation agent and also to adjust the rate of crystallization of the strippable layer. However, the DBS also initiated a rough surface at the interface between the strippable layer and the optical film, thereby providing the desired adhesion.

It has been demonstrated that when confined on the microscale, the nanoscale network morphology of DBS derivatives can be modified, simply by the dimensions of the confining space.[275] It is to be expected that this observation will be of importance in applications where such gel-phase materials are applied in optical or electronic device technology.

The compatibility of DBS with a variety of different solvents and other media suggests it has significant potential for further development in optical applications. This assumption can be based on the fact that DBS gels are transparent and can form nanoscale, non-light-scattering network as well as the rheology and dynamics of the gel network in term of switchability and responsiveness of the optical materials.

It seems likely that in the future, DBS, and modified versions of it have a lot to offer in terms of introducing activity into gel electrolytes in order to achieve simple

advances such as higher efficiency and capacity as well as innovative and new multi-functional energy storage devices. In particular, the ability of gels to bridge between hard and soft materials, for example being compatible with both biological tissue[276, 277] and electrode surfaces[65] means there is significant potential for being able to use these types of materials in a biological setting at the rapidly developing and all-important interface between electronic and biological systems.

2.5.6 Environmental remediation

The use of DBS and its derivatives for selective gelation of oil from an aqueous admixture, as a model oil spill remediation technology has been known since 1985 according to a patent.[278] It is interesting to note that the use of gels in this way has been an area of some activity amongst academic scientists working on gels of late, including some high profile publications (as discussed in Chapter 1 of this thesis).[76, 82, 103] In the original patent, the ability of DBS and its derivatives to solidify some organic liquids was exploited to entrap an oily layer in the presence of seawater. For instance, when a mixture of hydrophilic solvents such as *N*-methyl-2-pyrrolidone (NMP) and hydrophobic solvents such as liquid palm oil containing 5 % DBS and polyoxyethylene lauryl alcohol ether (1 %) was sprayed over a layer of kerosene on the surface of seawater for about 10 min. Interestingly, DBS rapidly and selectively gelled the oil layer within 10 minutes, leading to the recovery of 100 % of the kerosene with only 1 % water content. It should be noted that NMP has since been reported to cause cancer, although it does rapidly biodegrade and has low toxicity to aquatic life.[279] Other additives may be preferable. The use of 6wt% 1,3:2,4-di(p-methylbenzylidene)-D-sorbitol in another composition contributes to 95% of recovery of gasoline in seawater with only 0.3% of water content. The gelled oil was scooped with a net having 2 mm x 2 mm mesh opening and easily recovered by either dilution or distillation. These results, together with the high hardness of the gels make this approach a potentially powerful and simple technology for reclaiming spilled oil from water.

Even though, DBS has been known for over 100 years and its derivatives have demonstrated their prowess in various high-tech applications as discussed above, none of its derivatives till date has demonstrated highly effective and versatile gelation in

water. Therefore, in this Chapter of the thesis, the syntheses and gelation properties of new derivatives of DBS, including novel pioneer hydrogelators will be discussed.

This general overview about DBS and its derivatives has recently been published elsewhere by our group.

2.6 *Results and Discussion*

2.6.1 Synthesis of DBS and its derivatives

Dibenzylidene-D-sorbitol and its derivatives were synthesized by modifying a method reported elsewhere.[174] This method involves condensation / dehydration reaction between an appropriate benzaldehyde derivatives (2 moles) and D-sorbitol (1 mole) in the presence of an organic acid catalyst; *p*-toluenesulfonic acid (as shown in Scheme 2.6.1). The reactions were carried out in a mixture of large volume of cyclohexane and a little volume of absolute methanol at 70 °C. The hydrophobic solvent (cyclohexane) is necessary not only to precipitate the product but also to form a solvent azeotrope with the condensed water and the hydrophilic solvent (methanol).

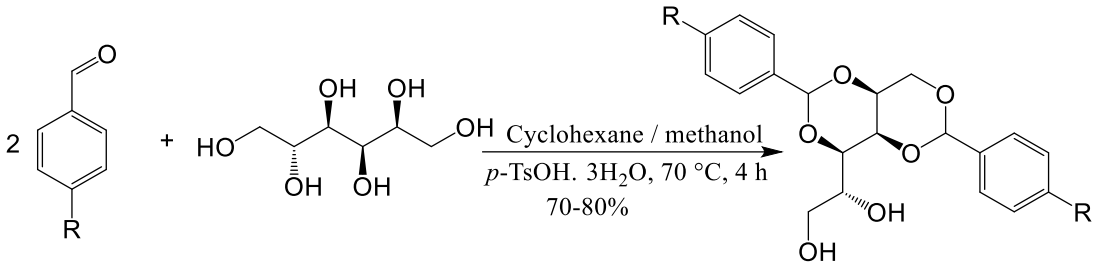

Scheme 2.6.1 Synthetic scheme for DBS and its derivatives

In all of the condensation / dehydration reactions, MBS and TBS were also formed, however, in a smaller yield. By taking advantage of the increased hydrophilicity of MBS and the hydrophobicity of TBS, the crude products were purified by washing with warm water (50 °C) and dichloromethane (DCM) to selectively remove MBS and TBS respectively. Similarly, the unreacted starting materials and the catalyst were removed from the crude products by washing with cold ethanol. The various DBS derivatives (**DBS, DBS-F, DBS-Br, DBS-SCH_3, DBS-NO_2**, and **DBS-$COOCH_3$**) synthesised were obtained in excellent yields (70-80 %). The products were characterised by NMR spectroscopy where resonances for the formed aromatic rings

were observed between 7.2 – 7.5 ppm in DMSO-d^6 for **DBS**, **DBS-F**, **DBS-Br** and **DBS-SCH$_3$** except for **DBS-COOCH$_3$** which appeared between 7.5 – 7.8 ppm in the same solvent. Another diagnostic signal corresponding to the benzylic proton appeared as a singlet at 5.7 ± 0.1 ppm. Additional peak corresponding to CH_3 in **DBS-SCH$_3$** and **DBS-COOCH$_3$** appeared as singlet at 2.5 and 3.8 ppm, respectively.

Interestingly, in this modified version of the method of Feng *et al*,[174] surfactants were not used to extract the target products neither were the final product neutralised with a base. It is important to mention that neutralization of the acid catalyst with NaOH always leaves alkaline impurities in the product, thereby limiting its gelation potential.[170]

The advantages of this method outweighed those of the conventional patented methods. The synthetic benefits included: shorter reaction time (less than 4 hours), high product yield (>70%) and low yields of by-products. It is also a relatively sustainable technique as the solvent can in principle easily be separated and re-used.

In order to further explore the synthesis of DBS-based hydrogelators, some of the derivatives above were further derivatised as discussed in the following subsection.

2.6.2 Synthesis of DBS acid (DBS-COOH)

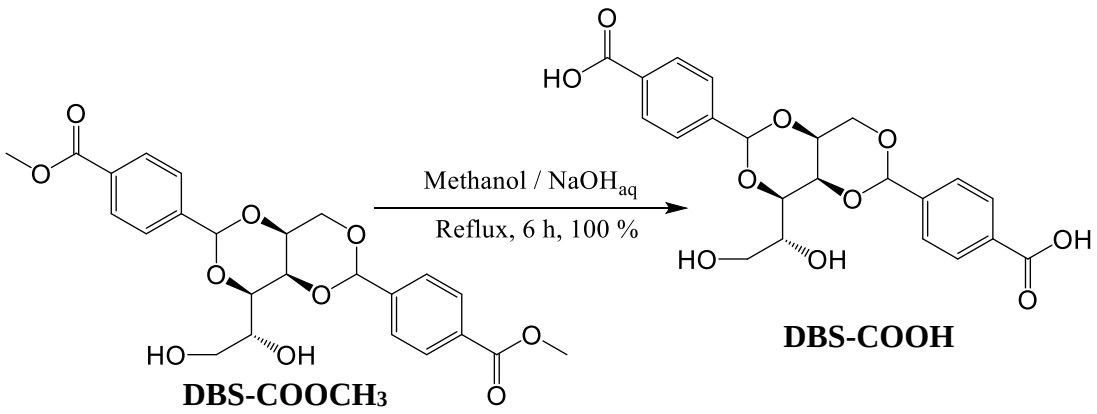

Scheme 2.6.2 Synthetic scheme for the synthesis of **DBS-COOH**

The methylester derivative of DBS (**DBS-COOCH$_3$**) was hydrolysed to obtain dicarboxylic acid DBS compound (**DBS-COOH**; as shown in Scheme 2.6.2). It is a standard method to transform methyl esters to carboxylic acids using a basic catalyst

at room temperature.[280] However, **DBS-COOCH$_3$** was not soluble in a methanolic solution of sodium hydroxide (NaOH) at room temperature. Therefore, a high temperature approach was employed. In this case, **DBS-COOCH$_3$** was dissolved in a 1:1 mixture of methanol and NaOH (1.0 M). The reaction mixture was refluxed for 6 h. The mixture turned colourless (from a white precipitate) due to dissolution of the ester as the reaction progressed. The formation of a colourless solution on cooling the reaction mixture could be attributed to the formation of sodium carboxylate (Na^{+-}OOC-DBS-COO^-Na^+). The solvents were removed under vacuum and the residue was diluted with deionized water. Acidification of the aqueous solution to pH 3 with 1.3 M $NaHSO_4$, caused the **DBS-COOH** to precipitate out of the solution as a white gelatinous substance. The white precipitate was filtered, washed thoroughly to remove the undesirable salts and the product obtained in quantitative yield. Appearance of a broad signal at 13.0 ppm in the ^{1}H-NMR spectrum of DBS-COOH confirms the transformation of ester group to the carboxylic acid group.

2.6.3 Synthesis of DBS hydrazide (DBS-CONHNH$_2$)

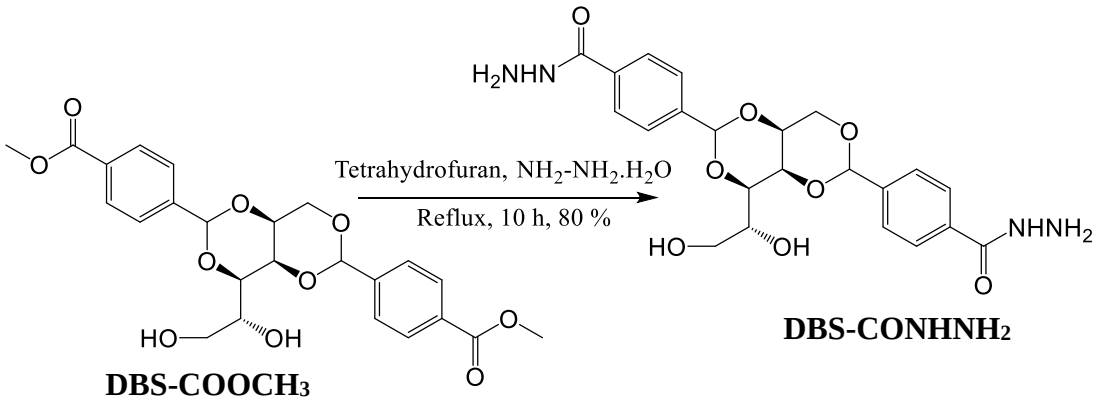

Scheme 2.6.3 Synthetic scheme for DBS hydrazide.

As part of our efforts to increase the hydrophilicity of **DBS**- therefore its hydrogelation ability and also to exploit the dynamics of its chelating potential, **DBS-CONHNH$_2$** was derived from the **DBS-COOCH$_3$** by a hydrazination[281] reaction. The synthetic route for our **DBS-CONHNH$_2$** is shown in Scheme 2.6.3. In this case, a suspension of the **DBS-COOCH$_3$** and excess hydrazine monohydrate were vigorously reacted in THF under reflux (65 ^{O}C) for 10 h. After the reaction, the white precipitate formed was filtered, washed with de-ionized water thoroughly and air-dried to afford the desired compound in high yield (80%). Excess of hydrazine was easily removed with

deionised water after the reaction due to its high polarity and can in principle be reused, however, its low cost would not make its recovery cost effective on a small scale.[282] ^{1}H-NMR spectrum of the product shows the presence of two separate singlet signals at 4.5 and 9.9 ppm in addition to other signals found in the spectrum of the ester analogue. This newly formed signals corresponds to the primary amine and the amide bonds respectively of **DBS-CONHNH$_2$**.

2.6.4 Synthesis of amino-DBS (DBS-NH$_2$)

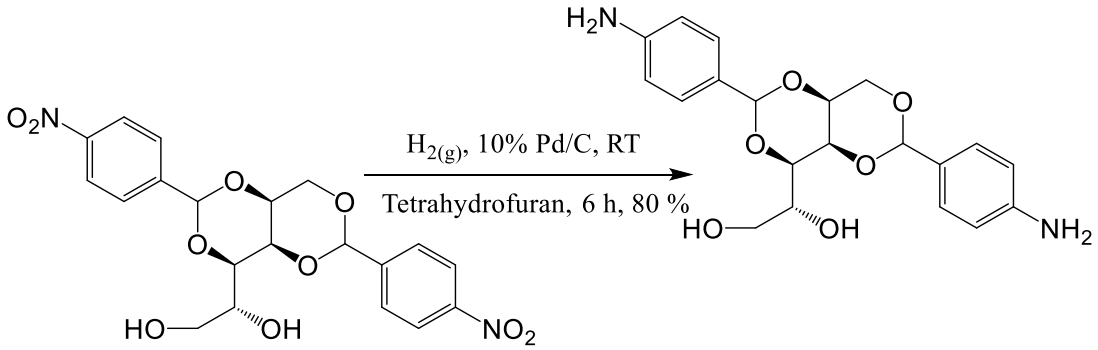

Scheme 2.6.4 Synthetic scheme for amino-DBS

Amino-DBS derivative was synthesized from the **DBS-NO$_2$** using a similar method to that reported by Raluca and co-workers.[283] In this case, the nitro-derivative of **DBS** was dissolved in THF and catalytically reduced with hydrogen gas in the presence of 10% Pd/C. The reaction was allowed to proceed at ambient temperature for 6 h. The yellow precipitate product, **DBS-NH$_2$** was obtained in high yield (90%). A singlet signal at 5.1 ppm which corresponds to the formation of a primary amine bond was observed in the ^{1}H-NMR spectrum of the new product in DMSO-d^{6}.

2.7 *Gelation studies*

2.7.1 Organogelation of DBS and its derivatives

The relative gel forming ability of each of the novel gelators- **DBS-F, DBS-Br, DBS-NO$_2$, DBS-SCH$_3$** and **DBS-COOCH$_3$**, was assessed by dissolving a known quantity of each potential gelator in different solvents contained in transparent sealed vials. The samples were sonicated and heated to form a clear homogenous solution and then allowed to cool to room temperature. In some cases, gels would form. A simple and reproducible tube inversion method was used to ascertain gel formation – i.e., if the

content of the vial did not flow under gravity upon inversion for a period of several minutes, then it was assumed to have formed a gel.[284] Table 2.7.1.1 shows that **DBS, DBS-F, DBS-Br, DBS-SCH$_3$** and **DBS-COOCH$_3$** are efficient organogelators as they only form stable gels in a range of organic solvents and oils but in not water. However, **DBS-NO$_2$** did not exhibit efficient gelation in most solvents investigated but efficiently gelled oils such as silicone oil, sunflower oil and olive oil- it can therefore be referred to as an oleogel and hence may be suitable for food processing applications.[285] It was also interesting to observe that none of the gelators in Table 2.7.1 formed gels in cyclohexane and water because cyclohexane is too apolar to dissolve the gelators and probably because water, even though polar, lacks the threshold solubility requirements to dissolve the gelators. As such, this observations exemplified the significant roles played by solvents in gelation events.[208]

Table 2.7.1 Gelation of **DBS** and its derivatives in various solvents. [gelator]= 10 mM

Solvent/Gelators	DBS	DBS-COOCH$_3$	CH$_3$S-DBS	NO$_2$-DBS	F-DBS	Br-DBS
Water	I	I	I	I	I	I
Ethanol	CG	CG	CG	S	CG	CG
DCM	CG	P	CG	P	CG	CG
Toluene	CG	CG	CG	TG	G	G
THF	CG	S	CG	S	CG	CG
DMF	S	S	S	S	S	S
DMSO	S	S	S	S	S	S
Acetonirile	CG	CG	CG	S	CG	CG
Ethylacetate	CG	P	CG	P	CG	CG
Cyclohexane	I	I	I	I	I	I
Acetone	CG	CG	CG	S	S	S
Silicon oil	CG	P	CG	CG	CG	CG
Xylene	CG	CG	CG	CG	CG	CG
Olive Oil	TG	P	TG	TG	TG	TG
Sunflower oil	TG	P	TG	TG	CG	TG

I= insoluble, CG= clear gel, P= precipitate, TG= translucent gel, S= solution

2.7.2 Hydrogelation of DBS and its derivatives

None of the derivatives of **DBS** in Table 2.7.1 could form stable gels in water but they all formed gels in water-ethanol mixtures down to ≤ 70% water in the solvent mixtures. Surprisingly, the gels formed in the presence of water were more thermally stable than

those formed in pure ethanol as demonstrated by the phase-transition temperature T_{gel} values (as shown in Figure 2.7.1). Although this observation appears to be counterintuitive because they formed solutions in polar solvents like dimethyl formamide (DMF), dimethyl sulfoxide (DMSO), but precipitated in pure water (also a polar solvent). DMF and DMSO are both H-bond acceptors while water is both H-bond acceptor and donor though. The rationale behind this could be adduced to solvophobic effects and the enhanced strength could be attributed to hydrogen bond donor-acceptor interactions between the pendant hydroxyl groups of the gelators and the water molecules. It is important to note that as % H_2O increases the gelators become less soluble – it forms a solid-like network until a threshold (70%) level is attained. As such, some water enhances the hydrophobic effect and gelation, but too much leads to complete insolubility and hence precipitation rather than gelation. This is in-line with the viewpoint that gels are colloidal materials that are likely balanced on a knife-edge between dissolution and crystallisation.[87, 213]

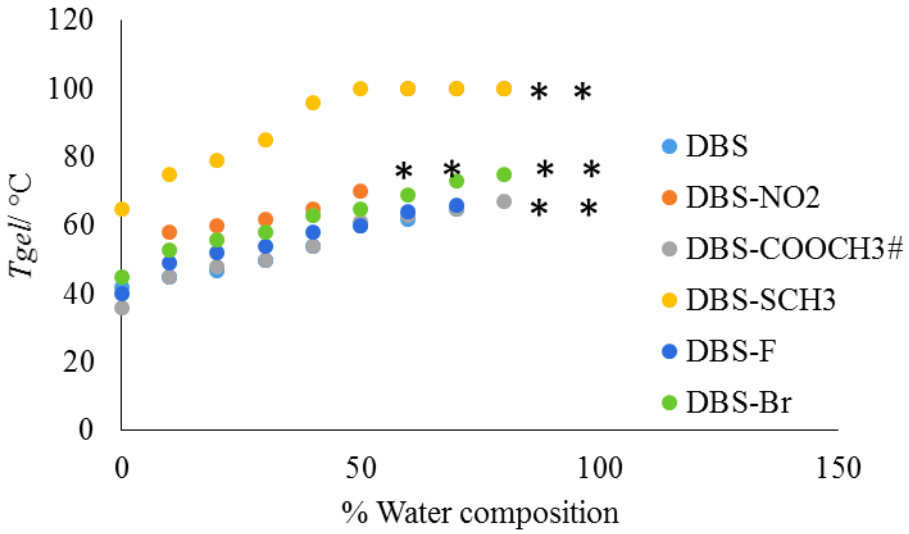

Figure 2.7.1 Effect of water as a co-solvent on the thermal stability of the hydrogels of **DBS** and its derivatives. (* implies no gelation at the %H_2O composition; # implies 6 mM of **DBS-COOCH$_3$** was used while 10 mM was used for others).

Moreover, the aggregation of **DBS** in water / ethanol mixture was further investigated with circular dichroism spectroscopy. As indicated in Figure 2.7.2, the chiral aggregation of **DBS** is controlled by the ratio of the two solvents. For example, gelation

of DBS in 50% water composition gives rise to a much stronger signal (λ_{max} = 222.5 nm) than obtained for ethanol gel (λ_{max} =220 nm), suggesting a more ordered packing structure of **DBS** molecules in the presence of water.[185, 191] This would agree with the view that the presence of water lowers the solubility and drives the assembly of **DBS** into pseudo-crystalline solid-like fibres. It is noteworthy that the signal at λ_{max} = 260 nm is more likely to be a fingerprint of the aromatic ring than the other signal at λ_{max} = 220.5 nm which is more likely to reflect chiral aggregation of the sugar backbone. Therefore, this is in agreement with some literature which suggest hydrogen bonding is dominant in less polar media and aromatic stacking becomes more important as the polarity increases.[182, 185]

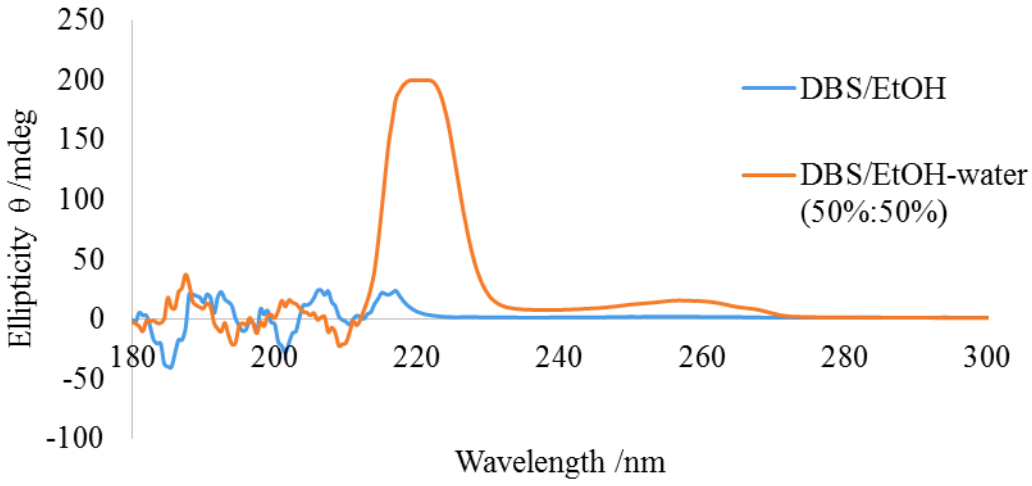

Figure 2.7.2 Circular dichroism spectral for a gel of **DBS** in pure ethanol (blue line) and ethanol-water mixture (50:50).

When searching for derivatives that could gel water, we serendipitously discovered that DBS hydrazide (**DBS-CONHNH$_2$**) and the DBS acid (**DBS-COOH**) could actually gel water without the addition of any organic co-solvent. This is probably because the two hydrophilic functional groups imparted the native **DBS** with the threshold hydrophilicity-hydrophobicity balance required for hydrogelation to occur. It can be suggested that this shifts **DBS** in Hansen space from being in the insoluble region into one of the gel-forming areas. Therefore, the duo can be considered as the pioneer DBS-based hydrogelators. DBS hydrazide formed stable hydrogels across a wide range of pH (2-10) by the simple and traditional heat-cool cycle. On the other

hand, DBS acid formed pH-tunable hydrogels by pH-switching, as fully discussed in Section 2.7.3. Interestingly, the duo congealed water (about 6000 molecule / gelator) at very low concentrations (minimum gelation concentration, MGC = 0.2% wt/vol), hence they can be referred to as ‘‘superhydrogelators’’.[82]

2.7.3 pH-induced hydrogelation of DBS-COOH

The traditional heat-cool method of gel-making was not suitable for DBS dicarboxylic acid (**DBS-COOH**) due to its poor solubility in all of the solvents chosen for this experiment, even at elevated temperature. However, it was found that **DBS-COOH** undergoes deprotonation under basic pH condition to form a homogenous solution in water. In this case, a known quantity of **DBS-COOH** was added to de-ionized water (0.5 mL) and sonicated for 10 minutes. Thereafter, NaOH (20 µl, 0.5 M) was added to deprotonate the gelator and the solution was further sonicated until a clear solution was obtained. In order to induce gelation of the carboxylate, two different acidification protocols were employed. On the one hand, an aqueous HCl solution (30µL, 0.5M) was placed in a separate sample vial and the pre-made **DBS-COOH** basic solution was added to the vial containing the HCl solution as quickly as possible to aid mixing. A gel was formed immediately. However, the gel formed was inhomogeneous due to microgel formation. The spatial inhomogeneity in the hydrogel could be attributed to the imbalance between the kinetics of gelation and kinetics of mixing. It is assumed that the speed of gelation is faster than the speed of mixing, thereby impairing the ability of the gelator molecules to become closely packed. On the other hand, the glucono-δ-lactone (GdL) protocol reported by Adams et al[286,287] was applied to induce the gelation of **DBS-COOH**. In this case, a known quantity of GdL was added to the basic **DBS-COOH** solution and shaken thoroughly until no solid GdL remained undissolved. Thereafter, the solution was allowed to stand while the solution slowly acidified and gelation took place over 4-8 h depending on the ratio of the GdL to the gelator concentration and the volume of 0.5 M NaOH used to basify the **DBS-COOH** solution. In this case, slow acidification is driven by GdL hydrolysis. Glucono-δ-lactone lends itself to this application due to its high water solubility, as well as its ability to undergo slow hydrolysis in water to give gluconic acid (as shown in Scheme 2.7.1). This method has previously been used[288] to induce the hydrogelaton of peptide-based LMWG. As expected, as the concentration of **DBS-COOH** increases, more

volume of 0.5 M NaOH was required to completely dissolve the gelator, therefore, a high concentration of GdL (or HCl) was added to the solution to induce gelation.

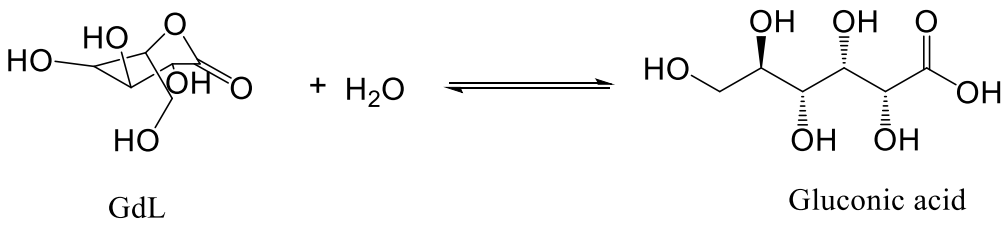

GdL Gluconic acid

Scheme 2.7.1 Hydrolysis of GDL to gluconic acid.

Change in pH values of the aqueous GdL solution at various concentrations of GdL with no **DBS-COOH** was measured (Figure 2.7.3). It is clear that the pH of the aqueous solution of GdL decreases with the increase in the concentration (µmol) of GdL as it is hydrolysed and the final pH of the solution is 4. This inter-conversion is most significant at high pH or when the solution is heated. The rate at which it dissolves and mixes in water is faster than the rate at which it undergoes hydrolysis, which is a reason for the uniform pH change throughout the solution, leading to the formation of uniform/ homogeneous hydrogels.[286]

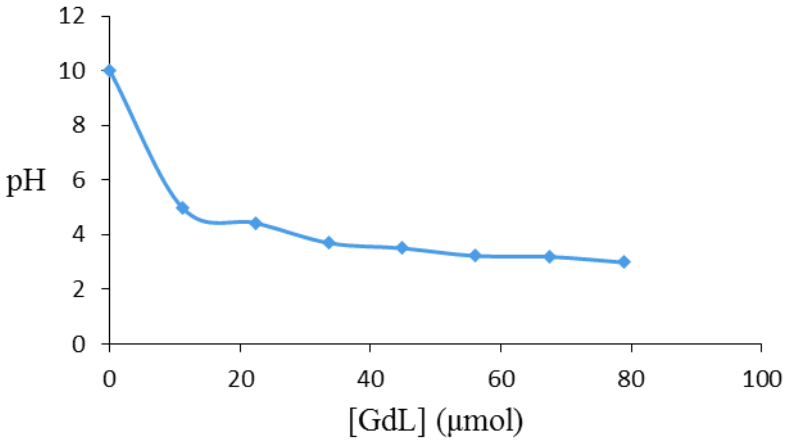

Figure 2.7.3 Variation of pH with the amount of GdL after hydrolysis for 12 h.

As a result of the slow hydrolysis of GdL, the kinetic of gelation, and hence assembly of LMWGs can be monitored. Figure 2.7.4 shows how UV-Vis technique was used to monitor self-assembly of DBS-COOH in the presence of *in situ* hydrolysed GdL over a period of time. The shift in the λ_{max} of DBS-COOH from 280 nm to 296 nm can be

attributed to the involvement of π-π stacking between the aromatic 'wings' of the gelator.

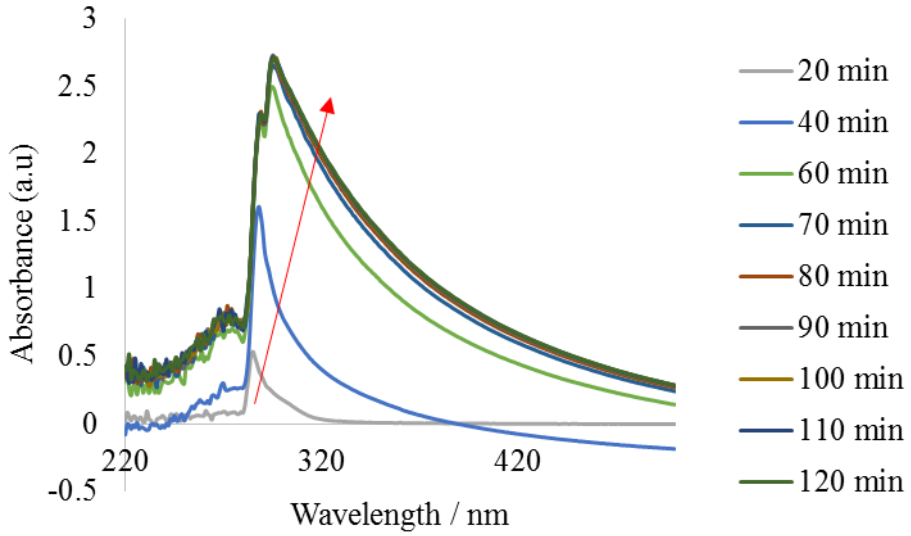

Figure 2.7.4 UV-Vis spectra for time-dependent self-assembly of **DBS-COOH** induced with GdL

Intriguingly, this system therefore offers the potential of making an ideal hydrogel with no spatial inhomogeneity. From an application point of view, this protocol should be important in areas where material properties such as optical clarity, uniform strength and uniform porosity are desirable. However, it should be noted that gluconic acid will be residual within the gel. It may in principle be removed by washing though. For the purpose of our experiment; uniform porosity of the hydrogel network is paramount. Moreover, Hayes and co-workers have also reported that slow kinetics of gel-formation are necessary to obtain stable hydrogels with long shelf-life/service-life.[96]

DBS-COOH formed stable gels at concentrations as low as 0.16% w/v, making it a super-hydrogelator. It is important to mention that 10:1 molar ratio of GdL:**DBS-COOH** is required to form a stable hydrogel.

2.8 *Effects of substituents on the chiral aggregation of DBS gelator*

Circular dichroism (CD) spectroscopy is a versatile tool for investigating chiral aggregation in supramolecular gels.[63, 138] In order to compare the assembly of the different **DBS** gelators, the chiral aggregation of **DBS, DBS-F, DBS-Br, DBS-NO_2, DBS-SCH_3, DBS-$COOCH_3$** in ethanol-water 1:1 mixture and **DBS-COOH** and **DBS-**

CONHNH$_2$ in water was investigated using this technique. In all cases, hot solution of each of the gelator was prepared in ethanol-water 1:1 mixture and was transferred into quartz cell with path length of 1 mm. The gels were allowed to set at room temperature and circular dichroism (CD) was measured between wavelength of 200 and 400 nm. Figure 2.8.1(a-f) shows that changing the substituent appended on the aromatic wings results in a remarkable alteration to the sign of the CD bands which would suggest they can significantly modify the chiral organisation of the fibres.

The gel of **DBS** and **DBS-F** exhibited a strong CD band at wavelength 220 nm and another weak band at 260 nm. This would suggest the aromatic stacking in the gels have CD bands at 260 nm – perhaps because they are less polar and assembled into helical stacks in 50/50 ethanol/water. **DBS-Br** exhibits a strong negative CD band at 245 nm. However, the CD spectra of **DBS-SCH$_3$** and **DBS-COOCH$_3$** gels exhibit bisignate CD spectra having negative CD bands at 223 and 255 nm and positive CD signals at 260 and 285 nm with crossover taking place at 255 and 267 nm respectively. As such, this observation could have been interpreted to mean an inversion of supramolecular aggregate to a direction opposite to that of **DBS-COOCH$_3$** and **DBS-CONHNH$_2$** as this is a common phenomenon with chiral aggregates when influenced by ambient factors such as solvent polarity, temperature and speed of gelation.[289, 290] But that is not the case with **DBS-SCH$_3$** as its bisignate CD signals are not directly opposite to those of the ester counterparts. Therefore, it could mean that **DBS-SCH$_3$** molecularly packed in a completely different orientation. On the other hand, the CD spectrum of **DBS-NO$_2$** hydrogel reveals additional long wavelength absorption at 350 nm which can be attributed to the nitro-group. Nitro-group is a chromophore which has the tendency to exhibit a CD band especially in an asymmetric environment due to n→π* transition.[291]

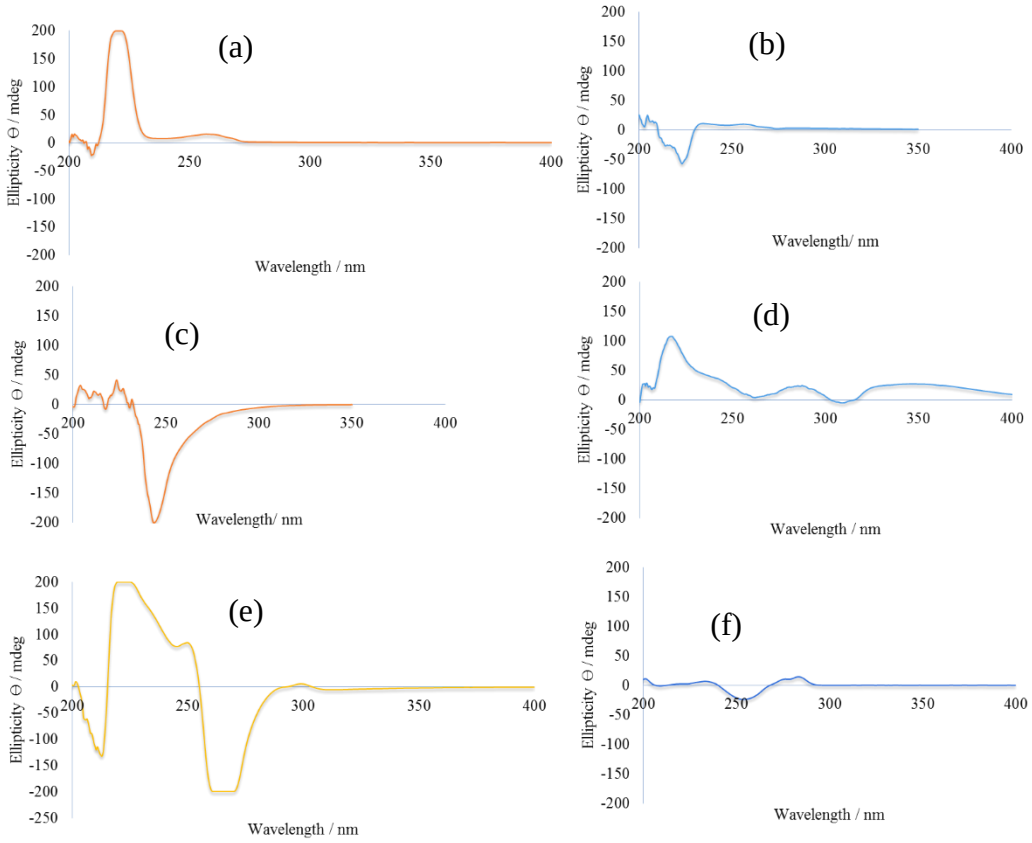

Figure 2.8.1 CD signal for the gel of (a) **DBS**, (b) **DBS-F**, (c) **DBS-Br**, (d) **DBS-NO$_2$**, (e) **DBS-SCH3**, (f) **DBS-COOCH$_3$** in water / ethanol (50: 50); [gelator] = 0.1% wt/vol.

In order to investigate effect of hydrazide functionality on the aggregation pattern of **DBS-CONHNH$_2$** and carboxylic acid group on **DBS-COOH,** hydrogel of **DBS-CONHNH$_2$** was prepared as described above but there was no addition of ethanol. But in the case of **DBS-COOH**, a cold hydrosol consisting of a homogenous aqueous solution of **DBS-COONa** and GdL was transferred into quartz cell. In both cases, transparent hydrogels were formed at room temperature over a period of 6 h and CD was measured between 190 and 350 nm. It is noteworthy that a gelator concentration of 0.2% wt/vol was used in both cases. As such, partial but transparent hydrogels were obtained. Figure 2.8.2a shows that **DBS-CONHNH$_2$** exhibits a bisignate CD spectrum having a negative CD band at 248 nm and positive CD band at 275 nm with crossover taking place at 250 nm. In addition to the first positive CD band, **DBS-CONHNH$_2$** exhibited a second positive Cotton band at 202 nm with crossover at 235 nm. This could be attributed to the assembly of the sugar backbone. The bisignate CD bands indicate strong exciton coupling between chromophores. It is also important to note

that the negative CD band at 248 nm and the positive CD bands at 275 nm imply a left-handed screw-sense of the electronic transition of the π-π interactions between the neighbouring chromophores. As such, this is an indication of helical organization of the aromatic chromophores.[290, 292] **DBS-COOH** exhibited a weak positive CD band at 280 nm and an intense negative CD band at 260 nm with cross-over at 270 nm (Figure 2.8.2b. The broad CD band at 228 nm corresponds to gluconic acid which results from hydrolysis of GdL.[293] It is important to note that the observed differences between the CD spectra of **DBS-CONHNH$_2$** and **DBS-COOH** hydrogels further suggest that the substituent on the hydrogels (like in the 50:50 EtOH:H_2O gels) can control chiral organisation.

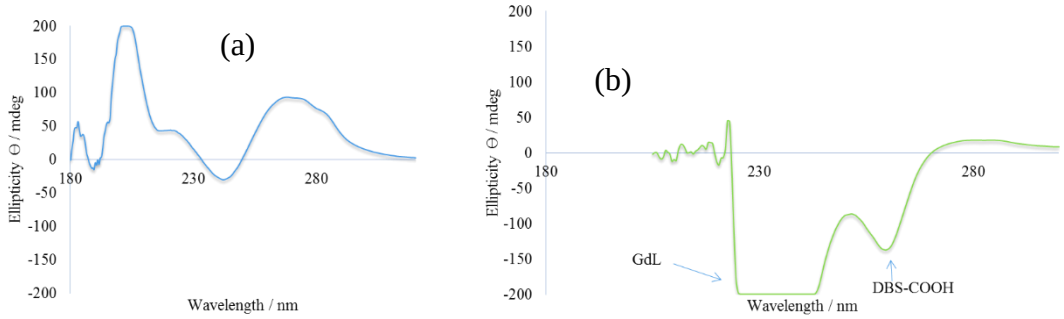

Figure 2.8.2 CD signal for the gel of (a) **DBS-CONHNH$_2$**, (b) **DBS-COOH**

Interestingly, scanning electron microscope images (Figure 2.8.3 (a-f)) further shows that various functionalities produce self-assembled nanofibres networks with different morphology. The hydrogel of **DBS** in 50:50 EtOH:H_2O is made up of very thin nanofibres having diameter of ca. 5 nm and some bundles of fibres having diameters of 8 – 10 nm. On the other hand, gel **DBS-NO$_2$** yielded parallel β-sheet nanotubes having diameters between 25-30 nm and several micron long. As such, the geometry of **DBS-NO$_2$** gel fibres is similar to those of nitrochalcones organogelators previously reported by Mesini and co-workers and it was confirmed by the authors that the alignment of the fibres in this way is due to the participation of the voluminous nitro group in the assembly process.[294] **DBS-F**, **DBS-Br** and **DBS-SCH$_3$** yielded tightly packed nanofibres having diameters between 8 - 10 nm. However, nanofibres of **DBS-COOCH$_3$** are similar to those of the unmodified **DBS** probably because they have similar solubility profile.

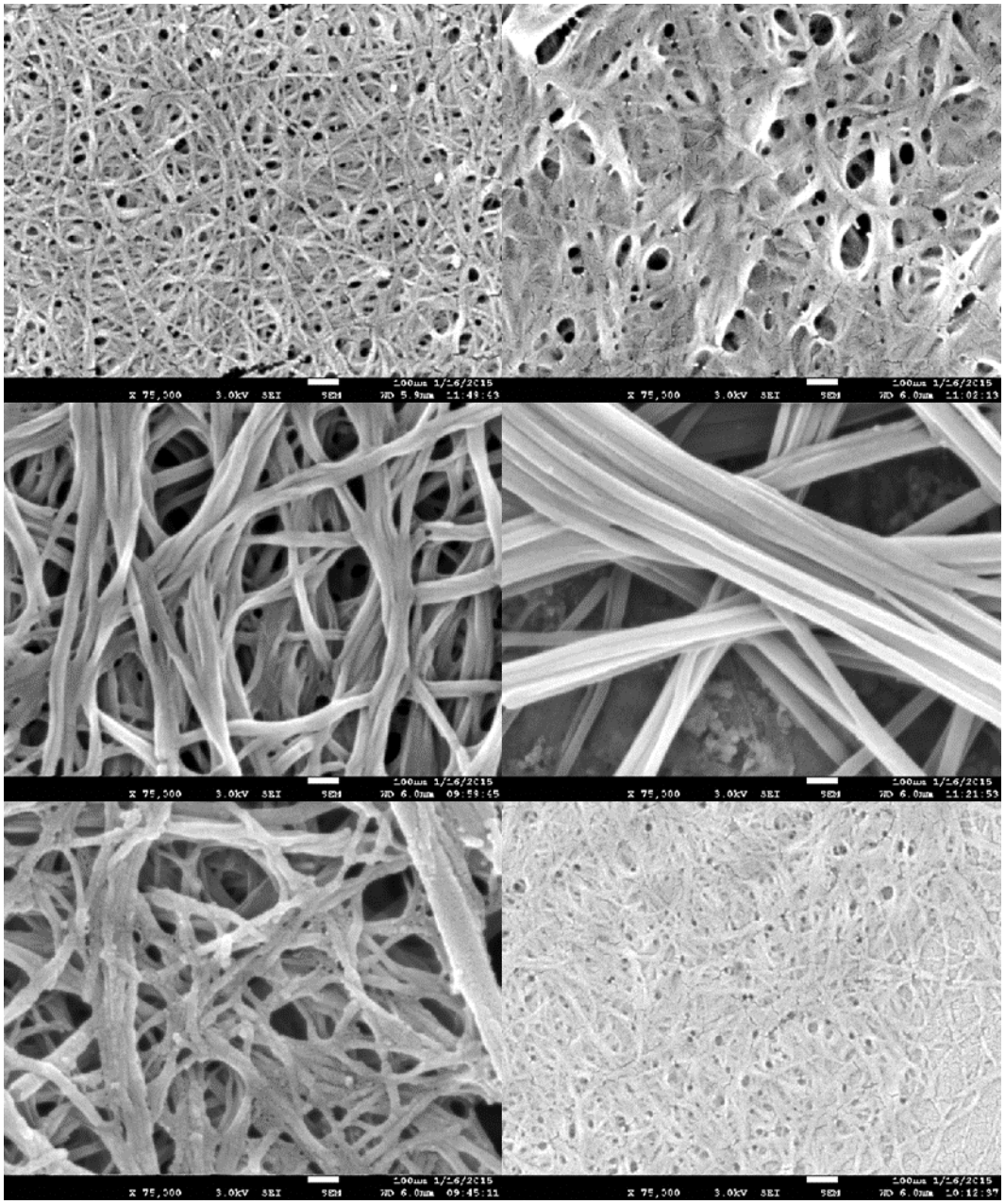

Figure 2.8.3 SEM image of the dried xerogel of (a) **DBS** (b) **DBS-F** (c) **DBS-Br** (d) **DBS-NO_2** (e) **DBS-SCH_3** (f) **DBS-$COOCH_3$** from 50:50 EtOH:H_2O. [gelator]= 0.4% wt/vol; Scale bar: 100 nm.

Similarly, both **DBS-$CONHNH_2$** and **DBS-COOH** hydrogels give twisted nanofibres of well-defined structures and width (Figure 2.8.4a and b). Figure 2.8.4a shows that the nanofibres of **DBS-$CONHNH_2$** hydrogel are thin (ca. 10 nm) and monodispersed which could suggests good compatibility with water and as such, may be ideal for a broad of applications. On the other hand, **DBS-COOH** hydrogel comprises of ribbon-like nanofibres having diameter and pitch of about 15 and 5 nm respectively.

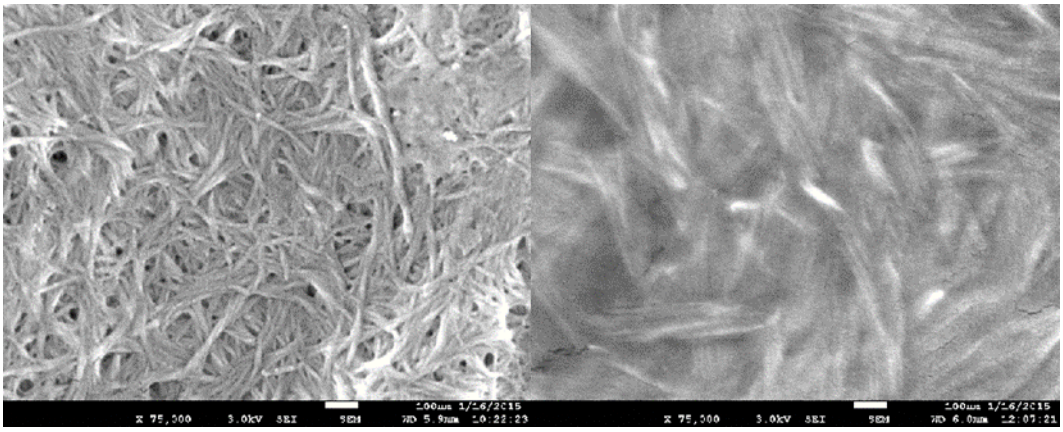

Figure 2.8.4 SEM image of the dried xerogel of (a) **DBS-CONHNH2** (b**) DBS-COOH** 100% H2O. [gelator]= 0.4% wt/vol; Scale bar: 100 nm.

Change in supramolecular chirality and aggregation mode of LMWGs gels networks due to variation in appended substituents groups to an aromatic ring has been reported by Liu and co-worker.[290] In this case, two pyrene-functionalized gelators were designed such that the pyrene group was linked to L-glutamide directly (**PyC0**) and with three methylene spacers (**PyC3**) respectively. Organogels of the two molecules exhibited different fluorescence, aggregation modes, supramolecular chirality, and responsiveness of chirality to polar and non-polar solvents as measured by SEM and CD spectroscopy (Figure 2.8.5). It was suggested in the article that H-bond between amide groups and π-π stacking between the pyrene moieties underpinned the gel formation while the spacer between the amide and the pyrene ring regulated the two interactions and as such, influenced the assembly mode as well as the resulting supramolecular chirality.

On these premises, it can be concluded that substituent groups on modified **DBS** gelators regulate the solubility, aggregation mode and supramolecular chirality of the **DBS** backbone.

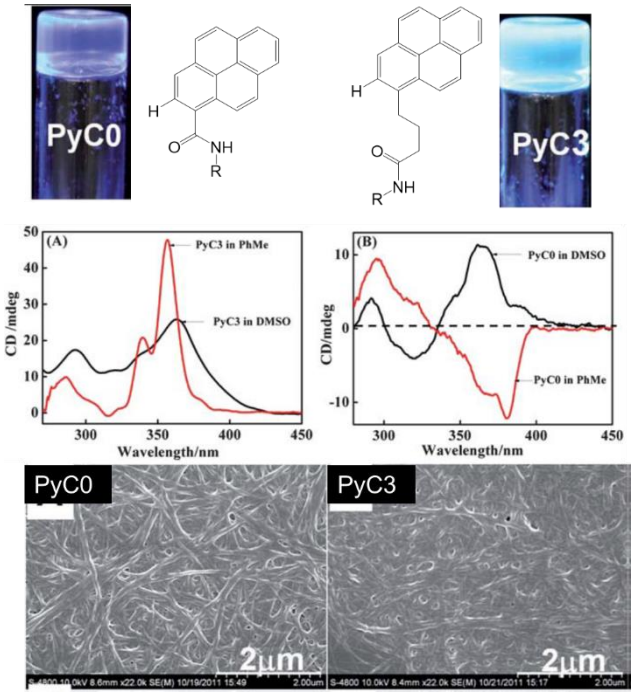

Figure 2.8.5 Chemical structures of pyrene-functionalized gelators **PyC0** and **PyC3**, photos of their fluorescent organogels, CD spectral and SEM images of their organogels in toluene. [Reproduced from ref. 290]

2.9 *Kinetics of hydrogelation of DBS-COOH and DBS-CONHNH$_2$*

The kinetics of fibre growth by **DBS-COOH** and **DBS-CONHNH$_2$** was investigated as they are transformed from a solution phase to a gel phase. Circular dichroism (CD) was used to follow the kinetics of the growth of the self-assembled fibrillar network (SAFINs) resulting from hydrogels (as shown in Figure 2.9.1). The gelator hydrosols were transferred with pipette into the CD cuvette prior to kinetic studies, and data were collected at 5 and 1 min intervals for **DBS-COOH** and **DBS-CONHNH$_2$** respectively. It is important to mention that **DBS-CONHNH$_2$** has the tendency to undergo instant hydrogelation, therefore, the cuvette was incubated at 100 °C prior to the transfer of its hot hydrosol into the cuvette and the kinetic studies. It was observed that gelators **DBS-COOH** and **DBS-CONHNH$_2$** had CD bands at 259.5 nm and 275 nm respectively and this can be attributed to the formation of β-sheet conformation resulting from the π-π stacking of the aromatic rings of the gelators. It is also worth noting that the molecular scale property (chirality) of the various gelators are transcribed up to the macroscopic scale material as they transform from solution phase to gel phase.[63]

It should also be noted that for **DBS-COOH** there was an incubation period prior to assembly as the pH lowers and before nucleation (which is a random stochastic event) occurs. There was also a short incubation time for **DBS-CONHNH2**, but there was no pH change required in this system and its nucleation was much faster.

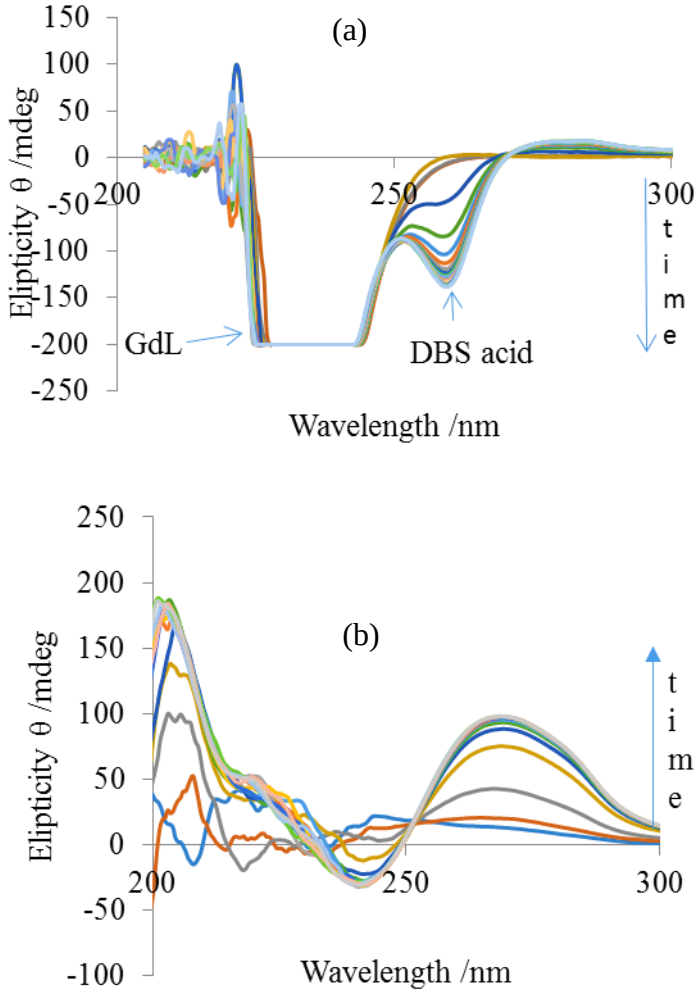

Figure 2.9.1 Time-dependent kinetic studies of the growth of (a) **DBS-COOH** (b) **DBS-CONHNH2** into 3-dimensional fibrillar network using CD spectroscopy. [gelator] = 0.1% wt/vol.

The kinetic data obtained from CD spectroscopy was treated with a statistical model based on Avrami equations. These exponential and logarithmic equations (2.9.1-2.9.3) were originally proposed to describe the crystal growth of polymer melts. This model has been previously applied to other low molecular weight gelators by some authors.[295, 296]

$$1 - X = e^{-kt^n} \qquad (2.9.1)$$

$$\ln(\ln\left(\frac{1}{1-X}\right)) = \ln k + n\ln t \qquad (2.9.2)$$

$$X(t)=(I(t)-I(0))/(I(\infty)-I(0)) \qquad (2.9.3)$$

According to Weiss and co-workers, X is the volume fraction of the gel phase, k is the fibre growth rate constant, n is the Avrami exponent and t is time. The most important parameter, n provides quantitative information about the nucleation mechanism and growth, while the Avrami rate constant, k provides a quantitative check on the course of assembly; it can be used to compare the nucleating abilities of different systems. The value of k depends on nucleation and growth-rate constants. The growth rate is unique for every material and depends on crystallization temperature. It is assumed that the growth rate is not influenced by nucleation.[297] The theoretical values of Avrami exponent, n, range from 1-4 depending on the nature of the crystal growth - the higher the Avrami number the greater the degree of branching.[298] A value of 1 is usually considered to represent pure one-dimensional growth.

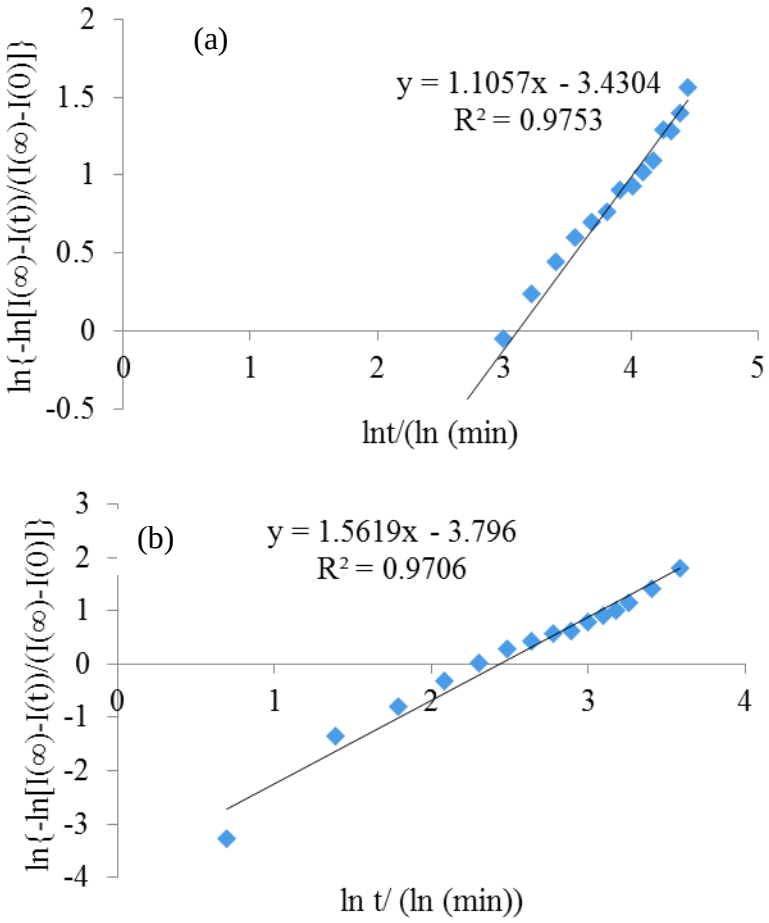

Figure 2.9.2 Kinetics of gelation of (a) **DBS-COOH** and (b) **DBS-CONHNH2** based on Avrami model.

Figure 2.9.2a and b shows that the values of the Avrami exponent *n* as deduced from the slopes of graphs are approximately 1.1 and 1.6 for **DBS-COOH** and **DBS-CONHNH2** respectively. These values imply a one-dimensional and interface-controlled growth pattern or a two-dimensional and diffusion growth pattern. The slightly higher value of n for **DBS-CONHNH2** hydrogel could as well mean that its fibres are more branched than the fibres resulting from the acid analogue. This hypothesis is partly validated by the TEM images of the hydrogels (as shown in Figure 2.9.3).

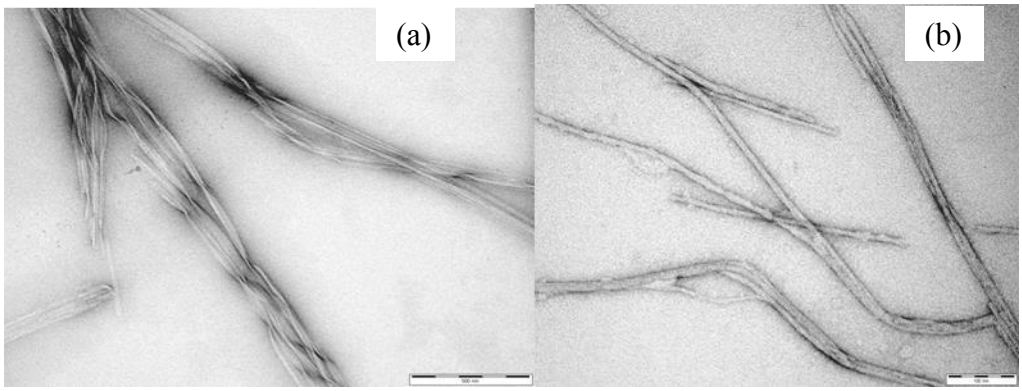

Figure 2.9.3 TEM images of the dried xerogel of (a) **DBS-COOH** and (b) **DBS-CONHNH$_2$**

2.10 *Thermo-reversibility and pH stability of DBS-CONHNH$_2$ hydrogels*

In order to probe the responsiveness of the chiral aggregate of **DBS-CONHNH$_2$** hydrogels to temperature, variable temperature circular dichroism (VT-CD) was carried out on the hydrogel. Interestingly, a decrease in the intensity of band at λ_{max} = 275 nm was observed (Figure 2.10.1. The VT-CD spectrum of the hydrogel showed a slow decrease in intensity from 20 °C to 40 °C but more sharply at elevated temperature presumably due to the breaking of intermolecular bonds. The observed disassembly of chiral aggregate suggests that the band can indeed be assigned to the assembled form of the gelator rather than the inherent chirality of the individual molecule or the presence of artefacts.

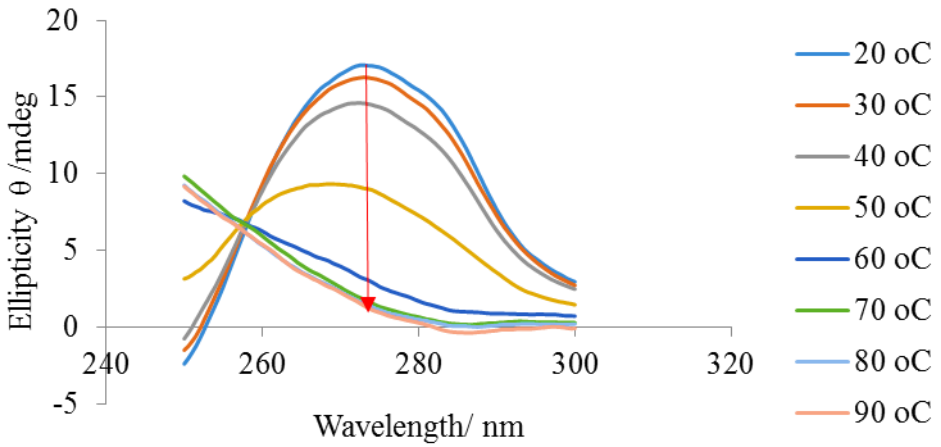

Figure 2.10.1 Spectra of VT-CD of **DBS-CONHNH$_2$** hydrogel; [gelator] = 0.05% wt/vol

In order to probe the effect of pH on the thermal responsiveness of **DBS-CONHNH$_2$** hydrogels, a tube inversion method was used to determine the T_{gel} values across a range of pH values (2-12) – pH values were adjusted with HCl (0.1 M) or NaOH (0.1 M). Figure 2.10.2 shows that **DBS-CONHNH$_2$** formed stable hydrogels across the wide range of pH values investigated and the T_{gel} values (*ca.* 68 °C) are insignificantly affected by pH. As such, this makes **DBS-CONHNH$_2$** hydrazide hydrogelators capable of pH-independent gelation and open up significant potential scope of applications for **DBS-CONHNH$_2$**.

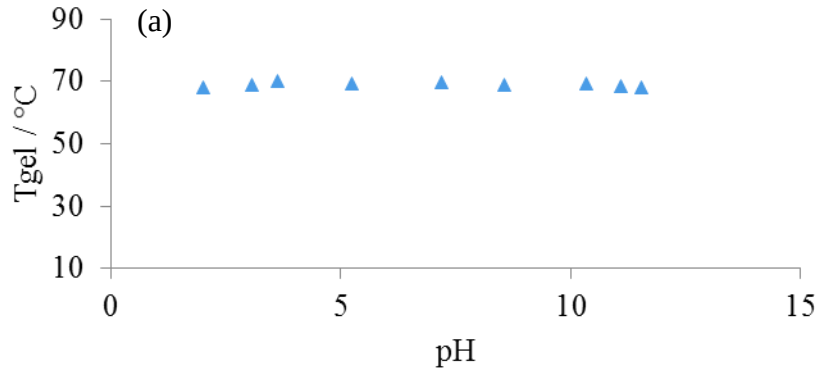

(b)

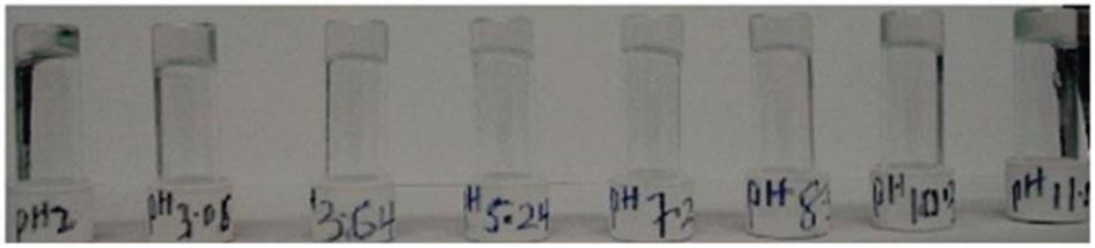

Figure 2.10.2 (a) Effect of pH on T_{gel} values and (b) photo of stable hydrogels of **DBS-CONHNH2** across a range of pH. [gelator] = 6 mM

In sharp contrast to this observation, in 2005 Sreenivasachary and Lehn demonstrated a pH-dependent hydrogelation of guanosine hydrazide (Figure 2.10.3).[299] The authors reported that gaunosine hydrazide only underwent thermally induced hydrogelation in the presence of monocationic species under neutral and slightly acidic pH conditions but not basic pH.

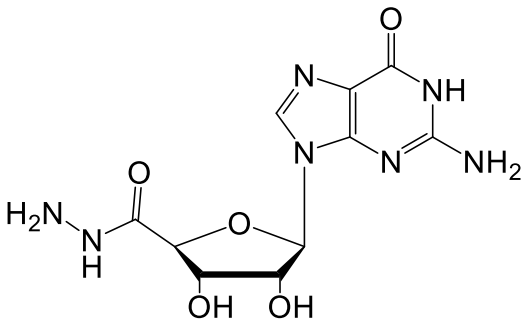

Figure 2.10.3 Chemical structure of guanosine hydrazide

2.11 *Summary and Conclusions*

Dibenzylidene-D-sorbitol is a remarkably versatile low molecular weight gelator which has been known for well-over 100 years and found many applications – it has

remained most patented LWMGs till date with over 100 derivatives. Therefore, it can be considered one of the best examples of supramolecular system, known even before the field or the terminology emerged.

DBS, **DBS-F**, **DBS-Br**, **DBS-SCH$_3$**, **DBS-NO$_2$** and **DBS-COOCH$_3$** were synthesised by an acid-catalysed dehydration - condensation reaction with MB and TBS derivatives as by-products which were easily removed by washing. **DBS-NO$_2$** and **DBS-COOCH$_3$** were further converted to **DBS-NH$_2$**, **DBS-CONHNH$_2$** and **DBS-COOH** via one synthetic step in quantitative yields.

DBS, **DBS-F**, **DBS-Br**, **DBS-SCH$_3$**, **DBS-NO$_2$** and **DBS-COOCH$_3$** demonstrated versatile and efficient self-assembly across a wide range of organic solvent by the interplay of non-covalent interactions predominantly H-bonding and π-π stacking. Although, they could not gel water but the thermal stability of their gels in ethanol – water mixture increases as % H_2O composition increases – because ethanol promoted the solubility in the admixture while water contributed to the H-bonding interaction. However, **DBS-CONHNH$_2$** and **DBS-COOH** formed stable hydrogels in water without adding ethanol as a co-solvent and as such, the two could be considered novel pioneer **DBS**-based hydrogelators – **DBS-CONHNH$_2$** formed gel by heating – cooling cycle while the pH responsive **DBS-COOH** formed hydrogel by acidifying its basic solution with HCl or GdL. As such, it is hopeful that the birth of these new hydrogelators will extend the scope of **DBS** to more a biologically – relevant applications.

Techniques such as SEM and CD spectroscopy show that substituent groups appended on the aromatic 'wings' of **DBS** have significant influence on aggregation mode and supramolecular chirality of the gels.

Having synthesized and characterised these gelators, the hydrogels of **DBS-CONHNH$_2$** and **DBS-COOH** in particular will be probed for some biologically – relevant applications in subsequent Chapters of this thesis

.

3 Chapter 3 – Supramolecular envirogels: Nanosorbents for sequestering dyes from water

Some of the results from this Chapter have been published in *Chem. Commun.*, 2013, 49, 11164-11166 and *Angew. Chem. Int. Ed.*, 2014, 53, 12461-12465.

3.1 Introduction

As described in detail in Chapter 1, dyes are not only useful to textile industries but also industries such as paints, plastics, rubbers, printing ink, leather, drug, food, paper and cosmetics.[300] It has been reported that about 128 tons of dyes are discharged daily into the aquatic environment.[301] Dyes even in low concentrations, present harmful and deleterious effects on the quality of our environment. Basic red 9 **3.1** and congo red **3.2** (Figure 3.1.1) have been rated the most toxic among the various classes of dye.[302, 303]

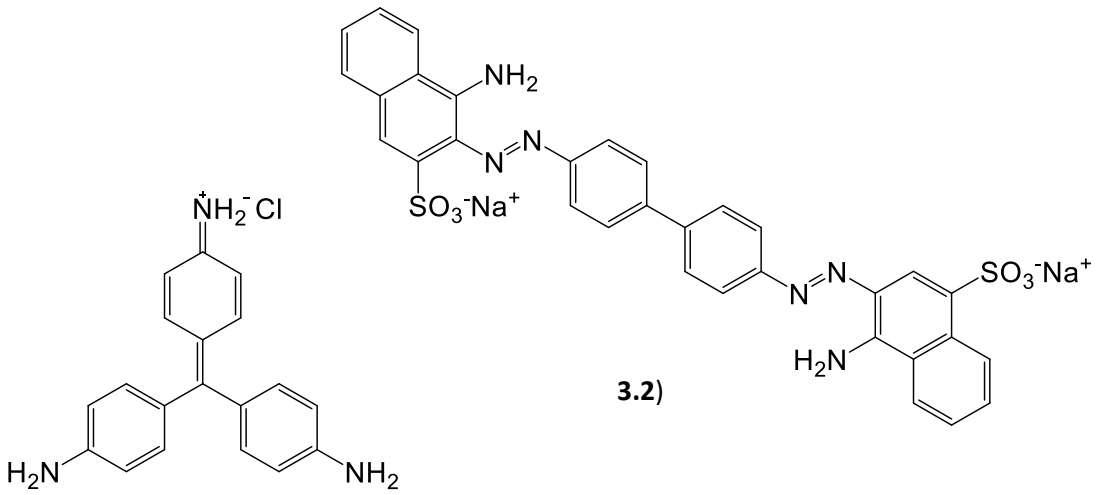

Figure 3.1.1 Chemical structures of basic red 9 **3.1** and congo red **3.2**

When dye is discharged as untreated industrial effluent into rivers, lakes, and oceans, it does not only affect the aquatic life and the food chain[*304*] but also predisposes human beings to certain health related problems such as cancer, abnormal structural genetic alteration, vomiting, cyanosis and liver dysfunction.[305] Several methods such as biological,[306-309] chemical[301, 310] and physical[311, 312] methods have been widely employed to remove dyes from water. Among these methods, adsorption is the best owning to its simplicity, ease of operation and handling, regeneration, near-to

complete removal of pollutants and economic feasibility. Activated carbons have been well exploited in the past centuries as efficient adsorbents for various colouring matters. Also, certain non-conventional adsorbents such as activated clay, alumina and zeolites are currently finding expression in environmental remediation.[51] However, certain limitations such as high cost of disposal of the spent adsorbent, low pollutant uptake and lack of selectivity remain with their application.

In recent years, attention has begun to focus on the use of gels for environmental remediation.[88, 90-96, 134] Gels are particularly good candidates for dye removal because they are solvated, yet highly porous materials with nanoscale fibres. This ensures a high surface area of contact between the solid-like network and the liquid-like phase, potentially offering attractive pollutant extraction. Furthermore, they are amphiphilic, making them suitable for removing dyes as the hydrophilic moiety can interact with water while the hydrophobic core adsorb the dyes or *vice versa*.

It is noteworthy that most currently reported low-molecular-weight envirogelators used for removing dyes from water are strongly pH-dependent, principally because the de/protonation of a carboxylic acid group (pK_a *ca.* 4-5) plays a vital role in their hydrogelation, which only occurs at lower pH values. It is also noteworthy that their syntheses require multiple steps and not easily amenable to scale-up. It therefore becomes imperative to develop hydrogels capable of sequestering dyes from water, having set the following criteria for their design; (i) simple synthetic procedures, (ii) pH-tolerant gels, (iii) well defined nanostructures, (iv) simple self-assembly and (v) selective pollutant uptake.[112]

3.2 Result and discussion

A simple synthetic strategy mapped out for designing a new class of envirogelators was achieved as discussed in Chapter 2 of this thesis. However, the hydrogels of **DBS-COOH** and **DBS-CONHNH$_2$** are the candidates of greatest interest for this purpose due to the fact that they are absolute hydrogelators, i.e., organic co-solvent is not required for their hydrogelation, as this might constitute a secondary pollutant in the water. Unfortunately, **DBS-COOH** being a carboxylic acid based gelator, also exhibits one of the negative features inherent in the previous envirogelators which contain

carboxylic acid functional groups and are, as such, highly pH dependent, only forming effective gels under conditions of controlled acidification, typically with pH ≤ 5. As such, the gels are pH intolerant. Therefore, **DBS-CONHNH$_2$** envirogels were our primary focus for this application due to its pH-tolerance. The pH-tolerant envirogel may be appropriate for dye adsorption across a wide range of pH. Hydrazide functionality is similar to a carboxylic acid analogue in that it has similar degree of hydrophilicity in its neutral state. However, this neutral state has greater pH stability.[313] More so, it should be noted that **DBS-CONHNH$_2$** forms gels at biologically relevant pH values – we therefore suggest that this hydrazide-functionalization approach system may be effective and hence a replacement for carboxylic acids in a wide range of other hydrogelators, to make them more pH-tolerant. Surprisingly, there have been very few reports of hydrogelators incorporating an acylhydrazide functional group.[299, 314, 315]

Further to the comprehensive discussion on **DBS-CONHNH$_2$** in Chapter 2, the method employed by Xu and co-workers[316] was used to investigate the effect of pH on the mechanical properties of **DBS-CONHNH$_2$** hydrogels. In this case, the hydrogels were submerged in aqueous solutions under acidic (pH 4), neutral (pH 7) or basic (pH 12) conditions for over 10 h. Oscillatory strain and frequency sweeps were used to probe the rheological properties of the hydrogels. Interestingly, Figure 3.2.1 shows that the maximum storage (*ca.* 12,000 Pa) and loss moduli (*ca.* 980 Pa) of the **DBS-CONHNH$_2$** hydrogels are effectively identical under the various pH conditions investigated. Figure 3.2.2 shows that the critical shear strain (*ca.* 7.5%) for the hydrogels also remains unaltered regardless of the ambient pH conditions. This provides quantitative confirmation of the hypothesis that **DBS-CONHNH$_2$** hydrogels are pH-tolerant. It is worthwhile mentioning again that pH-tolerant supramolecular hydrogels are very rare.[316]

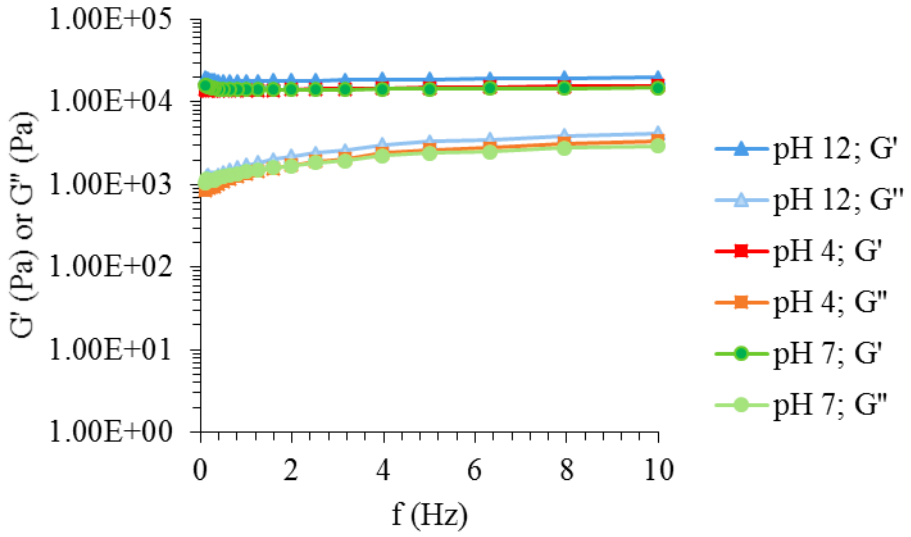

Figure 3.2.1 Dynamic frequency sweeps of the hydrogels of **DBS-CONHNH$_2$** after soaking in (a) acidic (pH 4) (b) neutral (pH 7) and (c) basic (pH 12) aqueous media. [gelator] = 0.4% wt/vol; strain = 0.2%

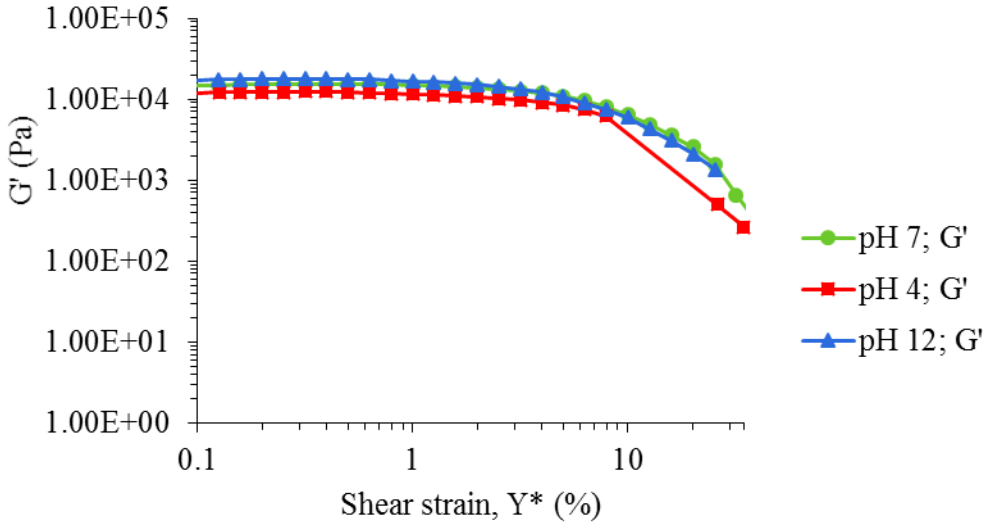

Figure 3.2.2 Dynamic strain sweeps of the hydrogels of **DBS-CONHNH$_2$** after soaking in (a) acidic (pH 4) (b) neutral (pH 7) and (c) basic (pH 12) aqueous media. [gelator] = 0.4% wt/vol; f = 1 Hz

3.2.1 Batch adsorption of dyes onto DBS-based envirogels

The ability of **DBS** based envirogels to sequester dyes of various kinds- methylene blue **MB**, acid blue 25 **AB25** and naphthol blue black **NBB**, **CR** (Figure 3.2.3) and congo red **3.1** (Figure 3.1.1) from water was demonstrated vis-à-vis dye uptake efficiency, kinetics and isotherms. Prior to the adsorption studies, ~ 95 µM stock solution of the dyes were prepared by dissolving a requisite amount (depending on the percentage purity- AB25 45%, CR 54%, NBB 80%, and MB 98%) of the dyes in water. For instance, acid blue (45% dye content), 6.7 mg (3.90 mg dye) was weighted and dissolved in a 100 mL volumetric flask. Standard solutions of the dyes were prepared from the stocks to plot the working curves (Appendix 2).

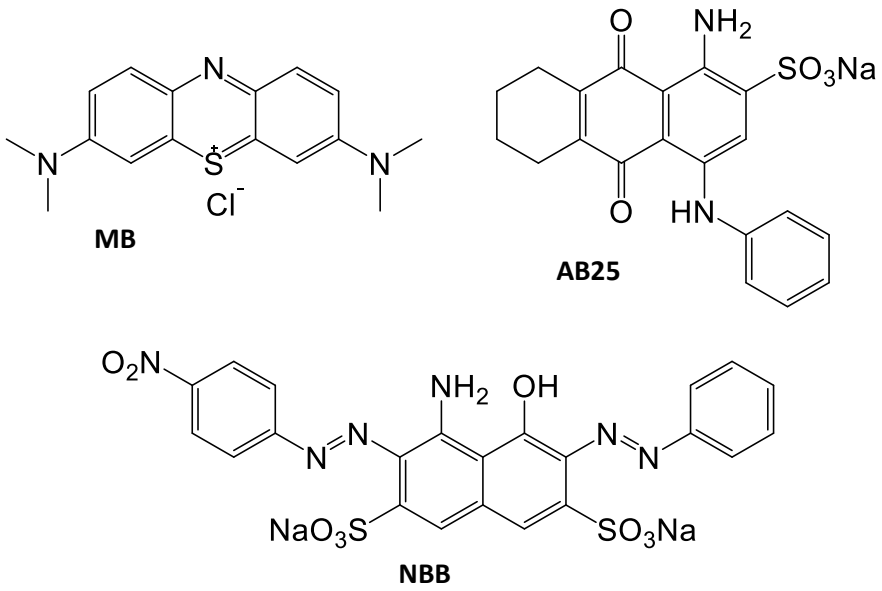

Figure 3.2.3 Chemical structure of methylene blue (**MB**), naphthol blue black (**NBB**) and acid blue 25 (**AB25**)

3.2.2 Probing dye adsorption onto DBS-COOH hydrogel nanofibres

Although **DBS-CONHNH$_2$** gels were thought to be optional, we also initially investigated **DBS-COOH** hydrogels for this application of dye uptake. Hydrogels of **DBS-COOH** were prepared as previously discussed in Chapter 2 of this thesis. A requisite amount (4 mg) of the gelator was dissolved in deionized water (1 mL) and NaOH (50 µL, 0.5 M) was added to deprotonate the gelator and thereby enables its solubility in water. After sonication for about 15 min, GdL (10 mg) was added to acidify alkali solution of the gelator and gelation was allowed to proceed under static

condition at ambient temperature. In order to probe its dye uptake potential, aliquot solutions (8 mL, 28 μM) of **MB** the vials containing the hydrogel. The system was allowed to stand at ambient temperature undisturbed (Figure 3.2.4a). A UV-Vis spectrophotometer was used to measure the absorbance of the dye **MB** remaining in the supernatant aqueous solution above the gel periodically over 24 hours and the concentration extrapolated from the calibration curves. The plot of absorbance against the λ_{max} shown in Figure 3.2.4b reveals a significance decrease in the concentration of the **MB** molecules remaining in the aqueous solution as the solution diffuses into the gel networks and as such demonstrated a maximum loading of 125 mg of **MB** /g of gelator. On the other hand, basic solution of **DBS-COOH** (as prepared above without GdL) was added to aliquot solution of **MB** and HCl (0.5 M, 200 μL) was added to the mixture. Interestingly, instant gelation was observed in the presence of **MB** on addition of HCl. However, as twice the maximum **MB** loading onto a preformed **DBS-COOH** hydrogel was obtained for hydrogel formed in situ – a maximum loading of 300 mg/g. As such, **DBS-COOH** hydrogel like other previously reported carboxylic acid envirogelators demonstrated a strong binding affinity for the cationic dye – **MB**.

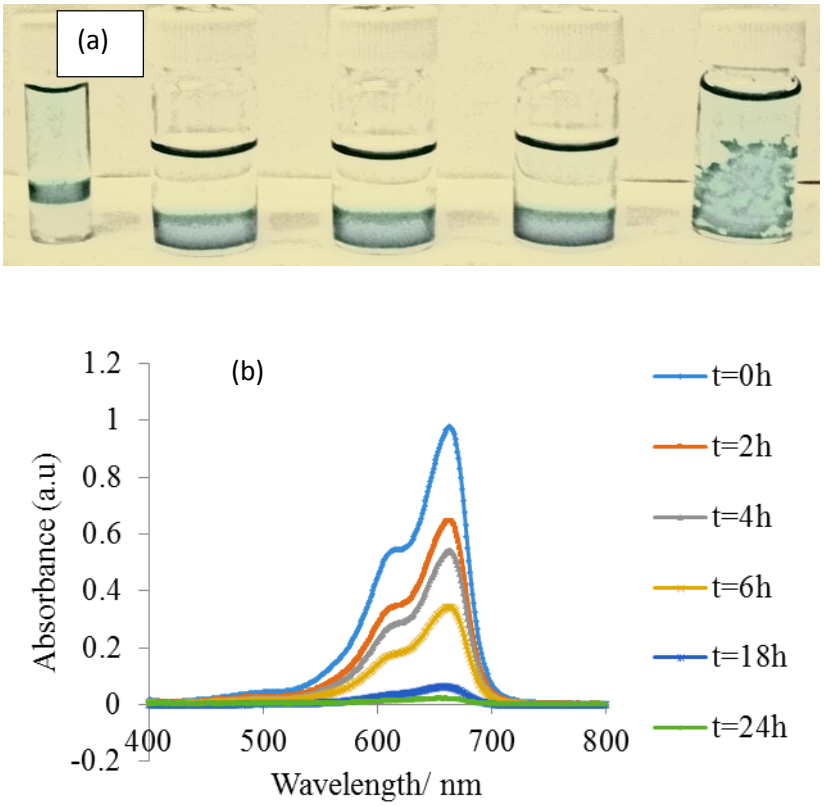

Figure 3.2.4 (a) Photo of **MB** adsorption onto **DBS-COOH** hydrogels (b) UV-Vis spectral for the time-dependent adsorption studies of methylene blue at ambient conditions.

The effect of extraneous substance (GdL), used to prepare **DBS-COOH** hydrogel, on rate of adsorbing **MB** onto **DBS-COOH** hydrogel was investigated. This was done by preparing two samples of **DBS-COOH** hydrogel with a fixed amount (3 mg) of **DBS-COOH** gelator but with 10 mg and 20 mg GdL respectively. While a dye solution containing 20 mg GdL but no hydrogel was used as the control. The time-dependent adsorption studies were carried out over a period of 52 h. Figure 3.2.5 shows that the presence of GdL may slightly have effect on the adsorption of **MB** unto the **DBS-COOH** hydrogel. This may be because the gluconic acid resulting from the hydrolysis of GdL is interacting to some extent with **MB**.

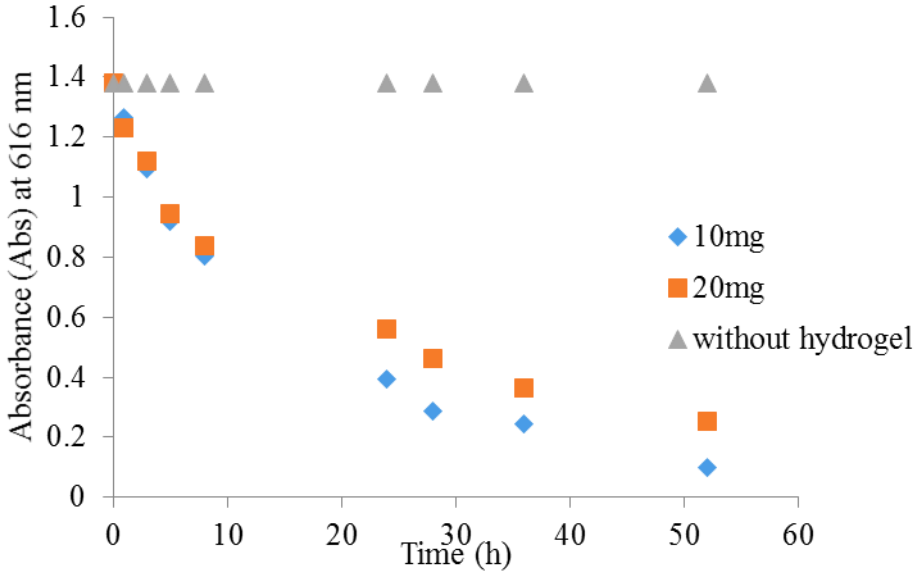

Figure 3.2.5 Effect of GdL on the kinetic of **MB** adsorption onto **DBS-COOH** hydrogel

In order to further investigate the mechanism underpinning its dye adsorption, Acid blue 25 (**AB25**), a molecule having primary amine functionality unlike **MB** which only has tertiary amine groups, was interacted with **DBS-COOH** hydrogel nanofibres for about 24 h. Figure 3.2.6 shows that the hydrogel adsorbed 60% of **AB25** within 24 h under ambient conditions. This suggests the hydrogel could demonstrate a significant uptake of amine based dye molecule. Similar observations have been previously reported by Hayes and co-workers.[96] However, **MB** and 1-pyrenemethyl amine **1-PyA** (Figure 1.4.19) were used in their studies.

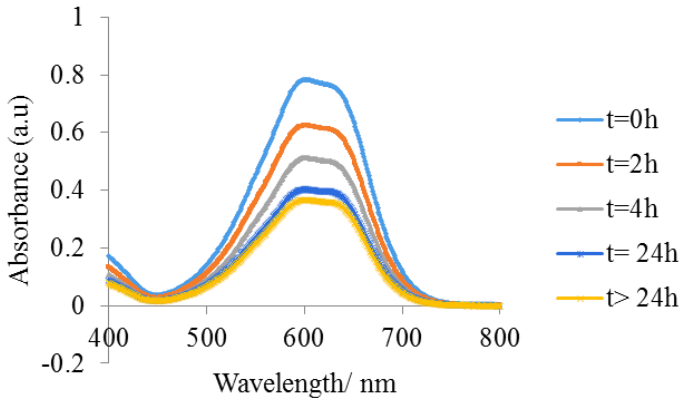

Figure 3.2.6 UV-Vis spectral for the time-dependent adsorption studies of Acid blue 25 (**AB25**) onto **DBS-COOH** hydrogels at ambient pH condition

The mechanism underpinning interactions between **MB** and **DBS-COOH** could be attributed to either intercalation of **MB** into the nanofibres or by an acid base interaction between the amine group of the dye molecule and the carboxylic acid group of the gelator. A comparison of SEM images (Figure 3.2.7) of **DBS-COOH** hydrogels with and without **MB** showed no significant difference in fibre structure, suggesting that acid– base interactions at the fibre periphery are probably the main cause of dye adsorption.[317] Intercalation would likely cause a significant change in fibre morphology as recently demonstrated by Hayes and co-workers.[96, 134] However, in that case the authors induced the gelation of the gelators in the presence of **MB** and hence adsorption took place as self-assembly proceeds whereas in our case dyes were adsorbed onto pre-formed hydrogel nanofibres. This might explain the contradiction between the two set of independent experiments.

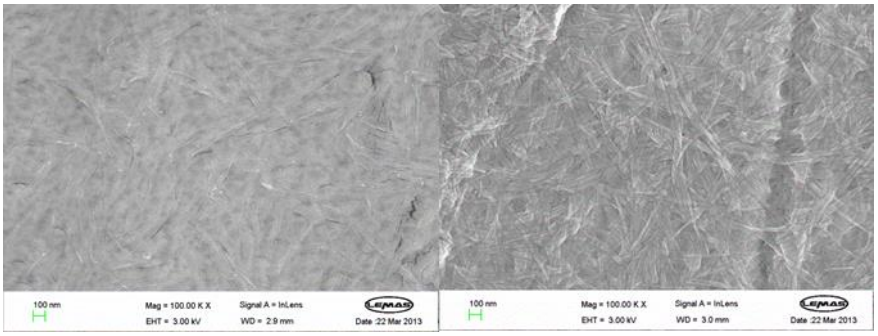

Figure 3.2.7 Scanning electron microscope (SEM) images of (a) native and (b) **MB** encapsulated **DBS-COOH** xerogel; Scale bars: 100 nm

3.2.3 Dye adsorption onto DBS-CONHNH$_2$ hydrogels

Hydrogels of **DBS-CONHNH$_2$** were prepared as previously discussed in Chapter 2 of this thesis. A requisite amount (4 mg) of the gelators was dissolved in deionised water (1 mL) and sonicated; heating-cooling cycle was employed to prepare hydrogels of **DBS-CONHNH$_2$**. Aliquot solutions (8 mL) of each of the dye solutions with different initial concentrations was added to each of the vials containing the gels. The systems were allowed to stand at ambient temperature undisturbed. The general batch adsorption process is schematically represented in Figure 3.2.8.

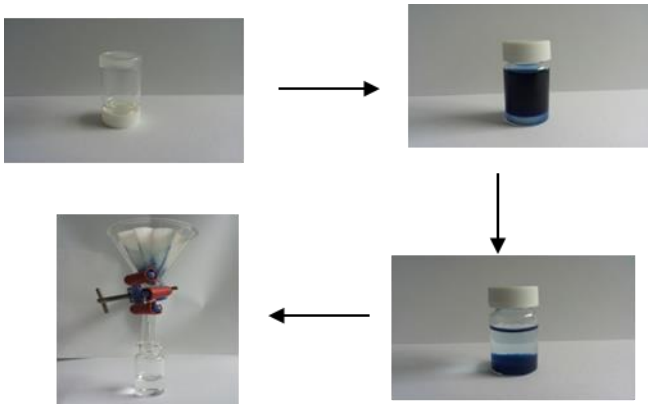

Figure 3.2.8 Schematic design for a batch adsorption model

A UV-Vis spectrophotometer was used to measure the absorbance of the dye remaining in the supernatant aqueous solution above the gel periodically over 24 hours and the concentration extrapolated from the calibration curves. The absorbance was measured at the maximum absorption wavelength (λ_{max}) of each dye CR (499 nm), MB (661nm), AB (601 nm) and NBB (619 nm). The plot of absorbance against the λ_{max} shown in Figures 3.2.3 and 3.2.4 reveals a significance decrease in the concentration of the dye remaining in aqueous solution as the solution diffuses into the gel networks. It should be noted that in the absence of any specific interactions between gel nanofibres and dye, the absorption of the supernatant should decrease 88.9% owing to simple dilution effects from the clean solvent present in the gel. In many cases the dye concentration decreased by significantly more than this factor.

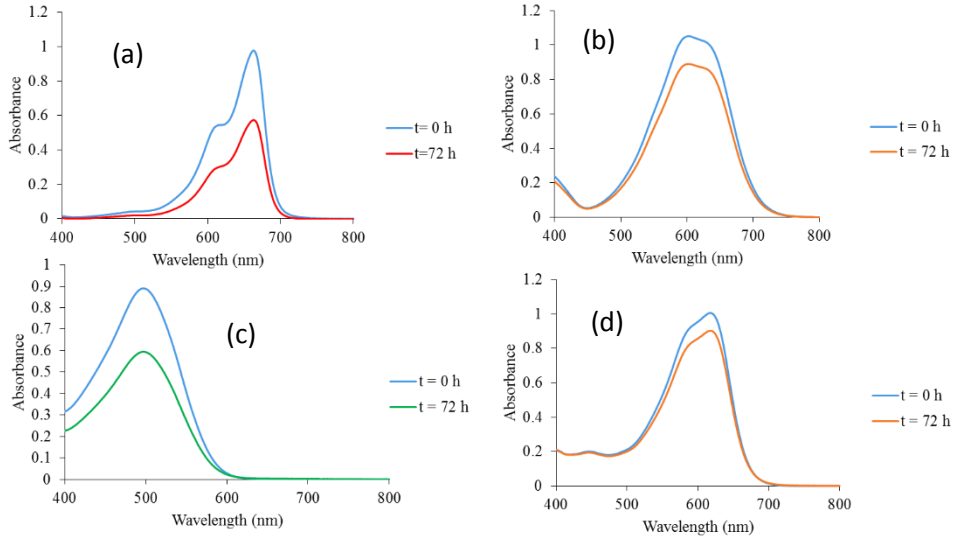

Figure 3.2.9 UV-Vis spectral for the time-dependent adsorption studies of (a) methylene blue (b) Acid blue25 (c) congo red and (d) naphthol blue black onto **DBS-CONHNH$_2$** hydrogels under neutral pH condition.

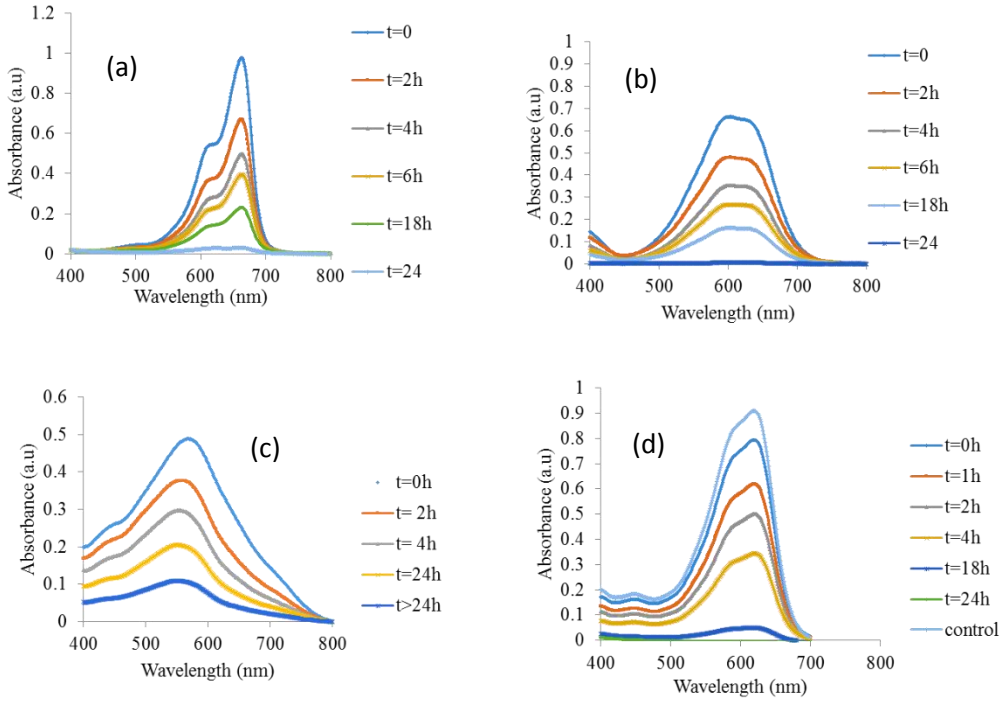

Figure 3.2.10 UV-Vis spectral for the time-dependent adsorption studies of (a) methylene blue (pH 9) and (b) Acid blue25 (c) congo red and (d) naphthol blue black (pH 4) onto **DBS-CONHNH$_2$** hydrogels.

The percentages of individual dye adsorbed by **DBS-CONHNH2** hydrogels increase from 33% **CR**, 40% **MB**, 17% **AB25**, and 10% **NBB** over a period of 72 h to 80%, 97% , 100%, and 100% respectively within a period of 24 h by changing the pH of the aliquot solutions of various dyes. The initial dye concentrations used for this experiment are 30 µM, 16 µM, and 72 µM for CR, **MB**, **NBB**, and **AB25** respectively. Drop-wise addition of 0.5M HCl to the aqueous solution of **AB25**, **NBB**, **CR** and 0.5 M NaOH to the aqueous solution of **MB**, enhanced the affinity of **DBS-CONHNH2** for these dyes. It is important to mention that **CR** changed colour from red (λ_{max} = 499 nm) to blue (λ_{max} = 590 nm) and underwent self-aggregation at pH ≤ 5. Therefore, the precise uptake of **CR** onto **DBS-CONHNH2** hydrogel at this pH value was difficult to quantify but Figure 3.2.11.

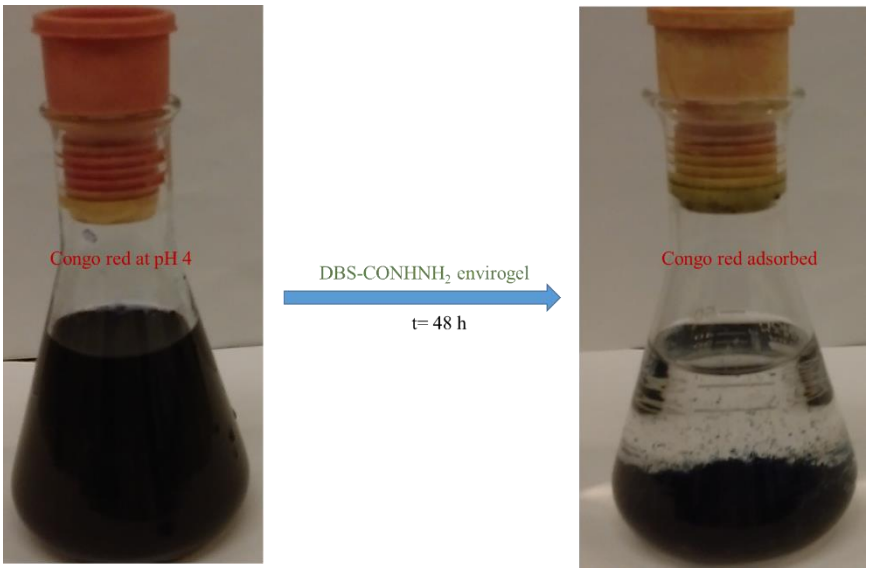

Figure 3.2.11 Congo red changes colour at acidic pH and was significantly adsorbed onto **DBS-CONHNH2** envirogel nanofibre after 48 h

Hydrogels of **DBS** and **DBS-COOCH3** prepared in water-ethanol mixture (50:50) were also able to efficiently adsorb 93% and 91% of **CR** respectively, but they showed no significant affinities for **MB**, **NBB** and **AB25** under this experimental condition.

Interestingly, **DBS-CONHNH2** demonstrates ambidextrous ability for dye uptake under various pH conditions. In order to consider the effect of pH on dye adsorption, it is informative to consider the structures of the dyes, and their functional groups. It should be assumed that all sulfonic acids, as strong acids, exist in anionic form across

the entire pH range, however, the amine groups (and phenols) will be protonated or deprotonated dependent on the p*Ka* values of the dyes. It can be suggested that the dyes are best adsorbed by the envirogels of **DBS-CONHNH2** in their lowest charged state. For **MB**, this will be at high pH, where the amines are not protonated and it only has +1 charge. For the other dyes it will be at low pH, where the amines are protonated, and can therefore somewhat counteract the negative charge of the sulfonate(s). Notably, **AB25** has two amine groups whereas **NBB** only has one (and phenol), and this possibly explains why the former dye is better adsorbed than the later as it will have a lower net charge. This suggests that when highly charged, these dyes prefer to be solvated in aqueous solution rather than interacting with the supramolecular envirogel fibres through simple hydrogen bond acid-base type interactions. As such, the gel fibres are able to distinguish between different types of dye (amine-based and sulfonate-based) under different conditions of pH.[112] In order to vindicate this hypothesis, reactive blue 4 **RB4** (Figure 3.2.12) – an anthraquinone dye with sulfonic acid group, was interacted with the envirogel nanofibres under the ambient neutral condition. Interestingly, about 64% of the initial dye concentration (0.5 g/l) was adsorbed within 18 h, perhaps as a result of acid-base interactions between the amine on the periphery of the nanofibres and sulfonic acids of the dye molecule.

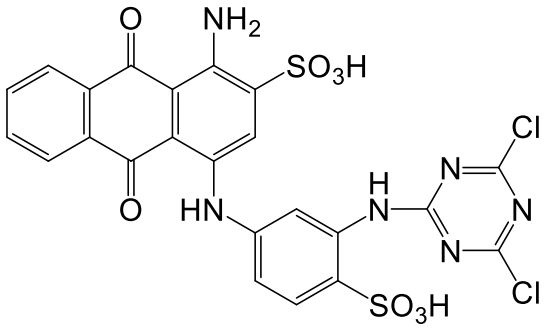

Figure 3.2.12 Chemical structure of reactive blue 4 **RB4**

For a representative example, transmission electron microscopy was used to investigate the interaction of NBB with the gel nanofibres. The patches and dark spots along the fibres suggests a close interaction of the dye with the gel nanofibres (as shown in Figure 3.2.13). It should be noted that the image is unstained, so the patches could not be attributed to staining effects and are more likely due to the heavy atoms present in the dye.

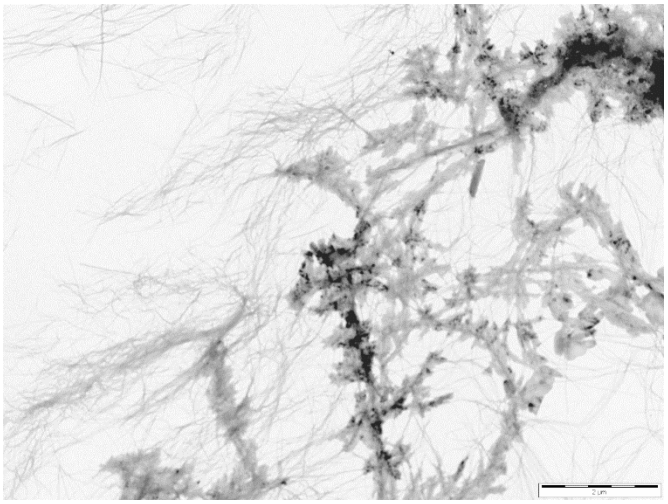

Figure 3.2.13 TEM image of dried **DBS-CONHNH$_2$** xerogel with **NBB** adsorbed

Infra-red spectroscopy is an informative technique for monitoring interactions within a nanostructured material. Interestingly, adsorption of **NBB** shifted the N-H stretch of **DBS-CONHNH$_2$** gelator from 1617 cm^{-1} shifted to a higher wavenumber by *ca.* 20 cm^{-1} while the O-H peak of the sorbitol backbone shifted from 3314 to 3382 cm^{-1} (these values are assigned with caution as they tend to overlap the characteristic peaks of the NH_2 and OH groups of **NBB**). The C=O peak was also shifted from 1644 cm^{-1} to a higher wavenumber by *ca.* 20 cm^{-1} while the C=C shifted from 1572 cm^{-1} to a lower wavenumber by *ca.* 15 cm^{-1} (Figure 3.2.14a).

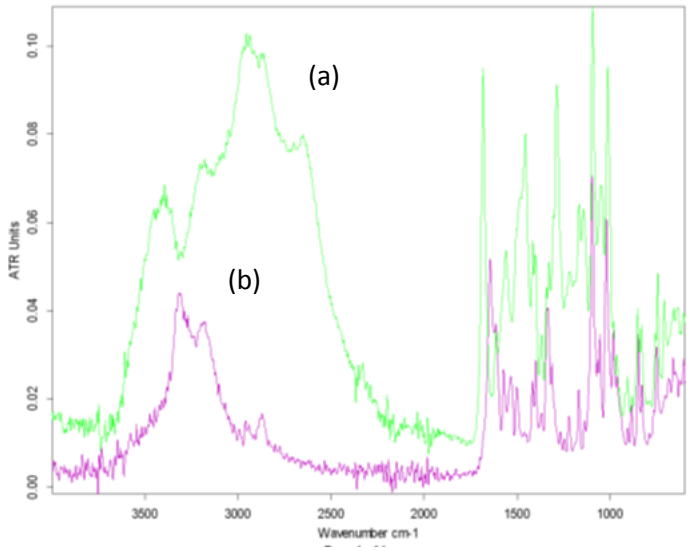

Figure 3.2.14 IR spectra for dried xerogel of **DBS-CONHNH2** (a) with (green line) and (b) without (pink) **NBB**

Interaction between **DBS-CONHNH2** and the adsorbed **NBB** was further explored by UV-Vis spectroscopy. Figure 3.2.15 shows the spectra of **NBB** in solution and when adsorbed onto the hydrogel of **DBS-CONHNH2**. The broadening of **NBB** spectrum and the bathochromic shift from 627 to 646 nm suggest a significant interaction between the dye molecule and nanofibres of **DBS-CONHNH2**.

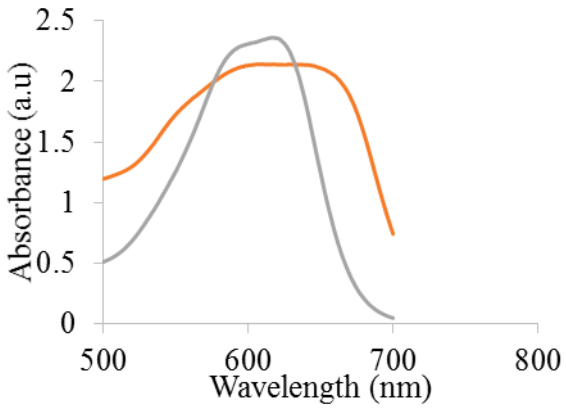

Figure 3.2.15 UV-Vis spectra for **NBB** in solution (grey) and on gel nanofibres (orange)

3.2.4 Adsorption efficiency of dyes onto DBS-CONHNH2 envirogels

In order to determine the maximum dye uptake by the envirogels of **DBS-CONHNH2**, concentrated solutions of the dyes were interacted with the gel nanofibres. An aliquot

of the supernatant was taken and diluted to measure concentration of the dye molecules remaining periodically using UV-Vis spectroscopy. All experiments were run so that the gels were becoming effectively saturated with dye by the end of each run. The dye uptake capacity of the envirogel increased with time until it nearly becomes a plateau- suggesting saturation of the envirogel with dye (as shown in Appendix B).

The maximum amount of dye adsorbed per gram of gelator used was then computed from Equation 3.2.1.

$$q_e = (Co - Ce)V/m \qquad \text{(Equation 3.2.1)}$$

q_e is the amount of dye adsorbed (mg/g), m is the weight of adsorbent used (g), C_e is the equilibrium concentration of dye in solution (mg/L), C_o is the initial dye concentration (mg/L) in solution, and V is the volume (L) of aqueous dye solution treated.

Figure 3.2.16 shows the maximum possible uptake of **MB**, **AB25**, **CR** and **NBB** under various pH conditions. In a basic pH 12 medium, **MB** (825 mg/ g) was remarkably adsorbed while **AB25** (1050 mg/ g), **CR** (~ 1500 mg/g) and **NBB** (700 mg/ g) were adsorbed better under acidic pH 2 conditions – approximate value of **CR** uptake is given because it underwent self-aggregation in the absence of gel at this pH condition. Besides the fact that these values are highly competitive with the best previous supramolecular envirogels, it also demonstrated a pH-dependent selectivity toward various dyes, making the **DBS-CONHNH$_2$** envirogel system quite different to the acid-functionalized gelators which can only adsorb dyes under neutral and acidic conditions as previously reported.[95, 96]

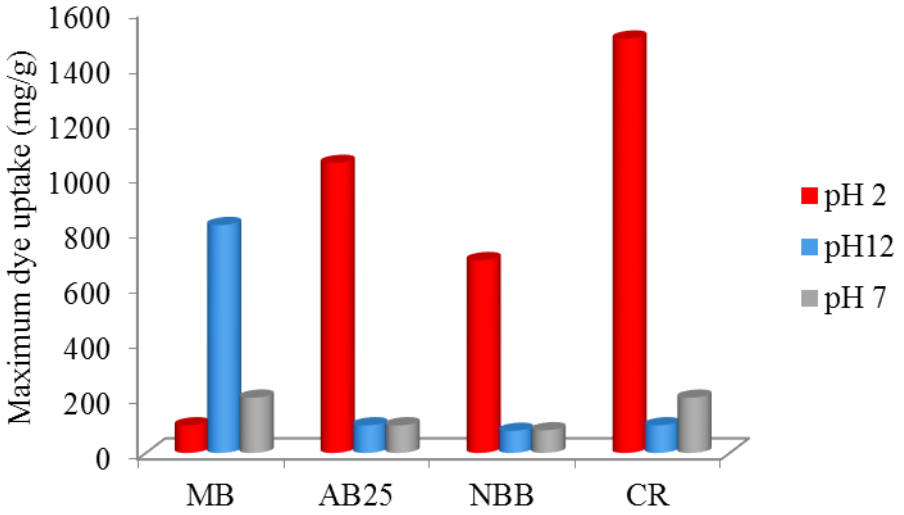

Figure 3.2.16 Maximum dye adsorption onto **DBS-CONHNH$_2$** envirogel under various pH conditions

It is difficult to calculate an accurate molar stoichiometry of uptake, as dyes are not purely obtained from commercial sources. Nevertheless, based on the indicated percentage purity, it was observed that the envirogelator can adsorb near stoichiometric amounts of dye – suggestive that every molecule which is self-assembled into the gel network has activity. This is predicated on the fact that the nanoscale fibres inherent within the gel network provide a highly accessible solid-like system with a remarkably high surface area in order to maximize dye uptake.

3.2.5 Adsorptive kinetics of dye adsorption onto DBS-COOH and DBS-CONHNH$_2$ envirogels

The kinetics of dye molecule - hydrogel interactions was investigated by fitting the kinetic data into pseudo first-order kinetic model of Lagereen and pseudo second-order kinetic models. It should be noted that the kinetics of adsorption was investigated under the pH condition most suitable for high uptake of various dyes. According to Bhattacharyya and Sharma,[318] when the adsorption process is preceded by diffusion through a boundary, then it is pseudo-first order and the kinetic model shown in Equation 3.2.2 holds in most cases.

$$\frac{dq}{dt} = K_1(q_e - q_t) \qquad \text{(Equation 3.2.2)}$$

By expression in a linear form, this gives;

$$\log_{10}(q_e - q_t) = \log_{10} q_e - \left(\frac{K_1}{2.303}\right) t \qquad \text{(Equation 3.2.3)}$$

K_1 = adsorption constant (l/min)

The plot of $\log_{10}(q_e - q_t)$ against *t* should give a straight line if the adsorption process obeys pseudo first -order Kinetics.

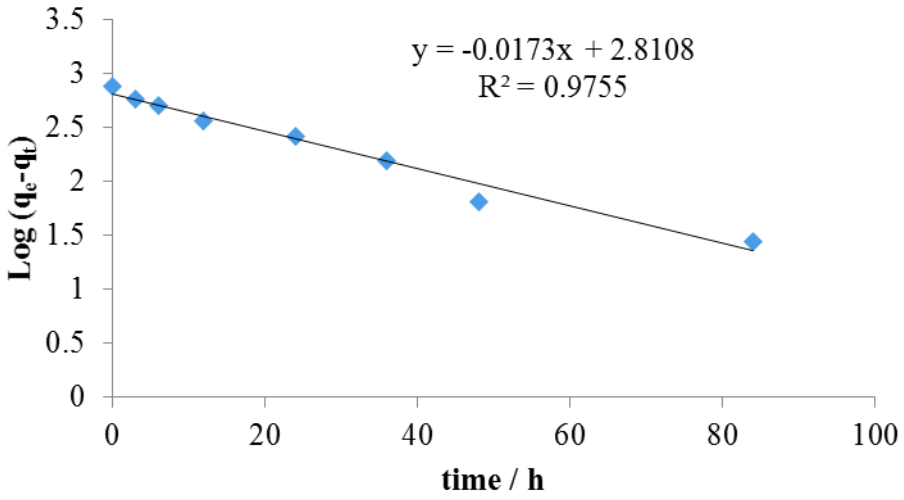

Figure 3.2.17 Pseudo first-order kinetic of **MB** adsorption onto **DBS-CONHNH2** envirogel under basic condition; [**MB**] = 1.27 g/l, [gelator] = 0.8% wt/vol

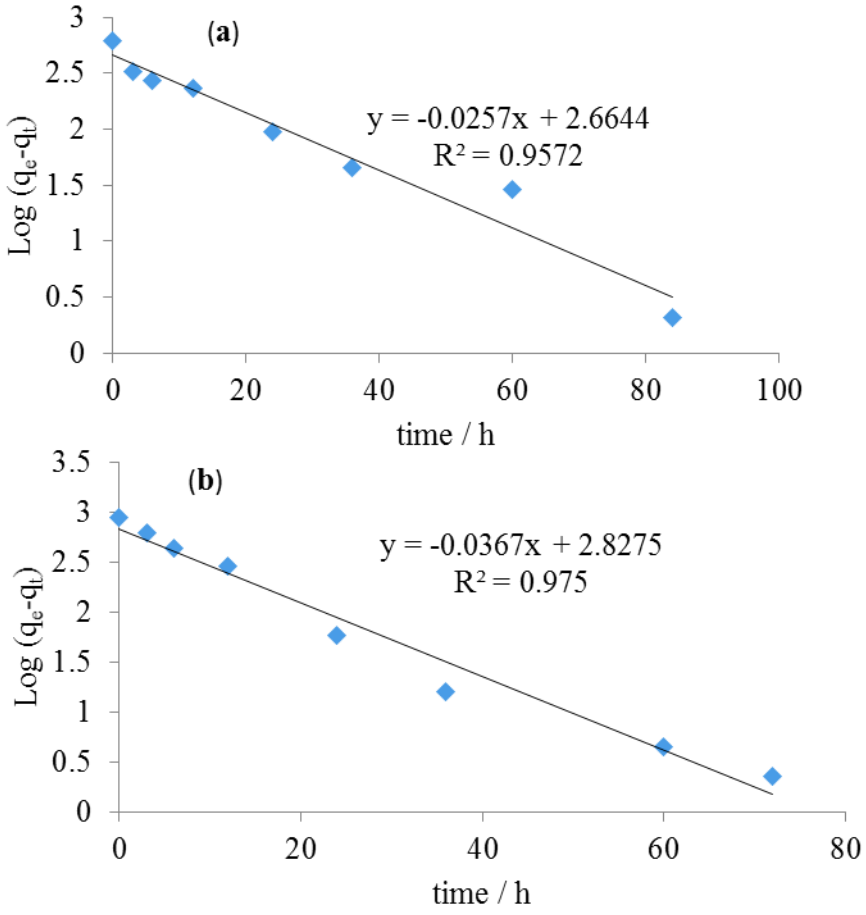

Figure 3.2.18 Pseudo first-order adsorptive kinetic of (a) **NBB** (b) **AB25** onto **DBS-CONHNH2** envirogel; [**NBB**] = 1.21 g/l, [**AB25**] = 1.51 g/l and [gelator] = 0.8% wt/vol

From Figure 3.2.17 and Figure 3.2.18, it was observed that the plot of $\log_{10}(q_e - q_t)$ against *t* yielded a fair correlation coefficient ($R^2 > 0.8$). However, pseudo second order kinetics was also investigated to see if it would yield a better fit.

According to Ho and Mckay (1998),[305] pseudo second-order kinetics is described by equations 3.2.4 and 3.2.5;

$$\frac{dq_t}{dt} = K_2(q_e - q_t)^2 \qquad \text{(Equation 3.2.4)}$$

Upon application of boundary condition t = 0 to t = t and $q_t = 0$ to $q_t = q_t$, followed by integration this results in;

$$\frac{t}{q_t} = \frac{1}{Kq_e^2} + t/q_e \qquad \text{(Equation 3.2.5)}$$

The plot of t/q_t vs t should give a straight line. This was the case with the dye-hydrogels system as shown in Figure 3.2.19 and Figure 3.2.20. It was also observed that the pseudo second-order adsorption kinetics yielded a better fit with higher correlation coefficients ($R^2 > 0.99$) for all the dyes.

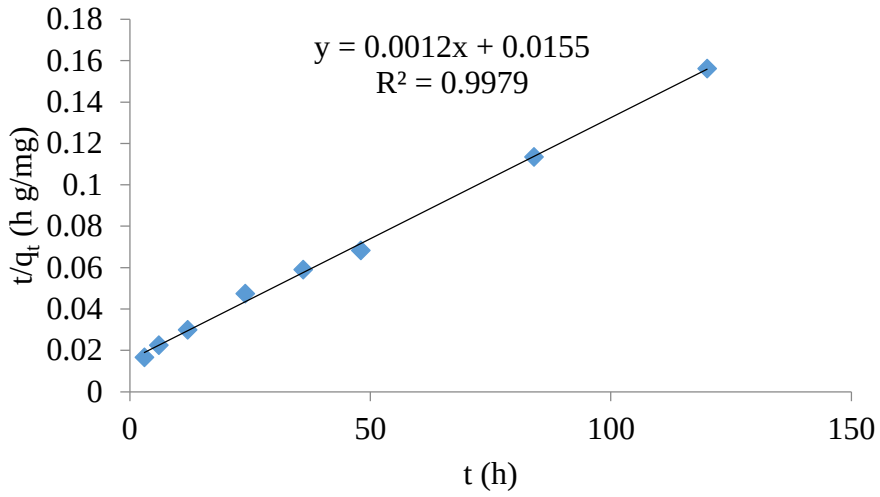

Figure 3.2.19 Pseudo second-order kinetic of **MB** adsorption onto **DBS-CONHNH$_2$** envirogel under basic condition; [MB] = 1.27 g/l, [gelator] = 0.8% wt/vol

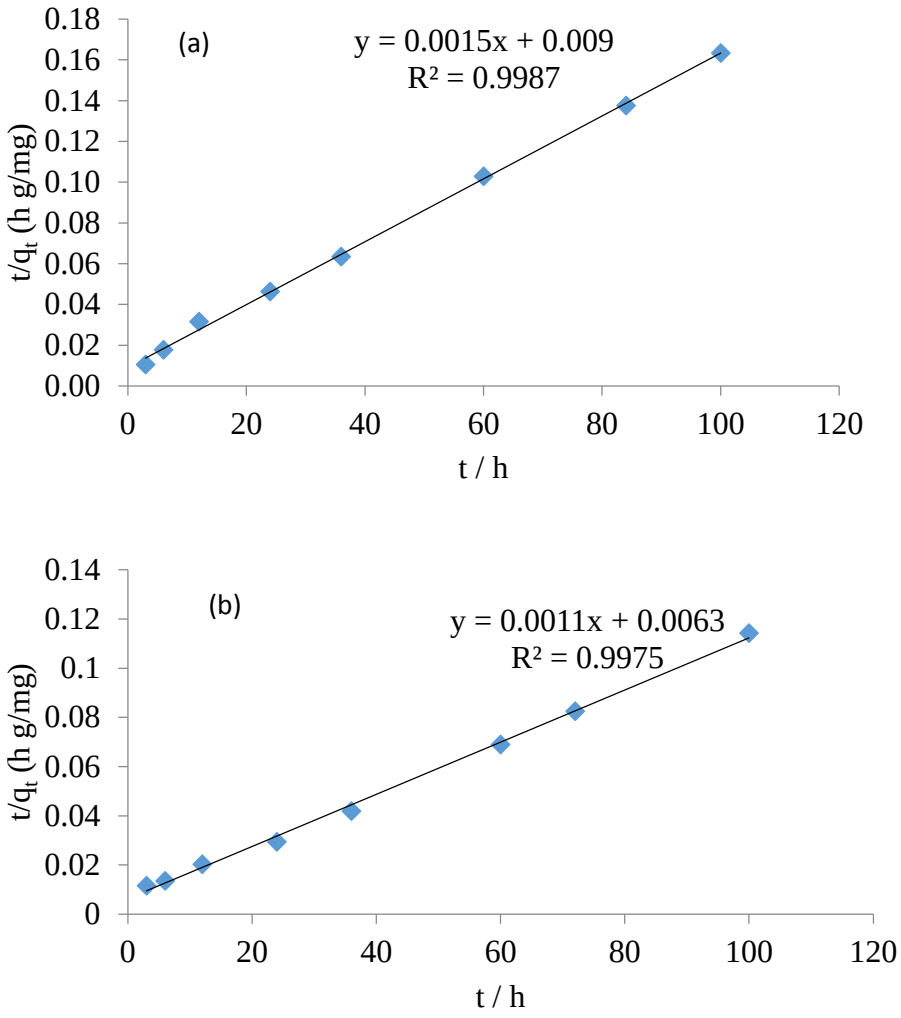

Figure 3.2.20 Pseudo second-order adsorptive kinetic of (a) **NBB** (b) **AB25** onto **DBS-CONHNH₂** envirogel; [**NBB**] = 1.21 g/l, [**AB25**] = 1.51 g/l and [gelator] = 0.8% wt/vol

In all cases, the kinetic data gave the best fit with pseudo second-order kinetics ($R^2 \geq 0.99$). This is often the case with adsorption of pollutants from water, and supports the view that chemically specific interactions between the gel nanofibres and the pollutant dyes underpin the adsorption process.[319, 320] All dyes showed significant rates of uptake, however, at pH 2.4 **AB25** and **NBB** were taken up significantly more quickly ($K_2 \sim 2.2 \times 10^{-4}$ g mg^{-1} h^{-1}) than MB at pH 12 ($K_2 \sim 1.0 \times 10^{-4}$ g mg^{-1} h^{-1}).

3.2.6 Adsorptive isotherms for dyes onto DBS-CONHNH$_2$ envirogel

The adsorption mechanism for the interactions between envirogel and dye was also investigated. Langmuir and Freundlich isotherm models were used to compute the adsorption isotherm fits. To do this, a range of concentration of aliquot dye solutions (10 – 90 mg/l) were added to a fixed concentration of gelator (0.8% wt/vol) assembled into envirogels. The adsorption process was allowed to proceed at ambient temperature for a period of time until there was no further change in the absorbance of the aliquot dye solution. At this point adsorption equilibrium is said to have been attained. Using the Langmuir isotherm model;

$$\frac{1}{q_e} = \frac{1}{q_{max}} + \frac{1}{q_{max} b} . 1/c_e \qquad \text{(Equation 3.2.6)}$$

q_e is the amount of dye adsorbed (mg/g) unto hydrogel, q_{max} is the maximum adsorption capacity according to Langmuir chemisorption (mg/g), c_e is the concentration (mg/l) of dye molecules remaining in the solution at equilibrium and b is the energy of adsorption (l/mg). The plot of $1/q_e$ vs $1/c_e$ should yields a straight line for a chemisorptive behaviour in which there are specific interactions between the dyes and the solid-like network.[305, 318]

According to Namasivayan and Kavitha,[304] the Langmuir equation can be further extended to obtain an equation for the dimensionless parameter (R_L) called the equilibrium parameter or separation factor.

$$R_L = 1/(1 + bC_0) \qquad \text{(Equation 3.2.7)}$$

C_o = Initial dye concentration (mg/l)

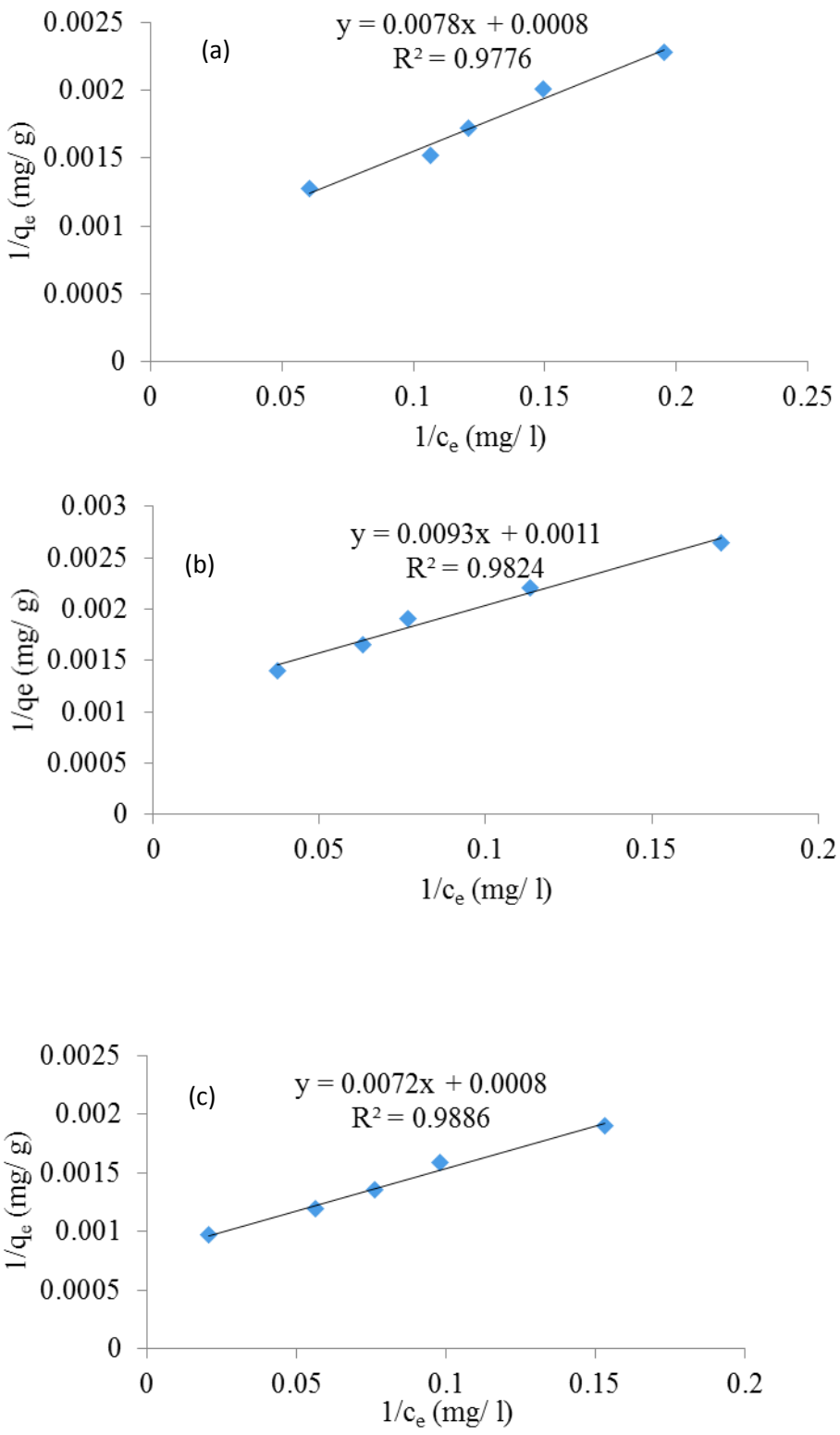

Figure 3.2.21 Langmuir isotherm for the adsorption of (a) **MB**, (b) **NBB** and (c) **AB25** onto **DBS-CONHNH$_2$** envirogel

On the other hand, the Freundlich isotherm describes a heterogeneous surface energy system. Its mathematical expression is shown in equations (Equation 3.2.8 and 3.2.9).

$$Q= K_f C^n \qquad \text{(Equation 3.2.8)}$$

When linearized becomes;

$$Log_{10} q_e = Log_{10} K_f + \frac{1}{n} Log_{10} C_e \qquad \text{(Equation 3.2.9)}$$

K_f = Freundlich constant, n = heterogeneity factor (g/l)

Both K_f and n are the Freundlich constants related to adsorption capacity and adsorption intensity respectively.

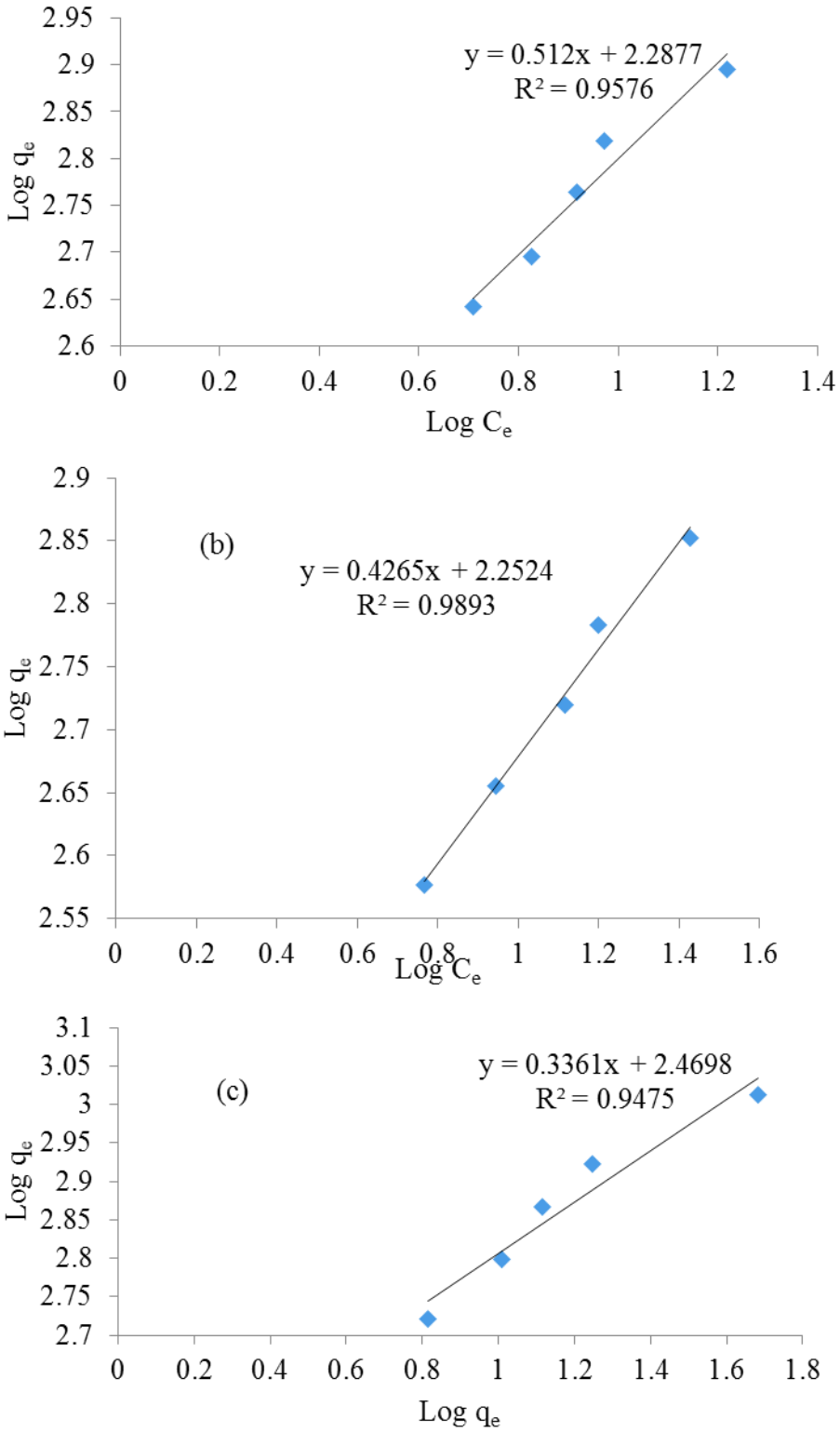

Figure 3.2.22 Freundlich isotherm for the adsorption of (a) **MB**, (b) **NBB** and (c) **AB25** onto **DBS-CONHNH$_2$** envirogel under optimum pH conditions

As shown in Table 3.2.1, the adsorption of the various dyes onto **DBS-CONHNH$_2$** envirogels fits the Langmuir isotherm (R^2 ~ 0.999) better than the Freundlich isotherm ($R^2 \leq 0.95$). Surprisingly, the maximum dye uptake capacity (Q_{max}) for **MB**, **AB25** and **NBB** are 1250, 1250 and 909 (mg g^{-1}) respectively as extrapolated from the Langmuir isotherm appears to be higher than the experimentally obtained values. This could be adduced to perhaps an incomplete equilibrium process during the experimental determination of the maximum dye uptake. The values of $R_L \leq 0.5$ and $n \leq 1$, therefore the adsorption of various dyes onto the envirogel nanofibres is favourable. Moreover, the low values of the energy of adsorption, b signifies beneficial adsorption with minimum energy requirement for all the hydrogels-dye interactions.

Table 3.2.1 Summary of the adsorptive isotherm parameter for dye-**DBS-CONHNH$_2$** interactions

Dye	**Solution pH**	**Langmuir isotherm**				**Freundlich isotherm**		
		Q_e (mg/g)	b(l/g)	R_L	R^2	K_f	n	R^2
MB	11.2	1250	0.10	0.45	0.98	194	0.5	0.95
AB25	2.4	1250	0.11	0.38	0.99	295	0.35	0.94
NBB	2.4	909	0.12	0.40	0.99	179	0.4	0.96

3.2.7 Recyclability and re-usability of DBS-CONHNH$_2$ envirogels

In order to probe the selectivity of the envirogel, an aqueous solution containing both **AB25** (60 µM) and **NBB** (25 µM) was interacted with **DBS-CONHNH$_2$** envirogel nanofibres under the optimum pH condition. It was revealed that a mixture of **AB25** and **NBB** could be simultaneously adsorbed from the acidic solution by the gel –

reflective of real-world conditions where mixtures of dyes may be present (Figure 3.2.23).

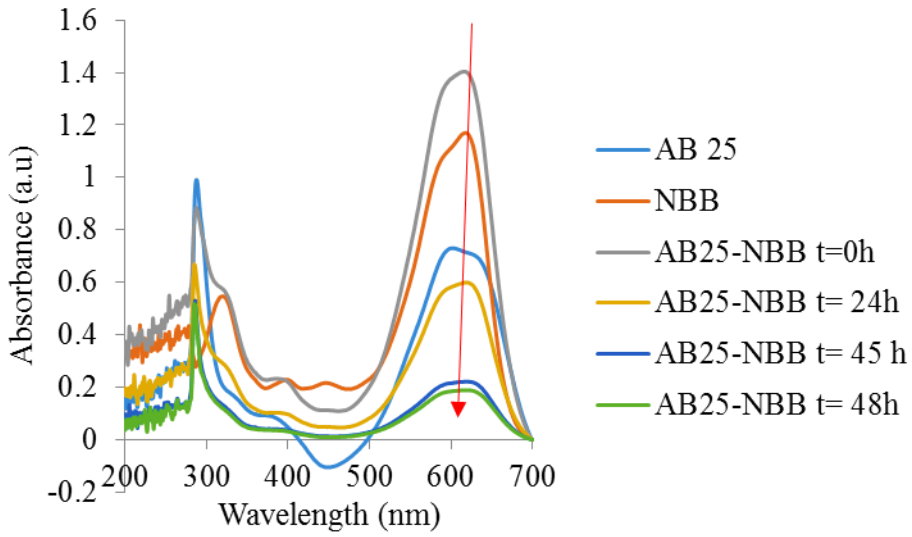

Figure 3.2.23 UV-Vis spectra for adsorption of an equimolar mixture of **AB25** and **NBB** onto **DBS-CONHNH$_2$** envirogel at pH 2.5

In order to recycle the envirogels, it was proposed that reversing the pH conditions may be a simple way of desorbing dyes from envirogel nanofibres. Figure 3.2.24a shows that envirogel nanofibres saturated with **AB25** and **NBB** released the dyes when exposed to a supernatant basic solution ($NaOH_{aq}$, 0.1 M). This cycle was repeated several times with 100% dye recovery after which the percentage recovery declined to about 80%. However, there was little or no visible damage to the macroscopic gel integrity (Figure 3.2.24b).

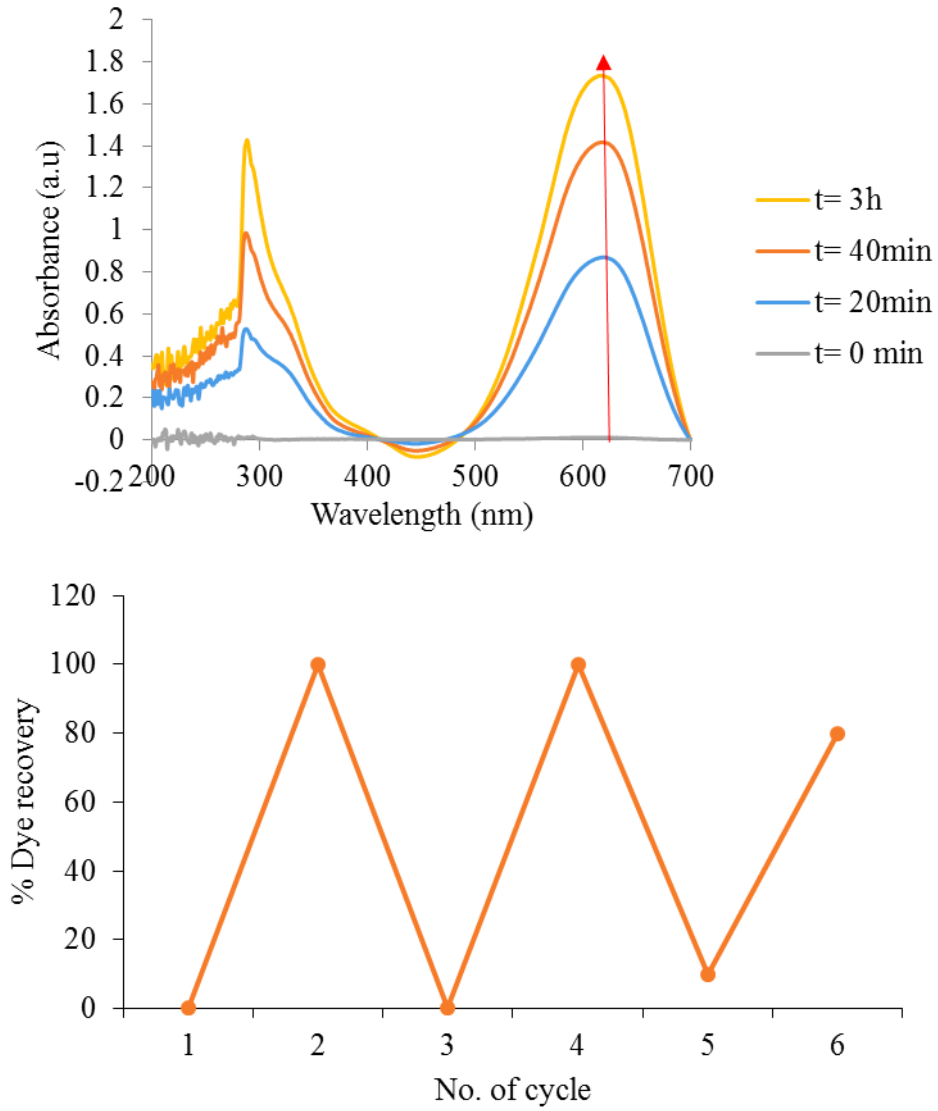

Figure 3.2.24 (a) desorption of dyes from envirogel nanofibres under basic conditions (b) repeatability of adsorption-desorption cycling

Therefore adsorption-desorption, with **AB25** and **NBB** being adsorbed in acidic conditions and then desorbed under basic conditions offers a simple mechanism for envirogel recycling. It is important to mention that the gels were exposed to deionised water for about 2 h between each cycle.

3.2.8 Flow-through experiment

In order to extend the scope of this adsorption experiment to a real life case study and explore the porosity of the envirogel, a column (as a laboratory model for a water filter) adsorption experiment was carried out. Although **DBS-CONHNH$_2$** demonstrated

efficient dye uptake under batch adsorption process but it was because its instant gel formation, it was difficult to make a uniform hydrogel of **DBS-CONHNH$_2$** in our in-house column and as such there was a massive eddy-diffusion of dyes through the gel nework. Therefore, **DBS-COOH** was used for this purpose due to the ease of in situ gel formation. In this case, a glass column (although 10 mL syringes were also used at some points) with an inner diameter of 10 mm and 20 cm height was filled with the pre-made **DBS-COOH** solution containing glucono-δ-lactone (GdL). The gelation was allowed to proceed as the GdL is hydrolysed in the solution (as shown in Figure 3.2.25) for the column hydrogel.

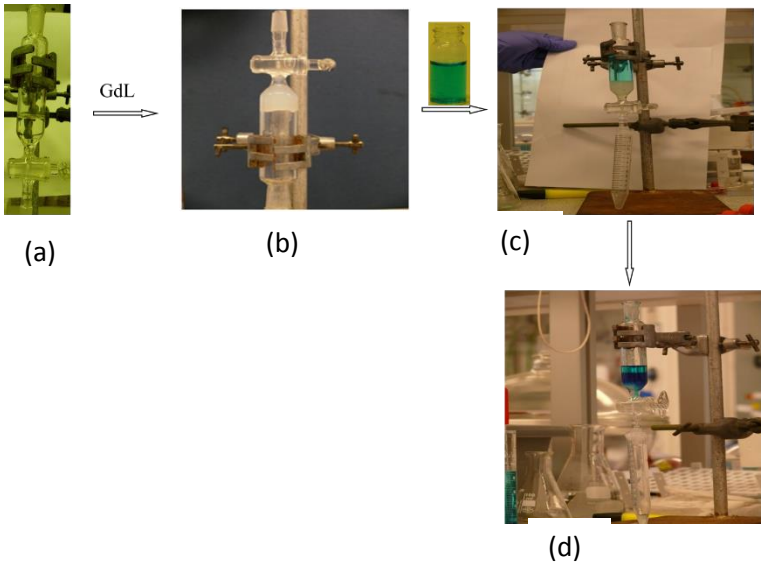

Figure 3.2.25 Scheme for a laboratory model for a gel-based water filter. (a) basified **DBS-COOH** solution (b) stable **DBS-COOH** hydrogel (c) influx of dye (**MB**) solution and (d) collection of clean water effluent

Deionised water was allowed to flow through the virgin column hydrogel before introducing the aliquot solution of **MB** into the column. This was done to fill any voids in the gel network and the column. The presence of void on the column walls might cause non-uniform diffusion of dye solution through the column wall- eddy diffusion. A correct gelator concentration was required to make a uniform column hydrogel. Several concentrations were tried - 0.3% wt/v, 0.4% wt/v, 0.44% wt/v, 0.5% wt/v, 0.57% wt/v and 0.67% wt/v. However, it was observed that concentrations below 0.5% wt/v yielded a highly porous hydrogel, leading to a rapid diffusion of the dye through the gel network. On the other hand, concentrations above 0.57% wt/v formed tightly packed fibrous networks, leading to limited porosity. As a result of this straitened pore

sizes, it took more than one week for 40 mL of clean effluent (void of dye molecules) to be collected at the column exit. Hence, 0.57% wt/v was found to be the optimum gelator loading for this experiment.

The feed solution of MB of known initial concentration was introduced from the column inlet. The aqueous dye solution was allowed to flow through the column under gravity. The effluent from the exit stream was collected in labeled 15 mL centrifuge tubes at desired intervals (although not constant) of time. The concentration of the dye solution emerging from the column was estimated by measuring the absorbance at λ_{max} = 664 nm with the aid of UV-Vis spectrophotometer and then interpolated into the calibration curve.

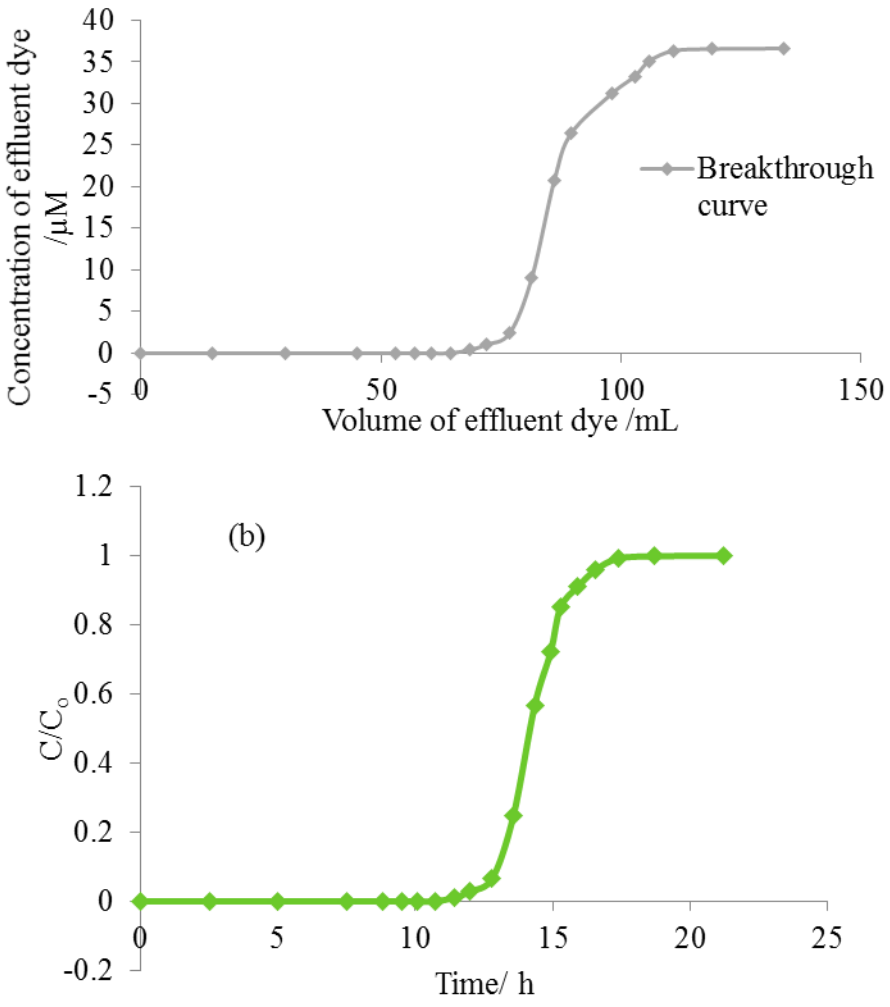

Figure 3.2.26 Breakthrough (a) volume and (b) time for the filtration of MB solution through **DBS-COOH** envirogel filter-bed

Figure 3.2.26 shows the way in which the dye molecules are distributed when an aqueous solution containing a constant concentration of **MB** migrates into the hydrogel network until the adsorbate dye emerges in the exit stream. When the adsorbate is first introduced into the clean filter bed, the hydrogel became saturated at the inlet interface of the bed and assumed equilibrium with the dye molecules in the aqueous inlet stream. The concentration of the dye molecules decreased gradually as the aqueous solution flows through the bed and the amount remaining at the exit stream becomes negligible. The volume and time attained before a significant amount of the adsorbate is first detected in the effluent are taken as the breakthrough volume and time respectively. It is obvious from Figure 3.2.26 a and b that it took about 12 h (ca. 75 mL) for the

breakthrough point to be attained. After the breakthrough point, the concentration of the adsorbate dye in the effluent stream rose steeply and become constant to assume the sigmoidal shape (S-shape) at the saturation point, until all the **MB** was simply eluting as the gel column was saturated.

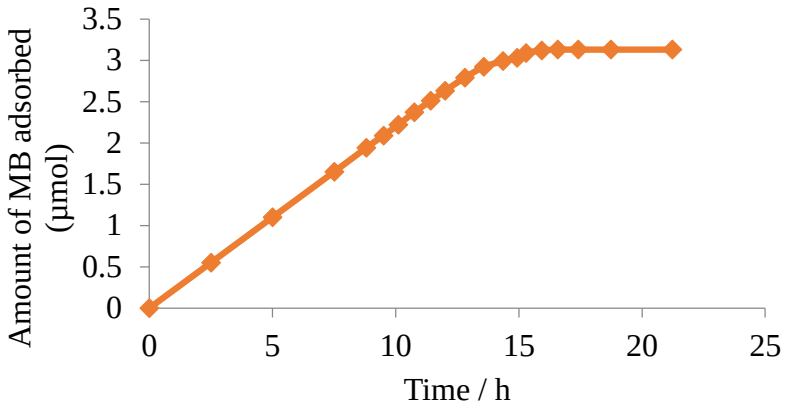

Figure 3.2.27 Adsorption rate for **MB** onto **DBS-COOH** under a gravity flow-through model

It is shown (Figure 3.2.27) that the adsorption increases steeply until the supposed maximum loading capacity is attained. The mass of **MB** adsorbed is computed to be 50 mg MB/ g of **DBS-COOH**. This value is expected to be less when compared with batch adsorption (ca. 125 mg **MB**/ g of **DBS-COOH** due to lower contact time and availability of active sites.

It is important to mention that any attempt to apply pressure to aid the flow through of the aqueous solution resulted in internal collapse of the gel network.

3.3 Conclusion and Summary

In order to kick-start the applications of the novel pioneer **DBS** based hydrogelators in a more biologically relevant area, **DBS-COOH** and **DBS-CONHNH$_2$** were used to remove pollutant dyes from water. In this initial study, **DBS-COOH** hydrogels like other pH-dependent carboxylic acid based hydrogelators reported in literature, significantly adsorbed methylene blue (**MB**), a basic cationic dye from water under

ambient condition but acid blue 25 (**AB25**), an anionic dye, to a lesser extent. Acid-base interactions were proposed as the underlying mechanism underpinning adsorption of the dyes onto **DBS-COOH** hydrogel nanofibres.

On the other hand, **DBS-CONHNH$_2$**, a pH-tolerant hydrogel, demonstrated a pH-dependent selective dye uptake towards methylene blue **(MB**), acid blue 25 (**AB25**), naphthol blue black (**NBB**) and congo red (**CR**). A significant amount of **MB** was adsorbed under basic pH condition while **AB25**, **NBB** and **CR** were efficiently adsorbed under acidic pH condition. It is hypothesized that hydrogen bonding acid-base type of interactions mediated the interaction between dye-hydrogel nanofibre interaction, and hence dye adsorption. Interestingly, techniques such as TEM, FTIR and UV-Vis spectroscopy shows there were obvious interactions between **NBB** and **DBS-CONHNH$_2$** hydrogel nanofibres at optimum pH condition.

Furthermore, adsorptive kinetic and isotherm studies reveal that uptake of dyes onto **DBS-CONHNH$_2$** hydrogel nanofibres fit pseudo second-order kinetic and the Langmuir model better than pseudo first-order kinetic and the Freundlich model. As such, both the kinetic and the isotherm parameters suggest that dye uptake onto the hydrogel nanofibres is a chemisorptive adsorption process rather than a physiosorptive phenomenon. The ability of **DBS-CONHNH$_2$** envirogel to simultaneously sequester acid dyes from their multicomponent aqueous mixture suggests its potential for a real-life water purification applications. The hydrogel could be recycle and reuse many times by a simple washing with $NaOH_{(aq)}$.

Due to the inherent nanoporous meshes in the hydrogels of **DBS-COOH** and **DBS-CONHNH$_2$**, they could be designed into a laboratory bench-scale nanofilter for water purification. **DBS-COOH** solution could easily be loaded into column and uniform hydrogelation obtained but **DBS-CONHNH$_2$** exhibited instant gelation and hence it was difficult to obtain uniform gel formation when loaded into the column. As such, **DBS-COOH** demonstrated better adsorption of **MB** as the aliquot solution of the dye elute through the gel column and clean water obtained as effluent until the whole column became saturated with dye.

Having established the adsorptivity of **DBS-COOH** and **DBS-CONHNH$_2$** envirogels towards various dye by using model polluted water, it is hoped that this studies would be carried out in the future using water obtained from river(s) polluted with various dye. Furthermore, a mechanically robust hybrid hydrogels comprising agarose/alginic acid/hyaluronic acid and **DBS-COOH**/**DBS-CONHNH$_2$** could be designed into a column for separation science applications.

4 Chapter 4 – Supramolecular envirogels: Nanosorbents for capturing heavy metals in water

4.1 ''Heavy Metals'' - A Misnomer?

''Heavy metal'' is one of the chemical phrases that has been persistently used in literature, policies, regulations and newspapers, with a diversity of definitions that do not have basis in IUPAC *Compendium of Chemical Terminology*,[321] leading to confusion and imprecise communication for over 70 years. This ambiguous misnomer which had previously been used to mean 'guns or shot of large size' or great ability[322, 323] was used for the first time by Bjerrum to provide a chemical definition for a certain class of elements.[324] In 2002, Duffus not only noted ''heavy metals'' as a meaningless term but also highlighted various ways people have defined this phrase.[28] There are more than 35 inconsistent definitions composed by different authors who independently used factors such as elemental density, atomic weight, atomic number and chemical properties as the yardsticks for classifying certain elements as heavy metals. For instance, Bjerrum defines heavy metals as those elements with density > 7.0 g/cm^3 [324] while other authors used densities ranging from 3.5 - 7.0 g/cm^3 and atomic mass 23 – 40 g/mol as the threshold levels for their definitions.[28] Because ''heaviness'' is currently likened to ''toxicity'', heavy metal is therefore a proverbial bogeyman used to describe some environmentally harmful elements such as mercury, lead, cadmium, arsenic and their compounds. However, the use of ''heavy metals'' to describe elements such as arsenic and tellurium is an aberration from the standard IUPAC classification and distribution of elements in the periodic table as these elements are metalloids.[325, 326] The use of this ill-defined term has been condemned by some authors[327-332] and some famous textbooks in toxicology like Casarett and Doull's Toxicology will not use this term at all.[333] Moving from semantics to pragmatics, Hübner et al have reported what has been suggested as alternatives to this widespread term.[331] A clarion call to return to the periodic table has been raised by Hodson[330] who preferred the fundamental classification of elements into s-, p-, d-, and f- block elements while Phipps reiterated the biologically significant properties of d- block elements and also, the strong interactions between high atomic number p- block elements and sulfur, which often leads to toxicity.[328] Nieboer and Richardson have used the preference of metals for certain ligands as a basis for classifying metals into

Class A, Borderline and Class B groups (Figure 4.1.1) and on this classification was based Pearson's soft and hard acids concept.[334] In this method of classification which appears to be more acceptable, Class A metals (s-block elements) are also referred to as 'hard metals' and Class B as 'soft metals' while the borderline groups exhibit intermediate properties.[327] The hard s-block metals bind poorly to soft ligands such as sulfur and rather form ionically-bound complexes with hard ligands such as oxygen donors.[334] The soft, high atomic number p- block metal ions on the other hand, exhibit strong affinity for soft ligands and form stable complexes, thereby making them threats to the environment and toxicants to living organisms. Borderline metal ions bind to either hard and soft donor ligands.[327] It is noteworthy to mention that the aforementioned classifications are based on empirical results, however, Klopman, used calculated orbital electronegativity (COE), a theoretical concept to classify metals. According to this author, metals with COE above 1.45 are Class A, while those with COE below -1.88 are Class B.[335] However, this system of classification is not all encompassing, as elements such as arsenic and tellurium are not accounted for, therefore, some authors[325] prefer to list individual elements in their articles rather than using any of the controversial terms.

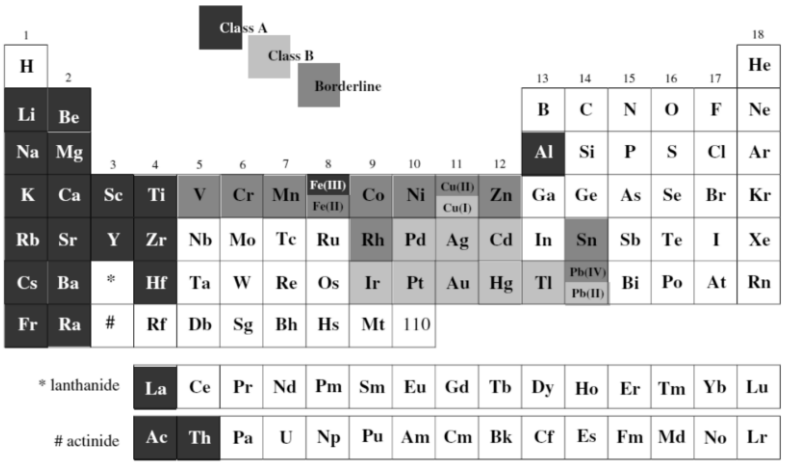

Figure 4.1.1 The periodic table showing the classification of metals into: Class A: hard metals (dark grey); Class B: soft metals (light grey); and Borderline: intermediate metals (intermediate grey). Reproduced from ref.[28]

Regardless of criticism of using the term ''heavy metal'' to denote lead (Pb), cadmium (Cd), mercury (Hg) and arsenic (As) among others, their presence in the biosphere has

caused more harm than not, to both plants and animals. As much as it is important to use scientifically definable terminology to represent these potential pollutants, it is equally not unessential to intensify efforts towards getting rid of them from the ecosystems and grouping them together is useful for public understanding of the science and the environment. Exposure to Pb, Cd, Hg and As can occur through contaminated air, water, food and soil. Anthropogenic activities such as mining, electronic waste recycling, wood treatment and battery production are the major sources of harmful metals and metalloids. The role of these elements in human health cannot be over-emphasized as some of them are systemic toxins with neurotoxic, carcinogenic, teratogenic, and fetotoxic effects.[13] The chemistry, uses and life threatening effects of these elements (Pb, Cd, Hg and As) will be discussed briefly in the following sections.

4.2 Chemistry and Toxicity of Lead, Cadmium, Mercury and Arsenic

4.2.1 Lead (Pb)

Lead is a soft, silvery white or grayish, metal which belongs to group 14 (IVA) of the periodic table. As one of the oldest known metals, its existence is dated back to the Bronze Age prior to the emergence of Roman Empire.[336] Pure elemental lead rarely exists in nature but rather as ores such as galena (PbS), cerussite ($PbCO_3$), anglesite (($PbSO_4$) and litharge (PbO). Lead has four stable isotopes (^{204}Pb, ^{206}Pb, ^{207}Pb and ^{208}Pb). ^{206}Pb, ^{207}Pb and ^{208}Pb are stable products of radioactive decay process. The two primary oxidation states of are Pb^{2+} and Pb^{4+}. The former predominates the inorganic chemistry of lead while the latter is commonly adopted by various organoleads.[337] Lead in +2 oxidation state is a soft class B metal while +4 oxidation state is borderline hard/soft (as shown in Figure 4.1.1). Like other metals, lead exhibits properties such as malleability, ductility, formability, low melting point, resistance to corrosion and have been applied for a variety of applications such as lead vats, cooking utensils, pots, vessels, water piping, statues, glazes, glass, pencil, coins, cosmetics, architecture and engineering, ammunitions, medicines, automobile, ornaments and seals from antiquity.[336, 337] The use of tetraethyl lead as an anti-knocking additive in gasoline was common until 1995 when its use was completely banned by the US Environmental

Protection Agency followed by other developed countries, while its use as an additive in pigments and paints was phased-out by the Consumer Products Safety Commission in 1978.[32] However, the use of leaded gasoline in developing countries like Nigeria is currently unabated.[338] Despite increasing efforts towards eradicating lead in the environment, the lead storage battery is currently rated the most common source of lead.[339, 340]

The toxicity of lead has been known since antiquity.[341] The upswing of use of lead and its toxicity in the environment became tremendous following the Industrial Revolution, especially in developing countries because of lack of regulatory measures against lead exposure.[342] However, efforts to stem the tide of its prevalence in our environment are currently increasing.

Lead poisoning can occur via the air, soil, food or water, often by inhalation or ingestion of lead. Drinking water is often contaminated from environmental sources such as effluents from industries and erosion or from municipal drinking water distribution systems such as leaching of lead from pipes.[183, 339, 343, 344] For example, a ‘‘plumbism’’ (lead poisoning) epidemic, claiming the life of about 400 children, occurred in 2010 in Nigeria as a result of leaching of lead from pipes into tap water.[345] The current permissible level of lead in drinking water is set at 15 ppb (15 µg/L) by the United State Environmental Protection Agency (US EPA), nonetheless, adherence to this value is debatable, as the leaching of lead from pipes cannot be ruled out and also, many of people in the US drink from well water systems that do not comply with the EPA action level.[32] In fact, some organizations have proposed that no amount of lead is safe for biological systems. Several authors have extensively reviewed close relationships between lead and ill-health.[32, 338] For instance, the effects of acute lead poisoning among adults and children have been widely reported.[32, 338, 346, 347] Children are the most vulnerable to lead poisoning due to factors such as an immature blood-brain barrier at the formative stage,[348, 349] higher basal uptake of lead and their oral exploratory behaviours - which predisposes them to direct ingestion of lead dust.[350] Lead poisoning has been established as a major cause of encephalopathy in children. Not only have studies shown that Blood Lead Level (BLL) > 10 µg/dl impaired the Intelligence Quotient (IQ) of children but it has also been demonstrated that dose-dependent effects of lead on the IQ of children is a non-linear relationship, as lower

lead exposure results in a greater rate of brain dysfunction than higher exposure.[351-353] Geographical location, societal and economic status of children influence the exposure of children to lead. Children from the ‘‘down’’ side of these strata are at higher risk of lead poisoning.[354] Lead-induced cognitive dysfunction in adulthood has been extensively reviewed.[355, 356] Impairment of cognitive function such as visuospatial ability, executive function, verbal memory, and dexterity are attributed to prolonged exposure to lead, especially at workplaces.[357] Cognitive decline has been linked to the destructive effects of lead on brain structure which results in cerebral ischemia, decrease in brain volume and these leads to attention deficits, impaired motor function and dementia if not managed at an early stage.[355, 358-360] Besides neurotoxicity and cognitive impairment, lead is also known to cause osteoporosis and dental caries due to its ability to interact with vitamin D, thereby depleting active vitamin D level in the body.[361] It has been proposed that its mechanism of neurotoxicity proceeds via the disruption of intracellular Ca^{2+}.[362] Other problems include cardiovascular diseases,[338] renal failure.[363] General symptoms of lead poisoning include; anaemia, hypertension, high blood pressure, vomiting, loss of weight, loss of appetite and abdominal colic.[364] The half-life of lead in the body is location dependent. For instance, the half-life of lead in the blood is about 36±5 days while it varies from a year to decades in bones.[32, 355, 361] As such bones are generally the ‘‘storage house’’ for lead in the human body.

4.2.2 Cadmium (Cd)

Like lead, Cd is a non-essential soft, lustrous, silver-white, malleable, ductile and corrosion resisting metal. It belongs to group 12 and the d-block in the periodic table sharing the same family with zinc (an essential element) and mercury. Cd does not exists freely in nature but commonly exist as CdS also known as greenockite, CdO or $CdSO_4$. It is often found in association with other metals such as zinc (Zn) and lead during mining process. The natural abundance of Cd is about 2 ppm and stable isotopes include ^{106}Cd, ^{108}Cd, ^{110}Cd, ^{111}Cd, ^{112}Cd, ^{113}Cd, ^{114}Cd and ^{116}Cd but among these eight (8) isotopes, ^{112}Cd and ^{114}Cd are the most common. However, the massive presence of Cd in the environment is as a result of anthropogenic activities.

Cadmium is a class B metal as shown in Figure 4.1.1. Due to its distinctive metallic properties, it has earned itself many applications in industries such as Ni–Cd batteries,

electro-galvanizing, electroplating, stabilizers for plastics, paints and pigments, glass and ceramic wares, laboratory reagent and catalyst, and in electronics.[365] Therefore, about 13,000 tons of Cd are produced annually worldwide mainly from the aforementioned applications.[366] Biological cadmium contamination can occur from foods. The use of phosphate fertilizers has been reported as one of the major sources of cadmium toxicity. Cd is an active component of phosphate rocks, therefore, when phosphate fertilizers are applied to crops, Cd is absorbed and becomes accumulated in the crop and further transfer to humans via food chains.[367-369]

Inhalation and ingestion are the major routes for the uptake of Cd into biological systems. Tobacco constitutes 50% of the total Cd exposure, therefore, it has been demonstrated that smokers of tobacco products are prone to a higher body burden of Cd than non-smoking individuals.[370, 371] Children are not exempted from Cd toxicity as recent investigations have shown that the level of Cd in babies' toys and low-cost jewellery exceed the regulated environmentally safe level, therefore, oral mobilization of Cd in their saliva as a result of oral exploratory behaviour is inevitable.[372] Common non-occupational sources of Cd contamination in drinking water include, zinc plated water storage tanks, leaching of Cd from soldered water pipes or leaching from contaminated soil. When Cd is absorbed into the body, it is usually bound to a thiol containing protein such as metallothionein, leading to an average of about 60% deposition in both the kidneys and liver while the rest is widely distributed all over the body. The half-life of Cd in the blood is estimated to be 75-128 days. However, this does not represent the time taken for complete removal of Cd from the body as it has been estimated that the half-life for clearance from the body is over two (2) decades.[373]

The epidemic of cadmium poisoning which happened in Japan between 1912 and 1959 remains an indelible ordeal in the history of humanity. This occurrence gave birth to *itai itai*; a local term used to represent the excruciating pain people suffered as a result of cadmium poisoning which occurred downstream of the Jinuz River basin in Japan.[374] A report has recently show that even though many decades have passed, the residual effects of cadmium poisoning still linger in the Toyama area.[375] Besides *itai itai* disease, several other problems triggered by Cadmium poisoning exist.[376] For instance, several authors have established a strong relationship between cadmium exposure and health problems such as oxidative stress,[377-379] male infertility,[380-384]

hypertension,[385, 386] epigenetic change of DNA,[387] impairment of mitochondrial related activities,[388-392] kidney damage,[393, 394] cancer,[395, 396] diabetes,[397] and disruption of heme synthesis.[398]

Mechanisms of Cd toxicity are multifactorial as the toxicity is organ dependent. Nonetheless, Cd impairs the functions of various organs by disrupting their modes of operation. For instance, Cd-induced cytotoxicity which leads to cell degeneration and/or transmutation is indirectly provoked by oxidative stress on DNA. The consequences of this include;induction of cellular proliferation, inhibition of the apoptotic mechanisms and blocking of the repair mechanisms of the DNA. Generally, oxidative stress occurs when the level of antioxidants in the body is depleted either by redox metals such as chromium and copper or redox-inactive metals such as lead and cadmium, leading to the excessive generation of reactive oxygen species (ROS) such as superoxide radicals ($O_2^{\cdot-}$), hydroxide radicals (HO^-) and hydrogen peroxide (H_2O_2).[366, 399]

4.2.3 Mercury (Hg)

Mercury is a chemical element otherwise known as quicksilver and formerly known as hydrargyrum. It is a heavy, silvery, highly toxic, d-block metal which shares the same group (12) with cadmium and zinc in the periodic table. Mercury is a unique metal, being the only one which exists as a liquid under the standard conditions for temperature and pressure. A large number of organic and inorganic compounds of mercury both in +1 (mercurous) and +2 (mercuric) oxidation states exist. The organic compounds of mercury, also known as organomercurial compounds such as methylmercury, are much more toxic than the inorganic analogues. Mercury is a naturally occurring metal but does not exist freely in nature, but rather as the ore cinnabar (HgS). Unlike lead and cadmium, huge amounts of mercury are often released into the environment from rocks, soils and volcanic eruptions. However, the amount of mercury released into the environment by human activities even outweighs that released by nature.[400] The anthropogenic sources of mercury include; burning of coal and oil, pyrometallurgical process, incineration of municipal and hospital wastes, mining discharge, industrial discharge and agricultural wastes.[400, 401]

The enormous benefits of mercury since antiquity, especially in the fields of medicine and chemistry cannot be underestimated. Mercury was historically used medically, albeit often unsuccessfully, to treat venereal diseases such as syphilis, dental caries, trachoma diseases, skin diseases, hand infections and as diuretic drug.[402, 403]

Despite the acute toxicity of mercury, the use of mercury is commonplace in our society nowadays. For example, the use of dental amalgam currently attracts serious controversy as some researchers consider it biocompatible[404] while others are throwing their weight against its use.[405-407] Mercury is currently a constituent of batteries, fluorescent light bulbs, thermometers, barometers, diffusion pumps and also as an electrode in electrolysis.

The toxicity of mercury is known since ancient times, but the most devastating catastrophes related to mercury poisoning in previous history include; Minamata Bay which occurred in Japan in 1957 as a result of people eating locally harvested fish from rivers previously contaminated by methymercury discharged in waste water from a chemical plant (Chisso Co Ltd).[408] Similar occurrences in Niigata and Iran in the 1960s and 1970s respectively have been reported.[409] Symptoms such as hearing loss, gait abnormality, ataxia, erosive bronchitis, respiratory insufficiency, tremor, excitability (also known as mercurial erethism), loss of weight, loss of memory, insomnia, excessive salivation, and tunnel vision are commonly associated with mercury poisoning.[410-412] In the UK, the saying 'mad as a hatter' emerged from the use of mercury for making felt for hats which caused neurological damage – mercury poisoning is still known today as 'Mad Hatter's' disease.

The route of absorption of mercury depends on whether it is organomercurial or an inorganic compound. Organomercurials are absorbed in the intestinal tract, but much more inhaled as vapour. The absorption rate of elemental Hg is less compared to organic analogues and absorption occurs mainly through inhalation with little ingested dose. Organic and elemental Hg are lipophilic and can cross the blood brain barrier, kidneys and placental barriers but the inorganic counterparts cannot.[413-415] As a result of the ability of organic mercury to cross placental barriers, several cases of post-natal effects of pre-natal exposure have been reported, especially from the contaminated fish consuming community in Japan and victims of mercury-poisoned wheat in Iran.[412, 416-

[418] Besides being a neurotoxin, other organ damage done to the body by organic mercury include oxidative stress, kidney damage, lipid peroxidation, and liver impairment.[419] The biological half-life of mercury in the brain is about 60 days while it is several years in the body.[420, 421]

4.2.4 Arsenic (As)

Arsenic is a multifaceted element having diverse chemical properties which are predicated upon its ability to exist in different oxidation states and bonding configurations, thereby giving rise to numerous inorganic and organic compounds which exist as solids, liquids or gases. Its reactivity is a function of the electronic configuration of its partially filled valence shell with which it both acts as an electron donor and also participate in covalent interactions by sharing of electrons. It is neither a metal nor a non-metal but exhibits properties of both groups, therefore is classified with other group V elements such as boron, as an ill-defined metalloid.[422] Its oxidation states varies from +5 to -3. Despite its high electronegativity (higher than nitrogen but similar to phosphorus), arsenic has a greater tendency to lose electrons (oxidation potential) than both nitrogen and phosphorus, a property which enables it to exhibit cationic character.[326, 423]

The applications of arsenic in human endeavour are paradoxical as it is a potential life terminator and also a potential life saver. For example, the tasteless, odourless, white sugar-like powder Arsenic trioxide (As_2O_3) was used in ancient time for eliminating enemies and aged relatives. It has also been used in metallurgy, pyrotechnics, warfare, pigment and paint.[422, 424] The same supposed poison has as well been used in past decades under the trade name TRISENOX ® as an effective drug against chronic promyelocytic leukemias.[425] In the early 20th century, Salvarsan was discovered as an effective drug for treating syphilis.[426] The use of organoarsenicals such as roxarson in livestock feeds was recently banned in U.S but its use still remains in other countries.[427] Arsenic is still currently finding applications as herbicides and fungicides for wood preservation.[428] It is also used as a component of semiconductors, light emitting diodes, lasers and transistors.

Arsenic has been adjudged one of the most toxic elements. However, the toxicity strongly depends on the oxidation state. For instance, As^{3+} is more toxic than As^{5+} but organoarsenicals are not toxic. The major cause of human arsenic toxicity is contamination of drinking water from geological origin.[429] For example, the notorious perennial arsenic toxicity in Bangladesh and southern India is attributed to the massive concentration of inorganic arsenics which leach from rocks into tube wells.[430] Arsenic toxicity can also occur through dietary and wine intake. The mysterious epidemic of arsenic poisoning which resulted from drinking contaminated beer at a bar somewhere in Manchester in 1900 led to over 6,000 casualties.[431, 432] The World Health Organisation (WHO) has recommended 10 part per billion (ppb) as the safe level for As in drinking water.[433] Accumulation of arsenic in the body can result in thickening and discoloration of skin, numbness in hands and feet, paralysis, blindness, cancer of the bladder, lungs, kidney, liver and prostate as arsenic has the potential to inhibit many enzymes, especially those involved in cellular mechanisms and DNA synthesis/repair.[428, 429]

4.3 Shifting paradigm: conventional adsorbents vs supramolecular envirogels

The use of metals to either trigger the gelation of low molecular weight gelators[434] or tune the properties of the resulting gel is a fast-growing area which has earned itself a special name among the various classes of supramolecular gels.[435] This class of gel is referred to as supramolecular metallogels.[436] Amongst such systems, the use of silver (Ag) to trigger the gelation of small organic molecules and afterward tune the properties of the resulting gel has been widely reported.[435, 437-439] For example, Wu and co-workers synthesized and triggered the gelation of a pyridyl-based gelator **4.1** (Figure 4.3.1) in toluene by adding an ethanolic solution of AgOTf to the solution of the gelator, with interactions between the pyridine ligand and Ag(I) being responsible for assembling a linear complex capable of gelation. The resulting metallogel also demonstrated an anion sensing ability as it underwent a gel-sol transition upon the addition of I^-.[440]

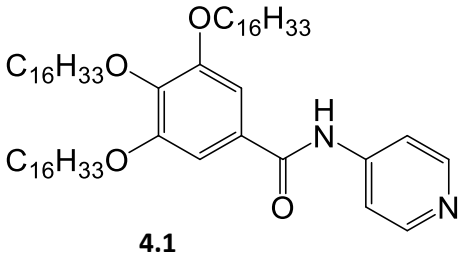

4.1

Figure 4.3.1 Chemical structure of metallogelator **4.1**

Hanabusa *et al* demonstrated the reinforcement of organogels derived from intermolecular interactions between compound **4.2** and **4.3** (Figure 4.3.2) by incorporating Cu^{2+} into the gel.[441] The T_{gel} values increased on the addition of $CuCl_2$ in triethylamine to the gel. The stability enhancement could be attributed to a strong metal-ligand interaction between the metal and the gel fibres.

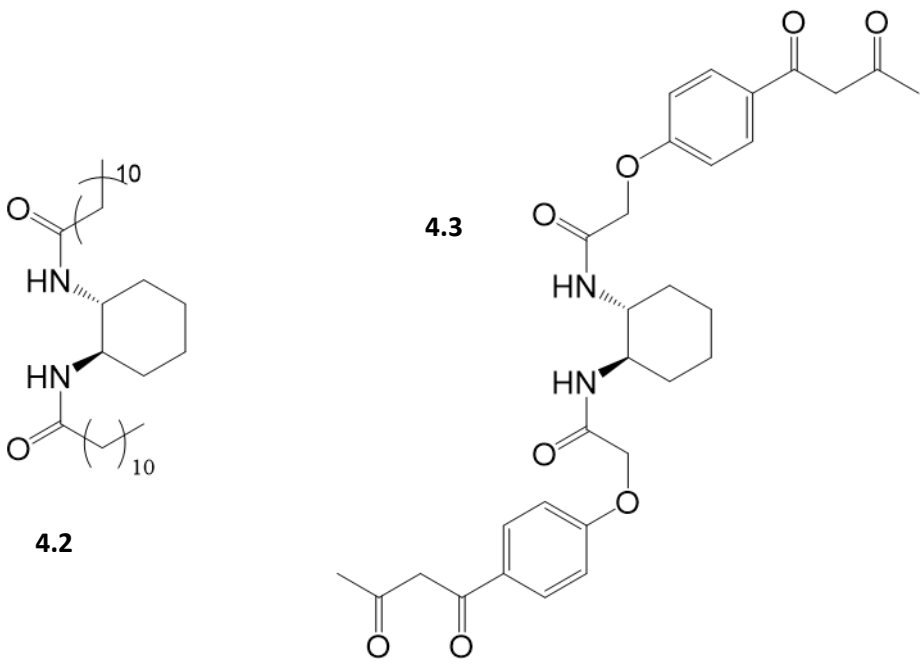

Figure 4.3.2 Chemical structure of gelators **4.2** and **4.3**

Several authors have demonstrated Cu^{2+} and Cu^{+} mediated metallogel formation and their potential applications in areas such as catalysis and anion sensing.[442-447] A number of palladium mediated metallogel formations have also been reported over the last decade. Nanofibres inherent within the gel network are potential solid supports for immobilizing catalysts. The first example of a Pd-metallogel - catalysed organic reaction was demonstrated by Xu *et al*. A wet metallogel of **4.4** and **4.5** (Figure 4.3.3)

doped with $[Pd(en)(H_2O)_2](NO_3)_2$ and $Pd(OAc)_2$ in dimethyl sulfoxide (DMSO) was used to catalyse the oxidation of benzyl alcohol to benzaldehyde with a high turnover rate. Intriguingly, the metallogel remained stable, even after several cycles.[448]

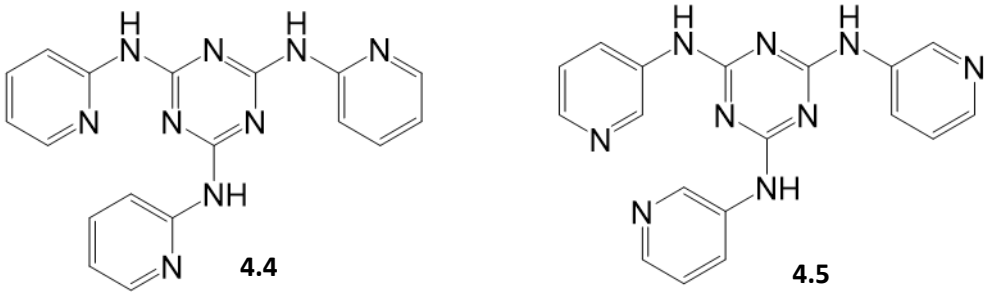

Figure 4.3.3 Chemical structures of gelator **4.4** and **4.5**

Other metals that have been used in in the past decades for metallogel formation include iron (Fe),[449, 450] cobalt (Co),[451] and lanthanides.[452, 453]

Most significantly, the use of heavy metals to induce metallogelation of LMWGs has recently been reported. Wei *et al* reported a family of hydrogelators (Figure 4.3.4).[454] All the gelators were screened for gelation individually and in the presence of Pb^{2+} in water and organic solvents. Only **4.6b** is an efficient hydrogelator both in the presence and absence of Pb^{2+} (Figure 4.3.4b). Surprisingly, it rapidly formed a stable metallo-hydrogel when mixed with $Pb(OAc)_2.3H_2O$ in water. Hydrogelator **4.6b** demonstrated a higher selectivity for Pb^{2+} in the presence of many divalent metals.

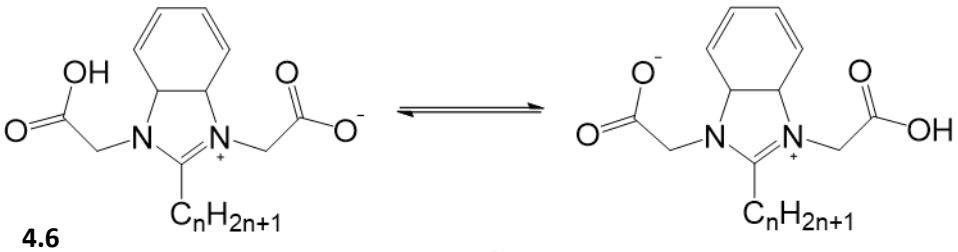

4.6

a: (*n* = 3), **b:** (*n* = 4),
c: (*n* = 5), **d:** (*n* = 7),
e: (*n* = 11)

(b)

Figure 4.3.4 (a) Chemical structures of ligand **4.6** and (b) metallo-hydrogels of **4.6b** / Pb^{2+}

It was also shown that the presence of Pb^{2+} enhances the thermo-reversibility of the metallo-hydrogel of **4.6b**. Interestingly, the metallo-hydrogel of **4.6b** demonstrated a significant degree of responsiveness to EDTA and pH-switching as it degraded when contacted with EDTA (a better chelator for Pb than **4.6b**) and disintegrated to a sol under acidic condition - protonation of the carboxyl group cleaved the **4.6-Pb** complex. This further justifies the importance of Pb as a trigger factor for metallo-hydrogelation of **4.6b**. The residual concentration of Pb^{2+} in the 1:0.5 sample was as low as 76 µM. As such, this material might provide a basis for capturing and removing lead from contaminated water.

Similarly, at about the same time Schneider and co-workers designed a metal binding hairpin peptide (VKVKVKV-CGPKEC-VKVKVKV-NH_2) whose hydrogelation was triggered by complexation with monomethyl arsonous acid (MMA), $ZnCl_2$, $CdCl_2$, $HgCl_2$ or $Pb(NO_3)_2$.[455] Interestingly, addition of stoichiometric amounts of metal ions

to the peptide solution yielded an amphiphilic β-hairpin which self-assembled into rigid self-supporting hydrogels as measured by rheology (Figure 4.3.5). It was hypothesized that formation of the nanostructural architecture is predicated on the foldability of the peptide which is triggered by the chelation of heavy metal ions to the two free cysteinyl thiols flanking the β-turn of the peptide. CD spectroscopy and mass spectroscopy were used to confirm a 1: 1 metal – peptide stoichiometry. TEM imaging shows that hydrogels formed in the presence of MMA and Zn^{2+} ions are composed of elongated, and twisted fibrils with high order laminates. Considering the laborious processes and synthetic costs of this peptide, it is important to mention that for a sustainable water purification system, a low-cost material is desirable.

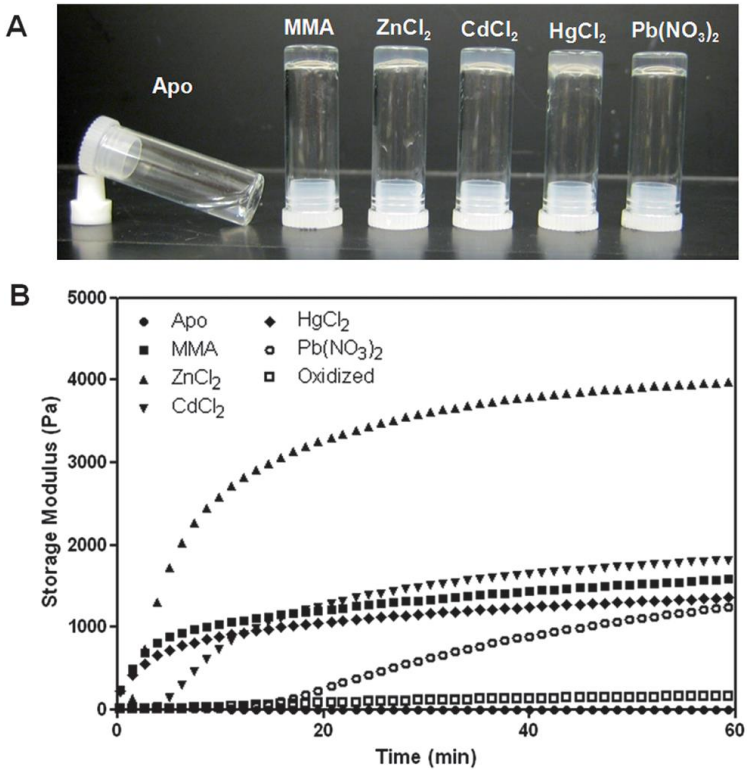

Figure 4.3.5 (A) Image of 1 wt% peptide bulk samples in pH 7.4 buffer (50mM BTP, 150 mM NaCl) at 25 °C in the presence and absence of 1.0 equivalent of MMA, $ZnCl_2$, $CdCl_2$, $HgCl_2$ and $Pb(NO_3)_2$. (B) Oscillatory rheological dynamic time sweeps of 1 wt% peptide in pH 7.4 buffer (50 mM MBTP, 150 mM NaCl) at 25 °C: reduced peptide, oxidized peptide, and reduced peptide in the presence of the metal ions introduced as their indicated salts.

Mercury(II) has also recently been used to trigger the organogelation of a library of quinoxalinone-based molecules **4.7**-**4.10** (Figure 4.3.6).[113, 114] Complexes of the ligands with Hg^{2+} form stable gels in organic solvents following the traditional sonication and heat-cool cycle. Surprisingly, instantaneous gelation of **4.7**-**4.10** by mixing of aqueous solutions of Hg^{2+} with methanolic solution of the ligands were observed. Similarly, aqueous solutions of Co^{2+}, Ni^{2+}, Cd^{2+}, Ba^{2+}, Cu^{2+}, Zn^{2+}, and Ag^{+} was independently added to the organosol of **4.7** but no gelation occurred. The preference of **4.7** for gelation with Hg^{2+} could be attributed to the linear geometry of the resulting complex **4.11** (as shown in Figure 4.3.6).

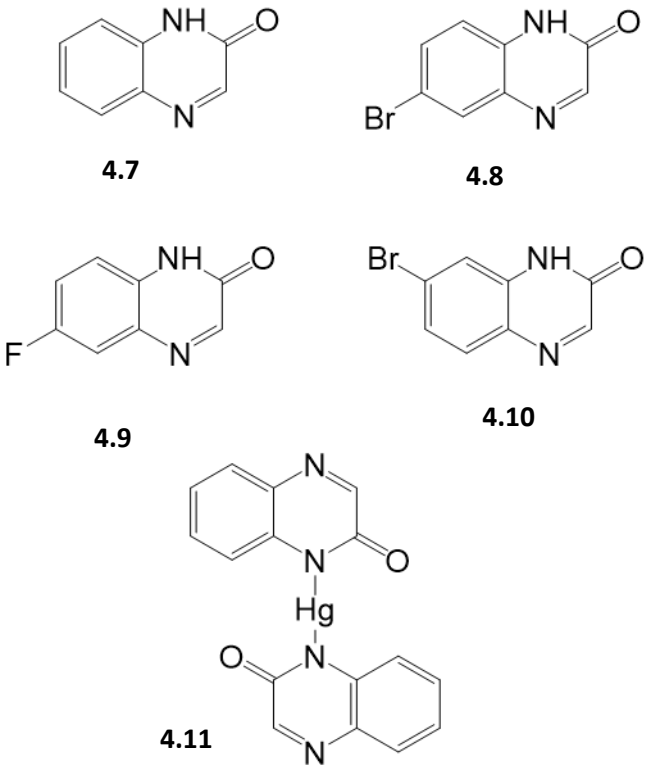

Figure 4.3.6 Chemical structures of quinoxalinone based gelators

As a proof of real-life applications, water samples (river, tap and bottled) contaminated with Hg^{2+} were examined. The concentrations of Hg^{2+} in the water samples were too low to detect so, $Hg(OAc)_2$ was added to the water prior to analysis. Gelator **4.10** formed stable gels when contacted with each of the treated waters, however, gelation was not observed without pre-treatment. Furthermore, **4.7** was able to reduce 3800 ppm Hg^{2+} to 289 ppm by *in situ* gelation of contaminated water. The gels also demonstrated resistance to various anions. As such this system can detect Hg^{2+}

contaminated water via a spontaneous gelation mechanism and also potentially mitigate against the pollution.

In 2014, Sengupta and Mondal demonstrated a dual purpose gel based approach for removing both toxic metals and dyes.[456] In this case, when aqueous solutions of lead acetate and cadmium nitrate were separately added to a DMF solution of pyridine-pyrazole based tris amide gelator **4.12** (Figure 4.3.7), gelation was observed on standing for few minutes. Addition of more than 1.5 equivalent of metal ions to the gelator solution led to precipitation. Similarly, the authors also reported the ability of the gelators to respond to the presence of silver salt in water.[457] Interestingly, besides responding to the presence of silver salt in water, the ligand also transformed Ag^+ ions into nanoparticles. Coordination of the metal ions with the pyridine-pyrazole moiety of the gelator could be attributed to the metallogelation observed. The Pb, Cd and Ag based gels also demonstrated efficient adsorption of cationic dyes. However, it is important to note that DMF is not biocompatible though.[458]

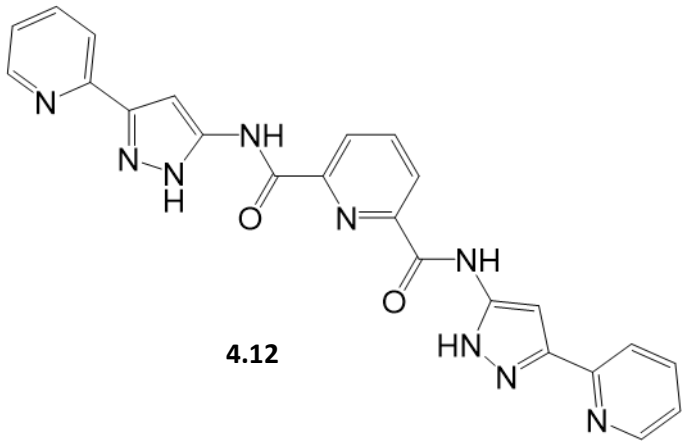

4.12

Figure 4.3.7 Chemical stucture of pyridine-pyrazole based tris amide gelator

Even though supramolecular envirogels hold a promising potential for sequestering pollutant from water resulting from their inherent properties such as large surface area, high porosity and tunability, many of them might be non-biocompatible. Furthermore, there are only very few examples of supramolecular gels that can remove heavy metals from water. Therefore, this project explores the potential of a library of derivatives of a simple gelators based on 1,3:2,4-dibenzylidene-D-sorbitol as nanosorbents for removing lead (Pb), cadmium (Cd), mercury (Hg) and arsenic (As) from a model

polluted water. Parameters such as selectivity, maximum uptake, adsorptive kinetics, adsorptive isotherms thermodynamics, limit of removal, regeneration and reusability of the envirogels will also be discussed.

4.4 Result and discussion

4.4.1 Screening of DBS based envirogels for the uptake of Pb^{2+} and Cd^{2+} ions

The capabilities of the gels of various derivatives of **DBS**, **DBS-NO_2**, **DBS-SCH_3**, **DBS-$COOCH_3$**, **DBS-COOH** and **DBS-$CONHNH_2$** to sequester hazardous metal ions, Pb^{2+} and Cd^{2+} ions from their aqueous nitrate solutions at ambient pH and temperature were investigated. It is important to mention that the gels of **DBS**, **DBS-NO_2**, **DBS-SCH_3** and **DBS-$COOCH_3$** were prepared in water-ethanol mixture (60:40), and are henceforth referred to, alongside the gels of **DBS-COOH** and **DBS-$CONHNH_2$** which were prepared in just water, as envirogels in this chapter. Aliquot solutions of Pb^{2+} and Cd^{2+} (600 mg/ l) were allowed to interact with the envirogels for about 24 h under ambient conditions of pH and temperature. This was achieved by standing the pollutant solution over the gels in sealed vials. The residual metal concentrations in the aqueous solution were then measured with inductively-coupled plasma mass spectrometry (ICP-MS).

Interestingly, all of the hydrogels demonstrated a significant uptake level of Pb^{2+} and Cd^{2+} ions from aqueous solutions with **DBS-$CONHNH_2$** hydrogel demonstrating the highest affinity for both metal ions (Figure 4.4.1). The maximum level of Pb^{2+} uptake onto **DBS**, **DBS-NO_2**, **DBS-$COOCH_3$**, **DBS-SCH_3**, **DBS-COOH** and **DBS-$CONHNH_2$** were 208 (0.36), 142 (0.31), 191(0.44), 120 (0.26), 103 (0.22) and 458 (1.05) mg/ g (mol mol^{-1}) respectively while for Cd^{2+}, they were 162 (0.52), 120 (0.48), 147 (0.62), 121 (0.48), 163 (0.65) and 312 (1.32) mg/ g (mol mol^{-1}) respectively. It should be noted that Cd (112 g mol^{-1}) has a lower atomic mass than (207 g mol^{-1}) Pb which can explain this difference. Generally, all the gelators are capable of capturing the metal ions due to coordinate bonds between the metals and the lone pairs of electron on the oxygen atoms of the hydroxyl groups and possibly the acetal oxygen.[459] As might be expected, the maximum uptake of metal ions observed for **DBS-$CONHNH_2$** is probably attributable to the peripheral amine group and, the most effective ligand for metal ion coordination. As such it was proposed that these ligands

are effectively displayed on the surface of the nanofibres and yield a nanostructure with significant affinity for these heavy metal ions.

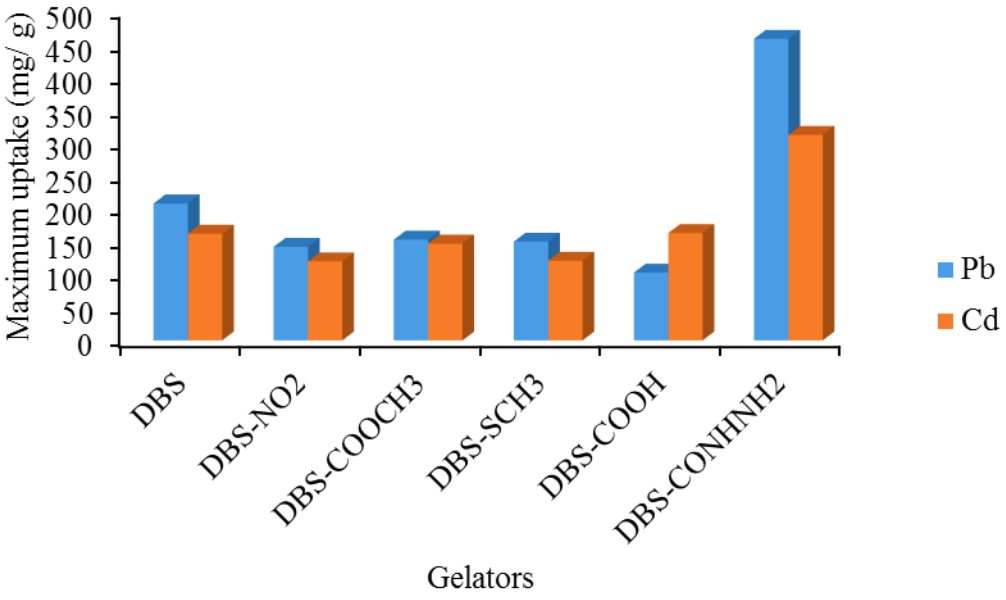

Figure 4.4.1 Maximum uptake of a) Pb^{2+} (blue bar) and b) Cd^{2+} (orange bar) ions onto the envirogels of various gelators

It is perhaps surprising that the envirogel of **DBS-COOH** shows little uptake of the metal ions. This could possibly be attributed the presence of gluconate anion **4.12** (Figure 4.4.2), the end product of GdL induced hydrogelation of **DBS-COOH**, being a better chelator than the protonated **DBS-COOH** within the gel fibres. As such, the metal ions would become concentrated into the supernatant as the complexes formed would be water soluble. The fact that gluconate is very soluble in water makes its removal from the hydrogel, prior to adsorption of metal ions, by simple washing easy.

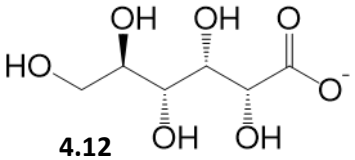

4.12

Figure 4.4.2 Chemical structure of gluconate anion

Consequently, on washing and removal of GdL prior to metal adsorption, the maximum uptake of Pb^{2+} and Cd^{2+} increased from 80 to 103 and 163 mg/ g respectively. The enhanced uptake could be attributed to the fact that in water at about physiological pH, **DBS-COOH** becomes partially deprotonated, hence the carboxylate becomes an additional binding site for the metal ions.

4.4.2 Envirogels of DBS-CONHNH$_2$ vs conventional adsorbents

The ability of the envirogel of **DBS-CONHNH$_2$**, the most effective among the envirogels, to bind heavy metals was compared with those of the conventional adsorbents. Aqueous solutions of Cd^{2+} ($Cd(NO_3)_2$), Pb^{2+} ($Pb(NO_3)_2$), Hg^{2+} ($Hg(NO_3)_2$) and As_2O_3 were therefore interacted with the envirogel and the conventional adsorbents for about 24 h under ambient conditions. However, a low concentration of As_2O_3 was used for the adsorption study due to its low solubility in water. Interestingly, the maximum uptake of the heavy metals onto the envirogels of **DBS-CONHNH$_2$** was 312 (1.32), 458 (1.02), 760 (1.80) and 156 (0. 50) mg/ g (mol/ mol) respectively while a commercially renowned conventional adsorbent (activate carbon (AC)) only uptake of 8, 30, 10 and 5 mg/ g respectively (Figure 4.4.3). This shows that the maximum uptake capacities of the various metal ions onto the envirogel are significantly larger than those of activated carbon. Starbon 800™ (starch-derived carbonaceous mesoporous material)[460] and partially cross-linked polyacrylic acid were also tested for removal of these metal ions but they had no better performance than AC. It is noteworthy that unlike others heavy metals which are cationic, and water-soluble, As species are anionic which cannot interact so well with **DBS-CONHNH$_2$**. As such, less is adsorbed onto the gel nanofibres than the other heavy metals.

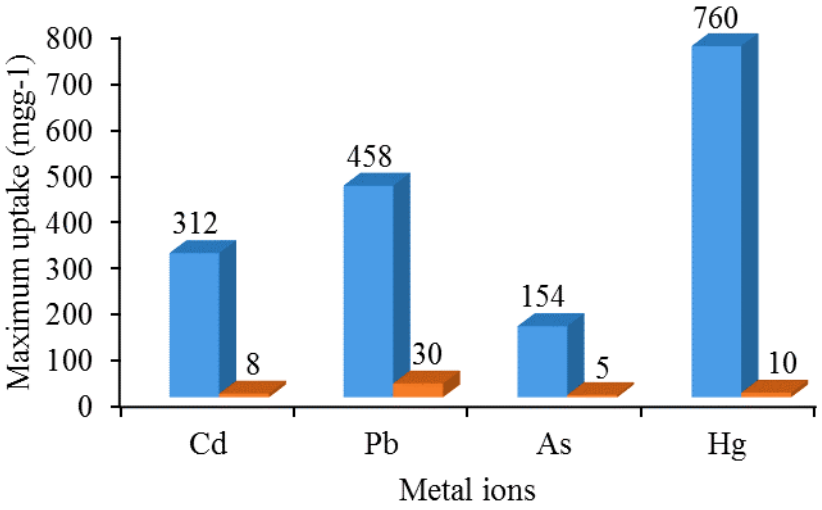

Figure 4.4.3. Maximum uptake of hazardous metal ions onto (a) DBS-$CONHNH_2$ (blue bar) (b) Activated carbons (orange bar); [**mass of adsorbent**] = 4 mg

It is noteworthy that as much as it is important for an adsorbent to have a large surface area for effective pollutant uptake and a large pore volume; factors that make activated carbon a global adsorbent for contaminants, it is equally important for an adsorbent to have a highly reactive surface.[461] The chemical structure of the gelator of **DBS-$CONHNH_2$** has additional functionalities such as the primary amine (NH_2) which are presumed to act as binding sites, and are located on the periphery of the solid-like nanofibres of the resulting hydrogels, for binding the metal ions.[462] Therefore, the highly reactive[463] hydrazide ($CONHNH_2$) functional group makes the nanofibres of **DBS-$CONHNH_2$** a better adsorbent than conventional counterparts and the reported up-to-date best adsorbents.[464-467]

4.4.3 Effect of pH on the uptake of Cd^{2+}, Pb^{2+} and Hg^{2+} ions onto DBS-$CONHNH_2$ hydrogels

Like chitosan[459, 464] and chitin[468] which are versatile adsorbents for environmental remediation, the nitrogen atoms of the amine may also be protonated which would then prevent the lone pair of electrons from effectively interacting with a metal ion. As such, the system may be pH dependent. The pH dependency was therefore investigated by quantifying the degree of metal extraction at different pH values.

The maximum amount of Pb^{2+}, Cd^{2+} and Hg^{2+} adsorbed onto **DBS-CONHNH$_2$** hydrogel fibres increases with increasing pH. Lowest uptake (125 mg Cd/g, 285 mg Pb/g, and 300 mg Hg/g) of the metal ions was observed at acidic pH (pH 4) while 313 mg Cd/g, 458 mg Pb/g and 760 mg Hg/g were observed under near neutral pH conditions (pH 6.5) and a further increase to pH 8 led to a further increase in the amount of Cd^{2+}, Pb^{2+} and Hg^{2+} being extracted to 542, 762 and 905 mg/g respectively (Figure 4.4.4). These high levels of metal extraction at pH 8 are particularly remarkable and suggestive of a highly porous, solvated and interactive gel nanostructure.

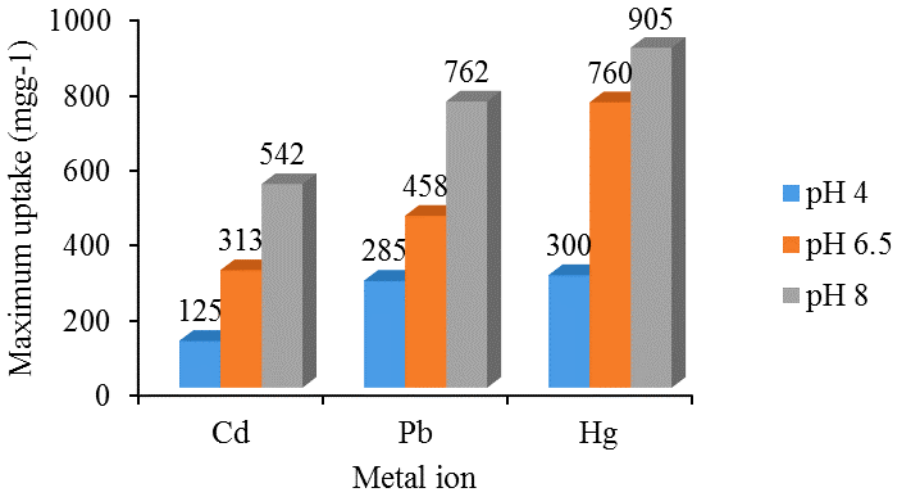

Figure 4.4.4 Effect of pH on the maximum uptake of Pb^{2+}, Cd^{2+} and Hg^{2+} onto the hydrogels of **DBS-CONHNH$_2$**

It is important to mention that at higher pH values (> 9), Pb and Cd solutions form white precipitates which may be attributed to the transformation of the metal ions (M^{2+}) into hydroxides; ($M(OH)_2^+$ and $(M(OH)_2)$,[469] and as such uptake onto the gel no longer occurred.

The low metal uptake at low pH (high acidic) condition is predicated on the fact that the amino groups of the gelator were becoming protonated, thereby leading to a reduction in the number of available binding sites as the metal ions have to compete with H^+ for binding sites. Therefore, inhibition of the mobility of metal ions to the

surface of the hydrogel nanofibres as a result of an electrostatic repulsion between the protonated amino groups (**DBS-CONHNH$_3^+$**) and the metal ions can explain the reason why metal adsorption capacity of the nanofibres diminishes with decrease in pH. At higher pH values, the nitrogen atoms of the amino groups are deprotonated and can undergo chelation with the metal ions on the surface of the gel nanofibre.

4.4.4 Selectivity of DBS-CONHNH$_2$ hydrogel for hazardous metals over beneficial metals

It is not only required that an ideal adsorbent for water purification demonstrates a high uptake of pollutants from water, but also exhibits their selective uptake in the presence of other beneficial components of water. Epidemiologically, essential metals such as calcium are invaluable for healthy living as their deficiencies in drinking water can trigger disorders such as osteoporosis, osteomalacia and hypertension.[470] The ability of **DBS-CONHNH$_2$** hydrogel nanofibres to selectively adsorb Pb^{2+} and Cd^{2+} ions from an aqueous solution of metal ions containing Pb^{2+}, Cd^{2+} ions (20 mg l^{-1}) and a 50-fold excess of both Na^+ and Ca^{2+} ions (1000 mg l^{-1}) was therefore investigated. Interestingly, the nanofibres selectively adsorbed 80% of Pb^{2+} and 60% of Cd^{2+} with an insignificant percentage of Na^+ and Ca^{2+} ions being removed (as shown in Figure 4.4.5).

Therefore, this highly selective heavy metal binding makes the hydrogel a potential adsorbent not only for a real-life applications in water purification but also in chelation therapies.[471, 472]

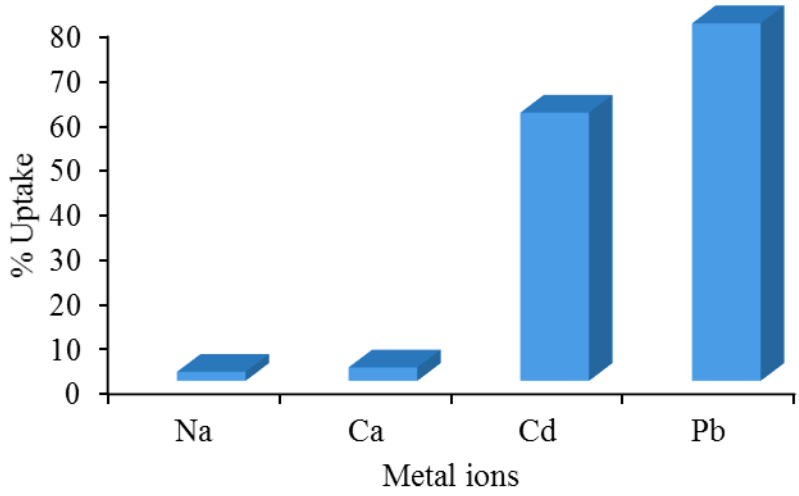

Figure 4.4.5 Selectivity of **DBS-CONHNH$_2$** hydrogel nanofibres for Pb^{2+} and Cd^{2+} ions in an aqueous metal solution containing excess Na^{+} and Ca^{2+} ions

The ability of **DBS-CONHNH$_2$** to discern between toxic and beneficial metal ions could be attributed to the chemical compatibility. According to Pearson's classification,[334, 473] Pb^{2+} and Cd^{2+} ions are regarded as soft acids while the hydrazide could be regarded as a soft base. The HOMO-LUMO transfer of electrons between the soft base and the soft acid underpins the Lewis acid-base interactions between ligand and toxic metals.[473-475] However, s-block metal ions such as Na^{+} and Ca^{2+} are hard acids with small ionic radii and therefore, in a competitive environment, they will be less preferably adsorbed by softer ligands such as hydrazide.[476]

It is also noteworthy that the higher selectivity of **DBS-CONHNH$_2$** for Pb^{2+} ions than Cd^{2+} could be attributed to the difference in their ionic radii. The ionic radius of Pb^{2+} is 119 pm while that of Cd^{2+} is 95 pm. The smaller the ionic radius, the greater the tendency to become hydrolysed (and the harder the metal ion) which leads to reduced adsorption.[477] This would also agree with the preferential uptake of Hg^{2+} (Figure 4.4.4) which is the largest of these three heavy metal cations.

4.4.5 Limit of Pb^{2+}, Cd^{2+} and Hg^{2+} ion uptake onto DBS-CONHNH$_2$ hydrogels

It has always been a general practice to adsorb toxic metals from water when they are present in large quantities but investigating the efficiency of an adsorbent with an extremely low concentration of toxic metal is relatively rare. The United States Environmental Protection Agency (US EPA) has enacted maximum contaminant limits for lead, cadmium and mercury in drinking water as 15, 10 and 2 ppb respectively.[32, 478, 479] It therefore becomes imperative for us to probe the ability of **DBS-CONHNH$_2$** hydrogels to detect and remove toxic metals from their extremely diluted aqueous solutions. It is interesting to see that the hydrogel was able to reduce Pb^{2+}, Cd^{2+} and Hg^{2+} ions in water from initial concentrations (I_o) of 120, 180 and 629 ppb to final concentrations (I_f) of 0, 3 and 2 ppb respectively (Figure 1.4.17). These values are found to comply with the U.S EPA regulated safe level for each of these toxic metals.

Table 4.4.1 Comparison between the limit of toxic metal detection (LDL) by **DBS-CONHNH$_2$** hydrogel and the regulated threshold limits in drinking water. Experimental results were obtained on ICP-MS and dilution effect has been accounted for.

Element	**Experimental LDL (ppb)**		**US EPA Safe Level (ppb)**
	I_o (ppb)	I_f (ppb)	
Hg	629	**2**	**2**
Pb	120	**0**	**15**
Cd	180	**3**	**10**

It is important to mention that the initial concentrations in this experiment were chosen arbitrarily to represent random polluted samples.

4.4.6 Probing interactions between DBS-CONHNH$_2$ ligand and metal ions

In order to understand the ligand-metal interactions responsible for the adsorption of Pb^{2+} and Cd^{2+} ions onto the envirogel nanofibres, techniques such as UV-Vis, Infrared and X-ray photoelectron spectroscopies were used to characterise the ligand-metal complexes formed.

When Pb was adsorbed onto **DBS-CONHNH$_2$** envirogel at higher pH values, the gel became yellowish after 72 h (as shown in Figure 4.4.6a). However, no colour change was observed for Cd under similar conditions. Figure 4.4.6b shows the Uv-visible spectra of **DBS-CONHNH$_2$** before and after Pb uptake at pH 8. The band observed at 288 nm of the virgin gel could be attributed to π-π^* transition of the aromatic rings of the gelator. After adsorbing Pb onto the gel nanofibres, the band shifted to 302 nm which suggests a slight alteration to the electronics of the gelator. The newly emerged band at 466 nm is assumed to be due to charge transfer between the hydrazide moiety of the gelator in **DBS-CONHNH$_2$**-Pb and the metal ion.

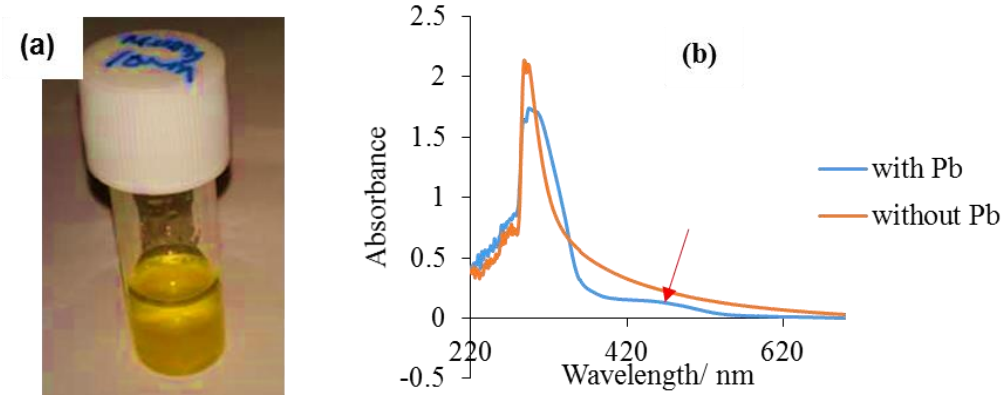

Figure 4.4.6 (a) Photo of **DBS-CONHNH$_2$** envirogel 72 h after Pb uptake (b) UV-Vis spectra of **DBS-CONHNH$_2$** with (blue line) and without (orange line) Pb adsorbed at pH 8.

Infrared spectroscopy was used to probe the interaction between nanofibres of **DBS-CONHNH$_2$** envirogels and metal ions. The spectra of the xerogel (i.e. lyophilized) of **DBS-CONHNH$_2$**, **DBS-CONHNH$_2$ – Pb** and **DBS-CONHNH$_2$ – Cd** are shown in Table 4.4.2. The band at 3315, 1097, 3178, 1644, 1600, 1019, 1573 and 1333 cm^{-1} corresponds to the vibrational frequency of O-H (stretching), C-O (stretching) of

alcohol, N-H (stretching), C=O (stretching), N-H (bending), C-O (stretching) acetal, C=C (aromatic) and C-N (stretching) respectively for the dried xerogel of **DBS-CONHNH$_2$**. However, the spectra for **DBS-CONHNH$_2$**-Pb show that the band of O-H, N-H (stretching), N-H (bending) and C-N shifted to 3309, 3200, 1620 and 1368 cm^{-1} respectively while for **DBS-CONHNH$_2$** – Cd, the bands shifted to 3281, 3205, 1615 and 1338 cm^{-1} respectively. The observed red shifts show that there is a significant interactions between the hydrazide (and OH) group on the surface of the nanofibres and the metal ions.

Table 4.4.2 FT-IR data for key functional groups on **DBS-CONHNH2** xerogels before and after Pb^{2+} and Cd^{2+} uptake

Functional group	DBS-$CONHNH_2$ xerogel (cm^{-1})	DBS-$CONHNH_2$-Pb xerogel (cm^{-1})	DBS-$CONHNH_2$-Cd xerogel (cm^{-1})
$OH_{(stretch)}$	3315	3309	3281
$N\text{-}H_{(stretch)}$	3177	3200	3225(overlap with OH)
$C\text{-}O_{(stretch)}$ alcohol	1097	1095	1090
$C{=}O_{(stretch)}$	1644	1645	1646
$N\text{-}H_{(sbend)}$	1600	1620	1615
$C\text{-}O_{(stretch)}$ acetal	1019	1021	1020
C=C (aromatic)	1572	1573	1574
C-N	1333	1368	1338

X-Ray photoelectron spectroscopy (XPS) is a non-invasive and powerful technique for investigating how metal ions bind to ligands. The chemical state of an element determines its XPS pattern and, hence, binding energy (BE). The binding energy of the photoelectron is characteristic of the element from which the electron is ejected. As such, XPS spectroscopy is a reliable technique that can be used to distinguish different forms of the same element in a material.[480] Therefore, XPS was used to characterize the xerogels of **DBS-CONHNH2** and its complexes with Pb^{2+} and Cd^{2+} ions.

Scheme 1.4.1 shows the XPS spectra for free **DBS-CONHNH2**. The narrow scan N 1s and O 1s were deconvoluted into two peaks corresponding to two different types of oxygen and nitrogen, each represented by a different binding energy. The two peaks, 396.5 and 401 eV under the nitrogen signal can be attributed to NH_2 and NH groups respectively. Structurally, **DBS-CONHNH2** has three types of oxygen; C-O-C, O=C and -OH but two peaks were observed on the O 1s deconvoluted spectra probably because of overlap of O=C and C–O-C as they tend to have similar binding energies. The two peaks, 532.5 and 530 eV under the oxygen signal are attributed to O=C / C-O-C and –OH respectively. The narrow scan of C 1s was deconvoluted into two peaks; 284.9 and 287.8 eV corresponding to two or more types of carbon against the many types of carbon on the structure of the gelator; adventitious C-C / C=C (aromatic), C-O / C-OH / N-C=O respectively.[481, 482] It is important to mention that the observed peak at BE of 283 eV could be attributed to a charging effect.

Figure 1.4.19 Chemical structure of urea based gelators **1.44** and **1.45,** (b) methylene blue **MB**, (c) 1-pyrenemethyl amine **1-PyA** and (d) spermine (**SP**) and Figure 1.4.19 shows the XPS spectra for **DBS-CONHNH2 – Pb** and **DBS-CONHNH2 – Cd** complexes. After Pb^{2+} and Cd^{2+} ions adsorption, new C 1s, O 1s and N 1s peak at BE of 280, 527.8 and 395.5 eV respectively is observed. More so, the N 1s peak at BE of 396.5 eV shifted to 398.5 eV which confirms a significant interaction between the gelator NH_2 appendage and the metal ions leading to the formation of **DBS-CONHNH2** – Metal complexes. The small shift (≈ 0.5 eV) in the BE of O 1s peak at 530 eV suggests that the contribution of lead – oxygen interaction to Pb^{2+} adsorption on the envirogel nanofibres was mainly through a physical adsorption via electrostatic attraction or a weak chemical interaction. The Pb 4f peaks at BEs of 134.5, 137.2, 139.5 and 143 eV suggest that Pb exists in different chemical states on the surface of the nanofibres. For example, the BEs at 139.5 and 143 eV correspond to Pb($4f_{7/2}$) and Pb($4f_{5/2}$) which belong to Pb^{2+} ions respectively.[483] On the other hand, the three Cd 3d peaks at binding energies of 400, 405.5 and 412.3 eV are characteristic of Cd^{2+} ions. BEs at 406 and 412 eV with a separation of 6.8 eV correspond to Cd($3d_{5/2}$) and Cd($3d_{3/2}$) orbit of Cd^{2+} respectively.[484] These observations and those from other spectroscopic techniques therefore confirm the formation of direct chemical interactions between **DBS-CONHNH2** and M^{2+}.

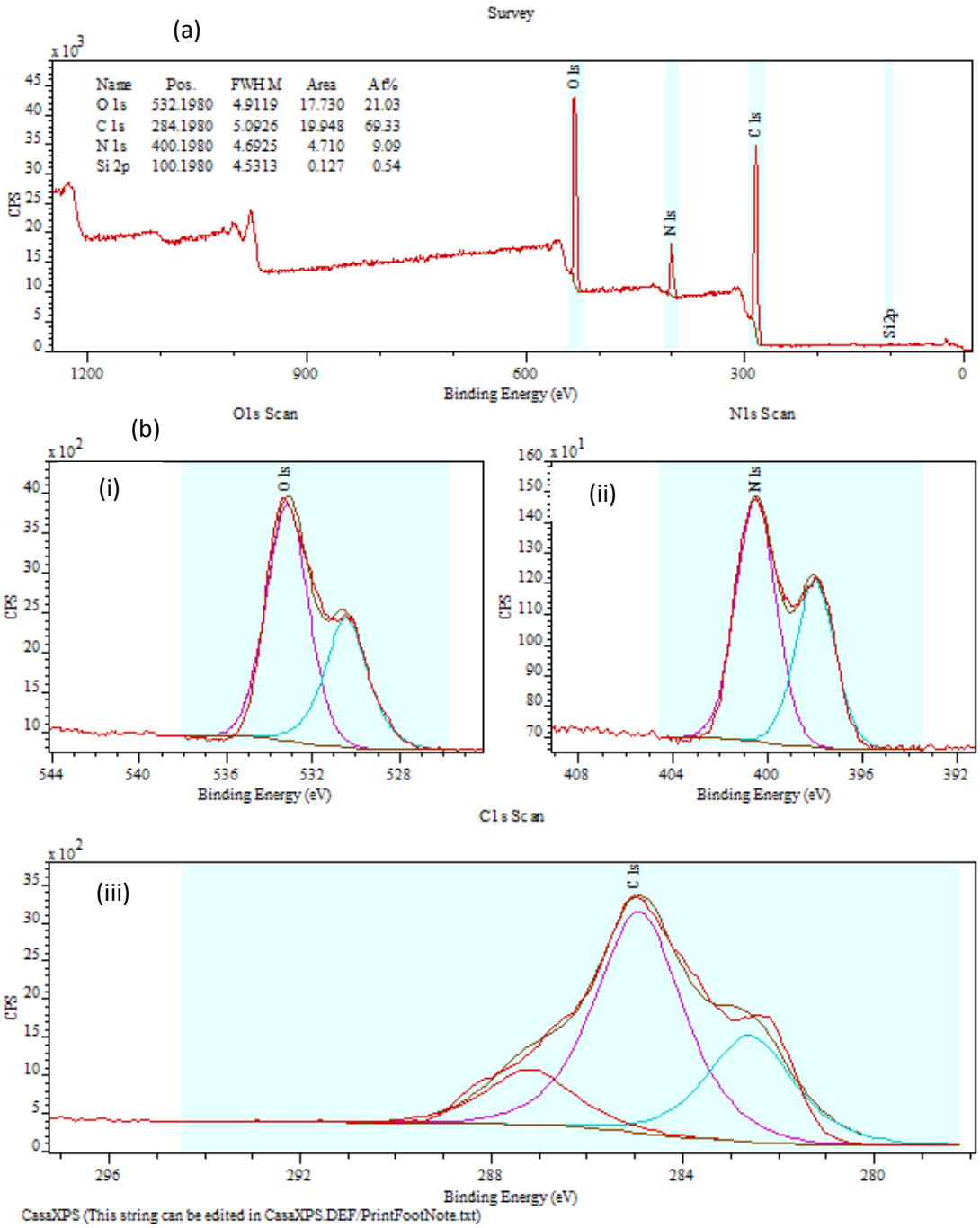

Figure 4.4.7 (a) XP spectrum for the xerogels of (a) native **DBS-CONHNH$_2$** (b) deconvoluted spectra of the narrow scan of (i) O 1s (ii) N 1s and (iii) C 1s.

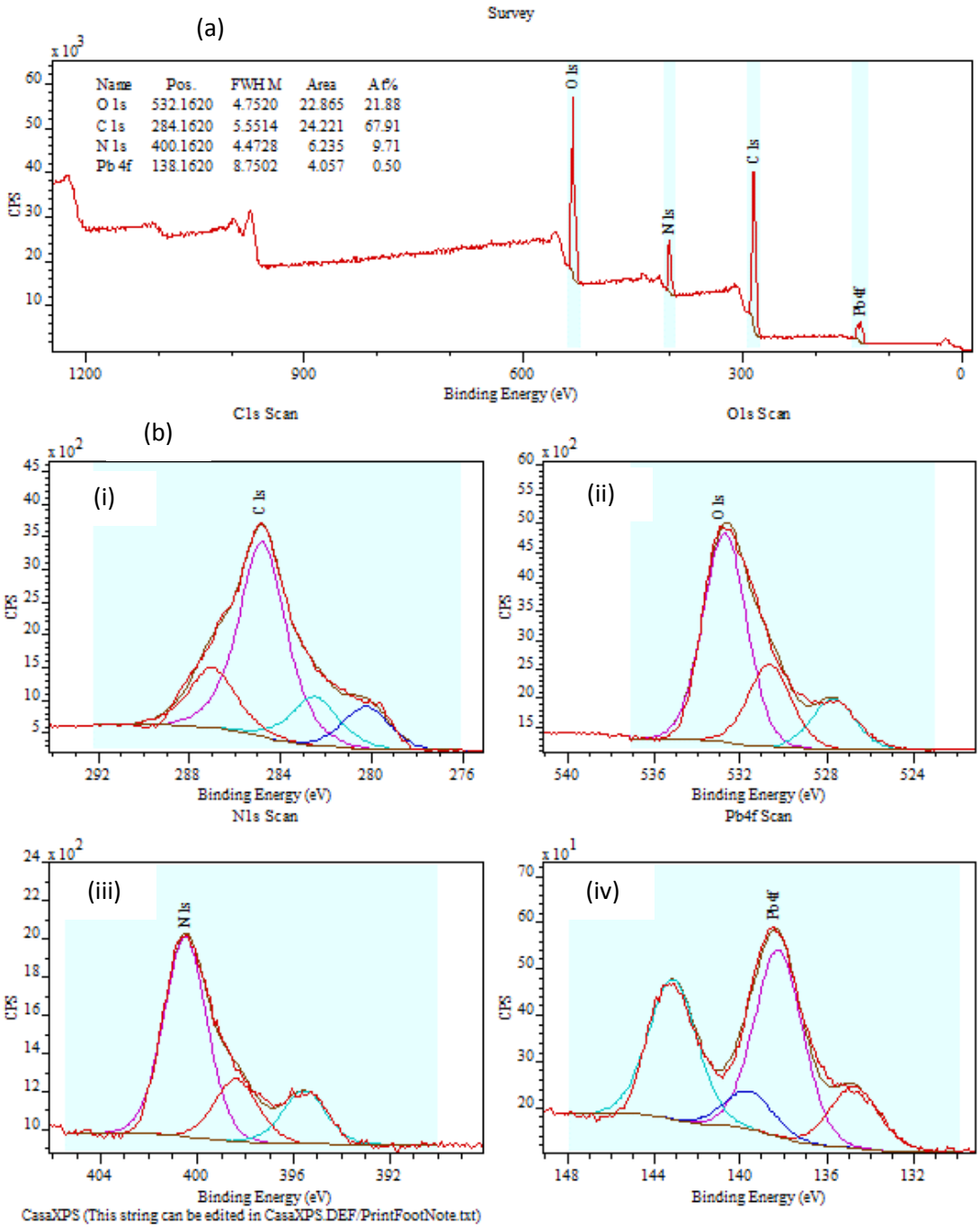

Figure 4.4.8 (a) XP spectrum for the xerogels of **DBS-CONHNH$_2$-Pb** complex (b) deconvoluted spectra of the narrow scan of (i) C 1s (ii) O 1s, (iii) N 1s and (iv) Pb 4f.

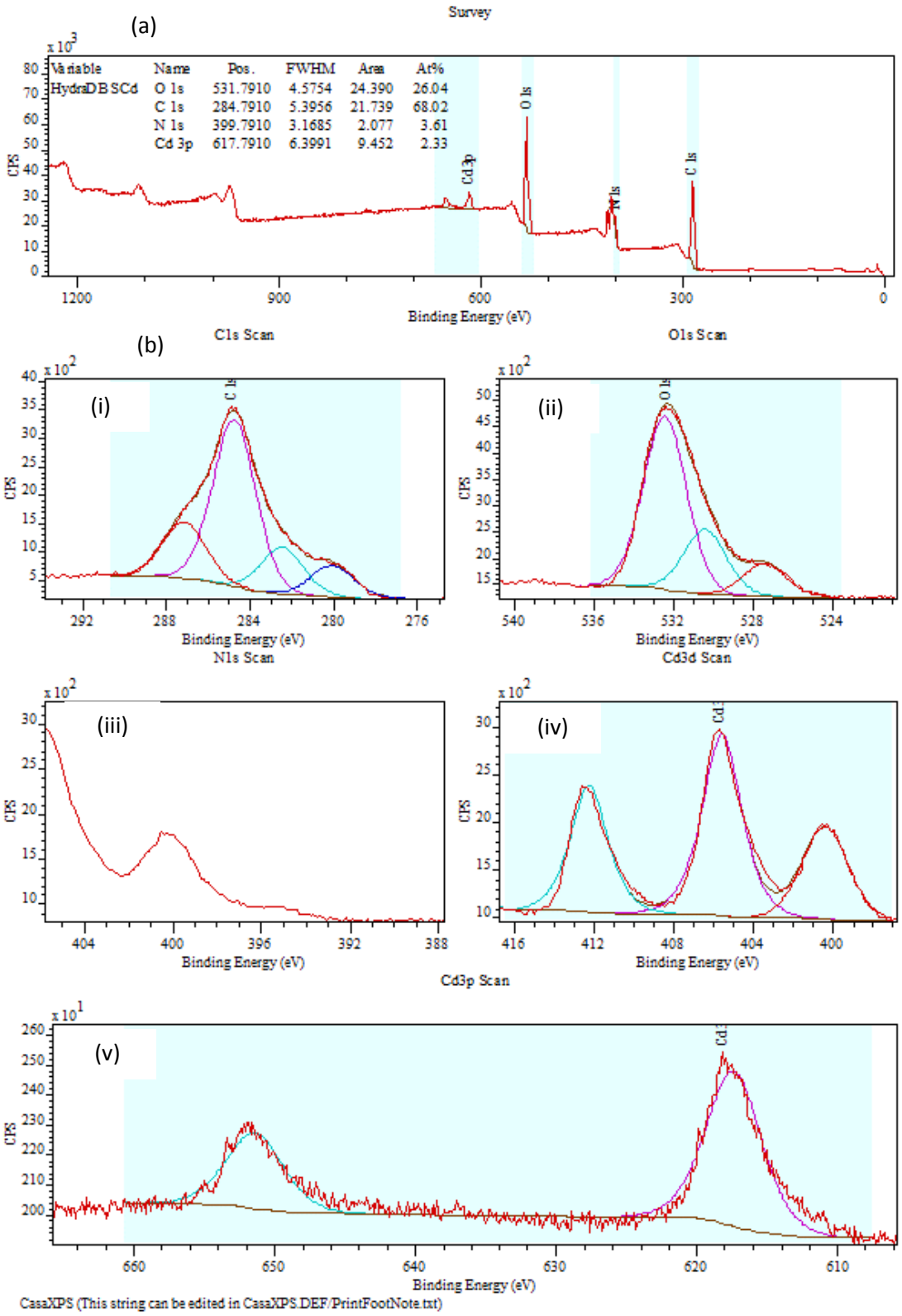

Figure 4.4.9 (a) XP spectrum for the xerogels of **DBS-CONHNH2-Cd** complex (b) deconvoluted spectra of the narrow scan of (i) C 1s (ii) O 1s, (iii) N 1s (iv) Cd 3d and (v) Cd 3p.

4.4.7 Adsorptive kinetic studies for the adsorption of Pb^{2+} and Cd^{2+} ions onto the nanofibres of DBS-CONHNH$_2$ hydrogels

The kinetics of the metal adsorption process were evaluated based on fitting to a pseudo-second-order model, which was characterised as the best kinetic model for **DBS-CONHNH$_2$**-pollutants systems in chapter 3 of this thesis. The experimental data were fitted to both pseudo-first-order and pseudo-second-order kinetics (Equation 3.2.3 and 3.2.5) but the correlation coefficients ($R^2 \approx 0.99$) for the pseudo-second-order kinetic were closer to unity than those for the pseudo-first-order kinetics. The maximum adsorption capacity ($q_{max,\ cal}$) of the envirogels were extrapolated from the intercepts of Figure 4.4.10 a and b. The values of $q_{max,\ cal}$; 454 mg Pb^{2+} / g and 312 mg Cd^{2+} / g for pseudo-second-order kinetics are almost equal to the experimental values ($q_{max,\ exp}$); 458 and 313 mg g^{-1} for Pb^{2+} and Cd^{2+} ions, respectively.

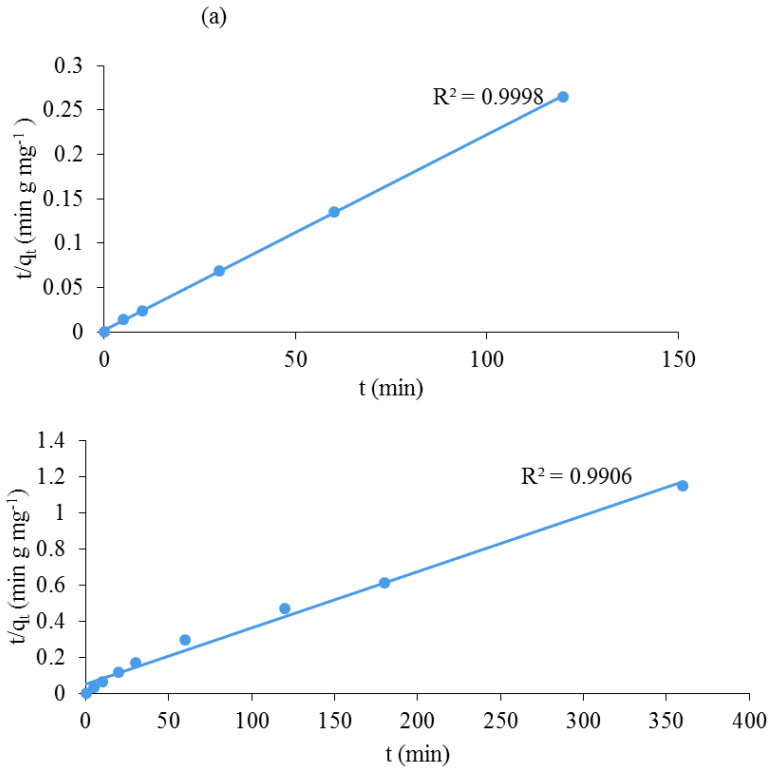

Figure 4.4.10. Pseudo-second-order adsorptive kinetics of (a) Pb^{2+} and (b) Cd^{2+} onto the hydrogel of **DBS-CONHNH$_2$**

The rate of Pb^{2+} ion uptake (2.4 x 10^{-3} g $mg^{-1}min^{-1}$) is much higher than that of the Cd^{2+} (1.0 x 10^{-4} g mg^{-1} min^{-1}) as shown in Table 4.4.3. This would suggest that the lead salt is better able to diffuse into the gel and interact with the gel nanofibres – lower ionic radius of Cd^{2+} means it is more ionic than Pb^{2+} and as such may hinder diffusion and uptake.

Table 4.4.3 Summary of pseudo-first-order and pseudo-second-order kinetics for the adsorption of Pb^{2+} and Cd^{2+} ions onto the hydrogel of **DBS-CONHNH2**

Pseudo 1st order kinetic			**Pseudo 2nd order kinetic**			**Metal ions**
Q_e(mg g^{-1})	**K_1 (min^{-1})**	**R^2**	**Q_e (mg g^{-1})**	**K_2(g$mg^{-1}min^{-1}$)**	**R^2**	
134	0.0510	0.6819	454	0.0024	0.9998	Pb
128	0.0016	0.8592	313	0.0001	0.9986	Cd

4.4.8 Isotherms and thermodynamics of the adsorption of Pb^{2+} and Cd^{2+} onto the hydrogels of DBS-CONHNH2

In order to further understand the mechanisms underpinning the adsorption of the hazardous metals onto **DBS-CONHNH2** the equilibrium data obtained were fitted into the Langmuir (Equation 4.4.1) and Freundlich isotherm equations.[318, 485, 486]

$$\frac{1}{q_e} = \frac{1}{q_{max}} + \frac{1}{q_{max} b} . 1/c_e \qquad \text{(Equation 4.4.1)}$$

Where q_e is the amount of metal adsorbed (mg/g) unto hydrogel, q_{max} is the maximum adsorption capacity according to Langmuir chemisorption (mg/g), c_e is the concentration (mg/l) of metal remaining in the solution at equilibrium and b is the energy of adsorption (l/mg). The plot of $1/q_e$ vs $1/c_e$ should yield a straight line (Figure

4.4.11) for chemisorptive behaviour in which there are specific interactions between the metals and the solid-like network.[305]

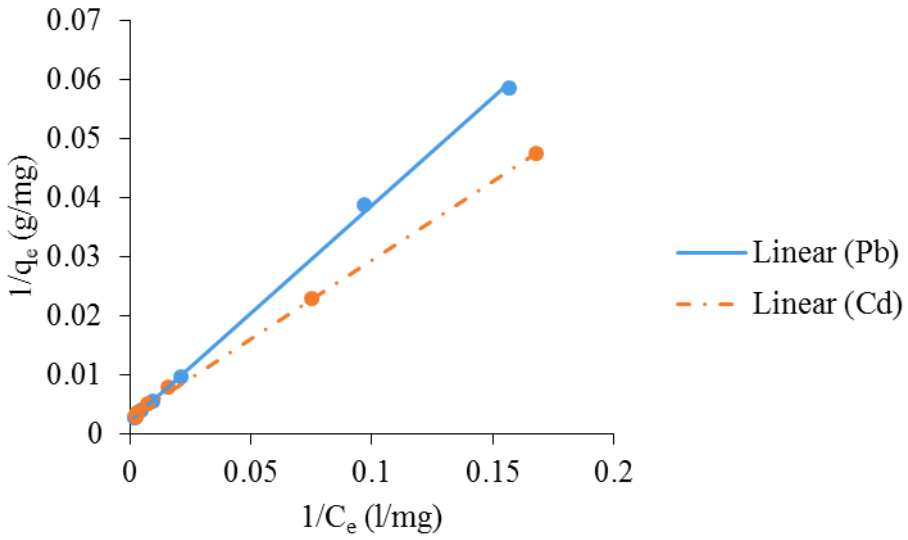

Figure 4.4.11 Langmuir isotherm for the adsorption of (a) Pb^{2+} and (b) Cd^{2+} ions onto hydrogels of **DBS-CONHNH2** at room temperature and ambient pH. (R^2 = 0.9992)

The Freundlich Isotherm describes a heterogeneous surface system. Its mathematical expression is shown in equations (4.4.2)

$$\text{Log}_{10}q_e = \text{Log}_{10}K_f + \frac{1}{n}\,\text{Log}_{10}C_e \qquad \text{(Equation 4.4.2)}$$

Where K_f = Freundlich constant and n = heterogeneity factor (g/l) are the slope and intercept for the plot of $\text{Log}_{10}\,q_e$ against $\text{Log}_{10}\,C_e$ respectively (Figure 4.4.12).

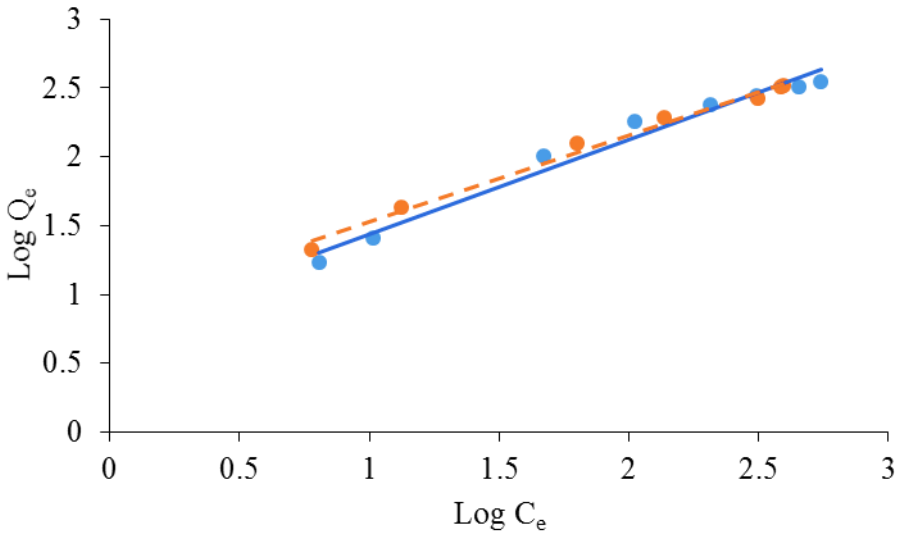

Figure 4.4.12 Freundlich isotherm for the adsorption of (a) Pb^{2+} and (b) Cd^{2+} ions onto hydrogels of **DBS-CONHNH$_2$** at room temperature and ambient pH

The correlation coefficients for the Langmuir isotherms for the adsorption Pb^{2+} and Cd^{2+} ions ($R^2 \approx 1.0$) are higher than those of the Freundlich isotherms ($R^2 \approx 0.96$). The high correlation coefficients for the Langmuir isotherm could be interpreted to mean that a single metal ion occupies a single surface site and there are no lateral interactions between the adsorbed Pb/Cd ions. Nonetheless, the observed high R^2 for the Freundlich isotherm would also support the heterogeneity of binding sites on the nanofibres of **DBS-CONHNH$_2$** hydrogels. As shown in Table 4.4.4, the values of maximum metal ion uptake (Q_{max}) onto the hydrogels deduced from the Langmuir isotherm equation only differ slightly from the experimentally - obtained maximum uptake (Q_{expt}) for both Pb^{2+} and Cd^{2+} ions.

Table 4.4.4 Adsorptive isotherm parameters for the adsorption of Pb^{2+} and Cd^{2+} ions onto the hydrogels of **DBS-CONHNH$_2$**

Metal ions	**Q_{expt} (mg/g)**	**Langmuir isotherm**			**R_L**	**Freundlich isotherm**		
		Q_{max} (mg/g)	**b(l/g)**	**R^2**		**K_f**	**n**	**R^2**
Pb	458	455	0.006	1.00	0.15	6.5	0.66	0.9655
Cd	312	313	0.008	0.9993	0.15	10.5	0.44	0.9644

The values (R_L = 0.15) of the dimensionless equilibrium parameter, R_L also known as separation factor, and the values (0.44 – 0.66) of n deduced from the Freundlich isotherm equation are used to establish the favourability of the adsorption systems.[318] Although there was a significant kinetic difference in favour of Pb, the thermodynamic preference is similar.

The effect of temperature on adsorption was investigated at four temperatures (283, 293, 303 and 308 K) with a constant weight of **DBS-CONHNH$_2$** gelator (4 mg) and a constant concentration of metal ions (0.6 g/ l). Figure 4.4.13 shows that when the ambient temperature was raised from 283 to 308 K, the maximum metal uptake, q_{max} was augmented from 400 to 625 mg/ g and 256 to 450 mg/ g for Pb^{2+} and Cd^{2+} ions respectively. This may suggest that the gel nanostructure is more open and accessible in order to maximise interactions between nanofibres and the metal ions at elevated temperature. It clearly suggests that binding is entropically driven

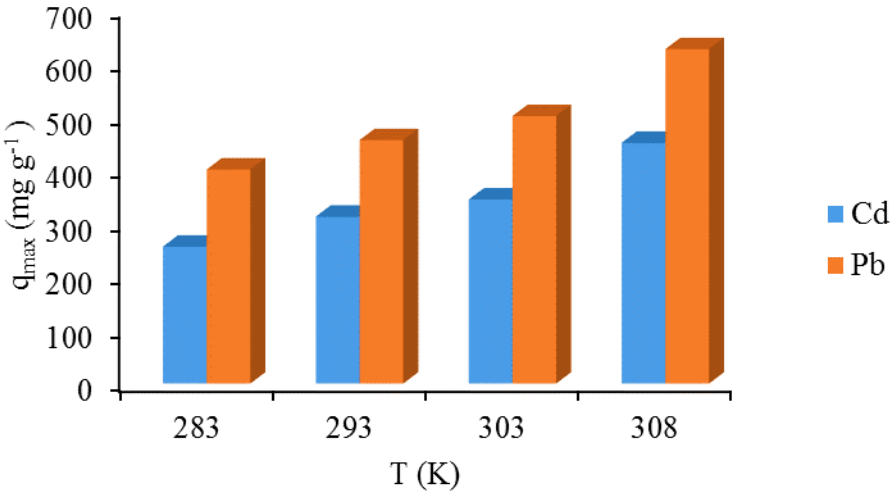

Figure 4.4.13 Effect of temperature on maximum metal uptake onto **DBS-CONHNH2** envirogel.

The thermodynamic properties associated with the adsorption systems were analysed using the classic van't Hoff equations and the well-known thermodynamic expressions (Equations 4.4.3- 4.4.5).

$$\log K = \log(c_s/c_e) = -\frac{\Delta G}{2.303RT} \qquad \text{Equation 4.4.3}$$

$$\Delta G = \Delta H - T\Delta S \qquad \text{Equation 4.4.4}$$

Therefore,

$$\log K = -\frac{\Delta H}{2.303RT} + \frac{\Delta S}{2.303R} \qquad \text{Equation 4.4.5}$$

Where K is the equilibrium constant, C_s (mg l^{-1}) is the concentration of metal adsorbed onto the hydrogel nanofibres at equilibrium, C_e (mg l^{-1}) is the equilibrium concentration of metal remaining in solution at equilibrium, ΔG (kJ mol^{-1}) is the Gibbs free energy change, ΔH (kJ mol^{-1}) is the change in enthalpy and ΔS (J mol^{-1} K^{-1}) is the entropy. The values of ΔH and ΔS were deduced from the slope and intercept respectively of the plot of logK versus1/T. The adsorption thermodynamic parameters for Pb^{2+} and Cd^{2+} ions at given initial metal ions concentrations (100, 200, 350, 600 and 900 mg/l) and temperature (283, 293 and 308 K) were investigated. The positive values of the enthalpy and the entropy suggest that the adsorption process is endothermic in nature and entropically driven for both Pb^{2+} and Cd^{2+} ions (as shown in Figure 4.4.14). This observation would suggest that desolvation of the metal ions on binding to the gel framework or desolvation of the gel network on binding to the metal, play very important roles in the binding event – this is reminiscent of chelate

binding which has a significant entropic component. The negative values of the ΔG suggests the spontaneity of the adsorption processes, especially at low concentrations of the adsorbates for both Pb^{2+} and Cd^{2+} ions respectively. Figure 4.4.15 shows that the negative values of ΔG for both Pb^{2+} and Cd^{2+} ions increases with increase in temperature. This could imply that the adsorption process is spontaneous and favourable at lower temperature. It is noteworthy that the positive values of ΔG at high initial metal concentration, especially for Cd^{2+} ions could be attributed to the fact that at high concentrations, the metal ions compete for available binding sites leading to electrostatic repulsion between two neighbouring metal ions and unfavourable uptake. But the case is slightly different for Pb^{2+} ions which could explain the reason why more Pb^{2+} ions were adsorbed than Cd^{2+} ions, even at high initial concentration – Cd^{2+} is more ionic, therefore, repulsions are more significant.

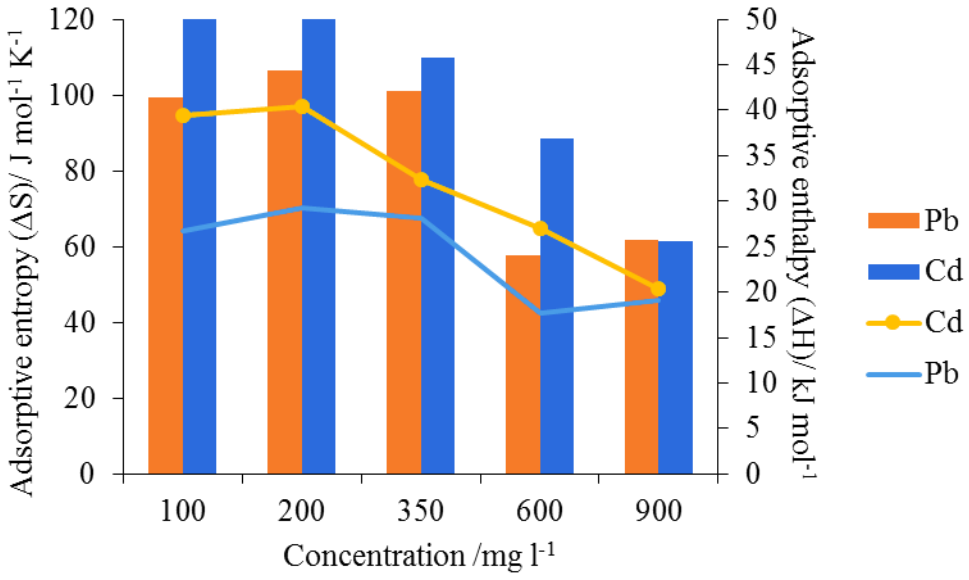

Figure 4.4.14 Adsorptive enthalpy (line graph) and entropy (bar graph) for $Pb^{2+}$and Cd^{2+} ions onto nanofibres of **DBS-CONHNH2** envirogels at various concentrations.

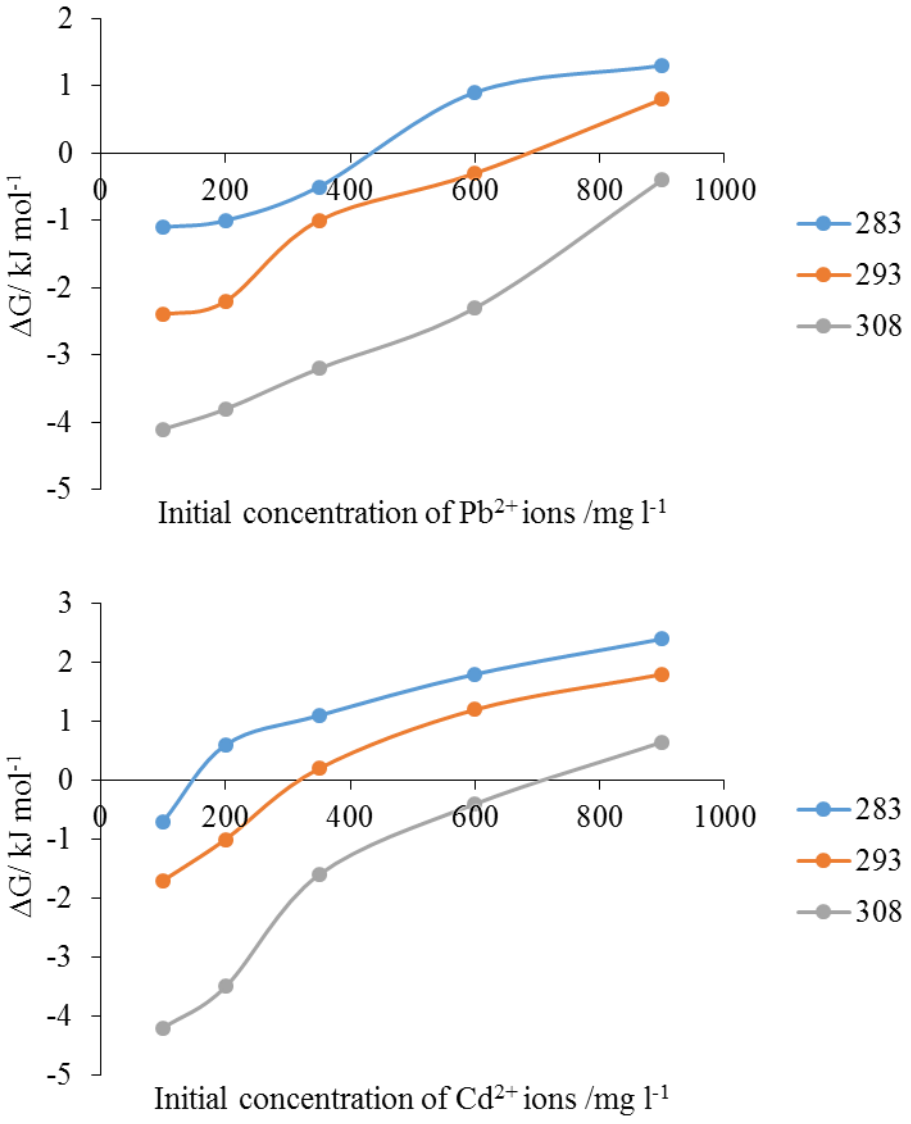

Figure 4.4.15 Gibbs free energy change for the adsorption of (a) $Pb^{2+}$and (b) Cd^{2+} ions onto nanofibers of **DBS-CONHNH$_2$** envirogels across a range of concentrations at 283, 293 and 308 K.

Similar trends of adsorptive thermodynamic properties have recently been reported for the adsorption of Pb^{2+} and Cd^{2+} ions onto modified chitosan adsorbents,[487] these systems are not gel – based. This is the first report in which self-assembled gels have been characterised in this way.

4.4.9 Recyclability of envirogels

Regeneration of spent envirogels after heavy metal uptake was investigated. In this case, ethylenediaminetetraacetic acid (EDTA, 0.1 M) was added on top of the envirogel and allowed to percolate at room temperature for 4 h. EDTA was chosen because it is a hexadentate ligand and as such, a better chelating agent than **DBS-CONHNH$_2$**.[471] The disappearance of the yellow colour of envirogel – Pb^{2+} complex formed at pH 8 was used to monitor the desorption of Pb^{2+} from gel nanofibres – under visual observation and concentration of Pb^{2+} ions desorbed into the supernatant aqueous layer was quantified by ICP-MS. This cycle was repeated four (4) times with little or no decline in the uptake capacity of the envirogel (Figure 4.4.16).

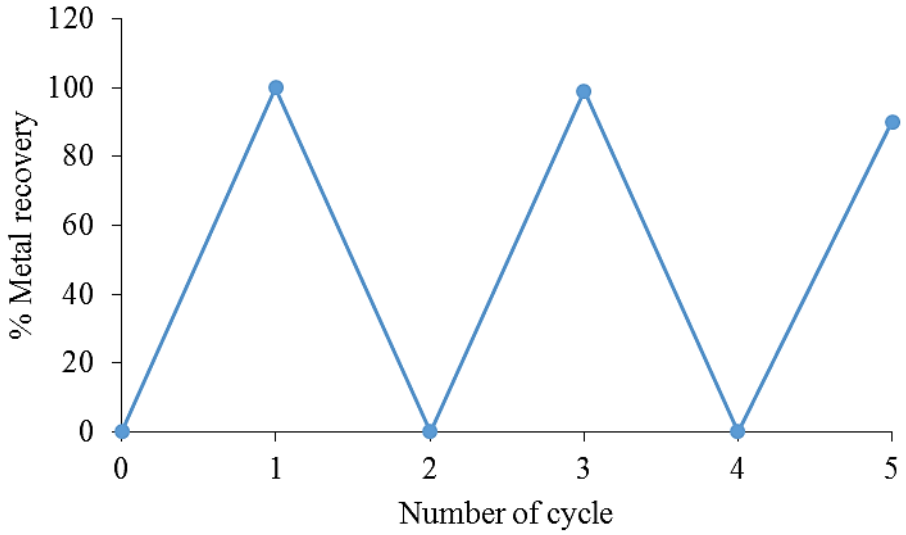

Figure 4.4.16 Regeneration of **DBS-CONHNH$_2$** envirogel by washing with EDTA

4.5 Conclusion and Future Work

Dibenzylidene-D-sorbitol (**DBS**) and its derivatives were used to adsorb heavy metals from model wastewater. Among the gelators investigated for this purpose, **DBS-CONHNH$_2$** envirogels demonstrated the highest uptake of hazardous metals and have the advantage of forming gels in 100% water. Therefore, its performance with regards to the uptake of Pb^{2+}, Cd^{2+}, Hg^{2+} and As_2O_3 was matched against that of conventional adsorbents such as activated carbon. It was observed that the metal uptake capacity of **DBS-CONHNH$_2$** envirogels increases with pH. The nanofibres of **DBS-CONHNH$_2$**

envirogels demonstrated a high selectivity for the heavy metals amidst beneficial metals and could also detect and capture heavy metals from aqueous solutions, reducing them to ultra-trace concentration.

Spectroscopic techniques such as FT-IR and in particular XPS reveal that the amine (NH_2) group of the hydrazide functionality is the principal binding sites for the metals. The kinetics of metal binding to the envirogel fits better to pseudo-second-order than pseudo first-order adsorptive kinetics while the adsorptive isotherm fits Langmuir model. The adsorptive thermodynamics of Pb^{2+} and Cd^{2+} ions on the envirogel nanofibres is spontaneous and entropically favoured but enthalpically disfavoured.

In order to recycle and reuse envirogels, EDTA was used to wash spent envirogels and the cycle was repeated more than four times without any noticeable decline in the metal uptake capacity of the envirogels.

The extreme potency of **DBS-CONHNH$_2$** towards heavy metal uptake compare with the commercial conventional adsorbent is attributed to its amphiphilicity, nanostructured morphology and specific programming for selective uptake. As such, **DBS-CONHNH$_2$** is a potential replacement for activated carbon.

In the future, it is hoped that the ability of the envirogels to simultaneously remove both toxic dyes and heavy metals from a model wastewater containing both will be investigated as this kind of mixture characterizes wastewaters from textile and tanning industries. It can also be envisaged that these envirogels would be able to remove radioactive wastes such as uranyl ions ($[UO_2]^{2+}$) present on wastewater generated from nuclear plants.

5 Chapter 5 - From supramolecular envirogels to conductive nanogels for high-tech applications

Results reported herein have been submitted for publication in *Angew. Chem. Int. Ed.*, 2015.

5.1 Introduction

The self-assembly of low molecular weight building blocks is a biomimetic approach for creating a wide range of supramolecular ‘‘organelles’’ having diversity of morphology and function.[111, 488-490] In these self-assembled nanostructures, the molecular blocks are held together by the interplay of non-covalent interactions such as hydrogen –bonding π-π stacking, van der Waals interactions. As such, the properties such as the shape and size of the material can be controlled at the micro and/or nanoscopic level.[491] Tunability of the resulting nanostructures has endowed them with many functions in material science. For example, the use of the self-assembled nanofibrillar network (SAFIN) of supramolecular gels as a template for inorganic nanoparticulates thereby yielding anisotropic nanostructures and hybrid materials with enhanced activity has attracted widespread attention in the past decades.[63-65, 492, 493] In the preparation of such systems, it is not only the synthesis of individual components that matters but also fabrication of dissimilar building blocks with pathways by which they can interact and influence each other and thereby leads to the generation of material with distinctive features.[494, 495]

Hydrogels, due to their high water content, biocompatibility and biodegradability are widely applied in regenerative medicine.[65] However, they are generally fragile and non-conductive. Therefore, in order to increase the scope of their applications, for example as bioactuators,[496] biorobotics, biosensors, fuel cells, energy storage,[497] super capacitors,[498] regulators of electro-active cells and 3-D electronic-tissue materials,[499-501] nanomaterials such as noble metals nanoparticles and carbon-based nanoparticles/tubes have been incorporated into hydrogels to impart both conductivity and mechanical strength onto the resulting hybrid hydrogels.[502] It is also worth noting that the hydrogel fibres sometimes help to align the nanoparticles into a well-defined three-dimensional arrays as well as immobilising them.[497] As such, conductive gels

are functional materials that synergize both the 3-dimensional nanostructure of gels and the conductivity of organic and/or inorganic conductors.[222, 260] Gel materials are suitable for applications involving transportation of charge due to the high aspect ratio of the inherent solid-like nanofibres – which favours the movement and separation of charges.[503] There are a number of commercially available conductive gels - ECG conductive gels, ePen conductive gels, Vector electrolysis- high conductivity electrolyte gels.[504-506] It also worth noting that despite the myriad of low molecular weight organogelators that have been used to fabricate gel-nanoparticles hybrid materials in the past decades,[222, 507] low molecular weight hydrogel – nanoparticles hybrid materials still remain relatively rare.[508, 509]

Syntheses and behaviour of gel network-templated metal nanoparticles with LMWG having functional groups capable of capping and binding nanoparticles have become a burgeoning field among many research groups in recent times. In 2004, Hanabusa and co-workers synthesised the first gel-nanoparticles in this category.[510] *Trans*-1,2-bis(alkylamide)cyclohexane **5.0** (Figure 5.1.1) appended with two thiol groups formed physical gels in a range of organic solvents via the traditional heat-cool cycle process. Gold nanoparticles (AuNPs) synthesized according to the method of Brust[149] were added to the gelator solution and the mixture heated above 60 °C to dissolve **5.0** then cooled down to room temperature to form a gel. Transmission electron microscopy (TEM) analysis was used to confirm the presence of AuNPs on the gel fibres.

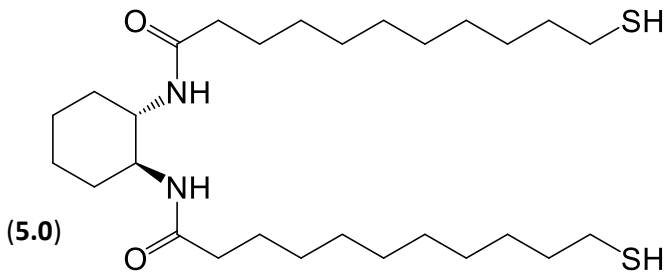

(**5.0**)

Figure 5.1.1 Gelator **5.0** containing thiol groups to bind to GNPs

Schenning and co-workers have developed gel-nanocomposites which comprise π-conjugated oligo(*p*-phenylenevinylene) (OPV1/OPV2) **5.2 / 5.3** (Figure 5.1.2) tapes and AuNPs.[492]

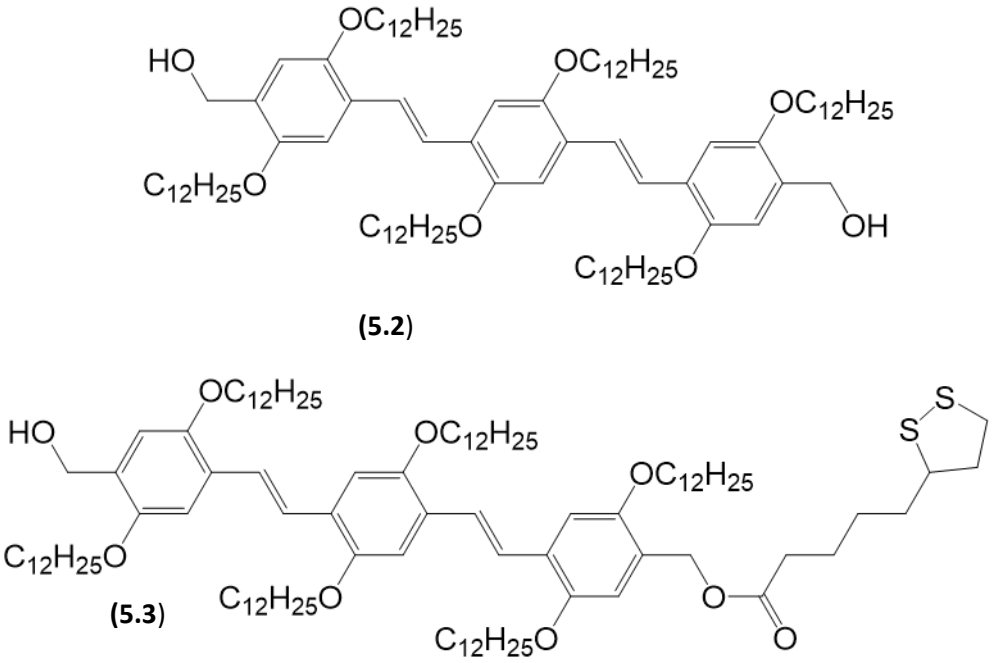

Figure 5.1.2 Structures of π-conjugated oligo(p-phenylenevinylene)

The OPV1/OPV2-AuNPs hybrid supramolecular tapes were formed by mixing OPV1 and OPV2-Au in toluene, followed by the traditional heating-cooling cycle. As shown in Figure 5.1.3, the AuNPs formed two parallel rows along the edges of the tape-like structures. The proximity of the gold nanoparticles to the π-conjugated tapes leads to energy transfer from the molecule to the metal nanoparticles in the gel state.

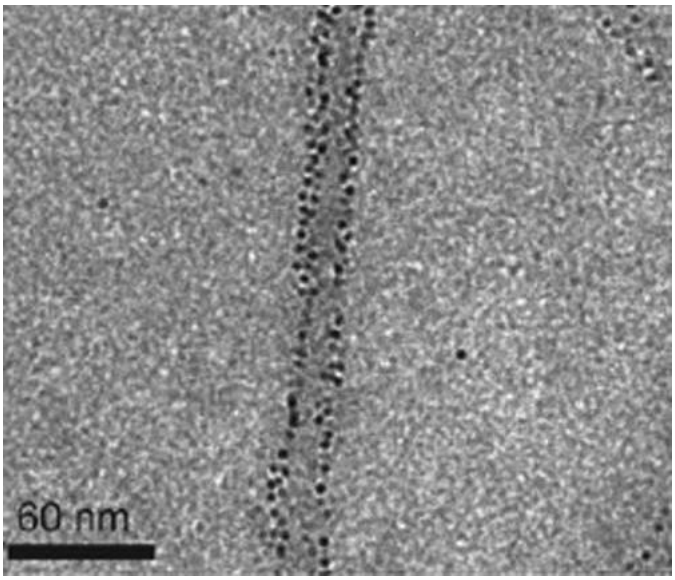

Figure 5.1.3 TEM images of the OPV1/OPV2–Au (100: 1) tapes deposited from toluene.

Bhattacharya and co-workers demonstrated that different capping agents have different effects on the morphology of gel fibres upon the addition of AuNPs.[511] Addition of AuNPs capped with alkanethiol (**5.4**)**,** cholesterol (**5.5**), and thiocresol (**5.6**) (Figure 5.1.4) to a hot solution of gelator **5.7** results in coalesced, rolled-tubular and platelet-like aggregates respectively. Rheological studies performed on the gels doped with alkanethiol and cholesterol stabilized AuNPs show that the incorporation of these nanoparticles rigidified the gel-network. The rigidity increased with increasing alkanethiol chain length, *m*. It was reasoned that this enhanced property could be attributed to the ability of the alkyl chains to interdigitate between the alkyl groups of the gelator. However, the addition of thiocresol capped AuNPs decreased the rigidity of the gel due to the inability of the aromatic moiety to interdigitate with the gelator.

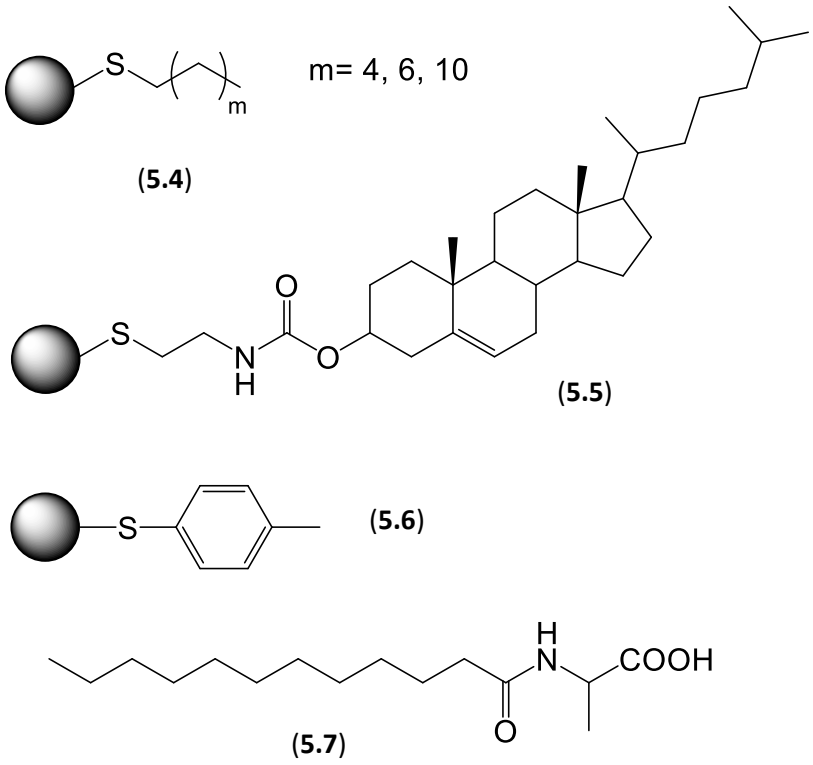

Figure 5.1.4 Gelaror **5.7** forms gel with different morphologies in the presence of different ligands (**5.4**, **5.5**, and **5.6**) stabilized AuNPs.

Bhattacharya and co-workers have also designed and developed two-component hydrogel systems comprising stearic acid (SA) or eicosanoic acid and diamines in specific molar ratios.[512] This hydrogel was further used to template the syntheses of

silver nanoparticles (AgNPs) by reducing $AgNO_3$ using $NaBH_4$ within the hydrosol of the two-component hydrogel systems and the thermoreversible gel-AgNPs composite was formed upon cooling. The spherical AgNPs (4-7 nm) were aligned along the gel fibres. This is tantamount to a symbiotic system whereby the gel fibres act as the host upon which the AgNPs become embedded during fibre formation.

Smith and co-workers have also formed AuNPs within the gel network of L-lysine based dendron via UV irradiation of the organogel of **5.8** (Figure 5.1.5) containing $HAuCl_4$ and tetraoctylammonium bromide (TOABr).[513] A solution of $HAuCl_4$ and TOABr was diffused into the gel followed by irradiation with a mercury vapour lamp. The change in colour from yellow to purple on irradiation was indicative of the formation of large AuNPs. With or without the disulfide link in the structure of gelator, AuNPs were formed uniformly within the gel network without being attached to the gel fibres, as indicated by TEM studies and the authors suggested they were trapped within pores in the gel network.

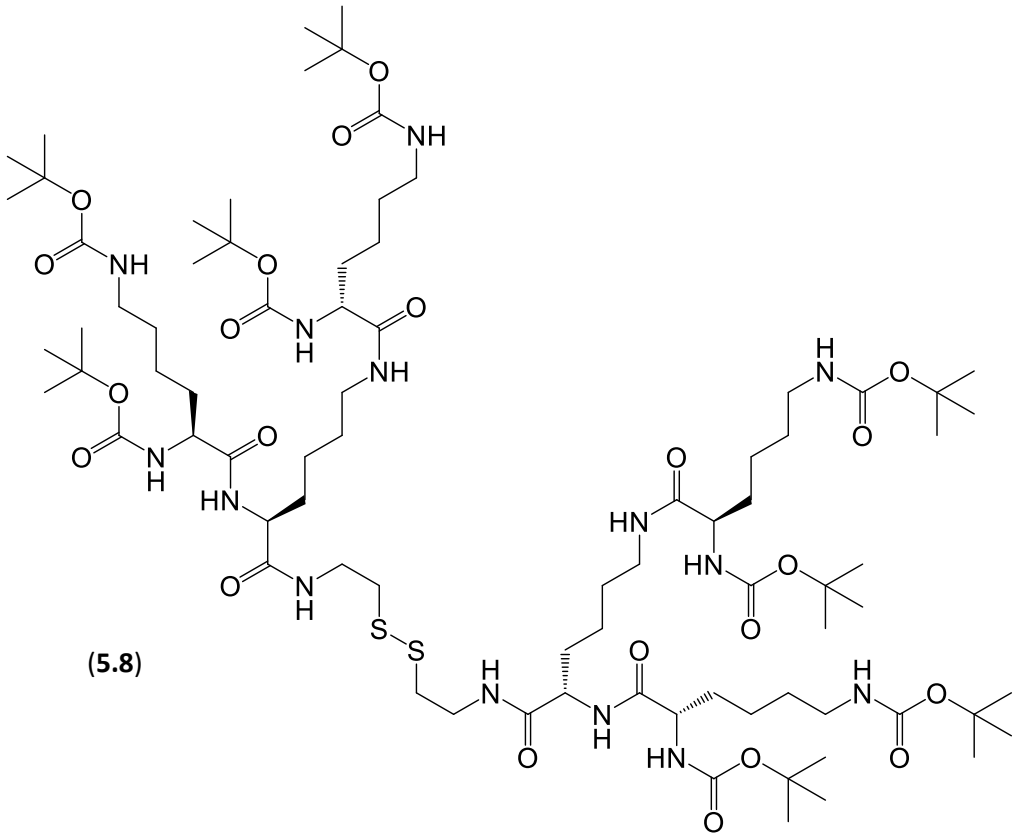

Figure 5.1.5 Disulfide dendritic gelator.

The same authors reported the design of gel-nanoparticle hybrid materials based on biologically derived building blocks. The cysteine-functionalized organogelators **5.9** (Figure 5.1.6) produces gold nanoparticles which align directly on the gel fibres via the S-Au interactions.[514] On the other hands, the non-sulfur based counterpart-tryptophan functionalized gelator **5.10**, could not form direct fibre-gold nanoparticles interactions, hence the nanoparticles aggregated into clusters loosely around the nanofibres. It was observed that the sizes of the nanoparticles increased from *ca* 1.4 nm to 3.1 nm as a result of Ostwald ripening when the xerogels of the hybrid gel-nanoparticles systems were heated on the TEM grid.[514]

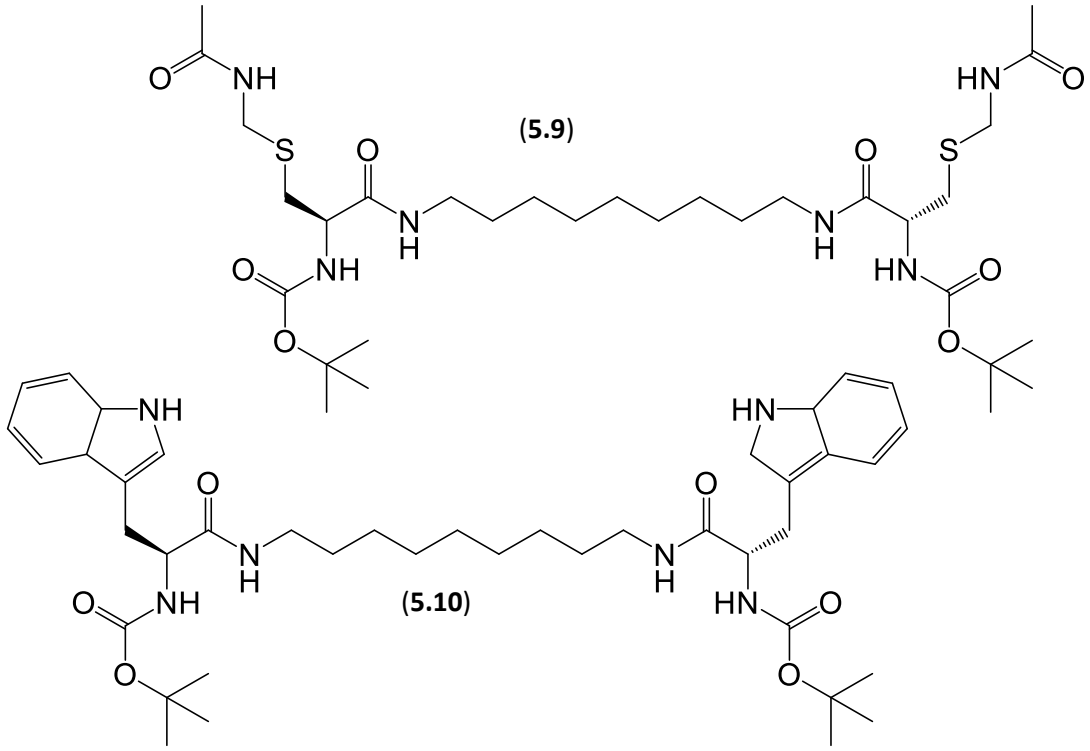

Figure 5.1.6 Structures of peptide gelators **5.9** and **5.10.**

Recently, Maitra and co-workers explored the use of a family of dimerized bile acid esters to engineer gold nanoparticles of different sizes and shapes and generate new gel−nanoparticle hybrid materials.[515] The gelator was dissolved in aromatic hydrocarbons containing $HAuCl_4.H_2O$, sonicated, heated at 60 °C and a yellow coloured gel was formed as the solution cooled down to room temperature. An aliquot solution of a reducing agent (tetraoctylammonium borohydride) was added to the top

of the gel. AuNPs of varying sizes and shapes were formed as the reducing agent diffuses into the gel-network.

The use of pre-formed metal nanoparticles or *in situ* formation of metal nanoparticles within the network of low molecular weight gels by the addition of external reducing agents in the construction of organic-inorganic nanocomposites is still common practice in this field. However, in recent years, synthesis of gelator molecules that will be able to reduce metal ions to form the corresponding nanoparticles without any external reducing agent have begun to attract attention.[144, 516-519] John and co-workers reported the first smart ambidextrous urea-based low molecular weight gelator **5.11** (Figure 5.1.7) which is able to perform the multiple functions of reducing, capping and binding nanoparticles *in-situ* in a gel. A mixture of **5.11** and $HAuCl_4$ were dissolved in a chosen solvent and heated until the gelator completely dissolved, then allowed to cool down. There was an initial colour transition from yellow to colourless solution, and finally a pink coloured gel was formed when the solution reached room temperature. Scanning electron microscopy was used to prove that the nanoparticles were attached to the edges of the gel platelets without causing obvious disruptions to the morphology of the gel. It was hypothesized that the terminal urea NH_2 is the active reducing agent for the gold from Au(III) to Au(0). This was confirmed by replacing the NH_2 group with a methyl group as in acetanilide, in which case gold nanoparticles formation did not occur.[509]

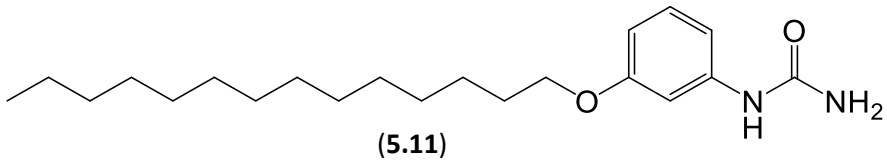

(**5.11**)

Figure 5.1.7 Gelator **5.11** which reduces Au (III) in situ

The same authors formed gold nanoparticles *in-situ* using low-molecular-weight gels based on ascorbic acid amphiphiles. Gelator **5.12** (Figure 5.1.8) was prepared enzymatically, formed gels in both polar (water) and non-polar solvents at a low gelator concentration (< 5 % wt/vol).[508] This ambidextrous nature is a rare occurrence among the gels of this class. It was observed that the thermal stability of the gel increased with increasing alkyl chain length. Gold nanoparticles were synthesized within the gel networks using the concept they initially adopted. However, the ascorbic

acid within the gel fibres acted as the reducing agent in this case. The formation of gold nanoparticles was confirmed by a colour change from yellow to pink and appearance of the surface plasmon band (520 nm) in the UV-Vis spectrum of the pink coloured gel. TEM revealed that the nanoparticles were distributed uniformly throughout the gel but did not assemble along the fibres. It is worth emphasising that this type of metal nanoparticle stabilization in an aqueous hydrogel is very rare.

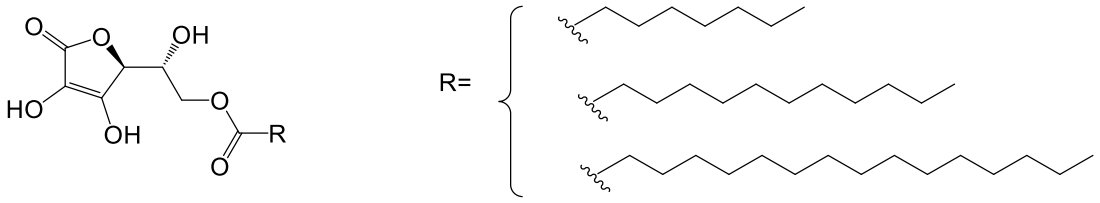

(**5.12**)

Figure 5.1.8 Gelator **5.12** which is able to form AuNPs *in situ*.

In sharp contrast to the conventional ideas of using synthetic organic molecules to control the organisation of nanoparticles, Amabilino and co-workers have demonstrated that gold nanoparticles can influence the organisation of a synthetic material.[507] In this case, a LMWG tetrathiafulvalene (TTF) **5.14** capable of acting as a semiconductor[520] in its own right was doped with gold nanoparticle capped with a derivative of TTF **5.15** that is capable of forming a hydrogen-bonding interaction with the gelator. The hybrid organogels were formed in hexane by heating-cooling method. It was shown by TEM that gold nanoparticles capped with hydrogen – bonding donor / acceptor group were included within the fibres of **5.14** while those capped with TTF derivative **5.16 (**with no hydrogen – bonding donor/acceptor moieties) did not exhibited intimate contact with the nanofibres of **5.14** (as shown in Figure 5.1.9). Current sensing atomic force microscopy (CSAFM) was used to show that the hybrid xerogel exhibits metallic conductivity (10 S cm^{-1}).

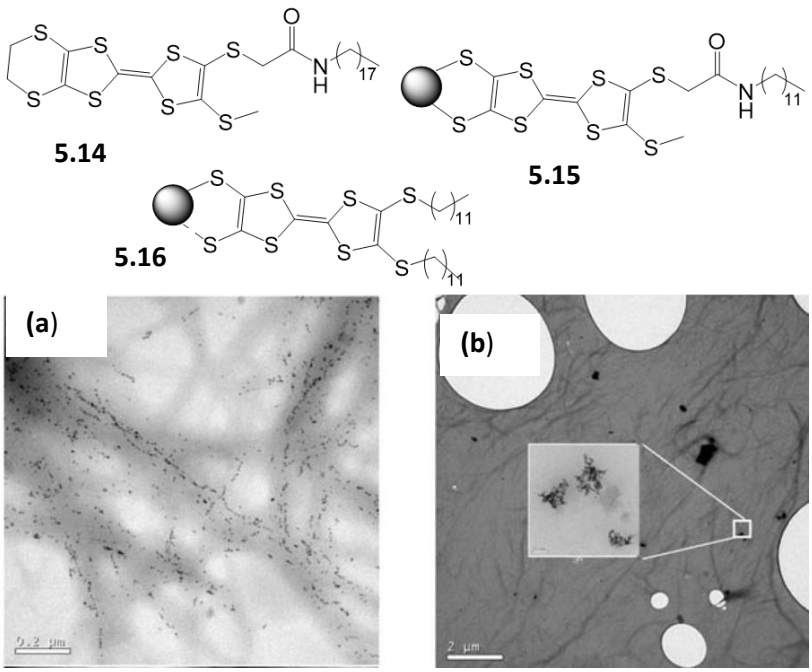

Figure 5.1.9 Top: Chemical structure of gelator **5.14** and schematic drawing of AuNPs capped with **5.15** and **5.16**. Bottom: TEM images of unstained xerogel of **5.15** in **5.14** (left) and **5.16** in **5.14**.

It is important to mention that noble metals mostly used in these nanoparticle – gel hybrid designs have been considered as ‘‘critical elements’’ owning to their economic importance and risk of supply – they are finite resources. Therefore, the awakening of research into e-wastes (waste electrical and electronic equipment) in the past decade brings along with it, a significant economic incentive for noble metal recovery not only from ores and consumer electronics but also from wastewater near, for example, mines.[145, 146] However, the conventional leaching method, which involves the use of inorganic cyanides, to recover gold from spent liquors often results in contamination of the environment via leakages.[147] Furthermore, a number of hydrometallurgical processes such as adsorption, chemical precipitation, coagulation, electrochemical technologies, ion exchange, and membrane technogologies have been used. However, certain limitations - high secondary waste generation, use of toxic chemical additives, high energy usage, high cost of operation, low metal uptake and poor efficiency at very low metal concentrations, remain with their uses.[521]

In order to circumvent problems associated with conventional methods, emerging bio-derived materials such as algae, fungi, yeasts, actinomycetes, bacteria, animal

products, agro-wastes and biopolymers have attracted a considerable deal of interests in the past decades (as for example schematically represented in Figure 5.1.10).[521-524] Nonetheless, difficulty in separation of biosorbent from reaction mixture, small particle size, non-suitability for batch process and high cost of production are among the characteristic disadvantages of a biosorption process tailored towards noble metal recovery.

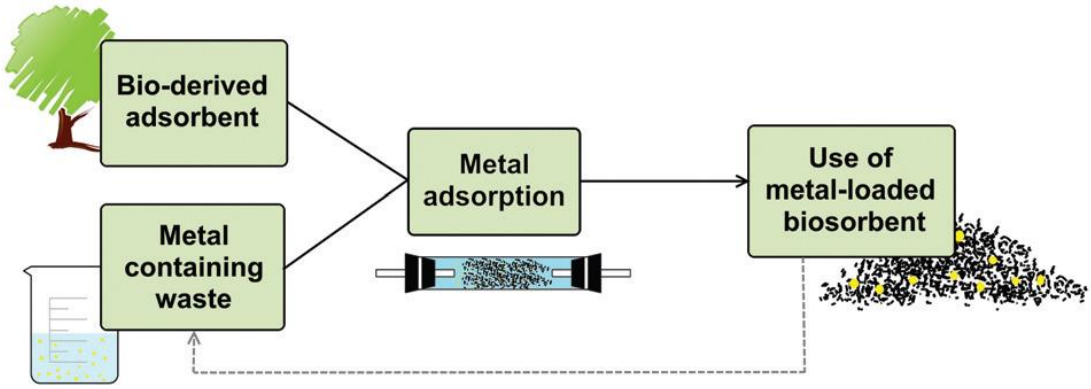

Figure 5.1.10 Schematic representation of metal recovery using biosorption process.

In 2015, while this work was in progress, Barthélémy and co-workers demonstrated for the first time, the use of a low molecular weight hydrogel to remove nanoparticle wastes from aqueous solutions.[525] In this case, hydrogels of a nucleoside-based amphiphile were interacted separately with aqueous solutions containing quantum dots (QDs), gold nanoparticles (AuNPs) and titanium dioxide nanoparticles (TiO_2-NPs). Interestingly, the emission peak at 622 nm, surface plasmon resonance (SPR) absorption peak at 510 nm and UV-visible absorption band at 280 nm corresponding to QDs, AuNPs and TiO_2-NPs were not observed in the supernatant liquids after 48 h (a representative example is shown in Figure 5.1.11).

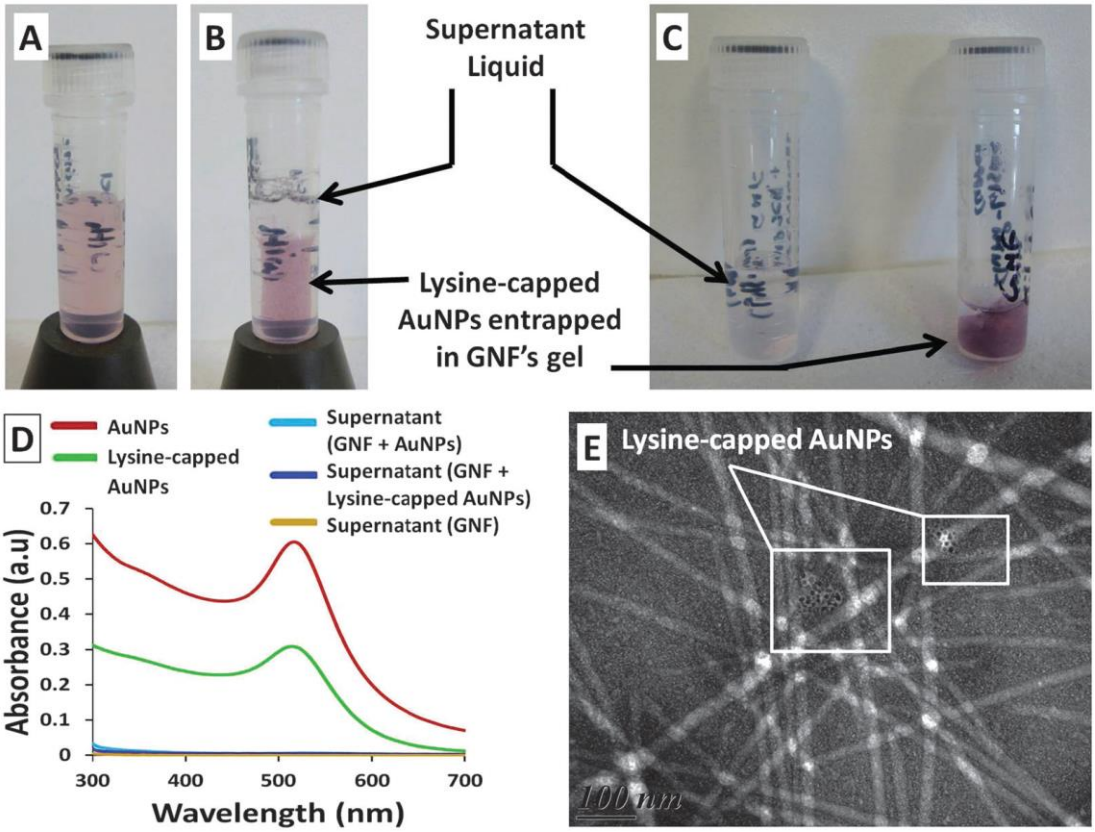

Figure 5.1.11 Lysine-capped AuNPs with GNF (0.1% (w/w)) (A) immediately after mixing (B) hydrogel formation after 48 h (C) supernatant liquid and hydrogel separated (D) UV-Vis absorption spectra (E) TEM image (scale: 100 nm).

The trapping ability of this supramolecular envirogel could be adduced to some interactions between the nanoparticles and the 3D network of the gel, thereby immobilising the nanoparticles.

However, recovery of noble metals (not in nanoparticulate form) from water with the use of supramolecular gel has not been reported to date. Therefore, developing an environmentally benign process for binding precious metals from water using a batch process, reducing them and converting them to a more useful nanostructured nanoparticles is not only important from green chemistry point of view but could also lead to more technologically viable nanodevices. Although several techniques exist for converting noble metals to nanoparticulates,[148-151] we rarely find any that could function as a self-reducing and stabilizing agent for nanoparticles synthesis without adding external reducing agents such as sodium borohydride ($NaBH_4$). The prime aim of this project is to further explore **DBS-CONHNH$_2$** and **DBS-COOH** envirogels as

archetypal 21st century nanosorbents for recovering gold from aqueous solutions at ambient conditions and as potential templates for *in situ* reduction, capping and binding of silver and gold in an aqueous medium - a simple and veritable technique for converting 'waste to wealth'. In addition to noble metal recovery, we aimed to produce useful hybrid organic – inorganic materials consisting of both organic nanofibres and inorganic nanoparticles and demonstrate their plausible use in high-tech applications as conductive hydrogels.

5.2 Results and discussions

5.2.1 Noble metals recovery with envirogels of DBS-CONHNH2

The ability of the **DBS-CONHNH2** envirogel nanofibres to sequester metal ions from water is further demonstrated with noble metals. Aqueous solutions (10 mM, 2.0 mL) of gold (Au) or silver (Ag) were added on top of the envirogels (0.4% wt/vol) and allowed to diffuse into the gel networks for about 48 h under ambient conditions. Aliquot solution of the supernatant liquid were analysed by ICP-MS for residual (equilibrium) concentrations of Au^{3+} and Ag^{+}. UV spectroscopy were also used to monitor the loss of Au^{3+} from the supernatant layer and the equilibrium concentration was extrapolated from the calibrated curve plotted for UV absorption at λ_{max} = 288 nm. Figure 5.2.1 shows that the concentration of Au^{3+} ions in the supernatant liquid decreases significantly and hence confirmed that Au^{3+} is being taking up by the envirogel nanofibres.

The maximum Au^{3+} loading, onto the hydrogel was calculated using Equation 5.2.1;

$$Q_{max} = \frac{(C_{initial} - C_{final})V}{m} \qquad \text{Equation 5.2.1}$$

Where q_{max} is the maximum amount of Au^{3+} loaded into the gel network (mg/g), *m* is the weight of hydrogelator used (g), C_{final} is the equilibrium concentration of Au^{3+} in solution (mg/L), $C_{initial}$ is the initial Au^{3+} concentration (mg/L) in solution, and *V* is the volume (L) of aqueous Au^{3+} solution.

The maximum Au^{3+} uptake capacity of the envirogel was estimated from the mass balance equation shown above (equation 5.2.1) to be as high as 2000 mg Au/ g **DBS-**

CONHNH$_2$ and 900 mg Ag/ g **DBS-CONHNH$_2$**. This uptake capacity is higher than most adsorbents reported in literature (i.e. biosorbents - chemically modified chitosans (70.8 mg g^{-1}), activated sugarcane bagasse (324 mg g^{-1}), etc.[521, 526] and magnetic nanoparticles (118.46 mg g^{-1}).[527] This uptake capacity is a little lower than what has recently been reported for Starbon® (3800 mg g^{-1}) by Clark and co-workers.[524] However, in terms of molar ratio of adsorbed Au to adsorbent, **DBS-CONHNH$_2$** is a better adsorbent than Starbon®. It is also important to mention that certain limitations such as high energy (MW heating) and non-suitability for batch adsorption among other things remain for the use of Starbon® in gold recovery. It is worthy of note that the envirogel collapsed at its maximum loading capacity (>2000 mg g^{-1}) and this could be attributed to the disruption of fibre – fibre interactions caused by build-up of layers of nanoparticles on the nanofibre networks.

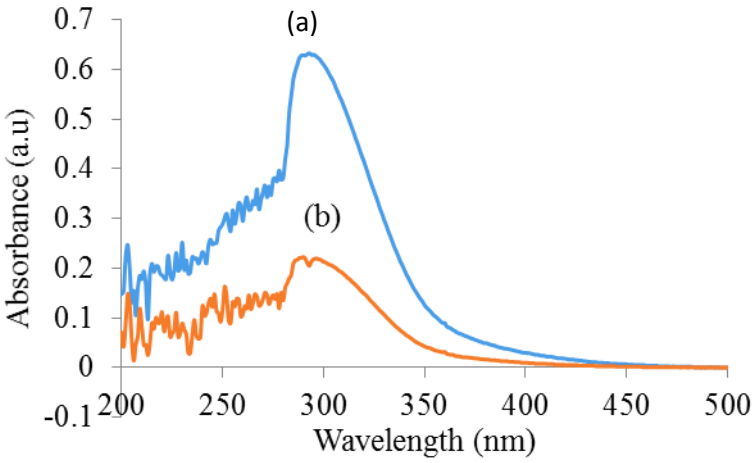

Figure 5.2.1 UV-Vis spectral of Au^{3+} solution (a) before adsorption at 20 times dilution and (b) after adsorption without dilution.

Interestingly, the gels changed colours to ruby red as Au^{3+} diffused into the gel networks. Also, adsorption of Ag^{+} changed the colour of the gel to yellow. These colours are characteristic features of nanoparticulate forms of these metals when capped with hydrazide functionality – which implies that the gel fibres have demonstrated a self-reducing and capping of noble metals nanoparticles (NPs) (as shown in Scheme 5.2.1A).[528, 529] Moreover, the ability of these gels to change colour in the presence of these noble metals make them a potential on-site sensor for Au^{3+}

and Ag^{+} ions in aqueous waste from electronics or mining industries as the gel was able to respond to an ultra-trace (< 5 nM) presence of Au^{3+} and Ag^{+} in water (Scheme 5.2.1B).

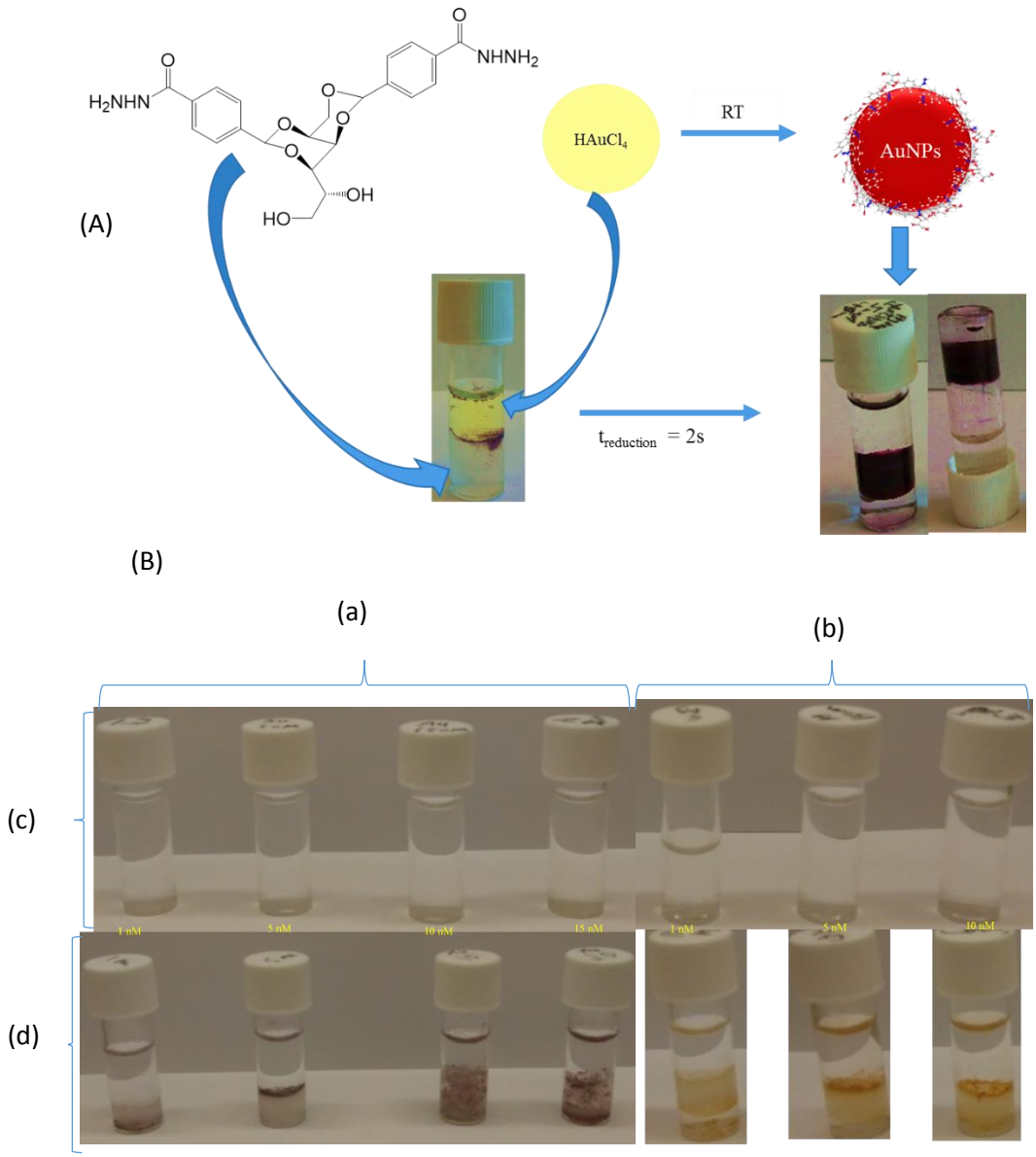

Scheme 5.2.1 A) Schematic representation for adsorption of gold to **DBS-CONHNH$_2$** envirogel and in situ gold nanoparticles formation, B) Ultra-trace (1.0 – 15.0 nM) concentrations of aqueous solution of Au^{3+} (a) and Ag^{+} (b) ions in the absence (c) and presence (d) of **DBS-CONHNH$_2$** hydrogels

It is worth noting that Au^{3+} ions changes colour within 2 s while the yellow colour of Ag^{+} ions was only observed after about 30 min of interaction with the gel nanofibres.

This could be attributed to the difference in their reduction potentials – for Au^{3+} ($Au^{3+} + 3e^- \rightarrow Au^0$, 1.50 V vs SHE) and Ag^+ ($Ag^+ + e^- \rightarrow Ag^0$, 0.80 V vs SHE). The reduction of $HAuCl_4$ and $AgNO_3$ occur as a result of the transfer of electrons from the amino group of the hydrazide to Au^{3+} and Ag^+ ions which resulted in the formation of Au^0 and Ag^0 according to the Scheme 5.2.2.[530]

$$HAuCl_{4\,(aq.)} + 3DBS\text{-}CONHNH_2 \rightarrow Au^0_{(s)} + 3DBS\text{-}CONHNH_2^+ + H^+ + 4Cl^-$$

$$AgNO_{3\,(aq.)} + DBS\text{-}CONHNH_2 \rightarrow Ag^0_{(s)} + DBS\text{-}CONHNH_2^+ + NO_3^-$$

Scheme 5.2.2 Reduction of Au^{3+} to Au^0 and Ag^+ to Ag^0 under the influence of the amino group on **DBS-CONHNH$_2$**.

The resulting metallic gold and silver then nucleates to form gold and silver nanoparticles respectively. The **DBS-CONHNH$_2$** can cap and stabilise the nanoparticles after reduction via electrostatic interactions.

From another perspective, the selectivity of **DBS-CONHNH$_2$** envirogels towards noble metals in the presence of earth - abundant elements was demonstrated. In this case, an aqueous solution (100 mg l^{-1}, 5 mL) of Ni^{2+}, Cu^{2+}, Zn^{2+}, Fe^{2+}, Pt^{2+}, Pd^{2+}, Au^{3+} and Ag^+ as a model wastewater from mine tailing was allowed to diffused into the envirogel network (mass of gelator 4 mg) for about 48 h at ambient conditions. Dilute HNO_3 (0.1 M) and NaOH (0.1 M) solutions were used to enhance the solubility of some of the metals in water. The supernatant liquid was analysed by ICP-MS for the residual concentrations of the metals. Figure 5.2.2 shows that **DBS-CONHNH$_2$** exhibited higher affinity towards the noble metals than the abundant earth metals as it adsorbed ≥ 99% of Pt^{2+}, Pd^{2+}, Au^{3+} and Ag^+ , but only 27, 30, 50 and 37% of Fe^{2+}, Ni^{2+}, Cu^{2+} and Zn^{2+} respectively.

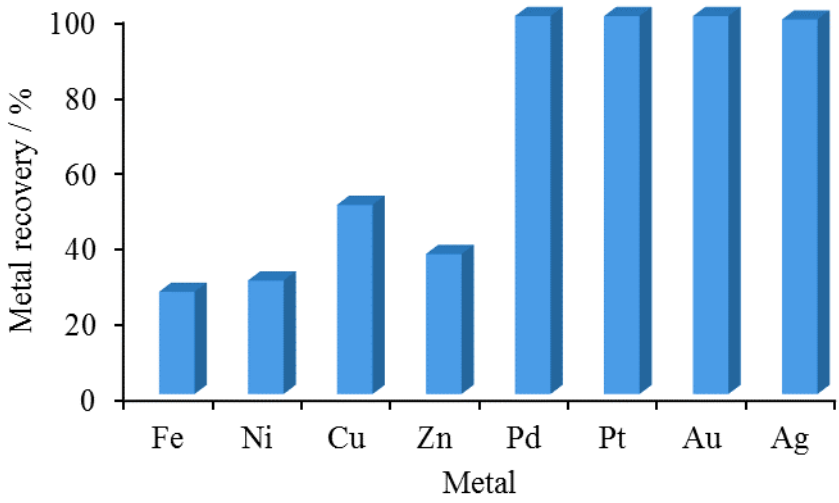

Figure 5.2.2 Metal recovery from a model wastewater from mineral, electronics or mining industries.

5.2.2 Characterisation of the emerged hybrid nanomaterials

In order to gain insight into the morphology of the nanoparticles and interactions between the nanocomponents materials, techniques such as UV-Vis, infrared (FT-IR) and X-ray photoelectron (XPS) spectroscopies and electron microscopy (SEM and TEM) were used to characterise the nanocomposites.

The hydrogel - encapsulated gold and silver nanoparticles were initially characterized by UV-Vis spectroscopy. Figure 5.2.3 a and b shows that the composite hydrogel-AuNPs/AgNPs system display strong absorption bands in the visible region at about λ_{max} = ca. 525 nm and hydrogel-AgNPs at λ_{max} = 420 nm. These absorption bands correspond to the Surface Plasmon Resonance (SPR) of spherical or roughly spherical gold and silver nanoparticles.[531-534] The observed strong SPR could be attributed to the interactions between light and electrons in the conduction bands of the metals at optical frequencies.

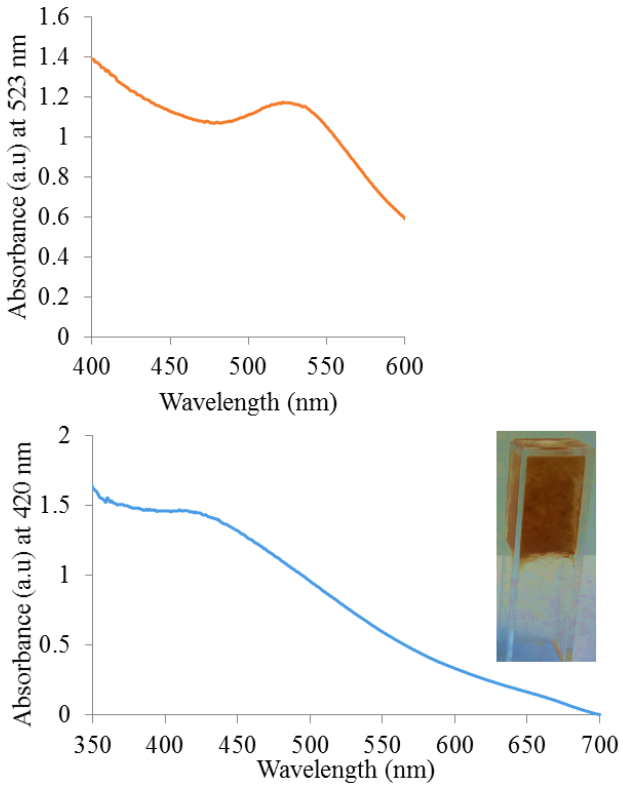

Figure 5.2.3 UV-Vis spectrum showing the surface plasmon band of **DBS-CONHNH$_2$** hydrogel-capped (a) AuNPs and (b) AgNPs. Inset: **DBS-CONHNH$_2$** hydrogel encapsulated AgNPs.

FT-IR spectroscopy data for the xerogels of **DBS-CONHNH$_2$**, **DBS-CONHNH$_2$**-AuNPs and **DBS-CONHNH$_2$**-AgNPs are presented in

Table 5.2.1. The characteristic bands for C-N, C=O, N-H (bending), N-H (stretching) and OH at 1333, 1600, 1644, 3178 and 3315 cm^{-1}, respectively shifted by 9, 15, 46, 48 and 90 cm^{-1} ,respectively when Au^{3+} and Ag^{+} ions were adsorbed onto the envirogels. It can be inferred from these shifts that the metals interacted with **DBS-CONHNH$_2$** envirogel nanofibres through carbonyl, amine and hydroxyl groups.

Table 5.2.1 FT-IR data for key functional groups on **DBS-CONHNH$_2$** xerogels before and after Au^{3+} and Ag^{+} uptake

Wavenumbers (cm^{-1})			
Functional group	DBS-CONHNH$_2$ xerogel	DBS-CONHNH$_2$-AuNPs xerogel	DBS-CONHNH$_2$-AgNPs xerogel
$OH_{(stretch)}$	3315	3297	3225
$N\text{-}H_{(stretch)}$	3177	3198	3225(overlap with OH)
$C\text{-}O_{(stretch)}$	1097	1095	1090
$C{=}O_{(stretch)}$	1644	1656	1690
$N\text{-}H_{(sbend)}$	1600	1615	1614
$C\text{-}O_{(stretch)}$ acetal	1019	1018	1015
C=C	1572	1573	1574
C-N	1333	1339	1341

XPS was employed to understand the surface chemistry of the xerogels of **DBS-CONHNH$_2$**-AuNPs and **DBS-CONHNH$_2$**-AgNPs. Figure 5.2.4 and Figure 5.2.5 show the spectra and deconvoluted peaks for each element constituting the hybrid materials. The narrow scan of C 1s was deconvoluted into two peaks; 284.9 and 287.8 eV corresponding to two or more types of carbon against the many types of carbon on

the structure of the native gelator; adventitious C-C / C=C (aromatic), C-O / C-OH / N-C=O respectively. However, when Au^{3+} was adsorbed onto the envirogels, the peaks at BEs of 284.9 and 287.8 eV are not visible while a new peak emerged at BE of 285.7 eV. The two peaks, 532.5 and 530 eV under the oxygen signals attributed to the presence of O=C / C-O-C and –OH respectively on the surface of the native xerogel were shifted to 532 and 528 eV respectively in the presence of AuNPs which confirms the interaction of the free hydroxyl groups of the sugar backbone of the gelator with AuNPs.[481, 482] The N 1s peak at BE of 397.5 and 400 eV for NH_2 and NH group on the native xerogel became very broad and are hence, non-diagnostic; however, the broadness could be due to a strong interaction of Au with these groups. Deconvolution of Au 4f peaks reveals that the peaks at BEs of 84 and 88 eV correspond to the $4f_{7/2}$ and $4f_{5/2}$ of Au in Au^0 oxidation state having a spin-orbit splitting (SOS) of 4 eV. These values of BEs and the SOS are similar to what have been reported in the literature. Interestingly, no values of BEs (85.9 and 89.6 eV) corresponding to Au^{3+} was observed and this confirmed a complete transformation of Au^{3+} into nanoparticulate form.[535]

On the other hand, in the presence of Ag, an additional C 1s peak to those at 284.9 and 287.8 eV appeared at 282.5 eV. The peaks at 532.5 eV under the oxygen signals due to the presence of O=C / C-O-C on the surface of the native xerogel shifted to 533.8 but the peak at 528 eV remained unchanged, however, a new peak emerged at 531.8 eV. This might suggests that Ag interacts preferentially with the C=O group than the O-H, and hence the oxygen atom of the carbonyl group witnessed a new chemical environment which gives rise to the new peak. Furthermore, the N 1s peaks also shifted to 395.8 and 401.3 eV respectively with the emergence of a new peak at 398.6 eV. Deconvolution of Ag 3d shows that the peaks at BEs of 368.2 and 374.4 eV correspond to Ag^0 suggesting reduction of Ag^+ to Ag^0 which further aggregated into a nanoparticulate form; no traces of Ag^+ were observed on the spectra.[536, 537] It is important to mention that the elemental compositional values obtained from the XPS survey spectra do not represent the maximum loading capacity of the envirogels, however, nearly 1:1 N:Au or N:Ag atomic ratio was observed on the spectra.

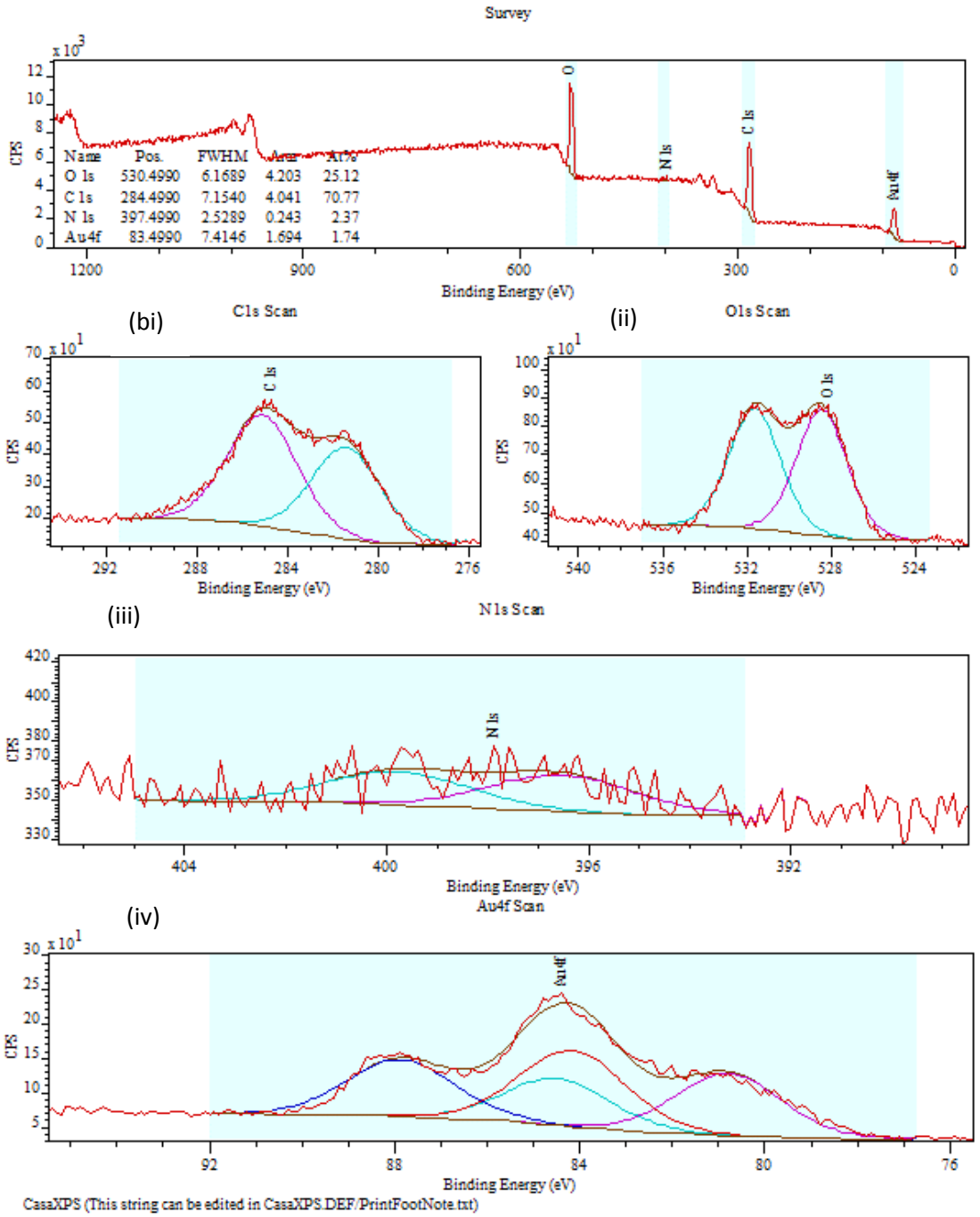

Figure 5.2.4 (a) XPS spectra for **DBS-CONHNH$_2$**-AuNPs and (b) deconvoluted spectra for (i) C 1s, (ii) O 1s, (iii) N 1s and (iv) Au 4f.

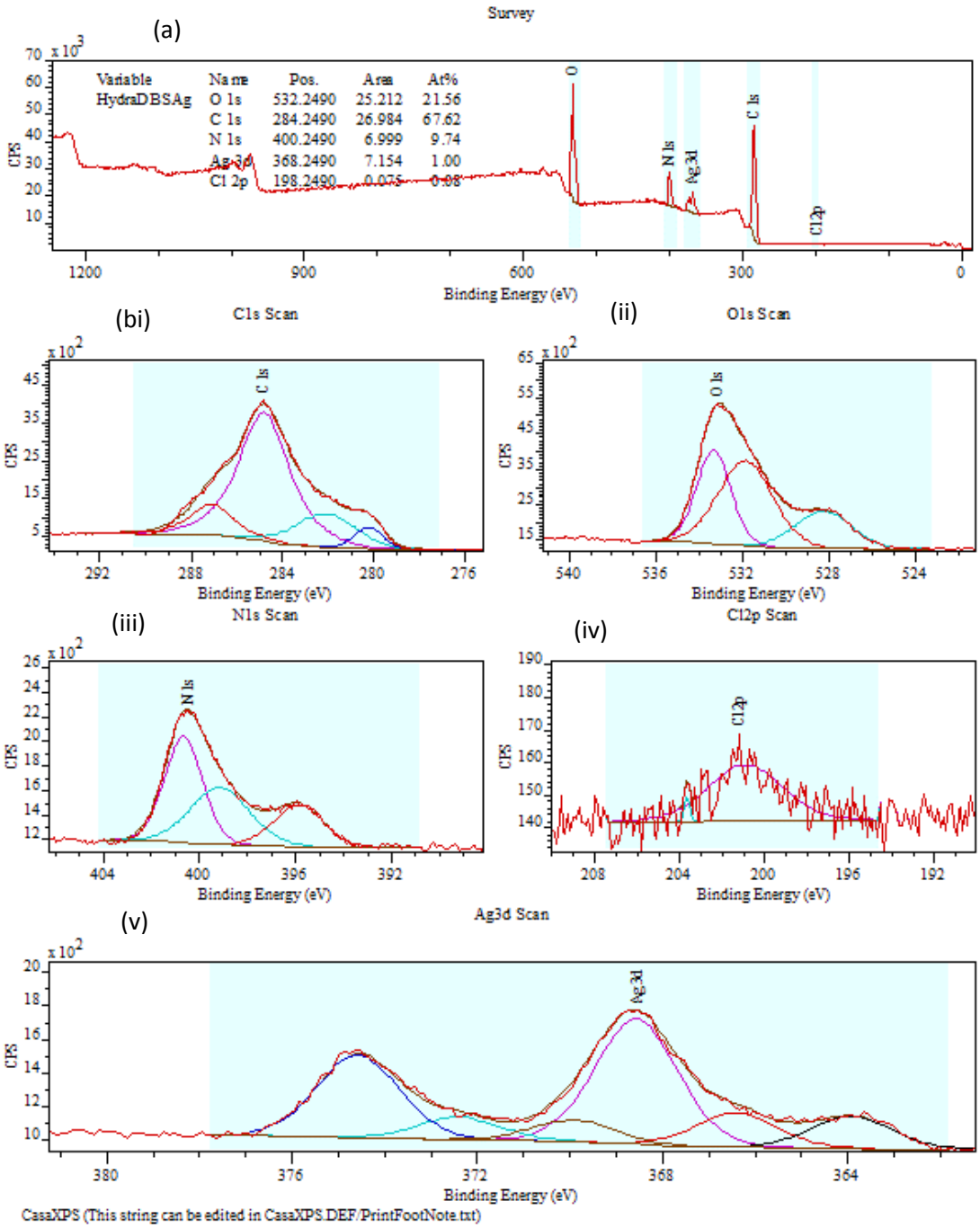

Figure 5.2.5 XPS spectra for **DBS-CONHNH$_2$**-AgNPs and (b) deconvoluted spectra for (i) C 1s, (ii) O 1s, (iii) N 1s and (v) Ag 3d.

In order to investigate the effect of nanoparticles on the morphology of the gel-network, TEM was used to investigate the self-assembled fibrillar network of the native **DBS-CONHNH$_2$** xerogel and **DBS-CONHNH$_2$**-AuNPs hybrid matrix. Interestingly, the nanoparticles (> 90%) were found to be mainly attached to the gel fibres rather than sitting in the solvent pocket within the gel-network (as shown in

Figure 5.2.6a). The imaging was done both on stained and unstained xerogels, so as to improve the contrast and thereby making the gel fibres visible. However, some of the weakly bonded nanoparticles were washed-off after staining. On the other hand, Figure 5.2.6b, shows that the spherical AgNPs (> 99%) were to some extent aligned along the extended nanofibrillar network.

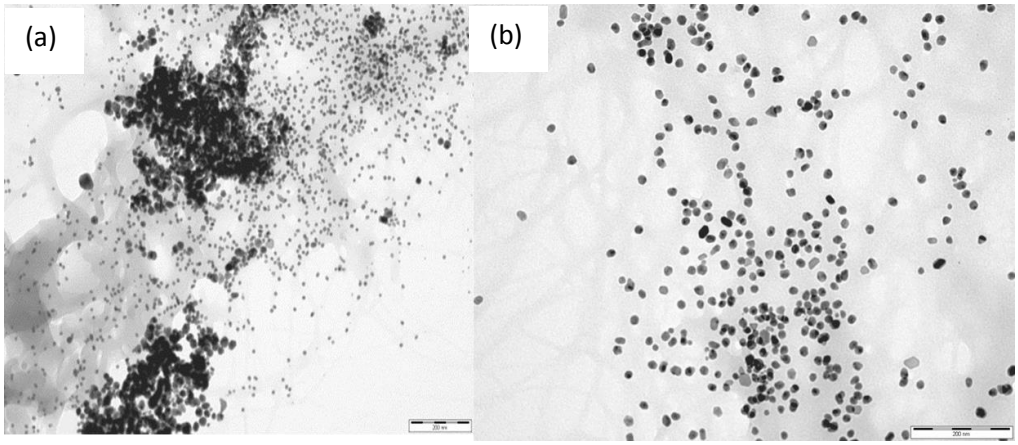

Figure 5.2.6 TEM image of unstained dried xerogel of (a) **DBS-CONHNH$_2$**-AuNPs (b) **DBS-CONHNH$_2$**-AgNPs. [Scale bar: 200 nm].

The observed organisation of nanoparticles on the nanofibres might be as a result of electrostatic interactions between the hydrazide functionalized gel fibres and the electron-deficient Au^{3+} and Ag^{+} ions leading to their reduction on the periphery of the gel nanofibres. Also, because the gel fibres were larger than the NPs, they may be able to act as hosts upon which the NPs were embedded, thereby becoming stabilized.

The average size of the particles was estimated with the use of TEM and IMAGEJ to be *ca* 5.0 and 10.0 nm for AuNPs and AgNPs respectively.

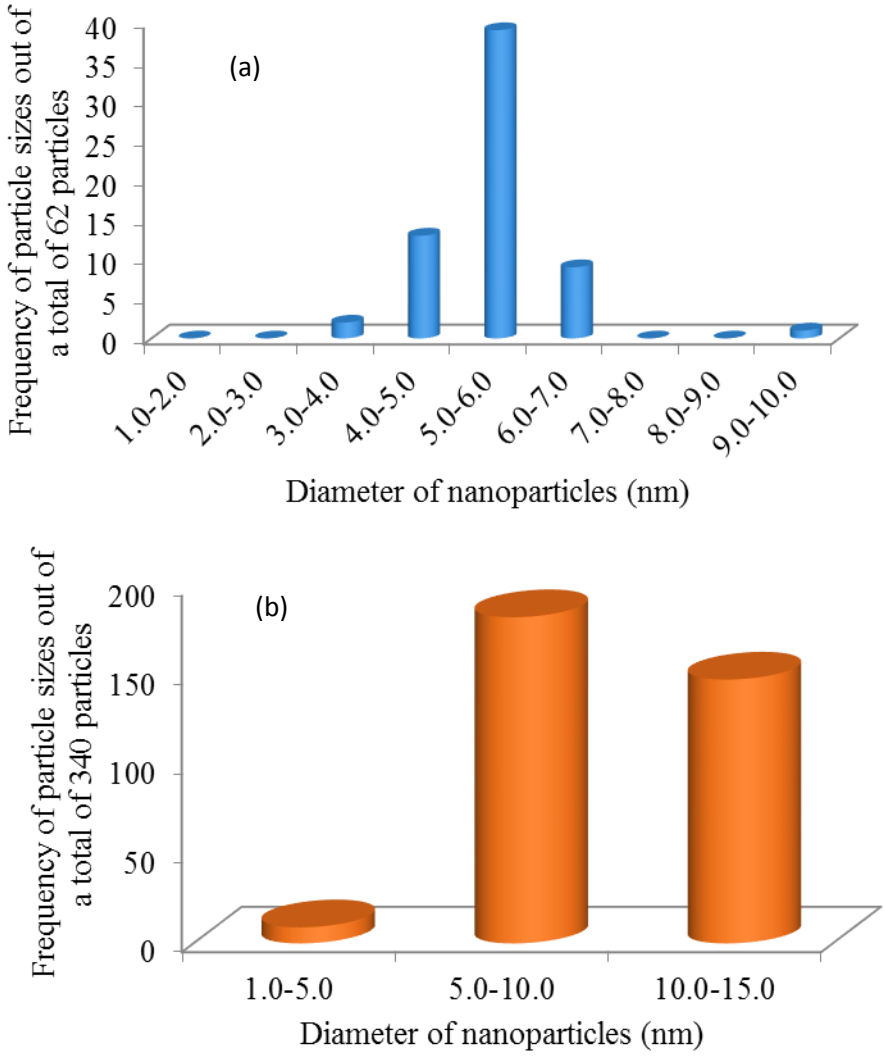

Figure 5.2.7 Particle size distribution of **DBS-CONHNH$_2$** hydrogel encapsulated (a) AuNPs and (b) AgNPs

5.2.3 Stability of DBS-CONHNH$_2$ hydrogel encapsulated AuNPs

The surface of gold nanoparticles is dynamic and greatly influenced by the local environment such as pH, ionic strength, temperature, light etc. However, different conditions will affect the particles in different ways, ranging from aggregation of particles to variation in shapes. Preventing aggregation of nanoparticles under various ambient factors and exposure time could be important depending on the potential application of these materials. The stability of nanoparticles can be probed using UV-Visible spectroscopy, dynamic light scattering or electron microscopy. It has been shown that the SPR of gold or silver nanoparticles varies with the size and shape of

the particle. The bigger the particle size, the longer the absorption wavelength (SPR).[538, 539]

Therefore, the stability of the DBS hydrazide-capped gold nanoparticles across a wide range of pH values was probed by measuring the SPR. The ambient pH was adjusted using 0.1 M HCl and 0.1 M NaOH solution. As shown in Figure 5.2.8, it was interesting to observe that the position of the SPR band of the gold nanoparticles in the hydrogel remains constant across the range of pH investigated, which suggest a high degree pH-tolerance. Besides stability to pH, the DBS hydrazide-capped gold/ silver nanoparticles also demonstrate a constant position of SPR band as measured using UV-Vis spectroscopy over an extended period of 90 days as shown in Figure 5.2.9 and Figure 5.2.10, which shows there is no detectable aggregation of AuNPs and AgNPs over extended periods of time.

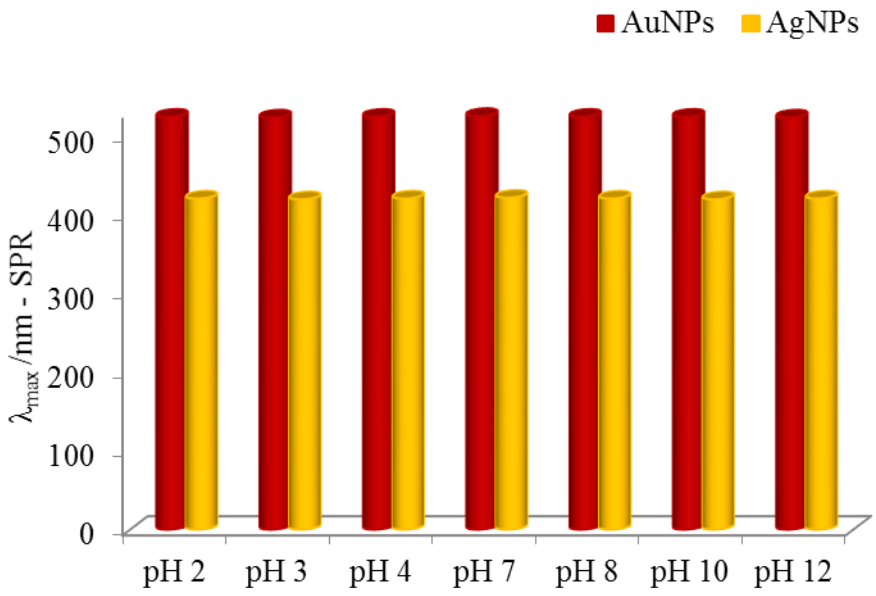

Figure 5.2.8 Stability of **DBS-CONHNH$_2$**-capped AuNPs/ AgNPs across a wide range of pH.

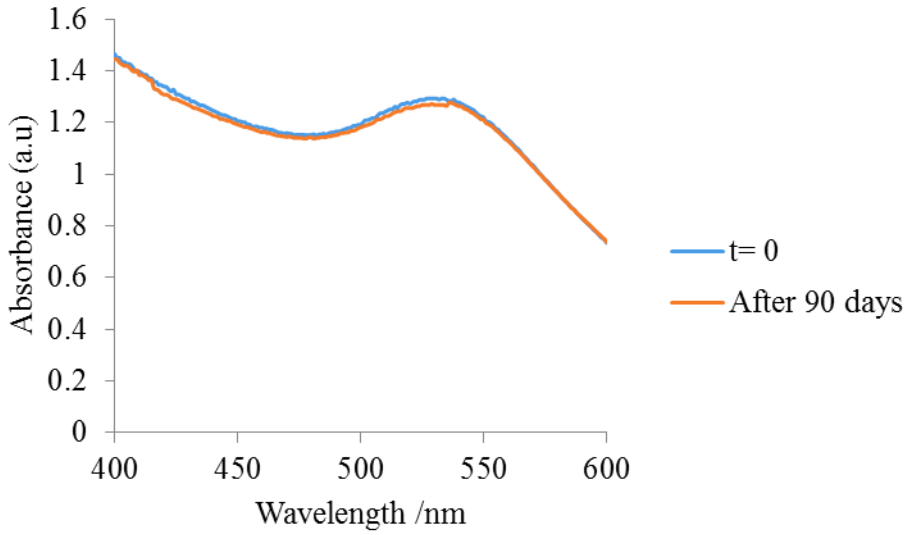

Figure 5.2.9 Stability of **DBS-CONHNH$_2$**-capped AuNPs over a period of 90 days.

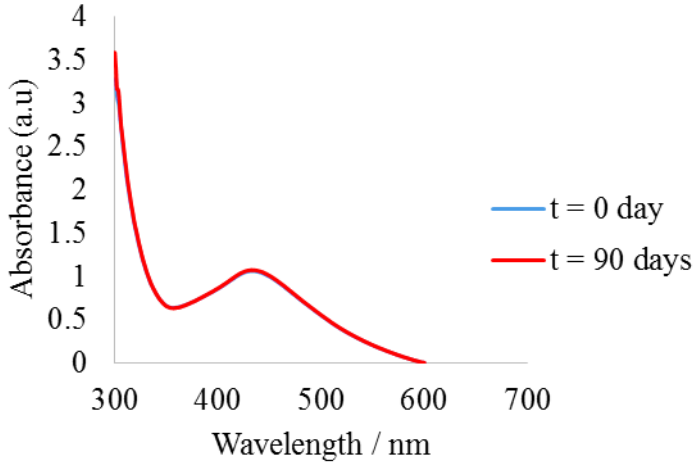

Figure 5.2.10 Stability of **DBS-CONHNH$_2$**-capped AgNPs over a period of 90 days.

5.2.4 Effect of nanoparticles on T_{gel} values of DBS-CONHNH$_2$ hydrogels

In order to probe the behaviour of the DBS hydrazide hydrogel-nanoparticle composite based on different concentrations of Au^{3+}, the transition temperature (T_{gel}) from a self-supporting gel state to a solution phase was determined by using tube-inversion. In this case, an aqueous solution (50 µL) of Au^{3+} across a range of concentrations was added to a hot hydrosol of a fixed concentration (10 mM) of the gelator molecule. In contrast to a previous report by Love *et al*, [513] there was no obvious change in the colour of the nanoparticles on heating the gel-nanoparticle composite. Moreover, Figure 5.2.11

shows that the phase transition temperature for the hydrogel increased from *ca* 65 °C to plateau at 87 °C with increasing concentration of Au^{3+}. Such improvement in the material properties of a gel material has previously been reported by Bhattacharya and co-workers,[511] and suggests that in the presence of small amount of nanoparticles the AuNPs may act to help crosslink the gel fibres.

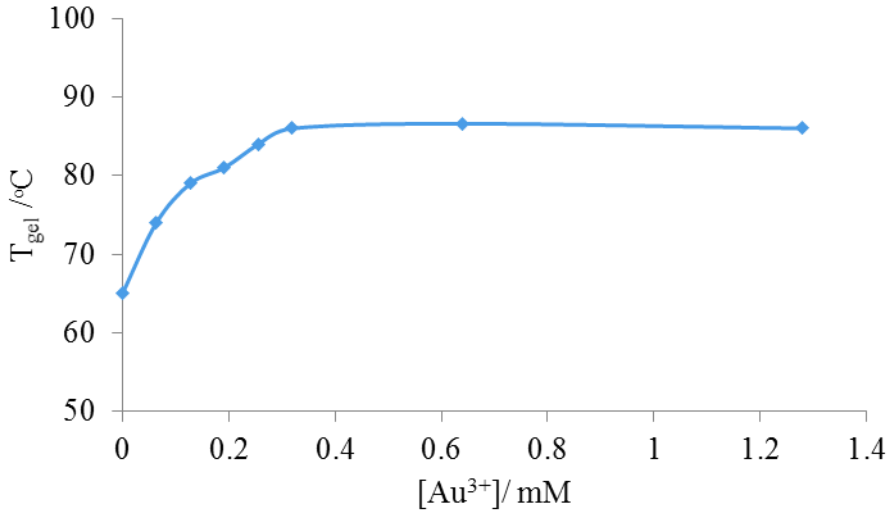

Figure 5.2.11 Curve showing the variation of gel-sol transition temperature of **DBS-CONHNH2** (10 mM) with respect to the concentration of Au^{3+}.

However, this gel-nanoparticle hybrid material collapsed at a 1:1 gelator/ Au^{3+} molar ratio. This breakdown in nanostructure could be attributed to the increased concentration of AuNPs coating the surface of the gel fibres thereby disrupting the fibre-fibre interactions as demonstrated by SEM coupled with low-angle backscattered electron (LABE) detector. This technique was used to improve the qualitative compositional images of nanofibre – nanoparticle hybrid with higher resolution than would have been obtained on conventional SEM – with this technique, brighter images represent component (AuNPs) with high atomic density while darker images (nanofibres) are those with low density (as shown in Figure 5.2.12). Also, it could potentially be attributed to the inability of the gelator to still reduce all of the Au^{3+}. It is also important to mention that at high gold concentrations, intra and intermolecular bonding otherwise known as aurophilic interactions between seemingly closed-shell gold centre, could also account for the observed disruption to gel ‘‘integrity’’.[540]

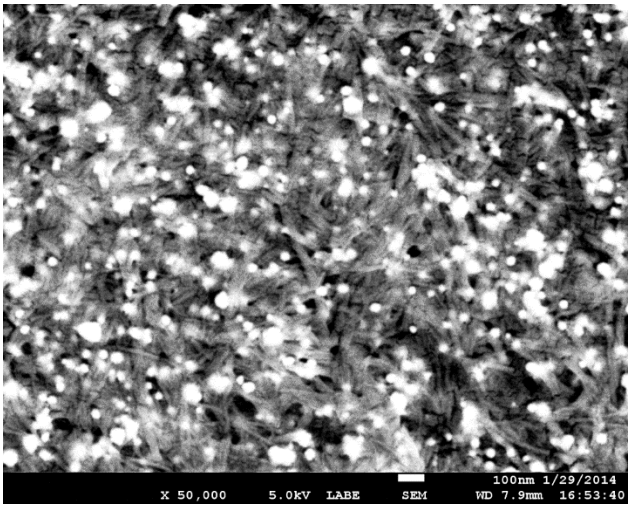

Figure 5.2.12 LABE - SEM image of a dried xerogel of **DBS-CONHNH$_2$-AuNPs** at maximum gold loading.

5.2.5 pH-Tunable nanogel – AuNPs

Unlike **DBS-CONHNH$_2$**, **DBS-COOH** is a pH-tunable hydrogelator. It forms a gel in water by switching from basic to acidic pH (Scheme 5.2.3). In a basic medium, **DBS-COOH** forms a homogeneous solution which self-assembles into a stable hydrogel upon acidification with either dilute HCl or Glucono-δ-lactone (GdL).[541] This process was discussed in more detail in Chapter 2.

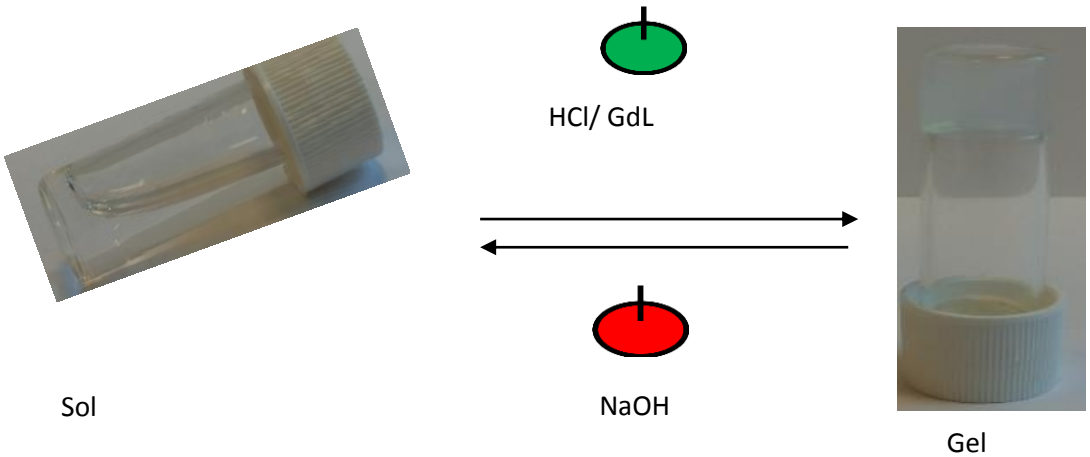

Scheme 5.2.3 ON/OFF Switching of **DBS-COOH** hydrogel

In this case, GdL was used to trigger hydrogelation of **DBS-COOH**, since the use of HCl gives rise to the formation of a non-uniform hydrogel. A diffusion method was used to load aqueous Au^{3+} solution into the gel network as previously discussed with

respect to the **DBS-CONHNH2** hydrogel. The solution diffuses through **DBS-COOH** hydrogel and formed two layers of AuNPs with different colours within the gel network - dark purple top and ruby red bottom layers (shown in Figure 5.2.13). This might implies that there are two driving forces responsible for the formation of gold nanoparticles *in situ* within the gel-network.

Figure 5.2.13 DBS-COOH hydrogel encapsulated AuNPs

UV-Vis spectroscopy was used to monitor the removal of Au^{3+} from the supernatant aqueous layer. Figure 5.2.14 shows that more than 90 % of the Au^{3+} has been withdrawn from the supernatant aqueous layer into the gel network where it is reduced and further converted into gold nanoparticles without the addition of any external reagents.

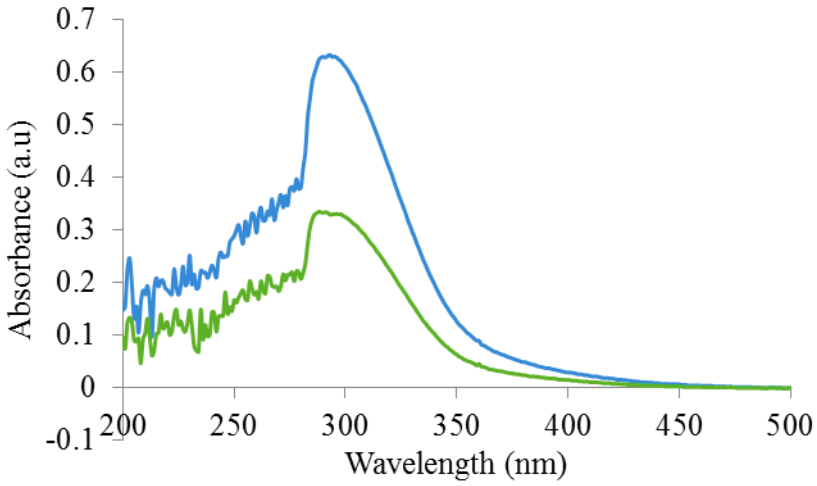

Figure 5.2.14 UV-Vis spectra of Au^{3+} solution (a) without gel (blue line, at 20 times dilution) and (b) at equilibrium with **DBS-COOH** hydrogel-AuNPs.

In order to understand the mechanism of gold nanoparticle formation within the **DBS-COOH** hydrogel, two sets of glucono-δ-lactone (without the gelator) were prepared with and without aqueous NaOH solution. The Au^{3+} solution was added to each of them. Purple colour was observed in the alkaline GdL solution within 30 min (shown in Figure 5.2.15) while there was no noticeable colour change with the neutral sample.

Figure 5.2.15 Aqueous colloids of glucono-δ-lactone (GdL) capped AuNPs.

This implies that gluconic acid which resulted from the alkaline hydrolysis of GdL played a key role in the *in situ* formation of gold nanoparticles within the network of this **DBS-COOH** hydrogel.

UV-Vis spectrometry was used to monitor the formation of AuNPs at 535 nm in the presence of GdL and 529 nm in both the absence and presence of **DBS-COOH** self-assembling from a hydrosol to hydrogel (shown in Figure 5.2.16a and b). These spectra show that Au^{3+} is reduced by GdL both in the absence and presence of the gel, however, at a faster rate in the absence of gel. This might suggests that GdL is interacting with **DBS-COOH**.

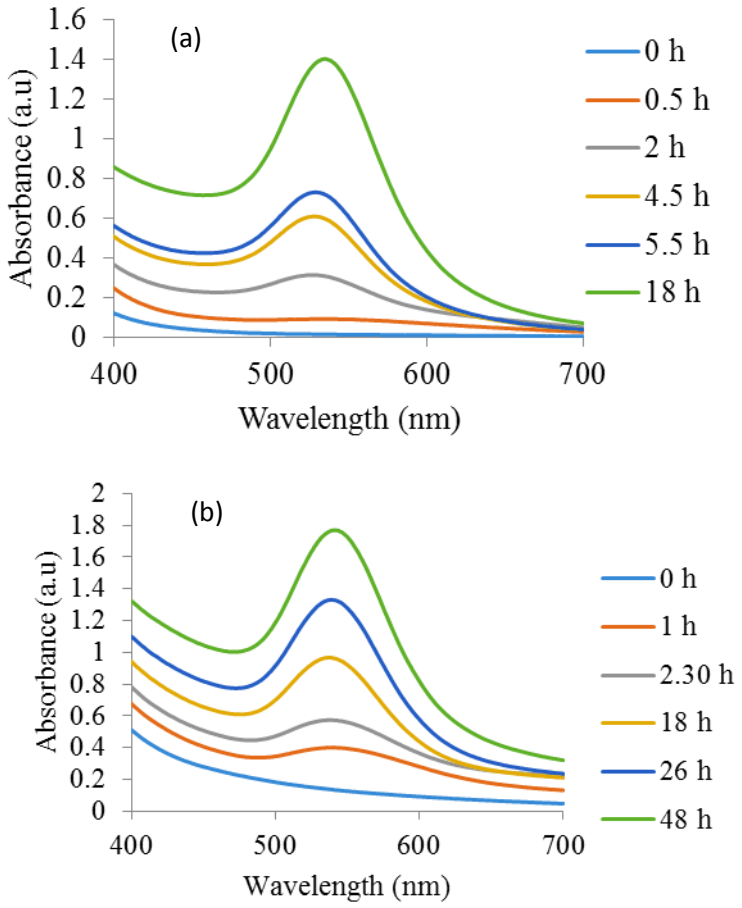

Figure 5.2.16 UV-Vis of AuNPs formation (a) without **DBS-COOH** hydrogel (b) with **DBS-COOH**

From the TEM images shown in Figure 5.2.17, it is evident that in the absence of **DBS-COOH**, GdL-capped gold nanoparticles form large aggregates which is an indication that although GdL can reduce Au^{3+} to gold nanoparticles, it cannot stabilize the resulting nanoparticles (Figure 5.2.17c). However with **DBS-COOH**, the gold nanoparticles are aligned along the gel fibres without any larger aggregates being formed. The sizes of the nanoparticles range from *ca* 6-10 nm. This confirms that the

gel nanofibres not only immobilize the gold nanoparticles but also confer a measure of stability on them.

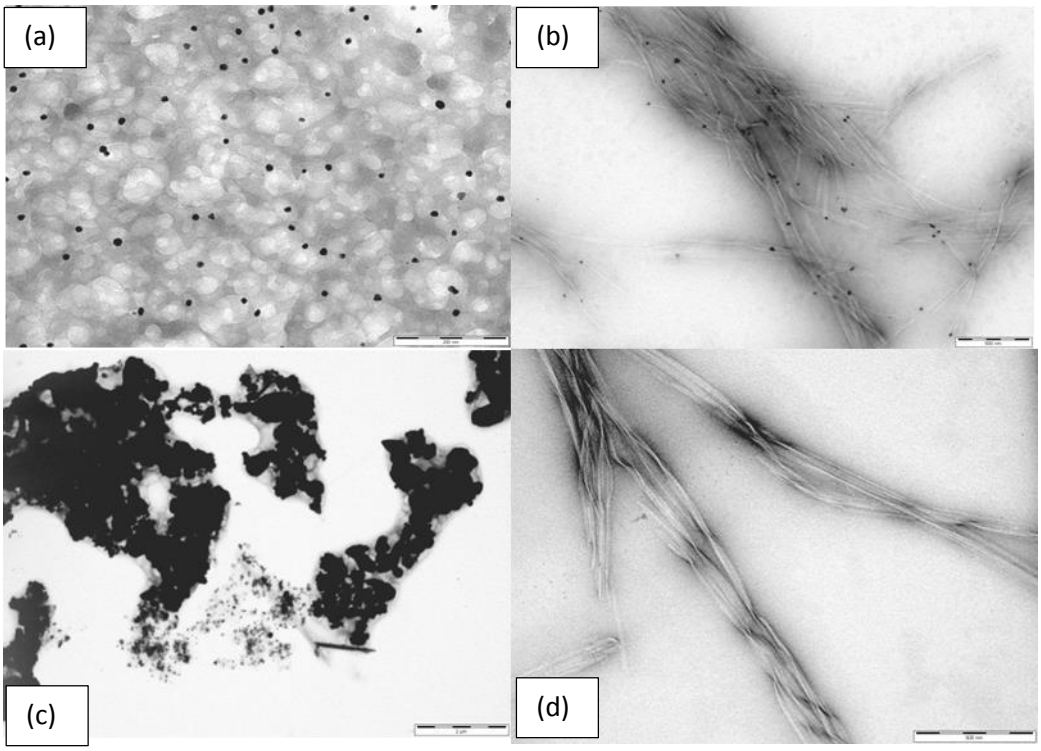

Figure 5.2.17 TEM image for the dried gel of (a) unstained **DBS-COOH**-capped AuNPs (b) Stained **DBS-COOH** capped AuNPs (c) GdL-capped AuNPs in the absence of gelator (d) virgin **DBS-COOH**.

Smith and co-workers have previously reported the orthogonal design and behaviour of a robust and responsive hybrid hydrogel system comprising agarose and **DBS-COOH**.[541] **DBS-COOH** is the responsive component (responsive to pH) while agarose is the robust component. We therefore, reasoned to design a responsive, yet strong gold nanoparticle- hybrid hydrogel composite based on this material. An aqueous solution of Au^{3+} (50 µl, 3.9 mM) was added to a solution of agarose and the low molecular weight gelator and the nanoparticles were allowed to form *in situ*. In order to probe the role of individual gelator components in the composite material, **DBS-COOH** gel was selectively converted into a sol in the presence of other component by diffusing an aqueous solution of NaOH (0.1 M, 100 µl) into the gel network. Universal indicator (UI) was used to monitor the total conversion of the **DBS-COOH** into hydrosol. TEM was used to investigate the morphological perturbation of the composite system. As shown in Figure 5.2.18, the gold nanoparticles prefer to stick

to the **DBS-COOH** gel fibres than the agarose counterpart. On the other hand, when **DBS-COOH** gel fibres were broken down, the nanoparticles coalesced and formed aggregates. This suggests that **DBS-COOH** gel fibres are vital in the stabilization of the AuNPs. This indicates how a pH stimulus can induce changes in one nanostructure (self-assembled gel fibres) which are then transmitted to a second (AuNPs).

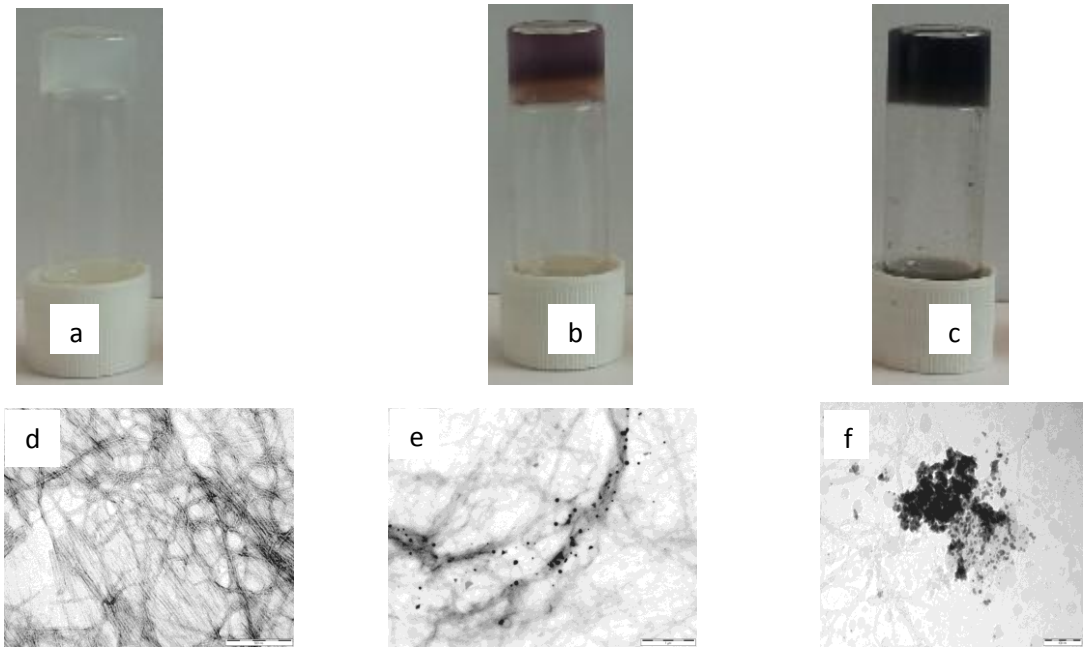

Figure 5.2.18 (a) Hybrid hydrogel (b) Hybrid hydrogel encapsulated AuNPs (c) Hybrid hydrogel-AuNPs + NaOH + UI; Stained TEM image of dried gel of (d) hybrid xerogel (e) hybrid hydrogel-AuNPs (f) Hybrid hydrogel-AuNPs + NaOH + UI

In the past decades, nanostructured stimuli-responsive hydrogels have been used to coat and immobilize gold nanoparticles for target delivery of pharmaceutics.[542-545] However, they are mostly polymer-based and the use of low molecular weight hydrogel to design such pH-responsive hydrogel – AuNPs is rare.[546] Therefore, **DBS-COOH** – AuNPs hydrogel offers a new and interesting potentials for biomedical applications.

5.2.6 High-tech applications of DBS-CONHNH$_2$ hydrogel – NPs hybrid materials

The inherent numerous nanofibrillar interconnections in a supramolecular gel network are vital for the transfer of properties such as electrical and optical conductivities for example in molecular electronics.[222] Many potential applications of conductive

hydrogels are schematically shown in Figure 5.2.19.[547] Therefore, the nanofibre – nanoparticle hybrid hydrogels were investigated for their electrical conductivity as interface between electrolyte and electrode or as a conductive bridge between two electrodes.

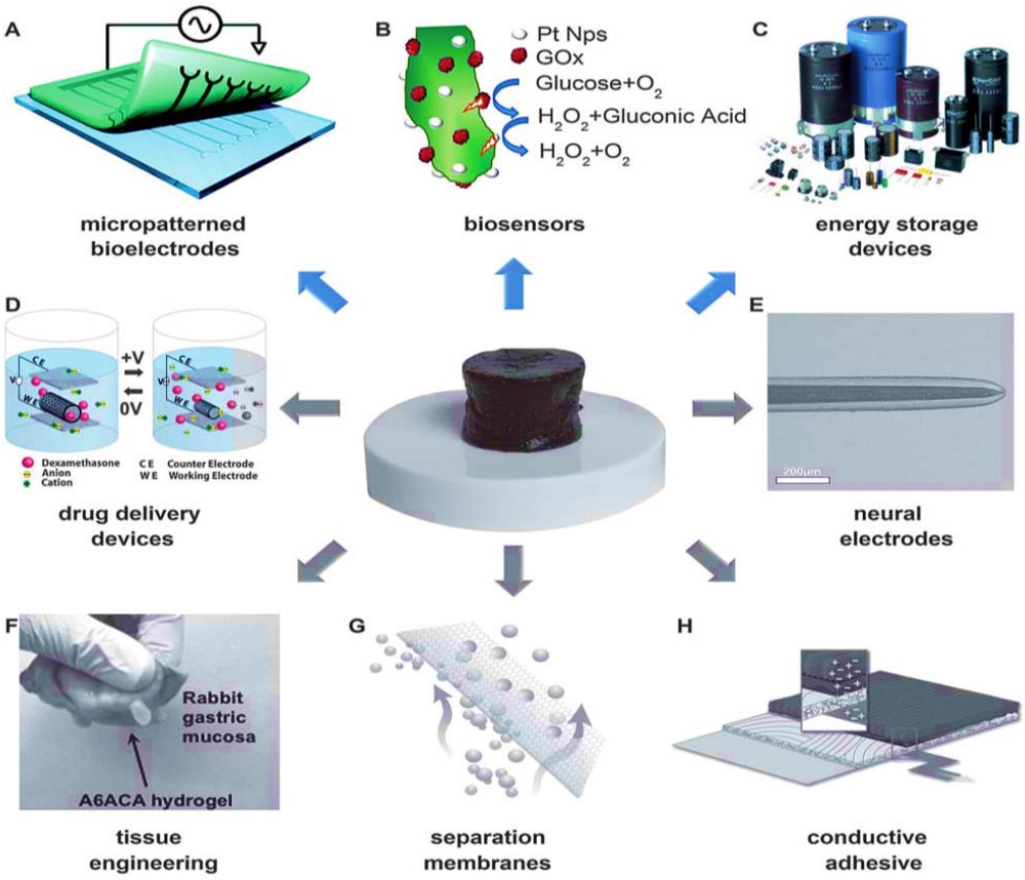

Figure 5.2.19 Representative applications of the hydrogels. (A) Bioelectrodes. (B) Biosensors. (C) Energy storage devices. (D) Drug delivery. (E) Neural electrodes. (F) Tissue engineering. (G) Separation membranes. (H) Conductive adhesives. [Reproduced from ref. 547].

Supramolecular gels are highly dynamic in nature, making them adaptive and responsive to stimuli. However, because their integrity relies on the non-covalent interactions that hold the network together; they are relatively weak and easily break down to a sol when perturbed. Some additives have recently been to enhance the material properties of gels – such as clay, polymers, etc.[258, 548-550] Most common among these additives are polymer-based additives. Therefore, in order to create a robust yet conductive nanogel, agarose (Figure 5.2.20) was compounded with **DBS-CONHNH2** gelator by simple mixing. Agarose, is a polysaccharide which self-assembles into a strong polymer hydrogel when subjected to a thermal heat-cool cycle, as a result of

non-covalent interactions between the polymer chains. It has found applications in separation science, purification of biomolecules and as a culture medium cells.[551-554] We reasoned that formulating our nanoparticle – gel hybrid materials with agarose would provide us with robust materials, which were easier to handle

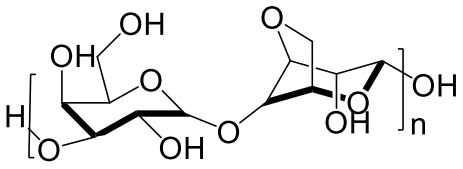

Figure 5.2.20 Chemical structure of agarose

5.2.7 Rheological properties of nanogel –nanofibre hybrid hydrogel

Gels are visco-elastic soft materials because they exhibit both the elastic properties of a solid and the viscous properties of a liquid, therefore, rheology is a versatile technique for investigating the mechanical properties of bulk gels. With the application of oscillating small strains 0.2% to the hydrogels of agarose, **DBS-CONHNH$_2$** and the hybrid agarose-**DBS-CONHNH$_2$**, two dynamic moduli; the storage or elastic modulus *G'*, a measure of the elasticity and the loss or viscous modulus *G''*, a measure of viscous components at a low oscillatory frequency sweep f were obtained. Figure 5.2.21 shows that the *G'* (storage modulus) is higher than *G''* (loss modulus) and both viscoelastic moduli only show slightly low dependence on frequency, which is the characteristic of a solid-liquid behaviour of gel-phase materials in the linear viscoelastic region.[555]

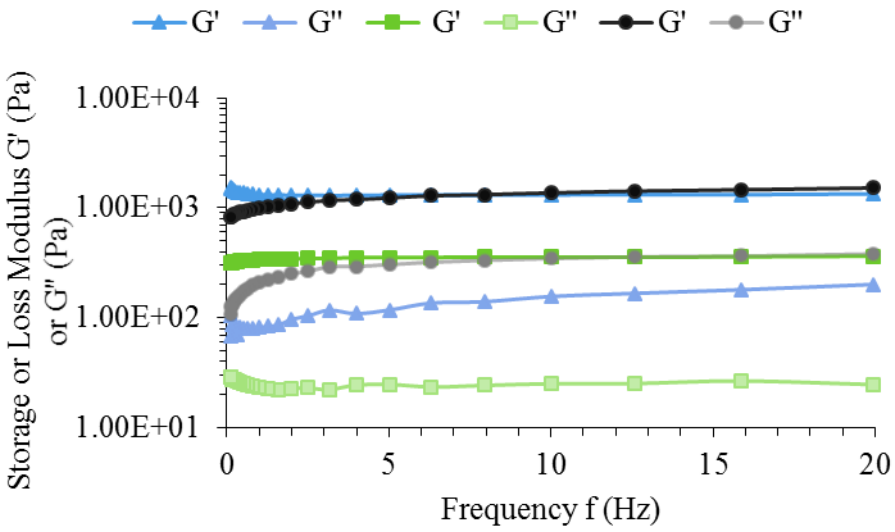

Figure 5.2.21 Frequency dependence of G' and G" for **DBS-CONHNH$_2$** (Δ), Agarose (□) and Agarose - **DBS-CONHNH$_2$** (o) at 25 °C [strain = 0.2%; [gelator] = 0.4% wt/ol]]

Intriguingly, the hydrogels of **DBS-CONHNH$_2$** are stronger and more elastic (G' = 1.36 kPa) than those of agarose (*G'* = 0.34 kPa) and as a result of this the hybrid gelator yields hydrogels with improved mechanical strength than the native agarose but a little lower than that of the low molecular weight gelator; **DBS-CONHNH$_2$** (*G'*= 1.09 kPa).

Oscillatory strain amplitude sweep measurements shown in Figure 5.2.22 also revealed that the critical strain amplitude[556] (a strain amplitude beyond which the behaviour of a material becomes non-linear and the storage modulus decreases) for hydrogels of the **DBS-CONHNH$_2$** is about 10 times than that of agarose. Thus, the hydrogel of the agarose becomes more brittle because the hydrogel structures break down at a smaller strain (1.2%) than those of the **DBS-CONHNH$_2$** (12%) counterparts. Moreover, it is interesting to see that the critical strain amplitude (6%) for the hybrid hydrogel is a little lower than that of the native **DBS-CONHNH$_2$** which implies that the self-assembled nanofibrillar networks of **DBS-CONHNH$_2$** hydrogel sandwiched within the networks of agarose hydrogel enhances the elasticity of agarose hydrogel but slightly lowers that of **DBS-CONHNH$_2$** hydrogel. Similarly, Yang and co-workers have recently demonstrated that the nanofibres of low molecular weight organogelator;

DBS, enhances the mechanical properties of poly (vinyl alcohol) based hydrogels as a result of its ability to dissipate stress around the polymer microdomains.[557]

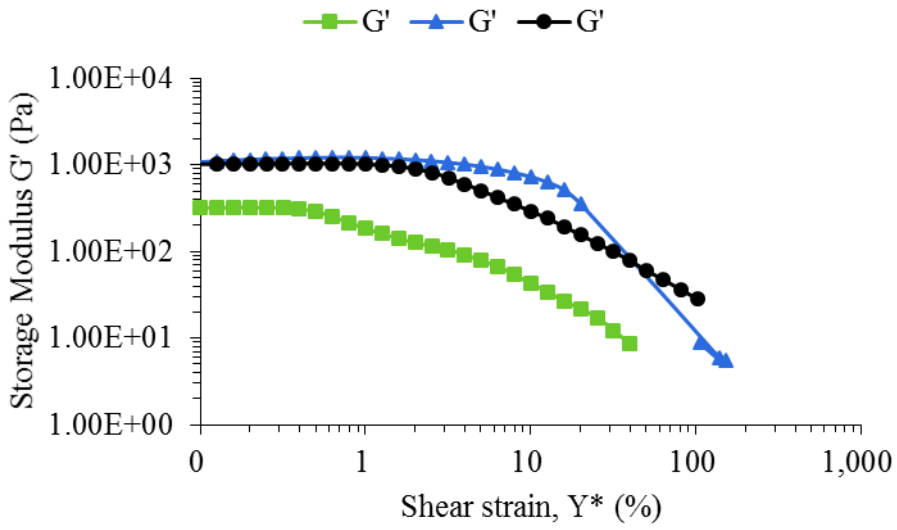

Figure 5.2.22 Strain amplitude dependence of G' for for **DBS-CONHNH2** (Δ), Agarose (□) and Agarose - **DBS-CONHNH2** (o) at 25 °C [frequency = 1 Hz; [gelator] = 0.4% wt/ol]]

The rheological behaviours act as fingerprints of differences in the networks of the various hydrogels as revealed by scanning electron microscopy (Figure 5.2.23). The nanofibres of agarose are fine while that of the **DBS-CONHNH2** have bundles of twisted nanofibres having larger diameters (*ca.* 10 nm), hence the reason for the disparity in their mechanical properties. The nanofibre network of the hybrid hydrogels reveals the interpenetration of the nanofibres of the agarose hydrogels within the self-assembled nanofibrillar network (SAFIN) of **DBS-CONHNH2** hydrogels. Moreover, the mechanical properties of a gel-phase material depend on the fibre density of the network and the degree of cross-linking/ interconnections between the fibres.[558] Vallon and co-workers have demonstrated that supersaturation is the prime driver of nucleation towards fibrillar network formation in agarose hydrogels; when supersaturation is very low, low fibre population and low connectivity among the fibres is inevitable, hence a flexible and weak hydrogel network is produced.[116] This probably buttresses the argument that **DBS-CONHNH2** hydrogels have a better network architecture even at a concentration as low as 0.4% wt/vol.

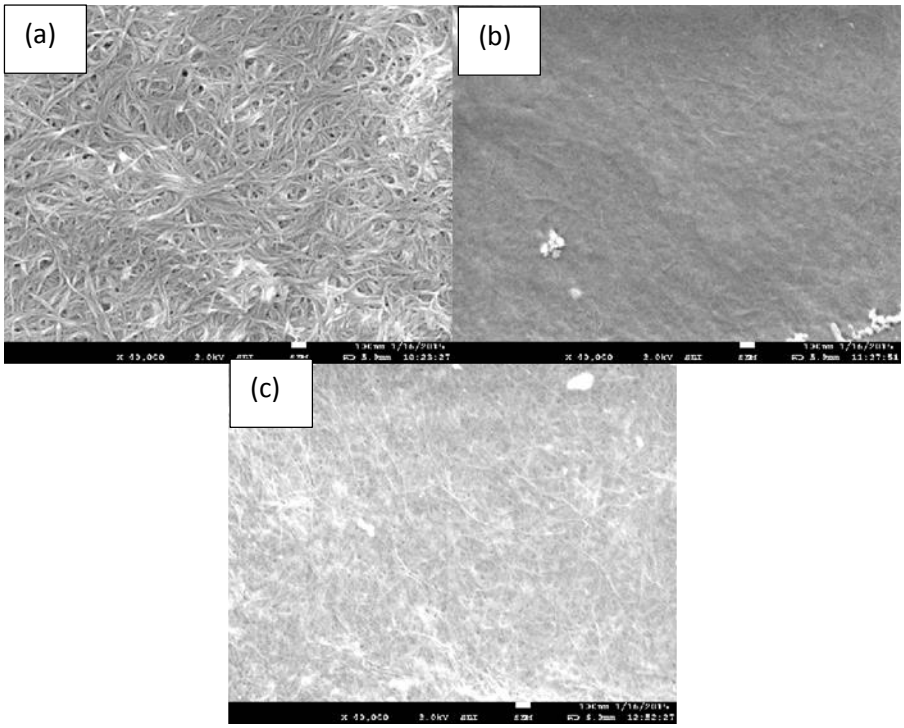

Figure 5.2.23 SEM image of dried xerogel of (a) **DBS-CONHNH$_2$** (b) Agarose and (c) Agarose - **DBS-CONHNH$_2$**

It could be expected that the hydrogel nanofibres would reflect the ‘‘symbiotic’’ relationship between the host nanofibres and the guest nanoparticles that constituted the inorganic-organic hybrid nanomaterial. Intriguingly, however, the hydrogels loaded with nanoparticles exhibit higher mechanical properties than the native hydrogels. Figure 5.2.24 and Figure **5.2.25** shows that when the hydrogels of **DBS-CONHNH$_2$-agarose** were doped with AuNPs, the G’ and the critical strain amplitude increase from 1.1 kPa and 6% to 1.7 kPa and 16% respectively, while they increased to 1.4 kPa and 20% when loaded with AgNPs. This shows that incorporation of NPs into the hydrogels modulated the hydrogel structures by bridging neighbouring nanofibres, thereby making them more compact and rigid than the native hydrogels, hence enhancing the mechanical strength of the hydrogels.[511, 559, 560]

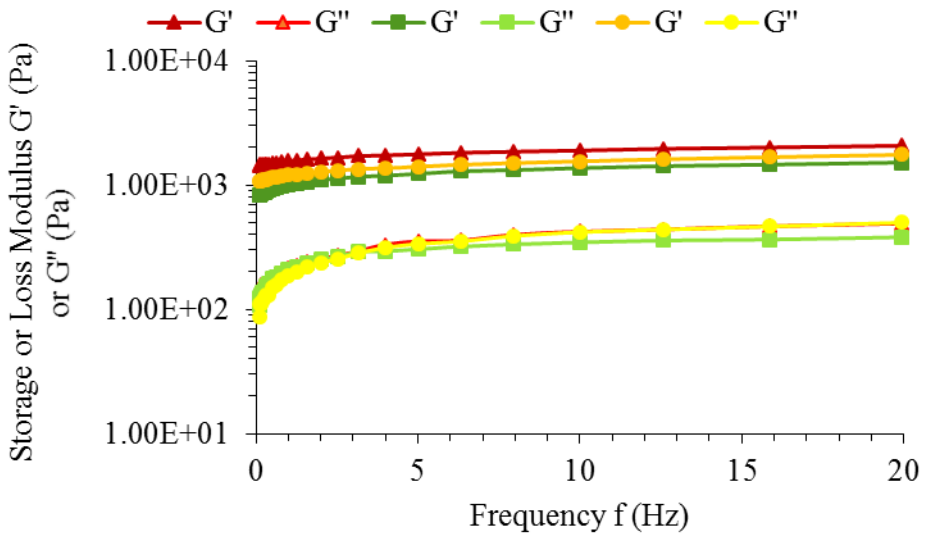

Figure 5.2.24 Frequency dependence of G' for nanogel + AuNPs (Δ), nanogel + AgNPs (o) and Agarose - **DBS-CONHNH$_2$** nanogel (□) at 25 °C [Strain = 0.2%; [gelator] = 0.4% wt/ol/ each]].

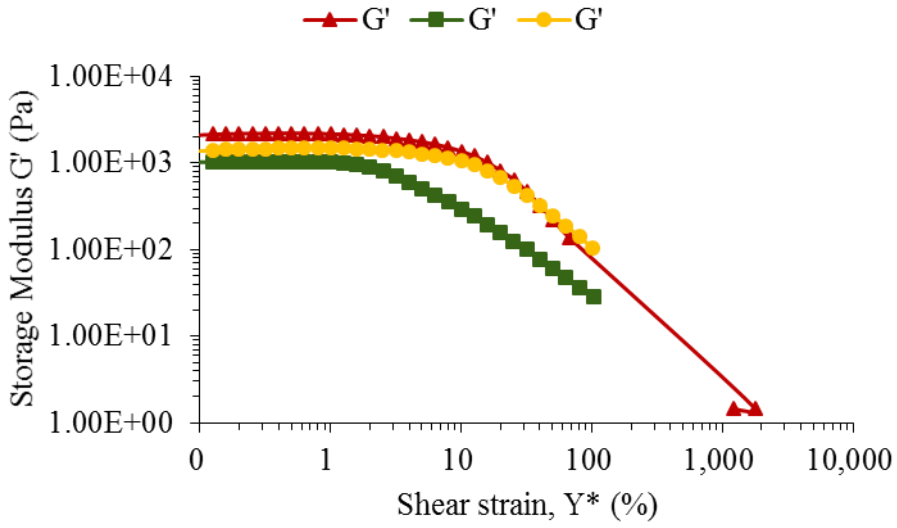

Figure 5.2.25 Strain amplitude dependence of G' for nanogel + AuNPs (Δ), nanogel + AgNPs (o) and Agarose - **DBS-CONHNH$_2$** nanogel (□) at 25 °C [frequency = 1 Hz; [gelator] = 0.4% wt/ol/ each]].

5.2.8 Electrocatalytic reduction of oxygen on nanogel-AuNPs nano-composite

Due to the importance of oxygen reduction, for instance fuel in cell applications, several materials have been employed with or without modifications as cathodes for the reduction of O_2 in different electrolytes. The use of gold and carbon-based materials have been widely reported.[561] However, bulk gold and carbon electrodes are poorly active towards many electrochemical reactions, hence, deposition of nanoparticles on the base electrodes makes them more electrochemically active because of the high catalytic activities of the nanoparticles.[562] Even though, electrochemical deposition and adsorption are commonly employed methods for depositing gold nanoparticles onto electrodes, limitations such as (i) formation of bulk gold and (ii) leaching of nanoparticles into electrolyte remains. Therefore, the use of gels, which can ‘‘wire’’ stabilized nanoparticles onto the electrode via the inherent nanofibrillar networks is a potential measure to circumvent the limitations associated with conventional methods of electrode modification. However, reports on this new technology are scarce except for a few polymer gels.[563-565] Therefore, we became interested in using **DBS-CONHNH$_2$** hydrogel, the first low molecular weight hydrogel applied in this regard, to synthesize a quasi-solid state conductive material having AuNPs embedded. The AuNPs were formed by diffusing Au^{3+} solution into the **DBS-CONHNH$_2$**-Agarose preformed on the surface of a carbon rod electrode (C). The Au^{3+} ions were reduced in situ to Au^0 which further aggregated into nanoparticles, as a result of the interactions with the free amine groups on the **DBS-CONHNH$_2$** nanofibres, hence no extraneous reducing agent was added. The presence of some unreacted Au^{3+} in the gel is unavoidable, hence, the hydrogel-AuNPs nano-composites were submerged into deionized water (200 mL) for 2 h and the water renewed until leaching of a yellow species, characteristic of Au^{3+} was no longer observe, at this point the hydrogels were adjudged ‘clean’. It is essential the free Au^{3+} ions are completely removed prior to electrocatalytic investigations, or else, they will diffuse into the electrolyte solution or become electroplated onto the surface of the electrode, hence, masking the true activities of the hydrogel-AuNPs nano-composites.

Intriguingly, no leaching of AuNPs from the hybrid gel was observed, which confirmed stable nanofibre - nanoparticle interactions. The **DBS-CONHNH$_2$**-agarose-AuNPs catalysed O_2 reduction process was investigated using a cyclic voltammetric

(CV) technique (Voltalab potentiostat) in a three electrode cell having; standard calomel electrode (reference electrode), platinum mesh cage (counter electrode), in-house carbon rod with or without modifications (working electrode) and sodium acetate (100 mM, electrolyte solution) (as shown in Figure 5.2.26). The potential was scanned between -0.25 V and 0.15 V at 20 mV/s for 5 cycles.

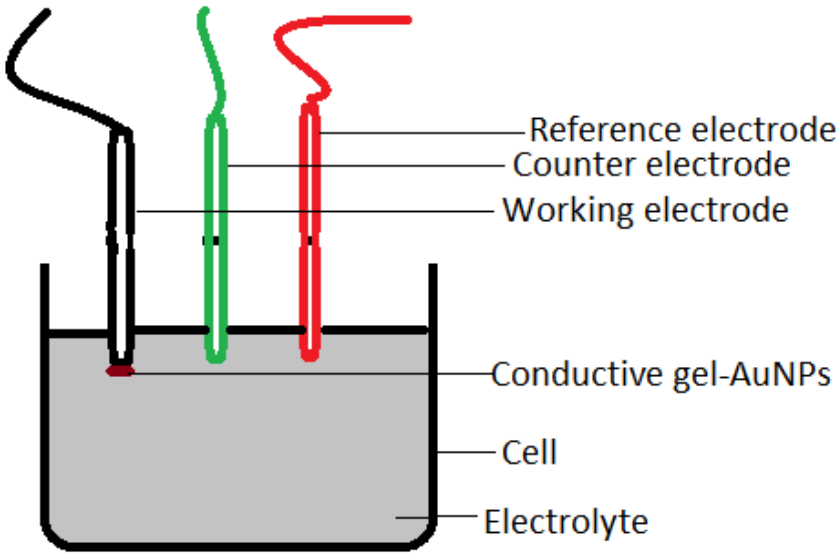

Figure 5.2.26 Schematic experimental set-up for electrochemical reduction of O_2 on carbon rod modified with conductive nanogel - AuNPs

The cyclic voltammograms for O_2 reduction on the bare carbon rod, carbon rod with hybrid hydrogel and carbon rod with hybrid hydrogel and AuNPs are presented in Figure 5.2.27.

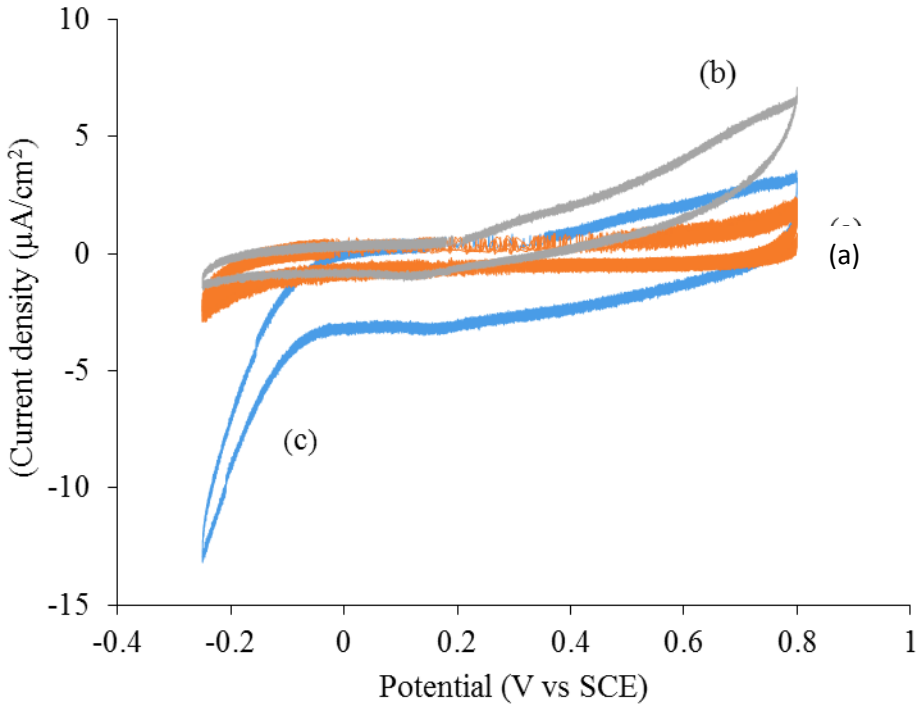

Figure 5.2.27 Cyclic voltammograms of O_2 reduction on a (a) bare carbon rod (b) carbon rod + hydrogel (c) carbon rod + gel +AuNPs. Protocol: [gelator] = 0.5 % wt/vol (10 µl) of each of **DBS-CONHNH2** and agarose, Au^{3+} (15 mM, 10 µl), diffusion time = 30 min, washing in deionised water (200 ml x 2).

It is noteworthy that the mechanism of O_2 reduction depends on the nature of the electrode material used as well as the pH of the medium. For instance, a crystalline gold electrode supports 2-electron reduction of O_2 to H_2O_2 in acidic media while the mechanism becomes a 4-electron reduction of O_2 to H_2O (or OH^-) at pH > 6 (as shown in Scheme 5.2.4).[566]

$O_2 + 2H^+ + 2e^- \longrightarrow H_2O_2$ (Acidic medium)

Eq. (1)

$O_2 + 2H_2O + 4e^- \longrightarrow 4OH^-$

Or (Alkaline medium)

Eq. (2)

$O_2 + H_2O + 2e^- \longrightarrow HO_2^- + OH^-$

Scheme 5.2.4 Mechanisms of O_2 reduction under acidic and alkaline conditions.

The bare carbon rod showed a typical non-Faradaic capacitive current response, however, the modified electrode with only the hybrid hydrogel on it produces a different shape of cyclic voltammogram to that of the unmodified carbon electrode with clear (positive) oxidative current at +0.42 V vs SCE which is indicative of the oxidation of hydrazide group. On the other hand, the current density of the electrode decreases from 5 μA/cm^2 to 3 μA/cm^2 when the hybrid hydrogel was added onto the carbon rod, hence the modified electrode is less conductive due to the insulating property of the layer of hybrid hydrogel. The observed shape of cyclic voltammogram is similar to the CV of native **DBS** gel reported in literature.[567] Interestingly, a much enhanced O_2 reduction was observed when the hybrid hydrogel was loaded with AuNPs. The large reductive current at about -0.18 V vs SCE is presumed to be the over-potential for AuNP catalysed O_2 reduction.[562] The increased electron current from 3 μA/cm^2 to 14 μA/cm^2 is an indication that besides catalysing the reduction of O_2, the AuNPs also create pathways for ionic and electronic transport at the interface between the electrolyte solution through the hybrid hydrogel to the carbon electrode, thereby increasing the effective surface area for a more efficient electrochemical process. Therefore, the gel-nanoparticle system demonstrates how metal nanoparticles can be aligned to communicate with a carbon electrode in a soft matter system and how such materials may have applications as modified electrodes. It is also worthwhile mentioning that the gel networks enables the transformation of planar carbon support surfaces into porous 3D structures of electrochemically active surfaces within a solvent network, and thereby overcoming traditional issues with solvent access to nanostructured carbon materials

In order to predict a likely mechanism for the reduction, it is worth knowing that the pH of the medium (sodium acetate) is alkaline (pH 9). Therefore, the mechanism of the O_2 reduction is most likely to proceed via a 4-electron reduction of O_2 to H_2O or 2-electron reduction to OH^-.

This conductive hybrid hydrogel is a potential substrate for immobilizing enzymes for direct electrochemistry as it might be able to enhance direct electron transfer between redox enzymes and the surface of electrodes without a need of a mediator.[568]

5.2.9 Electrode – electrode interface conductive nanogel-nanoparticle hybrid materials

In the past decades, numerous conductive polymer hydrogels,[497, 569, 570] and low-molecular-weight organogels[503, 507, 571-573] have been widely reported. However, the use of low-molecular-weight hydrogels – nanoparticle hybrid materials to construct electroconductive nanomaterials have not been reported to the best of our knowledge. Therefore, we explored the potential of the **DBS-CONHNH2**-agarose hydrogel to self-assemble into supramolecular nanowires (fibres) to ‘‘house’’ nanoparticles such as AuNPs and AgNPs which were synthesized *in situ*. In this case the hydrogels were made in a mould constructed with a 2 cm screw-capped vial. The vials are baseless, however the bases were temporarily glued to the vials with heat-shrinks prior to gel formation (Figure 5.2.28). This allows for easy extrusion of the hydrogels once they are set. With this design, hydrogels with identical dimensions would be obtained. The gel blocks were suspended into solutions of Au^{3+} and Ag^+ respectively and were allowed to adsorb and transform the noble metals into nanoparticles via hydrazide-mediated reduction.

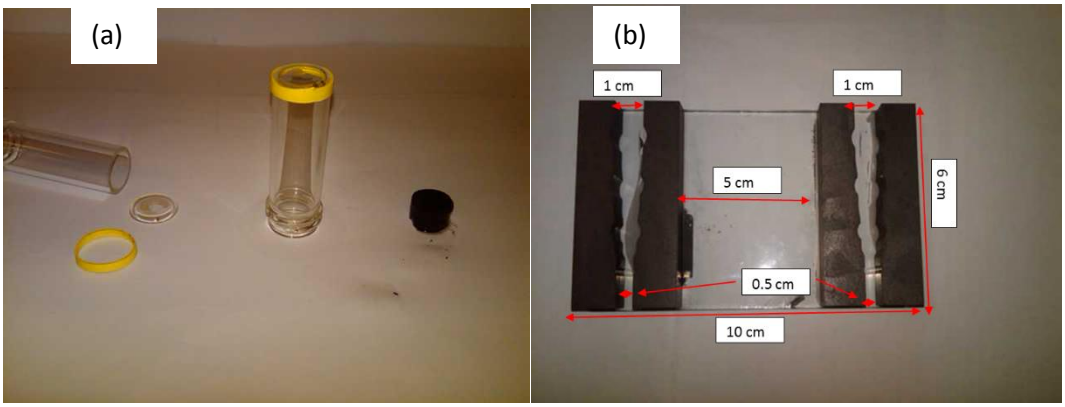

Figure 5.2.28 Photo of constructed (a) mould for hydrogel formation (b) graphite electrodes for conductivity measurement.

In order to have a reproducible device for measuring the conductivity of the conductive nano-composites, we constructed graphite block electrodes glued to a glass slab and separated by a fixed distance. However, the block-block surfaces were constructed such that they can accommodate various dimensions (Ø = 0.5 cm - 1.0 cm) of the gel blocks (Figure 5.2.28b). The electrodes were connected to the negative and positive nodes of a digital conductivity meter with crocodile clipped cables. Prior to measuring the conductivity of the nanogel-nanoparticle hybrid materials, the conductivity meter was calibrated with a range of resistors, water and aqueous solution of NaCl. This was done to check the consistency of the meter. The conductance of air between the two bare graphite rods was 0.009 µS. After calibration, a block of nanogel – nanoparticle was inserted one at a time into the space between the two graphite rods and conductivity measured. Figure 5.2.29 shows that the conductance of the bare nanogel, nanogel-AgNPs, nanogel-AuNPs and nanogel-SWNT are 20 µS, 62 µS, 100 µS and 101 µS respectively. As such, the nanoparticles have clearly imparted the organic nanofibres with enhanced electron conduction.

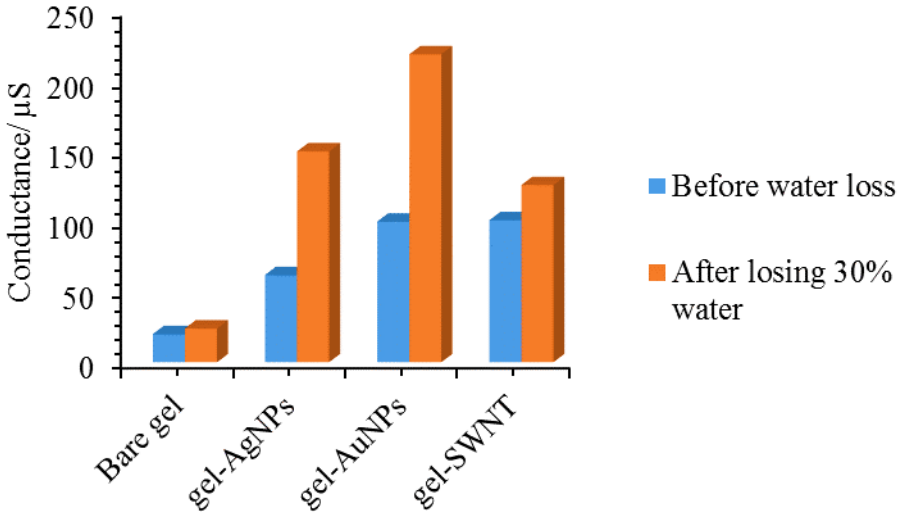

Figure 5.2.29. Conductance of hydrogel-nanoparticles composites before (blue bar) and after (orange bar) dehydration

In order to investigate the effect of water on the conductivity of the hybrid nanomaterials, the blocks of nanogel-nanoparticle composites were air-dried for about 3h. Interestingly, when 30 % of the water composition was lost via evaporation, the conductivities increased to 150 µS, 219 µS and 126 µS for the hydrogel-AgNPs, hydrogel-AuNPs and hydrogel-SWCNT nanocomposites respectively. The rationale behind this increase in conductivity is the fact that charge transport is mostly favoured when there is a high number of interconnected fibres. Although, there is a vast number of nanofibres in a wet hydrogel, they are highly solvated and therefore have few contacts with one another limiting conductivity.[222] Drying and water loss therefore increases network connectivity and conductivity. These conductive nanostructured nanocomposites are ideal for bridging the soft matter world of biology and the hard matter world of electronic devices. This approach has recently been demonstrated with gelatin – SWNT for engineering cardiac tissues.[570] It is important to mention that single walled carbon nanotube (SWNT) was used as a reference conductive material due to its widespread applications in constructing conductive nanomaterials for biological applications.

5.3 Conclusion and outlook

The **DBS-CONHNH$_2$** envirogels demonstrated high uptake of noble metals from water, thereby yielding clean water with selectivity towards them better than earth-

abundant metals. Due to the pendant hydrazide functionality on the gel nanofibres, these materials exhibited self-reducing and capping ability towards gold and silver, and transformed them into nanoparticulate forms. As such, the nanofibres hosted the nanoparticles by immobilizing them while the nanoparticles imparted the organic nanofibres with enhanced mechanical and thermal stability within optimum **DBS-CONHNH$_2$**: nanoparticles ratio. The nanogel – NPs are stable under a wide range of pH for about three (3) months. Furthermore, due to the inherent electrical conductivity and catalytic ability of noble metal nanoparticles, the hybrid nanostructured nanogel became conductive and electrocatalytically reduced oxygen.

On the other hand, **DBS-COOH** hydrogel demonstrated a significant uptake of Au^{3+} ion from water and reduced the adsorbed gold to AuNPs in situ. As such, a pH-responsive hydrogel encapsulated AuNPs was fabricated.

It is hoped that due to the conductivity and catalytic abilities of **DBS-CONHNH$_2$** hydrogel – NPs hybrids, they will find applications in areas as diverse as fuel cells, nanobioelectronics, conductive soft matter interfaces with biological systems, nanoreactors, conductive adhesives and antibacterial component for paint and surface coating, wound dressing and drug delivery. **DBS-COOH** – AuNP hybrid hydrogels also holds promising potential for biomedical applications.

6 Chapter 6 – Increasing the functionality of DBS-CONHNH$_2$ hydrogelator by incorporating a second component.

This project was carried out in conjunction with MChem student, Edward J. Howe and the findings have been published in – *Chem. Commun.* 2015, 51, 7451 - 7454 and has also featured as a research news item in *ChemistryWorld* magazine on 15th April, 2015 and *ScienceDaily* magazine on 1st April, 2015.

6.1 *Introduction*

Incorporation of materials such as drugs, nanoparticles and nanotubes into the network of supramolecular gels as cargoes or guests to enhance the functionalities of the gel is a burgeoning area of research. These additives could be mere residents in the pocket of the gel network or participate in the gelation process as a co-gelator. It has been demonstrated that when they act as co-gelators, a variety of nanostructures – worm-like micelles,[574, 575] spherical micelles, microemulsions,[576] nanotubes[78] and nanofibres,[577] crystals,[578] often emerge. The ultimate search for novel methods to circumvent the problems often associated with drug administrations such as poor water-solubility and low bioavailability[579, 580] has led to the development of numerous approaches- particle size reduction,[581 582] addition of surfactants,[580, 583] complex formation and physical entrapment,[584-587] adsorption onto nanoparticles,[588, 589] and PEGylation[590] for the controlled-delivery of drugs. However, these classical techniques are characterized with certain shortcomings such as tissue inflammation, cell death, burst release, non-biodegradability, non-biocompatibility, poor drug stability and shelf-life, loss of drug potency, first pass effects, systemic circulation, and multi-step syntheses.[591, 592]

6.1.1 Uses of supramolecular hydrogels in drug delivery technology

The use of hydrogels derived from polymers as robust drug delivery systems for various routes of administration has been extensively reviewed.[593, 594] The suitability of polymer-based hydrogels as drug carriers is predicated on their mechanical properties and ability to absorb large volume of solvents which make them swell to several hundred times their original sizes. However, when a polymer undergoes

degradation, it can lead to the generation of chains of different sizes that might be cytotoxic or trigger unhealthy side effects. In past decades, low molecular weight hydrogels also known as supramolecular hydrogels have begun to attract attention in various pharmacopeia as ‘‘intelligent’’ vehicles for both lipophilic and hydrophilic drugs owning to their highly solvated, porous and responsive networks.[595] Unlike, polymer-based gels, LMWGs are usually composed of < 1% gelator while the liquid component is usually about 99%, therefore, there is no need for a post-gelation solvent absorption which triggers swelling.

In most cases, LMWG and Active Pharmaceutical Ingredients (API) composites are usually formulated using one of two strategies: covalent conjugation and physical encapsulation.

6.1.2 Covalent Conjugation of API

In this case the drug molecule is covalently conjugated onto a known gelator, thereby creating a prodrug with amphiphilic properties that will enable it to self-assemble into nanofibrillar networks. The therapeutic agent will then be delivered slowly by hydrolytic or enzymatic degradation at the target part of the body. On other hand, a linker can be functionalized prior to a covalent conjugation to the API. Upon enzymatic cleavage of a labile part of the linker, the resulting amphiphilic prodrug can self-assemble into supramolecular hydrogel.[277] This method has the potential to circumvent problems such as low drug loading, uncontrolled release, rapid degradation of prodrug, hypersensitivity and surface neuropathy which are often associated with the formulation and administration of molecular prodrugs.[596-598] To pioneer research in this area, Xu and co-workers reported the first antibiotic, vancomycin - pyrene based low molecular weight hydrogelator **6.0** (Figure 6.1.2) that self-assembled into a thermo-reversible hydrogel with helical nanofibres via the cooperative influence of pi-pi interaction and hydrogen bonding between two gelator molecules.[599] It was demonstrated that only 0.36 wt % of the gelator was require to gel *ca* 23000 molecules of water, making it a supergelator. Interestingly, the hydrogel of **6.0** demonstrated significant potency against certain Gram-positive bacteria even at 8 -11 fold dilutions lower than the corresponding parent drug- vancomycin. It has been reasoned that this might be as a result of high local concentration of the drug which follows self-aggregation of the gelator at the surface of infected part (s).

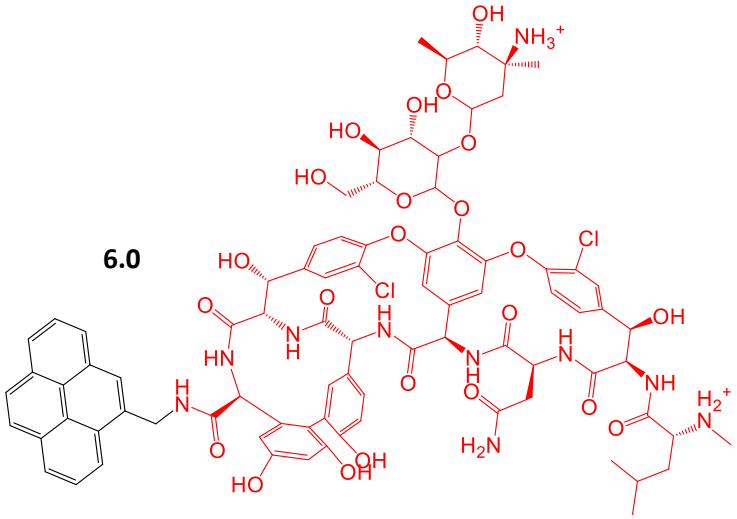

Figure 6.1.1 Structure of vancomycin-pyrene (**6.0)** based hydrogelator.

The modification of a commercially available anti-inflammatory drug- (*S*)-(+)-ibuprofen (**6.1**) has also been reported by Kim et al.[600] The drug molecule was functionalized with various L-amino acids to make dipeptidic prodrug hydrogelators (**6.2** and **6.3**, Figure 6.1.2). Among the various prodrugs, **6.2** demonstrated some ability to gel aqueous solution, but more efficiently 20%:80% ethanol:water mixture; the minimum gelation concentration (MGC) decreases from 0.9 to 0.25% wt/vol in the presence of ethanol. Compound **6.3** only formed a hydrogel (MGC = 0.5% wt/vol) in the presence of 20% ethanol reflecting the fact that the polarity of a solvent is an integral determinant of the gelation potential of a low molecular weight gelator.[208] In addition, hydrogels of the prodrugs formed bundles of nanofibres (Figure 6.1.3a and b). The release of **6.1** from the prodrug hydrogels was mediated by carboxypeptidase Y.

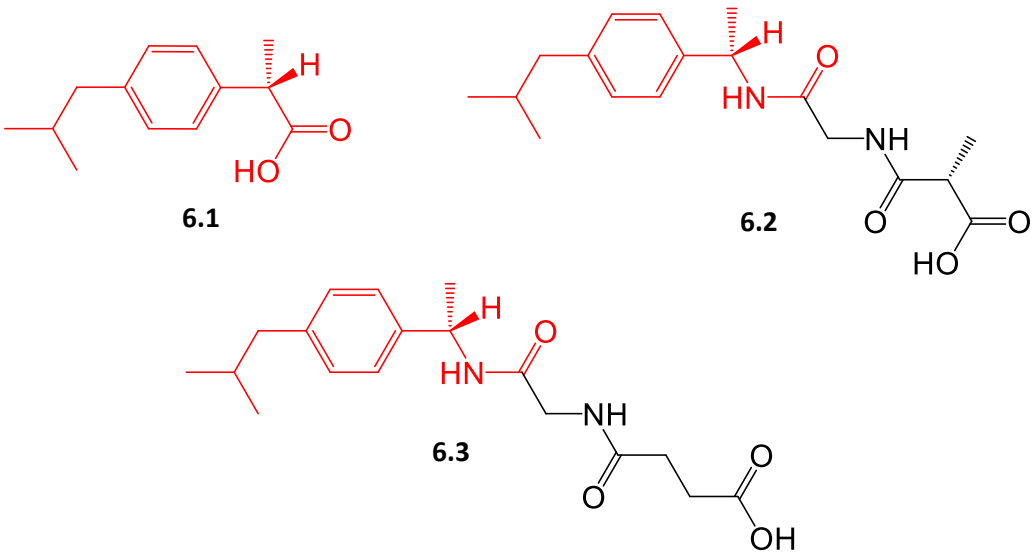

Figure 6.1.2 Structures of **6.1**, **6.2** and **6.3**

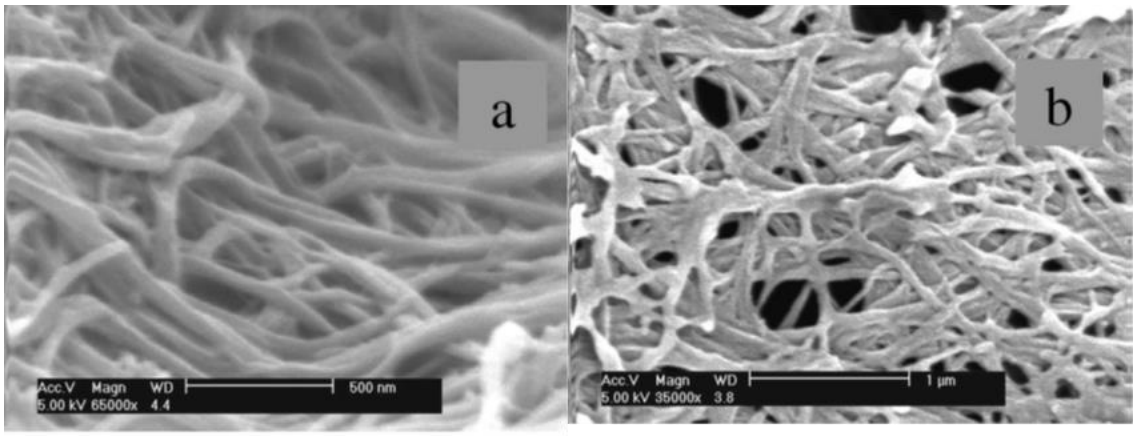

Figure 6.1.3 SEM of the dried xerogel of (a) **6.2** and (b) **6.3**

John and co-workers designed various amphiphilic and bolaamphiphilic acetaminophen **6.4** based prodrugs which self-assembled in water and alcohols to form thermoreversible hydrogels and organogels respectively.[601] The amphiphilic (**6.5 – 6.8**) and bolaamphiphilic (**6.9** and **6.10**) were synthesised by appending various biocompatible fatty acids onto the phenolic group of the parent acetaminophen. It was established that the ability of each of the prodrugs to self-assemble into varied nanostructures such as fibres and sheets is predicated upon the interplay of various non-covalent interactions such as hydrogen-bonding, π-π stacking and van der Waals forces between the gelator molecules.

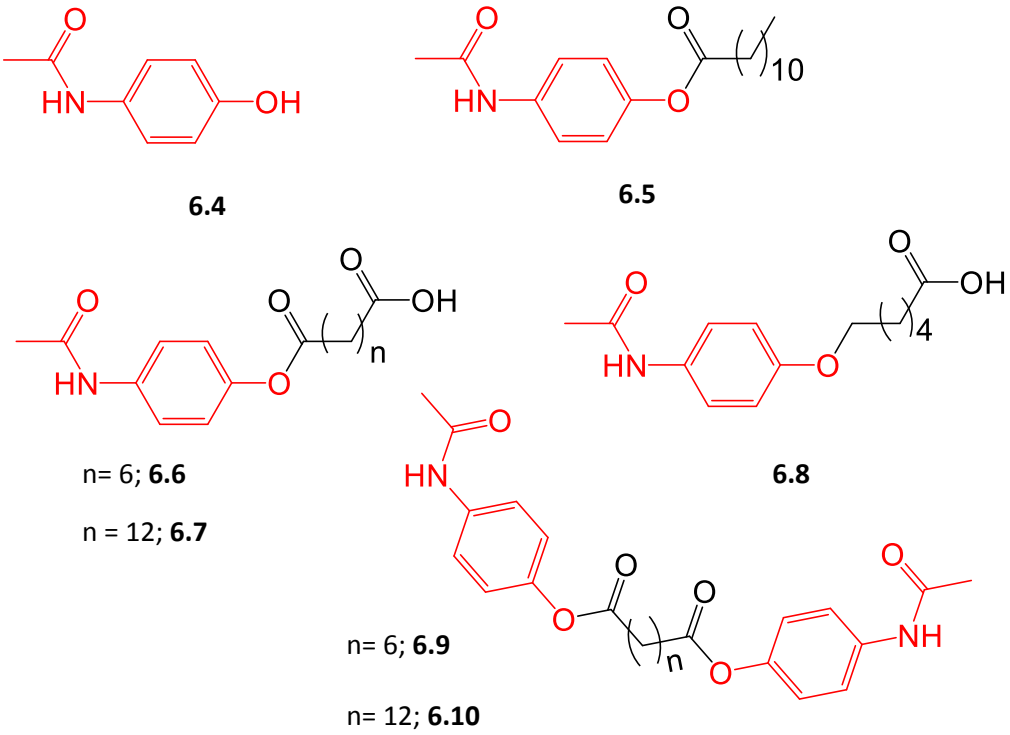

Figure 6.1.4 Structures of Acetaminophen based self-assembled prodrugs

Not only were the prodrugs able to act as self-deliverable vehicles but also encapsulate curcumin as a second drug via physical interactions (as shown in Scheme 6.1.1). Surprisingly, when exposed to an enzyme (esterase) at physiological temperature, the prodrug based hydrogels degraded, thereby releasing the two active drug molecules; acetaminophen and curcumin. However, no degradation was observed in the absence of an enzyme.

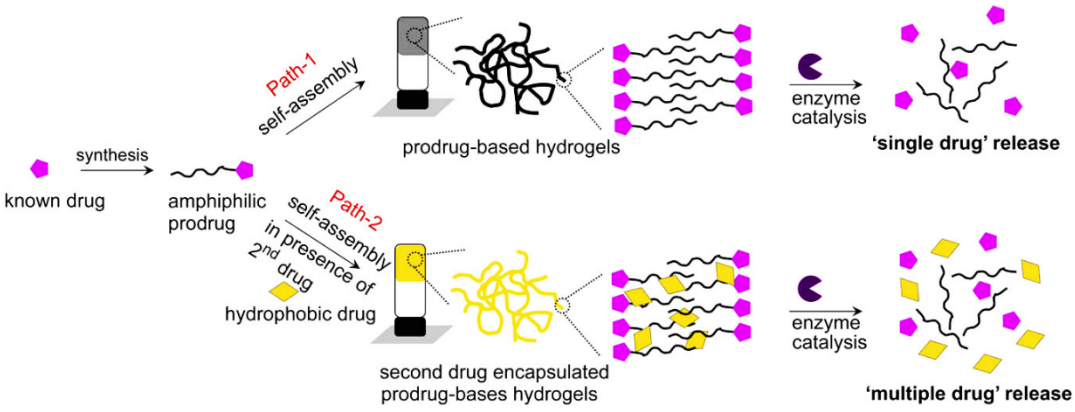

Scheme 6.1.1 Schematic representation of the design of degradable prodrug-based hydrogelators, therapeutic agents in the gel, and subsequent enzyme-triggered single (path-1) and multiple (path-2) drug-delivery. (Reproduced from ref. 601).

The design, synthesis and characterization of a nonsteroidal anti-inflammatory drug (NSAID) naproxen-based prodrug hydrogelator with selectivity for inhibiting cyclooxygenase-2 (COX-2) was demonstrated by Xu and co-workers.[602] The NSAID was functionalized with D-amino acids to form a library of naproxen-based prodrugs (shown in Scheme 6.1.2). The prodrugs formed stable hydrogels under different ambient conditions- enzymes, temperature and pH. The TEM images of the dried xerogels of the prodrug hydrogelators show that **6.18 – 6.23** prodrugs with various appendages (amino acids) self-assembled into nanofibres of varied sizes shapes. *In vitro* inhibition assays for both COX-1 and COX-2 enzymes shows that incorporation of D-amino acids makes naproxen highly selective towards COX-2 and reduce its adverse side effects.

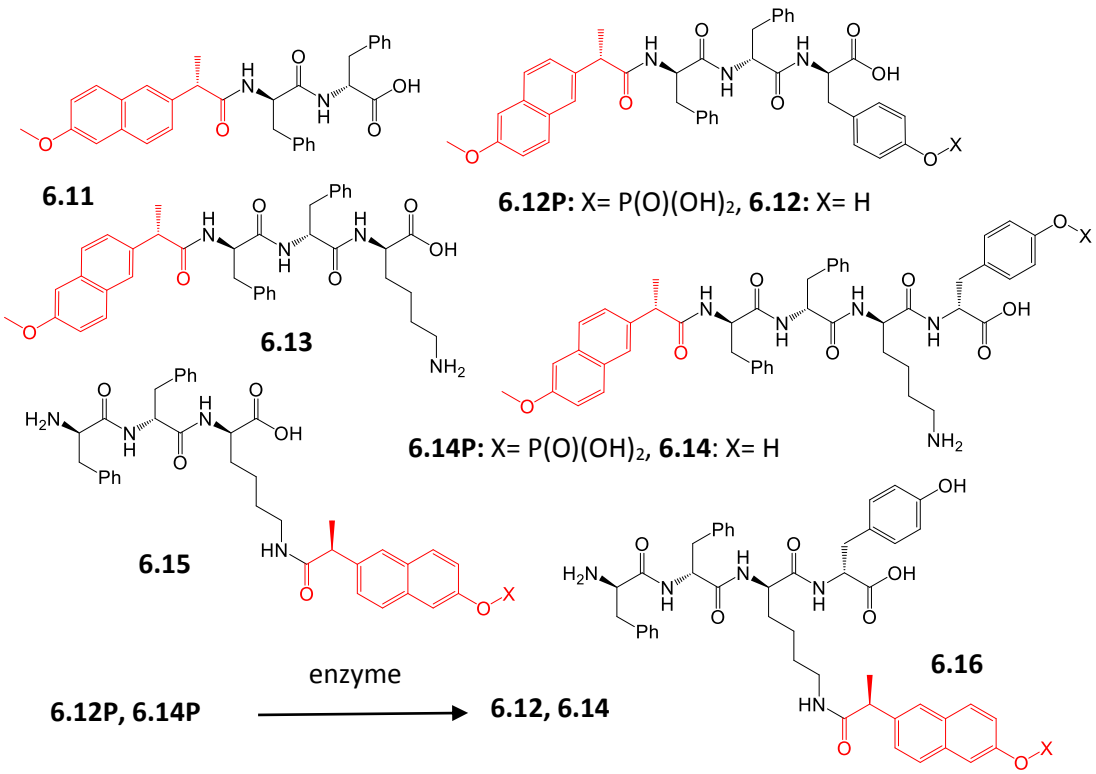

Scheme 6.1.2 Hydrogelators structures consisting of D-amino acid and naproxen.

It is important to mention these chemical modifications might cause a significant alteration to the physicochemical properties of the parent API, and hence cause adverse side effects in the body. Furthermore, many of the modifications require multiple synthetic steps to make the target prodrug – making the approach time consuming and tedious. As such, the market price of the drug becomes inflated. Therefore, physical

encapsulation of API rather than chemical modification offers some advantages in terms of simplicity and cost drug delivery.

6.1.3 Physical encapsulation of API

In this case, a drug molecule is physically entrapped within a gel matrix which may or may not interact with it. This has been reported by many authors.[598] This was demonstrated by Friggeri, and co-workers when they reported the first low molecular weight hydrogel for controlled drug release.[603] Cysteine-based molecule **6.7** (Figure 6.1.5) formed a stable gel in water, salt solution and buffer solutions by using either heat-cool cycle, pH-switching or adding co-solvent, while 8-aminoquinoline **6.8** and 2-hydroxyquinoline **6.9** were used as the model drug molecules. Phase transition (T_{gel}) experiments showed that the presence of **6.9** in the hydrogel has little or no effect on the T_{gel} value of **6.7**, however, the incorporation of **6.9**, at lower concentration resulted in *ca* 10 °C increase in the T_{gel} value – a feature which had previously been reported for a different additive.[604] On the other hand, when the concentration of **6.8** was increased to 1 molar equivalent of the gelator, the hydrogel was disrupted and a precipitate formed. Moreover, their release profiles from the hydrogel using NaOH as the release trigger shows that **6.8** has a higher binding constant to the gel fibres than **6.9**, hence the release kinetics of **6.9** were faster than those of **6.8** probably due to stronger interaction between the amine drug and the carboxylic acid based hydrogelator. It should be noted that many studies in this field have made use of model drugs rather than actual active pharmaceutical ingredients (APIs).

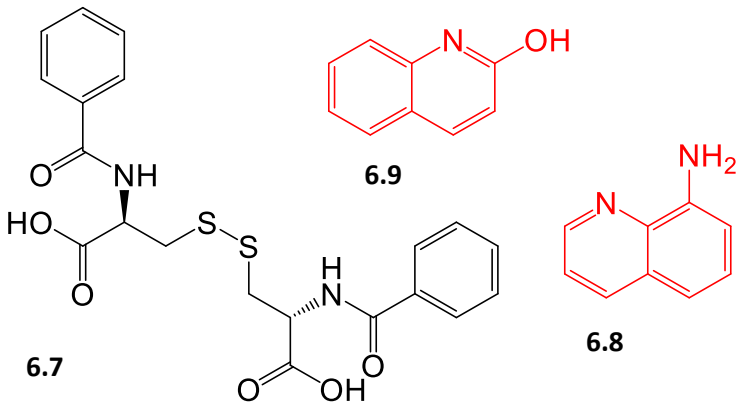

Figure 6.1.5 Structure of (a) *N*,*N*-dibenzoyl-L-cystine (**6.7**) (b) 8-aminoquinoline (**6.8**) (c) 2-hydroxyquinoline (**6.9**)

The syntheses and gelation properties of biotylated amino acids (**6.10**) have been reported by Kim et al.[605] The conjugates were designed such that the terminal carboxylic acid group of the amino acids were preserved. Even though, none of the individual components formed a stable hydrogel in their own right, the conjugated systems formed smart gels in water, NaCl solutions, buffers and variable pH conditions, regardless of the type of amino acid coupled (R= L-phenylalanine, L-leucine, L-methionine, L-isoleucine, L-valine, L-tyrosine, L-tryptophan, L-norvaline, L-norleucine, DL-2-aminoenantic acid and DL-2-aminocaprylic acid). Electron microscopy revealed that the self-assembled dried gels of **6.10** are characterized with varied type of structures - fibrous and lamellar, diameters of which range from 20 to 50 nm. Besides being able to bind Streptavidin, azidithymidine **6.11** was used as a model drug encapsulated within the biotylated L-norleucine based hydrogel. The release study of **6.11** from the hydrogel shows that *ca* 18 % of the drug was slowly released into the supernatant water layer on top of the gel over 9 h.

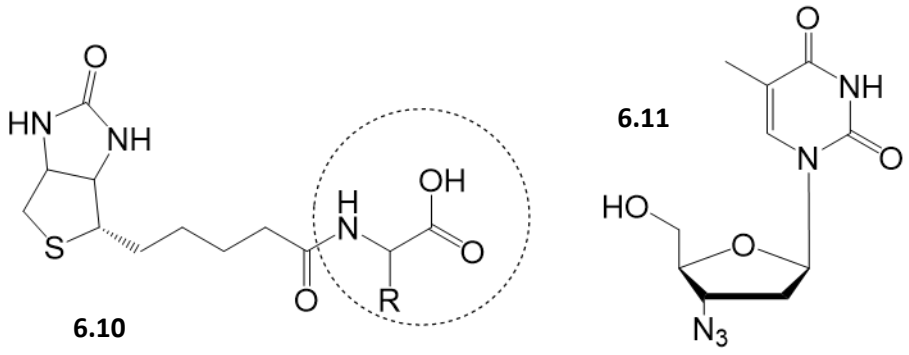

Figure 6.1.6 Chemical structure of (a) biotylated amino acid **6.10** (b) Azidithymidine **6.11**

The design of a 'green' hydrogel from amygdalin, a renewable resource by regioselective biocatalysis has also been reported by Vemula and co-workers.[606] The derivatives of amygdalin efficiently gelled water and organic solvents (MGC 0.05-0.2% wt/vol). The self-assembly of amygdalin in various solvents led to the formation of nanofibres of different shapes (helical ribbon) and sizes (40 -50 nm). As a proof of concept, the release of hydrophobic drug- curcumin, encapsulated within the gel network was triggered by using hydrolase enzyme which cleaved the ester group, thereby degrading the gel.

Yang and co-workers have investigated the entrapment and controlled release of salicylic acid (**6.12**) from L-phenylalanine-based (**6.13**, Figure 6.1.7) hydrogel which was made by the traditional heat-cool cycle. Release of the entrapped **6.12** was monitored using UV-Vis spectroscopy to measure the concentration of the supernatant layer in a static mode at selected time intervals. Scheme 6.1.3 is an outline of the release of **6.12** from the hydrogel. It was also demonstrated that **6.12** was best released into an acidic (pH 4) receiving solvent than basic and neutral receiving media.[607]

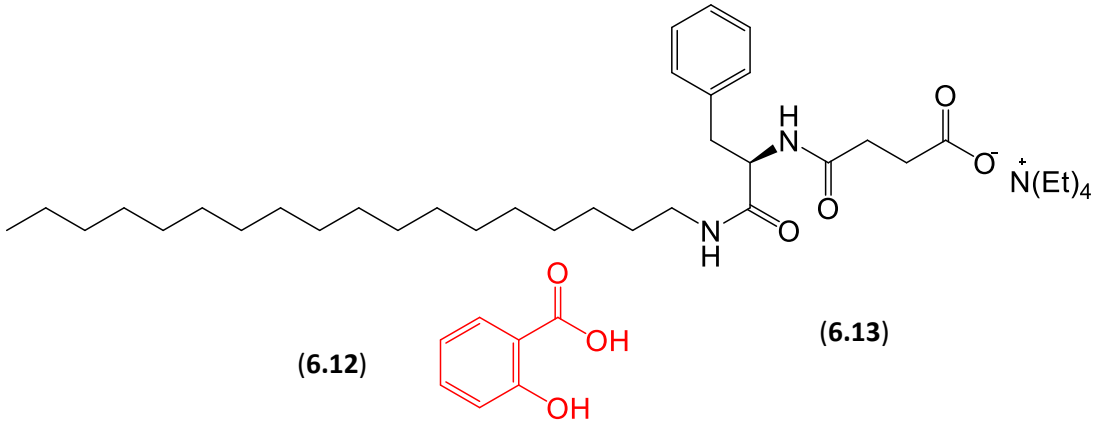

Figure 6.1.7 Structural formula of Salicylic acid (**6.12**) and L-phenylalanine-based gelator (**6.13**).

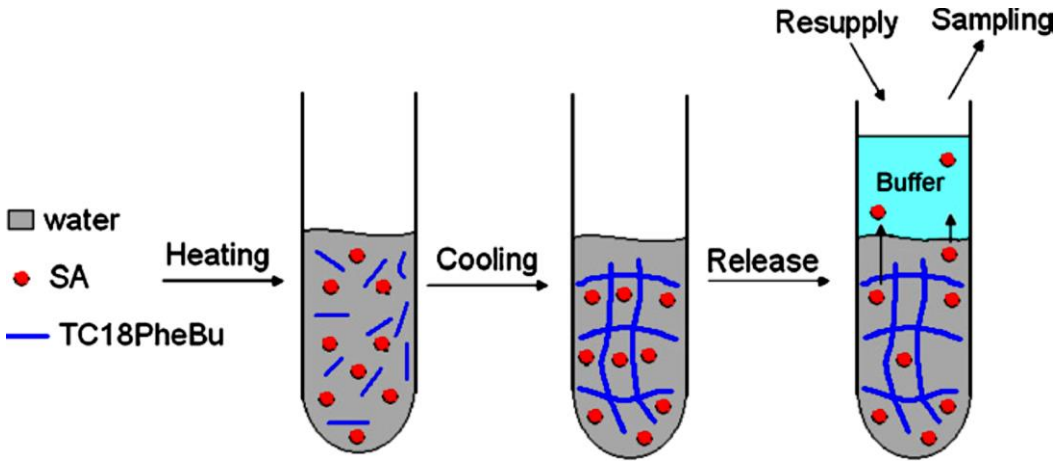

Scheme 6.1.3 Model design of **6.12** release from supramolecular hydrogel (Reproduced from ref. 607).

Besides the use of amino acids/ peptides, other LMWGs based on different molecular building blocks such as G-quartets,[315] imidazolium–based amphiphiles,[608] fatty acid–

modified disaccharides,[606] have been investigated for physical entrapment and controlled release of drugs.

Furuishi and co-workers patented a pharmaceutical formulation containging an organogel, a fatty acid ester and glycerolglycerin fatty acid ester that incorporated non-narcotic analgesics for external applications.[609] The use of **DBS** as an organogelator with 30% ethanol to furnish an organogel presented good skin permeability and high drug release – leading to efficient transdermal absorbable pharmaceutical compositions.

In a very recent patent by English and co-workers, pseudoephedrine **6.14** (Figure 6.1.8) a highly effective over-the-counter decongestant, was formulated within **DBS** organogel which acts as a controlled release formulation.[235] This invention is predicated upon a significant social problem often encountered with the abuse of over-the-counter pseudoephedrine. It is used for the illicit synthesis of methamphetamine **6.15** (crystal meth) – an extremely addictive stimulant drug.[610] By formulating pseudoephedrine within a gel it becomes much more difficult to use as a precursor for methamphetamine synthesis, as it is not possible to easily remove pure pseudoephedrine – the process is time-consuming and tedious. However, if pseudoephedrine is not removed from the gel, the reducing conditions for its conversion to methamphetamine lead to breakdown of **DBS**, wasting reductant and contaminating product. It is argued that this formulation may therefore allow continued use of pseudoephedrine as an over-the-counter medication.

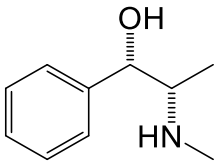

6.14

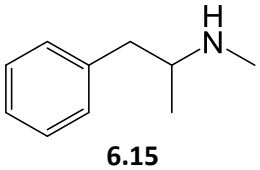

6.15

Figure 6.1.8 Chemical structure of (a) pseudoephedrine **6.14** and (b) methamphetamine **6.15**.

Despite the cleverness of these novel **DBS** technologies, they are limited by the use of organic solvents. Therefore, in these project, **DBS-CONHNH2**, one of the pioneer **DBS**-based hydrogelators developed in this thesis will be used to encapsulate certain

analgesics – ibruprofen (**IBU**), naproxen (**NPX**) and 5-amino salicylic acid (mesalazine, **MSZ**) (Figure 6.1.9) and explore its ability to demonstrate a controlled–release of the APIs under various pH conditions. It is important to mention that these APIs were chosen because they are acidic and as such, it is expected that the carboxylic acid group of the drug would interact with the amine group of **DBS-CONHNH$_2$** hydrogelator.

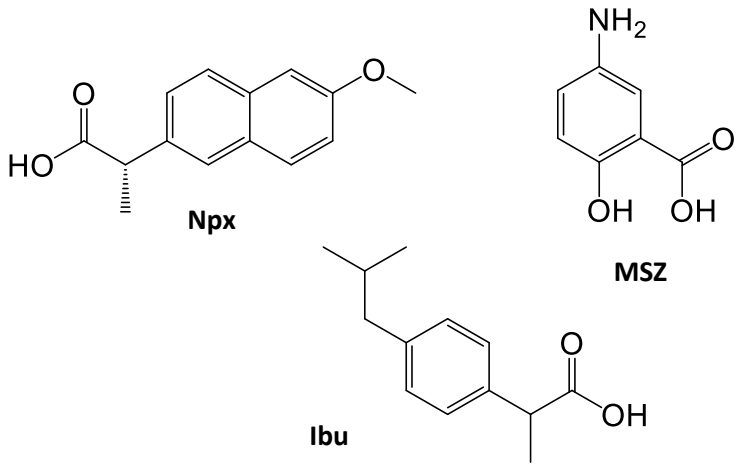

Figure 6.1.9 Structures of the APIs used.

6.2 *Results and discussion*

6.2.1 Formulation of DBS-CONHNH$_2$ hydrogel encapsulated APIs

The initial study involves exposing a pre-formed **DBS-CONHNH$_2$** hydrogel to a supernatant solution of **MSZ** (Figure 6.1.1.9). UV-Vis spectroscopy was used to monitor the withdrawal of the API from the supernatant liquid as it diffuses into the gel network. It is important to mention that due to sparing solubility of **MSZ** in pure water, acetate buffer (pH 4.65) was used to dissolve the API. Figure 6.2.1.1 shows that **DBS-CONHNH$_2$** hydrogel nanofibres demonstrated rapid and significant adsorption towards **MSZ** over a period of 24 h as it adsorbed ca. 1 molar equivalent (equivalent to an excellent API/gelator loading of 0.32 g/g). This observation suggests a specific amine – acid interactions between **DBS-CONHNH$_2$** and **MSZ**, with a 1:1 complex being formed.

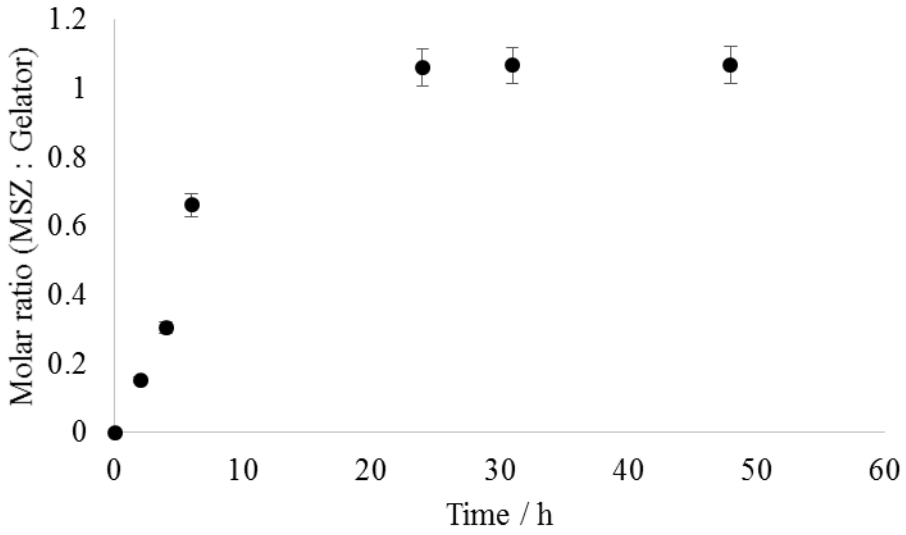

Figure 6.2.1 Uptake of **MSZ** from solution into **DBS-CONHNH$_2$** hydrogel.

Fitting the adsorption data into adsorptive kinetic models, pseudo–second order adsorption kinetics best described the uptake of **MSZ** unto the nanofibres – as we have demonstrated with dye and metal adsorption systems.[112] As such, **DBS-CONHNH$_2$** hydrogels hold great potential for sequestering pharmaceuticals from wastewaters.

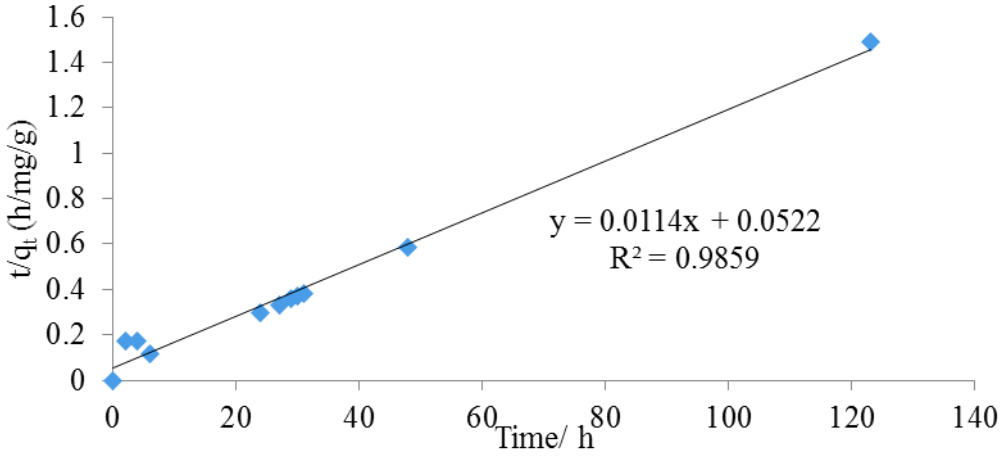

Figure 6.2.2 Pseudo - second order kinetics for uptake of **MSZ** into **DBS-CONHNH$_2$** hydrogel.

After loading MSZ, the T_{gel} value of **DBS-CONHNH$_2$** was lowered by *ca* 20 ºC. It is proposed that interactions of gel nanofibres with **MSZ** cause this, possibly because the complex is slightly more soluble than **DBS-CONHNH$_2$** alone.

It is worth noting that this concept for API loading could not be extended to the other selected APIs because they are insufficiently soluble in water. The logP values of **MSZ**, **IBU** and **NPX** are 1.2, 3.34 and 3.50 respectively, as such, **IBU** and **NPX** are significantly more hydrophobic and insoluble than **MSZ**. Thus, we devised an alternative method for loading these APIs into **DBS-CONHNH$_2$** hydrogels.

The ability of **DBS-CONHNH$_2$** hydrogel nanofibres to bind APIs, thereby enhancing the solubility of carboxylic acid functionalized drugs- naproxen (**NPX**), ibruprofen (**IBU**), and mesalazine (**MSZ**) was investigated by mixing equimolar amount of the APIs and the hydrogelator as solids. When the mixtures were heated in de-ionized water, transparent hydrosols were obtained, indicating that the gelator enhances the dissolution of each of the APIs in water upon heating as a consequence of complex formation. However, **NPX, IBU,** and **MSZ** will not dissolve in water on their own right, even when heated. Interestingly, the resulting hydrogel matrixes do not contain any precipitates upon cooling, which apparently shows that the API molecules did not precipitate from the gel network when fully formed (as shown in Figure 6.2.3). The enhanced solubility could be adduced to the formation of salt or hydrogen bonding interaction between the carboxylic acid group of the drug molecules and the terminal amine group of the gelator. However, at 1:2 gelator:**NPX, IBU** and **MSZ** molar ratio, the drugs did precipitate out of the hydrosol - supporting the view that there is a stoichiometric interaction between the acid-functionalized APIs and **DBS-CONHNH$_2$** gelator. The optimum drug loading with these systems are 0.32, 0.34, 0.41 and 0.49 g/ g for **SA**, **MSZ**, **IBU** and **NPX**/ gelator respectively – significantly higher than many values reported in literature for pharmaceutical uptake into an LMWG.[607]

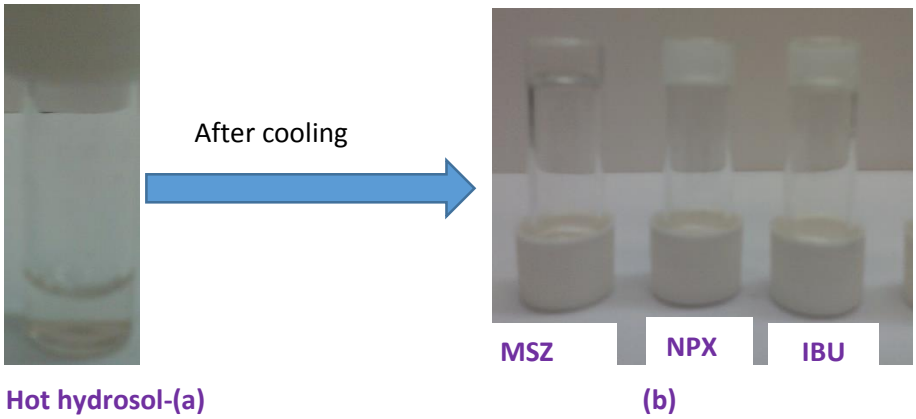

Figure 6.2.3: Photo of (a) a representative of the hot hydrosol of **DBS-CONHNH$_2$** containing various drugs (b) hydrogels of **DBS-CONHNH$_2$** containing various drugs, after cooling.

6.2.2 Effects of APIs on the self-assembled nanofibrillar networks of DBS-CONHNH$_2$ hydrogels

The effect of **NPX**, **IBU** and **MSZ** on the T_{gel} value of **DBS-CONHNH$_2$** hydrogel was probed by the tube inversion method. It was observed that the presence of equimolar amount of **NPX** and **IBU** enhances thermal stability of the hydrogel as the T_{gel} value increases from 92 to > 100 °C. However, the T_{gel} value of the hydrogel decreases from 92 to79 °C in the presence of **MSZ**. This difference could be correlated with the differences in the logP values of the APIs – higher logP values indicated lower solubility which will encourage better formation of gel network.

Contributions of a equimolar concentration of APIs to the rheological performance of hydrogels of **DBS-CONHNH$_2$** (10 mM) were investigated with a parallel plate geometry. Figures 6.2.4 – 6.2.7 shows that the storage modulus (G') of **DBS-CONHNH$_2$** increased in the presence of **IBU** and **NPX** from 14.5 to 19.6 and 33 kPa respectively while the loss modulus increased from 2.6 to 4.1 and 5.6 kPa respectively. However, G' and decreased to 10.2 and 1.8 kPa respectively in the presence of **MSZ**. This further corroborate the hypothesis that the more hydrophobic drugs (**IBU** and **NPX**) reinforce the 'solid-like' nature of these materials while the more hydrophilic drug (**MSZ**) decreases the ability of **DBS-CONHNH$_2$** to form a solid-like network.

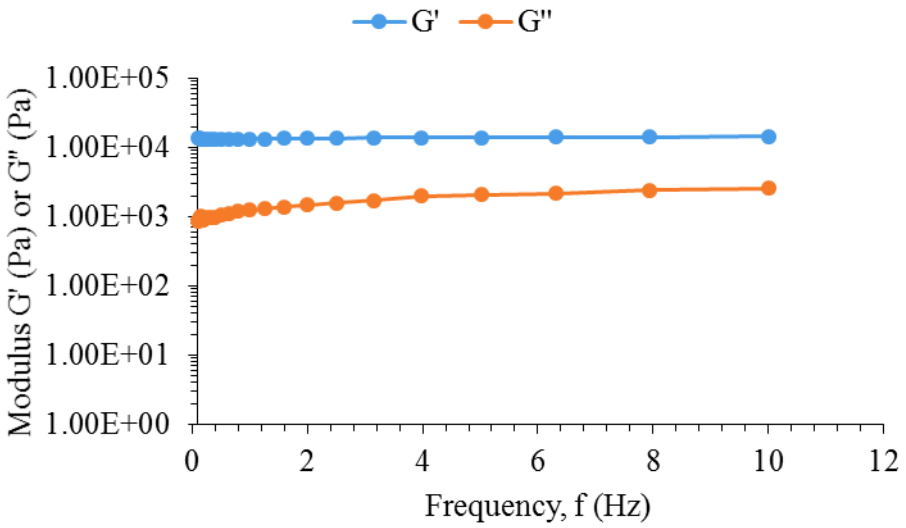

Figure 6.2.4 Frequency dependence of G' and G" of **DBS-CONHNH$_2$** hydrogel with no additive. [Shear strain = 0.2%].

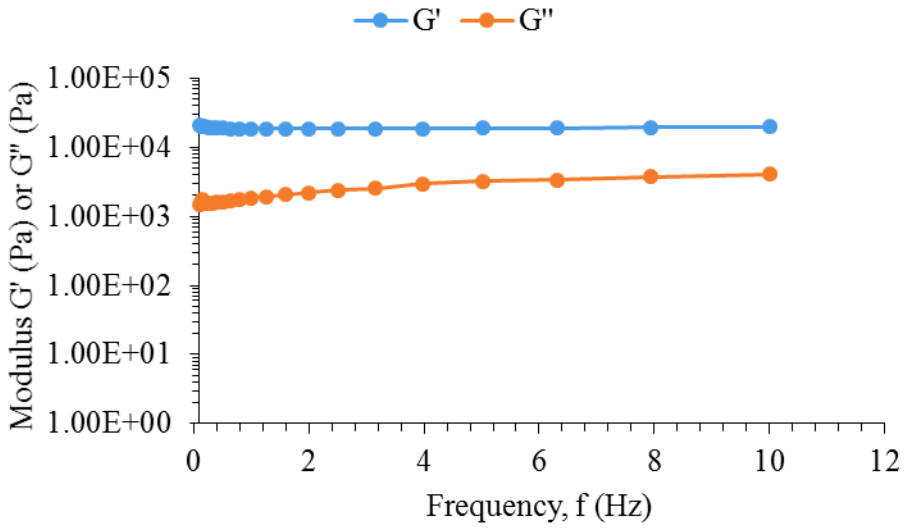

Figure 6.2.5 Frequency dependence of G' and G" of **DBS-CONHNH$_2$** hydrogel with **IBU**. [Shear strain = 0.2%].

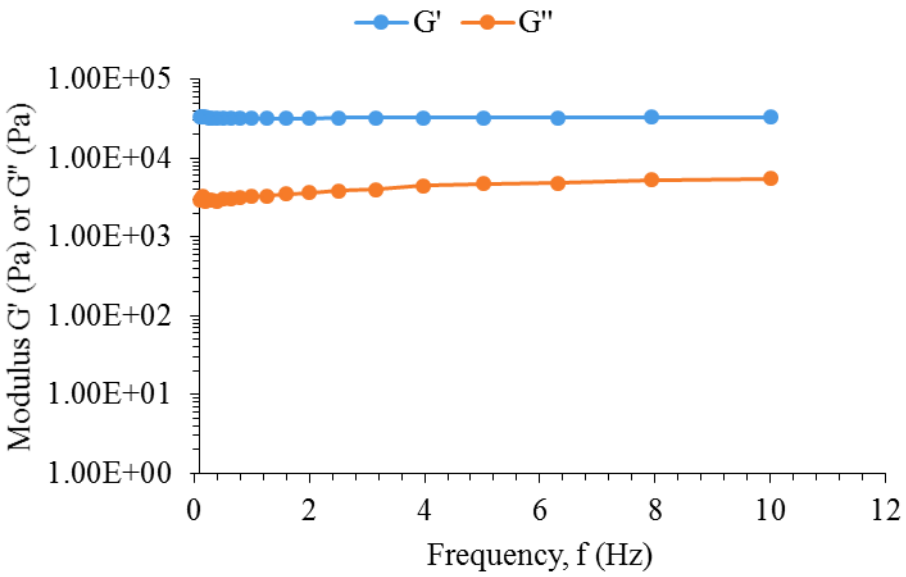

Figure 6.2.6 Frequency dependence of G' and G'' of **DBS-CONHNH$_2$** hydrogel with **NPX**. [Shear strain = 0.2%].

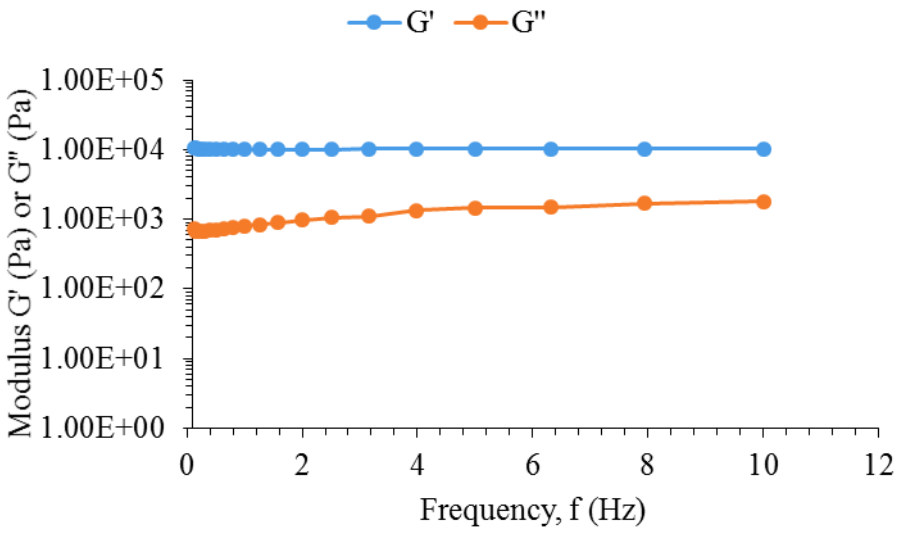

Figure 6.2.7 Frequency dependence of G' and G'' of **DBS-CONHNH$_2$** hydrogel with **MSZ**. [Shear strain = 0.2%].

In order to visualize the effect of APIs on the morphology of **DBS-CONHNH$_2$** hydrogel networks, scanning electron microscopy (SEM) was used to image the dried xerogels of the virgin hydrogel and API – hydrogel hybrids. Figure 6.2.8 shows that the virgin gel exhibited extended and intertwined bundles of nanofibres having

diameter of ca. 43 nm. In the presence of APIs the diameters of the nanofibre bundles are 36 nm, 29 nm and 29 nm respectively for the hybrid hydrogels with **IBU**, **NPX** and **MSZ**. The changes in fibre diameters suggest that the interaction of the APIs with nanofibres somewhat limits the ability of the fibres to bundle. However, the APIs did not inhibit gel assembly and no microcrystals (which might associate with unincorporated API) were observed – supportive of specific interactions between APIs and gelator fibres.

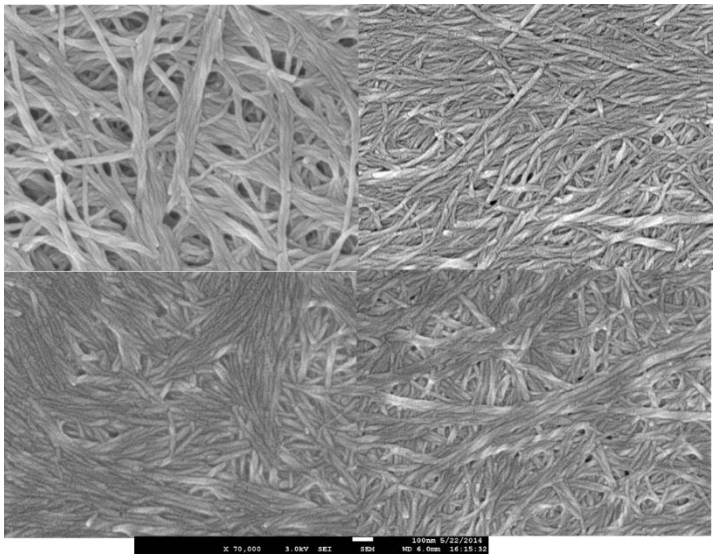

Figure 6.2.8 SEM images of dried xerogel of **DBS-CONHNH$_2$** presence of (a) no additive (b) **IBU** (c) **MSZ** and (d) **NPX**. Scale bar: 100 nm

The complex systems were probed with IR-spectroscopy. Interestingly, the presence of the drug molecules shifted the N-H stretch of gelator DBS-CONHNH$_2$ from 3194 cm^{-1} to lower wavenumber by up to 16 cm^{-1}. This would be consistent with the formation of interactions between this functional group and APIs. The O-H peak of sorbitol shifted by ca. 20 cm^{-1} to longer wavelength, consistent with possible involvement of this hydrogen bonding group. However, the C=O peak was less affected (max shift 6 cm^{-1}) and the aromatic C=C stretches and the C-O stretches were completely unchanged, which would appear to rule out pi - pi or solvophobic interactions between the gel fibres and these APIs. As such, IR supports specific interaction between the polar NH$_2$/OH units of the gelator and the carboxylic acid on these APIs.

Due to the unique chromophore of the naphthalene, which is different from **DBS-CONHNH$_2$**, CD spectroscopy was used to probe the effect of **NPX** on chiral aggregation of the gelator. A conspicuously broad CD band associated with chiral self-assembled **DBS-CONHNH$_2$** gel at ca. 275 nm can be attributed to the pi – pi stacking of the aromatic 'wings' of the gelator. This broad band was slightly blue shifted in the presence of **NPX**. Nonetheless, the key features of the nanostructured DBS-CONHNH$_2$ remain intact. As such, the API does not significantly disrupt chiral aggregation of the gelator and prehab bind to the periphery of the nanofibres rather than intercalating within the nanostructure. Fascinatingly, a CD signal associated with NPX also emerged as a small positive CD band at ca. 310 nm and a small negative band at 335 nm – suggesting that **NPX** is homogenously incorporated into the gel network in such a manner that its chiral signature can be observed (Figure 6.2.9).

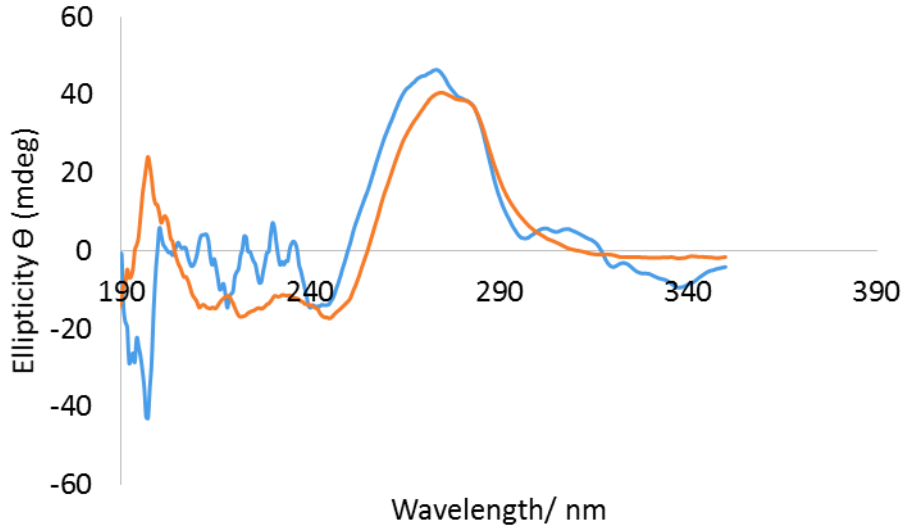

Figure 6.2.9 CD spectra for **DBS-CONHNH$_2$** hydrogel in the presence of (a) no additive (yellow line) and (b) NPX (blue line).

By monitoring the emergence of the **DBS-CONHNH$_2$** CD band over time, it is possible to gain insight into the kinetics of gel fibre growth. The dimensionality of the fibre can then be deduced by fitting the CD kinetic data into the Avrami model.[298] Figure 6.2.10 and 6.2.11 shows that the Avrami exponents n for the gel fibre growth in the absence and presence of **NPX** are 1.18 and 1.08 respectively and the gelation was completed in 5 min. It can be concluded that in both cases fibre formation is primarily one-dimensional, as supported by the SEM imaging.

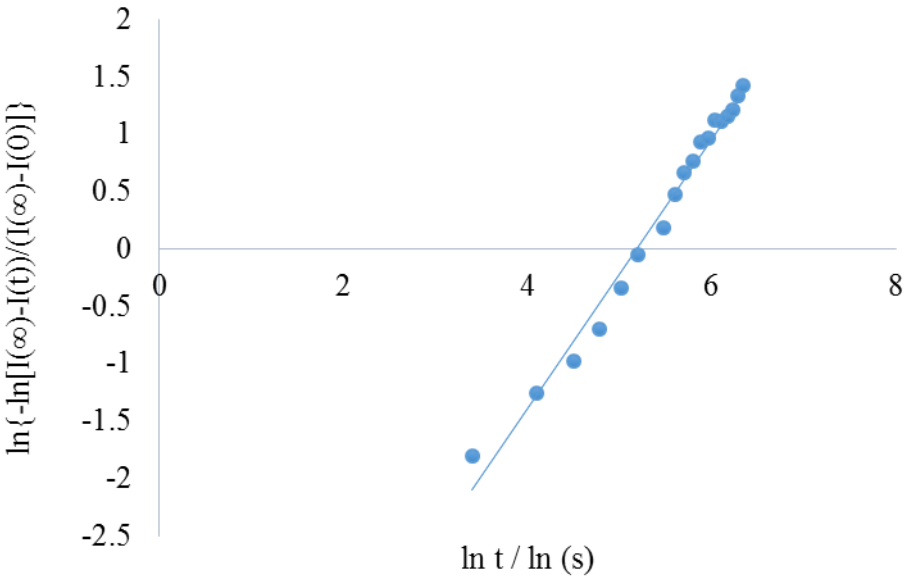

Figure 6.2.10 Avrami plot for **DBS-CONHNH$_2$** hydrogel fibre growth [R^2 = 0.98].

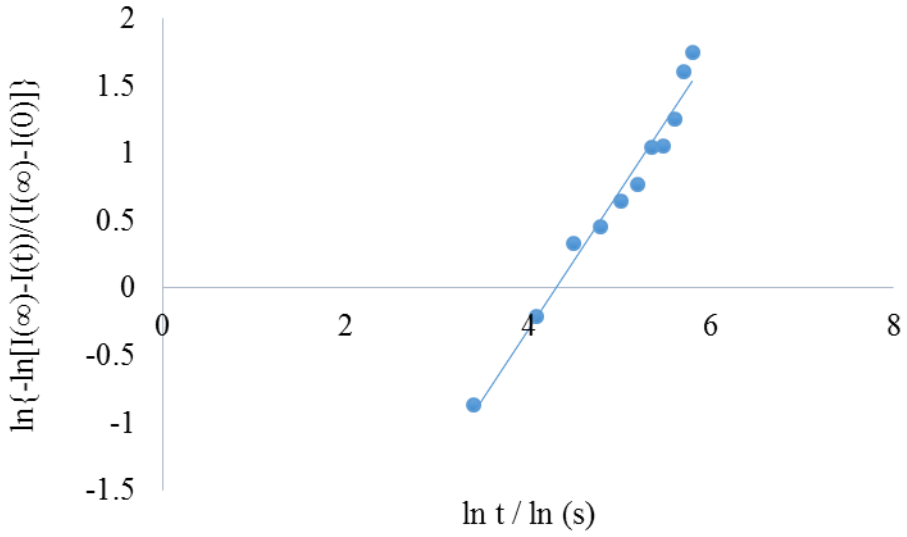

Figure 6.2.11 Avrami plot for **DBS-CONHNH$_2$** hydrogel fibre growth [R^2 = 0.98].

Fluorescent spectroscopy was also used to characterize the interaction between the gelator and **NPX** by using an excitation wavelength of 272 nm and comparing emission spectra of **DBS-CONHNH$_2$** in the presence and absence of **NPX**. Emission bands at 340 and 360 nm corresponding to **DBS-CONHNH$_2$** and **NPX** respectively were observed. Interestingly, for the gel – NPX hybrid, the gelator emission band disappeared while the band at 360 nm corresponding to **NPX** increased in intensity (Figure 6.2.2.9). Therefore, we reasoned that fluorescent resonance energy transfer

(FRET) - a distance-dependent radiationless transfer of energy from an excited donor fluorophore to a suitable acceptor fluorophore, might be responsible for the observed changes in fluorescent intensities. In which case, the excited state dimer of the gelator transfers its excitation energy to the **NPX** which is considered nearby in a non-radiative manner.[611-614]

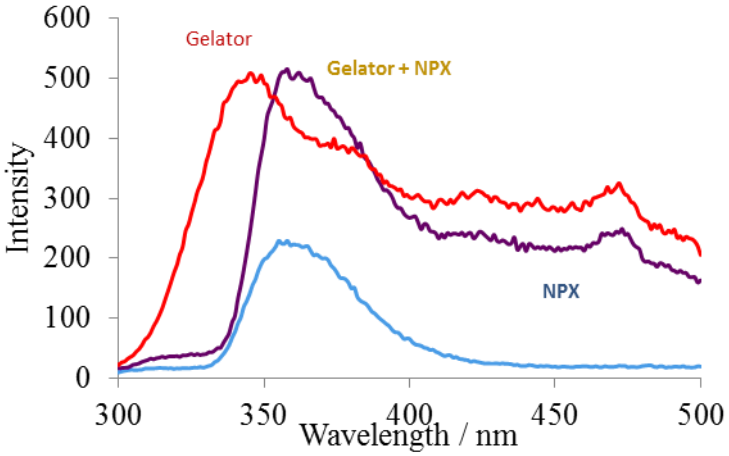

Figure 6.2.12 Emission spectra of a) **DBS-CONHNH$_2$**, b) **NPX** and c) equimolar mixture of **DBS-CONHNH$_2$** and **NPX**

6.2.3 Release studies of APIs from DBS-CONHNH$_2$ hydrogels

Further to the incorporation of APIs into the gel nanofibres, their controlled release were investigated under various pH regimes. Following solution–phase loading of preformed hydrogel with **MSZ**, the gel was exposed to clean water and 52% of the API was released over a period of 24 h. However, when the gel was further exposed to phosphate buffer (pH 8), 96% of the remaining **MSZ**, i.e., unreleased at pH 7 was then released from the gel. As such, **MSZ** release from these gels is pH–driven – basic conditions similar to those in the intestine can lead to greater levels of drug release, making this system potentially relevant to **MSZ** formulation.[615-617]

With the incorporation of APIs by two – component mixing, NPX showed a fascinating release profile. At pH 7, only 33% of the drug was released over 24 h, whereas at pH 8 the percentage released increased to ~ 100% (Figure 6.2.3.1). Using pH-adjusted water at pH 8, rather than buffered water slowed down the release rate,

which can be explained by API release gradually lowering the pH of the receiving solution in this case.

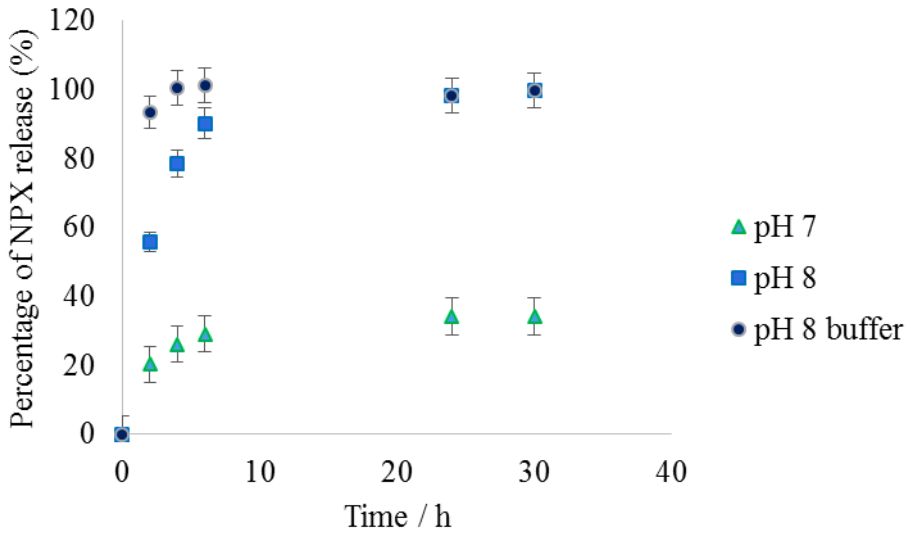

Figure 6.2.13 Release profiles of **NPX** from **DBS-CONHNH$_2$** hydrogel into a supernatant aqueous solution under different conditions of pH control.

The release of IBU could not be followed effectively in this assay owing to its lower solubility in water – this may be different in the presence of biomembranes and does not preclude the application of these gels with this drug.

Generally speaking, the ability of **DBS-CONHNH$_2$** hydrogel to demonstrate base-induced drug delivery could be attributed to deprotonation of the APIs and hence, disruption of API – gelator interactions. These gels are therefore ideal for release of **NPX** and **MSZ** at slightly elevated (e.g. intestinal) pH values. For instance, it has recently been disclosed that **NPX** has adverse effects, particularly on the stomach, if administered orally.[618] However, it should be noted that the gels became less stable in very low pH (pH 2) and this might limit its suitability for direct oral application. Nonetheless, such a problem could be solved by enclosing the gel–API within an enteric coated capsule. Alternatively, the gel can be reinforced by formulating the gel with a more stable gelator, thereby forming a strong and robust hybrid system.[220] It is also worth mentioning that these gels may be useful for slow release delivery technology with the gel forming in situ after for example subcutaneous injection.

6.3 *Conclusion and outlook*

In this project, a simple gelation system which encapsulates anti-inflammatory APIs as a result of direct 1: 1 API – gelator interactions in a novel two- component gelation system was investigated. Microscopic and macroscopic characterization of the hydrogel – API systems show that the presence of API did not disrupt gelation of **DBS-CONHNH$_2$**. Also, the solubility of APIs was enhanced in the presence of the gelator – as such no microcrystals of APIs were observed. The two-component co-assembled systems demonstrated strong pH–controlled and bio-relevant release of **NPX**. The release was more significant at pH 8 than 7 which is the validity for drug delivery in the small intestine.

DBS has been widely applied in cosmetic products[104] and nanoscale hydrazides have also been demonstrated to have good biocompatibility[463] and hence, **DBS-CONHNH$_2$** may be appropriate for drug delivery technology. Similar to existing self-assembled small molecule hydrogels with well-established routes to clinical application, it could be anticipated that our formulation systems might offer considerable potential.

In the future, further investigations such as capsulation of gel encapsulated drugs can be carried-out and first pass effects of the design be examined. Animal models can also be used to investigate potency of the system *in vivo*. Kinetics and thermodynamics of drug release could then be probed.

7 Chapter 7 - Experimental

7.1 General materials and methods

Reagents and solvents were commercially available and used as supplied without further purification. D-Sorbitol, various aldehydes, *p*-toluenesulfonic acid monohydrate, $HAuCl_4$. xH_2O, $AgNO_3$, $Pb(NO_3)_2$, $Cd(NO_3)_2$, $Hg(NO_3)_2$, As_2O_3, $NaNO_3$, $Ca(NO_3)_2$, $AuCl_3$, $PdCl_2$, $PtCl_2$, $ZnCl_2$, $NiCl_2$, $FeCl_2$, $CuCl_2$, and mercury atomic absorption spectroscopy standard solution (1000 µg/l Hg in 1 wt. % HNO_3), lead atomic absorption spectroscopy standard solution (1000 µg/l Hg in 1 wt. % HNO_3) and cadmium atomic absorption spectroscopy standard solution were purchased from Sigma-Aldrich. 1,3:2,4-Dibenzylidene-D-sorbitol and some of its derivatives were synthesized according to procedures previously reported in literature.[167, 619] The dyes were obtained in different levels of purity; Methylene blue (99%), Acid blue 25 (45%), Congo red (54%) and Reactive blue 4 (35%). The fraction of the dye content in the materials was calculated and weighed-out to prepare the aliquot stock solution of each of the dye. Thin layer chromatography was performed using Merck pre-coated silica gel 60-F254 plates. ^{1}H, ^{13}C, ^{1}H-^{1}H COSY, ^{1}H-^{13}C HSQC and ^{1}H-^{13}C HMBC NMR were recorded on a JEOL ECX 400 (^{1}H 400 MHz, ^{13}C 100 MHz) Spectrometer. Mass spectrometery data of the compounds synthesized were obtained on the ESI Bruker Daltonics Micro-TOF Mass spectrometer. ATR-FTIR was carried out using a Jasco FT/IR 4100 instrument fitted with a Pike MIRacle ATR sampling accessory. Absorbance bands are reported as the wavenumber of maximum absorbance (in cm^{-1}). Transparent screw-capped vials (2.5, 7.0 or 8.5 mL) were used at one point or the other for making gels. The T_{gel} values of the gels were determined on a thermostated oil bath at 10 ^{O}C ramp. Ultraviolet-visible spectrophotometer (SHIMADZU 2041 PC) was used to measure the absorbance of dye solutions. Inductively Coupled Plasma Mass Spectroscopy (ICP-MS) was carried out to measure the metal concentration in solution using an Agilent 7700x fitted with standard Ni sample and skimmer cones and coupled to a Mass Spectrometer (MS). The samples were run in He mode. The sample introduction line was rinsed for 60 s between samples using 5% HCl and 2% HNO_3. Samples were prepared by diluting 1 µL of the stock sample in 10 mL of ultra-pure water. ICP-MS data were collected by Darren Philip at Biorenewables Development Centre (BDC), University of York. Atomic absorption spectrophotometry (AAS 6300) was used to analyse the concentrations of

aqueous solution of Pb^{2+} and Cd^{2+} ions using Shimadzu AAS 6300 with Shimadzu Wizard software. The standard stock solutions (1000 ppm) were diluted to obtain working standard solutions ranging from 1 ppm to 10 ppm and stored at 4 °C. Nitric acid (0.1 M) was added to maintain solutions. A calibration curve was plotted between measured absorbance and concentration (ppm). Absorbance of aqueous solutions of Pb^{2+} and Cd^{2+} ions were measured before and after adsorption and their concentrations extrapolated from calibration curves. The spectrometer was auto zeroed by aspirating deionised water into the burner between various measurements. All samples were analysed in triplicate. Optimized operating parameters for AAS (Atomic Absorption Spectrophotometer) of various heavy metals are; slit = 0.7 nm, fuel (acetylene) flow rate = 1.8 l min^{-1}, oxidant (air) flow rate = 15 l min^{-1}, wavelength 283.3 and 228.8 nm for Pb and Cd respectively with deuterium arc background correction. Lead and Cadmium hollow cathodes lamps with current of ~6 mA were used.

Circular dichroism (CD) was measured with a Jasco J810 circular dichroism spectropolarimeter fitted with a Peltier temperature control unit using a quartz cell with a path length of 1 mm using the following settings: Data Pitch – 0.5 nm, Scanning Mode – Continuous, Scanning Speed – 100 nm min^{-1}, Response – 1 s, Bandwidth – 2 nm, Accumulation – 5. All CD data are presented as ellipticity and recorded in mdeg. The samples for scanning electron microscopy were prepared by being gently spread on an aluminium stub and dried. They were then coated with a 5 nm layer of Pt/Pd using an Agar High Resolution Sputter Coater and were imaged with JEOL JSM-7600F FESEM fitted with Gatan Alto 2500 cryo-system and Gatan MonoCL cathodoluminescence system. Transmission electron microscopy (TEM) was performed on copper backed TEM grids using a FEI Tecnai G fitted with a CCD camera. Samples were stained with a 1% aqueous uranyl acetate solution. Images were collected by Meg Stark at the Biology Technology Faculty, University of York. X-Ray photoemission spectra were obtained on VG Escalab 250. Wide spectrum survey scans were measured at pass energy of 150 eV, spot size 500 µm and each of the high resolution scans at a pass energy of 20 eV. The electron flood gun was on in order to compensate for the charging effect by using the following parameters: x-shift = -0.4 V; y-shift = -0.25 V; emission = 125 µA. Spectra were collected by Kellye Curtis at School of Physics and Astronomy, University of Leeds. Dynamic rheological measurements were performed using a Kinexus pro^{+} rheometer at 25 $^{\circ}$C with parallel

plate geometry (20 mm diameter) at a gap of 1 mm. All hydrogels (2 mL) were pre-formed in an in-house mould, de-moulded after being left to age for at least 20 hours and carefully loaded onto the sample stage. Caution, which include gradual gap closing and careful sample trimming was used to minimize internal damage to the hydrogel networks. Oscillatory frequency sweeps were performed from 0.1 Hz (0.68 rad^{-1}) to 20 Hz (125.6 rad^{-1}) under a strain of 0.5 %. The shear moduli (G' and G'') were measured at a frequency of 1 Hz. The oscillatory strain sweeps measurements were performed within the linear viscoelastic region. Data were processed using rSpace software.

7.2 Synthesis of gelators

7.2.1 Synthesis of 1,3: 2,4-dibenzylidene-D-Sorbitol (DBS)

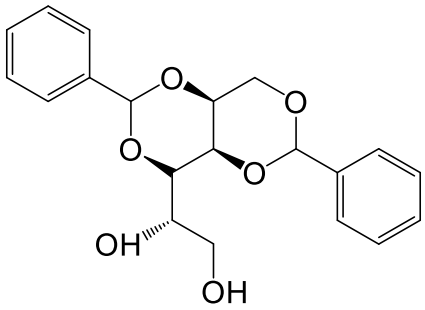

D-Sorbitol (9.7 g, 0.0533 mol) was added to methanol (60 mL) and stirred for 30 min (400 rpm). Benzaldehyde (11.4 ml, 0.112 mol.) and *p*-toluenesulfonic acid monohydrate (12.7 g, 0.0665 mol) was added to the reaction mixture and stirred for 10 h until a slurry paste is formed. In order to purify the crude product, cold methanol (150 mL) was added to the flask and stirring continued for another 1 h on ice/salt bath. The product was filtered off. The purification process was repeated twice and the product was filtered, air-dried for 48 h and pulverized to obtain a white powdered compound. TLC was used to ascertain the purity. Yield 6.5 g (34%). R_f = 0.45 (9: 1, CH_2Cl_2: MeOH). ^{1}H NMR(400 MHz, DMSO-d_6): δ 7.32-7.45 (10H, m, Ph-H); 5.64 (2H, s, PhCH); 4.80 (1H, CHOH); 4.38 (1H, CH_2OH); 4.16 (1H, d, *J* = 11.6 Hz, CH_2 – sugar, H^1) and 4.12 (1H, d, *J* = 11.6 Hz, CH_2 – sugar, H^1); 4.14 (1H, s, CH - sugar, H^3); 3.91 (1H, s, CH – sugar, H^2); 3.81 (1H, d, *J* = 10 Hz, CH – sugar, H^4), 3.74 (1H, m, CH – sugar, H^5); 3.57(1H, q, *J* = 11.6 Hz, CH_2 – sugar, H^6); 3.41 (1H, dd, *J* = 5.6

Hz and J = 11.2 Hz, CH_2 – sugar, H^6),. ^{13}C NMR (100 MHz, DMSO-d_6): δ 137.28 (Ph, C^1), 129.15 (Ph, C^p), 128.52 (Ph, C^m), 126.69 (Ar, C^o), 99.80 and 99.90 (Ph-C), 78.13 (CH – sugar, C^4), 70.61(CH – sugar, C^2), 69.85 (CH_2 – sugar, C^1), 68.93 (CH – sugar, C^3), 68.23 (CH – sugar, C^5), 63.82 (CH_2 – sugar, C^6). ATR-FTIR ν_{max} cm^{-1} 3246 (OH, alcohol), 2938 (CH, aliphatic), 1453 (C=C, aromatic), 1096 (C-O, acetal). ESI-MS: Calcd. $[M+H]^+$ ($C_{20}H_{23}O_6$), *m/z* = 359.1494; Obs. $[M+H]^+$, *m/*z =359.1498

7.2.2 Synthesis of 1,3:2,4-di-(*p*-nitrobenzylidene)-D-Sorbitol (DBS-NO_2)

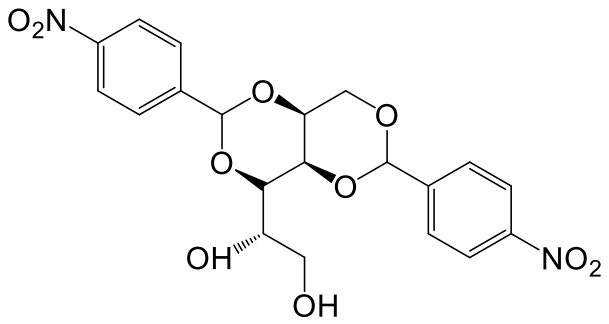

D-Sorbitol (2.45 g, 0.0135 mol) was weighed into a triple-neck round bottom flask equipped with Dean-stark apparatus. A mixture of cyclohexane (35 mL) and methanol (5 mL) was added to the flask and the mixture heated to 50 ^{O}C under $N_{2(g)}$ with continuous stirring (400 rpm) for about 20 min. A mixture of 4-nitrobenzaldehyde (4.0 g, 0.0265 mol) and *p*-toluenesulfonic acid hydrate (2.8 g, 0.0147 mol) was dissolved in methanol (20 mL) and stirred on a magnetic stirrer for about 20 min. The mixture was then dripped slowly into the flask containing the D-sorbitol in cyclohexane / methanol and the reaction was allowed to proceed at 78 ^{O}C for 3 h. During the reaction, the cyclohexane in the distillate was recycled to the reaction system and the mixture of water and methanol in the distillate was removed from the system via the Dean-Stark trap. To maintain the amount of solvent in the reaction system, some cyclohexane and methanol was added to the reaction system. The reaction mixture was allowed to cool down at ambient temperature and the white paste formed was thoroughly washed with boiled water (100 mL x7) and dichloromethane (50 mL x 2). The off-white powdered product was air-dried overnight, pulverized and further dried to a constant weight. The product was further purified using silica column chromatography in THF: DCM (8: 2). Yield 4.12 g (68 %). R_f = 0.39 (9: 1, CH_2Cl_2: MeOH).). ^{1}H NMR(400 MHz, DMSO-d_6): δ 8.25 (4H, d, J = 8.4 Hz, *p*-NO_2-Ph, H^m);

8.22 (2H, d, *J* = 8.4 Hz, *p*-NO_2-Ph, H^o); 7.70 (2H, t, *J* = 8.4 Hz, H^o); 5.80 (2H, s, *p*-NO_2-Ph); 4.94 (1H, d, CHOH); 4.46 (1H, t, CH_2OH); 4.24 (1H, d, *J* = 11.6 Hz, CH_2 – sugar, H^1) and 4.23 (1H, d, *J* = 11.6 Hz, CH_2 – sugar, H^1); 4.17 (1H, s, CH - sugar, H^3); 4.02 (1H, s, CH – sugar, H^2); 3.89 (1H, d, *J* = 10 Hz, CH – sugar, H^4), 3.75 (1H, m, CH - sugar, H^5); 3.57(1H, q, *J* = 11.6 Hz, CH_2 – sugar, H^6); 3.41 (1H, dd, *J* = 5.6 Hz and *J* = 11.2 Hz, CH_2 – sugar, H^6), ^{13}C NMR (100 MHz, DMSO-d_6): δ 148.17 (*p*-NO_2-Ph, C^1), 145.53 (*p*-NO_2-Ph, C^p), 128.09 (*p*-NO_2-Ph, C^m), 123.90 (*p*-NO_2-Ph, C^o), 98.47 and 98.37 (*p*-NO_2-Ph-CH), 78.01 (CH – sugar, C^4), 70.66 (CH – sugar, C^2), 69.83 (CH_2 – sugar, C^1), 69.04 (CH – sugar, C^3), 68.09 (CH – sugar, C^5), 63.02 (CH_2 – sugar, C^6). ATR-FTIR v_{max} cm^{-1} 3330 (OH, alcohol), 2944 (CH, aliphatic), 1451 (C=C, aromatic), 1541 (N=$O_{assym.}$, nitro), 1338 (N=$O_{sym.}$, nitro), 1090 (C-O, acetal). ESI-MS: Calcd. $[M+H]^+$ ($C_{20}H_{21}N_2O_{10}$), *m/z* = 449.1196; Obs. $[M+H]^+$, *m/z* = 449.1203.

7.2.3 Synthesis of *p, p*'-dithiomethyl-1,3: 2,4-dibenzylidene-D-Sorbitol (DBS-SCH_3

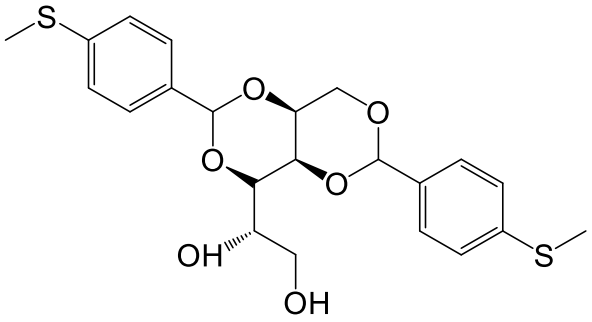

D-Sorbitol (8.5 g, 0.0467 mol) was weighed into a three neck round bottom flask to be used in a Dean-Stark experiment. Mixture of cyclohexane (50 mL) and methanol (50 mL) was added to the flask. The mixture was heated at 50 ^{O}C with continuous stirring under $N_{2\,(g)}$ for about 20 min. *p*-Thiomethylbenzaldehyde (12.0 g, 0.0788 mol) and *p*-toluenesulfonic acid hydrate (15.0 g, 0.0789 mol.) was dissolved in methanol (20 mL) and the mixture was stirred for 20 min after which the mixture was added drop wise to the D-sorbitol mixture. The reaction was allowed to proceed at 70 ^{O}C for 4 h. The reaction mixture was allowed to cool down to the room temperature and the white paste formed was washed with cold ethanol (100 mL x 3) to remove the unreacted starting materials. The crude product was dried under high vacuum for about

2 h and finally air-dried overnight. The mono-substituted derivative was removed from the product by washing with warm water (100 mL x 4). There was no tri-substituted product formed. The purity of the product was ascertained with the use of TLC. R_f 0.48 (9: 1, CH_2Cl_2: methanol) and the product was further characterized using NMR and MS. Yield is 17.59g (88%). δ 7.34 (4H, d, *J* = 8.4 Hz, *p*-CH_3S-Ph, H^m); 7.30 (2H, d, *J* = 8.4 Hz, *p*-CH_3S-Ph, H^o); 7.22 (2H, t, *J* = 8.4 Hz, H^o); 5.59 (2H, s, *p*-CH_3S-Ph -C<u>H</u>); 4.80 (1H, CHO<u>H</u>); 4.38 (1H, CH_2O<u>H</u>); 4.15 (1H, d, *J* = 11.6 Hz, CH_2 – sugar, H^1) and 4.11 (1H, d, *J* = 11.6 Hz, CH_2 – sugar, H^1); 4.13 (1H, s, CH - sugar, H^3); 4.02 (1H, s, CH – sugar, H^2); 3.86 (1H, d, *J* = 10 Hz, CH – sugar, H^4), 3.75 (1H, m, CH - sugar, H^5); 3.57(1H, q, *J* = 11.6 Hz, CH_2 – sugar, H^6); 3.41 (1H, dd, *J* = 5.6 Hz and *J* = 11.2 Hz, CH_2 – sugar, H^6), 2.46 (6H, s, SC<u>H</u>$_3$) ^{13}C NMR (100 MHz, DMSO-d_6): δ 139.16 (*p*-CH_3S-Ph, C^1), 135.95 (*p*-CH_3S-Ph, C^p), 127.28 (Ph, C^m), 125.91 (Ph, C^o), 99.54 (*p*-CH_3S-Ph -<u>C</u>H), 78.05 (CH – sugar, C^4), 70.54 (CH – sugar, C^2), 69.79 (CH_2 – sugar, C^1), 68.86 (CH – sugar, C^3), 68.25 (CH – sugar, C^5), 63.10 (CH_2 – sugar, C^6), 15.19 (S<u>C</u>H$_3$). ATR-FTIR ν_{max} cm^{-1} 3219 (OH, alcohol), 2941 (CH, aliphatic), 1520 (C=C, aromatic), 1091 (C-O, acetal). ESI-MS: Calcd. $[M+H]^+$ ($C_{24}H_{27}O_{10}$), *m/z* = 451.1249; Obs. $[M+H]^+$, *m/*z =451.1230.

7.2.4 Synthesis of 1,3:2,4-di-(*p*-bromobenzylidene)-D-Sorbitol (DBS-Br)

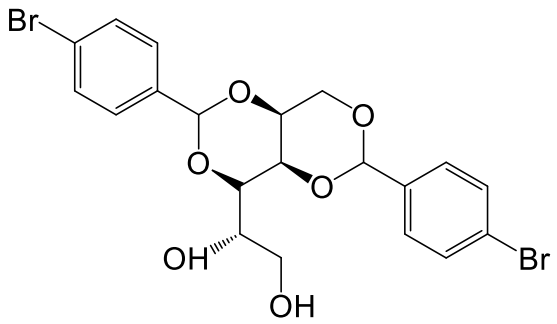

D-Sorbitol (7.5 g, 0.0405 mol) was weighed into a three neck round bottom flask to be used in a Dean-Stark experiment. A mixture of cyclohexane (50 mL) and methanol (50 mL) was added to the flask. The mixture was heated at 50 ^{O}C with continuous stirring under $N_{2\,(g)}$ for about 20 min. *p*-Bromobenzaldehyde (15.0 g, 0.0811 mol) and *p*-toluenesulfonic acid hydrate (15.0 g, 0.0789 mol.) was dissolved in methanol (20 mL) and the mixture was stirred for 20 min after which the mixture was added drop wise to the D-sorbitol mixture. The reaction was allowed to proceed at 70 ^{O}C for 4 h.

The reaction mixture was allowed to cool down to room temperature and the white paste formed was washed with cold ethanol (100 mL x 3) to remove the unreacted starting materials. The crude product was dried under high vacuum for about 2 h and finally air-dried overnight. The mono-substituted derivative was removed from the product by washing with warm water (100 mL x 4) and tri-substituted derivative with dichloromethane (50 mL x 3). The purity of the product was ascertained with the use of TLC. R_f 0.42 (9: 1, CH_2Cl_2: methanol) and the product was further characterized using NMR and MS. Yield is 12.60g (70%). δ 7.38-7.54 (8H, m, *p*-Br-Ph); 5.66 (2H, s, *p*-Br-Ph -C<u>H</u>); 4.89 (1H, CHO<u>H</u>); 4.38 (1H, CH_2O<u>H</u>); 4.17 (1H, d, *J* = 11.6 Hz, CH_2 – sugar, H^1) and 4.12 (1H, d, *J* = 11.6 Hz, CH_2 – sugar, H^1); 4.14 (1H, s, CH - sugar, H^3); 4.02 (1H, s, CH – sugar, H^2); 3.88 (1H, d, *J* = 10 Hz, CH – sugar, H^4), 3.70 (1H, m, CH - sugar, H^5); 3.57(1H, q, *J* = 11.6 Hz, CH_2 – sugar, H^6); 3.41 (1H, dd, *J* = 5.6 Hz and *J* = 11.2 Hz, CH_2 – sugar, H^6). ^{13}C NMR (100 MHz, DMSO-d_6): δ 135.95 (*p*-Br-Ph, C^1), 130.69 (*p*-Br-Ph, C^p), 128.40 (*p*-Br-Ph, C^m), 126.02 (*p*-Br-Ph, C^o), 98.15 (*p*-Br-Ph -<u>CH</u>), 77.15 (CH – sugar, C^4), 69.67 (CH – sugar, C^2), 69.79 (CH_2 – sugar, C^1), 68.91 (CH – sugar, C^3), 68.25 (CH – sugar, C^5), 62.19 (CH_2 – sugar, C^6). ATR-FTIR ν_{max} cm^{-1} 3219 (OH, alcohol), 2941 (CH, aliphatic), 1524 (C=C, aromatic), 1091 (C-O, acetal). ESI-MS: Calcd. $[M+Na]^+$ ($C_{20}H_{20}NaBr_2O_6$), *m/z* = 536.9525; Obs. $[M+Na]^+$, *m/*z =536.9500.

7.2.5 Synthesis of 1,3:2,4-di-(*p*-Fluorobenzylidene)-D-Sorbitol (DBS-F)

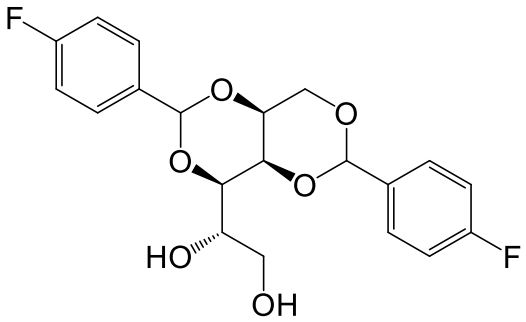

D-Sorbitol (7.4 g, 0.0403 mol) was weighed into a three neck round bottom flask to be used in a Dean-Stark experiment. A mixture of cyclohexane (60 mL) and methanol (40 mL) was added to the flask. The mixture was heated at 50 ^{O}C with continuous stirring under $N_{2\,(g)}$ for about 20 min. *p*-Fluorobenzaldehyde (10.0 g, 0.0806 mol) and *p*-toluene sulfonic acid hydrate (15.0 g, 0.0789 mol) was dissolved in methanol (20

mL) and the mixture was stirred for 20 min after which the mixture was added drop wise to the D-sorbitol mixture. The reaction was allowed to proceed at 70 ^{O}C for 4 h. The reaction mixture was allowed to cool down to room temperature and the white paste formed was washed with cold ethanol (100 mL x 3) to remove the unreacted starting materials. The crude product was dried under high vacuum for about 2 h and finally air-dried overnight. The mono-substituted derivative was removed from the product by washing with warm water (100 mL x 4) and tri-substituted derivative with dichloromethane (50 mL x 3). The purity of the product was ascertained with the use of TLC. R_f 0.4 (9: 1, CH_2Cl_2: methanol) and the product was further characterized using NMR and MS. Yield is 11.12g (70%). δ 7.19-7.49 (8H, m, *p*-F-Ph); 5.65 (2H, s, *p*-F-Ph-C<u>H</u>); 4.89 (1H, CHO<u>H</u>); 4.38 (1H, CH_2O<u>H</u>); 4.17 (1H, d, *J* = 11.6 Hz, CH_2 – sugar, H^1) and 4.12 (3H, m, CH_2 – sugar, H^1 and CH – sugar, H^3); 4.11 (1H, s, CH – sugar, H^2); 3.85 (1H, d, *J* = 10 Hz, CH – sugar, H^4), 3.70 (1H, m, CH - sugar, H^5); 3.57(1H, q, *J* = 11.6 Hz, CH_2 – sugar, H^6); 3.41 (1H, dd, *J* = 5.6 Hz and *J* = 11.2 Hz, CH_2 – sugar, H^6). ^{13}C NMR (100 MHz, DMSO-d_6): δ 163.35 (*p*-F-Ph, C^p), 135.95 (*p*-F-Ph, C^1), 128.40 (*p*-F-Ph, C^m), 118.02 (*p*-F-Ph, C^o), 98.95 (*p*-F-Ph-<u>CH</u>), 78.05 (CH – sugar, C^4), 70.54 (CH – sugar, C^2), 69.79 (CH_2 – sugar, C^1), 68.91 (CH – sugar, C^3), 68.25 (CH – sugar, C^5), 62.19 (CH_2 – sugar, C^6). ATR-FTIR ν_{max} cm^{-1} 3219 (OH, alcohol), 2941 (CH, aliphatic), 1522 (C=C, aromatic), 1091 (C-O, acetal). ESI-MS: Calcd. $[M+Na]^+$ ($C_{20}H_{20}NaF_2O_6$), *m/z* = 417.1128, Obs. $[M+H]^+$, *m/z* = 417.1126.

7.2.6 Synthesis of 1,3:2,4-dibenzylidene-D-Sorbitol-*p, p*'- dimethylester (DBS-$COCH_3$)

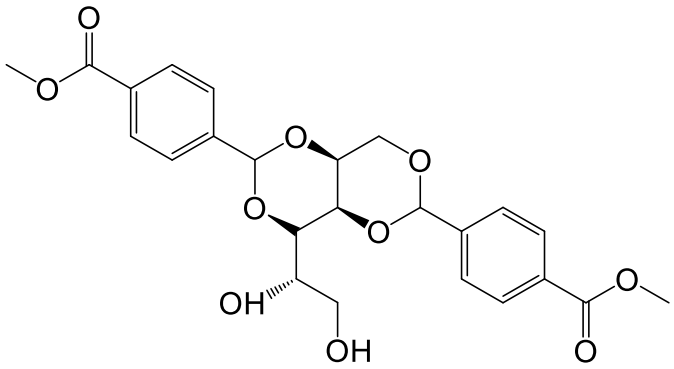

D-Sorbitol (4.9 g, 0.0253 mol) was weighed into a three neck round bottom flask to be used in a Dean-Stark experiment. A mixture of cyclohexane (35 mL) and methanol (10 mL) was added to the flask. The mixture was heated at 50 ^{O}C with continuous

stirring under $N_{2\,(g)}$ for about 20 min. 4-Methylformybenzoate (7.5 g, 0.0457 mol) and *p*-toluene sulfonic acid hydrate (1.0 g, 0.0526 mol.) was dissolved in methanol (20 mL) and the mixture was stirred for 20 min after which the mixture was added drop wise to the D-sorbitol mixture. The reaction was allowed to proceed at 70 ^{O}C for 2 h. The reaction mixture was allowed to cool down to room temperature and the white paste formed was washed with cold ethanol (100 mL x 3) to remove the unreacted starting materials. The crude product was dried under high vacuum for about 2 h and finally air-dried overnight. The mono-substituted and the tri-substituted derivatives were removed from the product by washing with warm water (100 mL x 4) and dichloromethane (100 mL x 3) respectively and the product was further characterized using NMR and MS. Yield 7.5g (70%). ^{1}H NMR (400 MHz, DMSO-d_6): δ 7.95 (4H, d, *J* = 8.4 Hz, *p*-CH_3OOC-Ph, H^m); 7.57 (4H, t, *J* = 8.4 Hz, *p*-CH_3OOC-Ph, H^o); 5.73 (2H, s, *p*-CH_3OOC-Ph-C<u>H</u>); 4.90 (1H, CHO<u>H</u>); 4.45 (1H, CH_2O<u>H</u>); 4.19 (1H, d, *J* = 11.6 Hz, CH_2 – sugar, H^1) and 4.17 (1H, d, *J* = 11.6 Hz, CH_2 – sugar, H^1); 4.15 (1H, s, CH - sugar, H^3); 3.98 (1H, s, CH – sugar, H^2); 3.87 (1H, d, *J* = 10 Hz, CH – sugar, H^4); 3.82 (6H, s, *p*-C<u>H_3</u>OOC-Ph); 3.75 (1H, m, CH - sugar, H^5); 3.57(1H, q, *J* = 11.6 Hz, CH_2 – sugar, H^6); 3.41 (1H, dd, *J* = 5.6 Hz and *J* = 11.2 Hz, CH_2 – sugar, H^6), ^{13}C NMR (100 MHz, DMSO-d_6): δ 166.52 (*p*-CH_3OO<u>C</u>-Ph, C^p), 143.86 (*p*-CH_3OOC-Ph, C^p); 136.20 (*p*-CH_3OOC-Ph, C^1); 130.29 (*p*-CH_3OOC-Ph, C^m); 127.03 (*p*-CH_3OOC-Ph, C^o); 99.05 (*p*-CH_3OOC-Ph-<u>CH</u>); 78.09 (CH – sugar, C^4); 70.70 (CH – sugar, C^2); 69.83 (CH_2 – sugar, C^1); 69.09 (CH – sugar, C^3); 68.05 (CH – sugar, C^5); 63.10 (CH_2 – sugar, C^6). ATR-FTIR ν_{max} cm^{-1} 3241 (OH, alcohol), 2956 (CH, aliphatic), 1722 (C=O, ester), 1579 (C=C, aromatic), 1090 (C-O, acetal). ESI-MS: Calcd. $[M+H]^+$ ($C_{24}H_{26}O_{10}$), *m/z* = 475.1604; Obs. $[M+H]^+$, *m/*z =475.1591.

7.2.7 Synthesis of 1,3:2,4-di-(*p*-Aminobenzylidene)-D-Sorbitol (DBS-NH_2)

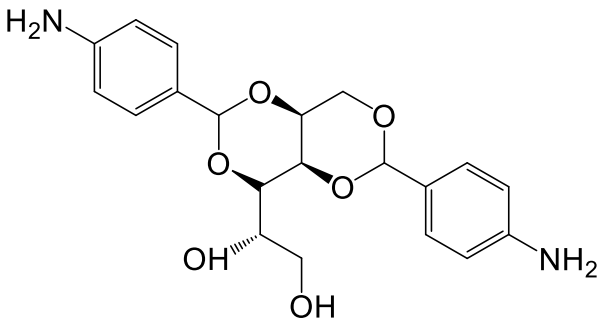

To a stirred solution of **DBS-NO$_2$** (1 .0 g, 2.2321 mmol) in THF (35 mL) kept under $N_{2\,(g)}$ for 30 min, 10% Pd/C (0.12 g) is added and then $H_{2\,(g)}$ immediately using a balloon. The reaction mixture was stirred for 10 h at room temperature. The catalyst was removed by filtration and the filtrate was concentrated on a rotary evaporator. The yellow solid obtained was washed with $CHCl_3$ (4 x 20 mL) and the product was dried under high vacuum for about 2 h and finally air-dried overnight. The product was further characterized using NMR and MS. Yield 0.92 g (90%). ^{1}H NMR (400 MHz, DMSO-d$_6$): δ 7.06 (4H, t, *J* = 8 Hz, *p*-NH$_2$-Ph, H^o); 6.45 (4H, d, *J* = 8 Hz, *p*-NH$_2$-Ph, H^m); 5.41 (2H, s, *p*-NH$_2$-Ph-C<u>H</u>); 4.71 (1H, CHO<u>H</u>); 4.39 (1H, CH$_2$O<u>H</u>); 4.03 (3H, m, CH$_2$ – sugar, H^1 and CH – sugar, H^3); 4.07 (1H, s, CH – sugar, H^2); 4.02 (1H, s, CH – sugar, H^4); 3.75 (1H, m, CH - sugar, H^5); 3.41-3.57(1H, m CH$_2$ – sugar, H^6). ^{13}C NMR (100 MHz, DMSO-d$_6$): δ 141.31 (*p*-NH$_2$-Ph, C^p), 126.71 (*p*-NH$_2$-Ph, C^o); 126.67 (*p*-NH$_2$-Ph, C^1); 112.23 (*p*-NH$_2$-Ph, C^m); 99.88 (*p*-NH$_2$-Ph-<u>CH</u>); 77.38 (CH – sugar, C^4); 70.67 (CH – sugar, C^2); 69.80 (CH$_2$ – sugar, C^1); 67.99 (CH – sugar, C^3); 67.35 (CH – sugar, C^5); 62.67 (CH$_2$ – sugar, C^6). ATR-FTIR ν_{max} cm^{-1} 3241-3600 (OH, alcohol and N-H, amine), 2956 (CH, aliphatic), 1618 (N-H), 1579 (C=C, aromatic), 1342 (C-N), 1092 (C-O, acetal). ESI-MS: Calcd. [M+H]$^+$ ($C_{20}H_{25}N_2O_6$), *m/z* = 389.1612; Obs. [M+H]$^+$, *m/*z = 389.1591.

7.2.8 Synthesis of 1,3: 2,4-Dibenzylidene-D-Sorbitol-*p, p*'-dicarboxylic acid

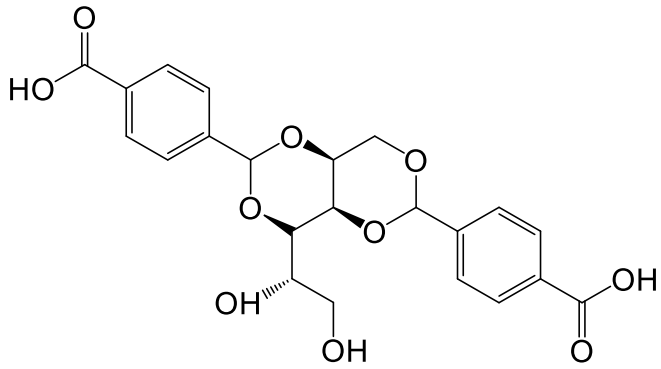

DBS-COOCH$_3$ (1.20 g, 2.53 mmol) was dissolved in methanol (35 mL) and NaOH $_{(aq)}$ (1.0 M, 35 ml) was added to the mixture. The mixture was heated overnight at 80 ^{O}C under reflux. Solvent was removed under vacuum and deionised water (50 mL) was added. The reaction mixture was acidified to pH 3 with $NaHSO_4$ which caused a white and stable gel to form. The product was filtered and washed thoroughly with

deionised water (100 mL x 4). The product was dried under high vacuum and finally dried to constant weight in the oven at 50 ^{O}C for 2 days. Yield 100% (1.12 g). ^{1}H NMR (400 MHz, DMSO-d_6): δ 12.99 (1H, s, *p*-HOOC-Ph); 7.93 (4H, d, *J* = 8.4 Hz, *p*-HOOC-Ph, H^{m}); 7.55 (4H, t, *J* = 8.4 Hz, *p*-HOOC-Ph, H^{o}); 5.72 (2H, s, *p*-HOOC-Ph-C<u>H</u>); 4.90 (1H, CHO<u>H</u>); 4.44 (1H, CH_2O<u>H</u>); 4.19 (1H, d, *J* = 11.6 Hz, CH_2 – sugar, H^{1}) and 4.17 (1H, d, *J* = 11.6 Hz, CH_2 – sugar, H^{1}); 4.15 (1H, s, CH - sugar, H^{3}); 3.98 (1H, s, CH – sugar, H^{2}); 3.87 (1H, d, *J* = 10 Hz, CH – sugar, H^{4}); 3.75 (1H, m, CH - sugar, H^{5}); 3.57(1H, q, *J* = 11.6 Hz, CH_2 – sugar, H^{6}); 3.41 (1H, dd, *J* = 5.6 Hz and *J* = 11.2 Hz, CH_2 – sugar, H^{6}), ^{13}C NMR (100 MHz, DMSO-d_6): δ 167.62 (*p*-HOO<u>C</u>-Ph, C^{p}); 129.68 (*p*-HOOC-Ph, C^{1}); 129.59 (*p*-HOOC-Ph, C^{m}); 126.85 (*p*-HOOC-Ph, C^{o}); 100 (*p*-HOOC-Ph-<u>CH</u>); 78.09 (CH – sugar, C^{4}); 70.69 (CH – sugar, C^{2}); 69.83 (CH_2 – sugar, C^{1}); 69.03 (CH – sugar, C^{3}); 68.13 (CH – sugar, C^{5}); 63.10 (CH_2 – sugar, C^{6}). ATR-FTIR ν_{max} cm^{-1} 3398 (OH, alcohol), 2871 (CH, aliphatic), 1687 (C=O, COOH), 1514 (C=C, aromatic), 1090 (C-O, acetal). ESI-MS: Calcd. [M+H]$^{+}$ ($C_{22}H_{23}O_{10}$), *m/z* = 447.1291; Obs. [M+H] $^{+}$, *m/z* = 447.1297.

7.2.9 Synthesis of *p, p*'-dihydraza-1,3: 2,4-dibenzylidene-D-Sorbitol

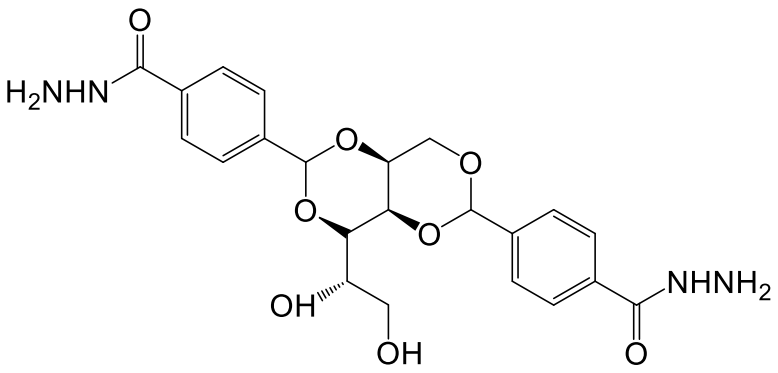

DBS-COOCH3 (1.10 g, 2.52 mmol) was weighed into a round bottom flask, THF (40 mL) was added and hydrazine monohydrate (6 mL, 6.192 g, 0.12 mol) was added to the reaction mixture. The reaction was allowed to proceed under reflux at 65 ^{O}C for 10 h. TLC was used to monitor the completion of the reaction. After the reaction, the white precipitate formed was filtered using sintered funnel and washed thoroughly with deionised water (100 mL x3). The white compound was dried under high vacuum, then oven-dried to a constant weight and pulverized. Yield 91% (1.00 g). ^{1}H NMR (400 MHz, DMSO-d_6): δ 9.77 (2H, s, *p*-H_2NHNOC-Ph); 7.79 (4H, d, *J* = 8.4 Hz, *p*-

H_2NHNOC-Ph, H^m); 7.48 (4H, t, *J* = 8.4 Hz, *p*-H_2NHNOC-Ph, H^o); 5.68 (2H, s, *p*-H_2NHNOC-Ph-C<u>H</u>); 4.95 (1H, CHO<u>H</u>); 4.45 (4H, s, CONHN<u>H_2</u>); 4.43 (1H, CH_2O<u>H</u>); 4.17 (1H, d, *J* = 11.6 Hz, CH_2 – sugar, H^1) and 4.16 (1H, d, *J* = 11.6 Hz, CH_2 – sugar, H^1); 4.14 (1H, s, CH - sugar, H^3); 3.95 (1H, s, CH – sugar, H^2); 3.85 (1H, d, *J* = 10 Hz, CH – sugar, H^4); 3.75 (1H, m, CH - sugar, H^5); 3.57(1H, q, *J* = 11.6 Hz, CH_2 – sugar, H^6); 3.41 (1H, dd, *J* = 5.6 Hz and *J* = 11.2 Hz, CH_2 – sugar, H^6), ^{13}C NMR (100 MHz, DMSO-d_6): δ 166.12 (*p*-H_2NHNOC-Ph, C^p), 141.34 (*p*-H_2NHNOC-Ph, C^1); 134.06 (*p*-H_2NHNOC-Ph, C^m); 127.28 (*p*-H_2NHNOC-Ph, C^o); 99.20 (*p*-H_2NHNOC-Ph -<u>CH</u>); 78.09 (CH – sugar, C^4); 70.63 (CH – sugar, C^2); 69.84 (CH_2 – sugar, C^1); 69.00 (CH – sugar, C^3); 68.13 (CH – sugar, C^5); 63.10 (CH_2 – sugar, C^6). ATR-FTIR ν_{max} cm^{-1} 3294 (NH and OH, hydrazide and alcohol), 2870 (CH, aliphatic), 1633 (C=O, $CONHNH_2$), 1568 (C=C, aromatic), 1091 (C-O, acetal). ESI-MS: Calcd. $[M+H]^+$ ($C_{22}H_{28}N_4O_6$), *m/z* = 475.1829; Obs. $[M+H]^+$, *m/z* = 475.1805.

7.3 Gel formation and characterization

7.3.1 Gelation by heat-cool cycle

A known weight (1-4 mg) of the sample of each of the gelators was mixed with the required solvent (0.5 mL) in a screw capped vial (2 mL), sonicated and heated until the solid was completely dissolved to give a clear solution. The solution was allowed to cool at room temperature for 5 h and gelation was visually observed by inverting the tube. Gelation was assumed to be successful if the gel sample did not exhibit gravitational flow in the inverted vial. In the case of gelation of **DBS-CONHNH$_2$** across a range of pH, 0.1 mM (50 µL) of HCl $_{(aq.)}$ and NaOH $_{(aq.)}$ were respectively added to aqueous solutions of the gelator to prior heating.

7.3.2 Gelation by pH-switching

A known quantity (1-3 mg) of **DBS-COOH** was mixed with de-ionized water (0.5 mL) in a capped vial; NaOH (0.5 M, 15 µL) was added and sonicated until the solid was completely dissolved. Glucono-δ-lactone, GdL (13 mg) was then added to the clear solution and shaken thoroughly. Gelation was allowed to occur without heating.

7.3.3 Kinetics of gelation of DBS-COOH by ^{1}H NMR spectroscopy

DBS-COOH (3 mg) was suspended in deuterated water (D_2O) and the suspension was sonicated for about 10 min. An equimolar quantity of NaOD (0.5 M, aq) was added and the solution was thoroughly shaken for about 10 minutes until a clear solution was formed. Dimethyl sulfoxide, DMSO (5 μmol) was added as an internal standard. The hydrogel was prepared by adding the solution to a measured quantity of GdL. The sample was loaded immediately into the spectrometer. ^{1}H NMR spectra were recorded at 500 MHz using a Bruker Avance 500 NMR spectrometer. Spectrum was collected at 10 min. interval. Data were analyzed using Topspin software.

7.3.4 Kinetics of gelation of DBS-CONHNH$_2$ and DBS-COOH by circular dichroism spectroscopy

A requisite weight (0.5 mg) of **DBS-CONHNH$_2$** was dissolved in water (0.5 mL) and heated on Eppendorf Aderman thermostat 5320 with the use of 1.5 mL Eppendorf tube until completely dissolved. The hot gelator solution was transferred within 15 s into a 1.0 mm quartz cell that was incubated in a thermostatted cell holder at 90 ^{O}C. It took about 30 s to attain temperature equilibration after sample transfer. Temperature of the cell compartment was allowed to cool to 15 ^{O}C while the Circular dichroism (CD) spectra were collected on a Jasco J810 circular dichromator fitted with a Peltier temperature control unit, at an interval of 2 min and 5 ^{O}C/min ramp. The infinite gelation time; point at which there was no more perceptible change in CD values following six (6) accumulations of the final scan, was attained within 3 h. CD spectra were fitted into the Avrami equations. On the other hand, a similar weight of **DBS-COOH** was weighed into deionised water (0.5 mL) and aliquot solution of NaOH (5 μL, 0.5 M) was added to dissolve the gelator by deprotonation. The solution was sonicated for about 10 min so as to aid complete dissolution of the gelator and the mixture transferred into a 1.0 mm quartz cell. The hydrogel of **DBS-COOH** was prepared by adding a requisite amount (10 mg) of glucono-δ-lactone and CD spectra were collected as described above but over a longer period of time (100 min).

7.3.5 Procedure for determining T_{gel} values

The temperature at which the gel sample was converted to a solution was determined by using a typical 'tube inversion' method. The gel was prepared in a 2 mL screw capped vial as described above. The vial was immersed in an oil-bath and heated slowly at 1 °C/min ramp. The temperature at which the gel-sol transition occurred was recorded as the T_{gel}. CD Variable temperature was further used to confirm the thermo-reversibility of the hydrogel of **DBS-CONHNH$_2$** prepared as described above by heating them at 10 °C/min ramp and CD spectra were collected on Jasco J810 circular dichromator fitted with a Peltier temperature control unit.

7.3.6 Procedure to determine stability of rheological properties of DBS-CONHNH$_2$ hydrogels to pH

In order to investigate the stability of **DBS-CONHNH$_2$** hydrogels (0.4% wt/vol) to pH, blocks of the hydrogels (d = 20 mm, h = 0.5 cm) were immersed in aqueous solution of HCl (1.0 M, 10 mL), deionised water (10 mL) or NaOH (1.0 M, 10 mL) for 10 h. The viscoelatic properties i.e. critical strain amplitude, storage modulus (G') and loss modulus (G'') of the hydrogels were measured by carrying out dynamic strain sweeps (f = 1 Hz) and dynamic frequency sweeps (Y = 0.2 %) were carried out on a parallel plate geometry (d = 20 mm).

7.4 Dye and metal uptake from model polluted water

7.4.1 Batch dye adsorption studies

The amount of dye adsorbed was monitored by adding 5 mL of each of the dye solutions; methylene blue (1.20 g/ l), reactive blue 4 (1.80 g/ l), acid blue 25 (1.54 g/ l) and naphthol blue black (1.20 g/ l) to 8 mL vials containing the hydrogel adsorbent (0.8 % wt/v). The time-dependent study of the adsorption of dyes was carried out under various pH conditions at room temperature. The pH of the dye solutions were adjusted with HCl (0.1 M, aq) and NaOH (0.1 M, aq). The supernatant (10 μL) was taken, diluted and the concentration of dye remaining in the solution was determined at various time intervals by using UV-Vis spectroscopy. The data obtained were used to compute the adsorption kinetics. The maximum dye uptake by the hydrogels was

determined at a point where there was no more significant adsorption. The dyes were calibrated beforehand and calibration curves are shown in Appendix 3.

7.4.2 Adsorption isotherm models

Adsorption isotherms were obtained by contacting a fixed amount (8 mg) of hydrogalor in wet gel form (0.8% wt/vol) with aliquot solution (5 mL) of each of the dyes investigated. A range of five different initial dye concentrations was prepared for each hydrogel-dye system. The amount of dye remaining in the aqueous solution was determined by UV-Vis spectrometry after 72 h. Langmuir and Freundlich models were used to describe the relationship between the amount of dye adsorbed and its equilibrium concentration in solution.

7.4.3 Desorption and reusability of DBS-CONHNH$_2$ hydrogels

Recyclability and reusability of **DBS-CONHNH$_2$** hydrogels for sequestering dyes from water was investigated by simple pH-switching. After the initial loading of an equimolar mixture of acid blue 25 (**AB25**) and naphthol blue black (**NBB**) into the hydrogels of **DBS-CONHNH$_2$** contained in a vial, NaOH (0.1 M, aq.) was added on top of the hydrogels and allowed to diffuse into the gel network. Deionised water was first added and allowed to diffuse into the gel network for 15 h. When no significant desorption emerged, aqueous basic solution was added to the top of the hydrogels and allowed to percolate the gel network for 6 h. UV-Vis spectroscopy was used to monitor the release of dyes from the gels.

7.4.4 Column preparation and flow-through experiment

A gel sample was made in a glass column (2.5-cm diameter and 15-cm length) or sometimes a 5 mL plastic syringe (1.0-cm diameter and 10-cm length). In both cases, gelator (20 mg) mixed with de-ionized water (0.3-0.5 mL), sonicated and NaOH (0.5 M, 30 μL) was added. The solution was shaken thoroughly until the solid was completely dissolved. GdL (20 mg) was added to the clear solution; was the solution was further shaken and transferred as quickly as possible into the vertically clamped column which was sealed at the bottom. The column was corked and gelation allowed to take place overnight. Thereafter, de-ionized water was added to the column and

allowed to flow through the column so as fill any voids in the gel network. The prepared column was then ready for the dye solution flow-through experiment.

The prepared dye solution (0.12 M Methylene blue) was charged into the column and the effluent was collected through the column exit at different time intervals.

7.4.5 Calibration of Pb^{2+} and Cd^{2+}

Commercially available $Pb(NO_3)_2$ and $Cd(NO_3)_2$ standards for AAS was used as the stock solution from which other concentrations were prepare by diluting varied concentration between 1-10 mg/l and 0.5-2.5 mg/l for Pb^{2+} and Cd^{2+} respectively with deionized water. Nitric acid (0.1 M) was added to the standard solutions in order to prevent precipitation of the metal ions. Figure 7.4.1a and b show the linearity of absorbance with concentration and hence, Beer-Lambert law is valid within this range.

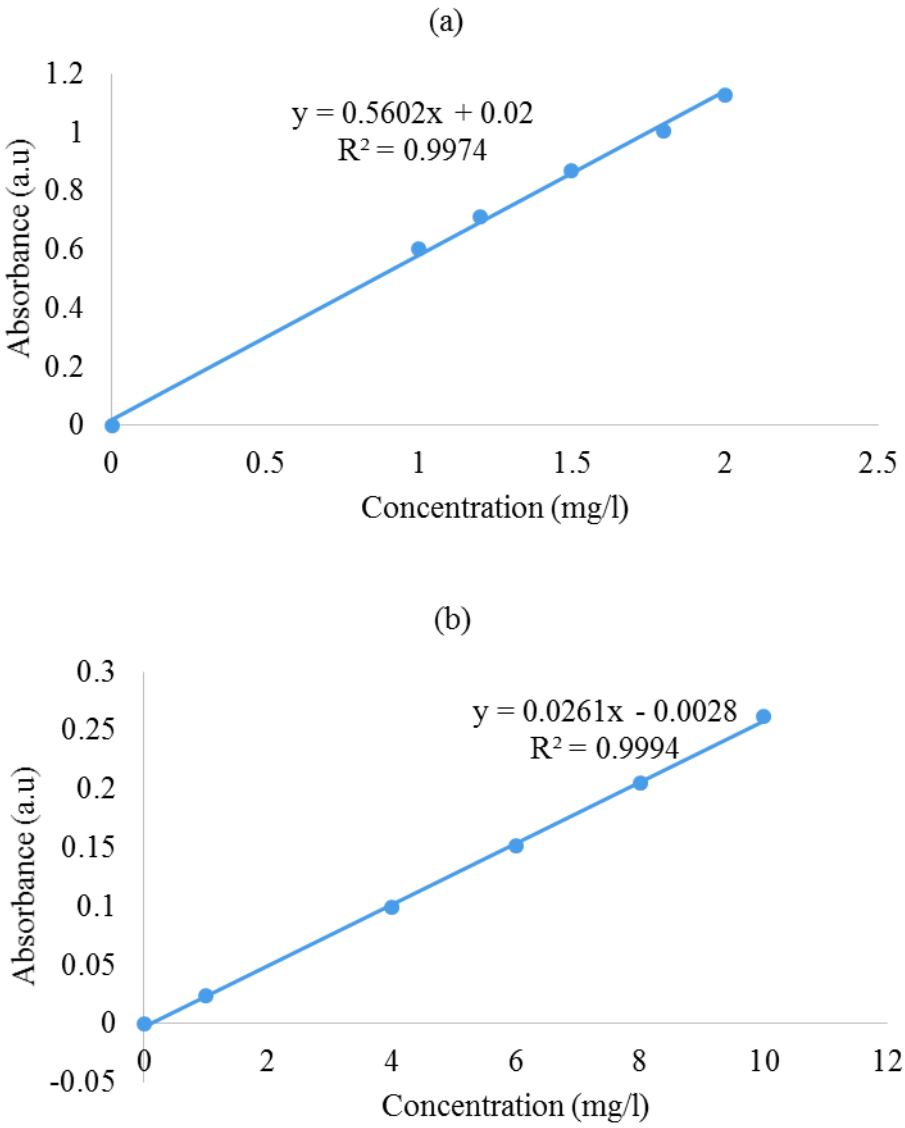

Figure 7.4.1 Calibration curves for aqueous solutions of (a) Pb^{2+} and (b) Cd^{2+}

7.4.6 Gelator screening for heavy metal adsorption

Hydrogels of **DBS-COOCH$_3$**, **DBS**, **DBS-F**, **DBS-Br**, **DBS-NO$_2$** and **DBS-SMe**, **DBS-COOH** and **DBS-CONHNH$_2$** were made by dissolving 4 mg of each gelator in 1.0 mL deionised water-ethanol mixture (40%-60%). The mixtures were sonicated, heated until the gelator fully dissolved to give a transparent solution and allowed to cool to room temperature. **DBS-CONHNH$_2$** on the other hand, did not require a co-solvent as it forms a stable hydrogel in 100% deionised water (1.0 mL). The hydrogel of **DBS-COOH** was made by dissolving a requisite weight of the gelator in deionised water (0.95 mL) followed by the addition of aqueous NaOH solution (0.5 M, 50µL).

The solution was sonicated until the gelator completely go into solution, after which glucono-d-lactone (15 mg) was added in order to trigger gelation at room temperature. All hydrogels were made in screw-capped 8 mL vials.

An aqueous solution of Pb^{2+} (600 mg/l, 6 mL) and Cd^{2+} (600 mg/l, 6 ml) was allowed to interact with the hydrogels for about 48 h. The hydrogel fibres were filtered-off and the residual concentrations of the metals were obtained using AAS by diluting 20 µL of the filtrate to 10 mL using aliquot solution of HNO_3 (0.1 M). For comparative performance, Activated carbon (4 mg), Starbon800 (4 mg), collected from Green Chemistry Centre, University of York and partially cross-linked Polyacrylic Acid (4 mg) were individually interacted with the same concentrations of Pb^{2+} and Cd^{2+}. The maximum metal ion uptakes were deduced from the equation of mass action shown in below

$$q_{max} = \frac{(C_o - C_e)V}{m} \qquad \text{Equation 7.4.1}$$

Where C_o and C_e are the initial and equilibrium concentration of the metal ions in mg/l respectively, V is the volume (L) of the aqueous metal ion added to the gel and m is the mass (g) of the gelator used.

7.4.7 Heavy metal screening for adsorption onto DBS-CONHNH$_2$

Aqueous solutions (600 mg/l, 6 mL) of $Hg(NO_3)_2$, $Pb(NO_3)_2$, $Cd(NO_3)_2$ and As_2O_3 (114 mg/l, 6 mL) was allowed to interact with the hydrogels of **DBS-CONHNH$_2$** for 48 h. This concentration was chosen for As^{3+} due to its low solubility in water at room temperature. Atomic absorption spectrophotometry (AAS 6300) was used to quantify the initial and the residual concentrations of Pb^{2+} and Cd^{2+} while Inductively Coupled Plasma-Mass Spectrometry (ICP-MS) was used for the analyses of Hg^{2+} and As^{3+}. Maximum uptake of heavy metals unto **DBS-CONHNH$_2$** hydrogels was computed using Equation 7.4.1. Adsorption studies of the heavy metals were carried out at ambient temperature and pH.

7.4.8 Effect of pH on adsorption of metal ions onto DBS-CONHNH$_2$.

The hydrogels of **DBS-CONHNH$_2$** were made as described in **7.3.1**. The pH of the aqueous metal ion solutions was adjusted with aliquot solutions of 0.1 M HCl and NaOH. Aqueous solution (6 mL) of Pb^{2+} and Cd^{2+} was allowed to interact with the nanofibres of **DBS-CONHNH$_2$** hydrogel for 48 h at room temperature. The equilibrium concentrations of Pb^{2+} and Cd^{2+} ions were measured using AAS and q_{max} deduced.

7.4.9 Adsorptive kinetics of Pb^{2+} and Cd^{2+} onto DBS-CONHNH$_2$ hydrogels.

Eight samples of **DBS-CONHNH$_2$** hydrogel were prepared for each of the metal ions by using a fixed weight (4 mg) of the gelator. Each time interval was studied with its own hydrogel, hence the hydrogels were labelled 5 min, 10 min, 30 min, 60 min, 120 min, 180 min, 240 min and 360 min. The time-dependent adsorption of Pb^{2+} and Cd^{2+} ions was investigated by adding a fixed concentration (950 mg/l, 6 mL) of each of the metal ions to each of the hydrogels. The mixture was shaken for 2 min and left undisturbed at ambient temperature to allow the metal ions to interact with the gel fibres. Mixtures of **DBS-CONHNH$_2$** hydrogel and metal solution were filtered when each time intervals elapsed and the residual concentration of the metal ions was used to compute the amount, q_t of Pb^{2+} and Cd^{2+} adsorbed after time, *t*. The data obtained were fitted into pseudo-first and pseudo-second order kinetics equations.

7.4.10 Adsorptive isotherm of Pb^{2+} and Cd^{2+} onto DBS-CONHNH$_2$

A range of concentrations (100-900 mg/l) of aqueous solutions of Pb^{2+} and Cd^{2+} was added to hydrogels made of **DBS-CONHNH$_2$** gelator (0.8% wt/vol). The mixture was thoroughly shaken to enable the metal ions and the gel fibres interact. The adsorption was allowed to proceed at 283K, 293K, 303K, 308K and ambient pH by for 72 h. The equilibrium concentrations and the amount of metal ions adsorbed were deduced. The data obtained were fitted into Langmuir and Freundlich isotherms models. The data and the isotherm parameters were further used to compute the thermodynamic properties of the adsorption process.

7.4.11 Selective uptake of heavy metals

An aqueous solution (5 ml) containing $NaNO_3$ (1264 mg/l), $Ca(NO_3)_2$ (1198 mg/l), $Pb(NO_3)_2$ (360 mg/l) and $Cd(NO_3)_2$ (357 mg/l) was added to the hydrogel of **DBS-CONHNH$_2$** (4 mg, 1.0 mL). The mixture was allowed to interact at ambient temperature and pH for 72 h after which the hydrogel was filtered off and the residual concentrations of metal ions were measured on an ICP-MS (Agilent 7700 series).

7.4.12 Minimum uptake level of heavy metals onto DBS-CONHNH$_2$ hydrogel

The ability of the hydrogel nanofibres to remove trace amount of toxic metals from water was investigated by interacting aqueous solutions of Pb^{2+} (120 ppb), Cd^{2+} (180 ppb) and Hg^{2+} (629 ppb) with **DBS-CONHNH$_2$** hydrogels at ambient temperature and pH for 48 h. The nanofibres were filtered-off and the residual concentrations of the metals were obtained by ICP-MS.

7.4.13 Recovery and reusability of DBS-CONHNH$_2$ hydrogels

DBS-CONHNH$_2$ hydrogels (0.8% wt/vol) were made in 8 mL vials and Pb^{2+} ions was adsorbed on the gel nanofibres with an evident yellow colour formation. An aqueous solution of ethylenediaminetetraacetic acid (EDTA, 0.1 M) was added on top of the gel – Pb complex system and allowed to interact with the gel for about 4 h. On the other hand, deionised water was used instead of EDTA. The concentration of Pb^{2+} in the supernatant liquid was obtained on ICP-MS.

7.4.14 Recovery of gold and silver from aqueous solution with DBS-CONHNH$_2$ hydrogels

A characteristic of Au^{3+} ions is the absorption of ultraviolet light at 293 nm. In order to calculate the molar extinction coefficient a curve was plotted correlating absorption with concentration for 0.025, 0.05, 0.075, 0.1, 0.15, 0.25 and 0.5 mM solutions of Au salts (as shown in Figure 7.4.2). This data was then used for calculating the ability of the gel to uptake Au^{3+}. Hydrogels of **DBS-CONHNH$_2$** were prepared in 3 mL screw–capped vials. An aqueous solution (10 mM, 2.0 mL) of $HAuCl_4.3H_2O$ or $AgNO_3$ was added on top of the hydrogels and allowed to diffuse into the gel network at ambient

and static conditions for 48 h. The equilibrium concentration of Au^{3+} ions in the supernatant liquid was extrapolated from the calibration curve and maximum gold loading onto the hydrogel was hence deduced from mass balance equation. On the other hand, $AgNO_3$ is colourless, hence it was impossible to use UV-Vis spectroscopy to determine equilibrium concentration of Ag^+, therefore, ICP-MS was used to quantify the residual concentration of Ag^+ ions in the supernatant liquid after 48 h. In all the experiments, glassware was rinsed with a mixture of HCl (30%): HNO_3 (70%).

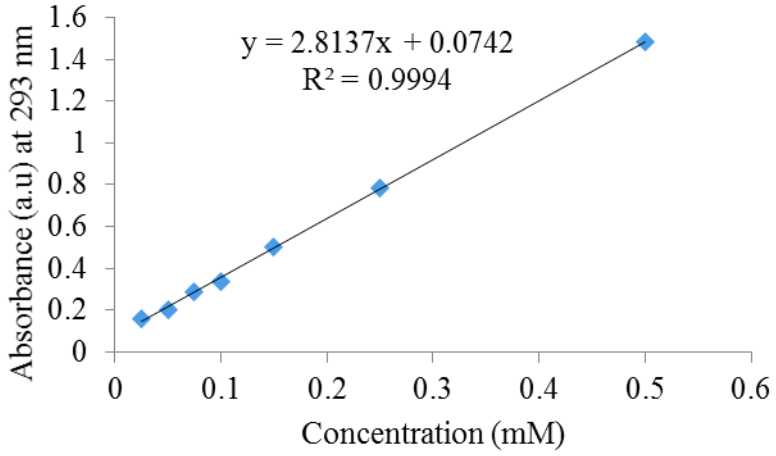

Figure 7.4.2 Calibration curve for Au^{3+} ions in an aqueous medium.

7.5 From precious metal recovery to conductive nanogel constructs

7.5.1 Selectivity of DBS-CONHNH$_2$ hydrogel for precious/noble metals

An aqueous solution containing an equimolar (100 mg/ l, 5 mL) concentration of $CuCl_2$, $NiCl_2$, $FeCl_2$, $ZnCl_2$, $AuCl_3$, $PtCl_2$, $PdCl_2$ and $AgNO_3$ was interacted with **DBS-CONHNH$_2$** hydrogel for about 72 h. The supernatant liquid was filtered and analysed on ICP-MS to obtain the residual concentrations of metal ions. Percentage selectivity of each of the metals was quantified by using Equation 7.5.1 shown below.

$$\text{Percentage metal uptake} = (C_{final} - C_{initial}) \times 100/C_{final} \quad \text{Equation 7.5.1}$$

7.5.2 **Synthesis of DBS-CONHNH2-Agarose hybrid hydrogels (Nanogels)**

The required weight of agarose (2.5 mg) and **DBS-CONHNH$_2$** (2.53 mg) were jointly dissolved in deionised water (0.5 mL). After sonicating the mixture, it was heated with shaking until the gelators completely go into solution, as judged by the formation of transparent hydrosol. The hydrosol was transferred into a removable-base (2 mL volume) with the base temporarily held on with a heat shrink plastic tubing. The hydrosol was allowed to cool down at room temperature as the hydrogel formed. Hydrogel formation was confirmed by its stability to inversion under gravity.

7.5.3 **Synthesis of DBS-CONHNH$_2$-Agarose-Nanoparticles hybrid hydrogel (Nanogel – NPs)**

The hydrogel blocks (diameter Ø = 0.8 cm and height h = 0.5 cm) as synthesized in **7.5.2** were immersed into aqueous solution of the Au^{3+} (15 mM, 3 mL) or Ag^{+} (10 mM, 3 mL) and allowed to interact with the metal solution for about 24 h. The colour change which confirmed formation of nanoparticles was observed.

7.5.4 **Measurement of the conductivity of the hydrogel-nanoparticles blocks**

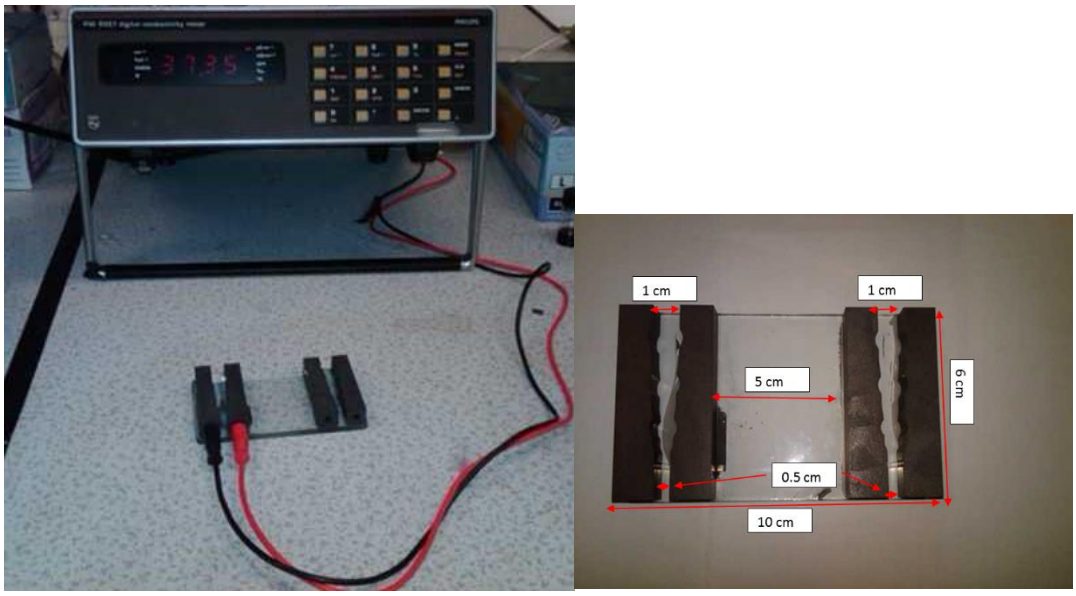

Figure 7.5.1 Fabricated in-house device for measuring the conductivity of hydrogels.

Prior to the measurement of the conductivity of the nanocomposites, a testing block (shown in Figure 7.5.1) was fabricated. The testing block comprises two pairs of

graphite pieces each with a dimension of 5.8 cm x 1.0 cm x 1.0 cm, glued onto a glass slab (10 cm x 6 cm x 0.4 cm) with a 5.0 cm separation between the two pairs. The gap between the left and right plates of one pair of blocks ranges from 0.5 cm-1.0 cm. The variations were made in order to accommodate gel blocks of various sizes. Each of the blocks had a drilled hole of depth 1.2 cm and diameter 4 mm in order to facilitate connection to the conductivity meter (PW9527 digital conductivity meter) via standard 4 mm plugs. The hydrogel-NPs composite was placed between the graphite blocks in order to bridge them and the conductance measured was in triplicate on a PW9527 digital conductivity meter.

7.5.5 Measurement of the electrocatalytic properties of DBS-CONHNH$_2$-Agarose hydrogel-nanoparticles composites

The working electrodes, designed for testing the electrochemical properties of the AuNP gel, were prepared as follows: the base of a carbon rod (diameter 5 mm) was encased in resin and then emery paper was used to reveal just the planar top face (area 0.1963 cm^2) of the carbon, with the resin acting to insulate the sides of the rod in contact with solution. The tip of the carbon rod was then fitted with PTFE tubing (Ø = 41 mm and l = 50 mm) to act as a mould for the gel. Into this mould, 5 μL of the hydrosol was applied and allowed to set into a gel for 10 min. An aqueous solution of Au^{3+} (10 μL, 15 mM) was subsequently dropped onto the modified electrode and allowed to diffuse into and interact with the gel fibres for 45 min as the nanoparticles formed *in situ*. The electrode was then immersed into deionised water for 1 h to remove excess metal ions.

The electrochemical experiments were performed by cyclic voltammetric (CV) measurement in a 100 mL Pyrex beaker using a computer-controlled PST050 VoltaLab potentiostat with VoltaMaster software. A platinum wire mesh and saturated Calomel electrode were the counter and the reference electrodes, respectively. Sodium acetate (100 mM) was employed as the electrolyte solution. The potential was scanned between -0.25 V to 0.15 V at 20 mV/s for 5 CV cycles.

7.5.6 Synthesis of DBS-CONHNH$_2$ hydrogel-AuNPs nanocomposite by direct addition to a hot DBS-CONHNH$_2$ hydrosol

DBS-CONHNH$_2$ (2.37 mg) was dissolved in deionised water (0.5 mL), sonicated for 15 min and heated in a sample vial until the gelator is completely dissolved. An aqueous solution of $HAuCl_4.3H_2O$ (3.2 mM, 100 µl) was added to the hot gelator solution (hydrosol), shaken and allowed to nucleate and grow as gelation takes place.

7.5.7 Effect of AuNPs on the T_{gel} of the hydrogel of DBS-CONHNH$_2$

DBS-CONHNH$_2$ hydrogel encapsulated AuNPs were prepared as described in **7.5.6**, however, the nanocomposites were made with a constant gelator concentration (10 mM) but a range of Au^{3+} concentrations (0.1-1.4 mM). The gel vials were immersed in an oil-bath and heated slowly at 5 ^{O}C/min ramp. The temperatures (T_{gel}) at which the hydrogel – AuNPs hybrids fell under gravity was determined by using a typical 'tube inversion' method.

7.5.8 Stability of DBS-CONHNH$_2$ Hydrogel Encapsulated NPs

Hydrosols of **DBS-CONHNH$_2$** (10 mM, 2 mL) containing *in situ* generated AuNPs/ AgNPs were transferred into cuvettes (x 8) with pipette and the hydrogels were allowed to set at room temperature. The pH of the nanocomposites was then adjusted by using HCl (0.1 M) or NaOH (0.1 M). Acid/base solutions (1 mL) prepared across a range of pH (2-12) were added to the top of the nanocomposite samples and were allowed 4 days for the supernatant acid/base solutions to diffuse into the hydrogel-AuNPs/ AgNPs composite samples. The effect of pH was assessed by measuring the SRP band using UV-Vis spectroscopy. Also, the change in SPR band of the **DBS-CONHNH$_2$** hydrogel-AuNPs/ AgNPs was recorded after 90 days.

7.5.9 Synthesis of pH-tunable hydrogel - AuNPs hybrid materials

A known quantity (2.24 mg) of **DBS-COOH** was mixed with de-ionized water (0.5 mL) in a capped vial; sonicated, NaOH (0.5 mM, 15 µL) was added and further sonicated until the solid was completely dissolved. GdL (13 mg) was added to the clear solution and shaken thoroughly. Gelation was then allowed to occur without heating.

An aqueous solution of $HAuCl_4.3H_2O$ (3.2 mM, 2.5 mL) was added to the top of the hydrogel and allowed to percolate the gel-network at room temperature. Removal of Au^{3+} from the top layer was monitored by measuring the absorbance of the supernatant with UV-Vis spectroscopy.

On the other hand, an aqueous solution of $HAuCl_4.3H_2O$ (3.2 mM, 200 µL) was added to the hydrosol of **DBS-COOH-GdL** (1.8 mL) in a cuvette at room temperature. Gelation of **DBS-COOH** was allowed to proceed simultaneously with nanoparticle formation. UV-Vis spectroscopy was used to monitor the growth of AuNPs within the gel-network by measuring the absorbance of the SPR band at various time intervals. A solution of GdL and $HAuCl_4.3H_2O$ without a gel present was used as the control.

7.6 Hydrogel-API formulation and release studies

7.6.1 Incorporation of mesalazine (MSZ) into DBS-CONHNH$_2$ hydrogel by batch adsorption process

A stock solution of **MSZ** (2.87 mM, 22 mg) in acetate buffer (50 mL) was prepared for adsorption experiments. Aliquot solutions was prepared across a range of concentrations (0.1 – 0.4 mM) to prepare a calibration curve for MSZ in acetate buffer.

An aliquot solution of **MSZ** (2.87 mM, 5.0 mL) was added carefully on top of a preformed **DBS-CONHNH$_2$** hydrogel (10 mM). Initially, 10 µL of the supernatant **MSZ** solution was withdrawn and diluted to 2 mL with acetate buffer. An initial absorption reading was taken and subsequent readings were taken every two hours. After 44 h, 2 mL of the solution was taken from the supernatant liquid. UV-Vis spectroscopy was used to quantify the residual concentration of **MSZ** in the supernatant liquid.

7.6.2 Incorporation of APIs into DBS-CONHNH$_2$ hydrogel nanofibres by direct mixing

An equimolar concentration (4 mM) of APIs – **NPX, IBU** and **MSZ** was simply mixed as solid with **DBS-CONHNH$_2$** gelator. To each of the mixtures, deionised water (0.5 mL) was added, sonicated for 10 min and the sample heated in a screw capped vial

until the mixture fully dissolves giving colourless aqueous solution. The hot hydrosol was allowed to cool at room temperature for 4 h. Formation of self-supported hydrogels was confirmed by the tube – inversion method.

7.6.3 Determination of T_{gel} values of hydrogel – APIs composites

Hydrogels comprising a range of concentration of APIs (0.5 – 4 mM) mixed with a fixed concentration of **DBS-CONHNH$_2$** (4 mM) were prepared as described in 7.6.2. The temperature at which the gel sample was converted to a solution was determined using a typical 'tube inversion' method. The gels were prepared in 2 mL screw capped vials. The vials were immersed in an oil-bath and heated slowly at 5 ^{o}C/min ramp.

7.6.4 Investigation of interaction between NPX and DBS-CONHNH$_2$ hydrogel

Fluorescence spectra were obtained on a Hitachi F-4500 spectrofluorimeter using excitation wavelength 272 nm. A requisite amount (0.29 mg) of NPX was dissolved in ethanol, loaded into a 1.0 cm path–length cuvette and excited at 272 nm to obtain an emission spectrum at 360 nm. On the other hand, 2.5 mM **DBS-CONHNH$_2$** with and without an equimolar concentration of NPX was prepared in deionised water, sonicated for about 15 min and heated until a transparent hydrosol was obtained. The hot hydrosol was transfer into 1.0 cm pathlength cuvette. The samples were excited at 272 nm before and after formation of partial and transparent gels. Emission spectra were obtained between 300 and 500 nm at a scan rate of 100 nm/min.

7.6.5 Controlled release studies of API from DBS-CONHNH$_2$ hydrogel nanofibres

Controlled release of APIs from **DBS-CONHNH$_2$** hydrogel nanofibres was investigated under four pH conditions – pH 1, 7, 8 and phosphate buffer 8. API – gelator hybrid hydrogels were prepared by mixing equimolar concentration (6 mM) of **DBS-CONHNH$_2$** (2.84 mg) and NPX (1.38 mg), IBU (1.22 mg) and MSZ (0.98 mg) respectively. Deionised water (1.0 mL) was added to the mixtures, sonicated for 10 min and heated until the components are fully dissolved. Hydrogels were allowed to be formed undisturbed at room temperature for 12 h.

Calibration curves were obtained by diluting API solutions with phosphate buffer at pH 8 and measuring of maximum absorbance at 316 nm and 297 nm using a UV-Vis spectrometer. The curves showed a linear relationships between maximum absorbance and concentration in the range of 0 – 1 mM and 0 – 0.4 mM for NPX and MSZ respectively. Five millilitres (5 mL) of water or buffer solution at various pH used as the receiving media for NPX and MSZ were carefully placed on top of each hydrogel in 8 mL vial. At designated time intervals, 2 mL of supernatant solution was removed and filtered. The absorbance at 316 nm and 297 nm for NPX and MSZ was measured and the concentration of APIs which has been released from the hydrogel was obtained from the calibration curves. The aliquot supernatant solution was carefully added to the receiving media after absorption measurement. After 12 h, the maximum absorbance of APIs in the receiving media was already above 1.0, therefore 20 µL aliquot solution was withdrawn from the supernatant solution and diluted to 2 mL prior to measurement.

8 Appendices

8.1 Appendix 1

8.1.1 Procedure for the *in silico* studies of DBS, DBS-COOH and DBS-CONHNH$_2$

These computational studies were carried out by Dr Dafna Kani (*Department of Biotechnology Engineering, ORT Braude College, Israel)* – see Appendix 1. Three simulation modules were used in this study (included in the molecular modelling package: "Material Studio" by Accelrys, as described elsewhere for a similar investigation.

DMOL3 - a quantum mechanics module used to model the electronic structure and energetics of molecules using density functional theory (DFT). DMOL3 was used to optimize the structure of a single and a pair of **DBS**, **DBS-COOH** and **DBS-CONHNH$_2$** molecules.

Discover - a force field simulation tool for performing Molecular Mechanics (MM) and Molecular Dynamics (MD) tasks.

Amorphous Cell - a simulation tool capable of building 3-D periodic boundary cells (PBC). Amorphous Cell and Discover modules were used to simulate pure **DBS**, **DBS-COOH** and **DBS-CONHNH$_2$**, pure water, and mixture of **DBS**, **DBS-COOH** and **DBS-CONHNH$_2$** with water as condensed phases at 300 K.

The simulation procedure was as follows:

(i) **DBS**, **DBS-COOH** and **DBS-CONHNH$_2$** were built as chiral molecules and were minimized using Discover module.

(ii) The geometry of the **DBS**, **DBS-COOH** and **DBS-CONHNH$_2$** molecules were optimized using DMOL3.

The molecules were subjected to 100,000 dynamics steps at 10000 K and were minimized in order to ensure that the minimum energy conformation is obtained, prior to optimization. This procedure was repeated for ten different conformations and the lowest energy conformation was then optimized using DMOL3. Angles and distances in the optimized structure were measured. The same procedure was repeated for two **DBS**, **DBS-COOH** and **DBS-CONHNH$_2$** molecules so as to obtain their inter- and intramolecular distances.

(iii) For the atomistic simulation, PBC (about 20 Å edge) were constructed for each of **DBS-COOH** and **DBS-CONHNH$_2$** in their pure states and the mixture of each of them with water. The boxes were built using Amorphous cell module at density of 1.3 g/cm3 for both pure **DBS-COOH** and **DBS-CONHNH$_2$**, and 1.0 g/cm^3 for the mixture of them with water. The simulation cubic cells of pure **DBS-COOH** and **DBS-CONHNH$_2$** contained 15 molecules each while the combined cells contained 250 molecules of water and two (2) molecules of each of **DBS-COOH** and **DBS-CONHNH$_2$**.

(iv) The cells containing pure **DBS-COOH** and **DBS-CONHNH$_2$** and a mixture of **DBS-COOH** and **DBS-CONHNH$_2$** with water were subjected to dynamic simulation in two stages:

a. The cells were brought to the appropriate density by dynamic simulation at constant pressure, temperature and cell mass (NPT) by 100,000 steps of 1 fs.

b. Equilibration and data collection steps were performed by dynamic simulation at constant volume, temperature and cell mass (NVT) by 300,000 steps of 1 fs. Frame output was recorded every 1000 steps (300 frames for each cubic cell).

The force field used in the simulation was COMPASS (condensed phase optimized molecular potentials for atomistic simulation studies). Electrostatic interactions were calculated by Ewald summation method, and Andersen thermostat was used.

(v) The resulted dynamic trajectories were analysed using Amorphous cell module analysis tools. The following properties were calculated:

a. Cohesive Energy Density (CED) and Solubility parameter of pure **DBS**, **DBS-COOH** and **DBS-CONHNH$_2$** and a mixture of **DBS-COOH** and **DBS-CONHNH$_2$** with water.

b. Radial distribution function: Also referred to as Pair correlation function is a measure of the probability.

8.1.2 Simulation of DBS, DBS-COOH and DBS-CONHNH2 hydrogels

This *in silico* studies were carried out by Dr Dafna Knani at Department of Biotechnology Engineering, ORT Braude College, Israel.

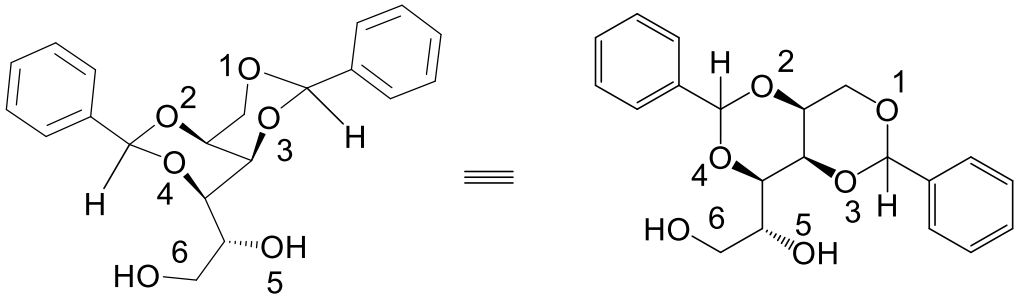

Figure 8.1.1 DBS molecular structure. The oxygen atoms are labelled for further discussion

8.1.3 Structural characterization and the interaction between two molecules of DBS, DBS-COOH and DBS-CONHNH2

DBS, **DBS-COOH** and **DBS-CONHNH2** molecules were constructed and optimized using DMOL3 (DFT based) quantum mechanical software and conformer search. The lowest energy conformations (Figures 8.1.2 - 8.1.4) were found to be those in which the two aromatic rings are almost perpendicular in the **DBS** and parallel in **DBS-COOH** and **DBS-CONHNH2**. The distances between various groups in the molecules were measured and are summarized in Tables 8.1.1 – 8.1.3. The hydrogen of the hydroxyl group O6 in **DBS** and **DBS-COOH** points towards the oxygen of the hydroxyl O5 group (distances of 2.038 and 2.074Å, respectively) but not in **DBS-CONHNH2** (3.965Å). Whereas in **DBS** and **DBS-CONHNH2** the hydroxyl group O5 is oriented towards O4, in **DBS-COOH** it points towards O3.

Following the intramolecular analysis of one molecule, two **DBS** molecules were constructed, and their distances and conformations were optimized. As shown in Figures 8.1.2 – 8.1.4 and in Tables 8.1.1 – 8.1.3, the two molecules of **DBS**, **DBS-CONHNH2** and **DBS-COOH** are attracted to each other by intermolecular hydrogen bonding formed between several groups. Whereas in **DBS** and **DBS-CONHNH2** the most significant intermolecular interaction (the shortest distance) is formed between H-O6 / O5 (distances of 1.722 and 1.733Å, respectively), in **DBS-COOH** it is formed between H-O5/O5 (2.403Å). Additional interactions are formed between the substituents, especially in **DBS-CONHNH2** (distance of 1.866Å between H-NHNH / O_ Carbonyl). The distance between H-O Carboxylate / O_ Carbonyl in **DBS-COOH** is (3.532Å).

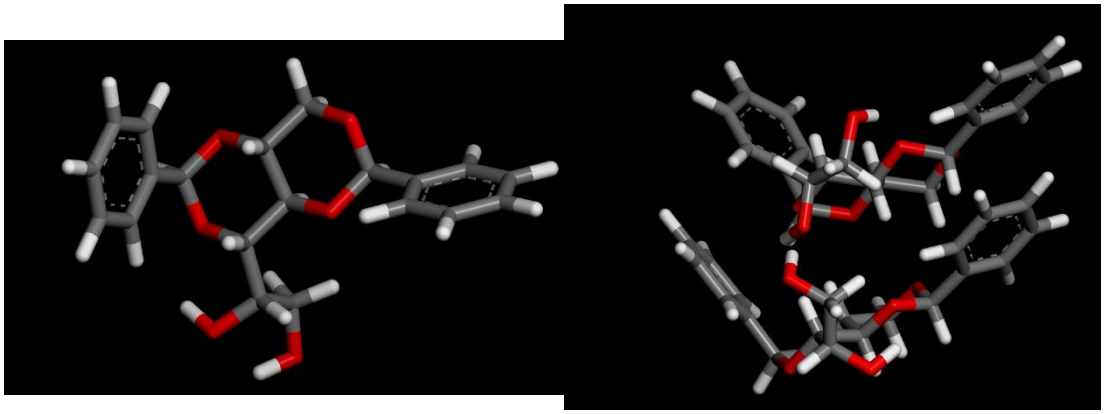

Figure 8.1.2 DBS molecule (left) and two **DBS** molecules (right) after optimization

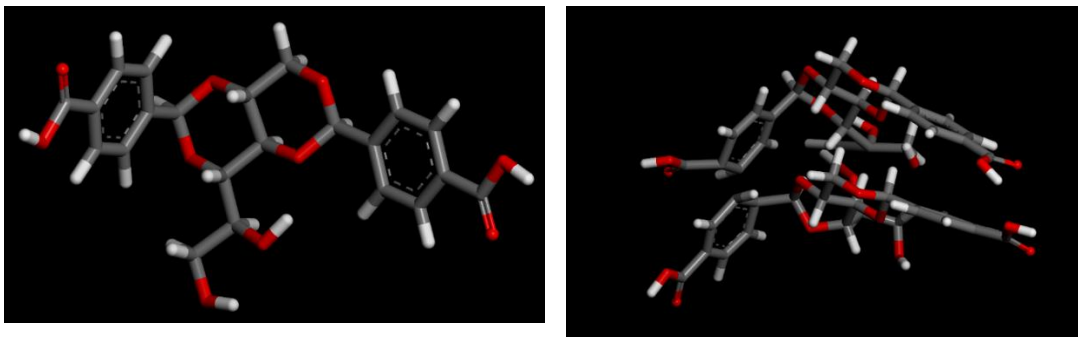

Figure 8.1.3 DBS-COOH molecule (left) and two **DBS-COOH** molecules (right) after optimization

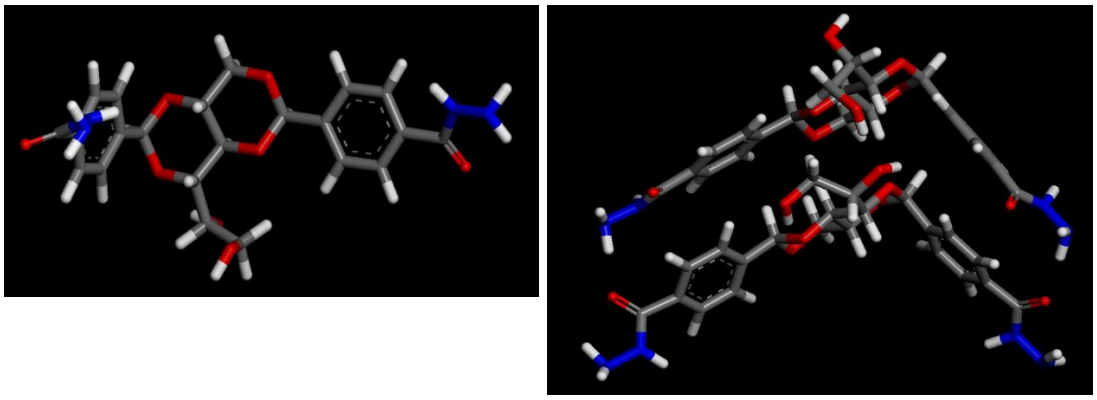

Figure 8.1.4 DBS-CONHNH$_2$ molecule (left) and two **DBS-CONHNH$_2$** molecules (right) after optimization

Table 8.1.1 Interaction distances calculated for optimized one and two molecules of **DBS**

Interaction between atoms	*One molecule*	*Two molecules*		
	Intramolecular interaction distance (Å)	*Intermolecular interaction distance (Å)**	*Intramolecular interaction distance (Å) ***	
O6 / H-O6	-	*4.575*	-	-
O6 / H-O5	*3.145*	*3.168*	*4.237*	*3.857*
O5 / H-O6	*2.038*	*1.722*	*3.894*	*4.095*
O5 / H-O5	-	*4.723*	-	-
O3 Acetal / H-O5	*4.623*	*3.767*	*4.428*	*2.162*
Acetal O3 / H-O6	*5.049*	*5.453*	*1.790*	*3.812*
O4 Acetal / H-O5	*2.024*	*3.836*	*1.955*	*3.677*
Acetal O4 / H-O6	*3.972*	*4.151*	*4.129*	*3.878*
Aromatic rings	-	*4.045*	-	-

* Shortest distances option
**A column for each of the two molecules

Table 8.1.2 Interaction distances calculated for optimized one and two molecules of **DBS-COOH**

Interaction between atoms	*One molecule*	*Two molecules*		
	Intramolecular interaction distance (Å)	*Intermolecular interaction distance (Å)**	*Intramolecular interaction distance (Å) ***	
O6 / H-O6	-	*4.139*	-	-
O6 / H-O5	*3.611*	*5.344*	*4.213*	*4.320*
O5 / H-O6	*2.074*	*3.616*	*5.616*	*3.889*
O5 / H-O5	-	*2.403*	-	-
O3 Acetal / H-O5	*1.861*	*4.340*	*6.659*	*4.340*
Acetal O3 / H-O6	*4.759*	*3.206*	*3.286*	*1.650*
O4 Acetal / H-O5	*3.792*	*2.922*	*4.749*	*1.833*
Acetal O4 / H-O6	*4.535*	*5.079*	*4.094*	*4.337*
Aromatic rings	-	*3.581*	-	-
H-O Carboxylate / O_ Carbonyl	-	*3.532*	-	-

* Shortest distances option, **A column for each of the two molecules

Table 8.1.3 Interaction distances calculated for optimized one and two molecules of **DBS-CONHNH2**

Interaction between atoms	***One molecule***	***Two molecules***		
	Intramolecular interaction distance (Å)	***Intermolecular interaction distance (Å)****	***Intramolecular interaction distance (Å)*** **	
O6 / H-O6	-	*4.015*	-	-
O6 / H-O5	*4.357*	*3.254*	*4.289*	*4.257*
O5 / H-O6	*3.965*	*1.733*	*4.113*	*3.903*
O5 / H-O5	-	*5.477*	-	-
O3 Acetal / H-O5	*4.044*	*4.011*	*3.806*	*4.584*
Acetal O3 / H-O6	*4.492*	*4.509*	*3.737*	*1.734*
O4 Acetal / H-O5	*2.426*	*4.161*	*2.717*	*1.760*
Acetal O4 / H-O6	*4.574*	*3.793*	*4.044*	*4.074*
Aromatic rings	-	*4.729*	-	-
H-NHNH / O_ Carbonyl	-	*1.866*	-	-

* Shortest distances option

**A column for each of the two molecules

Molecular dynamics simulations were performed in 300 K on pure **DBS**, **DBS-COOH** and **DBS-CONHNH2**, pure water and on their mixture. Simulation boxes of pure **DBS-COOH** and **DBS-CONHNH2** and their mixtures with water are shown in Figures 8.1.5 and 8.1.6.

8.1.4 Density and Solubility parameter calculation

Density, Cohesive Energy Density and solubility parameter δ (which is the square root of the CED) were calculated for pure **DBS, DBS-COOH** and **DBS-CONHNH2**, pure water and their mixture at 300 K using the amorphous cell module. As can be seen in Table 2, δ values of the pure gelators are much lower than that of pure water ($47.39(J/cm^3)^{0.5}$), because they are less polar than water. Therefore, it can be expected that the gelators will undergo phase separation when mixed with water, and this might explain the experimental observation that the gelator molecules self-organize into a nanofibrillar structure. The difference between the simulated values is an indication of the energetic benefit from mixing them together. The differences were quite small, indicating that the gelators do not mix well with water. The larger difference (1.37)

was observed for **DBS-COOH**, then **DBS-CONHNH$_2$** (0.76) and the smaller for DBS water 0.52). These results suggest that the solubility of **DBS-COOH** in water is the highest because the energetic benefit is the most pronounced. **DBS-CONHNH$_2$** is less soluble and **DBS** is even less soluble.

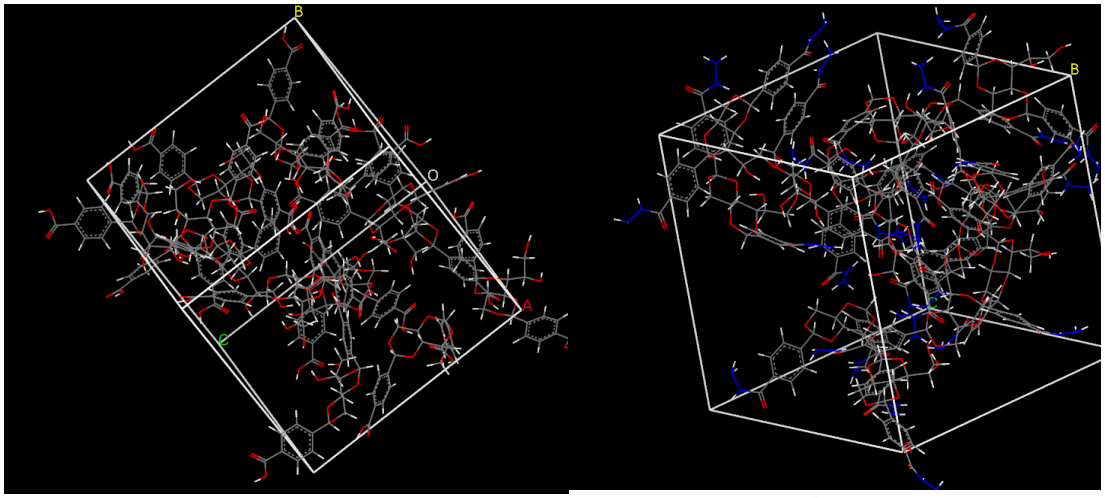

(a) **(b)**

Figure 8.1.5 Cubic cell containing *15* molecules of (a) **DBS-COOH** and (b) **DBS-CONHNH$_2$** at 300 K after 500 ns dynamic steps

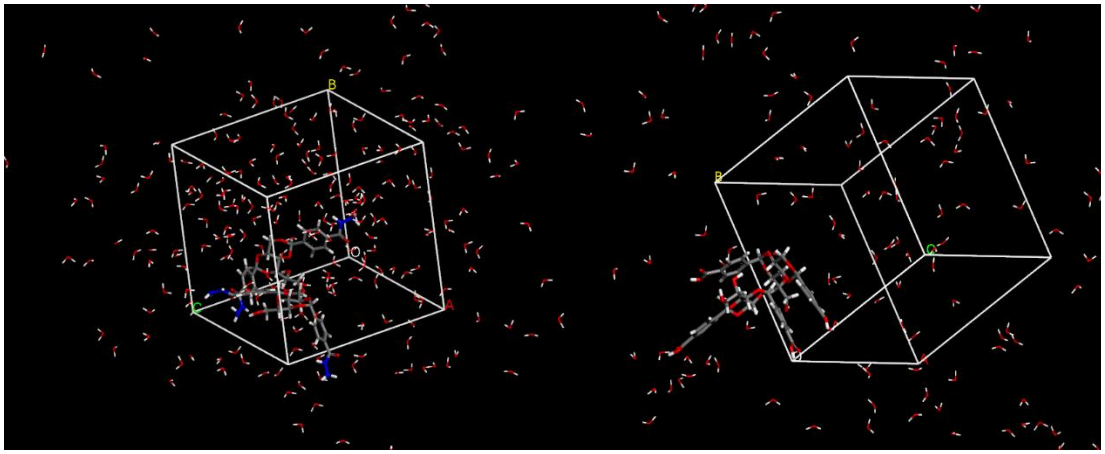

(a) **(b)**

Figure 8.1.6 Cubic cell containing *2* molecules of (a) **DBS-COOH** and (b) **DBS-CONHNH$_2$** and 250 water molecules at 300 K after 500 ns dynamic steps

Table 8.1.4 Calculated densities and solubility parameters of pure **DBS**, **DBS-COOH** and **DBS-CONHNH$_2$** and their mixture with water at 300 K

	Calculated densities (g/cm^3)*			***Solubility parameters δ [J/cm^3]$^{0.5}$***		
	DBS	*DBS-COOH*	*DBS-CONHNH$_2$*	*DBS*	*DBS-COOH*	*DBS-CONHNH$_2$*
Pure gelator	*1.228*	*1.310*	*1.306*	*22.04±0.01*	24.73±*0.01*	*25.80±0.014*
Gelator with water (simulated)	*0.992*	*1.034*	*1.012*	*44.43±0.016*	45.01±*0.03*	*44.39±0.03*
*Gelator with water (expected)**	-	-	-	43.91	*43.64*	*43.63*

**Calculated results for water: Density: 0.983 g/cm^3; Solubility parameters : 47.39 [J/cm^3]$^{0.5}$*

**Calculated Solubility parameters according to δ values and weight ratios of the constituents.

8.1.5 Radial Distribution Calculations

Inter- and intramolecular interactions, particularly hydrogen bonding, were calculated by pair correlation function for pure DBS and for its mixture with polypropylene. The distance between the groups is measured, and the peak height is proportional to the probability that the interacting groups will be at a certain distance from each other. Interaction intensities were calculated for the following pairs:

1. Between hydroxyl groups designated as:
   - **O6 / H-O6** (O6 and the hydrogen atom attached to O6)
   - **O6 / H-O5** (O6 and the hydrogen atom attached to O5)
   - **O5 / H-O6** (O5 and the hydrogen atom attached to O6)
   - **O5 / H-O5** (O5 and the hydrogen atom attached to O5)
2. Between hydroxyl groups and acetal group designated as:
   - **O3 Acetal / H-O5** (acetal group and the hydrogen atom attached to O5)
   - **O3 Acetal / H-O6** (acetal group and the hydrogen atom attached to O6)
   - **O4 Acetal / H-O5** (acetal group and the hydrogen atom attached to O5)
   - **O4 Acetal / H-O6** (acetal group and the hydrogen atom attached to O6)

3. Between aromatic rings
4. Between **H-O Carboxylate / O Carbonyl** in DBS-COOH and **H-NHNH / O Carbonyl** in DBS-$CONHNH_2$

The results of the calculated inter- and intramolecular interaction distances and peak heights (which correspond to the significance of the interaction) for DBS, DBS-COOH and DBS-$CONHNH_2$ and their mixture with water at 300 K appear in Tables 8.1.5 and 8.1.6 and Figures 8.2.1 - 8.2.6.

8.2 Intermolecular interactions between DBS, DBS-COOH and DBS-$CONHNH_2$ molecules

As can be seen in Table 8.2.1 and Figures 8.2.1 - 8.2.6, the intermolecular interactions are formed between the molecules of the three gelators in a similar manner. Intermolecular H-bonding interactions are formed between **O6 / H-O6**, **O5 / H-O6, O5 / H-O5** and **O6 / H-O5** of **DBS, DBS-COOH** and **DBS-$CONHNH_2$** molecules as pure substances (Figures 8.2.1 - 8.2.6). The interaction distance is between 1.65-1.85Å. On the other hand**, Acetal / H-O5** and **Acetal / H-O6** do not participate in intermolecular interactions. The interactions between aromatic rings were also elucidated, and no significant intermolecular π-π interaction was found. The interaction intensities in **DBS-$CONHNH_2$** are the lowest of the three, but an additional interaction is formed between the substituent **H-NHNH / O Carbonyl** groups compared to **DBS**. In **DBS-COOH** an interaction between **H-O Carboxylate / O Carbonyl** groups is also formed (Figure 8.2.5), at shorter distance and higher intensity than the interaction between **H-NHNH / O Carbonyl** groups in **DBS-$CONHNH_2$** (Figure 8.2.6). Overall, the interactions between DBS-COOH molecules are stronger than the interactions between **DBS-$CONHNH_2$** molecules.

The intermolecular interactions dramatically decrease in the presence of water. No significant interactions were detected for forming of intermolecular H-bonding interactions between **O6 / H-O6**, **O5 / H-O6, O5 / H-O5** and **O6 / H-O5** of DBS and also between **H-NHNH / O Carbonyl** groups in **DBS-$CONHNH_2$** molecules. Though, **DBS-COOH** molecules seem to interact in aqueous environment. H-bonds are formed especially between **O6 / H-O5,** and to a much lesser extent between **O5 /**

H-O6 and **H-O Carboxylate / O Carbonyl** group (Figure 8.2.5), which also forms interactions with the water molecules.

Table 8.2.1 Intermolecular interaction distances **(Å)** and relative frequencies calculated for pure **DBS, DBS-COOH** and **DBS-CONHNH$_2$** their mixture with water in a condensed phase at *300* K

Group	***DBS***	***DBS-COOH***	***DBS-CONHNH$_2$***	***DBS with water***	***DBS-COOH with water***	***DBS-CONHNH$_2$ with water***
O6 / H-O6	*1.65 (3.74)*	*1.65 (3.30)*	*1.65 (1.62)*	*No*	*No*	*No*
O6 / H-O5	*1.75 (3.97)*	*1.85 (3.66)*	*1.65 (2.21)*	*No*	*1.65 (3.97)*	*No*
O5 / H-O6	*1.75 (3.30)*	*1.65 (4.49)*	*1.75 (2.42)*	*No*	*3.15 (1.68)*	*No*
O5 / H-O5	*1.75 (2.23)*	*1.75 (2.50)*	*1.85 (1.05)*	*No*	*No*	*No*
O3 Acetal / H-O5	*No*	*No*	*No*	*No*	*3.65 (4.80)*	No
O3 Acetal /H-O6	*No*	*No*	*No*	*No*	*4.70 (2.45)*	No
O4 Acetal / H-O5	*No*	*No*	*No*	*No*	*No*	No
O4 Acetal /H-O6	*No*	*No*	*4.20 (1.69)*	*No*	*No*	*2.10 (2.71)*
Aromatic rings	*No*	*No*	*No*	*4.05 (1.99)*	*4.55 (2.11)*	*No*
H-O Carboxylate / O Carbonyl	-	*1.75 (3.65)*	-	-	*3.00 (2.13)*	-
H-NHNH / O Carbonyl	-	-	*2.00 (1.97)*	-	-	No
H-O Carboxylate / O water	-	-	-	No	*1.65 (3.03)*	No
H-NHNH / O water	-	-	-	No	No	No

8.2.1 Intramolecular interactions between DBS, DBS-COOH and DBS-$CONHNH_2$ molecules

The intramolecular interactions are presented in Table 8.2.2 and Figures 8.2.7 - 8.2.12 and it can be seen that they are formed between the molecules of the three gelators in a similar manner. Intramolecular H-bonding interactions are formed between **O6 / H-O5, O5 / H-O6** (Figures 8.2.7(a) and 8.2.8 (a))**, O3 Acetal / H-O5**, **O3 Acetal / H-O6** (Figures 8.2.9 (a) and 8.2.10 (a)) and also **O4 Acetal / H-O5** and **O4 Acetal / H-O6** (Figures 8.2.11(a) and 8.2.11 (a)) of **DBS, DBS-COOH** and **DBS-$CONHNH_2$** molecules as pure substances. The most significant intramolecular interaction appears to be formed between **O3 Acetal / H-O6** groups (distance of 1.85Å and intensity of around 4).

In contrast to the intermolecular interactions, the intramolecular interaction peak heights in water are much higher than for the pure gelators, though interaction distances do not significantly change. They are shown in Figures 8.2.7(b) and 8.2.8(b) for **O6 / H-O5** and **O5 / H-O6**, Figures 8.2.9(b) and 8.2.10(b) for **O3 Acetal / H-O5** and **O3 Acetal / H-O6**, and Figures 8.2.11(b) and 8.2.12(b) for **O4 Acetal / H-O5** and **O4 Acetal / H-O6**, respectively. In the presence of water the most significant intramolecular interaction is also formed between **O3 Acetal / H-O6** groups (distance of 1.65Å). It is interesting to note that the intensity of the intramolecular interactions in **DBS-COOH** molecules is lower than in **DBS** and **DBS-$CONHNH_2$.**

Table 8.2.2 Intramolecular interaction distances **(Å)** and relative frequencies calculated for pure **DBS**, **DBS-COOH** and **DBS-CONHNH2** their mixture with water in a condensed phase at 300 K

	DBS	***DBS-COOH***	***DBS-CONHNH$_2$***	***DBS with water***	***DBS-COOH with water***	***DBS-CONHNH$_2$ with water***
O6 / H-O6	-	-	-	-	-	-
O6 / H-O5	*2.25 (2.64)*	*2.15 (4.30)*	*2.55 (2.90)*	*2.55 (21.26)*	*2.45 (20.00) 2.75 (41.84)*	*2.45 (19.00)*
O5 / H-O6	*2.35 (2.29)*	*2.45 (2.22) 3.65 (3.68)*	*2.65 (3.30)*	*2.55 (18.16)*	*2.45 (9.40) 4.25 (33.25)*	*2.65 (21.14)*
O5 / H-O5	-	-	-	-	-	-
O3 Acetal / H-O5	*1.75 (2.48) 4.15 (2.15)*	*1.85 (2.24) 3.95 (1.81)*	*1.85 (1.57) 4.25 (2.26)*	*1.75 (7.12) 4.15 (17.14)*	*2.75 (2.20) 4.15 (23.00)*	*1.95 (8.02) 4.15 (19.53)*
O3 Acetal /H-O6	*1.85 (4.43)*	*1.85 (4.00)*	*1.85 (4.00)*	*1.65 (34.50)*	*1.65 (10.03)*	*1.65 (30.14)*
O4 Acetal / H-O5	*2.35 (3.93)*	*2.35 (1.94)*	*2.35 (2.33)*	*2.45 (33.43)*	*2.45 (33.43)*	2.55 (35.81)
O4 Acetal /H-O6	- *4.15 (1.30)*	*1.75 (1.34) 4.55 (1.31)*	*1.75 (1.42) 4.15 (1.55)*	- *4.25 (12.77)*	*1.65 (1.68) 5.05 (15.28)*	- *4.55 (17.87)*

8.2.2 Intermolecular interaction

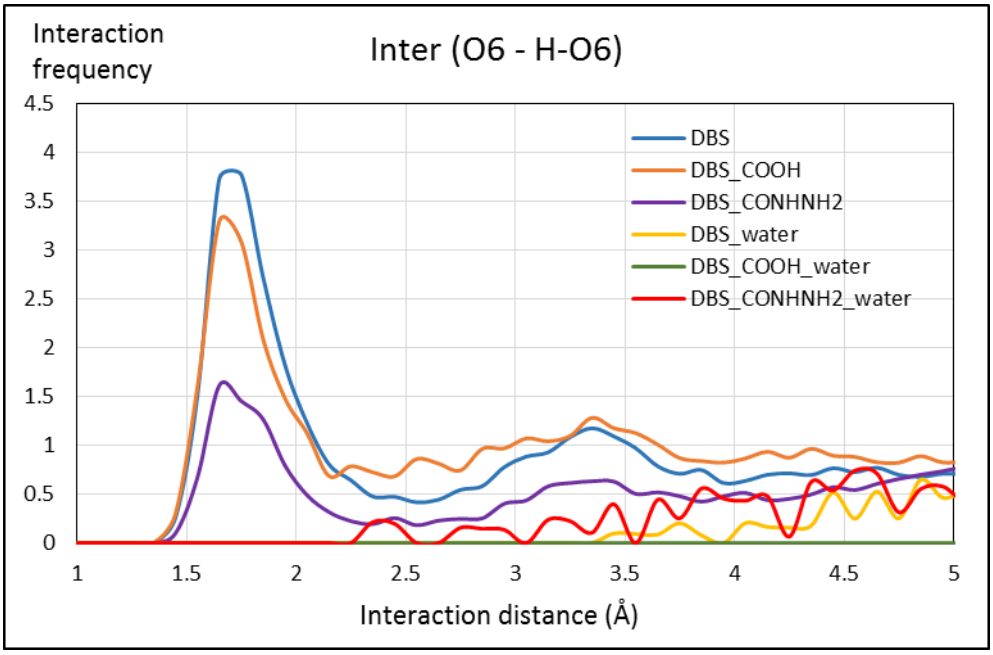

Figure 8.2.1 Intermolecular interaction intensities between **H-O6** and **O6** hydroxyl groups of pure **DBS, DBS-COOH** and **DBS-CONHNH$_2$** their mixture with water in a condensed phase at *300* K

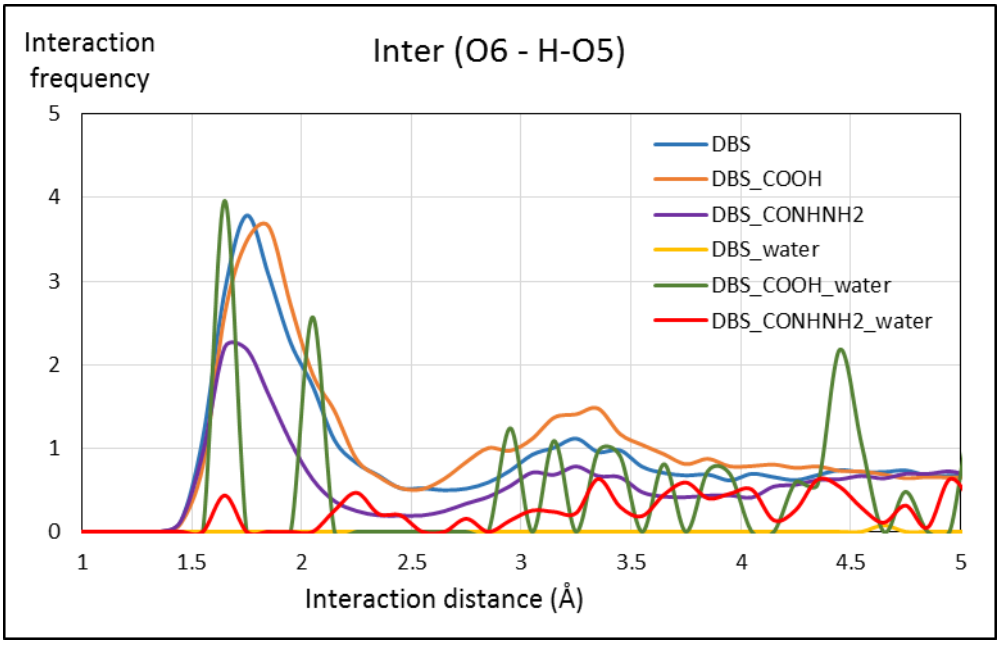

Figure 8.2.2 Intermolecular interaction intensities between **H-O5** and **O6** hydroxyl groups of pure **DBS**, **DBS-COOH** and **DBS-CONHNH$_2$** their mixture with water in a condensed phase at *300* K

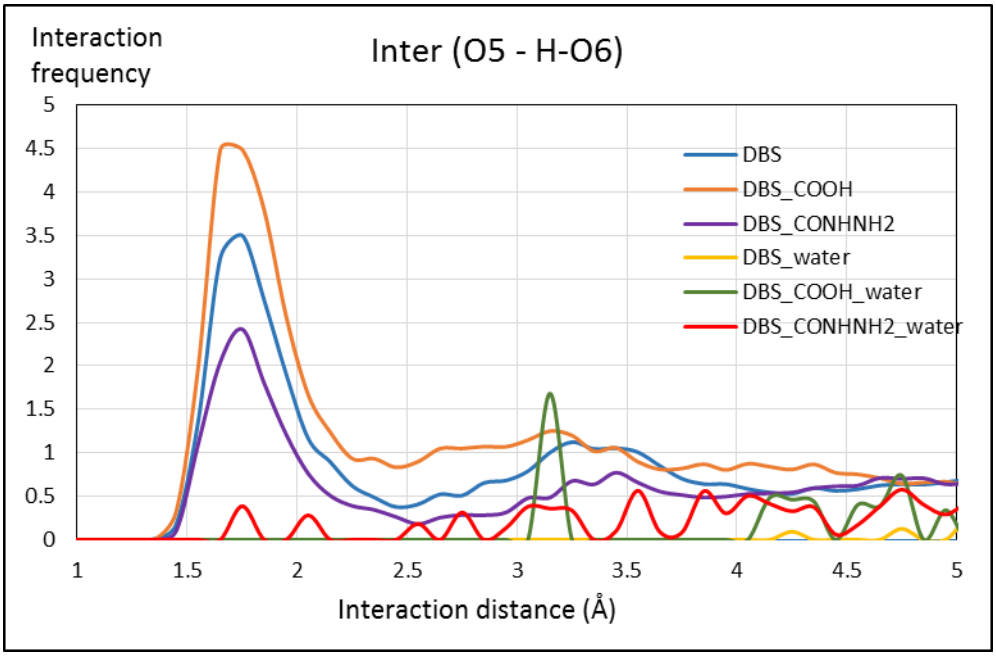

Figure 8.2.3 Intermolecular interaction intensities between **H-O6** and **O5** hydroxyl groups of pure **DBS, DBS-COOH** and **DBS-CONHNH$_2$** their mixture with water in a condensed phase at *300* K

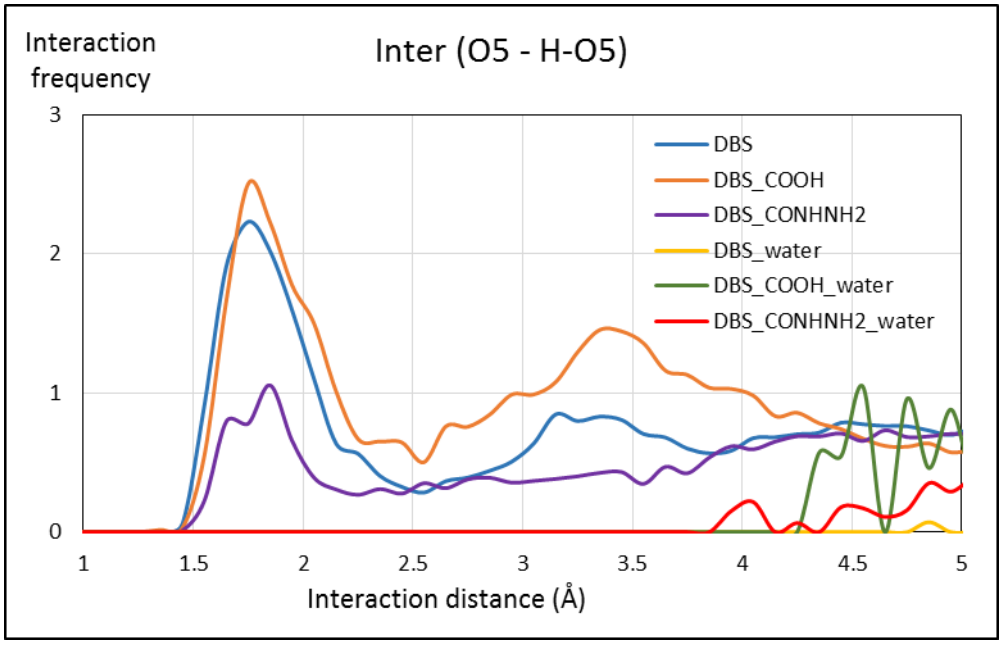

Figure 8.2.4 Intermolecular interaction intensities between **H-O5** and **O5** hydroxyl groups of pure **DBS, DBS-COOH** and **DBS-CONHNH$_2$** their mixture with water in a condensed phase at *300* K

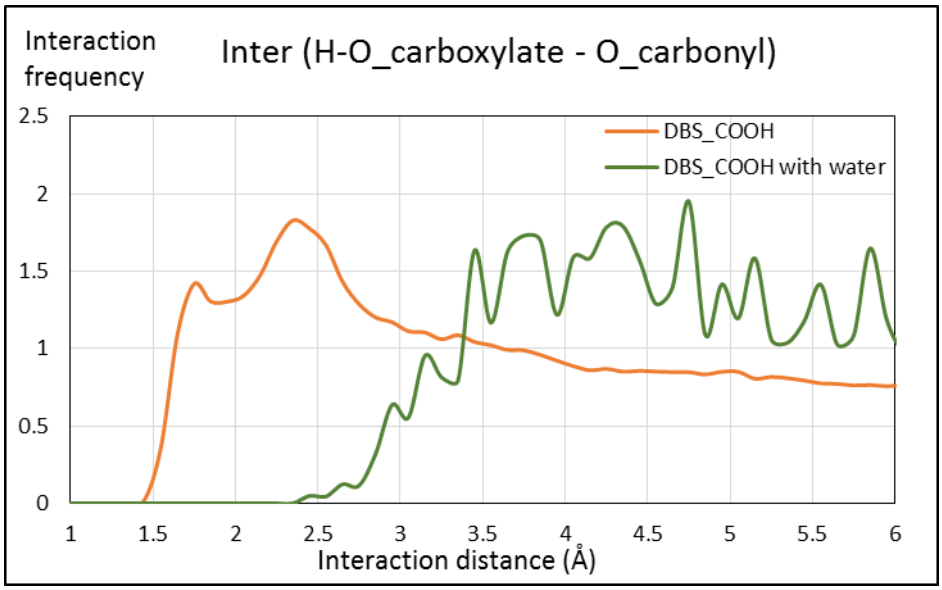

Figure 8.2.5 Intermolecular interaction intensities between **H-O Carboxylate / O Carbonyl** in **DBS-COOH** and its mixture with water in a condensed phase at 300 K

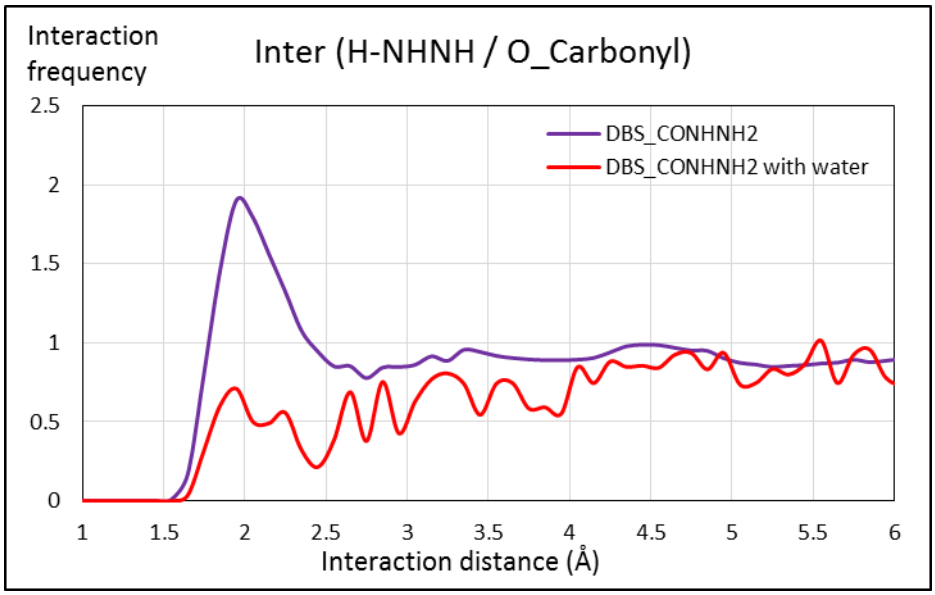

Figure 8.2.6 Intermolecular interaction intensities between **H-NHNH / O Carbonyl** in **DBS-CONHNH$_2$** and its mixture with water in a condensed phase at *300* K.

8.2.3 Intramolecular interactions

a)

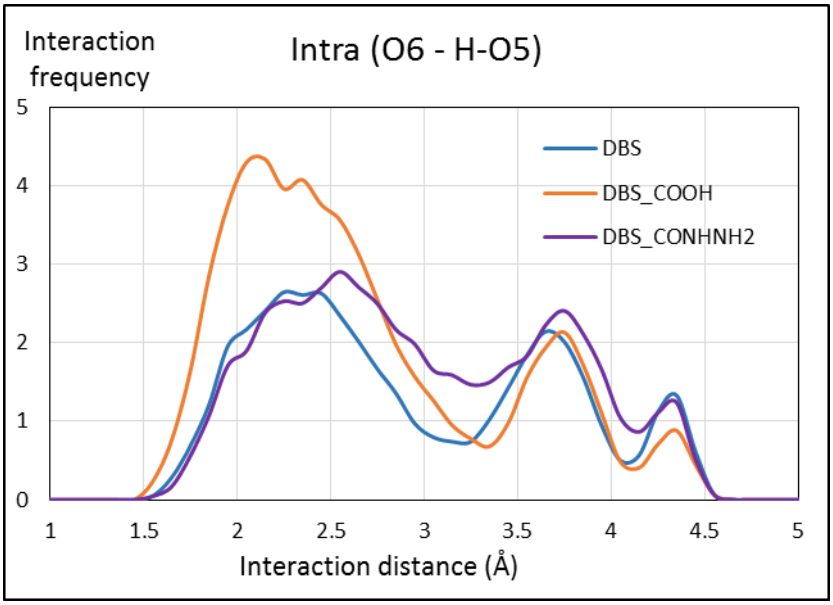

b)

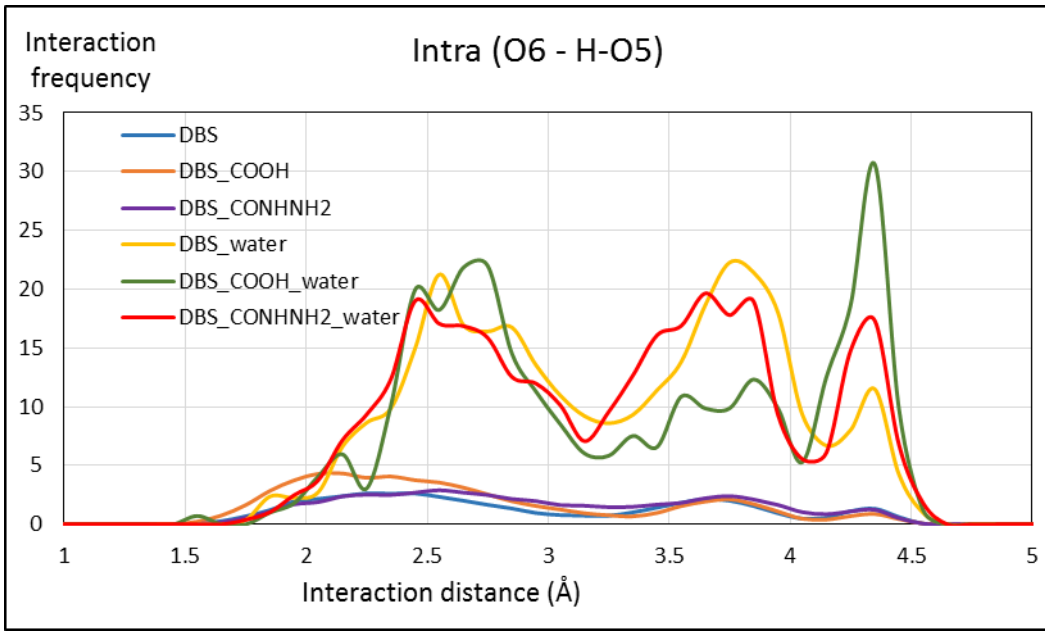

Figure 8.2.7 Intramolecular interaction intensities between **O6** and **H-O5** hydroxyl groups of (a) pure **DBS**, **DBS-COOH** and **DBS-CONHNH2** and (b) their mixture with water in a condensed phase at *300* K

(a)

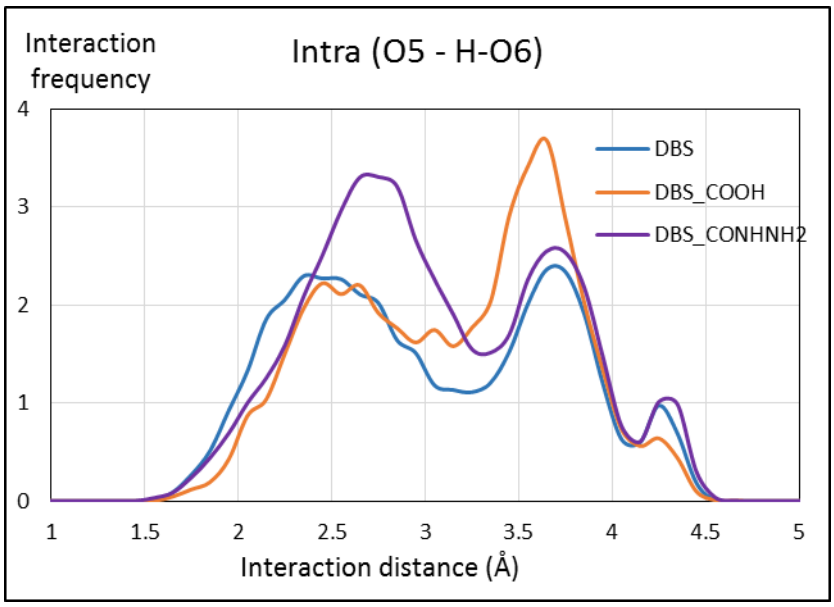

(b)

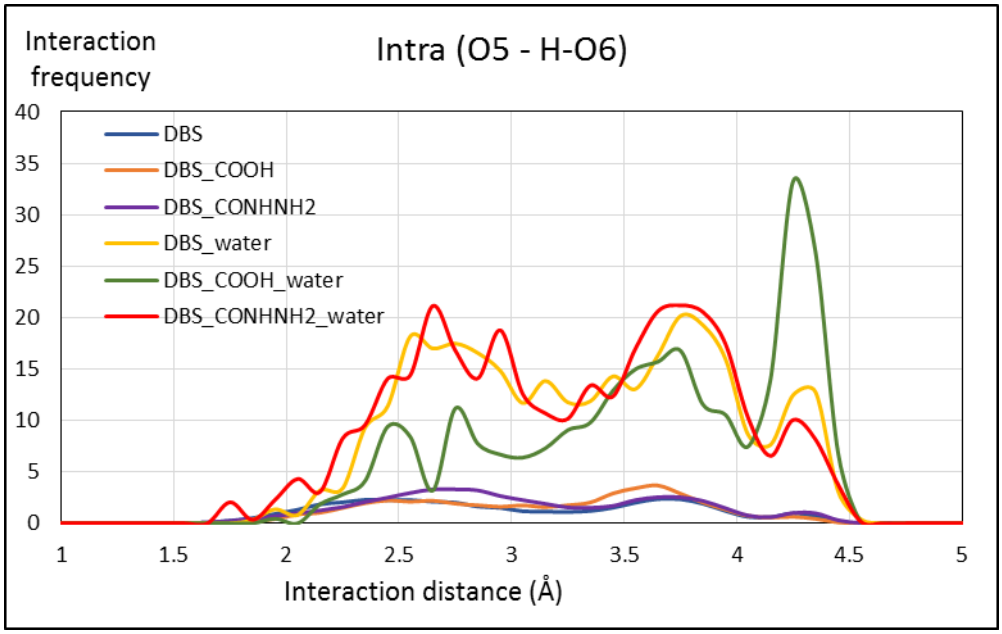

Figure 8.2.8 Intramolecular interaction intensities between **O5** and **H-O6** hydroxyl groups of (a) pure **DBS, DBS-COOH** and **DBS-CONHNH$_2$** and (b) their mixture with water in a condensed phase at *300* K

(a)

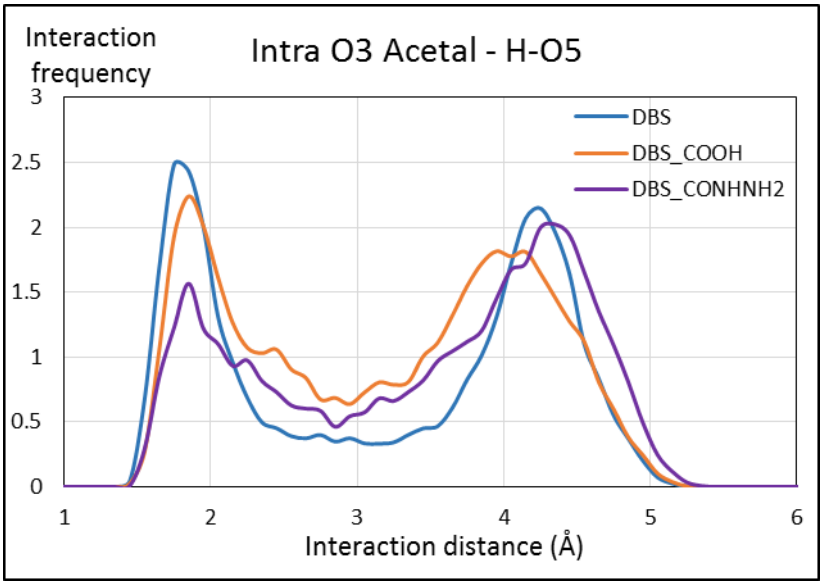

(b)

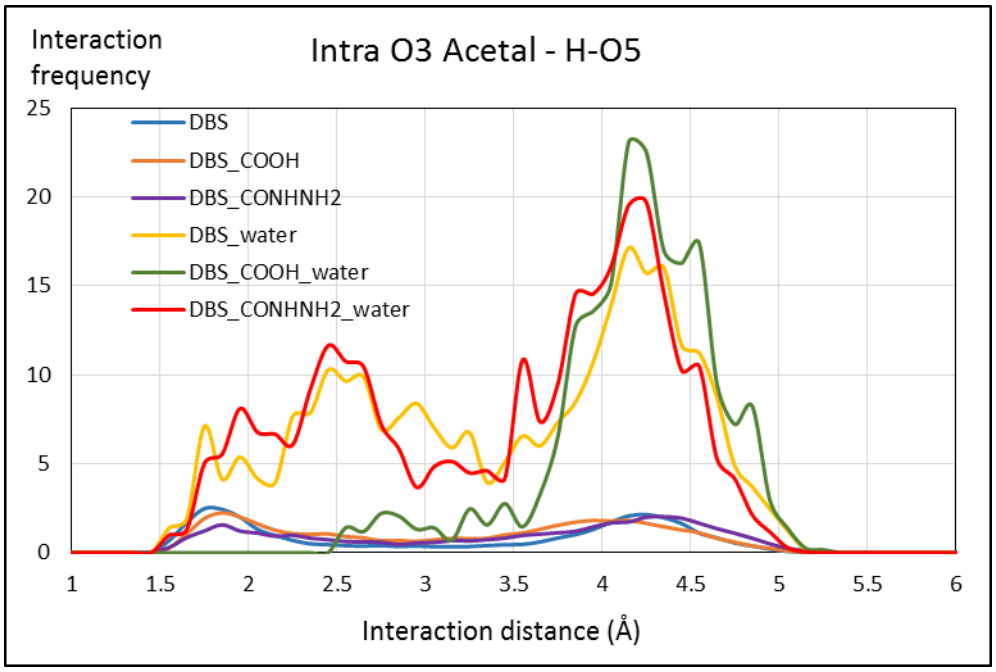

Figure 8.2.9 Intramolecular interaction intensities between **O3 acetal** and **H-O5** hydroxyl groups of (a) pure **DBS**, **DBS-COOH** and **DBS-CONHNH$_2$** and (b) their mixture with water in a condensed phase at *300* K

(a)

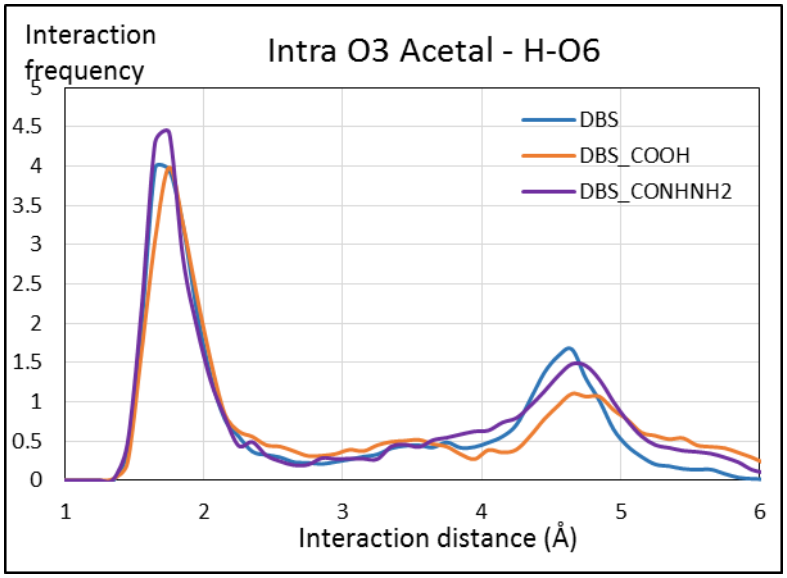

(b)

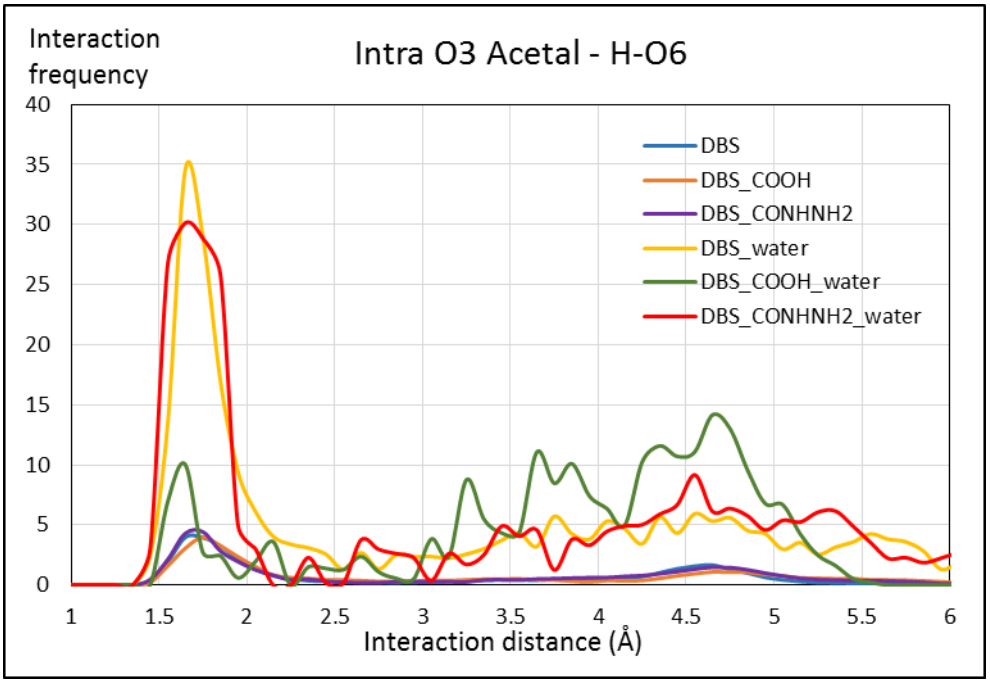

Figure 8.2.10 Intramolecular interaction intensities between **O3 acetal** and **H-O6** hydroxyl groups of (a) pure **DBS**, **DBS-COOH** and **DBS-CONHNH$_2$** and (b) their mixture with water in a condensed phase at *300* K

(a)

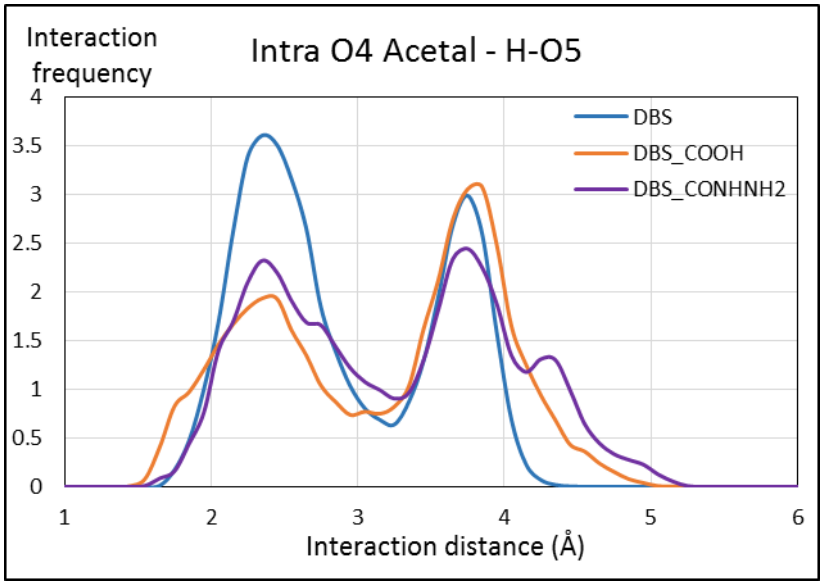

(b)

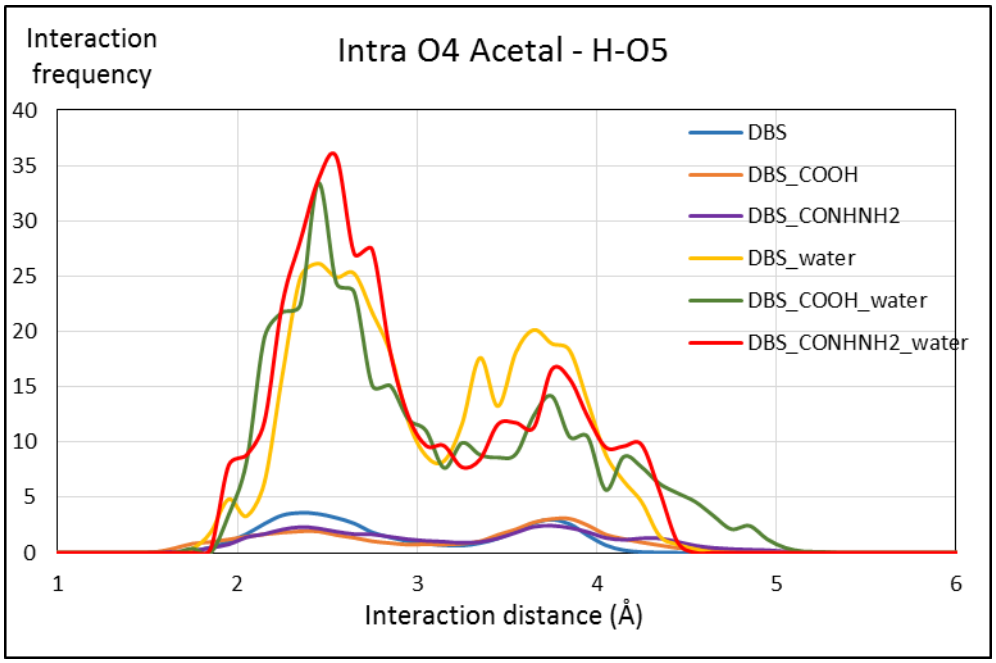

Figure 8.2.11 Intramolecular interaction intensities between **O4 acetal** and **H-O5** hydroxyl groups of (a) pure **DBS**, **DBS-COOH** and **DBS-CONHNH$_2$** and (b) their mixture with water in a condensed phase at *300* K

(a)

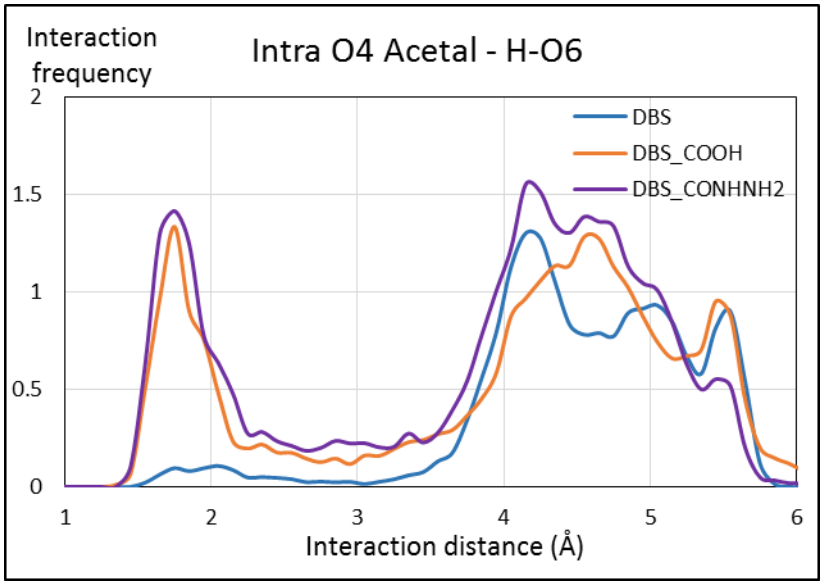

(b)

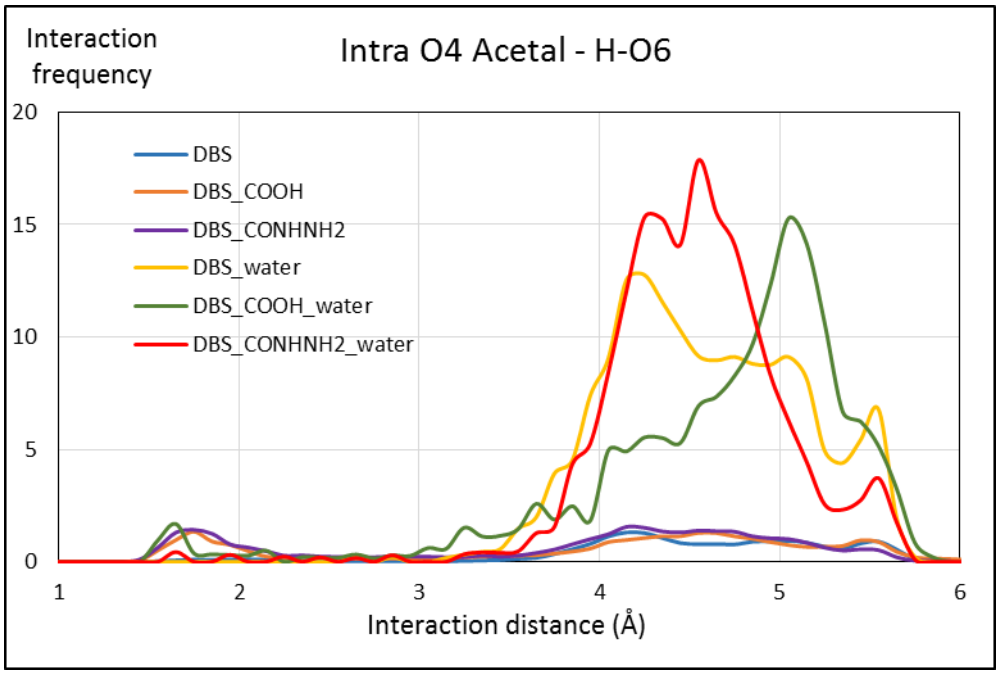

Figure 8.2.12 Intramolecular interaction intensities between **O4 acetal** and **H-O6** hydroxyl groups of (a) pure **DBS, DBS-COOH** and **DBS-CONHNH$_2$** and (b) their mixture with water in a condensed phase at *300* K

8.3 Appendix 2

8.3.1 Calibration curves for various dyes used

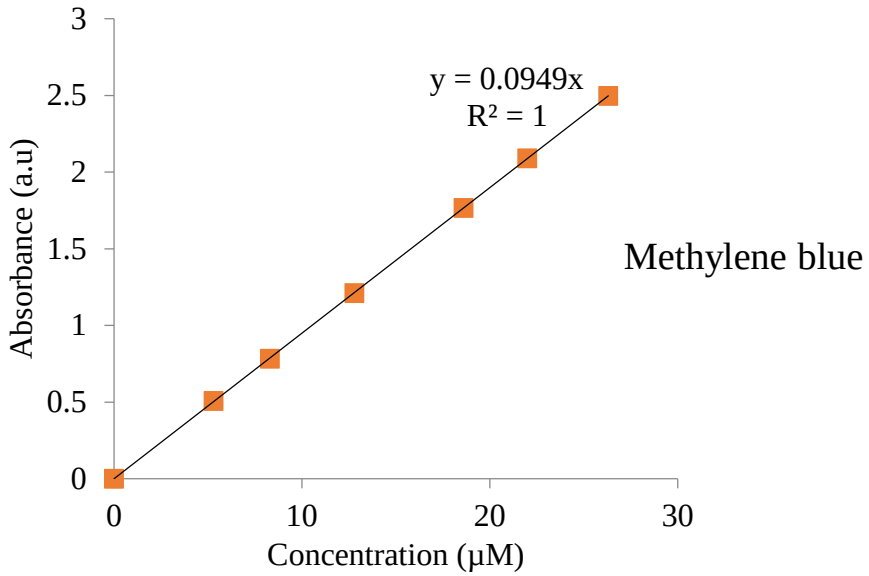

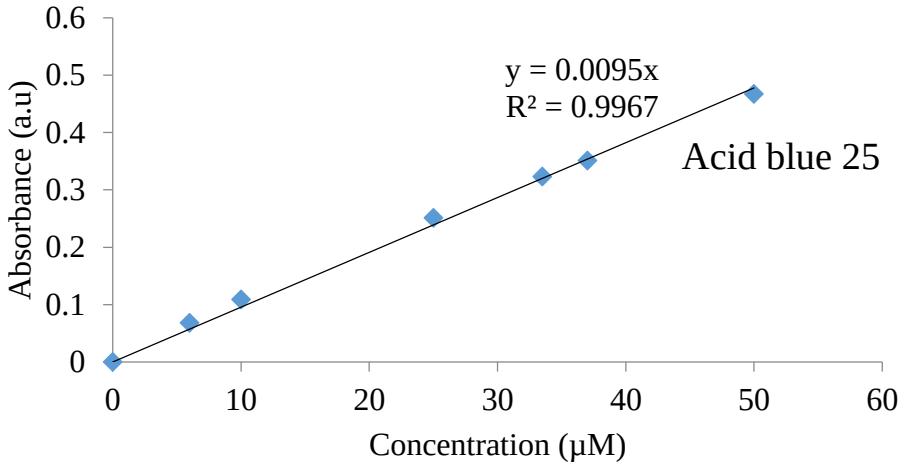

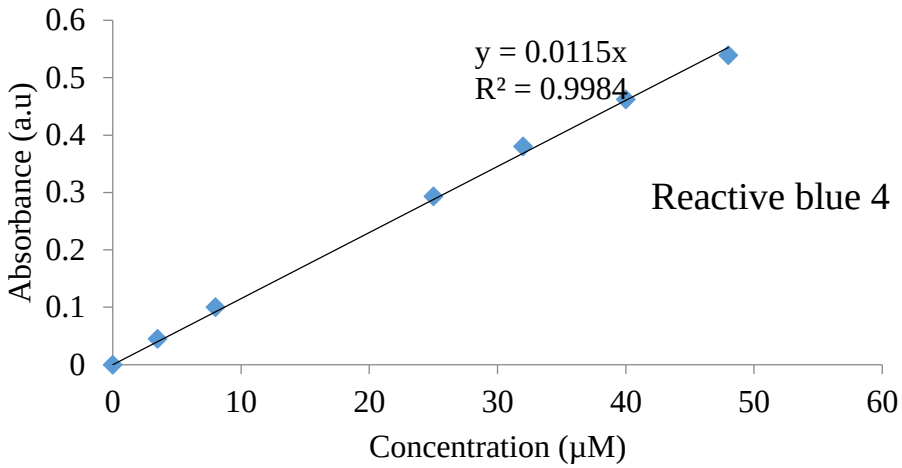
y = 0.0115x
R² = 0.9984
Reactive blue 4
Absorbance (a.u)
Concentration (µM)
0.6
0.5
0.4
0.3
0.2
0.1
0
0
10
20
30
40
50
60

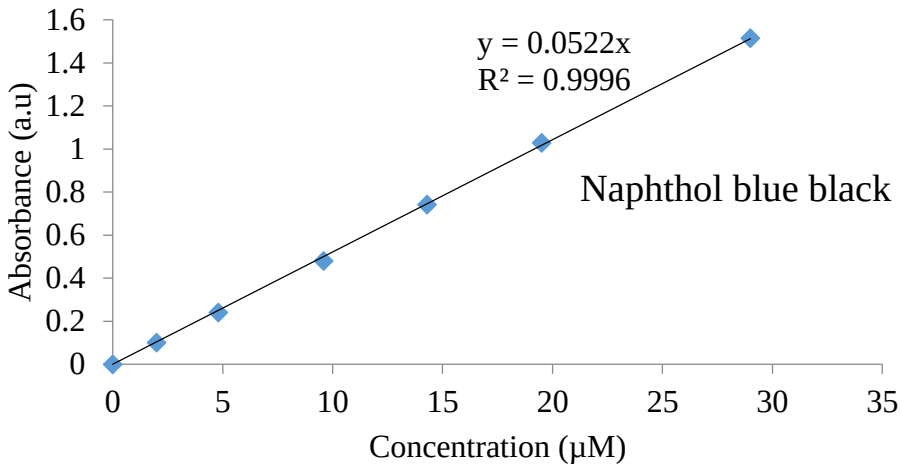
y = 0.0522x
R² = 0.9996
Naphthol blue black
Absorbance (a.u)
Concentration (µM)
1.6
1.4
1.2
1
0.8
0.6
0.4
0.2
0
0
5
10
15
20
25
30
35

8.3.2 Amount of dye uptake onto envirogels with time

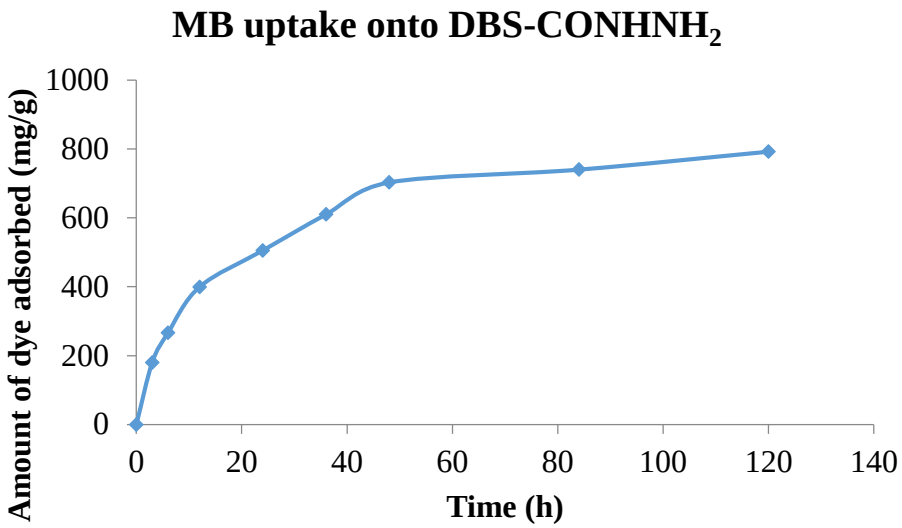

Abbreviations

Å	Angstrom
µA	Microampere
AAS	Atomic absorption spectrometry
AC	Activated carbon
AgOTf	Silver triflate
AgNPs	Silver nanoparticles
APIs	Active pharmaceutical ingredients
AuNPs	Gold nanoparticles
b	Energy of adsorption
BE	Binding energy
BET	Brunauer Emmette Teller
$Bi(OTf)_3$	Bismuth (III) triflate
Bf_3	Boron trifluoride
Bq	Becquerel
BLL	Blood lead level
Boc	tert-Butyloxylcarbonyl
C	Carbon
°C	Degree centigrade
C_0	Initial concentration
C_e	Equilibrium concentration
CD	Circular dichroism
CED	Cohesive energy density
COE	Calculated orbital electronegativity
COX-1	Cyclooxygenase-1
COX-2	Cyclooxygenase-2
CSAFM	Current sensing atomic force microscopy
Cm^3	Cubic centimetre
d	Doublet

DCC	Dicyclohexylcarbodiimide
DI	Deionised
DFT	Density functional theory
D_2O	Deuterium oxide
DMSO-d^6	Deuterated dimethyl sulfoxide
DNA	Deoxyribonucleic acid
EDTA	Ethylene diamine tetraacetic acid
ESI MS	Electrospray ionisation mass spectrometry
EtOH	Ethanol
eV	Electron volt
f	Frequency
$FeCl_2$	Iron (II) chloride
FRET	Fluorescent resonance energy transfer
FT-IR	Fourier transform infra-red spectroscopy
g	Gram
G’	Storage modulus
G’’	Loss modulus
ΔG	Gibb’s free energy change
GdL	Glucono-δ-lactone
h	hour
ΔH	Change in enthalpy
$HAuCl_4$	Chloroauric acid
HCl	Hydrochloric acid
HNO_3	Nitric acid
HOMO	Highest occupied molecular orbital
HSP	Hansen solubility parameter
Hz	Hertz
IBU	Ibuprofen
ICP-MS	Inductively coupled plasma mass spectrometry

IQ	Intelligent quotient
IR	Infra-red
J	Coupling constant
δ	Chemical shift
K	Equilibrium constant
K_f	Freundlich constant
L	Litre
LABE	Low-angle backscattered electron
$LiAlH_4$	Lithium aluminium hydride
LUMO	Lowest unoccupied molecular orbital
LMWG	Low-molecular-weight gelator
m	Multiplet
mdeg	Millidegree
MBTP	Metal binding hairpin peptide
MeI	Methyl iodide
mg	Milligram
MGC	Minimum gelation concentration
mL	Millilitre
mM	Millimolar
µL	Microlitre
µM	Micromolar
min	Minute
MD	Molecular dynamics
MM	Molecular mechanics
MSZ	Mesalazin
nm	Nanometer
NPX	Naproxen
NMR	Nuclear magnetic resonance
NSAID	Non-steroidal anti-inflammatory drug

o	Ortho
OPV	Oligo(*p*-phenylene vinylene)
p	Para
Pa	Pascal
ppb	Part per billion
ppm	Part per million
PTFE	Polytetrafluoroethylene
q_e	Equilibrium amount
q_{max}	Maximum amount
Ø	Diameter
R^2	Correlation coefficient
RE	Reference electrode
R_L	Separation factor
ROS	Reactive oxygen species
S	Siemens
SAFIN	Self-assembled nanofibrillar network
ΔS	Change in entropy
SEM	Scanning electron microscopy
SHE	Standard hydrogen electrode
SOS	Spin-orbit splitting
SPR	Surface plasmon resonance
T	Absolute temperature
t	Triplet
TEM	Transmission electron microscopy
T_{gel}	Gel-sol transition temperature
THF	Tetrahydrofuran
TLC	Thin-layer chromatography
TTF	Tetrathiafulvalene
UV	Ultraviolet

UV-Vis	Ultraviolet-visible
US EPA	United State Environmental Protection Agency
VT-CD	Variable temperature circular dichroism
XPS	X-Ray photoelectron microscopy.

References

1. A. Mishra and J. Clark, in *Green Materials for Sustainable Water Remediation and Treatment*, eds. A. Mishra and J. H. Clark, The Royal Society of Chemistry, Cambridge, 2013, pp. 1-10.
2. R. K. Sharma, A. Adholeya, M. Das and A. Puri, in *Green Materials for Sustainable Water Remediation and Treatment*, eds. A. Mishra and J. H. Clark, The Royal Society of Chemistry, Cambridge, 2013, pp. 11-29.
3. WHO/UNICEF, *Investing in water and sanitation: Increasing access, reducing inequalities*, World Health Organization, Geneva, 2014.
4. WHO/UNICEF, *Progress on drinking water and sanitation*, World Heealth Organization, Geneva, 2014.
5. WHO/UNICEF, *Water watch 2015: Are countries in Asia on track to meet target 10 of the MDGs*, World Health Organization, Geneva, 2015.
6. WHO, *Water- Fact sheets*, World Health Organization, Geneva, 2014.
7. M. Palaniappan, P. H. Gleick, L. Allen, M. J. Cohen, J. Christian-Smith and C. Smith, *Clearing the waters: A focus on water quality solutions*, United Nations Environment Protections, Nairobi, Kenya, 2010.
8. FAO, *Coping with water scarcity: An action framework for agriculture and food security*, Rome, 2012.
9. M. W. Rosegrant, X. Cai and S. A. Cline, in *Food policy report*, International Food Policy Research Institute, Washington D. C., USA, 2002.
10. S. Tanzeeba and T. Gan, *Climatic Change*, 2012, **112**, 355-386.
11. H. Bonsor, A. MacDonald and R. Calow, in *Sustainable Water*, The Royal Society of Chemistry, 2011, pp. 25-49.
12. WHO, *Guidelines for Drinking-Water Quality*, World Health Organization, Geneva, 1996.
13. R. K. Gautam, S. K. Sharma, S. Mahiya and M. C. Chattopadhyaya, in *Heavy Metals In Water: Presence, Removal and Safety*, ed. S. Sharma, The Royal Society of Chemistry, Cambridge, 2015, pp. 1-24.
14. J. E. Whitlock, D. T. Jones and V. J. Harwood, *Water Research*, 2002, **36**, 4273-4282.

15. WHO-UNICEF, *Meeting the Millenium Development Goal (MDG) drinking water and sanitation , the urban and rural challenge of the decade.*, Switzerland, 2006.
16. UNPF, *Development levels and environmental impact.*, UNFPA, New York, 2001.
17. USEPA, *2013 Toxics Release Inventory National Analysis*, http://www2.epa.gov/toxics-release-inventory-tri-program/2013-toxics-release-inventory-national-analysis, Accessed 28 January, 2015.
18. J. W. Readman, in *An Introduction to Pollution Science*, ed. R. M. Harrison, The Royal Society of Chemistry, Cambridge, 2006, pp. 77-121.
19. A. L. Batt, I. B. Bruce and D. S. Aga, *Environ. Pollut.*, 2006, **142**, 295-302.
20. D. Fatta-Kassinos, S. Meric and A. Nikolaou, *Anal Bioanal Chem*, 2011, **399**, 251-275.
21. T. Heberer, *Toxicol. Lett.*, 2002, **131**, 5-17.
22. D. Bendz, N. A. Paxéus, T. R. Ginn and F. J. Loge, *J. Hazard. Mater.*, 2005, **122**, 195-204.
23. A. Gulkowska, H. Leung, M. So, S. Taniyasu, N. Yamashita, L. Yeung and B. Richardson, *Water Res.*, 2008, **42**, 395.
24. E. Golet, I. Xifra, H. Siegrist, A. Alder and W. Giger, *Environ. Sci. Technol.*, 2003, **37**, 3243.
25. X. Peng, Z. Wang, W. Kuang, J. Tan and K. Li, *Sci. Tot. Environ.*, 2006, **371**, 314.
26. C. Zhang, K. Ning, W. Zhang, Y. Guo, J. Chen and C. Liang, *Env. Sci. Process. Impact.*, 2013, **15**, 709-714.
27. P. C. Rua-Gomez and W. Puttmann, *J. Environ. Monit.*, 2012, **14**, 1391-1399.
28. J. H. Duffus, *Pur. Appl. Chem.*, 2002, **74**, 793-807.
29. A. H. Welch, Westjohn, D.B., Helsel, D.R., and Wanty, R.B., *Ground Water*, 2000, **38**, 15.
30. N. R. Shinde, A. V. Bankar, A. R. Kumar and S. S. Zinjarde, *J. Environ. Manage.*, 2012, **102**, 115-124.
31. E. Ramírez, S. G. Burillo, C. Barrera-Díaz, G. Roa and B. Bilyeu, *J. Hazard. Mater.*, 2011, **192**, 432-439.
32. A. P. Neal and T. R. Guilarte, *Toxicol. Res.*, 2013, **2**, 99-114.

33. WHO, *Health risks of heavy metals from long-range transboundary air pollution*, World Health Organization, Copenhagen, Denmark, 2007.
34. M. M. Isam Salih, H. B. L. Pettersson and E. Lund, *Radiat. Prot. Dosimetry*, 2002, **102**, 249-258.
35. P. Milvy and C. R. Cothern, in *Radon, Radium and Uranium in drinking water* eds. C. R. Cothern and P. A. Rebers, Lewis publishers, inc, Michigan, 1990, pp. 1-16.
36. C. Nuccetelli, R. Rusconi and M. Forte, *Annali dell'Istituto Superiore di Sanità*, 2012, **48**, 362-373.
37. B. McGrath, in *World Socialist Web site*, ed. D. North, International Committee of the Fourth International (ICFI), 2015.
38. USEPA, *Basic information about radionuclides in drinking water*, http://water.epa.gov/drink/contaminants/basicinformation/radionuclides.cfm, Accessed 28 January, 2015.
39. WHO, *Guidelines for Drinking Water Quality*, World Health Organization, Geneva, 2011.
40. K. Singh and S. Arora, *Crit. Rev. Env. Sci.*, 2011, **41**, 807-878.
41. F. Fu and Q. Wang, *J. Environ. Manage.*, 2011, **92**, 407-418.
42. I. H. Lee, Y. C. Kuan and J. M. Chern, *J. Hazard. Mater.*, 2006, **138**, 549-559.
43. M. Černá, *Environ. Monit. Assess.*, 1995, **34**, 151-162.
44. M. A. Barakat, *Arab. J. Chem.*, 2011, **4**, 361-377.
45. E. A. López-Maldonado, M. T. Oropeza-Guzman, J. L. Jurado-Baizaval and A. Ochoa-Terán, *J. Hazard. Mater.*, 2014, **279**, 1-10.
46. L.K. Wang, D.A. Vaccari, Y. Li and N. K. Shammas, in *Chemical precipitation*, eds. L.K. Wang, Y.T. Hung and N. K. Shammas, Humana Press, New Jersey, 2004, vol. 3, pp. 141-198.
47. A. Efligenir, S. Déon, P. Fievet, C. Druart, N. Morin-Crini and G. Crini, *Chem. Eng. J.*, 2014, **258**, 309-319.
48. G. Kyzas, J. Fu and K. Matis, *Materials*, 2013, **6**, 5131-5158.
49. W. He, G. LÜ, J. Cui, L. Wu and L. Liao, *Chinese J. Chem. Eng.*, 2012, **20**, 659-664.
50. G. Crini, *Bioresource Technol.*, 2006, **97**, 1061-1085.
51. M. M. Khin, A. S. Nair, V. J. Babu, R. Murugan and S. Ramakrishna, *Energy Environ. Sci.*, 2012, **5**, 8075-8109.

52. P. Terech and R. G. Weiss, *Chem. Rev.*, 1997, **97**, 3133.
53. Z. Wei, J. H. Yang, J. Zhou, F. Xu, M. Zrinyi, P. H. Dussault, Y. Osada and Y. M. Chen, *Chem. Soc. Rev.*, 2014, **43**, 8114-8131.
54. B. R. Thakur, R. K. Singh, A. K. Handa and M. A. Rao, *Crit. Rev. Food Sci.*, 1997, **37**, 47-73.
55. J. Y. Song, Y. Y. Wang and C. C. Wan, *J. Power Sources*, 1999, **77**, 183-197.
56. J. H. van Esch, *Nature*, 2010, **466**, 193-194.
57. D. K. Smith, *Nat Chem*, 2010, **2**, 162-163.
58. J. Van Esch, F. Schoonbeek, M. De Loos, E. Marc Veen, R. Kellogg and B. Feringa, in *Supramolecular Science: Where It Is and Where It Is Going*, eds. R. Ungaro and E. Dalcanale, Springer Netherlands, 1999, vol. 527, pp. 233-259.
59. D. K. Smith, in *Supramolecular chemistry from molecules to nanomaterials*, eds. P. A. Gale and J. W. Steed, Wiley-Blackwell, Oxford, 2012, vol. 7, p. 20.
60. S. Fleming and R. V. Ulijn, *Chem. Soc. Rev.*, 2014, **43**, 8150-8177.
61. D. K. Kumar, D. A. Jose, A. Das and P. Dastidar, *Chem. Commun.*, 2005, 4059-4061.
62. K. Araki and I. Yoshikawa, in *Low Molecular Mass Gelator*, Springer Berlin Heidelberg, 2005, vol. 256, pp. 133-165.
63. D. K. Smith, *Chem. Soc. Rev.*, 2009, **38**, 684-694.
64. N. M. Sangeetha and U. Maitra, *Chem. Soc. Rev.*, 2005, **34**, 821.
65. A. R. Hirst, B. Escuder, J. F. Miravet and D. K. Smith, *Angew. Chem. Int. Ed.*, 2008, **47**, 8002-8018.
66. K. Huijer, in *Arctic and Marine Oilspill Program (AMOP) Technical Seminar*, International Tanker Owners Pollution Federation (ITOPF), Calgary, Canada, 2014.
67. L. Guterman, *Science*, 2009, **323**, 1558-1559.
68. M. O. Adebajo, R. L. Frost, J. T. Kloprogge, O. Carmody and S. Kokot, *J. Porous Mat.*, 2003, **10**, 159-170.
69. R. P. Swannell, K. Lee and M. McDonagh, *Microbiol. Rev.*, 1996, **60**, 342-365.
70. R. d. C. F. S. Silva, D. G. Almeida, R. D. Rufino, J. M. Luna, V. A. Santos and L. A. Sarubbo, *Int. J. Mol. Sci.*, 2014, **15**, 12523-12542.
71. R. R. Lessard and G. DeMarco, *Spill Sci. Technol. Bull.*, 2000, **6**, 59-68.
72. D. Dave and A. E. Ghaly, *Am. J. Environ. Sci.*, 2011, **7**, 423-440.

73. É. Pelletier and R. Siron, *Environ. Toxicol. Chem.*, 1999, **18**, 813-818.
74. K. Liu, P. He and Y. Fang, *Sci. China Chem.*, 2011, **54**, 575-586.
75. T. Saito, Y. Matsuzawa, S. Ninagawa, M. Honna, M. Takesada and M. Takehara, US 3969087 A, 1976.
76. S. Bhattacharya and Y. Krishnan-Ghosh, *Chem. Commun.*, 2001, 185-186.
77. D. R. Trivedi, A. Ballabh and P. Dastidar, *Chem. Mater.*, 2003, **15**, 3971-3973.
78. D. R. Trivedi, A. Ballabh, P. Dastidar and B. Ganguly, *Chem. Eur. J.*, 2004, **10**, 5311-5322.
79. A. Ballabh, D. R. Trivedi and P. Dastidar, *Chem. Mater.*, 2006, **18**, 3795-3800.
80. S. R. Jadhav, P. K. Vemula, R. Kumar, S. R. Raghavan and G. John, *Angew. Chem. Int. Ed.*, 2010, **49**, 7695-7698.
81. H. L. Hwang, S. R. Jadhav, J. R. Silverman and G. John, *J. Chem. Educ.*, 2014, **91**, 1563-1568.
82. A. Prathap and K. M. Sureshan, *Chem. Commun.*, 2012, **48**, 5250-5252.
83. J. Peng, K. Liu, X. Liu, H. Xia, J. Liu and Y. Fang, *New J. Chem.*, 2008, **32**, 2218-2224.
84. M. Xue, D. Gao, K. Liu, J. Peng and Y. Fang, *Tetrahedron*, 2009, **65**, 3369-3377.
85. S. Mukherjee, C. Shang, X. Chen, X. Chang, K. Liu, C. Yu and Y. Fang, *Chem. Commun.*, 2014, **50**, 13940-13943.
86. P. Lee and M. A. Rogers, *Langmuir*, 2013, **29**, 5617-5621.
87. N. Zweep and J. H. van Esch, in *Functional Molecular Gels*, eds. B. Escuder and J. F. Miravet, The Royal Society of Chemistry, Cambridge, 2014, pp. 1-29.
88. S. Ray, A. K. Das and A. Banerjee, *Chem. Mater.*, 2007, **19**, 1633.
89. M. Kumar and A. Puri, *Ind. J. Occup. Environ. Med.*, 2012, **16**, 40-44.
90. E. J. Cho, I. Y. Jeong, S. J. Lee, W. S. Han, J. K. Kang and J. H. Jung, *Tetrahedron Lett.*, 2008, **49**, 1076-1079.
91. S. Debnath, A. Shome, S. Dutta and P. K. Das, *Chem. Eur. J.*, 2008, **14**, 6870-6881.
92. B. Adhikari, G. Palui and A. Banerjee, *Soft Matter*, 2009, **5**, 3452.
93. S. Dutta, D. Das, A. Dasgupta and P. K. Das, *Chem. Eur. J.*, 2010, **16**, 1493-1505.

94. S. Song, L. Feng, A. Song and J. Hao, *J. Phys. Chem. B*, 2012, **116**, 12850-12856.
95. H. Wang, W. Xu, S. Song, L. Feng, A. Song and J. Hao, *J. Phys. Chem. B*, 2014, **118**, 4693-4701.
96. D. M. Wood, B. W. Greenland, A. L. Acton, F. Rodríguez-Llansola, C. A. Murray, C. J. Cardin, J. F. Miravet, B. Escuder, I. W. Hamley and W. Hayes, *Chem. Eur. J.*, 2012, **18**, 2692-2699.
97. B. C. Baker, A. L. Acton, G. C. Stevens and W. Hayes, *Tetrahedron*, 2014, **70**, 8303-8311.
98. M. Wallace, D. J. Adams and J. A. Iggo, *Soft Matter*, 2013, **9**, 5483-5491.
99. P. K. Sukul and S. Malik, *RSC Adv.*, 2013, **3**, 1902-1915.
100. Y.-T. Tang, X.-Q. Dou, Z.-A. Ji, P. Li, S.-M. Zhu, J.-J. Gu, C.-L. Feng and D. Zhang, *J. Mol. Liq.*, 2013, **177**, 167-171.
101. I. W. Hamley, *Soft Matter*, 2011, **7**, 4122-4138.
102. Y. Wang, H. Xu and X. Zhang, *Adv. Mater.*, 2009, **21**, 2849-2864.
103. S. Mukherjee and B. Mukhopadhyay, *RSC Adv.*, 2012, **2**, 2270-2273.
104. B. O. Okesola, V. M. P. Vieira, D. J. Cornwell, N. K. Whitelaw and D. K. Smith, *Soft Matter*, 2015, **11**, 4768-4787.
105. F. Vögtle, *Supramolecular chemistry*, John Willey & Sons, Chester, 1993.
106. R. M. Kellogg, *Rec. Trav. Chim. Pays-Bas*, 1993, **112**, 651-651.
107. M. F. Schneider, R. Zantl, C. Gege, R. R. Schmidt, M. Rappolt and M. Tanaka, *Biophys. J.*, 2003, **84**, 306-313.
108. S. Varghese, A. K. Lele and R. A. Mashelkar, *J. Chem. Phys.*, 2000, **112**, 3063-3070.
109. L. A. Estroff and A. D. Hamilton, *Angew. Chem. Int. Ed.*, 2000, **39**, 3447-3450.
110. L. A. Estroff, L. Leiserowitz, L. Addadi, S. Weiner and A. D. Hamilton, *Adv. Mater.*, 2003, **15**, 38-42.
111. L. A. Estroff and A. D. Hamilton, *Chem. Rev.*, 2004, **104**, 1201-1218.
112. B. O. Okesola and D. K. Smith, *Chem. Commun.*, 2013, **49**, 11164-11166.
113. K. N. King and A. J. McNeil, *Chem. Commun.*, 2010, **46**, 3511-3513.
114. K. K. Carter, H. B. Rycenga and A. J. McNeil, *Langmuir*, 2014, **30**, 3522-3527.
115. Y. Lan, M. G. Corradini, X. Liu, T. E. May, F. Borondics, R. G. Weiss and M. A. Rogers, *Langmuir*, 2014.

116. J.-Y. Xiong, X.-Y. Liu, J.-L. Li and M. W. Vallon, *J. Phys. Chem. B*, 2007, **111**, 5558-5563.
117. R. Wang, X.-Y. Liu, J. Xiong and J. Li, *J. Phys. Chem. B*, 2006, **110**, 7275-7280.
118. J.-L. Li and X.-Y. Liu, *Adv. Funct. Mater.*, 2010, **20**, 3196-3216.
119. J.-L. Li, X.-Y. Liu, R.-Y. Wang and J.-Y. Xiong, *J. Phys. Chem. B*, 2005, **109**, 24231-24235.
120. J.-L. Li, R.-Y. Wang, X.-Y. Liu and H.-H. Pan, *J. Phys. Chem. B*, 2009, **113**, 5011-5015.
121. R.-Y. Wang, X.-Y. Liu and J.-L. Li, *Cryst. Growth Des.*, 2009, **9**, 3286-3291.
122. M. A. Rogers, A. J. Wright and A. G. Marangoni, *Soft Matter*, 2008, **4**, 1483-1490.
123. M. A. Rogers and A. G. Marangoni, *Cryst. Growth Des.*, 2008, **8**, 4596-4601.
124. X. Dou, P. Li, D. Zhang and C.-L. Feng, *Soft Matter*, 2012, **8**, 3231-3238.
125. A. Wikström, H. Berglund, C. Hambraeus, S. van den Berg and T. Härd, *J. Mol. Biol.*, 1999, **289**, 963-979.
126. H. Cleaves, II, in *Encyclopedia of Astrobiology*, eds. M. Gargaud, R. Amils, J. Quintanilla, H. Cleaves, II, W. Irvine, D. Pinti and M. Viso, Springer Berlin Heidelberg, 2011, pp. 1079-1080.
127. J.-M. Lehn, in *Alkali Metal Complexes with Organic Ligands*, Springer Berlin Heidelberg, 1973, vol. 16, pp. 1-69.
128. J. F. Stoddart, *Angew. Chem. Int. Ed.*, 2012, **51**, 12902-12903.
129. D. N. Reinhoudt, J. F. Stoddart and R. Ungaro, *Chem. Eur. J.*, 1998, **4**, 1349-1351.
130. N. Ahmad, H. A. Younus, A. H. Chughtai and F. Verpoort, *Chem. Soc. Rev.*, 2015, **44**, 9-25.
131. V. Guillerm, D. Kim, J. F. Eubank, R. Luebke, X. Liu, K. Adil, M. S. Lah and M. Eddaoudi, *Chem. Soc. Rev.*, 2014, **43**, 6141-6172.
132. A. Brizard, R. Oda and I. Huc, in *Low Molecular Mass Gelators*, Springer Berlin Heidelberg, 2005, vol. 256, pp. 167-218.
133. D. A. S. Grahame, C. Olauson, R. S. H. Lam, T. Pedersen, F. Borondics, S. Abraham, R. G. Weiss and M. A. Rogers, *Soft Matter*, 2011, **7**, 7359-7365.
134. F. Rodriguez-Llansola, B. Escuder, J. F. Miravet, D. Hermida-Merino, I. W. Hamley, C. J. Cardin and W. Hayes, *Chem. Commun.*, 2010, **46**, 7960-7962.

135. M.-A. Gagnon and M. Lafleur, *Pharm. Dev. Technol.*, 2011, **16**, 651-656.
136. Y. Kuang, J. Shi, J. Li, D. Yuan, K. A. Alberti, Q. Xu and B. Xu, *Angew. Chem. Int. Ed.*, 2014, **53**, 8104-8107.
137. T. Vermonden, R. Censi and W. E. Hennink, *Chem. Rev.*, 2012, **112**, 2853-2888.
138. V. J. Nebot and D. K. Smith, in *Functional Molecular Gels*, eds. Beatriu Escuder and J. F. Miravet, The Royal Society of Chemistry, 2014, pp. 30-66.
139. J. A. Foster, D. W. Johnson, M.-O. M. Pipenbrock and J. W. Steed, *New J. Chem.*, 2014, **38**, 927-932.
140. C. A. Lagadec and D. K. Smith, *Chem. Commun.*, 2012, **48**, 7817-7819.
141. Y. E. Shapiro, *Prog. Polym. Sci.*, 2011, **36**, 1184-1253.
142. R. G. Weiss and P. Terech, *Molecular Gels: Materials with Self-Assembled Fibrillar Networks*, Springer., Dordrecht, Netherlands, 2006.
143. S. Debnath, A. Shome, D. Das and P. K. Das, *J. Phys. Chem. B*, 2010, **114**, 4407-4415.
144. S. Dutta, A. Shome, S. Debnath and P. K. Das, *Soft Matter*, 2009, **5**, 1607-1620.
145. M. R. Shumon, S. Ahmed and M. T. Islam, *Environ. Earth Sci.*, 2014, 1-11.
146. S. Sthiannopkao and M. H. Wong, *Sci. Tot. Environ.*, 2013, **463–464**, 1147-1153.
147. S. Syed, *Hydrometallurgy*, 2012, **115–116**, 30-51.
148. J. Turkevich, P. C. Stevenson and J. Hillier, *Discuss. Faraday Soc.*, 1951, **11**, 55-75.
149. M. Brust, M. Walker, D. Bethell, D. J. Schiffrin and R. Whyman, *J. Chem. Soc., Chem. Commun.*, 1994, 801-802.
150. J. Kimling, M. Maier, B. Okenve, V. Kotaidis, H. Ballot and A. Plech, *J. Phys. Chem. B*, 2006, **110**, 15700-15707.
151. C. Schliebe, K. Jiang, S. Schulze, M. Hietschold, W.-B. Cai and H. Lang, *Chem. Commun.*, 2013, **49**, 3991-3993.
152. M. Watase and H. Itagaki, *Bull. Chem. Soc. Jpn.*, 1998, **71**, 1457-1466.
153. T. Sterzynski, M. Lambla, H. Crozier and M. Thomas, *Adv. Polym. Tech.*, 1994, **13**, 25-36.
154. M. J. Meunier, *Ann.Chim. Phys.*, 1891, **22**.
155. P. Thomas and M. Sibi, *Compt. Rend.*, 1926, **183**, 282-284.

156. J. K. Wolfe, R. M. Hann and C. S. Hudson, *J. Am. Chem. Soc.*, 1942, **64**, 1493-1497.
157. S. J. Angyal and J. V. Lawler, *J. Am. Chem. Soc.*, 1944, **66**, 837-838.
158. L. v. Vargha, *Ber.*, 1935, **68**, 1377-1384.
159. T. G. Bonner, E. J. Bourne and D. Lewis, *Carbohyd. Res.*, 1966, **2**, 421-425.
160. R. M. C. Douglas J. Brecknell, Jeffrey J. Kibby and a. L. T. Nicholas, *Aust. J. Chem.*, 1976, **29**, 5.
161. G. Akazome, Y. Choshi, T. Kobayashi, K. Murai and A. Tsuji, *US Patent* 3721682 A, 1973.
162. K. Murai, T. Kobayashi and K. Fujitani, *US Patent* 4429140 A, 1984.
163. H. Uchiyama, *US Patent* 4267110 A, 1981.
164. H. Uchiyama, *US Patent* 4131612 A, 1978.
165. J. P. Salome and G. Fleche, *US Patent* 5023354A, 1991.
166. C. Xie, J. Li and J. Xia, *US Patent* 20060079720 2006.
167. J. Song, H. Sun, S. Sun and R. Feng, *Trans. Tianjin Uni.*, 2013, **19**, 319-325.
168. G. Machell, *US Patent* 4562265 A, 1985.
169. T. Kobayashi, *US Patent* 5120863 A, 1992.
170. J. M. Gardlik and R. V. Burkes, *US Patent* 5106999 A, 1992.
171. W. A. Scrivens and J. M. Salley, *US Patent* 5731474 A, 1998.
172. J. G. Lever, D. L. Dotson, J. D. Anderson, J. R. Jones and S. R. Sheppard, *US Patent* 6500964 B2, 2002.
173. P. V. Uppara, P. Aduri, M. Sakhalkar and U. Ratnaparkhi, *US Patent* 20130281716, 2014.
174. R. Feng, L. Chen, Z. Hou and J. Song, *Trans. Tianji Univ.*, 2007, **13**, 6.
175. W. Wan, W. Gao, G. Ma, L. Ma, F. Wang, J. Wang, H. Jiang, S. Zhu and J. Hao, *RSC Adv.*, 2014, **4**, 26563-26568.
176. R. Stan, N. Chira, C. Ott, C. Todasca and E. Perez, *Rev. Chim.*, 2008, **59**, 273-276.
177. J. Raeburn and D. J. Adams, *Chem. Commun.*, 2015, **51**, 5170-5180.
178. R. Stan, C. Ott, N. Sulca, A. Lungu and H. Iovu, *Mater. Plast.*, 2009, **46**, 230-235.
179. Gérard Malle and T. Luukas, *US Patent* 20130039862, 2013.
180. M. Fariya, A. Jain, V. Dhawan, S. Shah and M. S. Nagarsenker, *Adv. Pharm. Bull.*, 2014, **4**, 483-491.

181. C. Xie, L. R. Rieth and T. D. Danielson, *US Patent* 7662978, 2010.
182. S. Yamasaki and H. Tsutsumi, *Bull. Chem. Soc. Jpn.*, 1995, **68**, 123-127.
183. R. Renner, *Environ. Health Perspect.*, 2009, **117**, A543-A547.
184. S. Yamasaki, Y. Ohashi, H. Tsutsumi and K. Tsujii, *Bull. Chem. Soc. Jpn.*, 1995, **68**, 146-151.
185. M. Watase, Y. Nakatani and H. Itagaki, *J. Phys. Chem. B*, 1999, **103**, 2366-2373.
186. H. Shen, L. Niu, K. Fan, J. Li, X. Guan and J. Song, *Langmuir*, 2014, **30**, 9176-9182.
187. M. L. Muro-Small, J. Chen and A. J. McNeil, *Langmuir*, 2011, **27**, 13248-13253.
188. J. Chen, J. W. Kampf and A. J. McNeil, *Langmuir*, 2010, **26**, 13076-13080.
189. E. A. Wilder, R. J. Spontak and C. K. Hall, *Mol. Phys.*, 2003, **101**, 3017-3027.
190. D. Alperstein and D. Knani, *Polym. Adv. Technol.*, 2013, **24**, 391-397.
191. J. Li, K. Fan, X. Guan, Y. Yu and J. Song, *Langmuir*, 2014, **30**, 13422-13429.
192. P. F. Deng, Y. Q. Feng, F. H. Xu and J. Song, *Fine Chemicals*, 2007, **24**, 1056-1060.
193. G. McKenna, K. Francois and J. Sauveur, *Polym. Prepr.*, 1991, **32**, 455-456.
194. S. Yamasaki and H. Tsutsumi, *Bull. Chem. Soc. Jpn.*, 1994, **67**, 2053-2056.
195. W. C. Lai, S. J. Tseng and Y. S. Chao, *Langmuir*, 2011, **27**, 12630-12635.
196. W. C. Lai, S. J. Tseng, S. H. Tung, Y. E. Huang and S. R. Raghavan, *J. Phys. Chem. B.*, 2009, **113**, 8026-8030.
197. D. J. Mercurio and R. J. Spontak, *J. Phys. Chem. B* 2001, **105**, 2091-2098.
198. W. Frassdorf, M. Fahrlander, K. Fuchs and C. Friedrich, *J. Rheol.*, 2003, **47**, 1445-1454.
199. E. A. Wilder, C. K. Hall and R. J. Spontak, *J. Colloid Interface Sci.*, 2003, **267**, 509-518.
200. E. A. Wilder, C. K. Hall, S. A. Khan and R. J. Spontak, *Langmuir.*, 2003, **19**, 6004-6013.
201. M. Tenma, N. Mieda, S. Takamatsu and M. Yamaguchi, *J. Polym. Sci. Part B: Polym. Phys.*, 2008, **46**, 41-47.
202. M. Kühne and C. Friedrich, *Rheol. Acta*, 2009, **48**, 1-9.
203. W. C. Lai and C. H. Wu, *J. Appl. Polym. Sci.*, 2010, **115**, 1113-1119.

204. P. S. Santos, M. G. Abiad, M. A. Carignano and O. H. Campanella, *Rheol. Acta*, 2011, **51**, 3-11.
205. R. H. C. Janssen, V. Stumpflen, M. C. W. Van Boxtel, C. W. M. Bastiaansen, D. J. Broer, T. A. Tervoort and P. Smith, *Macromol. Symp.*, 2000, **154**, 117-126.
206. H. Takeno and Y. Kuribayashi, *Adv. Mater. Res.*, 2014, **896**, 300-304.
207. G. Zhu and J. S. Dordick, *Chem. Mater.*, 2006, **18**, 5988-5995.
208. W. Edwards, C. A. Lagadec and D. K. Smith, *Soft Matter*, 2011, **7**, 110-117.
209. S. Yamamoto, *Kogyo Kagaku Zasshi*, 1942, **45**, 695.
210. S. Liu, W. Yu and C. Zhou, *Soft Matter*, 2013, **9**, 864-874.
211. K. K. Diehn, H. Oh, R. Hashemipour, R. G. Weiss and S. R. Raghavan, *Soft Matter*, 2014, **10**, 2632-2640.
212. P. Santos, M. Abiad, M. Carignano and O. Campanella, *Rheol. Acta*, 2012, **51**, 3-11.
213. K. K. Diehn, H. Oh, R. Hashemipour, R. G. Weiss and S. R. Raghavan, *Soft Matter*, 2014, **10**, 2632-2640.
214. C. M. Hansen, *Prog. Org. Coat.*, 2004, **51**, 77-84.
215. J. Gao, S. Wu and M. A. Rogers, *J. Mater. Chem.*, 2012, **22**, 12651-12658.
216. M. Watase and H. Itagaki, *Bull. Chem. Soc. Jpn.*, 1998, **71**, 1457-1466.
217. E. A. Wilder, C. K. Hall, S. A. Khan and R. J. Spontak, *Langmuir*, 2003, **19**, 6004-6013.
218. J. M. Smith and D. E. Katsoulis, *J. Mater. Chem.*, 1995, **5**, 1899-1903

219. E. A. Wilder, C. K. Hall, S. A. Khan and R. J. Spontak, *Research Signpost*, 2002, **3**, 93-115.
220. D. J. Cornwell and D. K. Smith, *Mater. Horiz.*, 2015, **2**, 279-293.
221. R. G. Weiss, *J. Am. Chem. Soc.*, 2014, **136**, 7519-7530.
222. J. Puigmarti-Luis and D. B. Amabilino, in *Functional Molecular Gels*, eds. B. Escuder and J. F. Miravet, RSC, 2014, pp. 195-254.
223. E. L. Roehl, US Patent 4,346,079, 1982.
224. E. L. Roehl and H. B. Tan, US Patent 4,154,816, 1979.
225. T. Schamper, M. Jablon, M. H. Randhawa, A. Senatore and J. D. Warren, *J. Soc. Cosmet. Chem.* , 1986, **37**, 225-231.

226. T. J. Schamper, M. M. Perl and J. D. Warren, US Patent 4,720,381, 1988.
227. R. B. Kasat, W. Lee, D. R. McCarthy and N. G. Telyan, US Patent 5,490,979, 1996.
228. J. P. Luebbe, P. R. Tanner and J. D. Melanson, US Patent 4,816,261, 1989.
229. M. H. Randhawa and T. J. Schamper, US Patent 4,719,102, 1988.
230. J. Mattai, C. Ortiz, E. Guenin and J. Afflitto, US Patent 6,338,841, 2002.
231. A. Esposito, T. Schamper and E. C. Henry, US Patent 7,799,318, 2010.
232. G. Malle and T. Luukas, US Patent 20130039862, 2013.
233. T. Saito, T. Teshigawara, M. Reger, H. Hoffmann, Y. Sugiyama and M. Kitajima, US Patent 2014/0134255, 2014.
234. T. Furuishi, K. Tomono, T. Suzuki, T. Fukami and K. Kunimasu, US Patent 20120264742, 2012.
235. C. R. King, D. W. Bristol and M. L. English, *US Patent* 20140178480 A1, 2014.
236. E. A. Vogler, T. A. Shepard and J. C. Graper, US Patent 5,547,577, 1996.
237. W.-C. Lai, *J. Phys. Chem. B*, 2011, **115**, 11029-11037.
238. J. Cao, K. Wang, W. Cao, Q. Zhang, R. Du and Q. Fu, *J. Appl. Polym. Sci.*, 2009, **112**, 1104-1113.
239. T. D. Danielson, J. Rockwood and N. A. Mehl, US Patent 8,653,165, 2014.
240. J. Xu, J. Li, B. W. Bolt, K. D. Lake, J. D. Sprinkle, B. M. Burkhart and K. A. Keller, US Patent 8,022,133, 2011.
241. B. Fillon, A. Thierry, B. Lotz and J. Wittmann, *J. Therm. Anal. Calorim.*, 1994, **42**, 721-731.
242. T. A. Shepard, C. R. Delsorbo, R. M. Louth, J. L. Walborn, D. A. Norman, N. G. Harvey and R. J. Spontak, *J. Polym. Sci. Part B: Polym. Phys.*, 1997, **35**, 2617-2628.
243. A. Thierry, B. Fillon, C. Straupé, B. Lotz and J. C. Wittmann, in *Solidification Processes in Polymers*, eds. J. F. Janssson and U. W. Gedde, Steinkopff, 1992, vol. 87, pp. 28-31.
244. M. Kristiansen, M. Werner, T. Tervoort, P. Smith, M. Blomenhofer and H.-W. Schmidt, *Macromolecules*, 2003, **36**, 5150-5156.
245. M. Gahleitner, C. Grein, S. Kheirandish and J. Wolfschwenger, *Inter. Polym. Process.*, 2011, **26**, 2-20.
246. G. R. Titus and J. L. Williams, US Patent 4,808,650, 1989.

247. K. Hamada and H. Uchiyama, US Patent 4,016,118, 1977.
248. Y. Kawai, K. Sasagawa, M. Maki, H. Ueda and M. Miyamoto, US Patent 4,314,039, 1982.
249. H. Uchiyama, US Patent 4,483,956, 1984.
250. J. W. Rekers, US Patent 5,049,605, 1991.
251. J. You, W. Yu and C. Zhou, *Ind. Eng. Chem. Res.* , 2013, **53**, 1097-1107.
252. S. Liu, W. Yu and C. Zhou, *Macromolecules*, 2013, **46**, 6309-6318.
253. J. Lipp, M. Shuster, G. Feldman and Y. Cohen, *Macromolecules*, 2007, **41**, 136-140.
254. J. Siripitayananon, S. Wangsoub, R. H. Olley and G. R. Mitchell, *Macromol. Rapid Commun.*, 2004, **25**, 1365-1370.
255. L. Wei-Chi and T. Shen-Chen, *Nanotechnology*, 2009, **20**, 475606.
256. W.-C. Lai, *Soft Matter*, 2011, **7**, 3844-3851.
257. G. Tan, M. Singh, J. He, V. T. John and G. L. McPherson, *Langmuir*, 2005, **21**, 9322-9326.
258. J. R. Moffat, I. A. Coates, F. J. Leng and D. K. Smith, *Langmuir*, 2009, **25**, 8786-8793.
259. W.-C. Lai, S.-J. Tseng and Y.-S. Chao, *Langmuir*, 2011, **27**, 12630-12635.
260. T. Kar and P. K. Das, in *Functional Molecular Gels*, The Royal Society of Chemistry, 2014, pp. 255-303.
261. E. A. Wilder, K. S. Wilson, J. B. Quinn, D. Skrtic and J. M. Antonucci, *Chem. Mater.*, 2005, **17**, 2946-2952.
262. E. A. Wilder and J. M. Antonucci, *Macromol. Symp.*, 2005, **227**, 255-264.
263. N. M. Sulca, A. V. Munteanu, R. G. Popescu, A. Lungu, R. Stan and H. Iovu, *U.P.B. Sci. Bull., Series B.*, 2010, **72**, 25-36.
264. V. R. Basrur, J. Guo, C. Wang and S. R. Raghavan, *ACS Appl. Mater. Interfaces*, 2013, **5**, 262-267.
265. W.-C. Lai and C.-C. Chen, *Soft Matter*, 2014, **10**, 312-319.
266. N. Mohmeyer, P. Wang, H.-W. Schmidt, S. M. Zakeeruddin and M. Gratzel, *J. Mater. Chem.*, 2004, **14**, 1905-1909.
267. C. M. Pereira, J. M. Oliveira, R. M. Silva and F. Silva, *Anal. Chem.*, 2004, **76**, 5547-5551.
268. F. Silva, M. J. Sousa and C. M. Pereira, *Electrochim. Acta*, 1997, **42**, 3095-3103.

269. K. Miyakawa, I. Ishizu, T. Koga, S. Sakagami and A. Takase, *Liq. Cryst.*, 2005, **32**, 373-380.
270. N. Mizoshita, K. Hanabusa and T. Kato, *Adv. Mater.*, 1999, **11**, 392-394.
271. R. H. C. Janssen, S. Volker, C. W. M. Bastiaansen, D. J. Broer, T. A. Tervoort and P. Smith, *Jpn. J. Appl. Phys.*, 2000, **39**, 2721.
272. R. H. C. Janssen, V. Stümpflen, D. J. Broer, C. W. M. Bastiaansen, T. A. Tervoort and P. Smith, *J. Appl. Phys.*, 2000, **88**, 161-167.
273. T. Kato, *Science*, 2002, **295**, 2414-2418.
274. B. Chien, J. Strobel, M. Strobel, C. Jones, J. Getschel and E. Bosl, *US Patent* 20060093845, 2006.
275. H. Chen, X. Kou, Z. Yang, W. Ni and J. Wang, *Langmuir*, 2008, **24**, 5233-5237.
276. D. M. Ryan and B. L. Nilsson, *Polym. Chem.*, 2012, **3**, 18-33.
277. K. J. Skilling, F. Citossi, T. D. Bradshaw, M. Ashford, B. Kellam and M. Marlow, *Soft Matter*, 2014, **10**, 237-256.
278. T. Kobayashi, Y. Kawashima, M. Yoshimura, M. Sugiura, T. Nobe and S. Fujimoto, *US Patent* 4502975, 1985.
279. WHO, *N-Methyl-2-pyrrolidone*, World Health Organization, Geneva, 2001.
280. P. G. M. Wuts and T. W. Greene, in *Greene's Protective Groups in Organic Synthesis*, John Wiley & Sons, Inc., 2006, pp. 533-646.
281. A. Counotte-Potman and H. C. Van Der Plas, *J. Heterocyclic Chem.*, 1983, **20**, 1259-1261.
282. N. Ballard and S. A. F. Bon, *Polym. Chem.*, 2014, **5**, 6789-6796.
283. R. Stan, C. Ott, S. Rosca, A. Badanoiu, S. Stoleriu and G. Voicu, *U.P.B. Sci. Bull., Series B,*, 2008, **70**, 1-10.
284. S. Raghavan and B. Cipriano, in *Molecular Gels*, eds. R. Weiss and P. Terech, Springer Netherlands, 2006, pp. 241-252.
285. T. A. Stortz, A. K. Zetzl, S. Barbut, A. Cattaruzza and A. G. Marangoni, *Lipid Technol.*, 2012, **24**, 151-154.
286. D. J. Adams, *Macromol. Biosci.*, 2011, **11**, 160-173.
287. D. J. Adams, M. F. Butler, W. J. Frith, M. Kirkland, L. Mullen and P. Sanderson, *Soft Matter*, 2009, **5**, 1856-1862.
288. A. S. Côté, W. Smith and P. J. Lindan, in *Democritus*, eds. A. S. Côté, W. Smith and P. J. Lindan, CCLRC Daresbury Laboratory, Warrington, UK, 2000.

289. S. Brahma, S. A. Ikbal, A. Dhamija and S. P. Rath, *Inorg. Chem.*, 2014, **53**, 2381-2395.
290. L. Zhang, C. Liu, Q. Jin, X. Zhu and M. Liu, *Soft Matter*, 2013, **9**, 7966-7973.
291. G. Snatzke, *J. Chem. Soc.*, 1965, 5002-5015.
292. Q. Sun, Y. Bai, G. He, C. Duan, Z. Lin and Q. Meng, *Chem. Commun.*, 2006, 2777-2779.
293. X. Mu, K. M. Eckes, M. M. Nguyen, L. J. Suggs and P. Ren, *Biomacromolecules*, 2012, **13**, 3562-3571.
294. F.-X. Simon, T.-T.-T. Nguyen, M. Schmutz, G. Decher, J.-F. Nicoud and P. J. Mesini, *New J. Chem.*, 2009, **33**, 2028-2033.
295. P. Terech, *J. Coll. Interface Sci.*, 1985, **107**, 244-255.
296. X. Y. Liu and P. D. Sawant, *Adv. Mater.*, 2002, **14**, 421-426.
297. N. Markovic, M. Ginic-Markovic and N. K. Dutta, *Polym. Int.*, 2003, **52**, 1095-1107.
298. X. Huang, P. Terech, S. R. Raghavan and R. G. Weiss, *J. Am. Chem. Soc.*, 2005, **127**, 4336-4344.
299. N. Sreenivasachary and J.-M. Lehn, *Proc. Natl. Acad. Sci. USA*, 2005, **102**, 5938-5943.
300. R. V. B. Pratimo Rao, *Nutrition & Food Scienc*, 2003, **33**, 5.
301. E. S. Beach, R. T. Malecky, R. R. Gil, C. P. Horwitz and T. J. Collins, *Catal. Sci. Technol.*, 2011, **1**, 437-443.
302. P. Gregory, *Dyes and Pigments*, 1986, **7**, 45-56.
303. H. Motschi and E. A. Clarke, *Rev. Prog. Color. Relat. Top.*, 1998, **28**, 71-79.
304. C. Namasivayam and D. Kavitha, *Dyes and Pigments*, 2002, **54**, 47-58.
305. Y. S. Ho and G. McKay, *Can. J. Chem. Eng.*, 1998, **76**, 822-827.
306. L. K. Archna and R. K. Siva, *J. Biochem. Tech.*, 2012, **3**, S177-S180.
307. J. Maier, A. Kandelbauer, A. Erlacher, A. Cavaco-Paulo and G. M. Gübitz, *Appl. Environ. Microbiol.*, 2004, **70**, 837-844.
308. M. D. Chengalroyen and E. R. Dabbs, *World J. Microbiol. Biotechnol.*, 2013, **29**, 389-399.
309. R. G. Saratale, G. D. Saratale, J. S. Chang and S. P. Govindwar, *Biodegradation*, 2010, **21**, 999-1015.
310. S. B. Sadr Ghayeni, P. J. Beatson, R. P. Schneider and A. G. Fane, *Desalination*, 1998, **116**, 65-80.

311. G. Ciardelli and N. Ranieri, *Water Res.*, 2001, **35**, 567-572.
312. B. Van der Bruggen, G. Cornelis, C. Vandecasteele and I. Devreese, *Desalination*, 2005, **175**, 111-119.
313. S. Raddatz, J. Mueller-Ibeler, J. Kluge, L. Wäß, G. Burdinski, J. R. Havens, T. J. Onofrey, D. Wang and M. Schweitzer, *Nucleic Acids Res.*, 2002, **30**, 4793-4802.
314. B. Buchs, W. Fieber, F. Vigouroux-Elie, N. Sreenivasachary, J.-M. Lehn and A. Herrmann, *Org. Biomol. Chem.*, 2011, **9**, 2906-2919.
315. N. Sreenivasachary and J.-M. Lehn, *Chem. Asian J.*, 2008, **3**, 134-139.
316. F. Zhao, Y. Gao, J. Shi, H. M. Browdy and B. Xu, *Langmuir*, 2011, **27**, 1510-1512.
317. D. J. Cornwell, B. O. Okesola and D. K. Smith, *Angew. Chem. Int. Ed.*, 2014, **53**, 12461-12465.
318. K. G. Bhattacharyya and A. Sharma, *J. Environ. Manag.*, 2004, **71**, 217-229.
319. F.-C. Wu, R.-L. Tseng, S.-C. Huang and R.-S. Juang, *Chem. Eng. J.*, 2009, **151**, 1-9.
320. Y. S. Ho, J. C. Y. Ng and G. McKay, *Sep. Purif. Rev.*, 2000, **29**, 189-232.
321. A. D. McNaught and A. Wilkinson, *Compendium of chemical terminology : IUPAC recommendations*, 2nd edn., Blackwell Science, Oxford 1997.
322. J. Ogilvie, in *The Comprehensive English Dictionary*, Blackie, London, 1884.
323. A. M. Williams, in *The English Encyclopedic Dictionary*, Collins, London, 1930.
324. W. Foster, *J. Chem. Educ.*, 1936, **13**, 349.
325. E. Resongles, C. Casiot, R. Freydier, L. Dezileau, J. Viers and F. Elbaz-Poulichet, *Sci. Tot. Environ.*, 2014, **481**, 509-521.
326. B. Perks, *Chemistry in Its Element - Arsenic*, http://www.rsc.org/chemistryworld/podcast/interactive_periodic_table_transcripts/arsenic.asp, Accessed January 20, 2015, 2015.
327. E. Nieboer and D. H. S. Richardson, *Environ. Pollut. Ser. B, Chem. and Phys.*, 1980, **1**, 3-26.
328. D. A. Phipps, in *Effect of Heavy Metal Pollution on Plants*, ed. N. W. Lepp, Springer Netherlands, 1981, pp. 1-54.
329. G. W. VanLoon and S. J. Duffy, *Environmental Chemistry: A Global Perspective*, Oxford University Press, Oxford, 2000.

330. M. E. Hodson, *Environ. Pollut.*, 2004, **129**, 341-343.
331. R. Hubner, K. B. Astin and R. J. H. Herbert, *J. Environ. Monit.*, 2010, **12**, 1511-1514.
332. L. Madrid, *Geoderma*, 2010, **155**, 128-129.
333. C. D. Klaasen, *Casarette and Doull's Toxicology- The basic Science of Poisons*, 6th edn., McGraw-Hill, New York, 2001.
334. R. G. Pearson, *J. Chem. Educ.*, 1968, **45**, 581.
335. G. Klopman, in *Chemical Reactivity and Reaction Paths*, ed. G. Klopman, Wiley, New York, 1974.
336. J. O. Nriagu, *Lead and Lead poisoning in antiquity*, John Wiley, New York, 1982.
337. J. S. Casas and J. Sordo, in *Lead: Chemistry, Analytical Aspects, Environmental Impact and Health Effects*, eds. J. S. Casas and J. Sordo, Elsevier, Oxford, First edn., 2006.
338. O. Orisakwe, *North. Am. J. Med. Sci*, 2014, **6**, 61-70.
339. T. Bahadir, G. Bakan, L. Altas and H. Buyukgungor, *Enzyme Microb. Technol.*, 2007, **41**, 98-102.
340. A. Davidson, J. Ryman, C. A. Sutherland, E. F. Milner, R. C. Kerby, H. Teindl, A. Melin and H. M. Bolt, in *Ullmann's Encyclopedia of Industrial Chemistry*, Wiley-VCH Verlag GmbH & Co. KGaA, 2000.
341. D. E. Woolley, *NeuroToxicology*, 1984, **5**, 353-362.
342. M. H. Azizi and F. Azizi, *The international journal of occupational and environmental medicine*, 2010, **1**, 81-87.
343. M. Edwards, S. Triantafyllidou and D. Best, *Environ. Sci. Technol.*, 2009, **43**, 1618-1623.
344. R. Renner, *Environ. Health Perspect.*, 2010, **118**, A202-208.
345. C. A. Dooyema, A. Neri, Y. C. Lo, J. Durant, P. I. Dargan, T. Swarthout, O. Biya, S. O. Gidado, S. Haladu, N. Sani-Gwarzo, P. M. Nguku, H. Akpan, S. Idris, A. M. Bashir and M. J. Brown, *Environ. Health Perspect.*, 2012, **120**, 601-607.
346. P. J. Landrigan and A. C. Todd, *Western J. Med.*, 1994, **161**, 153-159.
347. H. Schroeder, K. A. Shuler and S. R. Chenery, *Am. J. Phys. Anthropol.*, 2013, **150**, 203-209.

348. K. Kostial, D. Kello and S. Jugo, *Environ. Health Perspect.*, 1978, **VOL. 25**, 81-86.

349. P. A. Johansson, K. M. Dziegielewska, S. A. Liddelow and N. R. Saunders, *BioEssays*, 2008, **30**, 237-248.

350. D. Rosner, G. Markowitz and B. Lanphear, *Public Health Rep.*, 2005, **120**, 296-300.

351. B. P. Lanphear, R. Hornung, J. Khoury, K. Yolton, P. Baghurst, D. C. Bellinger, R. L. Canfield, K. N. Dietrich, R. Bornschein, T. Greene, S. J. Rothenberg, H. L. Needleman, L. Schnaas, G. Wasserman, J. Graziano and R. Roberts, *Environ. Health Perspect.*, 2005, **113**, 894-899.

352. T. S. Bowers and B. D. Beck, *NeuroToxicology*, 2006, **27**, 520-524.

353. R. L. Canfield, C. R. Henderson, D. A. Cory-Slechta, C. Cox, T. A. Jusko and B. P. Lanphear, *New Engl. J. Med.*, 2003, **348**, 1517-1526.

354. L. F. Scott and L. Nguyen, *Int. Arch. Occup. Environ. Health*, 2011, **84**, 513-522.

355. J. Weuve and M. G. Weisskopf, in *Aging and Vulnerability to Environmental Chemicals: Age-related Disorders and their Origins in Environmental Exposures*, ed. B. Weiss, RSC, Cambridge, 2013, pp. 1-26.

356. J. V. B. Rao, B. Vengamma, T. Naveen and V. Naveen, *J. Neurosci. Rural Pract.*, 2014, **5**, 161-163.

357. R. A. Shih, H. Hu, M. G. Weisskopf and B. S. Schwartz, *Environ. Health Perspect.*, 2007, **115**, 483-492.

358. W. F. Stewart, B. S. Schwartz, C. Davatzikos, D. Shen, D. Liu, X. Wu, A. C. Todd, W. Shi, S. Bassett and D. Youssem, *Neurology*, 2006, **66**, 1476-1484.

359. B. Caffo, S. Chen, W. Stewart, K. Bolla, D. Yousem, C. Davatzikos and B. S. Schwartz, *Am. J. Epidemiol.*, 2008, **167**, 429-437.

360. M. G. Weisskopf, H. Hu, R. V. Mulkern, R. White, A. Aro, S. Oliveira and R. O. Wright, *Environ. Health Perspect.*, 2004, **112**, 620-625.

361. J. E. Puzas, C. A. Muzytchuk and J. D. Holz, in *Aging and Vulnerability to Environmental Chemicals Age-related Disorders and their Origins in Environmental Exposures*, ed. B. Weiss, RSC, Cambridge, 2013.

362. J. E. Puzas, J. Campbell, R. O'Keefe and R. Rosier, in *Nutrition and Bone Health*, eds. M. Holick and B. Dawson-Hughes, Humana Press, 2004, pp. 363-376.

363. L. P. Rong, Y. Y. Xu and X. Y. Jiang, *Chinese J. Contemp. Pediatr.*, 2014, **16**, 325-329.
364. I. Mazumdar and K. Goswami, *Ind. J. Clin. Biochem.*, 2014, **29**, 257-259.
365. G. F. Nordberg, K. Nogawa, M. Nordberg and L. T. Friberg, in *Handbook on the Toxicology of Metals (Third Edition)*, eds. G. F. Nordberg, B. A. Fowler, M. Nordberg and L. T. Friberg, Academic Press, Burlington, 2007, pp. 445-486.
366. A. Rani, A. Kumar, A. Lal and M. Pant, *Int. J. Environ. Health Res.*, 2014, **24**, 378-399.
367. C. A. Grant and S. C. Sheppard, *Hum. Ecol. Risk Assess.*, 2008, **14**, 210-228.
368. A. R. Jafarnejadi, G. Sayyad, M. Homaee and A. H. Davamei, *Environ. Monit. Assess.*, 2013, **185**, 4087-4096.
369. Q. Q. Huang, X. Liu, Q. Zhang, Y. H. Qiao, D. C. Su, R. F. Jiang, Y. K. Rui and H. F. Li, *Spectrosc. Spect. Anal.*, 2014, **34**, 1403-1406.
370. S. V. Adams, P. A. Newcomb, M. M. Shafer, C. Atkinson, E. J. A. Bowles, K. M. Newton and J. W. Lampe, *Sci. Tot. Environ.*, 2011, **409**, 1632-1637.
371. P. A. Richter, E. E. Bishop, J. Wang and M. H. Swahn, *Int. J. Environ. Res. Public Health* 2009, **6**, 16.
372. M. Guney, A. Nguyen and G. J. Zagury, *J. Environ. Sci. Health - Part A* 2014, **49**, 1218-1227.
373. L. Jarup, A. Rogenfelt, C. G. Elinder, K. Nogawa and T. Kjellström, *Scand. J. Work Environ. Health*, 1983, **9**, 327-331.
374. R. H. Friis, in *Essential Public Health*, ed. R. Riegelman, Jone and Bartlett, Canada, 2007.
375. K. Aoshima, *Nippon Eiseigaku Zasshi (Japanese Journal of Hygiene)*, 2012, **67**, 455-463.
376. R. A. Bernhoft, *Sci. World J.*, 2013, **2013**, 7.
377. V. Matović, A. Buha, Z. Bulat and D. Dukić-ĆOsić, *Arhiv za Higijenu Rada i Toksikologiju*, 2011, **62**, 65-76.
378. R. C. Patra, A. K. Rautray and D. Swarup, *Vet. Med. Int.*, 2011, **2011**.
379. A. Cuypers, M. Plusquin, T. Remans, M. Jozefczak, E. Keunen, H. Gielen, K. Opdenakker, A. R. Nair, E. Munters, T. J. Artois, T. Nawrot, J. Vangronsveld and K. Smeets, *BioMetals*, 2010, **23**, 927-940.

380. A. J. Wyrobek, S. M. Schrader, S. D. Perreault, L. Fenster, G. Huszar, D. F. Katz, A. M. Osorio, V. Sublet and D. Evenson, *Reprod. Toxicol.*, 1997, **11**, 243-259.

381. J. Jurasović, P. Cvitković, A. Pizent, B. Čolak and S. Telišman, *BioMetals*, 2004, **17**, 735-743.

382. J. Mendiola, J. M. Moreno, M. Roca, N. Vergara-Jurez, M. J. Martínez-García, A. García-Snchez, B. Elvira-Rendueles, S. Moreno-Grau, J. J. Lápez-Espín, J. Ten, R. Bernabeu and A. M. Torres-Cantero, *Environ. Health*, 2011, **10**, 1-7.

383. L. Giaccio, D. Cicchella, B. De Vivo, G. Lombardi and M. De Rosa, *J. Geochem. Explor.*, 2012, **112**, 218-225.

384. J. J. Wirth and R. S. Mijal, *Syst. Biol. Reprod. Med.*, 2010, **56**, 147-167.

385. T. S. Nawrot, E. Van Hecke, L. Thijs, T. Richart, T. Kuznetsova, Y. Jin, J. Vangronsveld, H. A. Roels and J. A. Staessen, *Environ. Health Perspect.*, 2008, **116**, 1620-1628.

386. M. V. Varoni, D. Palomba, S. Gianorso and V. Anania, *Vet. Res. Commun.*, 2003, **27**, 807-810.

387. E. Kobayashi, Y. Suwazono, R. Honda, M. Dochi, M. Nishijo, T. Kido and H. Nakagawa, *Toxicol. Lett.*, 2008, **176**, 124-130.

388. G. Cannino, E. Ferruggia, C. Luparello and A. M. Rinaldi, *Mitochondrion*, 2009, **9**, 377-384.

389. G. Cannino, E. Ferruggia, C. Luparello and A. M. Rinaldi, *J. Inorg. Biochem.*, 2008, **102**, 1668-1676.

390. G. Cannino, E. Ferruggia, C. Luparello and A. M. Rinaldi, *Mol. Cell. Biochem.*, 2009, **328**, 75-84.

391. D. Liu, J. Yang, Y. Li, M. Zhang and L. Wang, *PLoS ONE*, 2013, **8**.

392. S. A. Jancic and B. Z. Stosic, in *Vitamins and Hormones*, 2014, vol. 94, pp. 391-425.

393. H. Hagar and W. Al Malki, *Environ. Toxicol. Pharmacol.*, 2014, **37**, 803-811.

394. Y. D. Kim, D. H. Yim, S. Y. Eom, S. I. Moon, C. H. Park, G. B. Kim, S. D. Yu, B. S. Choi, J. D. Park and H. Kim, *Environ. Toxicol. Pharmacol.*, 2014, **38**, 272-278.

395. F. Thévenod and W. K. Lee, in *Metal Ions in Life Sciences*, 2013, vol. 11, pp. 415-490.

396. M. B. Martin, H. James Voeller, E. P. Gelmann, L. Jianming, E. G. Stoica, E. J. Hebert, R. Reiter, B. Singh, M. Danielsen, E. Pentecost and A. Stoica, *Endocrinology*, 2002, **143**, 263-275.
397. G. G. Schwartz, D. Il'Yasova and A. Ivanova, *Diabetes Care*, 2003, **26**, 468-470.
398. H. Horiguchi, *Nippon Eiseigaku Zasshi (Japanese journal of hygiene)*, 2007, **62**, 888-904.
399. M. Filipič, *Mutat. Res-Fund. Mol. M.*, 2012, **733**, 69-77.
400. Q. Wang, D. Kim, D. D. Dionysiou, G. A. Sorial and D. Timberlake, *Environ. Pollut.*, 2004, **131**, 323-336.
401. P. Pai, D. Niemi and B. Powers, *Fuel Process. Technol.*, 2000, **65–66**, 101-115.
402. E. R. Caley, *J. Chem. Edu.*, 1928, **5**, 419.
403. S. Norn, H. Permin, E. Kruse and P. R. Kruse, *Dansk Medicinhistorisk Arbog*, 2008, **36**, 21-40.
404. Y. Uçar and W. A. Brantley, *Int. J. Dent.*, 2011.
405. K. G. Homme, J. K. Kern, B. E. Haley, D. A. Geier, P. G. King, L. K. Sykes and M. R. Geier, *BioMetals*, 2014, **27**, 19-24.
406. G. M. Richardson, *Hum. Ecol. Risk Assess.*, 2014, **20**, 433-447.
407. G. M. Richardson, R. Wilson, D. Allard, C. Purtill, S. Douma and J. Gravière, *Sci. Tot. Environ.*, 2011, **409**, 4257-4268.
408. M. Harada, *Crit. Rev. Toxicol.*, 1995, **25**, 1-24.
409. J. C. Clifton Ii, *Pediatr. Clin. North Am.*, 2007, **54**, 237.e231-237.e245.
410. S. Takaoka, T. Fujino, N. Hotta, K. Ueda, M. Hanada, M. Tajiri and Y. Inoue, *Sci. Tot. Environ.*, 2013, **468-469**, 950-957.
411. J. E. Saunders, B. G. Jastrzembski, J. C. Buckey, D. Enriquez, T. A. MacKenzie and M. R. Karagas, *Audiol. Neurotol.*, 2013, **18**, 101-113.
412. H. Satoh, in *Aging and Vulnerability to Environmental Chemicals: Age-related Disorders and their Origins in Environmental Exposures*, ed. B. Weiss, RSC, Cambridge, 2013.
413. N. Gaur, G. Flora, M. Yadav and A. Tiwari, *Environ. Sci. Process. Impact*, 2014, **16**, 180-193.

414. M. Korbas, J. L. Odonoghue, G. E. Watson, I. J. Pickering, S. P. Singh, G. J. Myers, T. W. Clarkson and G. N. George, *ACS Chem. Neurosci.*, 2010, **1**, 810-818.
415. S. Nishigaki and M. Harada, *Nature*, 1975, **258**, 324-325.
416. K. Suzuki, K. Nakai, T. Sugawara, T. Nakamura, T. Ohba, M. Shimada, T. Hosokawa, K. Okamura, T. Sakai, N. Kurokawa, K. Murata, C. Satoh and H. Satoh, *Environ. Res.*, 2010, **110**, 699-704.
417. L. Amin-Zaki, M. A. Majeed, T. W. Clarkson and M. R. Greenwood, *Br. Med. J.*, 1978, **1**, 613-618.
418. L. Amin-Zaki, M. A. Majeed, M. R. Greenwood, S. B. Elhassani, T. W. Clarkson and R. A. Doherty, *J. Appl. Toxicol.*, 1981, **1**, 210-214.
419. D. Joshi, M. D. Kumar, S. A. Kumar and S. Sangeeta, *J. Environ. Pathol. Toxicol. Oncol.*, 2014, **33**, 167-182.
420. J. B. Cavanagh, *Br. J. Ind. Med.*, 1988, **45**, 649-651.
421. L. Kosta, A. R. Byrne and V. Zelenko, *Nature*, 1975, **254**, 238-239.
422. P. A. O'Day, *Elements*, 2006, **2**, 77-83.
423. A. L. Allred and A. L. Hensley Jr, *J. Inorg. Nucl. Chem.*, 1961, **17**, 43-54.
424. W. H. Miller, H. M. Schipper, J. S. Lee, J. Singer and S. Waxman, *Cancer Res.*, 2002, **62**, 3893-3903.
425. D. Douer, W. Hu, S. Giralt, M. Lill and J. DiPersio, *The Oncologist*, 2003, **8**, 132-140.
426. S. H. E. Kaufmann, *Nat Rev Drug Discov*, 2008, **7**, 373-373.
427. K. E. Nachman, G. Raber, K. A. Francesconi, A. Navas-Acien and D. C. Love, *Sci. Tot. Environ.*, 2012, **417-418**, 183-188.
428. W. R. Cullen, - *Is Arsenic an Aphrodisiac? The sonochemistry of an element*, RSC, Cambridge, 2008.
429. R. N. Ratnaike, *Postgrad. Med. J.*, 2003, **79**, 391-396.
430. UNICEF, *Bangladesh Multiple Indicator Cluster Survey 2009*, Bangladesh Bureau of Statistics UNICEF, Bangladesh, 2010.
431. H. S. Satterlee, *New Engl. J. Med.*, 1960, **263**, 676-684.
432. K. L. Cottingham, R. Karimi, J. F. Gruber, M. S. Zens, V. Sayarath, C. L. Folt, T. Punshon, J. S. Morris and M. R. Karagas, *Nutr. J.*, 2013, **12**.
433. USEPA, *Arsenic in Drinking Water*, USEPA, 2006.
434. W. Edwards and D. K. Smith, *Chem. Commun.*, 2012, **48**, 2767-2769.

435. K. Murata, M. Aoki, T. Nishi, A. Ikeda and S. Shinkai, *J. Chem. Soc., Chem. Commun.*, 1991, 1715-1718.
436. A. Y.-Y. Tam and V. W.-W. Yam, *Chem. Soc. Rev.*, 2013, **42**, 1540-1567.
437. S. Zhang, S. Yang, J. Lan, S. Yang and J. You, *Chem. Commun.*, 2008, 6170-6172.
438. P. Bairi, B. Roy and A. K. Nandi, *J. Mater. Chem.*, 2011, **21**, 11747-11749.
439. K. Chen, L. Tang, Y. Xia and Y. Wang, *Langmuir*, 2008, **24**, 13838-13841.
440. Q. Liu, Y. Wang, W. Li and L. Wu, *Langmuir*, 2007, **23**, 8217-8223.
441. K. Hanabusa, Y. Maesaka, M. Suzuki, M. Kimura and H. Shirai, *Chem. Lett.*, 2000, **29**, 1168-1169.
442. S. A. Joshi and N. D. Kulkarni, *Chem. Commun.*, 2009, 2341-2343.
443. A. Westcott, C. J. Sumby, R. D. Walshaw and M. J. Hardie, *New J. Chem.*, 2009, **33**, 902-912.
444. L. Applegarth, N. Clark, A. C. Richardson, A. D. M. Parker, I. Radosavljevic-Evans, A. E. Goeta, J. A. K. Howard and J. W. Steed, *Chem. Commun.*, 2005, 5423-5425.
445. Y. He, Z. Bian, C. Kang, Y. Cheng and L. Gao, *Chem. Commun.*, 2010, **46**, 3532-3534.
446. Q. Jin, L. Zhang, H. Cao, T. Wang, X. Zhu, J. Jiang and M. Liu, *Langmuir*, 2011, **27**, 13847-13853.
447. M.-O. M. Piepenbrock, N. Clarke and J. W. Steed, *Soft Matter*, 2010, **6**, 3541-3547.
448. B. Xing, M.-F. Choi and B. Xu, *Chem. Eur. J.*, 2002, **8**, 5028-5032.
449. M. George, G. P. Funkhouser, P. Terech and R. G. Weiss, *Langmuir*, 2006, **22**, 7885-7893.
450. J. Zhang, X. Wang, L. He, L. Chen, C.-Y. Su and S. L. James, *New J. Chem.*, 2009, **33**, 1070-1075.
451. H. Lee, S. H. Jung, W. S. Han, J. H. Moon, S. Kang, J. Y. Lee, J. H. Jung and S. Shinkai, *Chem. Eur. J.*, 2011, **17**, 2823-2827.
452. J. B. Beck and S. J. Rowan, *J. Am. Chem. Soc.*, 2003, **125**, 13922-13923.
453. W. Weng, J. B. Beck, A. M. Jamieson and S. J. Rowan, *J. Am. Chem. Soc.*, 2006, **128**, 11663-11672.
454. T. Wei, J. Dang, Q. Lin, H. Yao, Y. Liu, W. Zhang, J. Ming and Y. Zhang, *Sci. China Chem.*, 2012, **55**, 2554-2561.

455. P. J. Knerr, M. C. Branco, R. Nagarkar, D. J. Pochan and J. P. Schneider, *J. Mater. Chem.*, 2012, **22**, 1352-1357.
456. S. Sengupta and R. Mondal, *J. Mater. Chem.*, 2014, **2**, 16373-16377.
457. S. Sengupta, A. Goswami and R. Mondal, *New J. Chem.*, 2014, **38**, 2470-2479.
458. T. H. Kim and S. G. Kim, *Saf. Health Work*, 2011, **2**, 97-104.
459. J. R. Rangel-Mendez, R. Monroy-Zepeda, E. Leyva-Ramos, P. E. Diaz-Flores and K. Shirai, *J. Hazard. Mater.*, 2009, **162**, 503-511.
460. R. J. White, N. Brun, V. L. Budarin, J. H. Clark and M.-M. Titirici, *ChemSusChem*, 2014, **7**, 670-689.
461. J. Li, X. Xiao, X. Xu, J. Lin, Y. Huang, Y. Xue, P. Jin, J. Zou and C. Tang, *Sci. Rep.*, 2013, **3**.
462. F. C. Bersworth, *US Patent* 3507892, 1970.
463. D. Zhao, S.-M. Ong, Z. Yue, Z. Jiang, Y.-C. Toh, M. Khan, J. Shi, C.-H. Tan, J. P. Chen and H. Yu, *Biomaterials*, 2008, **29**, 3693-3702.
464. Y. Zhang, W. Yan, Z. Sun, C. Pan, X. Mi, G. Zhao and J. Gao, *Carbohydr. Polym.*, 2015, **117**, 657-665.
465. Y. Zhang, Y. Liu, X. Wang, Z. Sun, J. Ma, T. Wu, F. Xing and J. Gao, *Carbohydr. Polym.*, 2014, **101**, 392-400.
466. A. Lim and A. Aris, *Rev Environ Sci Biotechnol*, 2014, **13**, 163-181.
467. O. Valdés, C. E. Vergara, M. B. Camarada, V. Carrasco-Sánchez, F. M. Nachtigall, J. Tapia, R. Fischer, F. D. González-Nilo and L. S. Santos, *J. Environ. Manage.*, 2015, **147**, 321-329.
468. D. Zhou, L. Zhang and S. Guo, *Water Res.*, 2005, **39**, 3755-3762.
469. R. Leyva-Ramos, P. E. Diaz-Flores, A. Aragon-Piña, J. Mendoza-Barron and R. M. Guerrero-Coronado, *Sep. Sci. Technol.*, 2005, **40**, 2079-2094.
470. F. Kožíšek, *Health significance of drinking water Calcium and Magnesium*, http://www.alkaway.com.au/downloads/hard-water-report.pdf, Accessed 16 January, 2015.
471. S. J. S. Flora and V. Pachauri, *Int. J. Environ. Res. Public Health*, 2010, **7**, 2745-2788.
472. G. Chauhan, K. K. Pant and K. D. P. Nigam, *Environ. Sci.: Processes Impacts*, 2015, **17**, 12-40.
473. R. G. Pearson, *J. Am. Chem. Soc.*, 1963, **85**, 3533-3539.
474. T.-L. Ho, *Chem. Rev.*, 1975, **75**, 1-20.

475. T.-F. Liu, L. Zou, D. Feng, Y.-P. Chen, S. Fordham, X. Wang, Y. Liu and H.-C. Zhou, *J. Am. Chem. Soc.*, 2014, **136**, 7813-7816.
476. M. Kirberger and J. J. Yang, *J. Inorg. Biochem.*, 2008, **102**, 1901-1909.
477. D.-L. Mitic-Stojanovic, A. Zarubica, M. Purenovic, D. Bojic, T. Andjelkovic and A. L. Bojic, *Water SA*, 2011, **37**, 303-312.
478. USEPA, *Basic information about cadmium in drinking water*, EPA, Washington, DC, 2013.
479. USEPA, *Drinking Water Contaminants*, EPA, Washington, DC, 2014.
480. A. K. Arof, N. M. Morni and M. A. Yarmo, *Mater. Sci. Eng.*, 1998, **55**, 130-133.
481. R. S. Vieira, M. L. M. Oliveira, E. Guibal, E. Rodríguez-Castellón and M. M. Beppu, *Colloids and Surfaces A: Physicochem. Eng. Aspects*, 2011, **374**, 108-114.
482. L. Dambies, C. Guimon, S. Yiacoumi and E. Guibal, *Colloids and Surfaces A: Physicochem. Eng. Aspects*, 2001, **177**, 203-214.
483. T. Yoshida, T. Yamaguchi, Y. Iida and S. Nakayama, *J. Nucl. Sci. Technol.*, 2003, **40**, 672-678.
484. Y. Ding, Y. Wang, L. Zhang, H. Zhang and Y. Lei, *J. Mater. Chem.*, 2012, **22**, 980-986.
485. G. Z. Kyzas, P. I. Siafaka, D. A. Lambropoulou, N. K. Lazaridis and D. N. Bikiaris, *Langmuir*, 2013, **30**, 120-131.
486. I. Langmuir, *J. Am. Chem. Soc.*, 1918, **40**, 1361-1403.
487. G. Z. Kyzas, P. I. Siafaka, D. A. Lambropoulou, N. K. Lazaridis and D. N. Bikiaris, *Langmuir*, 2014, **30**, 120-131.
488. P. Terech and R. G. Weiss, *Chem. Rev.*, 1997, **97**, 3133-3159.
489. M. George and R. Weiss, in *Molecular Gels*, eds. R. Weiss and P. Terech, Springer Netherlands, 2006, pp. 449-551.
490. M. de Loos, B. L. Feringa and J. H. van Esch, *Eur. J. Org. Chem.*, 2005, **361**, 5.
491. J. W. Steed, *Chem. Commun.*, 2011, **47**, 1379-1383.
492. J. van Herrikhuyzen, S. J. George, M. R. J. Vos, N. A. J. M. Sommerdijk, A. Ajayaghosh, S. C. J. Meskers and A. P. H. J. Schenning, *Angew. Chem. Int. Ed.*, 2007, **46**, 1825-1828.

493. M. O. M. Piepenbrock, G. O. Lloyd, N. Clarke and J. W. Steed, *Chem. Rev.*, 2010, **110**, 1960.

494. P. M. Mendes, A. H. Flood and J. F. Stoddart, *Appl. Phys. A*, 2005, **80**, 1197-1209.

495. A. Greiner, J. H. Wendorff, A. L. Yarin and E. Zussman, *Appl Microbiol Biotechnol*, 2006, **71**, 387-393.

496. S. R. Shin, S. M. Jung, M. Zalabany, K. Kim, P. Zorlutuna, S. b. Kim, M. Nikkhah, M. Khabiry, M. Azize, J. Kong, K.-t. Wan, T. Palacios, M. R. Dokmeci, H. Bae, X. Tang and A. Khademhosseini, *ACS Nano*, 2013, **7**, 2369-2380.

497. D. R. Rolison, J. W. Long, J. C. Lytle, A. E. Fischer, C. P. Rhodes, T. M. McEvoy, M. E. Bourg and A. M. Lubers, *Chem. Soc. Rev.*, 2009, **38**, 226-252.

498. L. Pan, G. Yu, D. Zhai, H. R. Lee, W. Zhao, N. Liu, H. Wang, B. C.-K. Tee, Y. Shi, Y. Cui and Z. Bao, *Proc. Natl. Acad. Sci. USA*, 2012, **109**, 9287-9292.

499. P. Schwille, *Science*, 2011, **333**, 1252-1254.

500. K. T. Sapra and H. Bayley, *Sci. Rep.* , 2012, **2**, 848.

501. A. Guiseppi-Elie, *Biomaterials*, 2010, **31**, 2701-2716.

502. T. Dvir, B. P. Timko, D. S. Kohane and R. Langer, *Nat Nano*, 2011, **6**, 13-22.

503. F. S. Schoonbeek, J. H. van Esch, B. Wegewijs, D. B. A. Rep, M. P. de Haas, T. M. Klapwijk, R. M. Kellogg and B. L. Feringa, *Angew. Chem. Int. Ed.*, 1999, **38**, 1393-1397.

504. Y. H. Chen, M. Op de Beeck, L. Vanderheyden, E. Carrette, V. Mihajlović, K. Vanstreels, B. Grundlehner, S. Gadeyne, P. Boon and C. van Hoof, *Sensors*, 2014, **14**, 23758-23780.

505. K. Y. Lin, D. Y. Chen and S. Y. Lee, in *Frontiers in Artificial Intelligence and Applications*, 2015, vol. 274, pp. 1052-1061.

506. C. J. Anderson and J. T. Gumbusky, *US Patent* 3998215 A, 1976.

507. J. Puigmartí-Luis, Á. Pérez del Pino, E. Laukhina, J. Esquena, V. Laukhin, C. Rovira, J. Vidal-Gancedo, A. G. Kanaras, R. J. Nichols, M. Brust and D. B. Amabilino, *Angew. Chem. Int. Ed.*, 2008, **47**, 1861-1865.

508. P. K. Vemula, U. Aslam, V. A. Mallia and G. John, *Chem. Mater.*, 2007, **19**, 138-140.

509. P. K. Vemula and G. John, *Chem. Commun.*, 2006, 2218-2220.

510. M. Kimura, S. Kobayashi, T. Kuroda, K. Hanabusa and H. Shirai, *Adv. Mater.*, 2004, **16**, 335-338.
511. S. Bhattacharya, A. Srivastava and A. Pal, *Angew. Chem. Int. Ed.*, 2006, **45**, 2934-2937.
512. H. Basit, A. Pal, S. Sen and S. Bhattacharya, *Chem. Eur. J.*, 2008, **14**, 6534-6545.
513. C. S. Love, V. Chechik, D. K. Smith, K. Wilson, I. Ashworth and C. Brennan, *Chem. Commun.*, 2005, 1971-1973.
514. I. A. Coates and D. K. Smith, *J. Mater. Chem.*, 2010, **20**, 6696-6702.
515. A. Chakrabarty and U. Maitra, *J. Phys. Chem. B*, 2013, **117**, 8039-8046.
516. S. Ray, A. K. Das and A. Banerjee, *Chem. Commun.*, 2006, 2816-2818.
517. Y. Li and M. Liu, *Chem. Commun.*, 2008, 5571-5573.
518. R. N. Mitra and P. K. Das, *J. Phys. Chem. C*, 2008, **112**, 8159-8166.
519. D. Das, S. Maiti, S. Brahmachari and P. K. Das, *Soft Matter*, 2011, **7**, 7291-7303.
520. T. Kitamura, S. Nakaso, N. Mizoshita, Y. Tochigi, T. Shimomura, M. Moriyama, K. Ito and T. Kato, *J. Am. Chem. Soc.*, 2005, **127**, 14769-14775.
521. N. Das, *Hydrometallurgy*, 2010, **103**, 180-189.
522. I. S. Yunus and S.-L. Tsai, *RSC Adv.*, 2015, **5**, 20276-20282.
523. J. R. Dodson, H. L. Parker, A. Munoz Garcia, A. Hicken, K. Asemave, T. J. Farmer, H. He, J. H. Clark and A. J. Hunt, *Green Chem.*, 2015, **17**, 1951-1965.
524. A. Munoz Garcia, A. J. Hunt, V. L. Budarin, H. L. Parker, P. S. Shuttleworth, G. J. Ellis and J. H. Clark, *Green Chem.*, 2015, **17**, 2146-2149.
525. A. Patwa, J. Labille, J.-Y. Bottero, A. Thiery and P. Barthelemy, *Chem. Commun.*, 2015, **51**, 2547-2550.
526. R. Asadi-Kesheh, S.-A. Mohtashami, T. Kaghazchi, N. Asasian and M. Soleimani, *Sep. Sci. Technol.*, 2014, **50**, 223-232.
527. T.-L. Lin and H.-L. Lien, *Int. J. Mol. Sci.*, 2013, **14**, 9834-9847.
528. D. J. Vyas, B. A. Makwana, H. S. Gupte, K. D. Bhatt and V. K. Jain, *J. Nanosci. Nanotechnol.*, 2012, **12**, 3781-3787.
529. B. A. Makwana, D. J. Vyas, K. D. Bhatt, V. K. Jain and Y. K. Agrawal, *Spectrochim. Acta Part A: Mol. Biomol. Spectrosc.*, 2015, **134**, 73-80.
530. J. D. S. Newman and G. J. Blanchard, *Langmuir*, 2006, **22**, 5882-5887.

531. P. K. Jain, K. S. Lee, I. H. El-Sayed and M. A. El-Sayed, *J. Phys. Chem. B*, 2006, **110**, 7238-7248.
532. S. Eustis and M. A. El-Sayed, *Chem. Soc. Rev.*, 2006, **35**, 209-217.
533. S. Mohanty, S. Mishra, P. Jena, B. Jacob, B. Sarkar and A. Sonawane, *Nanomedicine: Nanotechnol. Biol. Med.*, 2012, **8**, 916-924.
534. M. Guzman, J. Dille and S. Godet, *Nanomedicine: Nanotechnol. Biol. Med.*, 2012, **8**, 37-45.
535. K. Juodkazis, J. Juodkazyt, V. Jasulaitien, A. Lukinskas and B. Šebeka, *Electrochem. Commun.*, 2000, **2**, 503-507.
536. Z. Yuan, N. Cai, Y. Du, Y. He and E. S. Yeung, *Anal. Chem.*, 2014, **86**, 419-426.
537. X. Yang, L. Gan, L. Han, E. Wang and J. Wang, *Angew. Chem. Int. Ed.*, 2013, **52**, 2022-2026.
538. A. A. Keller, H. Wang, D. Zhou, H. S. Lenihan, G. Cherr, B. J. Cardinale, R. Miller and Z. Ji, *Environ. Sci. Technol.*, 2010, **44**, 1962-1967.
539. T. C. Prathna, N. Chandrasekaran and A. Mukherjee, *Colloids and Surfaces A: Physicochem. Eng. Aspects*, 2011, **390**, 216-224.
540. H. Schmidbaur and A. Schier, *Chem. Soc. Rev.*, 2008, **37**, 1931-1951.
541. D. J. Cornwell, B. O. Okesola and D. K. Smith, *Soft Matter*, 2013, **9**, 8730-8736.
542. J.-H. Kim and T. R. Lee, *Chem. Mater.*, 2004, **16**, 3647-3651.
543. A. Riedinger, M. Pernia Leal, S. R. Deka, C. George, I. R. Franchini, A. Falqui, R. Cingolani and T. Pellegrino, *Nano Lett.*, 2011, **11**, 3136-3141.
544. D. Liu, E. Cheng and Z. Yang, *NPG Asia Mater.*, 2011, **3**, 109-114.
545. J.-K. Chen and C.-J. Chang, *Materials*, 2014, **7**, 805-875.
546. I. Odriozola, I. Loinaz, J. A. Pomposo and H. J. Grande, *J. Mater. Chem.*, 2007, **17**, 4843-4845.
547. Y. Zhao, B. Liu, L. Pan and G. Yu, *Energy Environ. Sci.*, 2013, **6**, 2856-2870.
548. J. R. Moffat, G. J. Seeley, J. T. Carter, A. Burgess and D. K. Smith, *Chem. Commun.*, 2008, 4601-4603.
549. M.-O. M. Piepenbrock, N. Clarke, J. A. Foster and J. W. Steed, *Chem. Commun.*, 2011, **47**, 2095-2097.
550. E. R. Zubarev, M. U. Pralle, E. D. Sone and S. I. Stupp, *Adv. Mater.*, 2002, **14**, 198-203.

551. C.-B. Laurell, *Anal. Biochem.*, 1966, **15**, 45-52.
552. D. Tautz and M. Renz, *Anal. Biochem.*, 1983, **132**, 14-19.
553. A. Broomfield and D. Bourn, *J. Laryngol. Otol.*, 1998, **112**, 230-234.
554. J.-F. Giot, in *J. Med. Biochem.*, 2010, vol. 29, p. 9.
555. S. Ikeda and K. Nishinari, *J. Agric. Food Chem.*, 2001, **49**, 4436-4441.
556. V. Breedveld, A. P. Nowak, J. Sato, T. J. Deming and D. J. Pine, *Macromolecules*, 2004, **37**, 3943-3953.
557. H. Huang, W. Li, H. Wang, X. Zeng, Q. Wang and Y. Yang, *ACS Appl. Mater. Interfaces*, 2014, **6**, 1595-1600.
558. J. M. Poolman, J. Boekhoven, A. Besselink, A. G. L. Olive, J. H. van Esch and R. Eelkema, *Nat. Protocols*, 2014, **9**, 977-988.
559. D. Das, T. Kar and P. K. Das, *Soft Matter*, 2012, **8**, 2348-2365.
560. Y. Li, Y. Ding, M. Qin, Y. Cao and W. Wang, *Chem. Commun.*, 2013, **49**, 8653-8655.
561. N. J. Ronkainen, H. B. Halsall and W. R. Heineman, *Chem. Soc. Rev.*, 2010, **39**, 1747-1763.
562. M. S. El- Deab and T. Ohsaka, *Electrochem. Commun.*, 2002, **4**, 288-292.
563. É. Lojou and P. Bianco, *J. Electroceram.*, 2006, **16**, 79-91.
564. S. Cosnier, *Electroanalysis*, 2005, **17**, 1701-1715.
565. M. Tosoni, M. Schulz and T. Hanemann, *Int. J. Electrochem. Sci.*, 2014, **9**, 3602-3617.
566. S. Štrbac and R. R. Adžić, *Electrochim. Acta*, 1996, **41**, 2903-2908.
567. T. M. Nahir, Y.-J. Qiu and J. L. Williams, *Electroanalysis*, 1994, **6**, 972-975.
568. X. Kang, J. Wang, H. Wu, I. A. Aksay, J. Liu and Y. Lin, *Biosens. Bioelectron.*, 2009, **25**, 901-905.
569. T. Dvir, B. P. Timko, M. D. Brigham, S. R. Naik, S. S. Karajanagi, O. Levy, H. Jin, K. K. Parker, R. Langer and D. S. Kohane, *Nat. Nano*, 2011, **6**, 720-725.
570. J. Zhou, J. Chen, H. Sun, X. Qiu, Y. Mou, Z. Liu, Y. Zhao, X. Li, Y. Han, C. Duan, R. Tang, C. Wang, W. Zhong, J. Liu, Y. Luo, M. Xing and C. Wang, *Sci. Rep.*, 2014, **4**, 3733.
571. M. Joergensen, K. Bechgaard, T. Bjoernholm, P. Sommer-Larsen, L. G. Hansen and K. Schaumburg, *J. Org. Chem.*, 1994, **59**, 5877-5882.

572. T. Kitahara, M. Shirakawa, S.-i. Kawano, U. Beginn, N. Fujita and S. Shinkai, *J. Am. Chem. Soc.*, 2005, **127**, 14980-14981.
573. Thierry L. Gall, C. Pearson, Martin R. Bryce, Michael C. Petty, H. Dahlgaard and J. Becher, *Eur. J. Org. Chem.*, 2003, **2003**, 3562-3568.
574. K. Hashizaki, H. Taguchi and Y. Saito, *Colloid Polym. Sci.*, 2009, **287**, 1099-1105.
575. M. Pernetti, K. van Malssen, D. Kalnin and E. Flöter, *Food Hydrocolloids*, 2007, **21**, 855-861.
576. K. Trickett, H. Brice, O. Myakonkaya, J. Eastoe, S. E. Rogers, R. K. Heenan and I. Grillo, *Soft Matter*, 2010, **6**, 1291-1296.
577. P. K. Vemula and G. John, *Acc. Chem. Res.*, 2008, **41**, 769-782.
578. H. M. Schaink, K. F. van Malssen, S. Morgado-Alves, D. Kalnin and E. van der Linden, *Food Res. Int.*, 2007, **40**, 1185-1193.
579. G. Amidon, H. Lennernäs, V. Shah and J. Crison, *Pharm. Res.*, 1995, **12**, 413-420.
580. D. Bolten, R. Lietzow and M. Türk, *Chem. Eng.Technol.*, 2013, **36**, 426-434.
581. M. Türk, *J. Supercrit. Fluids*, 2009, **47**, 537-545.
582. M. Türk and D. Bolten, *J. Supercrit. Fluids*, 2010, **55**, 778-785.
583. P. A. Bhat, G. M. Rather and A. A. Dar, *J. Phys. Chem. B*, 2009, **113**, 997-1006.
584. M. E. Brewster, W. R. Anderson, K. S. Estes and N. Bodor, *J. Pharm. Sci.*, 1991, **80**, 380-383.
585. M. Cirri, F. Maestrelli, G. Corti, S. Furlanetto and P. Mura, *J. Pharm. Biomed. Anal.*, 2006, **42**, 126-131.
586. J. Buse and A. El-Aneed, *Nanomedicine*, 2010, **5**, 1237-1260.
587. S. Mignani, S. El Kazzouli, M. Bousmina and J.-P. Majoral, *Adv. Drug Deliv. Rev.*, 2013, **65**, 1316-1330.
588. D. Wesselinova, *Curr. Cancer Drug Targets*, 2011, **11**, 164-183.
589. B. Haley and E. Frenkel, *Urologic Oncology: Seminars and Original Investigations*, 2008, **26**, 57-64.
590. R. B. Greenwald, Y. H. Choe, J. McGuire and C. D. Conover, *Adv. Drug Deliver. Rev.*, 2003, **55**, 217-250.
591. R. Sinha, G. J. Kim, S. Nie and D. M. Shin, *Mol. Cancer Ther.*, 2006, **5**, 1909-1917.

592. M. C. Branco and J. P. Schneider, *Acta Biomater.*, 2009, **5**, 817-831.
593. W.-W. Yang and E. Pierstorff, *J. Lab. Autom.*, 2012, **17**, 50-58.
594. A. Vashist, A. Vashist, Y. K. Gupta and S. Ahmad, *J. Mater. Chem. B*, 2014, **2**, 147-166.
595. G. Cirillo, S. Hampel, U. G. Spizzirri, O. I. Parisi, N. Picci and F. Iemma, *BioMed Res. Int.*, 2014, **2014**, 17.
596. R. B. Weiss, R. C. Donehower, P. H. Wiernik, T. Ohnuma, R. J. Gralla, D. L. Trump, J. R. Baker, D. A. Van Echo, D. D. Von Hoff and B. Leyland-Jones, *J. Clin. Oncol.*, 1990, **8**, 1263-1268.
597. A. ten Tije, J. Verweij, W. Loos and A. Sparreboom, *Clin. Pharmacokinet.*, 2003, **42**, 665-685.
598. P. K. Vemula, N. Wiradharma, J. A. Ankrum, O. R. Miranda, G. John and J. M. Karp, *Curr. Opin. Biotech.*, 2013, **24**, 1174-1182.
599. B. Xing, C. W. Yu, K. H. Chow, P. L. Ho, D. Fu and B. Xu, *J. Am. Chem. Soc.*, 2002, **124**, 14846-14847.
600. S. Bhuniya, Y. J. Seo and B. H. Kim, *Tetrahedron Lett.*, 2006, **47**, 7153-7156.
601. P. K. Vemula, G. A. Cruikshank, J. M. Karp and G. John, *Biomaterials*, 2009, **30**, 383-393.
602. J. Li, Y. Kuang, Y. Gao, X. Du, J. Shi and B. Xu, *J. Am. Chem. Soc.*, 2012, **135**, 542-545.
603. A. Friggeri, B. L. Feringa and J. van Esch, *J. Control. Release*, 2004, **97**, 241-248.
604. S.-i. Kawano, N. Fujita, K. J. C. v. Bommel and S. Shinkai, *Chem. Lett.*, 2003, **32**, 12-13.
605. S. Bhuniya, S. M. Park and B. H. Kim, *Org. Lett.*, 2005, **7**, 1741-1744.
606. P. K. Vemula, J. Li and G. John, *J. Am. Chem. Soc.*, 2006, **128**, 8932-8938.
607. S. Cao, X. Fu, N. Wang, H. Wang and Y. Yang, *Int. J. Pharm.*, 2008, **357**, 95-99.
608. M. Rodrigues, A. C. Calpena, D. B. Amabilino, M. L. Garduno-Ramirez and L. Perez-Garcia, *J. Mater. Chem. B.*, 2014, **2**, 5419-5429.
609. T. Furuishi, K. Tomono, T. Suzuki, T. Fukami and K. Kunimasu, *US Patent* 2012/0264742 A1, 2012.
610. L. Karila, A. Weinstein, H.-J. Aubin, A. Benyamina, M. Reynaud and S. L. Batki, *Br. J. Clin. Pharmacol.*, 2010, **69**, 578-592.

611. L. Chen, S. Revel, K. Morris and D. J. Adams, *Chem. Commun.*, 2010, **46**, 4267-4269.

612. A. Wada, S.-i. Tamaru, M. Ikeda and I. Hamachi, *J. Am. Chem. Soc.*, 2009, **131**, 5321-5330.

613. S. S. Babu, V. K. Praveen and A. Ajayaghosh, *Chem. Rev.*, 2014, **114**, 1973-2129.

614. Y. Cai, Y. Shi, H. Wang, J. Wang, D. Ding, L. Wang and Z. Yang, *Anal. Chem.*, 2014, **86**, 2193-2199.

615. H. Tozaki, T. Odoriba, N. Okada, T. Fujita, A. Terabe, T. Suzuki, S. Okabe, S. Muranishi and A. Yamamoto, *J. Control. Release*, 2002, **82**, 51-61.

616. K. Mladenovska, R. S. Raicki, E. I. Janevik, T. Ristoski, M. J. Pavlova, Z. Kavrakovski, M. G. Dodov and K. Goracinova, *Int. J. Pharm.*, 2007, **342**, 124-136.

617. X. Li, J. Li, Y. Gao, Y. Kuang, J. Shi and B. Xu, *J. Am. Chem. Soc.*, 2010, **132**, 17707-17709.

618. J. E. N. Bhala, A. Merhi, S. Abramson, N. Arber, J. A. Baron,, C. C. C. Bombardier, M. E. Farkouh, G. A. FitzGerald, P. Goss,, H. Halls, E. Hawk, C. Hawkey, C. Hennekens, M. Hochberg, L. E. Holland, P. M. Kearney, L. Laine, A. Lanas, P. Lance, A. Laupacis, J. Oates, C. Patrono, T. J. Schnitzer, S. Solomon, P. Tugwell, K. Wilson, J. Wittes and C. Baigent, *The Lancet*, 2013, **382**, 769-779.

619. R. Feng, L. Chen, Z. Hou and J. Song, *Trans. Tianjin Univ.*, 2007, **13**, 35-41.